Lateral connectivity : propagation of network belief and hallucinatory-like states in the primary visual cortex

Benoît Le Bec

Sorbonne Université

Ecole doctorale Cerveau, Cognition et Comportement

Thèse de Doctorat de Neuroscience Cognitive

Benoît Le Bec

Lateral connectivity: propagation of network belief and hallucinatory-like states in the primary visual cortex

Thèse Dirigée par Yves Frégnac et Marc Pananceau
Présentée et soutenue publiquement le : lundi 03 décembre 2018

Devant le Jury composé de :

Dr. Laurent Perrinet	Rapporteur
Dr. Rufin VanRullen	Rapporteur
Dr. Jean-Marc Edeline	Examinateur
Pr. Stéphane Charpier	Examinateur
Dr. Yves Frégnac	Directeur de thèse
Dr. Marc Pananceau	Co-directeur de thèse

“When you open your mind to the impossible, sometimes you find the truth...Based on our findings we developed a window of sorts, a way of looking into this neighboring world. This window works by capturing errant photons from the universe beside ours. The window essentially stretches the membrane between our worlds and allows us to see their image from our side...Geometry and harmonic vibrations, that’s how we did it, Belly and I. Send Belly’s Monte Carlo from this universe to the other side. As I’ve said before, the two universes vibrate at different frequencies so we set up three harmonic rods arranged as an equilateral triangle and then we activated the rods. When the car began to vibrate at just the right frequency—that’s how we sent Belly’s car to the other side...I designed a device intended to cross the time-space continuum and retrieve my dying son...This is the boy I showed you, the other Peter. It was the only way I could save him...Elizabeth, don't. He's not ours. I have to take him back...I realized at that moment that despite what I'd promised, what I fully intended to do, that I could never take Peter back. The way she looked at him. I saw in her what I feared most in myself when I saw him: I couldn't lose him again. It was the first hole, Olivia. The first breach. The first crack in the pattern of cracks. Spaces between the worlds. And it's my fault. You can't imagine what it's like to lose a child...You and I both know there are certain things we take for granted. The laws of nature, for example that are not necessarily binding. There are places on this Earth where two plus two most definitely does not equal four. You figured out how to bend time. But you're only interested in traveling to the past. Your goal, your next jump, is the 18th of May....Then allow me to serve as a precautionary tale. There will be repercussions if you pull Arlette from that car. You don't know how things will be changed by your actions, but they will. It's not our place to adjust the universe. And you will never be able to look at her again without knowing that, just like every time I look at my son. I have traveled through madness to figure this out. And you will too.”

Walter Bishop, Fringe

Remerciements - Acknowledgements

Il n'est jamais aisé de trouver des mots pour retranscrire souvenirs et émotions d'une portion de vie. Le langage semble bien souvent insuffisant pour en refléter l'étendue. Si j'ai bien appris quelque chose lors de ces années de thèse, c'est qu'il n'existe pas de voie toute tracée ; contrairement aux idéaux naïfs du néophyte, je crois que nous ne pouvons que tenter de faire de notre mieux, continuellement, et que c'est déjà beaucoup. Il est donc venu le temps pour moi de refermer un chapitre, de tourner une page. Le vingt-trois décembre deux mille treize qui marque le début de cette histoire, mon frère et moi partîmes en voiture de notre Bretagne natale pour que j'aille visiter l'Unic. Après plus de trois heures de discussion avec Yves Frégnac, nous nous serrâmes la pogne et je rentrai chez moi pour Noël sous vent de tempête avec une idée en tête : faire une thèse en neuroscience.

Je remercie tout d'abord les membres de mon jury : Laurent Perrinet et Rufin VanRullen pour leur accessibilité et l'intérêt qu'ils ont porté à ce travail en acceptant d'être rapporteurs de ma thèse, Stéphane Charpier pour sa disponibilité et sa gentillesse ainsi que Jean-Marc Edeline dont la bienveillance, le calme et la curiosité scientifique m'ont toujours inspiré. Je remercie également Jean Lorenceau pour ses précieux conseils et son accompagnement lors de ma thèse.

Je remercie Yves Frégnac pour m'avoir accueilli au sein de son laboratoire, pour m'avoir donné ma chance et pour m'avoir fait confiance. Yves, tu m'as laissé les coudées franches en t'assurant que j'étais entouré d'un noyau solide pour avancer. Je crois que ce qui me marquera le plus sont tes arrivées au labo, suivies du fameux « réunion en salle de vie dans cinq minutes ». C'est seulement couche par couche, pas à pas, que j'ai progressivement découvert ton univers de recherche. Richesse qui vient de l'intérieur, que l'on parle de l'Unic intra-muros ou d'une cellule. C'est ton recul scientifique, nourri par ton goût de la rigueur étymologique qui m'inspire le plus grand respect, et sans lequel ma thèse ne serait pas ce qu'elle est aujourd'hui. Tu as su m'aider, m'encourager et me soutenir pendant l'écriture du manuscrit. En tout cela trouve mon amitié et un grand merci !

Marc, il y'a tellement de choses à dire… Que ce soit ta gentillesse ou les fous rires…C'est bien simple, sans toi, je ne connaitrais rien de l'intra. Je garde précieusement en mémoire les moments de délire ou, à quatre heures du mat, on empale une cellule sur du David Gilmour. Des choses qui m'impressionnent le plus chez toi, je retiens ton humilité et ta pédagogie. Combien de fois nous ne nous sommes pas retrouvés en manip à attendre ton retour providentiel, après lequel ni une ni deux, on retrouve espoir. Pour toutes les discussions également, passionnées, endiablées, you are the star ! Merci pour tes conseils, ta compréhension et ta présence dans les moments difficiles. De tes blagues répétées sur le chouchen, je garde le rythme et j'enchaîne. De toi, je garde l'image que tu m'as donnée : celle d'une goutte d'eau qui coule, déroule, toujours vers l'aval ! La première fois aperçue, dit-on, dans une rivière de Durtal.

J'en viens maintenant à toi Chris, mon collègue de bureau, mon binôme. Qu'est-ce qu'on a pu en voir tous les deux ! Toujours sur le pont du lundi au dimanche, toujours avec ta joie de vivre, ton envie de voir le verre à moitié plein. C'est en grande partie grâce à toi que j'ai tenu toutes ces années,

sans aucun doute. Non seulement tu m'as épaulé, mais tu m'as également porté par moments. Ta souplesse d'esprit, ton empathie et la finesse de tes analyses ont réellement fait de toi le cœur de notre esprit d'équipe, contre vents et marées. Un baroudeur kayakiste qui bricole de ses mains, chercheur, véto, anesthésiste qui d'un seul geste esquisse le travail de demain. Ce qui frappe le plus dans ta manière d'enseigner n'est pas la certitude de ce que tu assènes, mais la façon dont tu distribues les clés qui permettront de te convaincre. Prendre l'air, discuter avec toi de tout et de rien, je n'aurais pu rêver d'un meilleur voisin !

Merci à toi Xoana pour les moments passés ensemble. Comme tu l'as dit, travailler de nuit, ça crée des liens ! Tantôt à la rame, tantôt à la proue, on a souqué ferme pour aller jusqu'au bout. De toi je garde l'extrême rigueur scientifique, l'analyse, l'argumentation. Je crois que j'ai appris auprès de toi plus que je ne m'en rends compte. De la Galice à paris tu as fait beaucoup de chemin. Maintenant que ta voile tend vers de nouveaux horizons, le meilleur pour toi et les tiens !

Gérard, sans toi cette section aurait peu de sens puisqu'elle n'existerait probablement pas. J'ai découvert en toi tout un monde qui s'exprime davantage par les actes que par la parole. Et puis j'ai commencé à envahir ton bureau, venant te voir de plus en plus, apprenant. Tu es la personne qui a donné un sens à ma thèse, me fournissant chaque jour de nouveaux buts, des objectifs à atteindre quand ma boussole n'indiquait plus le nord. En un tour de main, l'air de rien, toujours avec tact et sans jamais un mot plus haut que l'autre, j'ai bien vite compris la nécessité d'écouter et d'observer pour plonger de plus en plus profondément dans ta logique de la programmation. Et j'y ai pris goût, tu ne peux pas savoir à quel point ! Jeux vidéo, technologie et romans, pas étonnant que j'ai rappliqué si souvent ! Tu es brillant mais jamais je ne t'ai entendu le crier à tout vent. Des merveilles d'Elphy qui ont dépassé les frontières, tu es l'unique, dépositaire. Au-delà de la pure réflexion, de tes propres mains, avec Solange, tu as même rebâti ta maison ! Tu as cependant gardé une âme d'enfant, que ce soit au ping pong ou en bricolant ! Ton héritage s'étend cependant au-delà d'Elphy car je ne sais pas quel sentier je suivrai, mais comme d'autres avant moi l'on dit, j'espère qu'il portera ton empreinte. Et si un jour je m'égare, je penserai à toi, merci Gérard.

Cyril, les discussions avec toi ont toujours été instructives. Merci pour ton oreille attentive, tes conseils et ton aide. Merci également pour tadadam… Univision ! Correctement implémenter des stimulations visuelles tient parfois à peu de chose… ne serait-ce qu'un seul pixel.

Merci à Valérie pour ton énergie communicative, à Isabelle pour ta force tranquille, à Evan pour ton punch et à Matias pour tes conseils avisés et ton recul. Merci également à toi Dan pour ta sollicitude, ton calme et ton oreille attentive.

Merci Andrew pour ton aide, Michelle pour ton grain de folie, Claude pour ton pragmatisme fondamental. Jan pour ton sens critique, Luc Foubert pour l'arbre et tant d'autre chose, Luc Estebanez pour ton rire, Bartosz pour ta joie de vivre et la facilité avec laquelle tu viens aider les autres.

Merci Gilles, que ce soit pour m'apprendre à chlorurer un fil, commander des headers, venir tester du voltage clamp ou alors plaisanter et discuter sur la terrasse. Qu'il fasse beau ou qu'il pleuve, tu as toujours été là. Le meilleur pour Francesca, Nell et toi !

Merci à Irina et Katherine pour toujours veiller au grain.

Merci Rémi pour les délires en Time lapse, Tony et Alvino pour les coups de mains et William pour ton aide. Je n'oublie pas Paul, qui m'a aidé à m'adapter à la vie à l'Unic, ainsi que Thomas pour le temps que tu as su m'accorder, ta patience et ta pêche.

Roland, merci à toi, je ne garde que de bons souvenirs de boutades douteuses combinées à des moments de galère et de discussions permettant de s'évader. Hélissande, Shailesh, Joffrey, Lungsi, Onur, Elodie, Matthieu et bien sûr Pedro, pour toutes les bonnes soirées à la brasserie. Vous formez une super bande.

Sylvia, je n'ai toujours pas vu « la mouche » mais je compte bien y remédier ! C'était génial de discuter avec toi, tu m'as bien souvent remonté le moral même lorsque tu me réveillais le matin en tapant sur la vitre de la terrasse comme une furie, mais toujours avec style…

Une pensée toute particulière pour Jean-Paul qui bien souvent a dû me rattraper par le col ! Merci pour l'écoute, la patience, le soutien. C'est en partie dans notre lien que j'ai trouvé la sagesse de temporiser, un phare dans une mer déchaînée qui a permis la traversée.

Merci également à Cyrille Vaillend et Rémi Chaussenot, deux compères avec qui j'ai débuté le travail de recherche et à qui je dois beaucoup.

A ceux qui m'ont enseigné : Jacqueline, Jean François, Daniel et Alain, merci.

Aurélie, sans toi notre travail ne serait pas ce qu'il est. Je te remercie mille fois pour m'avoir appris les fondamentaux de l'expérimentation et pour ta présence avec nous en manips. Sans toi les thésards qui arrivent seraient bien vite dépassés. Ta présence, ton aide et ta disponibilité ont été une bouffée d'air frais qui soufflera encore bien des années.

Justine, ta patate et ton sourire manquent au labo. La chef de file de l'équipe des chocovores me restera longtemps en mémoire. Jour après jour, pour tout le monde, tu n'as jamais ménagé tes efforts, toujours la première à installer le sapin de Noël. Merci pour ta bonne humeur communicative et ta patience pour intégrer chacun.

Guillaume, maître de la révélation histologique, j'ai toujours adoré ton sens pratique. Pas susceptible pour un rien, toujours à trouver une solution, juste serein. De la tête du lundi matin à celle du vendredi aprem, ça déroule les vannes, ça enchaine ! Y'a pas à dire, t'est un pro, de la préparation des solutions au timing des pots ! Sur la même longueur d'onde, on a bien déconné tous les deux, alors à bientôt et merci mon vieux.

Aline…ah Aline… Tant de choses à dire et si peu de mots pour l'écrire ! Trouver une gestionnaire métalleuse fan de l'assassin royal était encore moins probable que d'obtenir des résultats dans la seconde partie de ma thèse, c'est pour dire... Ton caractère bien trempé et tes regards assassins m'ont toujours fait marrer et jouer au taquin. Mais Derrière tes murailles d'art, barricadées de tourelles se cache un univers rare où le respect est naturel. Merci de ta franchise et de ta présence quotidienne, toi qui entre deux cartes rassemblées, de l'Unic reste la gardienne.

Yannick le magnifique. Mine de rien, on en a fait du chemin…De nos débuts de galère, beaucoup me revient. L'important, c'est que j'ai toujours pu compter sur toi, ramant côte à côte, sans que l'on sache vraiment vers ou on allait. Qu'importe, on l'a fait ! Roublard comme pas deux, ténor de l'impro, tu as su apporter de la vie au labo. Sans savoir ce que demain nous réserve, merci pour tout, je ne m'inquiète pas, car le mercato n'attend que toi !

Margot, pour te lancer dans une thèse parallèle sur le RER B, il n'y a que toi. Non pas que je m'inquiète car je sais que tu y arriveras ! Générer des images n'est pas artificiel, garde le dans ton escarcelle, ça te servira. Tu atteins maintenant la dernière phase de la flèche décochée, en approche de la cible, prête à la moucher ! Tu es une vraie bosseuse et cela paiera, malgré les bosses parfois nombreuses que l'on rencontre… Le meilleur pour la suite car cela va arriver vite.

Domenico, garde ta barbe, elle te va à merveille ! Entre le cortex et le thalamus, tu n'as pu choisir… alors tu as relié les deux, juste pour le plaisir. Ton calme olympien combiné à ton humour taquin ont fait de toi le grand frère de tous les thésards. Mais dans l'âme tu as su rester un gamin et c'est là ta plus grande force. Toujours à me bousculer, l'air de rien, je veux juste garder l'image de Gilles et toi au magasin de bricolage…Merci pour tout, et à bientôt sous la houle bretonne !

Pauline, de notre promo de Master 2 à la fin de ta thèse, je ne sais pas ou tu as trouvé toute cette énergie ! Travailleuse acharnée, collègue du weekend au cœur de l'été comme au solstice d'hiver, aucun thésard n'a fait autant de kilomètres que toi ! Tantôt au bureau, en manip ou à l'atelier mécano, tu as toujours tenu la ligne de front. Et du labyrinthe que tu as toi-même construit, tu as su t'extraire, merci et bravo pour ta grande force de caractère.

Merci Alex pour ton peps et les beers on the grass. Aamir, Dorian, Sebastian, vous êtes sur la bonne voie ! Merci Jonathan, Eugenia et Yann, le thésard le plus stylé que je connaisse.

Je pense également à mes collègues de Fac : Guillaume, Kévin, Aurélien, Anthonin, Anthony. Bien que nos chemins se soient éloignés, votre voix, parfois retentit.

Mario, you're the most stubborn person that I have ever met. Without our chessgames and our talks, I wouldn't have had the occasion to breathe. I learned so much with you bro but above all, you made me truly understand and accept that whatever happens in life, we've got to deal with it and that in the end, that's all that matters. I don't see in you the categorization that society craves for, just the man under the béret, and that's enough. Valar Morghulis.

Steeve, tu m'as pris sous ton aile alors que tu pipetais encore au CNPS. Depuis, je n'ai jamais vu quelqu'un qui soit si ouvert d'esprit et qui ne juge pas. Des parties de dés avec Amina chez moi aux soirées avec Rémi, Florian, Pilou, Quentin et Alex à la pizzeria, j'ai toujours eu le même ressenti : peu importe le temps qui s'écoule, quand on se retrouve, on se comprend sans avoir à parler. Ton rhum réchauffe les cœurs, richesse venant de l'intérieur chez toi, merci l'ami pour le Genkidama !

Jonathan et Jé, vous restez là.

Merci aux zozos de la batri pour m'avoir accueilli quand j'en avais besoin.

Nico, Will, Yann, Fab, Pierre, Benj, Laurence, Dam, Sophie, vous tenez la marée !

Al pour ton amour de la nature, Typhaine pour qui tu es.

Lilian, Charlotte, Agathe, Ol, Lambert, Ivan, Marion, Loïc, Mago, Cédric, Rémi et Sophie, quand vous voulez on ressort le bilig et c'est reparti !

Hélène et Jean-Pierre, c'est toujours un plaisir de vous voir, merci pour toutes les fois où vous m'avez accueilli chez vous et celles à venir !

Lolo, le boss du poteau. Délirer avec toi depuis toutes ces années ne se fait qu'en franchissant de nouveaux paliers !

Meryl le baroudeur qui ne se laisse pas enfumer, pourtant fumiste à tes heures, tu sais comment rigoler !

Pour Adri, toi le comptable dont la tolérance à l'alcool n'a d'égal que l'habileté à jongler avec les chiffres, merci !

Le voici le meilleur, triste clown à l'allure de chasseur. Jean-Bapt, 25 ans depuis la maternelle, sur les côtes du Finistère, on te dit lost in the swell. Toi le waverider avec qui j'ai tant partagé, mon roc fait d'écume et de fumée. Non content de faire des vagues, tu sais aussi les surfer ! Mais du bac à sable à aujourd'hui toujours le même, on déchaine les envies, Carpe Diem ! Le jah work ça te parle, tu caracoles sur un tube à ta façon, avec Foxy, sur ta board, tu traces ton propre horizon. Et quand claque le ressac dans le plus grand fracas, on te voit toujours debout, la victoire au bout des doigts ! Merci pour le pire, merci pour le meilleur, petit loup toujours fou mais surtout au grand cœur.

De mes grands parents, qui m'ont tant montré, je n'oublie pas et je pense à vous.

A mes parents Catherine et Georges et à mon frère Arnaud, sans votre soutien je n'aurais pu arriver à bon port. Cette thèse vous est dédiée, merci.

Lateral connectivity: propagation of network belief and hallucinatory-like states in the primary visual cortex

Abstract

Because of its reported anisotropic patchy aspect spanning several hypercolumns, lateral connectivity has long been presented as the biological substrate of iso-preference binding in the electrophysiological and psychophysical cortical literature. From a functional point of view, the preferential iso-binding of lateral connections has been associated with center-surround facilitatory effects between elements iso-aligned in the visual field. At the psychophysical level, this view corresponds to the perceptual "association field" concept. To a large degree, the role of long distance horizontal connectivity in influencing the response gain within the classical receptive field, and in particular in boosting it for specific center-surround stimulus conditions remains an issue of debate. More precisely, a remaining unsolved issue is to determine to which extent horizontal connections, intrinsic to V1, are already instrumental to the neural implementation of Gestalt psychophysical laws of perceptual binding in low level perception. Traditionally, binding in space and across time are thought to be implemented in separate cortical areas, respectively in V1 and MT. The work of this thesis is based on *in vivo* intracellular recordings of the primary visual cortex of the anaesthetized animal.

In the first part of this thesis, we examined the functional impact of centripetal apparent motion sequences of stimuli originating from the far periphery and converging towards the receptive field center of individual cells along their preferred orientation axis. We show that at high saccadic speed, the anisotropic congruency of individual elements embedded in a coherent motion flow is crucial in the lateral broadcast and effective integration of contextual information. Those results are translated at the electrophysiological level by a latency advance and amplitude gain of the response at the sub- and under certain circumstances, suprathreshold level when compared to the sole feedforward stimulation of the RF center. Our results highlight the existence of a dynamic association field that allows to bind form and motion as early as V1. Second, in a subset of cells, coherent apparent motion sequences restricted to the silent periphery resulted in a prediction invasion of activity filling-in the unstimulated RF. Our results shade a new light on a potential generalisation of the Hierarchical Predictive Coding framework by suggesting that V1 possesses its own mechanism of lateral diffusion of a predictive "network belief" allowing to solve the motion extrapolation problem.

In the second part of this thesis we focused on the possibility that geometric hallucinations reflect a long distance spatial opponency of the horizontal connectivity in V1. We posit that cortical adaptation to a geometric inducer constrain the exploration of neighbouring orientation domain transition, as observed in the cat ongoing activity and developed a phenomenological model of hypercolumns interactions resulting in the formation of stripes of activity on V1 surface. We designed visual stimuli in which the perturbation by a $1/f^{\alpha}$ noise possessing natural spatio-temporal statistics of a *highly* biased network adapted to a geometric planform (radial fans shapes and concentric annuli) resulted in the emergence of dynamic opponent percepts reflecting waves of activity orthogonal to the geometric physical inducers. We manipulated the center of the geometric inducers position in order to render the perceived wavefront of the propagating percepts locally parallel to the preferred orientation of individual cells. Our preliminary results suggest that such waves of hallucinatory-like activity do emerge in the primary visual cortex and are detectable at the single cell level under the form of oscillations of the membrane potential matching the perceived dynamic of the propagating percepts. Moreover, their geometric distribution in the cortical space is of paramount importance in the detectability of their oscillatory signature.

Keywords: Primary visual cortex, lateral connectivity, form, motion, binding, filling-in, prediction, neurogeometry, opponent planforms, oscillations

Connectivité latérale : propagation d'une croyance de réseau et états hallucinatoires dans le cortex visuel primaire

Résumé

De par son aspect anisotrope formant des patchs couvrant plusieurs hypercolonnes, la connectivité latérale a depuis longtemps été présentée comme le substrat biologique du liage préférentiel entre éléments iso orientés dans la littérature corticale électrophysiologique et psychophysique. D'un point de vue fonctionnel, le liage préférentiel entre éléments iso orientés par les connections latérales s'est vu associé aux effet facilitateurs entre le centre et le pourtour d'éléments iso alignés dans le champ visuel. Au niveau psychophysique, cette notion correspond au concept de champ d'association perceptuel. Dans une large mesure, au sein du champ récepteur classique, l'influence des connections horizontales longue distance dans le gain de réponse contextuel et, en particulier dans son amplification lors de stimulations centre-pourtour particulières font toujours débat. Plus précisément, il reste à déterminer dans quelle mesure les connections horizontales propres à V1 sont déjà nécessaires à l'implémentation neurale des lois psychophysiques du lien perceptuel de la Gestalt dans la perception bas niveau. Il est traditionnellement considéré que le liage dans l'espace et le temps sont implémentés dans différentes aires corticales qui correspondent respectivement à V1 et MT. Le travail de cette thèse est basé sur des enregistrements intracellulaires *in vivo* dans le cortex visuel primaire d'animaux anesthésiés.

Dans la première partie de cette thèse, nous avons examiné l'impact fonctionnel de séquences de mouvement apparent centripète prenant son origine dans la périphérie lointaine et convergeant vers le champ récepteur de cellules individuelles le long de leur axe d'orientation préféré. Nous montrons qu'à haute vitesse saccadique, la congruence anisotrope d'éléments individuels composants un mouvement cohérent est cruciale, à la fois dans la diffusion latérale et dans l'intégration d'information contextuelle. Ces résultats se traduisent au niveau électrophysiologique par une avance de latence et un gain d'amplitude des réponses sous, et dans certaines circonstances, supraliminaires par rapport à la seule stimulation du centre du champ récepteur. Nos résultats soulignent l'existence d'un champ d'association dynamique qui permet de lier forme et mouvement dès V1. Deuxièmement, les réponses d'un sous-groupe de cellules ont montré l'invasion du champ récepteur non rétinotopiquement stimulé par une activité prédictive lorsque le mouvement apparent était restreint à la périphérie silencieuse du champ récepteur. Nos résultats mettent en évidence une potentielle généralisation du codage prédictif hiérarchique en suggérant que V1 possède son propre mécanisme de diffusion latérale d'activité prédictive sous la forme d'une "croyance de réseau" lui permettant de résoudre le problème d'extrapolation du mouvement.

Dans la deuxième partie de cette thèse nous nous sommes concentrés sur la possibilité que les hallucinations géométriques reflètent une opposition spatiale longue distance de la connectivité horizontale. Nous postulons que l'adaptation corticale à un inducteur géométrique contraint l'activation transitoire de domaines d'orientation adjacents, phénomène déjà observé dans l'activité spontanée du chat et avons développé un modèle phénoménologique d'interactions entre hypercolonnes expliquant la formation de bandes d'activité sur la surface de V1. Nous avons créé des stimuli visuels dans lesquels la perturbation par un bruit en $1/f^{\alpha}$ possédant des statistiques spatio-temporelles naturelles d'un réseau fortement adapté à des inducteurs géométriques (hélices radiales et anneaux concentriques) induit la perception de planforms dynamiques opposés reflétant des vagues d'activités orthogonales aux inducteurs géométriques. Nous avons manipulé la position du centre des inducteurs géométriques afin que les fronts d'onde des percepts induits soient localement parallèles à l'orientation préférée de cellules individuelles. Nos résultats préliminaires montrent que de telles vagues d'activité hallucinatoire émergent bel et bien dans V1 et sont détectables au niveau de cellules individuelles sous la forme d'oscillations du potentiel de membrane correspondant à la dynamique des percepts se propageant. De plus, leur distribution géométrique dans l'espace cortical est cruciale dans la détectabilité de leur signature oscillatoire.

Mots clés : cortex visuel primaire, connectivité latérale, forme, mouvement, liage, complétion, prédiction, neurogéométrie, planforms opposées, oscillations

Content

General Introduction

1.1 The construction of a global percept

Addressing the notion of perception first requires an approach of its definition, settling a common ground upon which further discussion can be developed. The word perception derives from the Latin *perceptio* "action of grasping by the mind", itself derived from *percipere* "to collect". According to the French Larousse dictionary, the definition of perception is the following: "cognitive event in which a stimulus or an object present in the immediate environment of an individual is represented to him in its internal psychological activity, in principle in a conscious manner". Two conclusions directly emerge from that definition: first, our perception is not a replica of the external world but an internal reconstruction of this latter, second, the action of grasping confers an active role to the mind of the individual, under the form of a state referred to as conscious. From the first conclusion, we deduce that there is an initial step of transformation or processing of information of the sensory input detected by the peripheral sensory organs (eye, ear, skin…). That step corresponds to the transduction of the sensory receptors of those different organs, classified into distinct senses or modalities, transforming photons for vision, acoustic vibrations for hearing, mechanical pressure for the haptic sense and volatile or dissolved chemicals for taste and olfaction into electric activity transmitted in the brain. This initial transduction corresponds to sensations and does not necessarily require an active contribution of the mind or, in other words, does not requires consciousness. Perception then resembles more to a progressive processing of information within the brain than to an abrupt jump in information integration as we see that some operations involved in perception are already performed without any active contribution of the mind. The so called "conscious" wall that we erected to reach perception might then delineates a barrier that is much blurrier than commonly accepted. We do not argue here that the emergence of consciousness does not heavily impacts perception by providing attentional processes but simply aim to discard the dichotomy between conscious perception and unconscious sensations to highlight the scope of intermediate physiological processes involved in perception.

Low level perception is a step that can be defined as the neural-based computations building unconscious or self-generated inferences under the form of perceptual primitives in early primary sensory cortical areas (Fregnac and Bathellier, 2015). It does not necessarily requires attentional processes but is a necessary step where operations reformate sensory input in a neuronal language which will allow more abstract processing by higher cognitive-like areas. Perceptual primitives are inferences that emerge effortlessly ("pop out"), reflecting an automatic interpretation of our environment or expectations of the brain about what is to be perceived. They are based on already built-in mechanisms forged from past sensory experiences (Schulz and Fregnac, 2010). Thus, exposure to our environment shape and conditions low level neural-based computations via plasticity mechanisms occurring mostly during critical stages of development but also during later

stages of life. This allows us to infer meaning, by confronting real time sensory evaluation and past experiences built on the previous evaluation of appropriate/inappropriate behaviours. The choice of the behaviour evaluated as appropriate is then applied in order to adapt ourselves to our continuously varying environment. However, sensory illusions prove that our sensory evaluation is not always "correct" as they do not reflect the pure physical reality, leading sometimes to "erroneous inferences" about the sensory input. Those illusions are the perceptual manifestation of stimulus inference in the brain where what we see (perceive) is not what we get (receive). Our perception of the world does not rely on the sole physical description of the features composing our environment but rather on their overall integration, leading to the extraction of a global "picture" of the current state in which our organism is. This imply a confrontation between sensory inferences provided by different modalities (polymodal congruence) where the combination of multimodal expectations provides a context that allows to solve ambiguity in the case of erroneous inference provided by one modality, for example during a visual illusion. Memories or previous occurrences of the combination of such contextual information are then searched for/recalled or act as a continuous weft forming a comparison basis, allowing us to establish a confidence of what we accept as our most immediate reality.

Polymodal integration provides a multi contextual framework in which each modality is a referential sampling a given type of information. Below this level of integration, at the level of a single sensory modality, context also matters as in order to fully capture and analyse a type of information (sound, texture…), our receptors must be able to *discriminate* information among a wide range of variations reflecting the environment. It implies that our sensory receptors compose a wide panel of sensors, sensitive to specific features of the modality they belong to (frequency for sound, position for vision…) and spatially clustered in the brain, forming a topographic map dedicated to the treatment of the overall range of information provided by specialized sensory receptors. The resulting sensory inference is then composed of a mixture of features that, in order to form a perceptual skeleton, must be integrated as a whole. It means that the overall integration of information during the formation of sensory inference relies on the interaction between local neural-based computations. Ignoring on purpose anatomical evidence of bottleneck taking place in the Central Nervous System (CNS), let's imagine on the contrary a modality (our retinal sensory receptors and their first cortical targets) where each receptor is only represented by one cortical neuron that does not communicate with others. If we take the example of spatial representation, how can we position ourselves in space in that configuration lacking interplay? More precisely, how can we build a representation of our own position in space if the elements composing that representation are not linked together? Such a link would provide a global framework in which meaning can only emerges from a *relative* integration of features leading to the construction of a global percept.

That observation leads to the idea that a common reference involving interplay between neurons treating the different sources of information of our environment is necessary for the brain to

generate a coherent and relevant percept. This relativist approach of the construction of a global percept inscribes itself in the *Gestalt* 's school of though. This school was founded by psychologists like Wertheimer (1923), Koffka (1935), Köhler (1947) or Kanisza (1980) who focused on visual perception and developed a set of psychophysical rules dissecting the principles of visual scene decomposition. Those principles allow the construction of a visual scene representation by operations like figure/ground segregation and segmentation. By opposition to the *structuralism*, the *Gestalt* (shape) conception postulates that visual percepts are more than the sum of their individual parts and that emergent properties arise from the binding of individual elements that none of them possesses on their own. As an example, a group of stars forms a percept corresponding to the Big Dipper (Figure 1.1 A) that contains information about curvature, length, regularity/irregularity and homogeneity that none of the points possesses if taken individually. On the other hand, the structuration of the whole influences the perception of each element composing it.

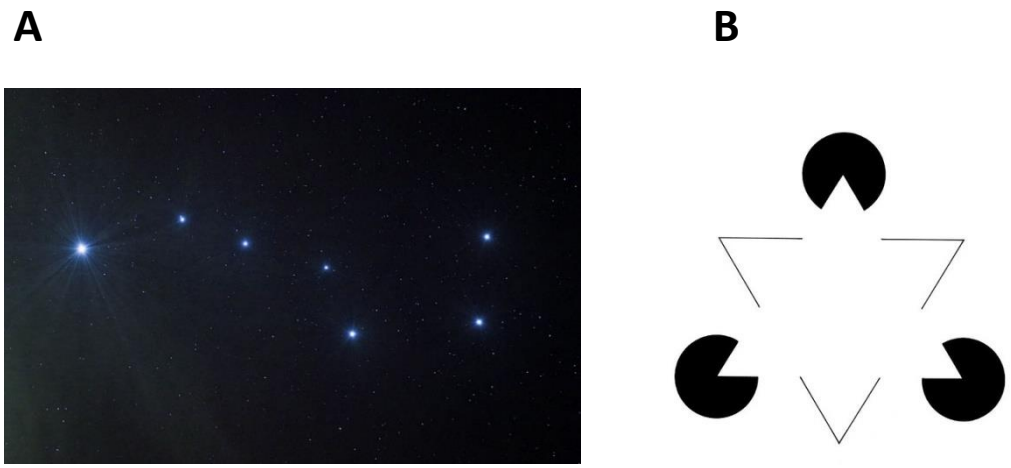

Figure 1.1: ***Examples of emergent properties****. A. From a set of stars global properties arise, the overall shape of the Big Dipper, the curvatures of some parts, the spatial regularity between some of them and irregularities between others bound together by the principle of similarity (each of the stars composing the constellation being bigger and having a higher luminance than the ones in the background). B. Illusory triangle of Kanisza. Illusory contours of a white empty triangle appear given the geometric configuration of the three partially unfilled black circles. Another triangle of black contours appears behind the white one even though none of these triangles exists if we consider each element independently.*

1.1.1 Psychophysical rules underlying perceptual binding and information extraction

The set of psychophysical rules postulated by Wertheimer explains the grouping of disparate elements according to the principle of similarity (1) described above, proximity (2), “good continuation” (3), of common fate (4) motion or spatial grouping if the elements move together in the same direction or remain inscribed in a common region of space (5) (Figure 1.2). Symmetry can be seen as another example of similarity. Those principles account for the perceptual binding of elements that only acquire saliency if bound together and not with others. This seems to be the consequence of a direct attempt of the brain to decompose and classify features in order to extract what is relevant and reject what is not. According to Wertheimer, through evolution, those principles would derive from a learning process that reflects the regularities of the world.

From a systemic point of view, the principle of Gestalt spatiotemporal continuity is consistent with the extraction of relevant information. This selection can be seen as a detection of spatial correlations over time operating on various parameters (position, shape, color, orientation) defining the constraints of the formulated rules. This extraction allows to segregate what matters in a scene (the information) and to exclude what does not (the “noise”), highlighting the principle of efficient coding first introduced in neuroscience by Barlow (1961). The efficient coding hypothesis is derived from information theory (Shannon, 1948). It considers sensory pathways as communication channels where neuronal spiking is the code that represents information provided by sensory signals. Due to anatomical constraints such as the number of neurons and energetic limitations intrinsic to metabolic consumption of energy to produce spikes, information transmission must be optimized. An efficient coding implies that a given system like the visual processing system must have a strategy to maximise the amount of relevant information transmitted and optimizes available channel capacity by reducing redundancy between channels. Because of the system’s limitations, the amount of transmitted information must be reduced or “compacted” in order to extract relevant information and reduce redundancy.

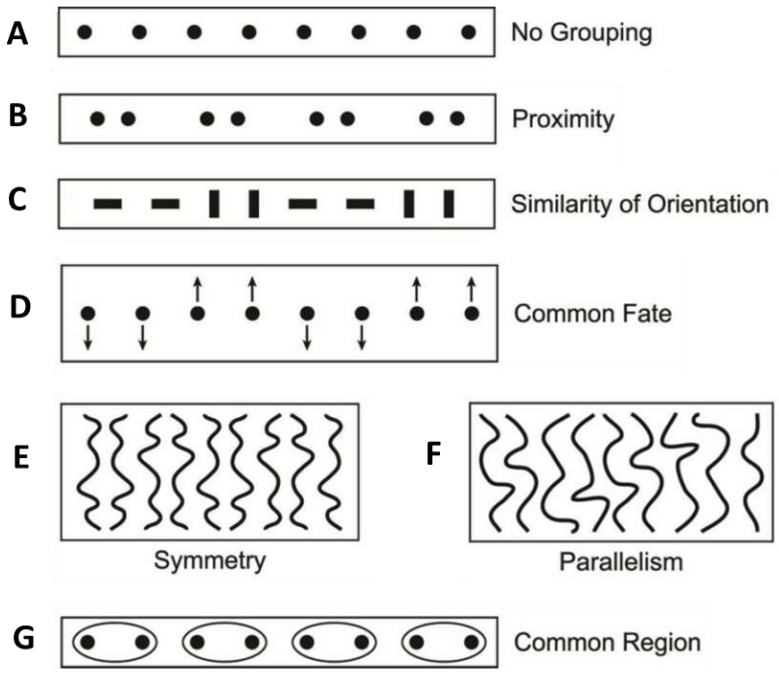

Figure 1.2: ***Principles of binding****. A. According to the context defined by the rectangle surrounding the dots, there is no grouping between the identical elements. B. Given the differences in spatial repartition of the dots, they tend to be grouped by their relative proximity. C. Similarity of the elements, here in terms of orientation. D. Groups of dots moving spatiotemporally in the same direction exhibit coherence. Contours presenting symmetry (E) or parallelism (F) can be grouped together. G. Here the spatial distribution of the dots is not different than the one in (A), the ellipse surrounding the pairs of dots is what provokes their binding. Despite the similarity of the dots here, dissimilar elements can be grouped together if they are in common regions of space. (Adapted from Wagemans et al., 2012).*

Now that we provided a basis to the decomposition of a visual scene that involves the extraction and the construction of a global percept by binding elements according to a set of rules relying on psychophysical evidence, remains the question of the physiological support of those phenomena. What are the operations performed by the brain? What are the neuronal properties and mechanisms underlying those operations, where do they take place and what is our current knowledge of the physiological implementation of these psychophysical rules? We will start by defining physiological “sensory units” before detailing their different types, respective operations and distribution along the visual pathway together with an anatomo-functional description of the hierarchy of information processing along the visual system.

1.2 Receptive fields along the visual pathway

The concept of receptive fields (RFs) is a crucial one in neuroscience. It links the external world to an internal representation of features composing this latter. It is classically defined in the visual system as the region of space/retina (assuming that the relationship between the two is fixed and known a priori) sensitive to visual stimulation that results in a modulation of activity of specific neurons in the brain. This first definition of a spatially restricted area of afferent receptors on the sensory sheet will be challenged as we go deeper into its description through the evolution of discoveries.

In 1938, Hartline is the first to use the term "receptive field" to define the retinal region through which isolated ganglion cells of the horseshoe crab and of the frog respond to illumination of the retina in a given fiber. E. A. Adrian (1932 Nobel prize of medicine) already observed in 1927 by recording action potentials in the optic nerve of the conger-eel that the spiking rate of neurons increases and the latency of responses decreases when the luminous intensity increases.

Following the work of Hartline, Kuffler in the cat and Barlow in the frog characterized for the first time in 1953 the receptive field of retinal ganglion cells. Kuffler demonstrated their concentric opponent spatial organization composed of a light sensitive "ON" center and dark sensitive "OFF" surround (or vice-versa) "OFF" center and "ON" surround, receptive fields similar than the one of the Lateral Geniculate Nucleus (LGN) (Figure 1.3 A). This arrangement seems to be universal as it was also found in the spider monkey (Hubel and Wiesel, 1960) and rabbit (Barlow et al., 1964). That discovery led to the interpretation that those receptive fields were isotropic local contrast detectors whose configuration allows a first filtering of information transmitted to other visual areas for further processing.

From the studies mentioned above, it is evident that the type of modulation provided by the surround of retinal ganglion cells receptive fields is inhibitory since there is an optimal diameter for the luminous patch presented in the RF center of ON center and OFF surround units beyond which the response is reduced or suppressed. For OFF center and ON surround units, even though the strength of the response reduction is weaker and the tolerance for surrounding illumination annulus size is higher, lateral inhibitory signals originating from the far surround are also found. In the retina, lateral inhibition is produced by interneurons (horizontal and amacrine cells) that pool signals over a neighbourhood of presynaptic feedforward cells (photoreceptors and bipolar cells) and send inhibitory signals back to them (Enroth-Cugell and Robson, 1966; Perlman and Normann, 1998; Lee et al., 2010; Thoreson and Mangel, 2012). Early physiological studies originally reported a spatial extent of retinal interneurons extending from 100 to 300 µM (Shapley and Enroth-Cugel, 1984; Enroth-Cugel and Robson, 1966; Benardete and Kaplan; 1999 a,b; Kaplan and Benardete, 2001). However more recent studies showed in mouse and monkey that retinal interneurons extend up to 500-1000 µM (Kolb, 1997; Packer and Dacey, 2002, 2005; Lin and Masland, 2006; Manoonkin et al., 2015) as well as an extra classical RF surround mechanism of suppression in the cat and the macaque monkey (Passaglia et al., 2001; Solomon et al., 2002; Alitto and Usrey, 2015).

That is why the typical center-surround spatial profile of contrast sensitivity of retinal and LGN RFs is classically modelled as a Difference Of Gaussians (DOG). In this model, the standard deviations of the center and of the surround Gaussians functions reflect the RF sizes of the excitatory feedforward and inhibitory lateral signals, respectively, resulting in the famous "Mexican hat" profile of retinal and LGN RFs spatial contrast sensitivity (Rodieck and Stone, 1965; Enroth-Cugell and Robson, 1966; Fiorentini, 1972) (Figure 1.3).

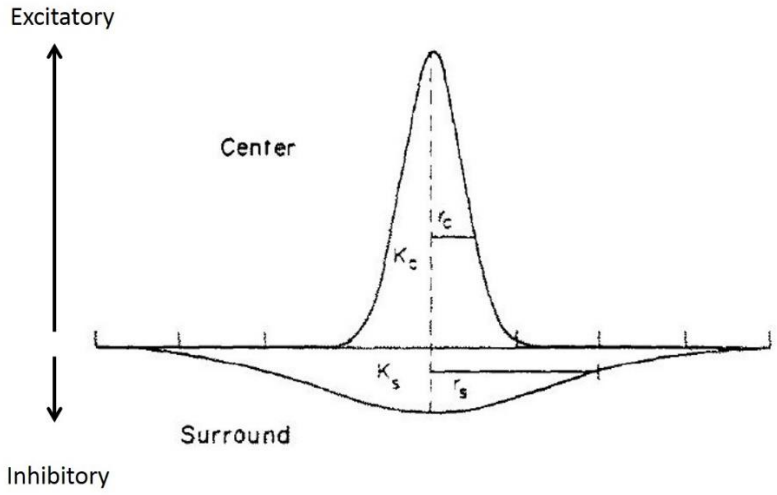

Figure 1.3: ***Difference of Gaussians model of retinal and LGN receptive fields****. The original DOG model. It is assumed that the spatial profiles of RFs center and surround mechanisms are Gaussians that are concentrically positioned, meaning that the receptive field is spatially symmetric. Typically, the model is characterized by four parameters: Kc and Ks, respectively the strength of the center and of the surround mechanisms; rc and rs, respectively the extent of the center and surround mechanisms. The spatial profile of excitation of the center is represented by a narrow Gaussian (Y positive axis) representing feedforward excitatory effects and the spatial profile of the surround by a much broader Gaussian (Y negative axis) representing lateral inhibition coming from the surround. The Difference of those two curves gives a Mexican hat profile representing the overall spatial contrast sensitivity of the RFs. (Adapted from Dawis et al., 1984).*

If we think about it in the framework of efficiency that we introduced, an "ON" center "OFF" surround cell would be optimally activated if the center of its receptive field is illuminated and simultaneously its surround gets less illumination than the background. On the contrary, that cell would not be optimally activated if its surround is illuminated too, limiting the transmission of a relatively irrelevant visual context if the visual field has a uniform luminance. Lateral inhibition is a key mechanism in efficient coding: it allows the encoding of the difference in activity between a cell and its surround: in this manner, large homogeneous areas in the scene generate little neural activity and can be represented with fewer resources (Yeonan-Kim and Bertalmio, 2016). This process, already seen at the retinal level, could be the first step of redundancy reduction and

extraction of relevant information by “compacting” or reducing the amount of information transmitted. This is consistent with the necessity of information compaction formulated in the principle of efficient coding stated by Barlow. Furthermore, reducing the information flow has to be a necessity, given anatomical evidence of bottleneck between the huge number of retinal photoreceptors (cones and rods) projecting onto fewer ganglion cells (Atick and Redlich, 1990). We already see a picture drawing itself: the *filter* role of the receptive field, consistent with both functional evidence and the efficient implementation of information transmission in the brain.

Retinal ganglion cells are composed of two types: the midget ganglion and parasol ganglion cells (P an M types, respectively). The P type represents 70-75 % of retinal ganglion cells, which have small receptive fields, display sustained responses with a rather slow velocity conduction and are sensitive to color (Xu et al., 2001). The M type represents 10-15 % of retinal ganglion cells, with larger RFs and transient responses. Beyond ganglion cell layers, the optic tracts, composed by the LGN axons, project onto the LGN situated in the dorsal part of the thalamus, where P and M cells project respectively on Parvocellular and Magnocellular cells situated in separated layers of the LGN. As already mentioned, the RFs of that structure are similar to the ones of retinal ganglion cells. That is why the LGN is often considered as a simple relay from the retina to the cortex. However, evidence shows that thalamo-cortical feedforward and feedback loops could confer a “gate keeper” role to the LGN (O’Connor et al., 2002; Wunderlich et al., 2005; Kastner et al., 2006). The Magnocellular and Parvocellular cells form different streams (respectively X and Y streams and cell types in the cat) that project in primates respectively onto layer 4cα and 4cβ of the primary visual cortex before both projecting on cells of layer 4B (Yabuta et al., 2001).

However, the picture seems different in the cat. Even though both anatomical and functional evidences indicate that Y cells project onto the primary visual cortex, area 17 or V1 of the cat (Cleland et al., 1971; Hoffman & Stone, 1971; Gilbert & Wiesel, 1979; Freund et al., 1985; Humphrey et al., 1985), it seems that they project preferably onto area 18 (V2). Movshon et al. (1978) clearly identified in area 17 of the cat “sustained cells” preferring relatively high spatial frequencies and responding well to low and moderate temporal frequencies, characteristics classically attributed to thalamic X cells. They also found, but only in area 18 and not in area 17 “transient cells” preferring relatively low spatial frequencies and high temporal ones, classical characteristics of the Y stream. They highlighted the surprising findings that there are virtually no cells in area 17 whose properties resemble those of area 18, suggesting that Y cells could subserve different roles in area 17 (where they are only a fraction of the afferent relay) and in area 18 (where they are the dominant component) in the cat. Moreover, LeVay and Ferster (1977) claimed that the neurons projecting to area 18 from the LGN are different than the ones projecting to area 17. In addition, the medial interlaminar nucleus of the LGN sends a substantial projection of Y cells to area 18 and does not project to area 17 (Rosenquist et al., 1974; Mason, 1975; LeVay and Ferster, 1977; Hollander and Vanegas, 1977). It is therefore possible that in the cat, differences in areas 17 and 18 responses could come from a lack of X cells projections to area 18 and from a group of LGN Y cells that only project to area 18 and not to area 17. Ferster (1990) also highlighted differences into functional properties of X and Y projections onto area 17 and 18 of the cat. By electrically

stimulating the optic tracts with different thresholds (a relatively low one activating large Y cells and a higher threshold activating X cells), he recorded intracellularly the evoked responses in area 17 and 18. Even though intracellular recordings can introduce a bias in the sampling of a neuronal population, among 58 recorded cells in all layers of area 17, only 4 presented Y mediated substantial excitation, among which 3 were found near the area 17/18 border against 24 out of 24 recorded cells in area 18. He suggested that the type of synaptic input that Y projections provide to area 17 evokes much smaller excitatory and inhibitory postsynaptic potentials (EPSPs and IPSPs) than in area 18.

1.2.1 Simple and complex cells of the primary visual cortex

The primary visual cortex (V1, area 17 in the cat or striate cortex) is the principal target of LGN cells afferents and the first cortical area treating visual inputs. Thanks to the work of Hubel and Wiesel (1981 Nobel prize of Medicine), two principal types of receptive fields were described in the cat V1. The first type is called simple cells. Those latter possess spatially oriented RFs composed of spatially separated single or multiple elongated sub regions sensitive either to positive or negative contrast change (Figure 1.4 B). The global spatial sensitivity profile is classically modelled by anisotropic Gabor functions (Jones and Palmer, 1987). That peculiar organisation makes them sensitive to bars brighter or darker than the background and moving slowly (1-5° of visual angle per second) across the visual field, eliciting an optimal response when the bar is parallel to the orientation of the elongated sub regions of the RF with the direction of motion being orthogonal to it. When a bright oriented bar enters the “ON” sub region of the receptive field of a simple cell (or when it leaves an OFF region) with the optimal orientation, an important spiking response is observed. This spiking response is boosted when the stimulus direction sweeps the OFF subzone before entering the ON region. That discovery founded the interpretation that simple cells are edge detectors. That was the first evidence of an actual operation of reconstitution of the external visual world taking place into the cortex. The orientation selectivity of simple cells in the cortical recipient zone of LGN axons is supposed to come from the geometrical combination of thalamo-cortical afferents of LGN cells, where afferents of a given type tend to be preferentially aligned along the “preferred orientation” (Figure 1.5 A) (Hubel and Wiesel, 1962; Chapman et al., 1991; Reid and Alonso, 1995). Intracortical mechanisms of facilitation and inhibition would also contribute to the refinement of orientation selectivity shaping (Ferster and Miller, 2000).

Complex cells were also described by Hubel and Wiesel in the primary visual cortex. Their RFs have a spatial superposition of ON and OFF responses, making them sensitive to both bright and dark stimuli presented in the same region of space (Figure 1.4 C). Those properties are often thought of as a non-linear combination of multiple simple cells projecting onto one complex cell (Figure 1.5 B). Both simple and complex cells are also sensitive to the stimulated eye (ocular dominance), motion direction, speed, spatial and temporal frequencies of the presented stimulus.

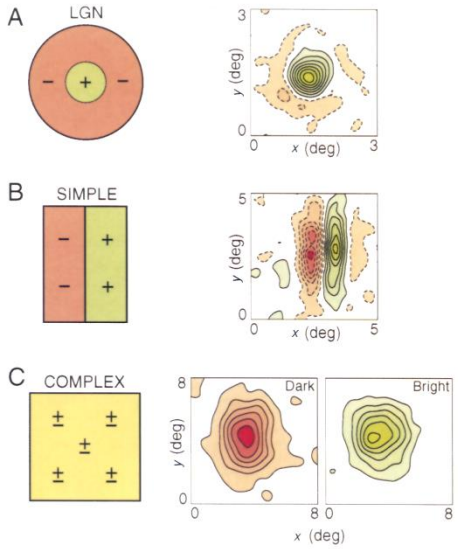

Figure 1.4: ***Thalamo-cortical description of cat spatial RFs properties.*** *Schematic profiles (left) and experimental ones (right) of different cell types.* ***A****. LGN cell with an ON center and an OFF surround.* ***B****. 2 regions simple cell of V1.* ***C****. Complex cell of V1, separated representation of ON and OFF regions overlapping in space. The spatial maps representing the experimental profiles of the RFs are obtained from a reverse correlation between the evoked responses and the spatial presentation of bright and dark elementary stimuli presented in different spatial positions. (Adapted from DeAngelis et al., 1995).*

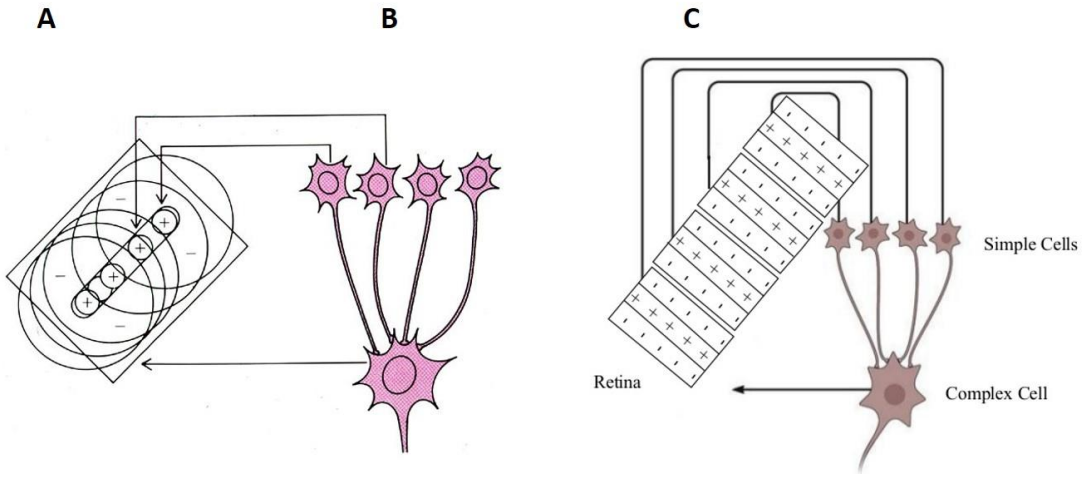

Figure.1.5: ***Hierarchical model of cortical receptive fields proposed by Hubel & Wiesel.*** *A. DOG RF, at the retinal and thalamic level. The receptive field can be described by opponent subzones with circular symmetry. B. The specific projection of LGN cells having concentric ON centers and OFF surrounds RFs spatially adjacent projects onto one simple V1 cell having an oblique (45°) preferred*

orientation and composed by three sub regions: one central ON region surrounded by two OFF regions. C. Four simple cells having similar RFs than in B project onto one complex cell. The hierarchical schema of Hubel and Wiesel supposes that information is serially processed first through isotropic opponent contrast detectors feeding simple RFs in area 17, before being pooled and relayed by complex RFs in area 18, projecting onto higher-order feature extraction in hypercomplex RFs (area 19).

1.2.2 A columnar organization

Going further into the architectural description of those functional properties, Hubel and Wiesel described in 1962 and 1963 a columnar organization of orientation representation orthogonal to the surface of the cortex in primary and secondary visual cortices of the cat. That organization obeys to the cortical spatial distribution of neuronal responses representing visual space. The cortical representation of visual space is not uniform but distorted by a differential magnification factor between the area centralis and the periphery onto the cortical sheet in a non-linear manner. That organisation is said to be retinotopic. Together with spatial representation and clustered distribution of orientation, Hubel and Wiesel (1962, 1963) also found a clustered distribution of ocular dominance maps, each cell responding dominantly or only to the stimulation of one eye (Figure 1.6). Taken with evidence of increasing complexity of the RFs along the visual pathway, the clustered distribution of superimposed maps reflecting distinct functional properties embedded into the same cortical tissue led to the thought that the processing of visual information was composed of a serial and hierarchical circuit where the role of vertical feedforward connectivity was predominant in the transmission of more and more complex information from retina to primary and higher cortical visual areas.

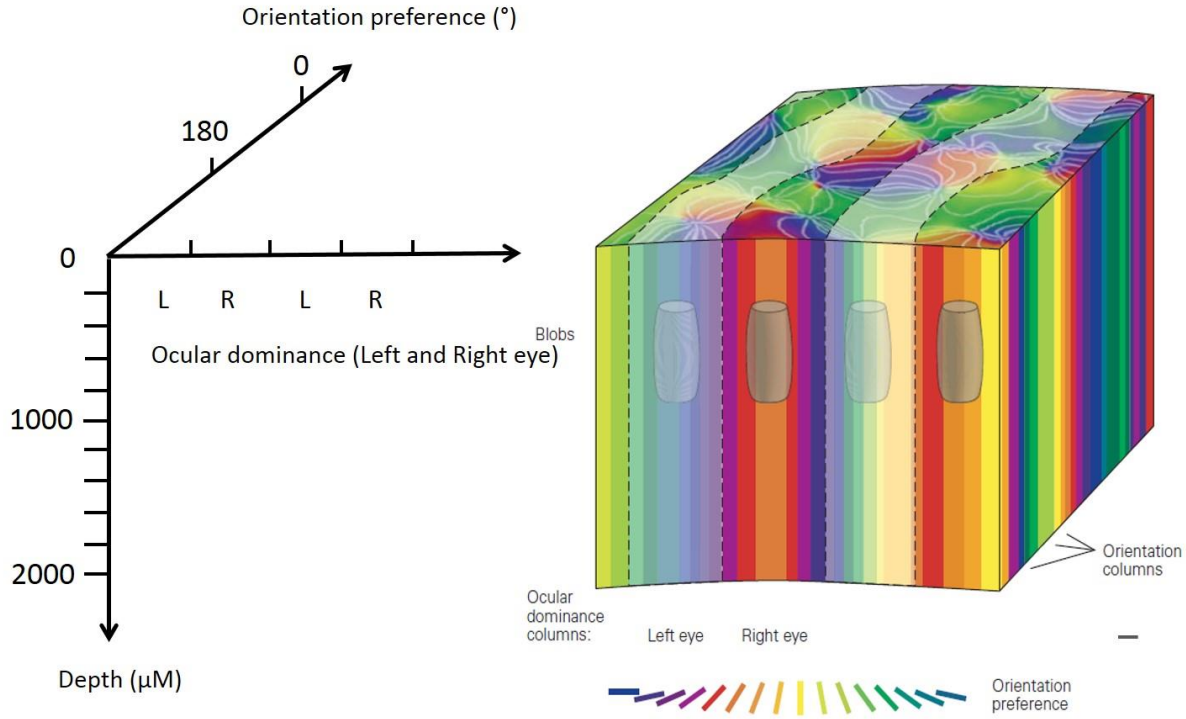

Figure 1.6: ***Columnar organization of orientation selectivity and ocular dominance in cat primary visual cortex.*** A chunk of cortical tissue, roughly 1 by 1 mm in cat visual cortex contains an orientation hypercolumn (a full cycle of orientation columns), one full cycle of left and right ocular dominance columns and blobs and interblobs. The composite (aggregate) receptive field of all cells within this cortical block encodes for the same region of visual space (all receptive fields overlap). Cortical regions where all orientations are spatially adjacent represent pinwheels: areas where neurons of orthogonal preferred orientation can be found in close vicinity (discontinuity in the spatial orientation gradient). This module would presumably contain all of the functional and anatomical cell types of primary visual cortex and would be repeated hundreds of times to cover the visual field. Grey scale bar: 100 µm. (Adapted from Kandel et al., 2013).

1.2.3 A hierarchical processing of information

Beyond V1, several areas have been identified to further process visual information. Dozens of cortical areas (more than thirty) seem to be involved in the processing of visual information in the macaque (Felleman and Van Essen, 1991; Maunsell, 1988; Kravitz et al., 2013, Chang and Tsao, 2017) (Figure 1.6 B). Each of those areas possesses its own architecture, connectivity, topographical organization and functional properties (DeYoe et al., 1996) (Figure 1.7 A). Their distinct contribution to visual perception is not yet very well understood, due to the complexity of inter areas

connections, the difficulty to generate stimuli of increasing complexity matching specific, complex and unknown operations performed by each area, experimental limitations and large differences across species. However, some properties are known. For instance, V2's RFs are bigger than the one of V1 and are sensitive to illusory contours in the macaque (Von Der Heyt and Peterhans, 1984, Baumann et al., 1997); they also play a role in figure-ground segregation (Lamme, 1995; Lee et al., 1998; Zhou et al., 2000; Zipser et al.,1996). V4 seems to be involved in the analysis of color (Shipp and Zeki, 1985) and in attentional processes (Desimone and Duncan, 1995). From the posterior inferior temporal cortex (including V4 and areas projecting onto it) we observe a loss of retinotopic representation.

More recent studies revealed a more elaborate distribution of information treatment in the emergence of illusory contours that relies on inter area interactions. Indeed, in humans, fMRI studies demonstrated a robust activation of V1 and V2 during perception of illusory contours (Seghier and Vuilleumier, 2006) but also activations of other areas, notably of V4 (Mendola et al., 1999; Montaser-Kouhsari et al., 2007). This is consistent with electrophysiological studies in the monkey where cells responding to illusory contours are found in V1 and V2, but these responses emerge a few tens of milliseconds later than in downstream areas such as V4 (Von der Heydt et al., 1984; Lee and Nguyen, 2001), suggestive of a top-down cortico-cortical feedback origin. The contribution of V1, V2 and V4 in the perception of illusory contours was dissected by Pan et al. (2012) in the macaque, confirming the results of a previous study in the cat (Sheth et al., 1996). Pan and collaborators showed by combining optical imaging in anaesthetized rhesus macaque with extracellular electrophysiological recordings in awake animals that orientation preference maps for drifting gratings and stimuli inducing the perception of illusory contours are shifted by the angle between the gratings physically presented and the perceived illusory contour in V1 and V2. On the other hand, no shift is observed in V4 where orientation maps for drifting gratings and illusory contours are undistinguishable despite the angle between them. In the same study, electrophysiological recordings confirmed a "salt and pepper" distribution of cells sensitive to illusory contours in V1 and V2, thus, orientation domains of those early visual areas mainly capture and encode local physical features of the inducer stimulus whereas a complete overlap of orientation domains only emerging in V4 allow to process both real and illusory contours. The decoding of illusory visual contours then seems to obey a hierarchical model of information treatment distributed over several early visual areas which individual computation converge in a feedforward manner further downstream the hierarchy of visual information processing (Frégnac and Bathellier, 2015).

Certain structures have RFs covering almost the entire visual field (AIT and PIT), responding to complex and specific objects like faces or hands (Tanaka et al., 1991, 1996). The area MT (V5) receives direct inputs from V1 and has a large proportion of cells sensitive to the direction of a moving stimulus and to depth characteristics (DeAngelis and Newsome, 1995). Even more complex dynamic features of motion seem to be represented in MST, which receives projections from MT, like rotation, contraction or expansion and would participate to ocular pursuit behaviour. MT

projects onto areas 7a, LIP and VIP that would participate to the preparation of action like ocular motion.

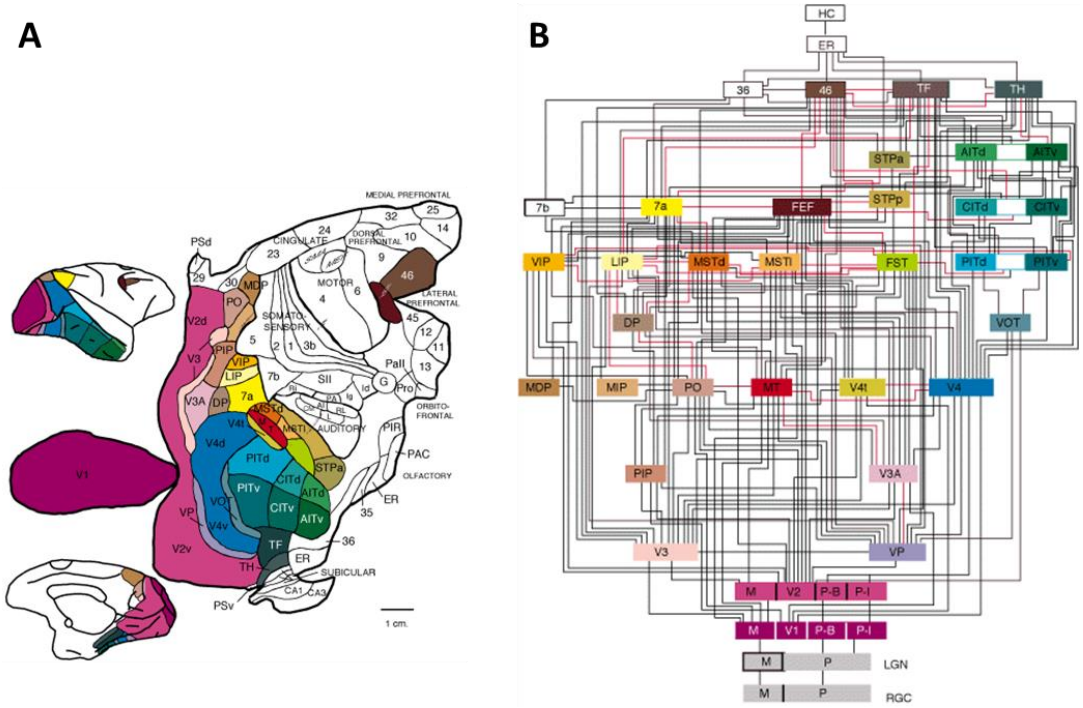

Figure 1.7: ***Anatomical and schematic representation of the macaque brain connectivity.*** *A. Flattened map of the macaque monkey brain representing visual (colored) and non-visual (uncolored) areas. B. Hierarchy of visual areas. This Hierarchy shows 32 visual areas, colored according to the same scheme as in A. These areas are connected by 187 linkage, most of which have been demonstrated to be reciprocal pathways (Adapted from Felleman and Van Essen, 1991).*

Despite this complicated and fragmented picture, it seems that the cortical treatment of visual information can roughly be divided in two pathways: the dorsal pathway of the “where” or “how”, specialized in space and motion detection, action planning and the ventral pathway of the “what” specialized in form and object perception (Figure 1.7 and 1.8). The former is composed of areas V1, V2, MT, MST, LIP, VIP and PP and the latter includes areas V1, V2, V4, PIT and AIT (Felleman and Van Essen, 1991; DeYoe et al., 1996, Markov et al., 2013, 2014 a and b).

Combined evidence of clustered and specialized functional maps having their own architecture and anatomical connections with higher order areas performing more complex operations depicts a rather hierarchical processing of information where each structure would extract more and more complex features. Visual scene processing would then be modular (each structure having a rather strong specialisation) and serial: each operation would be based on the extraction of characteristics of lower levels in primary areas, tending towards a perceptual interpretation in higher areas. This

seems to be consistent with the increasing selectivity of the receptive fields described earlier and reinforces their filter role.

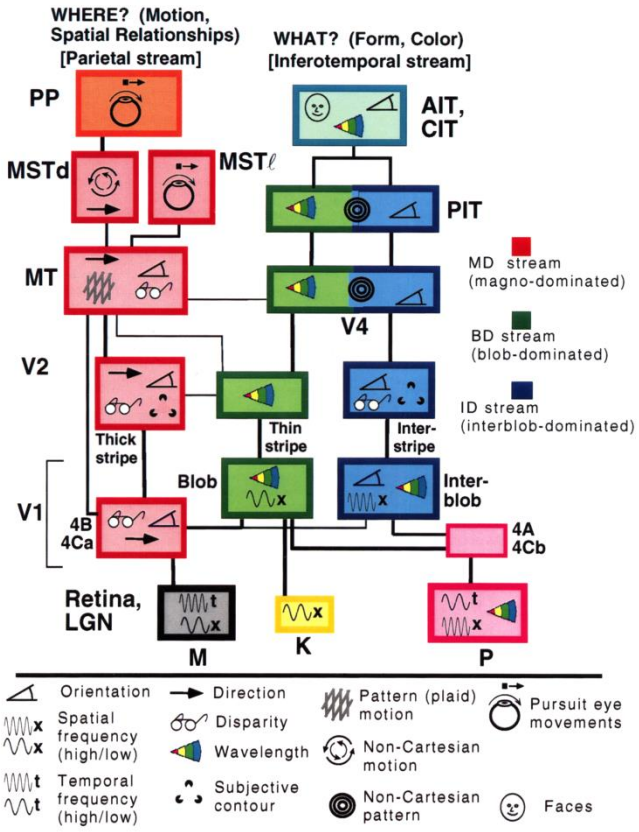

Figure 1.8: ***Hierarchical organization of concurrent processing streams in the macaque monkey.*** *Boxes represent visual areas, compartments within an area, and subcortical centers; solid lines represent major connections between structures (usually reciprocal pathways); and icons represent characteristic neurophysiological properties. Subcortical streams in the retina and lateral geniculate nucleus (LGN) include the M, K, and P streams, i.e Magno, Konio and Parvo cellular streams (grey, yellow, and pink, respectively). Cortical streams at early and intermediate stages include the MD, BD, and ID streams (red, green, and blue, respectively). The Postero-Parietal (PP) complex is shown in orange. The Infero-Temporal complex (IT) includes Posterior Infero-Temporal areas (PIT), which are components of the BD and ID streams, and Central and Anterior Infero-Temporal areas (CIT and AIT) (Van Essen and Gallant, 1994).*

1.2.4 Questioning the hierarchical model

However, a certain number of inconsistencies, both theoretical and anatomical contradict the pure hierarchical model of serial feature extraction of the visual system (Bullier and Nowak, 1995; Burr, 1999). A pure serial and parallel processing of elements composing a scene would imply that

the binding between those elements, necessary to build a relevant global percept would take place *after* the treatment of local information. We saw previously that the perception of an ensemble can modify the perception of each element composing a percept. How can we reconcile psychophysical evidence of a global percept introduced by the Gestalt's psychologists with a serial parallel treatment of local individual elements?

Moreover, the linear convergence of more and more complex filters would face a drastically increasing combinatory problem, filters of the same order potentially sharing a large number of common inputs from lower order filters. As an example, inconsistencies appear if we consider RFs covering the whole visual field in higher areas combined with the loss of retinotopic representation and the necessity of the system to be able to discriminate differences in localization of high-order features across the visual field.

Furthermore, anatomical evidence of cross-talk between the ventral and the dorsal pathways has been described (Bullier and Nowak, 1995). As we saw in figure 1.7 and 1.8, top-down connections from higher to lower areas (a feedback connectivity, as opposed to the feedforward one) provide constant exchanges of modulatory signals between cortical areas, having different time-scales and spatial distributions according to their relative connectivity. Finally, there are long distant horizontal connections within each cortical area linking neurons whose RFs are spatially distant in the retinotopic representation of space (V1, Gilbert et al., 1996; V2, Levitt et al., 1994; V4, Yoshioka et al., 1992; IT, Fujita and Fujita, 1996; PFC, Levitt et al. 1993; Amir et al., 1993).

All those evidences diverge drastically from a pure hierarchical and serial processing of information. The existence of feedback connections from higher areas highlights the presence of down-stream modulations of the first pre-treatment of information taking place in early visual areas such as V1. Long distance horizontal connectivity linking neurons retinotopically distant already indicates an intra-area specific communication between neurons across the visual field. Such interactions make very good candidates as substrates for the physiological implementation of Gestalt's psychophysical rules of perception allowing the binding of disparate elements composing a visual scene by providing modulatory signals *carrying contextual information*. Those modulatory signals would compose complementary operations taking place in parallel of the pure bottom-up extraction of more and more complex features.

Moreover, at the functional level, there are electrophysiological evidence of contextual modulations as early as the retina between the center of a receptive field and its surround. Center-surround interactions specific of the cortical stage *are orientation sensitive* (Blakemore and Tobin, 1972; Nelson and Frost, 1978; Allman et al., 1985, Gilbert and Wiesel, 1990, Li and Li, 1994, Silito et al., 1995; Walker et al., 1999). On top of that, they are rather complex and compose a huge panel of different effects. Those effects are both suppressive and facilitatory, their sign and amplitude depending on the spatial characteristics and the relative configuration between stimuli placed in the surround and in the center of the RF, especially their contrast, orientation, separation and alignment (DeAngelis et al., 1995; Frégnac et al, 1996; Gilbert, 1998; Wörgötter and Eysel, 2000).

What are we talking about when we mention the binding of different elements composing a global percept? What are the center-surround modulations that this binding involves? What are the actors of their physiological implementation at the level of V1, the anatomical types of connectivity contributing to those operations and how can the spatial scale of those interactions be accounted for? We first need to answer those questions to set in place a proper definition and origin of center-surround interactions in V1 in order to establish a link between physiological operations, properties and the construction of a perceptual skeleton translated at the psychophysical level into perceptual phenomena.

1.3 Center-surround interactions: physiological definition, spatial scale, connectivity's origins across species and link with perception

It is well known that stimuli presented far beyond the receptive field may strongly influence neuronal responses to stimuli presented within the RF center, both in the retina and LGN, (Mcllwain, 1964, 1966; Cleland et al., 1971; Ikeda & Wright, 1972 a,b; Krüger and Fischer, 1973; Fischer and Krüger, 1974; Krüger, 1977; Marrocco et al., 1982). However, retinal and thalamic center-surround modulations are weakly orientation sensitive.

On the contrary, at the cortical stage, center-surround interactions are orientation sensitive (Blakemore and Tobin, 1972; Nelson and Frost, 1978; Allman et al., 1985, Gilbert and Wiesel, 1990, Li and Li, 1994, Silito et al., 1995; Walker et al., 1999). The cortical sheet, especially the primary visual cortex and its center-surround modulations represents the level of information processing and operations in which we are interested in in the context of this thesis and that we will develop in this section. At the level of V1, the surrounding of simple and complex cells RFs are also regions responsive to visual stimuli that, although not sensitive enough to evoke spikes when stimulated in isolation have substantial effects on cell responsiveness whether the RF is stimulated or not. That surrounding region has been called by Li and Li (1994) the Integration Field (IF). The effects of this region can be either facilitatory or inhibitory (Blakemore & Tobin, 1972; Bishop et al*.,* 1973; Maffei & Fiorentini, 1976; Rizzolatti & Camarda, 1977; Nelson & Frost, 1978, 1985; Hammond & Mackay, 1981; De Valois et al*.,* 1985; Allman et al., 1985; Gilbert and Wiesel, 1990; DeAngelis et al., 1994; Sillito et al., 1995; Levitt and Lund, 1997a; Walker et al., 1999).

In area V1 of cats and monkeys, the integration field, or larger non-classical receptive field (nCRF) surrounding the excitatory classical receptive field (CRF), also called the minimum Response field (mRF) or minimum Discharge Field (mDF), is defined as the smallest spatial area of the visual field eliciting spiking responses and is generally determined by extracellular electrophysiological recordings of single neurons. Even though both signs of modulation have been observed, the stimulation of the IF has however been more frequently reported to be suppressive (Allman et al.,

1985; DeAngelis et al., 1994; Gulyas et al., 1987; Hammond & MacKay, 1981; Li & Li, 1994; Sadakane et al., 2006; Sengpiel et al., 1997; Sillito et al., 1995). In those studies, both the extent and the stimulus selectivity of the IF has been estimated. For instance, Bishop et al., (1973) were able to map out powerful, but non-orientation-selective inhibitory regions that extended 2-6° of visual angle beyond the sides of the RF in the cat. In the same species, using intracellular recordings, Creutzfeldt et al. (1974) mapped an inhibitory area of 3-4° that overlapped the excitatory center. Still in the cat, Li and Li (1994) estimated the average size of V1 RFs to be of about 3° of visual angle on average and the overall extent of the IF between 2 and 5 times the size of the RF, extending from 6 to 15° of visual angle around the RF center.

1.3.1 Contrast-dependent spatial summation of the Receptive field

However, the stimulus contrast is an important parameter to take into account in the functional characterization of receptive fields spatial extent and final output as it influences the balance between excitation and inhibition: both the CRF and nCRF size expands when the stimulus contrast is varied from high to low, in the LGN and at the cortical level (Chen et al., 2014; Chen, Song, & Li, 2013; Wang et al., 2009, Kapadia et al, 1999; Sceniak et al., 1999). Those findings demonstrate a differential *spatial summation* of the RF size as a function of the contrast of the stimuli used. The contrast-dependent spatial summation is important for the visual system. At high stimulus contrast, saturation of V1 RF response by thalamic inputs may explain the shrinkage of RF center and the predominance of strong surround suppression where accurate smaller receptive fields may be used by the visual system for precisely extracting focal features. However, responses to a low contrast visual stimulus are weaker. Larger size of the IF and smaller surround suppression at low contrast may unmask subjacent surround excitatory influence that allows cortical neurons to extract more visual information to improve image detection and object recognition in a contextual manner (Frégnac and Bathellier, 2015; Chen et al., 2014; Frégnac, 2012; Shulz and Frégnac, 2010, Frégnac et al., 1996). Several studies have characterized the spatial organization of excitation and inhibition at high and low contrasts in the macaque V1 (Sceniak et al., 2001; Shushruth et al., 2009). Electrophysiological studies have shown that monkey neurons exhibit more suppression than those in the cat: of about 56-86% of cells in the cat but more than 90% in the monkey show significant surround suppression (Jones et al., 2001; Series et al., 2003; Sengpiel et al., 1997; Walker et al., 1999).

Using extracellular recordings, Levitt and Lund (2002) mapped in the macaque monkey V1 the spatial extent of receptive field using gratings stimuli of increasing size centered on the RF at high contrast (75%) to disentangle between discrepancies in spatial summation RFs profiles reported in the literature, mostly due to a great variety of stimuli like flashed oriented bars that does not fully activate the overall receptive field. In that line of evidence, they found, using high contrast extending gratings centered on the RF, minimum response field ranging from 0.8 and 1.6°of visual angle in layer 4C, at a retinal eccentricity from 2 to 8° from the area centralis, contradicting conclusions of Blasdel and Fitzpatrick (1984) which obtained in the same layers, between the same

eccentricities and also at high contrast minimum spatial summation fields ranging from 0.1 to 0.4° of visual angle by using flashed oriented dark and bright bars. Basing themselves on experimental evidence of increase of the receptive field spatial summation area by a factor of 2-3 when the contrast is lowered (Sceniak et al., 1999), Angelluci et al., (2002 a) estimated that the extent of the receptive field that they measured could reach between 2.4 and 4.8° if measured at low contrast.

1.3.2 Thalamo-cortical contribution of macaque LGN inputs to V1 center-surround modulations

The same authors (Angelucci et al., 2002a) also estimated the potential contribution of thalamic LGN inputs offered to each macaque layer 4C cell by overlapped, retinotopically organized thalamic axons. The cortical neuron dendritic field (about 200 μm in diameter) could receive direct input from a total overlap of thalamic arbors equivalent to approximately two adjacent, non-overlapped, thalamic axon terminal fields (Figure 1.9 a). Using published values of magnification factor (MF) of the macaque monkey in V1 at 5-8° of eccentricity from the area centralis (MF = 2,3-3,03 mm/degree at 5° of eccentricity and 1,43-2,06 mm/degree at 8° of eccentricity, Van Essen et al., 1984; Tootell et al., 1988; Blasdel and Campbell, 2001), the arbor size of single thalamic axons on the cortex (1,2 mm; Blasdel and Lund, 1983) covers a retinotopic area of 0,4°-0,8°. Thus, layer 4Cα neurons postsynaptic to the largest M axons could receive direct thalamic input from 0,8 to 1,6 ° of visual field (twice the retinotopic area covered by a single M axon terminal arbor (Figure 1.9 a and b). Contrarily to Sceniak et al. (2001), the estimations of Angelucci, Levitt, Lund and collaborators (Levitt and Lund, 2002; Angelluci et al., 2002 a,b) in the macaque V1 are in accordance with their measure of the minimum response field at high contrast and predict that LGN input to layer 4C could underlie the high contrast spatial summation field of V1 neurons. However, even the largest size of direct thalamic input field is still not likely to underlie the large sizes of layer 4Cα cell summation fields (2,4-4,8°) measured at low contrast.

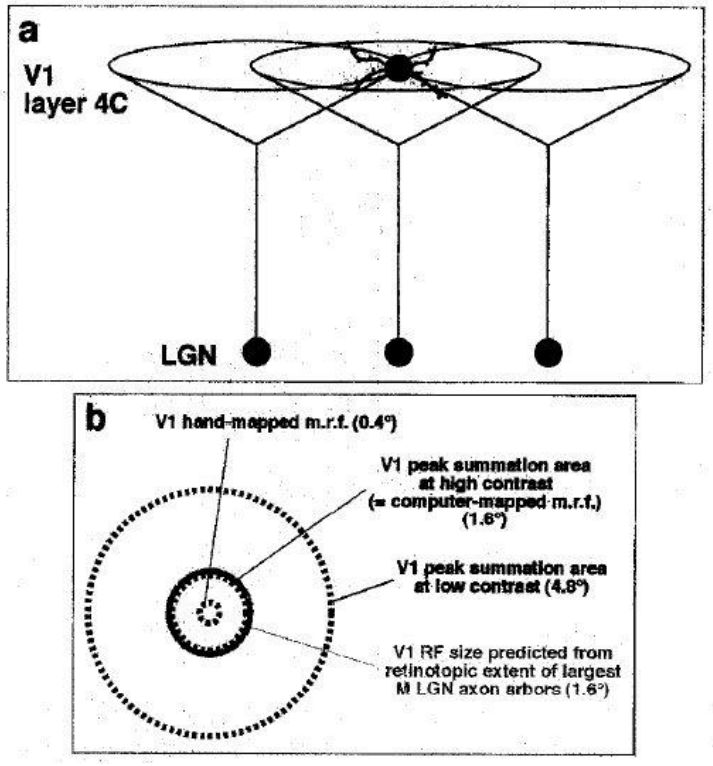

Figure 1.9: ***Schematic diagram illustrating the potential contribution of thalamic inputs to the receptive field diameter of a macaque V1 layer 4C spiny stellate neuron. a.*** *Given the small size of a layer 4C neuron dendritic arbor (about 200 µm in diameter), and assuming orderly retinotopic organization of thalamic afferents in layer 4C, then each layer 4C neuron can receive information from a number of overlapped axons providing visual field information equivalent to approximately two adjacent nonoverlapped thalamic axon terminal arbors.* ***b.*** *Dashed circles indicate largest receptive field (RF) sizes of layer 4C neurons at 8° of retinal eccentricity measured using different methods to map the size of cortical neurons' RFs. Gray circle: largest V1 RF size of layer 4C neuron predicted from the retinotopic extent of two adjacent, nonoverlapped largest M thalamic axon arbors. Thalamic inputs can predict the largest high stimulus contrast summation area of V1 layer 4C neurons, but are too small to cover the size of the spatial summation area measured at low contrast. m.r.f: minimum response field. (Adapted from Angelucci et al. 2002a).*

1.3.3 Aggregate receptive field and intra V1 lateral connectivity's contribution to macaque V1 near and far surround modulation

In the pursuit of the anatomical substrate of surround modulations of the integration field extending beyond the high contrast minimum response field that they found, Angelucci et al., (2002b) compared physiological measures of RF size with measures of the retinotopic extent of

anatomically labelled intra-V1 lateral connections to an injected point in layer 4B, upper layer 4C and layer 2/3 of macaque area V1. They represented the visual field retinotopic extension of intra V1 lateral connections as a function of the Aggregate Receptive Field (ARF) size. The concept of ARF reflects the cumulative spatial extent of all neurons RFs of a given cortical hypercolumn containing all orientations and corresponding roughly to the same retinotopic stimulation of space. The ARF is therefore, by definition, larger than the individual neurons RFs of the hypercolumn. Angelucci and collaborators estimated its size from their data by adding to the retinotopic extent of the labeled zone diameter the mean RF size of neurons at the edge of the labelled field and the scatter in RF center position (Angelucci et al., 2002a).

They found that when the receptive field is characterized by small flashed bars at high contrast, the retinotopic diameter of V1 lateral connections is of 3° of visual angle, or 2,2-fold greater than the high contrast ARF of the cells of origins, thus linking ARF representing distinct neighboring hypercolumns from each side of the RF center. However, we saw that this type of stimulus (small bar flashed at high contrast) does not allow to characterize the full extent of RFs spatial sensitivity, as opposed to circular gratings of increasing size presented at low contrast. Using this latter stimulus, the group of Angelucci estimated that V1 lateral connections retinotopically extend to a visual area similar to the ARF size when calculated with the neuron's peak summation spatial area at low contrast. Therefore, they concluded that at low contrast, the thalamic drive is not sufficient to reach saturation of the response and lateral connections account very well for the spatial extension of RFs as this connectivity seems to reach almost exactly the spatial extension of RFs when characterized with low contrast stimuli.

On their population sample (n=10), they found that the retinotopic extent of V1 lateral connections in layers 2/3 and 4B/ upper 4Cα of the macaque V1 range between 1.2 and 4.3 times the size of the minimum response ARF at high contrast (mean = 2.7) and between 0.3 and 1.6 times (mean = 0.9) the size of the peak spatial summation ARF at low contrast. On average, the low contrast ARF size of V1 lateral connections is 1.7 times the size of the low contrast ARF of the injected neurons. We see that the average ratio between V1 lateral connections retinotopic extent and low contrast ARF extent represent well the one to one ratio that they highlight in their interpretation (mean = 0.9) but that that there is a huge variability (from 1.2 to 4.3 times at high contrast) and a V1 lateral spread of 1.7 times the low contrast ARF of injected neurons *on average*, thus largely superior to 1 and potentially capable to reach neighboring low contrast ARF corresponding to non-overlapping distinct hypercolumns. This variability probably reflects the laminar heterogeneity that they used to calculate their estimate average by combining layers 2/3, 4B and upper 4Cα. Indeed, the anatomical staining part of their study shows that horizontal connections in layer 2/3 and 4B can reach up to 10 mm in total length (with an average of 6-7 mm).

Angelucci et al. (2002 a,b) therefore concluded that surround modulation mediated by lateral connectivity could not extend beyond the monosynaptic reach of horizontal connections and acknowledged that the low contrast summation receptive field revealed extracellularly reflect the

monosynaptic extent of the facilitatory subthreshold depolarizing field of lateral connections found intracellularly in the cat V1 by Bringuier et al. (1999). The group of Angelucci (2002 a,b) argued that collinear facilitation at low contrast of a central target presented in the RF center by iso-oriented flankers would come from an extension of the receptive field spatial summation at low contrast. The dominant surround suppression would then be reduced, unmasking the concomitant excitatory influence of the surround region. Facilitation by neighboring flankers iso-oriented would emerge because the flankers would fall into an overlapping region where distinct V1 neurons would share common orientation preference properties derived from thalamic inputs. This would result in two activity zones where one belonging to the surround of a given cell would be activated and laterally propagate a depolarizing wave of activity reaching the center of that cell, thereby facilitating its response at low contrast (Figure 1.10 a). According to them, this is only beyond the extent of the low contrast summation ARF (about 5° of visual angle), at a cortical distance corresponding to 6-7 mm from each side of the RF where no common inputs are shared that lateral monosynaptic activation cannot explain longer range modulatory effects from the surround (Figure 1.10 c), which would correspond to a maximal lateral surround field of about 10 and 5.5° at respectively 8 and 5 ° of eccentricity. Instead, according to their data, longer range modulatory effects would come from more spatially extended feedback connections from extrastriate areas, explaining their findings that V1 modulatory surround fields can extend up to and likely more than 13 ° of visual angle in diameter at the same eccentricities, hence 6.5° or more from each side of the RF center (Figure 1.11).

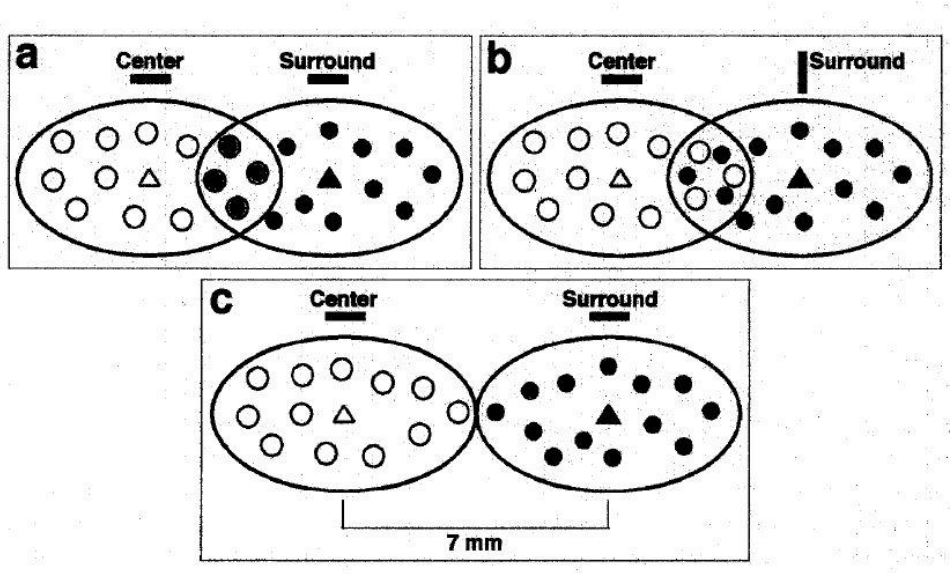

Figure 1.10: ***Schematic diagram illustrating three different conditions of interaction between lateral connectional fields as a possible substrate for surround modulation of V1 neurons center responses.*** *Empty and filled triangles: pyramidal neurons whose receptive fields (RFs) are directly driven by the center or surround stimuli, respectively. Empty and filled circles: patches of lateral*

connections made by the "center" and "surround" pyramidal neuron, respectively. ***a.*** *When center and surround cells are driven by stimuli of similar orientation (e.g. horizontal), surround modulation of the center cell's response could occur because patches of connections shared by the overlapping lateral connectional fields of the center and surround cells are coactivated by both the center and surround stimulus.* ***b.*** *When center and surround cells are driven by stimuli of orthogonal orientation (e,g. horizontal and vertical, respectively), surround modulation of the center cell's response would not occur, even though the lateral connectional fields of the center and surround stimulated cells overlap. Lack of surround modulation in this condition would result because patches of connections pertaining to the center and surround connectional fields interdigitate rather than overlap, and would thus be activated only by the center or surround stimulus, but not by both. Although no surround modulation of the center response is most commonly observed for center and surround stimuli of orthogonal orientation, this stimulus configuration can evoke surround modulation of the center response in a subset of V1 neurons.* ***c.*** *No surround modulation of the center cell's response would occur when the lateral connectional fields of center and surround neurons are not overlapped, i.e. at distances > 7 mm. This distance would thus represent the spatial limit of the surround modulatory fields of V1 cells if overlap of active lateral connection fields were the origin of surround modulation. (Angelucci et al. 2002 a).*

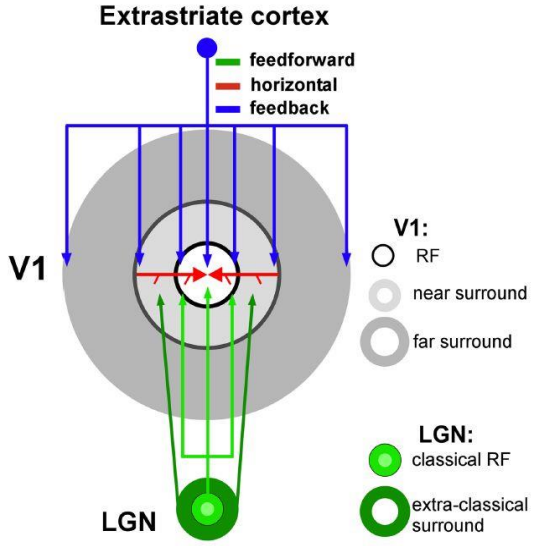

Figure 1.11: ***Presumptive anatomical circuits for macaque surround modulation***
Different components of the RF (white area) and surround (gray areas) of a V1 neuron and their presumptive underlying circuits (arrows). Monosynaptic horizontal connections in V1 (red) extend into the near surround; their spread is commensurate with the size of a V1 neuron's spatial summation area measured at low contrast (Angelucci et al., 2002 a,b), which is on average about twice the diameter of the cell's RF, or spatial summation area measured at high contrast (Sceniak et al., 1999). The spread of feedforward connections to V1 from the LGN (Angelucci and Sainsbury,

2006) added to the size of suppressive surrounds of LGN cells (Sceniak et al., 2006; Alitto and Usrey, 2008) (dark green) is commensurate with a V1 cell's near surround. Inter-areal feedback connections (blue) are commensurate with the far surround (Angelucci et al., 2002 a,b) and contribute to all components of the RF and surround, but are the only connections contributing to the far surround. (Shushruth et al., 2013).

Here comes the crucial necessity to define the spatial scale and anatomical support of what we call center-surround modulations, based on the physiological findings reported above. Since response facilitation by collinear flankers is often observed when the target contrast in the RF center is low, a network driven, primarily excitatory dynamic (Sceniak et al., 1999) must be responsible for those facilitatory effects and for enlargement of the RF at low contrast. If we examine the proposition of Angelucci et al. (2002), a collinear flanker presented in the surround of the classical receptive field would fall into the larger integration field and facilitate the response to a low contrast central target. But how would this facilitation at the level of the center cell be orientation dependent since the flanker would not fall into the cortical recipient of thalamic afferents restricted to the high contrast minimum response field, thalamic afferents at the origin of orientation selectivity at the cortical level? This imply the existence of a cooperative mechanism of cortical origin allowing the diffusion of facilitatory activity in an anisotropic dependent manner. As previously proposed, this cooperativity would come from the concomitant activation by the flankers of distinct population of cells retinotopically distant from the RF center of the target cell (falling into its low contrast surrounding field or on the limit of this latter) but sharing similar orientation properties. Those population of cells belong to neighboring orientation columns composing distinct surrounding hypercolumns having their own ARF. The further away we get from the ARF of the target cell, the fewer ARF of neighboring hypercolumns overlap. Indeed, as we previously saw, the size of an hypercolumn is of roughly 1 by 1 mm in cortical distance parallel to the cortex surface, a distance largely covered by the spatial extent of horizontal connectivity (with an average of 6-7 mm in the macaque V1 according to Angelucci et al. (2002a), which is about 3 mm on each side of the RF center on average).

One of the main characteristic of horizontal connectivity is that it preferably links columns sharing the same orientation preference across different hypercolumns. It is therefore straightforward to acknowledge that horizontal connectivity is likely responsible for the extent of the low contrast summation field of V1 receptive fields, and that its extent is sufficiently large to account for the interaction of a large number of hypercolumns. It does so by preferentially linking columns sharing the same orientation preference, thereby conveying facilitatory signals responsible for iso-orientation facilitation and from a broader perspective, anisotropic center-surround modulations observed at the level of V1. Those functional units: low contrast summation receptive field interactions and the subjacent hypercolumns interactions as well as high contrast receptive field summation involving much less hypercolumns overlap compose the unitary radius length of sensitivity of the contextual anisotropic modulations that we are interested in in the context of this thesis.

1.3.4 Lateral connectivity, collinear facilitation and link with perception

However, an important question remains: to which extent does lateral connectivity can provide far surround anisotropic contextual modulatory effects and what are the implications at the perceptual level? Orientation dependent surround facilitatory effects are reflected in human psychophysics by the facilitation of contour integration by collinear flankers in the static association field (Field et al., 1993; Hess and Field, 1999) (Figure 1.12 a) and in the "perceptual pop out" of collinear elements in a sea of randomly oriented patches of Gabor (Figure 1.12 b) that emerge effortlessly, reflecting a sensory inference resulting from an already built-in mechanism in early visual areas. The precise contribution of long-range horizontal and feedback connections as anatomo-functional source of activity modulation providing long distance contextual information still remains controversial but distinguishing the origin and anatomical substrate of near and far surround modulations remains crucial, that is why we will discuss results and conclusions from the literature on plausible substrates thought to contribute to those distinct phenomena in the cat, monkey and human.

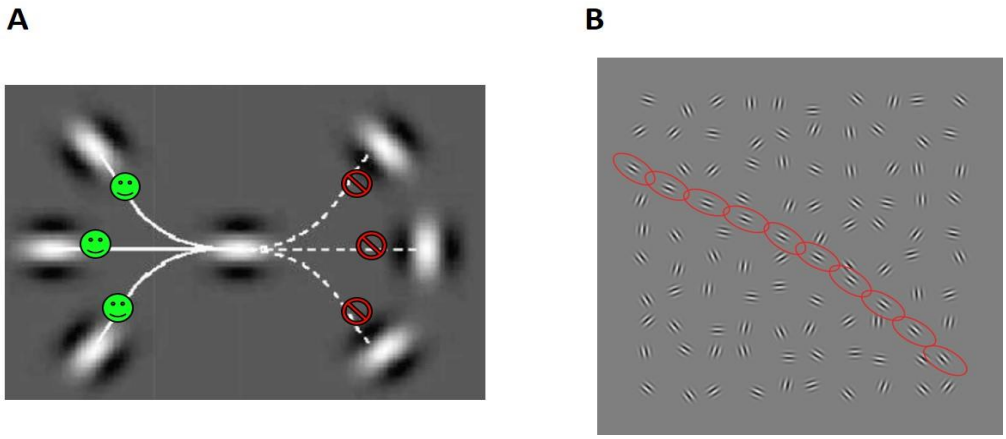

Figure 1.12: ***Psychophysical principle of collinear facilitation in contour detection. A.*** *Perceptual static association field described by Hess et al. (1993) demonstrating that the strength of linking between elements depends on their orientation. The strength is greater for elements that lie along the same axis, or close to it (solid lines), than for those that are orthogonal to each other (dotted lines), it is therefore easier to bind spatially distant elements that share a certain degree of collinearity. This imply the existence of anisotropic lateral interactions at the perceptual level.* ***B.*** *Stimuli made up of test elements (in this case Gabor patches – blobs composed of a 1-D sinusoid multiplied by a 2-D Gaussian) embedded in a background field of identical, randomly-oriented elements. Gabor patches surrounded by red ellipses are nearly collinear and compose a path that is almost straight. The high degree of collinearity of those elements in a sea of randomly oriented*

patches of Gabor provokes a perceptual "pop-out" reflecting the facilitation of contour detection by collinear elements. (Adapted from Hess and Field, 1999).

Although the main effect of surround suppression in striate cortex is thought to be suppression, cellular behavior is more complicated when stimulated with a compound stimulus made of two concentric, drifting grating patches: strong cross-orientation facilitation was observed both in monkey and cat striate cortex when the CRF was weakly stimulated ("at low contrast" or at a non-optimal orientation, Sillito et al., 1995). However, using similar concentric drifting gratings, those effects were not found in other studies on either primate (Levitt and Lund, 1997 a,b) or cat striate cortex (Walker et al., 1999) where response suppression prevailed when center and surround stimuli had matching orientation. The consensus seems to lie in the facilitation at low contrast of the center target surrounded by higher contrast coaligned surrounding flankers. Using contrast reversal of patches of Gabor, rather than drifting gratings, Mizobe et al. (2001) argue in their cat study to have minimized the possible contribution of feedback afferents from extrastriate areas in which motion sensitive cells prevail (Hupé et al., 1998) in favor of lateral connections. In those conditions, by stimulating the CRF of single V1 cells at its optimal orientation with neighboring flankers at high contrast presented at a distance up to 12-15° from each side of the RF, they found that both facilitation and suppression occurred in a quantitatively equivalent manner in their sample (n > 100), distance potentially twice superior as what was previously described in the literature (Maffei and Firorentini, 1976; Li and Li, 1994). On top of that, the facilitation that they observed was present while they used high contrast collinear flankers and central target, at a distance extending well beyond the monosynaptic reach of lateral connections. More precisely, they found that flanker excitation is overlaid on suppression *along the optimal orientation axis of the CRF*, closely resembling the perceptual association field reported by Hess et al., (1993) (see Figure 1.12 and 1.13) in human. The large effective distance between target on the CRF and surround flankers (up to 12-15°) combined with the strong anisotropic dependency of the facilitation may imply that the spatial organization shown in Figure 1.13 is more suitable for long-range polysynaptic lateral interactions than short-range interactions within the immediate vicinity of the CRF and extend well beyond the monosynaptic lateral neighboring low contrast ARF described by Angelucci et al., (2002 a) in the macaque. This is consistent with reports that V1 surround suppression is less orientation tuned than surround facilitation in the cat (Bishop et al., 1973; Maffei and Forentini, 1976; Walker et al., 2000), in the alert (Knierim and Van Essen, 1992) and anaesthetized macaque (Nothdurft et al., 1999), highlighting a spatial distribution of surround facilitation more narrowly orientation tuned and extensive along the preferred orientation axis of the cell than surround suppression.

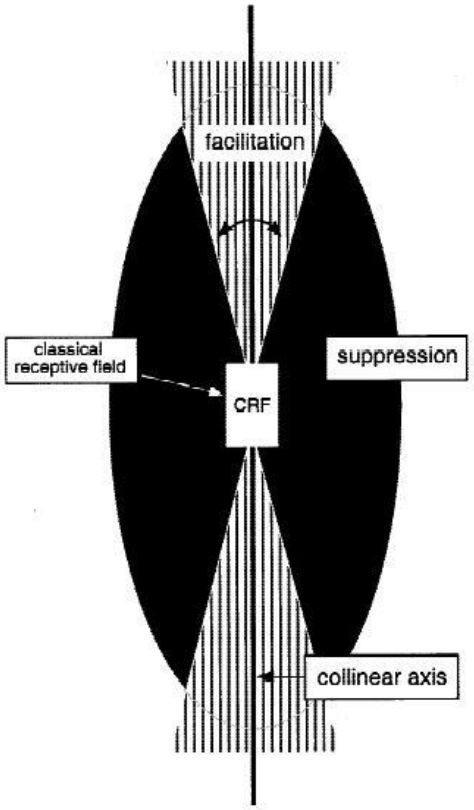

Figure 1.13: ***A cortical model of perceptual grouping based on extracellular recordings of the spatial organization of facilitative and suppressive modulatory fields around the CRF of cat single striate cells.*** *Facilitation is overlaid on suppression along the optimal orientation axis of the CRF. That is, facilitation is organized along the optimal orientation of the cell in a collinear manner. Suppression is less selective for orientation or spatial frequency and distributed diffusely, especially toward its periphery, around the cell's CRF (e.g. Walker et al., 2000). The dynamic balance between the two mechanisms, primarily dictated by the cell's contrast threshold, controls the cell's firing behavior upon visual stimulation with compound stimuli. The total dimensions of the modulatory field can be as large as 24 ° or more (Kitano et al., 1994). (Mizobe et al., 2001).*

Mizobe and collaborators also conducted other studies, still in the cat (Chen and Kasamatsu, 1998; Chen et al., 2001) in which they confirmed and largely extended precedent results: they found different lateral modulatory signs as function of target contrast: the existence of lateral facilitative increase at high target and collinear flankers contrast (expansive facilitation). In 1995, Kapadia et al., had indeed already reported in the awake monkey that in many cells of V1, presenting a high-contrast single bar of optimal orientation in the CRF resulted in facilitation when a second collinear bar at high contrast was presented outside the receptive field. The former effect of Mizobe et al., (2001) (expansive facilitation) was present in a large subgroup of the cells they studied (29%). According to them, this high contrast facilitation would come from cooperation of a certain type of cells having a large CRF which show expansive facilitation upon increase in contrast. They presented a sensitivity-modulation model in the general framework of contrast gain control where activation of neighboring cells changes the sensitivities of the target both to the direct feedforward input and inhibitory divisive feedback from neighboring cells (Chen et al., 2001). Those

findings are consistent with more recent studies in the cat V1 reporting that the low contrast rate of expansion for the suppressive space is substantially lower than for the excitatory space (Chen et al., 2013; Wang et al., 2009). The excitatory and suppressive space appear to overlap extensively and a relatively large part of the suppressive space is masked at low contrast. If the excitatory space exceeds the suppressive space, even at high contrast, surround suppression will disappear. According to Mizobe et al. (2001) and Chen et al. (2014), expansive facilitation (at high contrast) may be due to the variation in spatial summation of cells having large CRF extending well beyond the suppressive space. They also noted that low suppression and surround facilitation was more apparent in studies using low luminance values: from 3 to 10 cd/m² (in the alert monkey: 3cd/m², Kapadia et al., 1999; in the cat: 8,3 cd/m², Li and Li, 1994; 9 cd.m², Wang et al., 2009), consistent with their own data in the cat (10 cd.m², Chen et al., 2014).

In the same line of evidence Song et al. (2010) have related in the cat spatial summation properties to cell morphology and found in their study two cell types divided in two categories according to the modulatory sign of the receptive field surrounding: Facilitatory Extra-Classical Receptive Field (F-ERF) and Suppressive Extra-Classical Receptive Field (S-ERF) neurons. Using intracellular recordings, they characterized the size of F-ERF and S-ERF neurons at a medium contrast (0,4) and stained them using biocytin. At the anatomical level, they found that both F-ERF and S-ERF neurons are mainly pyramidal cells. However, an F-ERF neuron has a more complex dendritic arborization, higher spine density and a larger soma. At the physiological level, they found that an F-ERF neuron has a larger extra classical receptive field than an S-ERF neuron (0,34 vs 0,22 mm on average, respectively). According to them the axons of most F-ERF neurons form a plexus of long-range connections that expands horizontally over a wide area, extending up to 2.5 mm parallel to the surface of the cortex with an average of 1,2 mm against 0,4 mm for S-ERF neurons. Those results are consistent with the findings reported above (Chen and Kasamatsu, 1998; Chen et al., 2001, 2013, 2014; Wang et al., 2009; Mizobe et al., 2001) where neurons displaying facilitatory surround effects have larger CRF and nCRF than surround suppressive neurons. The former category extends beyond the suppressive space and display surround facilitatory effects upon increase of a centered drifting grating at a given medium contrast and display a much larger spread of horizontal connections than the suppressive extra classical receptive field neurons. This confirm that both the contrast-dependent extension of the modulatory summation area of the receptive field and that the facilitatory surrounding effects are mediated by lateral connections, conclusions strongly reinforced by the anisotropic nature of surround modulatory effects whereas lateral connections are known to link columns of similar orientation preference.

1.3.5 Differences and similarities between cat and monkey's lateral connectivity: implication for perception

As we previously saw, surround facilitation by collinear flankers can extend up to 12-15 ° from each side of the RF in the cat V1 (Mizobe et al., 2001), distance extending well beyond the monosynaptic reach of horizontal connections. On top of that, the spatial summation enlargement of facilitatory surround modulation extend further than the suppressive space (Chen et al., 2013; Wang et al., 2009; Mizobe et al., 2001), and further than the monosynaptic reach of neighboring low contrast ARF, along the preferred orientation of the CRF (in the cat: Mizobe et al., 2001; Gérard-Mercier et al., 2016; in the monkey: Kapadia et al., 2000; Gilbert and Li, 2012). It is also mediated by excitatory influence conveyed by lateral connections (Bringuier et al., 1999; Song et al., 2010). The spatial distribution of facilitatory and inhibitory surround of the CRF (Mizobe et al., 2001; Gilbert and Li, 2012; Gérard-Mercier et al., 2016) closely mirror the perceptual static association field reported in humans (Field et al., 1993; Hess and Field, 1999). It is also consistent with psychophysical reports in humans of collinear facilitation of target detection even at high contrast of target and flankers, but to a smaller spatial extent: up to 3 ° from each side of the target (Polat and Sagi, 1993, 1994 a,b; Polat and Norcia, 1996) which claimed that far surround collinear facilitation of target detection (by lowering the contrast threshold necessary to perceive the central target) by high contrast flankers would come from long distance disinhibition of local inhibitory circuits at the target level. This interpretation is in accordance with reports of long distance polysynaptic excitatory horizontal connections and concord with the view of the group of Angelucci and collaborators in the macaque who estimated the spread of monosynaptic horizontal connections involved in collinear facilitation to extend up to 3° of visual space on each side of the RF (Angelucci et al., 2002 a), a distance largely inferior than the 12-15° found in the cat by Mizobe et al., (2001) and much closer to the psychophysical findings of collinear facilitation up to 3° of visual angle in humans (Polat and Sagi, 1993, 1994 a,b; Polat and Norcia, 1996). Facilitation by high contrast flankers and target was also found at the physiological level in the cat where Chen and Kasamatsu, (1998), Chen et al., (2001) and Mizobe et al., (2001) reported that 29% of the cells they examined (n > 100) presented a facilitatory summation area increase when the contrast of both target and flankers was increased (expansive facilitation) and in the awake monkey (Kapadia et al., 1995).

In addition, the results of Mizobe et al., (2001) in the cat appear to differ substantially from those of Levitt and Lund (1997 a,b) in the macaque in that the former saw much more collinear facilitation at low contrast flankers than did Levitt and Lund which almost always saw suppression. The former argued that the stimulus configuration that they used: contrast reversal of small, localized Gabor patches following the stimulus configuration which decreased the contrast detection threshold in human psychophysics (Polat and Sagi, 1993, 1994 a,b) account for the difference observed by Levitt and Lund (1997) which used concentric, drifting gratings that psychophysically lowered (suppressed) the perceived contrast of the central target (Cannon and

Fullenkamp, 1991). Angelucci et al., (2002 a,b), Shushruth et al., (2009, 2012, 2013), Nurminen and Angelucci, (2014) however continued to use concentric annular drifting gratings in their macaque studies. However, Mizobe et al., (2001) argue that the use of this type of stimulus cannot probe contour integration but are rather more relevant to surface representation, for example figure ground segregation or image segmentation, as other authors also claimed (Knierim and Van essen, 1992; Nothdurft et al., 1999). Still according to Mizobe et al., (2001), remote activation by the use of small localized patches of Gabor may activate a different neural mechanism for perceptual grouping of various features belonging to a single, large object (Polat and Tyler, 1999; Solomon and Morgan, 2000), consistent with the idea that grouping mechanisms operate in the formation of contour and image boundaries, obeying laws of Gestalt psychology (continuity, similarity, proximity). The collinear facilitation found by Mizobe et al., (2001) using this latter type of stimulus extended up to 12° or more, distance large enough to group separate patterns belonging to the same object.

According to the group of Angelucci, even though in principle polysynaptic circuits of horizontal connections could underlie long-range center-surround interactions, it is unlikely to them for several reasons. First, they argue that the strong inhibitory nature of most surround effects would preclude propagation of signals through a cascade of lateral connections (Angelucci et al., 2002 b). However, they do not distinguish the differential spatial distribution of excitation that is stronger and more extended than inhibition along the preferred orientation axis of cells compared to surround inhibitory effects that are much more broadly tuned in the cat (Mizobe et al., 2001; Gérard-Mercier et al., 2016; Bishop et al., 1973; Maffei and Forentini, 1976; Walker et al., 2000), in the alert (Knierim and Van Essen, 1992; Kapadia et al., 2000; Gilbert and Li, 2012) and anaesthetized macaque (Nothdurft et al., 1999). Their argument relies on evidence that lateral axons are known to target the same population of neurons at every synaptic location in the macaque (about 80% of excitatory and 20 % of inhibitory neurons; McGuire et al., 1991). However, they do not envision the likely possibility highlighted by Polat et al., (1998) that facilitation interactions may be preferentially organized for collinear elements that comprise extended contours where long distance excitatory lateral influence from a collinear flanker may end up on a local inhibitory interneuron, thereby favoring its activation and detection by disinhibition (Polat and Sagi, 1993). Suppression would be a more general feature, occurring across all orientations and over a broad region around the CRF (Knierim and Van Essen, 1992; Li and Li, 1994; Kapadia et al., 1995; Sillito et al., 1995; Mizobe et al., 1996; Kitano et al., 1994; Levitt and Lund, 1997 a,b) explaining that it has been most commonly found. On the other hand, it remains true that even though facilitation might be preferentially arranged along the cell's preferred orientation axis, surround facilitation in monkey may however be much harder to find as monkey neurons do indeed exhibit more suppression than those of the cat: of about 56%-86% of cells in the cat but more than 90% in the monkey show significant surround suppression (Jones et al., 2001; Series et al., 2003; Sengpiel et al., 1997; Walker et al., 1999). Non-specific suppression may act to rescale the contrast-response function to maximize differential sensitivity in the face of high image contrast.

In the same line of evidence than Mizobe et al., (2001), a recent intracellular study of the group of Frégnac (Gérard-Mercier et al., 2016) in the cat provided experimental data consistent with the interpretation of Polat and Sagi, (1993) reported above. They showed in the anaesthetized cat V1 that responses to elementary stimuli flashed along the preferred orientation axis of a cell as far as 10-12° away from the MDF could evoke significant subthreshold depolarizing responses. In some cells, stimuli flashed at 9° of eccentricity from the MDF could evoke spiking responses, distances well beyond the monosynaptic reach of lateral connections. The latency of evoked responses is consistent with the conduction speed of horizontal axons. This is against the interpretation of Angelucci et al., (2002 a,b; Angelucci and Bressloff, 2006), Shusruth et al., (2009, 2012, 2013) and Nurminen and Angelucci, (2014) who consider polysynaptic lateral influence as largely inhibitory in monkey center-surround modulations. On the other hand, a more targeted view advocate for the facilitatory influence of the surround, relayed by polysynaptic lateral connections (Gérard-Mercier et al., 2016) and overpowering inhibition along the cell's preferred orientation axis (in the cat: Walker et al., 2000; Mizobe et al., 2001; Gérard-Mercier et al., 2016; in the behaving monkey: Kapadia et al., 2000; Gilbert and Li, 2012). In the cat, when stimulated in a spatio-temporally coherent manner, lateral and feedforward activity act together to shape the spread of lateral excitatory activity over large cortical territory (Jancke et al., 2004; Chavane et al., 2011; Gérard-Mercier et al., 2016). The anisotropic spread of lateral activity polysynaptically propagated is maximized when collinear stimuli cooperate to shape the overall spread of lateral activity via multiple relays (Chavane et al., 2011; Gérard-Mercier et al. 2016).

Secondly, the group of Angelucci (Nurminen and Angelucci, 2014) stated that horizontal connections only produce subthreshold responses in their target neurons (Hirsch and Gilbert, 1991) and therefore cannot relay surround influences across extensive visual field regions in the absence of feedforward stimulation, something that has been observed experimentally (Ichida et al., 2007; Nurminen et al., 2010; Shushruth et al., 2009). This might be true to a certain extent in monkeys, but here again the results of Gerard-Mercier et al., (2016) contradict this statement in the cat as unitary Gabor patches presented in isolation, without direct feedforward activation of the minimum discharge field center evoked spiking responses when flashed up to 9° in some cells and subthreshold depolarizing responses were evoked up to 10-12° away from the MDF center along the preferred orientation axis of cells. This first argue against the pure inhibitory nature of cascadic activation of lateral connectivity and highlight the substantial contribution of laterally propagated activity across several synaptic relays in the absence of feedforward stimulation. The findings of Chavane et al., (2011) in the anesthetized cat V1 also conferred a much more prominent role to horizontal connectivity. Using Voltage Sensitive Dye Imaging (VSDI), they showed that maximizing stimulus cooperativity using a grating embedded in a surrounding annulus of the same orientation evoked the anisotropic propagation of activity filling in the feedforward unstimulated cortical central region of the annulus at a speed consistent with lateral connectivity's velocity conduction. Moreover, Polat and Sagi (1994b) showed psychophysically in humans that the detection of a central target was facilitated by collinear flankers and that the spatial range of this detection facilitation was increased by a factor of three upon learning of the detection task (up to 3° from

each side of the central target). They suggested that the induced longer-range facilitation is a result of increase in lateral connections efficiency consistent with a plasticity of the early visual system governed by Hebbian rules. Therefore, the relatively unsubstantial contribution of laterally propagated activity described by Angelucci and collaborators is rather relative, depends on and must take into account the statistics of the environment of each individual/each specie and cannot be considered as a rigid phenomenon.

Thirdly, Nurminen and Angelucci (2013) argued that the conduction velocity of horizontal axons is too slow (Bringuier et al., 1999; Girard et al., 2001) to account for polysynaptic propagation of activity modulating the very fast onset of orientation-tuned surround suppression in macaque V1 cells (Bair et al., 2003) and human vision (Kilpeläinen et al., 2007). They added that if horizontal connections mediated far-surround modulation, the latency of suppression should be strongly distance dependent, but that experiments show that it is nearly independent of the distance of the surround stimulus from the RF (Bair et al., 2003). To analyze the validity of those interpretations, we must first take a step back and weight the relevancy of those assertions by thoroughly dissecting the contribution of the temporal factor in the results that we presented before.

If we take the perceptual “pop-out” of nearly collinear static patches of Gabor almost forming a straight path in a sea of randomly oriented Gabor patches (Figure 1.12 B), we must first consider the argument that Angelucci et al., (2002 a) introduced themselves. In the cat as well as in the monkey and human, all the elements of the figure stimulate retinotopically distant V1 RFs at the same time in a feedforward manner. Without having do add up the latency of monosynaptic laterally propagated activity for each patch of Gabor from one patch at the edge of the picture to the furthest on the other side, the simple neighbour to neighbour introduction of collinear elements falling into the slightly overlapping adjacent low contrast ARF mediated by monosynaptic lateral connections would facilitate the response to each neighboring patch of Gabor (Angelucci et al., 2002 a). This would happen within a time window corresponding to a single monosynaptic delay of lateral activity propagation, facilitating the response to each neighboring patch of Gabor of the scene almost instantaneously (with a latency of propagation slightly increasing with eccentricity from the area centralis to the periphery due to the difference in magnification factor). Just as in Figure 1.12 B, this could happen even at high contrast of the elements (expansive facilitation, Chen and Kasamatsu, 1998; Chen et al., 2001), by a population of cells whose RF surrounding is facilitative and extends beyond the suppressive space via more extended lateral connections (Song et al., 2010, Chen et al., 2013; Wang et al., 2009; Mizobe et al., 2001). This population of cell simultaneously activated would cooperate to induce the anisotropic spread of activity along the path formed by the elements, filling in between each of them (Chavane et al., 2011) and account for the relative amplification of response to elements of that orientation, explaining the facilitation of their binding at the perceptual level. In a second time, polysynaptic lateral connectivity would propagate over larger distances (10-12°, Mizobe et al., 2001; Gérard-Mercier et al., 2016). It could sustain/amplify the relative increase in activation of previously activated loci by feedforward-lateral monosynaptic activity as non-linear facilitative summation of feedforward and laterally propagated

activity was observed when the membrane potential was depolarized (Yoshimura et al., 2000; Gérard-Mercier et al., 2016).

This last argument is crucial when we aim to disentangle the contribution of horizontal connectivity in the propagation of contextual information. From a broader perspective, as mentioned above, the temporal factor must be introduced and several configurations composing more realistic natural stimuli must be apprehended to fully describe V1's center surround interactions. Whether we consider the monkey or the cat, the assertion of Nurminen and Angelucci (2013) remains nonetheless true: lateral connectivity's speed conduction cannot account for the very fast onset of responses facilitation when a target is only surrounded by two collinear flankers presented in the far surround (10-12°) as opposed to feedback connectivity. However, the role and importance of horizontally propagated activity and especially of long distance subthreshold depolarizing influence in the *spatio-temporal preparation of the network* is of paramount importance. It first reflects that even though spikes represent the unit of information transmission in the brain, they are not generated randomly and strongly depend on the overall electrical context of the brain. Even though space seems to be included in most of the studies leading to the findings presented above, when we search to characterize the contextual stimulation of the V1 network, the contribution of the temporal domain is very often neglected, findings and conclusions obtained therefore do not realistically describe information processing at the cortical level.

That is what Gérard-Mercier et al., (2016) demonstrated in their cat study where they also used pairs of Gabor patches flashed in a sequential manner. They showed that when, and only when, the subthreshold depolarizing wave of activity evoked by the first Gabor patch stimulating the adjacent low contrast ARF propagated in phase with the feedforward stimulation of the intracellularly recorded RF, the response was amplified and emerged faster than the sole feedforward stimulation. They found that a minimum time window is necessary for the cell to integrate the laterally propagated activity as this latter must arrive slightly before the feedforward stimulation of the RF center in order to observe a supralinear interaction between feedforward and horizontal activity. Those findings were only obtained for Gabor patches collinear to the preferred orientation axis of the cell and *converging* towards the RF center in a centripetal manner, highlighting the existence of a dynamic association field at the synaptic level of cat V1 RFs, favoring the integration of local (collinear orientation) and global (motion's direction) features composing the flows. This stimulus configuration is of importance as we may encounter it very often in natural circumstances when our gaze sweeps a continuous contour where the periphery is sequentially activated before the center of a receptive field. Moreover, Using VSDI, Jancke at al., (2004) tested the cortical activation of the anesthetized cat V1 during the presentation of an illusory effect: the line motion illusion in which a static bar flashed after a static small square evokes the perception of a bar progressively extending over space and time. Using that paradigm, they showed that the presentation of a small square evoked a lasting wave of depolarization that spatially facilitated the consecutive cortical feedforward activation to a bar presented after, inducing the anisotropic spread of activity along the trajectory composed by the bar from the initial site of activation

towards the end of the bar. The speed of propagation of activity was consistent with the speed of lateral connectivity's conduction and undistinguishable from the activity evoked by an actual bar extending progressively at the same speed than horizontal activity's speed propagation. The interaction between feedforward and lateral activity as well as the percept disappeared when the presentation between the square and the bar was elongated. Firstly, this highlight the existence of a spatio-temporal range necessary for the two waves to interact, in accordance with the observations of Gérard Mercier et al., (2016) and secondly, this points out a striking similarity between the polysynaptic propagation of lateral activity characterized at the physiological level in the cat and the functional integration at the perceptual level in humans.

Differences across species must however be taken into account, especially between monkey and cat because our understanding of vision neuroscience first comes from a large majority of data obtained in the cat since the pioneer studies of Hubel and Wiesel. Non-Human Primates (NHP) are on the other hand closer to human than the cat in the phylogenic tree, the understanding of sensory integration of NHP is therefore more relevant than the cat when compared to human. Angelucci et al., (2002 a,b) first reported their surprise to find that horizontal connections in macaque are isotropic in visual space. This contrasted especially with results in other species in which these cortical connections are anisotropic along an axis collinear to the optimal orientation in the visual field map, (tree shrew: Bosking et al., 1997, cat: Schmidt et al., 1997, owl monkey: Sincich and Blasdel, 2001). They argued that the visual space anisotropy of V1 lateral connections seen in other species might instead reflect the longer length summation receptive fields of V1 cells, demonstrated at least in the tree shrew (Bosking an Fitzpatrick, 1995). In the same line of evidence, other studies reported that summation fields in macaque V1 are generally isotropic (Sceniak et al., 2001; Levitt and Lund, 2002), the group of Angelucci therefore argued at that time that long distance anisotropic surround modulatory effects would come from feedback connections in the macaque V1 rather than lateral connections.

However, more recent studies disproved the isotropic RF surroundings of macaque horizontal connectivity: a more recent review of Gilbert and Li, (2012) based on a previous work (Kapadia et al., 2000) showed the existence of a neural facilitation field favoring the integration of local collinear flankers up to 5° from each side of V1 RFs in the macaque. Nurminen and Angelucci, (2014) later reported that in monkey, as well as in cat and tree shrew, horizontal connections are millimeters-long axonal projections (Gilbert and Wiesel, 1983; Rockland and Lund, 1982, 1983) prominent in layers 2/3, arising from excitatory neurons, targeting both excitatory and inhibitory neurons and linking V1 neurons with similar orientation preference (Bosking et al., 1997; Malach et al., 1993; Schmidt et al., 1997; Sincich and Blasdel, 2001), thereby conveying contextual anisotropic modulations. In a previous study (Shushruth et al., 2013), the group of Angelucci had already found that in macaque, similarly to cat V1 (Hashemi-Nezhad and Lyon, 2011), surround modulation is sharply orientation tuned when measured with stimuli confined to the spatial extent of monosynaptic horizontal connections, while broadly tuned when measured with stimuli placed in the far surround corresponding to the spatial extent of feedback connections. Notably, they found

that the orientation tuning of lateral connections corresponding to their definition of the near surround in macaque V1 RFs is stronger in supra-granular layers than in the infra-granular ones. They concluded that the orientation-tuned component of surround modulation, in a general manner, involves horizontal connections in layers 2/3 of the macaque and of the cat.

In the same study (Shushruth et al., 2013), the authors also measured the statistical dependencies between responses of V1 RF-like filters to natural images as a function of orientation and distance between the filters, and compared those measurements to surround suppression in macaque V1 neurons and human perception. They found that the orientation dependence of the mutual information shared by two RFs filters closely resembled the orientation tuning of near-surround suppression that they measured in both human vision and macaque V1 cells. Moreover, they found that the mutual information between center and far-surround RFs filters became progressively less orientation tuned as the distance between central target and distant flanker increased. This is similar in both macaque V1 cells and human vision, where far-surround suppression mediated by feedback connections was clearly more broadly tuned for orientation than near-surround laterally mediated suppression (Nurminen et al., 2014, Shushruth et al., 2013).

Once again, conclusions on their findings focus on the suppressive center-surround type of modulation that is the predominant type in monkey: of about 56%-86% of cells in the cat but more than 90% in monkey (Jones et al., 2001; Series et al., 2003; Sengpiel et al., 1997; Walker et al., 1999). However, the neural facilitation field found by Kapadia et al., 2000 (see also Gilbert and Li, 2012) shows that collinear surrounding stimuli *along the preferred orientation axis of the cell* and extending up to 5° from each side of the RF *are facilitative* in the macaque. The set of stimuli used by Nurminen et al., (2014) was composed of drifting gratings, stimuli though to lower (suppress) the perceived contrast of the central target (Cannon and Fullenkamp, 1991) and considered as activating neuronal population more involved in surface representation like figure/ground segregation or image segmentation (Knierim and Van essen, 1992; Nothdurft et al., 1999) than perceptual grouping of various features belonging to a single, large object (Polat and Tyler, 1999; Solomon and Morgan, 2000). They arguably attributed the more broadly tuned component of far-surround suppression that they found to feedback connections because their stimuli were composed of gratings presented simultaneously, configuration that limit extensive study of the contribution of the temporal factor in the propagation of contextual information within the network. They concluded that V1 lateral connectivity serves to the extraction of object boundaries by locally facilitating adjacent collinear contours belonging to a same object of a visual scene or inhibiting adjacent elements of dissimilar orientation in a spatially dependent manner consistent with natural image statistics (Coen-Cagli et al., 2012). On the other hand, according to them, feedback connections quickly detect and guides saccadic eye movements to salient parts of the visual scene by increasing the saliency of dissimilar orientation in the visual scene.

To summarize, it cannot be denied that even though the role of lateral connectivity was less thoroughly studied in monkey than in the cat, horizontally-mediated anisotropic contextual

modulations are less spatially extensive and more inhibitory in NHP than in the cat. To understand the differences reported above, we must take into account that environmental statistics provided to monkey and cat are different. It seems logic to differentiate what we call “near” and “far” modulations between NHP and other mammals and we must take caution when we aim to compare physiological results obtained in NHP and cat to psychophysical phenomena in human as the visual scene content is different between species. In Non-Human Primates (Angelucci et al., 2002 a,b; Shusruth et al., 2013, Nurminen and Angeluci, 2014), cortico-cortical feedback has taken a more prominent role than long-range horizontal connections intrinsic to a given primary cortical area, e.g V1 for vision in ferret, cat or tree shrew (Gérard-Mercier et al., 2016). In the cat, horizontal connections extend over larger regions than in NHP, spanning up to 8-10 mm of cortex, which correspond to 8-10° of visual angle (Gilbert and Wiesel, 1989; Callaway and Katz, 1990; Kisvarday et al., 1997). In primates, on the other hand, the reach of long-distance axons only represents a few degrees in foveal vision: between 4-6 mm, corresponding to 1-3° (Angelucci et al., 2002 a,b; Angelucci and Bressloff, 2006). That distance is closer to the psychophysical results of collinear facilitation obtained in humans (up to 3°: Polat and Sagi, 1993, 1994 a,b, 1998) where cortico-cortical loops of feedback connections are also probably more involved than horizontal connectivity in the transmission of far-surround modulation beyond the limit of monosynaptic lateral connections. This change in spatial scale comes from the refined grain of the retinotopic map in NHP (resulting in an increase in retino-cortical magnification factor) and from the relative size increase of cortical areas that are the product of evolutive pressure. Very long-range horizontal connections may have become insufficient in primate (potentially too slow, too diluted or too expensive) to mediate long distance center-surround interactions in the visual field (Frégnac and Bathellier, 2015). Therefore, the control of feedback projections on V1 lateral connections is very likely much more important in primate than in the cat, ferret or tree shrew. Despite the difference in spatial scale, horizontal connectivity remains similar between cat and monkey in its functional essence and essential as it was preserved throughout evolution.

Now that we set in place a proper definition of center-surround modulations and of their substrate, we saw that feedback projections from extrastriate areas and intra V1 lateral connections are the two types of connectivity underlying near and far surround anisotropic contextual information in V1. What are exactly the other types of connectivity that can be distinguished? What are their main anatomical and functional properties and what is their contribution to center-surround orientation selective modulations? Those questions need to be addressed more precisely in order to fully decompose our knowledge of the operations performed by the brain and precise the role of distinct connectivities and mechanisms of V1 in the implementation of Gestalt laws of perception.

1.4 Connectivity types and canonical circuits involved in lateral processing

1.4.1 Thalamo-cortical feedforward connectivity's contribution to V1 center-surround modulations

The cortical circuit can be divided into its excitatory components, generated by pyramidal and spiny cells, and its inhibitory components, formed by smooth stellate cells. Using intracellular injections of Horseradish Peroxidase (HRP) in the cat, Gilbert and Wiesel (1979, 1983) found that inputs from the LGN arborize within layer 4, the upper part of layer 6 and layer 1 of V1. The intracortical columnar processing is then organized as following: layer 4B spiny stellate cells project to layer 4A, which in turn feeds superficial layers 2/3 (Lund et al., 1979). Layer 2/3 cells then project down to layer 5 that in turn projects to layer 6. Layer 6 cells back project to layer 4 cells via feedback connections, closing a loop of intrinsic excitatory connections (Figure 1.14, Gilbert, 1993). In addition to these spiny neurons there is a population of smooth stellate cell, corresponding to approximately 20% of cortical neurons within V1, which mediates intracortical inhibition. The laminar pattern of thalamic projection to area 17 is roughly similar to the one of area 18 (Levay and Gilbert, 1976), even though differences between the X and Y pathways projections exist in the cat (Rosenquist et al., 1974; Mason, 1975; Hollander and Vanegas, 1977; LeVay and Ferster, 1977; Movshon et al., 1978; Ferster, 1990). In the primary visual cortex of the macaque monkey (Lund, 1973; Lund and Boothe, 1975; Callaway, 1998), the basic laminar organization of excitatory local circuitry and geniculate projections is similar to that described in the cat (Gilbert and Kelly, 1975; Lund et al., 1979; Gilbert and Wiesel, 1979, 1983 a,b, 1985). In the macaque monkey, at the level of V1, the principal targets of thalamocortical projections are also situated in layer 4 even though they also contact, but less frequently, cells situated in other layers (layer 5 and 6 and blobs of layers 2/3) (Gilbert and Wiesel, 1985; Callaway, 1998; Dantzker and Callaway, 2000). However, unlike the cat V1, where it appears that patterned inputs from the lateral geniculate nucleus to layer 4 provide the basis for orientation selectivity (Hubel and Wiesel, 1962; Ferster and Miller, 2000), neurons in layer 4C of primate V1 are insensitive to stimulus orientation. Instead, sharp orientation tuning is found in layers 2/3 and 4B, one synapse removed from the thalamic input (Hubel and Wiesel, 1968; Dow, 1974; Bullier and Henry, 1980; Blasdel and Fitzpatrick, 1984; Anderson et al., 1993; Ringach et al., 1997). Consequently, orientation selectivity in primates arises from intracortical circuitry. Macaque neurons in layer 4Cβ provide patterned inputs to the superficial layers 2/3, building up orientation sensitivity in a manner analogous to the thalamic input to layer 4B in the cat (Lund et al., 1979; Sincich and Blasdel; 2001). Layer 4 cells then represent the largest source of input to layer 2/3 cells in the cat, corresponding to layers 2-4B in the monkey (Lund et al., 1979; Callaway, 1998), layers in which center-surround modulations have been mainly described and where they seem to be more pronounced (Jones et al., 2001).

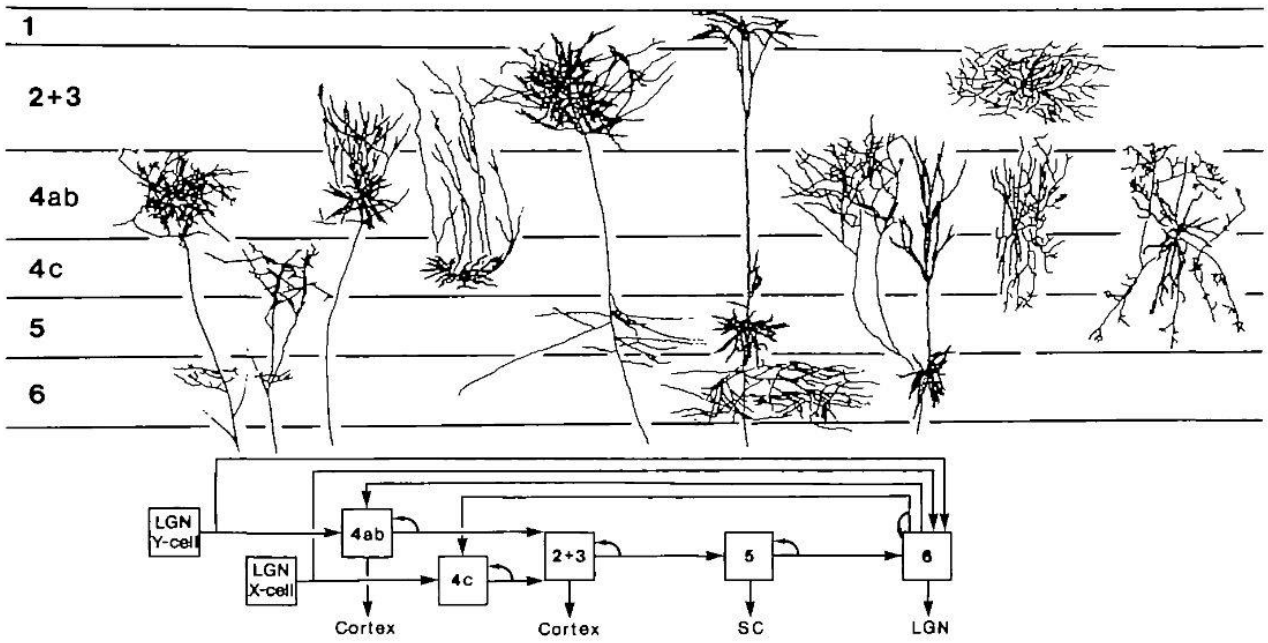

Figure 1.14: ***Schematic diagram of the intracortical connections of the cat's striate cortex, determined by intracellular HRP injections (Gilbert and Wiesel, 1979)****. The spiny stellate and pyramidal cells are responsible for excitatory connections, and their intracortical and efferent connections are summarized in the block diagram below. Smooth stellate cells, several types of which are shown on the upper right mediate inhibitory interactions in the cortex (Gilbert and Wiesel, 1983). (Gilbert, 1993).*

We can then suppose that some center-surround modulatory effects, even though weakly orientation sensitive, are already present at subcortical levels (retina and LGN) and would be transmitted directly to V1 via ascending connections. Indeed, a certain number of center-surround modulations also exists both in the retina and the LGN of cat (McIlwain, 1964, 1966, Fischer and Krüger, 1974; Krüger and Fischer, 1973; Derrington and Fuchs, 1979; Funke et al., 1996) and monkey (Krüger et al, 1975; Krüger, 1977). Those modulations are called the “peripheral” and the “shift” effects, which both affect the firing of ganglion cells of the retina and the LGN without direct stimulation of their RF center. However, those effects do not affect the response of the cat primary visual cortex (Rizzollatti and Camarda, 1977). Moreover, as we already saw, suppressive center-surround interactions exist in the LGN (cat: Cleland et al., 1983; Sillito et al., 1993, Walker et al, 1999; Jones et al., 2000, Felisberti and Demington, 1999, primate: Jones et al., 2001; Felisberti and Demington, 2001). On top of that, Naito et al. (2007) in the cat and Solomon et al. (2002) in the marmoset observed modifications of spatial summation function of the contrast and an enlargement of LGN RFs at weak contrast, just as in V1. However, some differences can be distinguished between V1 and LGN center-surround modulations.

First, in the cat or monkey V1, nearly all the modulations observed are sensitive to the orientation of the surrounding stimuli. That dependency also exists in the cat LGN but, contrarily to V1, the large majority of suppressive surrounding stimulus orientation is not fixed but depends on the orientation of the stimulus presented in the RF center (Naito et al., 2007). Those anisotropic modulations would come from feedback connections from V1 (Silito et al., 1993; Naito et al., 2007). In the marmoset LGN however, modulatory effects seem to be completely independent of the orientation of the stimuli (Solomon et al., 2002).

Secondly, the majority of center-surround modulatory effects observed in the LGN are suppressive, in contrary to cat and primate V1 where both facilitation and suppression can be more easily detected, at least along the preferred orientation axis of cells. Molotchnikoff et al., (1986) however showed in the anaesthetized and paralyzed rabbit that presenting a moving stimulus in a receptive field of the superior colliculus could either increases or decreases responses to the stimulation of a geniculate RF spatially distant in the visual field. This highlights the existence of islands of excitatory and inhibitory modulations in the LGN originating from stimulation of colliculus receptive fields spatially distant in the visual field (Molotchnikoff and Cerat, 1992). Lee and Malpeli (1998) also reported in the cat a large post-saccadic facilitation of LGN responses following a modest suppression before and during eye movements, results that were confirmed in the awake macaque monkey (Royal et al., 2005).

Thirdly, in the cat (Salin et al., 1989) and in the monkey V1 (Perkel et al., 1986), the thalamic spread of projections converging within one hypercolumn of V1 is about 0.4 mm, hence approximately twice the size of two adjacent nonoverlapped thalamic axon arbors reaching their layer 4C cells cortical recipient (about 200 µm in diameter) in the macaque monkey (Figure 1.8a, Angelucci et al., 2002a). That distance is inferior to the size of the entire hypercolumn (about 1 mm in diameter), and thus cannot reach the overall panel of retinotopically distant neighbouring orientation columns to provide anisotropic contextual information.

In cat and monkey, both LGN neurons (Alitto and Usrey, 2008; Bonin et al., 2005; Levick et al., 1972; Sceniak, et al., 2006; Solomon et al., 2002) and retinal ganglion cells (Solomon et al., 2006) exhibit surround modulation. Thus, large stimuli induce surround suppression in the LGN, resulting in a withdrawal of feedforward excitation at the level of V1. However, due to the limited anatomical spread of geniculo-cortical connections (Angelucci and Sainsbury, 2006) and the small size of LGN suppressive surround fields (Alitto & Usrey, 2008; Sceniak, et al., 2006), this thalamic drive is insufficient to account for all center-surround modulations in V1, as those latter are orientation tuned and spatially more extensive than surround suppression observed in the LGN. It appears that feedforward projection from the LGN contributes partially to V1 surround modulation but its contribution is spatially confined to the near surround of V1 RFs.

Indeed, the blockade of intra-V1 inhibition does not completely abolish near-surround suppression in cat V1 cells, signature of a remaining contribution of thalamo-cortical afferents to V1 center-surround modulations (Ozeki et al., 2004). Moreover, the spatio-temporal tuning of V1 surround modulations exceeds the range which drives most cortical neurons (Webb et al., 2005),

resembling the tuning of LGN cells, which suggests that at least part of the modulation in V1 originates subcortically. This feedforward component of surround modulation in V1 is fast (comparable with the pure feedforward latency of RF activation). It is also untuned to orientation (Henry et al., 2013), just as surround suppression in the LGN, which is untuned to orientation in primates (Solomon et al., 2002; Webb et al., 2002), or much less orientation-tuned than V1 suppression in the cat (Bonin et al., 2005; Ozeki et al., 2009 but see Naito et al., 2007).

Contrast normalization is a computation that allows V1 neurons to handle the wide range of contrasts existing in natural scenes, despite the neurons limited dynamic range (Carandini and Heeger, 2012). For instance, divisive normalization can account for experimental evidence that despite saturation of V1 responses at high contrast, the ratio of neurons responses with different orientation preferences remains independent of the contrast (Albrecht and Hamilton, 1982). This is an important requirement, because it allows contrast-invariant recovery of stimulus orientation from the overall neuronal population response (Heeger, 1992). That is why Nurminen and Angelucci (2014) proposed that the untuned component of center-surround modulation in V1 originating from the feedforward drive of geniculo-cortical projections serves to normalize V1 responses but does not account for long range anisotropic modulatory effects.

1.4.2 Feedback connectivity

As discussed before, V1 modulations could be the retroaction product of a more elaborate treatment by superior cortical areas in the visual pathway hierarchy, from areas that V1 directly innervate (V2, V3 or MT/V5) or not (V4, TEO, TE) (Salin and Bullier, 1995). Feedback connections have been identified as targeting mainly pyramidal cells (Johnson and Burkhalter, 1996) in all V1 layers except layer 4. Their role was originally thought to be mainly excitatory (Shao and Burkhalter, 1996), but Anderson and Martin (2009) showed that top down connections from V2 to V1 target both excitatory and inhibitory neurons in layers 1, 2/3, 4B and 6 of the macaque monkey.

The influence of feedback projections can be very fast, in the same range as the Y pathway and comparable to feedforward speed conduction in V1 and V2 (around 3.5 m/s) according to Girard et al. (2001) (Angelucci and Bullier, 2003; Briggs and Usrey, 2007) and are therefore very well suited to mediate the very fast far-surround modulation observed in V1 (Bair et al., 2003; Kilpeläinen et al., 2007). Indeed, to the opposite of what is generally assumed in hierarchical processing (Thorpe and Imbert, 1989; Thorpe et al., 1996; Oram and Perret, 1992; Hung et al., 2005) the conduction speed of those connections is sufficiently high to modulate the pre-treatment of information of early visual areas and contributes to elaborate cognitive processes like rapid visual categorization of natural and artificial stimuli. Although the proportion of cells displaying short latency of feedforward activation tends to decrease as we progress in cortical hierarchy, there is a large overlap of latency distribution across visual areas ranging from V1 to MT (Ouellette and Casanova, 2006; Schmolesky et al., 1998; Nowak and Bullier, 1997, Nowak et al., 1995). Thus, feedback

connections from higher areas can facilitate V1 activity from the beginning of the responses (Martinez-Conde et al., 1999; Hupé et al., 1998). They could provide information about more complex treatment realized by RFs of higher cortical areas (for instance sensitivity to more global structures of shape and motion). V2 and MT, directly innervated by V1, also display center-surround anisotropic modulations. In addition, their receptive fields are much larger than the ones of V1, implying that the integration of center-surround modulations at the level of their RF center is longer than in V1. Therefore, the type of feedback information provided to the striate cortex by those higher areas at a very early stage of the response, before the integration of center-surround modulations at the level of their receptive field center is unclear. From a broader perspective, due to the larger size of V2, V3 and MT RFs, feedback connections coming from those areas and projecting onto V1 are spatially less precise than feedforward ascending connections from the LGN. However, they remain retinotopic on a mesoscale: the gravity center of V1 receptive fields reached by V2, V3 and MT top down connections roughly corresponds to the RF parent cell from which feedback axons originates. It means that one V1 cell receives top down projections from neurons whose RFs are sufficiently spatially more extended to carry far-surround contextual information. We can then imagine that larger receptive fields in V2, V3 and MT integrate more spatially distributed information about the visual scene and could be responsible for far surround modulations observed in V1 via feedback influence.

Experimental evidence indeed shows the implication of feedback connections on V1 response modulation: feedback connections from MT serve to amplify and focus activity in lower order areas as inactivation of MT by cooling mainly provokes a reduction of V1, V2 and V3 responses in the macaque monkey. More precisely, they facilitate the responses to objects moving within the classical RF and are involved in figure-ground discrimination as they enhance suppression evoked by surrounding background stimuli and have strongest effects for stimuli of low visibility (Hupé et al., 1998, Lamme et al., 1998a, Bullier et al., 2001, Bullier, 2001).

In the macaque, V3 RFs are bigger than the ones of V1 by a factor of 10 and the ones of MT by a factor of 25 (Albright and Desimone, 1987). MT Feedback connections conserve the retinotopy of back projections on V1 (Shipp and Zeki, 1989; Sillito et al., 2006), including projections to layer VI (Shipp and Zeki, 1989; Rockland and Knutson, 2000) where it has access to cortico-geniculate feedback projections. Via this route, MT feedback temporally affects the early stage of responses of both V1 and LGN cells (Hupé et al., 2001a, Pascual-Leone and Walsh, 2001; Sillito et al., 2006; Briggs and Usrey, 2007, 2008, Jones et al., 2013).

In the cat, feedback connections from V2 also project retinotopically onto V1 (Bullier et al., 1988; Martinez-Conde et al., 1999; Salin et al., 1992; Salin and Bullier, 1995). In the monkey, feedback connections from V2 convey information corresponding to a region of visual space 5 to 6 times superior to the size of one V1 RF (Angelucci et al., 2002 b). In the cat, those connections cover a region of about 15° of visual angle on a population of cells whose cumulated RFs covers 5°, hence a factor 3 times superior (Salin et al., 1989). We can then speculate that spatially more extended

integration of information by larger RFs of V2, V3 and MT allows those areas to directly modulate the responses of V1 in an orientation-dependent manner via top down connections.

There are indeed indications in V1 layers 2/3 and 4B of the macaque monkey that the spatial distribution of feedback connections could be anisotropically organized, presenting an irregularity or "patchiness" suggesting a distribution that could contact spatially clustered areas spanning orientation columns (Angelucci et al., 2002b), but not in layers 1 and 4 (Angelucci and Bressloff, 2006). Shmuel et al. (2005) also did report orientation specific feedback connections from V2 to V1 in layers 2/3 of the owl monkey. In the cat, Gilbert and Wiesel (1989) showed that area 17 and 18 are preferably connected by feedback connections when they share similar orientation preference. Feedback could then compose a laminar dependent system orientation specific in some layers but not in others. However, the functional role of the feedback component to surround orientation specific modulations remains unclear as those findings were not confirmed in the macaque by Stettler et al. (2002) who showed an orientation non-specific arrangement of feedback connections from V2 to V1. Moreover, there are reports of anatomically widespread feedback connections in the macaque and rhesus monkey (Rockland and Pandya, 1979; Maunsell and Van Essen, 1983; Rockland, 2003). In macaque V1 cells and in human vision, more recent studies from the group of Angelucci showed that the orientation tuning of far-surround modulation mediated by feedback connections progressively decreases with eccentricity from a central RF target, by opposition to near surround laterally mediated influence that remains strongly orientation tuned. (Nurminen and Angelucci, 2014; Shushruth et al., 2013).

What are exactly the characteristics of V1 responses that are affected by top down connections and, more specifically, to which degree is that connectivity responsible for the orientation tuning of center-surround response modulations in V1? We saw that the inactivation by cooling of MT confers a prominent role to feedback connections from that area in response facilitation of some V1 neurons to a moving bar presented into the classical receptive field and participates to the suppression of responses to moving textures presented in the surround of macaque V1's RFs (Hupé et al., 1998). More precisely, inactivation of MT can either suppress or increase V1 responses whether a static or a moving stimulus is presented (Hupé et al., 2001a). Whatever the sign of the modulation, MT affects V1, V2 and V3 during the early stage of the response in the anaesthetized macaque monkey (Hupé et al., 2001a). It has been hypothesized that MT top down connections are involved in figure ground segregation during the late phase of the response (after 100 ms in V1) and that this late influence is only found in awake animals (monkey: Lee et al., 1998b; Lamme et al., 1998b, 1999; cat and monkey: Lamme et al., 1998a), suggesting a prominent role of attention in response modulation. On the other hand, inactivation of V2 does not impact facilitatory and suppressive center-surround modulatory effects specific to orientation observed in V1, when a bar is flashed into the RF center and is surrounded by iso or cross aligned surrounding ones but merely decreases the response of about 10% of the neurons recorded by Hupé et al., (2001b).

Taken together, those results indicate that V2 and MT, higher areas than V1 in the hierarchy of visual processing and receiving direct inputs from it influence the responses evoked in the primary

visual cortex by feedback connections and contribute to center-surround interactions. Despite several evidence of anisotropy of feedback connections, it however seems that feedback connections do not systematically influence the orientation preference of V1 neurons. Indeed, as in monkey experiments, despite the anatomical bias of iso-binding, inactivation studies of higher areas in the cat have shown that feedback has no effect on RF size, surround modulation size nor orientation preference, but it does modulate the amplitude of the evoked response and broadens, or alternatively sharpens tuning width in some cells (Wang et al., 2000, 2007, 2010; Galuske et al., 2002; Huang et al., 2004, 2007; Shen et al., 2006, 2008; Liang et al., 2007). According to those studies, feedback networks generate a context-dependent modulation of the horizontal network over a large region at the level of the primary visual cortex (Ito and Gilbert, 1999) via a rapid and multiplicative scaling action (Wang et al., 2010).

The “near” and “far” surround modulatory effects (based on their proximity regarding the RF center) was proposed by Angelucci and collaborators to be subserved by different anatomical circuits (Angelucci and Bressloff, 2006). The large spatial extent (Levit and Lund, 2002; Shushruth et al., 2009) and fast onset (Bair et al., 2003) of far surround suppression in V1 suggest that modulation comes from highly divergent (Angelucci et al., 2002b) and fast-conducting (Girard et al., 2001) feedback connections from extrastriate cortex. Hashemi-Nezhad and Lyon (2012) reported in the cat that the suppression caused by stimulation of the far surround was more broadly tuned to orientation than the suppression caused by the stimulation of the full surround, including near and far surround stimulation. Although compatible with the findings of Nurminen and Angelucci, (2014) and Shushruth et al., (2013) in the macaque, Hashemi-Nezhad and Lyon (2012) did not address the specific contribution of the near surround stimulation alone, probably responsible for the enhancement of orientation tuning seen in their data. That is why Shushruth et al. (2013) used oriented stimuli confined to the near- and far-surround (extending beyond the monosynaptic extent of horizontal connections) of V1 receptive fields both in the macaque monkey and in human psychophysics. Their findings point out a similarity between surround suppression in macaque V1 and human vision and strengthen evidence of distinct mechanisms of near- and far-surround modulation where far-surround modulations mediated by feedback connections are less orientation-biased than intra-V1 horizontal circuits. Contrarily to Hashemi-Nezhad and Lyon (2012), the visual stimuli used by Shushruth et al., (2013) allowed them to observe an interesting difference: they observed in their data that far-surround suppression was stronger than near surround suppression at near-orthogonal orientation. Whether this is due to an anatomo-functional difference between cat and macaque monkey or a shared characteristic has not yet been tested. Shushruth et al. (2013) hypothesized that broadly tuned far-surround suppression mediated by feedback connections could serve to detect large orientation differences in distant edges, useful for perception of global contours and to direct saccades or attention to salient visual field locations that are markedly different from their surrounding (Petrov and McKee, 2006; Shushruth et al., 2013; Nurminen and Angelucci, 2014). However, strong anisotropic dependency of V1 RFs modulation is observed even in the far surround of the cat CRF (up to 12°, Mizobe et al., Gérard-Mercier et al., 2016), effects that cannot be attributed to extrastriate feedback connections broadly tuned to orientation at those distances (Hashemi-Nezhad and Lyon, 2012).

1.4.3 A laminar dependency?

Center-surround modulations have been mostly described in layer 2/3 where they seem stronger (Jones et al., 2001). However, facilitation of responses for surrounding stimuli cross-oriented to the non-optimal one presented in the center is present in all layers, for simple and complex cells alike (cat and monkey: Sillito et al., 1995; monkey: Levitt and Lund, 1997b). Those results were confirmed by other studies (cat: Walker et al., 2000; monkey: Jones et al, 2001) where the authors described that center-surround modulations differences were weak between layers. The presence in all V1 layers of those contextual interactions precludes the role of a single layer responsible for the emergence of those modulations via interlaminar connectivity.

Moreover, feedback connections target cells of every V1 layer except layer 4 (Salin and Bullier, 1995), layer who display nevertheless center-surround modulations, strengthening both the interpretation that feedback connections do not suffice to explain those specific interactions and highlighting a relative homogeneity of back projections distribution, hence a lack of specific laminar target. Despite the lack of orientation sensitivity of layer 4C cells in the macaque, layer 4B and A are orientation sensitive and display center-surround interactions (Hubel and Wiesel, 1968; Dow, 1974; Bullier and Henry, 1980; Blasdel and Fitzpatrick, 1984; Anderson et al., 1993; Ringach et al., 1997). Although responses from layer 4 and 2/3 cells are influenced by layer 6, this type of modulation does not account for orientation specific modulations including “end-stopping” and “side-inhibition” (suppression of the response when a certain bar length or width are reached, respectively). It is the case because those phenomena are also found in layer 6. However, layer 2/3 cells, where plexuses of horizontal connections are longer than in other layers (cat: song et al., 2010; macaque: Levitt and Lund, 2002; Angelucci et al., 2002 a,b; Angelucci and Bressloff, 2006) display larger and more extended facilitatory extra classical receptive field along their preferred orientation axis.

1.4.4 Local recurrent connectivity

When we aim to study local connectivity, a problem immediately appears: how local is local? The local circuit level, defined as regional groups of interconnected neurons links the microscopic level (several tens of µm describing a discrete nerve cell as a morphological entity with integrative properties) to the macroscopic level (several millimetres linking brain areas) via the mesoscopic level where stereotyped patterns of synaptic connections, or motifs form neuronal subunits. There is however no consensus in the measure of dimension of the mesoscopic connections as no precise, universal definition exists (Horton and Adams, 2005; da Costa and Martin, 2010; Rockland, 2010). In the search of “elementary” subgroups or motifs, there is no clear-cut evidence that different types of axonal pathways innervate distinct cellular types or sub cellular pre- and postsynaptic domains. Song et al., (2005) analysed in vitro quadruple whole cell recordings of rat visual cortex

pyramidal cells and concentrated their analysis on three neuron groups for which there was 16 different possible topological subgraph configurations. Using their estimate of uni/multi directional and reciprocal connection probabilities, they generated random networks and indeed found that three neuron motifs occurred more frequently than expected by chance. Perin et al., (2011) followed a similar approach by recording in vitro simultaneously up to 12 cells in the somatosensory cortex of the rat and also identified specific three and four neurons overrepresented motifs.

Outside of these biologically extrapolated models, experimental data show that most of V1's cells synaptic inputs come from local neurons situated less than 1mm away (Albus et al., 1991), taking place inside the hypercolumn functional unit first described by Hubel and Wiesel (1962). At the level of the primary visual cortex, recurrent local connectivity involves interactions between different orientation columns belonging to and composing the hypercolumn functional block. V1 local excitatory connectivity does not spread beyond 500 µm (Malach et al., 1993; Weliky et al., 1995; Kisvarday et al., 1997, Yousef et al., 1999, 2001, Das and Gilbert, 1999). In the cat area 18, the group of Kisvarday quantitatively analysed in layer 4 (Karube et al., 2011) and layer 6 (Karube et al., 2017) the clustering of synaptic boutons by combining intrinsic optical imaging with three-dimensional reconstruction. They found over 44 cells that pyramidal cells boutons of clusters ranged from 394 to 442 µm of diameter on average. However, they distinguished a first order core cluster embedded in a more extended second order cluster where distances from cell's soma to the cluster center ranged from 711 to 850 µm. They found a weak anisotropy of boutons alignment on orientation map, with a similar number of iso- and non-iso orientation cluster sites. It seems that in the cat (Das and Gilbert, 1999; Karube et al., 2011, 2017), as well as in the tree shrew (Fitzpatrick, 1996) the distribution of local connectivity is isotropic, radially contacting cells of various preferred orientation. Thus, cross orientation suppression of a cell's response when a bar orthogonal to the preferred orientation of a cell is presented in its RF and abolishes the response to the presentation of an optimally oriented bar seems to involve local connectivity that act in a competitive manner with the feedforward activation of a receptive field (Priebe and Ferster, 2006). However, in the ferret, Roerig and Chen (2002) found by combining in vivo optical imaging with in vitro photostimulation that both excitatory and inhibitory inputs to pyramidal cells preferentially originated from regions with similar orientation preference in area 17 and 18. This is consistent with previous results of Dalva et al., (1997) but in addition to those latter, Roerig and Chen (2002) found that ferret recurrent local connectivity is more broadly tuned to orientation for inhibitory inputs than excitatory ones in layer 2/3 and 5/6. In the visual cortex of the mouse (Dräger, 1975; Mangini and Pearlman, 1980; Metin et al., 1988) and rat (Wiesenfeld and Kornel, 1975; Parnavelas et al., 1981; Girman et al., 1999), there are no orientation maps nor orientation columns and hypercolumn, even though neurons are sharply tuned to orientation. Indeed, a "salt and pepper" organization of orientation preference is found in those species (mouse: Wang et al., 2006; Sohya et al., 2007; rat: Ohki et al., 2005). This contrasts with the organization of the visual cortex that we previously described in higher order mammals (tree shrew, ferret, cat, primate). In spite of this striking difference, Ho Ko et al., (2011) found that as in the ferret, local connectivity of mouse cortex is anisotropic: inputs to nearby layer 2/3 neurons connected two times more iso-oriented neurons than cross-oriented ones. According to Douglas and Martin (1991), the feedforward

thalamic drive provides the basis for orientation selectivity at the cortical level whereas local intracolumnar recurrent connections further shape tuning properties of cortical neurons.

The spatial reach of local recurrent connectivity being relatively limited, its role in center-surround interactions between distinct hypercolumns can be questioned, though from a probabilistic point of view, outside of pinwheels areas, spatially limited contacts would preferentially connect cells belonging to neighbouring orientation columns. Due to its radial isotropic distribution in the cat, this connectivity could play an enhancer role of local information. An important point remains: the question of the relative contribution of excitation and inhibition converging on a single cell and their relative role in activity modulation. Indeed, being the largest source of connections of V1 neurons, even if this connectivity is not the substrate of center-surround orientation selective modulations, the balance between excitation and inhibition received by a single neuron has to be essentially controlled by local recurrent connectivity (Somers et al., 1998; Dragoi and Sur, 2000).

The precise role of local connectivity is still unknown. Fournier et al. (2011) showed in the cat using binary sparse noise and ternary dense noise that the spatial extent of both linear and nonlinear kernels of RFs and their relative weights depend on the spatio-temporal density of the stimulus used. The simple-like component of V1 RFs could then come from the feedforward drive and complex-like components would result from recurrent local connections. This local connectivity could underlie the extraction and amplification of local information that would be modulated by a long range anisotropic connectivity providing more global information between the elements composing a visual scene (Frégnac and Bathellier, 2015).

1.4.5 Horizontal connectivity

The existence of horizontal connectivity parallel to the surface of the cortex was first highlighted by Fisken et al., (1975) and Creutzfeld et al., (1977). Later on, thanks to the use of retrograde transport of Horse Radish Peroxidase (HRP), several intracellular studies (Gilbert and Wiesel, 1979, 1983; Martin and Whitteridge, 1984) in the cat, extracellular ones in the tree shrew (Rockland and Lund, 1982) and in the monkey (Rockland and Lund, 1983) showed, after tridimensional reconstruction the existence of a long-range connectivity of presumably excitatory axons that links pyramidal cells of a same cortical area over several millimetres in V1. Those results highlight an apparent contradiction between the classical “Mexican hat” profile of surround inhibition taking place at the retinal and thalamic level where long distance surrounding influence is inhibitory (Figure 1.3) whereas long distance lateral connections are excitatory at the cortical stage. It seems that there is an inversion of the kernel of surround modulation that emerges at the level of the cortical sheet. Computational approaches have been successful in describing center surround modulations at the cortical level by assuming long distance suppressive surrounding influence. One

has to assume that the success of computational predictions based on long distance inhibitory influence relies on long excitatory lateral axons ending up on local inhibitory interneurons.

Gilbert and Wiesel (1989) confirmed anatomically the relationship between the organization of horizontal connectivity projections and the periodicity of cortical columns of orientation in layers 2/3 of the cat. Using a staining technique of retrograde transport of a fluorescent marker (the rhodamine) combined with a staining of the orientation map by 2-deoxyglucose (a radioactive marker which is incorporated but not metabolized by active cells), they showed that rhodamine stained neurons only appeared in orientation columns having the same preferred orientation than the site of injection. This indicates that horizontal connectivity does link cells of the same preferred orientation.

Contrarily to cat local connectivity, the horizontal one is not radially organized in all directions around a given cell. On the opposite, it is organized in patchy motifs regularly spaced by 0.5 to 1 mm, a periodicity corresponding to the distance between cortical columns (Gilbert and Wiesel, 1979, 1983 a,b; Rockland and Lund, 1983; Mitchison and Crick, 1982). Mitchison and Crick (1982) proposed that horizontal connectivity links neurons of the same preferred orientation according to a particular direction: orthogonal or collinear. According to them, collinear links of neurons having the same preferred orientation could be the anatomical support of facilitatory/inhibitory messages responsible for “end-stopping” (inhibition when a certain bar’s length is reached) while “side-inhibition” (inhibition when a certain bar width is reached) would come from lateral connections orthogonal to the cell’s orientation axis. Certain cells displaying both end and side inhibition have been found in the cat V1 (DeAngelis et al., 1994) and called Length-Width Inseparable (LWI) cells (Lui et al, 2007).

From a functional point of view, Michalsky et al., (1983) described in the cat a strong cross correlation between spiking responses of cells belonging to different columns of similar orientation and ocular dominance, illustrating the principle of “who fires together (or are alike) tends to be wired together” evoked by Shatz (1992), results confirmed by Ts’o et al. (1986). However, the picture is not that clear cut since more recent studies did not confirm those results (Das and Gilbert, 1999). The lateral iso binding of distant orientation columns sharing orientation properties doesn’t seem to be the rule as reports of lateral connections mediated by interneurons (Kisvarday et al., 1994; Buzas et al., 2001), layer 4 stellate neurons (Yousef et al., 1999) and pyramidal neurons close to pinwheel areas (Yousef et al., 2001) also connect orientation columns in a cross-oriented manner. Moreover, local and selective inactivation of lateral connections showed that lateral suppression comes from both iso- and cross-oriented sites (Crook and Eysel, 1992; Crook et al., 1998). This heterogeneity probably reflects the huge panel of center-surround modulatory effects that does not only include collinear facilitation between iso-oriented columns but also modulations whose sign, orientation tuning and preference differ according to specific stimuli configurations (Blakemore and Tobin, 1972; Maffei and Fiorentini, 1976; Nelson and Frost, 1978; Gilbert and Wiesel, 1990; Li and Li, 1994; Sillito et al., 1995; Levitt and Lund, 1997 a; Sengpiel et al., 1997; Polat et al., 1998).

More specifically, in primates, extensive lateral circuitry was found in layers 2/3 and 4B (Rockland and Lund, 1983). These intralaminar projections capture the spatial geometry of a line stimulus by recapitulating retinotopy, specifically by distributing axon terminals along retinotopic axes in squirrel and owl monkeys, just as in the tree shrew (Bosking et al., 1997). The total reach of these projections corresponds to approximately three times the receptive field dimension in the macaque monkey, which limits the retinotopic extent of monosynaptic influences to neurons representing adjacent receptive fields (Sincish and Blasdel, 2001) and is in accordance with the smaller spatial extent of horizontal connectivity in NHP than in the cat. Those results in NHP are also closer to psychophysical findings in humans where the near extent of collinear facilitation presumably mediated by lateral connections is confined to the near surround of V1 RFs and reach up to 3° of visual angle on each side of a central target (Polat and Sagi, 1993, 1994 a,b).

In the monkey, the small spatial extent (Angelucci et al., 2002 a,b; Angelucci and Bressloff, 2006) and slow conduction velocity (Grinvald et al., 1994; Bringuier et al., 1999; Girard et al., 2001) of intra-V1 horizontal axons suggests that they are responsible for near-surround modulations extending up to the monosynaptic reach of horizontal connections and encompassing the untuned modulatory surround of geniculo-cortical feedforward afferents(Shushruth et al., 2013; Nurminen and Angelucci, 2014). In the cat, the spatial spread of intra V1 horizontal connectivity is much more important and encompass bot near and far surround spatial regions around the RF (Gilbert and Wiesel, 1989; Callaway and Katz, 1990; Kisvarday et al., 1997), especially along the preferred orientation axis of cells (Chen and Kasamatsu, 1998; Chen et al., 2001, 2013, 2014; Wang et al., 2009; Walker et al., 2000; Mizobe et al., 2001; Gérard-Mercier et al., 2016).

The consensus that horizontal axons predominantly link neurons with similar response properties i.e., orientation, relies on anatomical data. However, functional data are not easy to reconcile with anatomical data because first, functional evidence of cross orientation modulation via lateral connections are also found (Crook and Eysel, 1992; Crook et al., 1998). The rule for iso-binding of similar orientation columns is therefore not absolute but a bias. This bias of lateral connections linking iso oriented columns is only partial, it has been quantified in the cat as only 1,5 times superior than expected by chance (Kisvarday and Eysel, 1993; Kisvarday et al., 1994, 1997; Schmidt et al., 1997; Yousef et al., 1999, 2001; Buzas et al., 2001; Buzas et al., 2006). Moreover, plexuses of lateral connections are, even though on average superior for facilitative extra classical receptive field cells, heterogeneously distributed among cortical cell types (F-ERF vs S-ERF neurons in Song et al., 2010). On top of that, lateral connectivity spread and tuning estimates are controversial, potentially because of methodological issues (injection site, marker type, type of stimuli, anaesthetized versus awake state, level of anesthesia) and species differences. The picture seems even more complex as iso-orientation selectivity of lateral connectivity revealed at the anatomical level decreases with distance (Kisvarday et al., 1994, 1997; Buzas et al., 2006). This is also the case at the functional level (in the macaque monkey: Shushruth et al., 2013, in the cat: Chavane et al., 2011, Hashemi-Nezhad and Lyon, 2012). That is why the combination of distinct techniques must be used in order to fully capture similarities and discrepancies between results and species. Intracellular recordings allow to access the subthreshold depolarizing influence of

lateral connections with a remarkable temporal precision whereas VSDI experiments allow to capture subthreshold effects spatially distributed and highlight masked subthreshold depolarizing influence undetectable by classical extracellular electrophysiological recordings.

1.5 Role of V1 lateral connectivity in low level perception

From the characteristics of the different types of connectivity described above, the horizontal and feedback ones are the most plausible substrate for center-surround modulations observed in V1. Responses in that area depend on the spatial configuration in which stimuli are presented, based on complex mechanisms of center surround interactions involving facilitation or suppression of responses that are function of the relative geometric organization of oriented stimuli and of their contrast. In this context, the receptive field cannot be considered as a rigid filter extracting only bottom-up information, composing a pure hierarchical model of serial features extraction of increasing complexity.

Attributing a given and unchanging role to brain areas ranging from relatively simple operations to more complex ones then seems reductive and even though practical, counterproductive in the complete depiction of more subtle “hidden” operations performed by the brain. That is why the role of early visual areas is more and more put back in question, since we don’t understand precisely the subtlety of the overall operations that they perform, their contribution to visual information processing is not as simple as initially thought. Even our understanding and description of visual information processing have to be questioned, the functional characterization of low level areas operations only relying on relatively simple stimuli which complexity does not allow a direct confrontation to the external visual world, potentially underlying a huge number of complementary regimes of information treatment. Because it is the basis of the hierarchical model, challenging the serial view of information processing throughout the visual pathway necessarily includes a re-evaluation of the receptive field concept, especially the complexity of operations performed under more naturalistic stimulations involving contextual modulations and their origin.

The dominant view is that contextual long-range interactions, studied at the spiking level, rely on cortico-cortical feedback (from higher-order cortical areas onto V1) and on attention (Lamme & Roelfsema, 2000; Schwabe et al., 2010; Gilbert & Li, 2013; Bastos et al., 2015; Nassi et al., 2013). The implementation of Gestalt’s psychological laws of perceptual binding strongly depends on top-down control signals in the behaving non-human primate (Li et al., 2006; Gilbert and Li, 2013). Indeed, Gilbert and Li (Kapadia et al., 2000; Gilbert and Li, 2012) saw contextual facilitation of responses to a central target by collinear flankers in the alert macaque extending up to 5° of visual angle on each side of V1 RFs (Kapadia et al., 1995, 2000; Gilbert and Li, 2012). However, Gilbert, Li and collaborators failed to see contextual modulation in the presence of anaesthesia (Li et al., 2006, 2008). By opposition, the working assumption of our group is that the implementation of Gestalt’s

psychological laws of perceptual binding requires an intra-V1 stimulus-driven bottom-up process, which operates *even in the absence of attentional processes.*

Indeed, in the cat, neuronal correlates of collinear facilitation can be searched for, even in the low level perceptual state of the anesthetised animal using intracellular recordings, revealing subthreshold influence undetectable by extracellular recordings. There is ample evidence from anesthetized cat experiments that pleads for the existence of contextual facilitation to a central target by collinear flankers (Polat et al., 1998; Mizobe et al., 2001; Kasamatsu et al., 2010). However, Kasamatsu et al., (2010) reported in the anesthetized cat that V1 collinear facilitation was independent of receptive field expansion at low contrast. This is in direct opposition to the interpretation of Mizobe et al., (2001) who found facilitation by collinear flankers in the anesthetised cat for stimuli placed as far as 12° of eccentricity from the RF center. More recent studies in the cat V1 reported that the low contrast rate of expansion for the suppressive space is substantially lower than for the excitatory space (Chen et al., 2013; Wang et al., 2009). The excitatory and suppressive space overlap extensively and a relatively large part of the suppressive space is masked at low contrast. According to Mizobe et al. (2001) and Chen et al. (2014), cells displaying collinear facilitation, even at high contrast (expansive facilitation) have large CRF and long range horizontal connections (Song et al., 2010) that extend well beyond the suppressive space, by opposition to suppressive extra classical receptive field cells that does not form extended lateral connections and only display surround suppression with no particular response facilitation by collinear flankers. Kasamatsu et al., (2010) argued that the low contrast expansion of the RF, classically attributed to horizontal connections, cannot account for collinear facilitation first because low contrast RF expansion is not universal and second because in half of the cells they examined, the strength of collinear facilitation continually increased with target contrast, while the RF center size should in principle be shrinking under those conditions. Thus, according to them, collinear facilitation is certainly not a consequence of the RF expansion at low contrast. Their interpretation is surprising since previous studies of the same group (Chen and Kasamatsu, 1998; Chen et al., 2001, Mizobe et al., 2001) reported that over more than a hundred cells that they examined, a third exhibited an expansion of their RF upon increase in contrast, phenomena that they termed expensive facilitation. Moreover, Kasamatsu et al., (2010) argued that collinear facilitation could not emerge from RF expansion because the spatial extent of RF expansion was smaller than the one of collinear facilitation. Even though the spatial extent of RF expansion is smaller than the extent of collinear facilitation, concomitant stimulation of two adjacent RF of the same preferred orientation can form overlapping connectional fields of lateral activity. This overlap can mutually facilitate the response of each locus of activation for distances extending at least up to the extent of monosynaptic lateral connections (Angelucci et al., 2002 a,b). Laterally mediated activity linking receptive fields of similar orientation and facilitating their detection at the V1 level can thus very well account for emergent properties, such as feature grouping by form similarity, spatial proximity and perceptual facilitation for collinear visual elements, operations funding the principles of Gestalt's psychophysical laws of perceptual binding (Kovacs and Julesz, 1993; Polat and Sagi, 1993, 1994 a,b; Polat and Tyler, 1999). The influence of lateral connectivity can thus be

described at a more holistic level by a perceptual “association field”, operating in the spatial (Figure 1.14) (Field et al., 1993; Hess and Field, 1999), and temporal (Neri et al., 1998) domains.

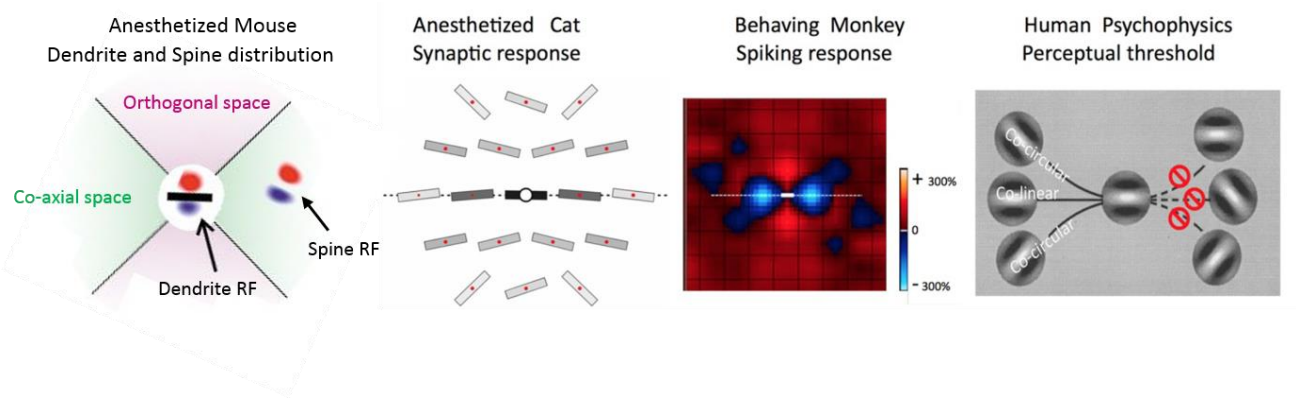

Figure 1.15: ***Horizontal connectivity, Visual Space and the Association field concept.*** *From left to right: example V1 dendrite RF with a retinotopically displaced spine RF showing the preferential distribution of synaptic input co-oriented and co-aligned along the retinotopic representation of visual space in the anesthetized mouse (Iacaruso et al., 2017). Synaptic association field represented by the distribution of orientation sensitivity of V1 RFs surround and center in the anesthetized cat, the strength of synaptic responses obtained by intracellular recordings is color coded from darker for stronger responses to brighter for weaker ones (Gerard-Mercier et al., 2016). Neural facilitation field of awake behaving monkey revealed by extracellular recordings showing the facilitation of V1 RFs spiking responses to collinear flankers (blue, facilitatory; red, inhibitory influence) (Gilbert and Li, 2012). Association field described in human psychophysics: elements sharing a certain degree of collinearity are easier to bind than elements cross oriented breaking continuity in visual space (Hess and Field, 1999).*

Recent work from our lab showed in the anesthetized cat the existence of a synaptic bias intrinsic to V1 for the integration of local collinear features across the visual field (Figure 1.15, second column, Gérard-Mercier et al., 2016). That synaptic “footprint” first reveals a structural organization already present in V1, corresponding to a synaptic association field that mirrors the perceptual static association field seen in human psychophysics (Field et al., 1993; Hess and Field, 1999). Second, it shows that intracellular recordings can reveal neuronal correlates of perceptual phenomena in the low level perceptual state of the anesthetised animal. That structural bias was forged during critical stages of development by plasticity mechanisms obeying Hebbian rules following exposure to natural statistics of the external visual world. In the adult cat, it appears that the integration of collinear contours is already inscribed in the synaptic echoes of V1, revealing an already built in mechanism for the integration of continuous contour that does not require consciousness. It accounts very well for the emergence of sensory inference in the brain, or predictions about what is to be perceived without any active contribution of the mind, like the perceptual pop out for contour integration presented in Figure 1.12 B. Attentional processes are

not the basis of contour grouping phenomena but act upon mechanistic constraints of “automatic” information processing.

Traditionally, binding in space and across time are thought to be implemented in separate cortical areas, respectively in V1 and MT (Heeger et al., 1996). In spite of the hierarchy in cortical specialization (Felleman and Van Essen, 1991; Serre et al., 2007), the contribution of intra-V1 mechanisms such as recurrent amplification and lateral propagation is largely unknown (Frégnac and Bathellier, 2015). More precisely, a remaining unsolved issue is to determine to which extent horizontal connections, intrinsic to V1, are already instrumental to the neural implementation of Gestalt psychophysical laws of perceptual binding in low level perception. The second part of our study (Gérard-Mercier et al., 2016) revealed that the synaptic bias for the integration of collinear elements was not restricted to the spatial domain. Indeed, using an Apparent Motion (AM), pairs of Gabor patches were presented in a cellulo centric referential centred on the subthreshold depolarising field. Those experiments revealed that the synaptic bias for the integration of collinear contour was not restricted to the spatial domain but also included the temporal one as it extended to collinear elements forming a centripetal flow converging onto V1 RFs, encompassing both local (element’s orientation) and global (direction of the flow) features of motion. These findings reveal the existence of an intra V1 dynamic association field that adds a temporal component to the “neural facilitation field” found in the awake non-human primate (NHP) (Kapadia et al., 2000, Gilbert and Li, 2012). It participates actively to the processing of non-stationary stimuli in human like the “speed-up” effect (Georges et al., 2002) and the illusory “line-motion” effect (Jancke et al., 2004). In the non-human primate, it may be involved or complementary to the processing of non-stationary stimuli by rolling waves of activity that does not require horizontal’s connectivity (Reynaud et al.,2012, Muller et al., 2014).

The framework of this thesis posits in a first time that horizontal connectivity participates to the propagation of a network-based belief, resulting in the propagation of a “prediction” travelling through the V1 network. This notion is to distinguish from the classical “predictive coding” scheme (Rao and Ballard, 1999) where the information conveyed laterally or through feedback is the error message itself, based on the confrontation with expectations from higher cortical areas rather than the global perceptual information propagation postulated here. When the contrast is high, horizontal propagation of contextual information coming from the periphery leads to a suppression of redundancy in V1 (Martin and Von der Heydt, 2015). By opposition, when the feedforward signal is weak (low contrast or stimulus absence in “illusory contours”), maximising the lateral broadcast of relevant contextual information matching the spatio-temporal bias of the dynamic association field would boost the gain of feedforward-related activity (Frégnac et al., 1996), resulting in the propagation of a prediction. We tested the hypothesis that laterally propagated and feedforward activity interact in order to boost sensory responsiveness. By sequentially activating the periphery of a receptive field at a speed corresponding to lateral connectivity’s conduction velocity before stimulating its center, we tested whether local: orientation of the elements (collinear or orthogonal

to the cell's preferred orientation) and global features of the AM flow (direction of the flows converging towards or diverging from the RF center) impacted cell's responsiveness. We expected a reduction of the intracellularly recorded cell latency activation and an amplification of its response by setting the comparison basis to the sole feedforward activation of the RF center. We also tested whether the stimulation of the periphery alone could induce filling-in/predictive responses and manipulated the AM flows speed to probe the implication of horizontal connectivity.

The second part of this thesis is less data-driven and more exploratory. We focused on the possibility that geometric hallucinations and similar induced percepts like the Mackay's after effect reflect a long distance spatial opponency of the horizontal connectivity in V1. We posit that cortical adaptation to a geometric inducer constrain the exploration of neighbouring orientation domain transition observed in the cat's ongoing activity (Kenet et al., 2003). The perturbation by a $1/f^{\alpha}$ noise possessing natural spatio-temporal statistics of a highly biased network adapted to a geometric planform result in the emergence of opponent waves of activity orthogonal to the physical inducer, revealing interactions between the imposed sensory-driven input constraint and the consequent adaptation of self-organized activity. We developed visual stimuli containing radial fan shape or concentric annulus geometric inducers embedded in a $1/f^{\alpha}$ noise whose statistics were adapted to optimize the percept of opponent planforms propagating on the visual field. We manipulated the center of the geometric inducers position in order to render the perceived propagating percept wavefront locally parallel to the preferred orientation of individual cells recorded intracellularly. Our working hypothesis was that the induced waves of activity and their geometric nature would be detectable at the single cell level when their wavefront is parallel to the preferred orientation of a cell under the form of oscillations of the membrane potential matching the perceived dynamic of propagation of the percept.

Part I – Lateral connectivity and the propagation of network belief

I-1. Background

General features of horizontal connectivity

I-1.1 Anatomy

I-1.1.1 Iso-orientation bias in excitatory horizontal connectivity?

A major issue in the study of the functional role of horizontal connectivity is to determine first, to which extent does it convey contextual modulation and second, to which type of modular functional properties of V1 (orientation distribution, ocular dominance…) does it apply. Indeed, being able to determine to which degree the horizontal network overlaps with the representation of orientation in V1 and what is its action at different scales (short range modulation of neighboring hypercolumns or long-distance modulation of distant hypercolumns) is of paramount importance. In order to study the anatomical organization of horizontal connectivity (HC), injection of HRP (Horse Radish Peroxidase) intracellularly in the cat (Gilbert and Wiesel, 1979, 1983 a,b; Martin and Whitteridge, 1984), extracellularly in layers I-III of the tupaia (Rockland and Lund, 1982) and in layers II/III of the monkey (Rockland and Lund, 1983), showed, after three-dimensional reconstruction that long distance horizontal connections tend to remain in the supragranular layers and link retinotopically distant points of visual space. HC mainly links excitatory pyramidal cells of the same cortical area over several millimetres. Moreover, this connectivity is heterogeneously distributed and organized in patchy motifs (Figure 2.1) regularly spaced by 0.5 to 1 mm, a periodicity corresponding to orientation cortical columns (Gilbert and Wiesel, 1979, 1983 a,b; Rockland and Lund, 1983; Mitchison and Crick, 1982).

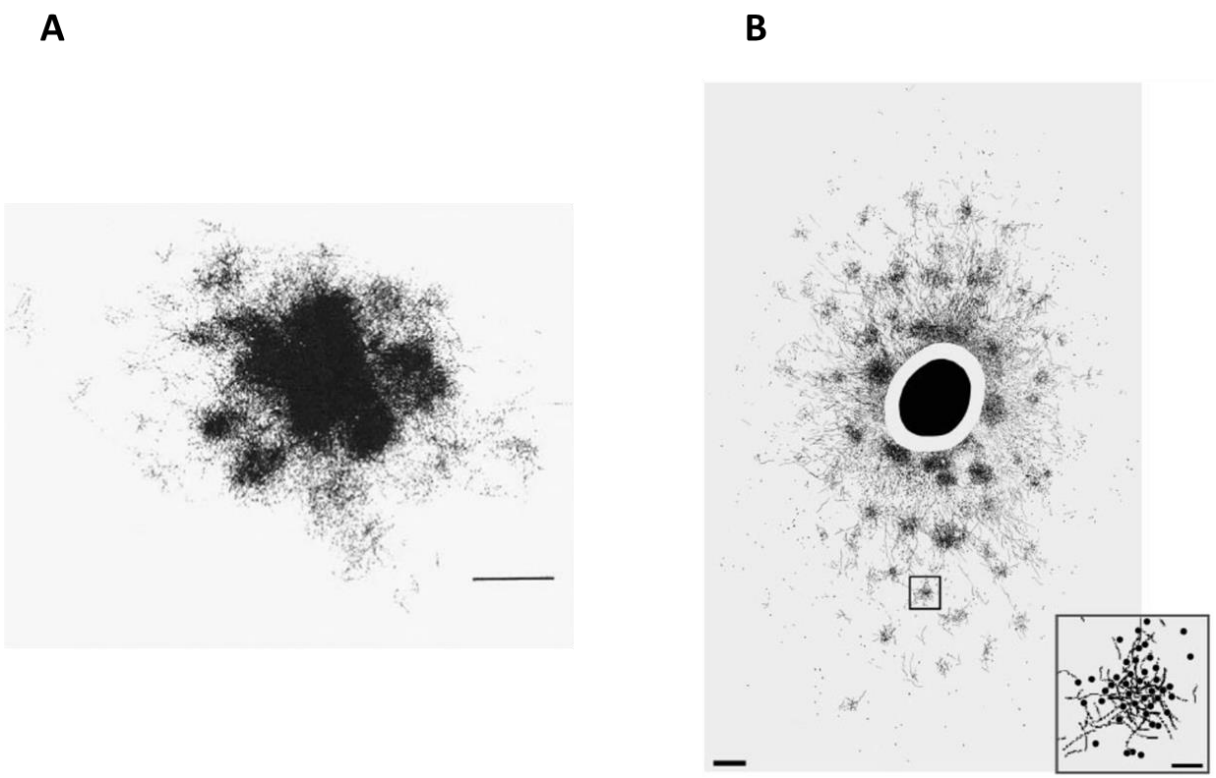

Figure.2.1: ***Patchy horizontal connections in layers 2/3 of cat and macaque V1.***
A. *Reconstruction of lateral connections in cat area 17. Distribution of synaptic boutons labelled anterogradely from a biocytin injection site (dark region in the center). Each dot represents one single bouton; excitatory and inhibitory boutons are plotted together. At least 20 distinct patches can be discriminated but interpatch regions are also heavily innervated. Scale bar: 1000 µm. (Kisvarday et al., 1997).* ***B.*** *2D view of macaque V1 surface. Black oval: Cholera Toxin B (CTB) uptake zone. Blank annulus: region of heavy label. Scale bar: 500µm. Small square: high-power drawing of a patch displayed in the inset showing labelled fibers and somata (dots), indicating reciprocity of connections. Scale bar: 100 µm. (Angelucci et al., 2002b).*

The comparison between the staining of cells horizontally connected by retrograde transport of rhodamine and the staining of orientation map by 2-deoxyglucose (2-DG) allowed Gilbert and Wiesel (1989) to confirm in the cat that rhodamine stained neurons only appeared in orientation columns having the same preferred orientation, highlighting the anisotropic property of horizontal connectivity in layer 2/3. However, all cells stained by 2-DG did not exhibit a staining by rhodamine, establishing that long distance horizontal connections do link neurons with similar orientations but that all neurons of a given orientation are not laterally connected with all matching distant orientation columns. It must be emphasized that the configuration of HC strongly depends on the given local sites of injection and on the position of those sites of injection within the orientation map (near or far away from pinwheels).

In the macaque monkey, using in vivo intrinsic imaging and extracellular staining by biocytin (an anterograde marker) Malach et al. (1993) showed similar results but nuanced them: the iso orientation of horizontal connectivity is only partial, i.e., HC does not only link neurons with the

exact same orientation but a third of this connectivity displays a higher tolerance, linking neurons having orientations preference differing of 45°. Using the same techniques combined with extracellular recordings in layers II/III of V1 in the Tupaia, Fitzpatrick (1996) and Bosking et al. (1997) aligned the synaptic buttons that were stained in their studies with orientations maps. They observed within their sample that stained buttons situated further than 500 µM from the injection site always contacted areas of orientation similar to the site of injection. Beyond the spread of the local excitatory isotropic connectivity, longer range horizontal connectivity parallel to the cortex surface becomes anisotropic. Taking all their results into account without distinguishing close (inferior or equal to 500 µM) and long-distance contacts, about 60% of buttons that they identified contact a preferred orientation site with a tolerance of ± 35° from the orientation of the injection site.

Similar results were found in the cat using the same techniques (Kisvarday et al., 1997; Schmidt et al., 1997 a,b): about 55% of excitatory horizontal connectivity buttons of excitatory pyramidal cells link iso-oriented regions of ± 30° of difference regarding the injection site, 30% link oblique orientations areas (± 30°- ± 60°) and 15% link cross-oriented areas. Even though long distance horizontal projections also innerve inter-patch regions not iso-oriented, especially for distances inferior to 0.5 mm, they mainly project to iso-oriented areas.

Overall, in different species (cat, monkey, tupaia) and with different techniques, reproducible results indicate that long distance HC preferentially link iso-oriented neurons. However, this selectivity is partial (50-60%) and disappear for short distances (< 500-800 µM). In addition, it seems that HC displays a rather strong layer-dependent heterogeneity: mainly studied in layer 2/3, to the contrary of V1, excitatory and inhibitory horizontal connections of layer 4 of the cat V2 do not present the “patchy” aspect characteristic of supragranular layers and seem isotropic (Yousef et al., 1999). However, Kisvarday et al., (1993 a,b) reported the existence of a long-distance network of inhibitory connections between basket cells both in supra and infragranular layers of area 18 that was different than the patchy aspect of excitatory pyramidal connections.

The selectivity of lateral connectivity projection patterns also concerns ocular dominance. König et al., (1993) observed that during early stage of development, induction of squint in kittens can modulate lateral connectivity between neurons dominated by different eyes as synchronicity between them is reduced while left unaffected between neurons having similar ocular dominance. Malach et al. (1993) observed in the macaque that injections in monocular areas mainly led to a staining of cells having the same ocular preference, neurons situated in binocular regions being linked to binocular cells. Similarly, as for iso-orientation binding, the ocular dominance selectivity is partial (Yoshioka et al., 1996).

I-1.1.2 Spatial spread of horizontal connections

An important issue in integrative and computational studies of V1 is to determine the « diffusion » radius of visual information relayed by horizontal connectivity and the corresponding radius of space representation across species. Pioneers studies were made in the cat, where it was shown that retrograde transport of rhodamine via HC covers a large area of 8 to 10 mm of diameter around the injection site, corresponding to 8-10° of visual angle (Gilbert and Wiesel, 1989; Callaway and Katz, 1990; Kisvarday et al., 1997). Similar estimates have been found on the basis of cross-correlation studies and synchronization effects (Schwarz and Bolz, 1991; Gray et al., 1989). In the tupaia, it can reach 4 mm of radius, corresponding to 2 to 3 times the size of a low contrast RF in the area of injection, covering up to 20° of visual angle due to the difference in magnification factor of that species (Bosking et al., 1997). In the platyrrhines (new world monkeys), the spread of HC is much smaller, of about 1-2 mm, representing a distance of one low contrast spatial summation RF on each side of the RF of a given cell (Sincich and Blasdel, 2001). In the macaque, HC spread over 4-6 mm on the cortex surface on average, which correspond to 1-3° of visual angle (Levitt and Lund 2002; Angelucci et al., 2002 a,b, Angelucci and Bressloff, 2006). This dispersion distance in non-human primates, measured in visual coordinates, is much more reduced than that found in the cat, which corresponds to 3 times the size of the high contrast minimum discharge field and equates the spatial extent of the summation field at weak contrast. From a broader perspective, the change in spatial scale covered by HC between cat and non-human primate comes mostly from the refined grain of the retinotopic map in NHP (resulting in an increase in retino-cortical magnification factor) and from the relative size increase of cortical areas.

The use of optical intrinsic imaging to determine orientation selectivity maps combined with anatomical staining of afferent and efferent connections at the level of pinwheels allowed Yousef et al., (2001) to show that the spread and organization of the horizontal connectivity strongly depends on the cell's position in the orientation map. Indeed, in cat V1 pinwheels, horizontal connectivity connects reciprocally cells of various orientations in a radius of 300-400 µM but *do not belong to a long distance horizontal network*: those connections reach 1.6 mm on average in pinwheels, by opposition to 3.5 mm in orientation domains outside of pinwheel areas (Gilbert and Wiesel, 1989; Kisvarday et al., 1997).

I-1.1.3 Iso-orientation binding across the retinotopic map

On top of preferentially connecting cells having the same preferred orientation, it already appeared from pioneer studies that axonic arborisations of individual neurons are elongated along the cortical surface, spreading over larger distances and displaying more connections *along a particular axis of the cortical map* (cat: Gilbert and Wiesel, 1983, 1989; macaque: McGuire et al., 1991; Malach et al., 1993; Grinvald et al., 1994). The anisotropy of horizontal connectivity had

mainly been studied along the vertical axis of retinotopic space, it was then difficult to determine to which extent the preferential binding of iso-oriented cells was due to the cortical magnification factor, more important along that axis. The group of Fitzpatrick (Fitzpatrick, 1996; Bosking et al., 1997) quantified precisely the differential spatial spread of horizontal connectivity along that particular axis in layers 2/3 of the tupaia. They found that horizontal connections in those layers spread systematically over larger distances and make more connections (superior by a factor of 4 on average) *along an axis that correspond to the preferred orientation axis of a neuron* compared to an orthogonal axis, regardless of the given neuron's preferred orientation. The systematic relationship between the elongation axis and the orientation preference cannot then be explained by a mesoscopic anisotropy property like the magnification factor. From those results, not only does the horizontal connectivity tend to bind neurons having the same preferred orientation but it binds them preferentially if they are collinear in the retinotopic representation of visual space.

Those results were confirmed in the cat (Schmidt et al., 1997a) where the authors reported that neurons having iso-oriented *and* iso-aligned RFs in the visual field are more frequently inter-connected and over larger distance than neurons iso-oriented but not iso-aligned in visual space, although those later remains more frequently connected than neurons having different preferred orientations. The retinotopic collinearity property of the lateral connectivity's anisotropy was also observed in the squirrel monkey (Sincish and Blasdel, 2001) where long distance projections of layer 3 cells are also retinotopically aligned with preferred orientation in that species, with a smaller degree of tolerance (12°) between the RF orientation and the orientation of lateral projections sites.

I-1.1.4 Excitatory versus inhibitory horizontal connectivity

According to Kisvarday and Eysel (1993), in the cat, inhibitory lateral connections only come from GABA related basket cells. To the contrary of excitatory horizontal connectivity, the distribution of inhibitory interneurons collaterals does not present the orientation selective "patchy" aspect of excitatory lateral connectivity. It seems to be more uniform and to cover a smaller distance of about 2.5 mm (Albus et al., 1991; Kisvarday and Eysel, 1993; Kisvarday et al., 1994, 1997). In those regions, cells contact both pyramidal cells and interneurons, forming a relatively large inhibitory field, but also a des-inhibitory field reaching 4 to 5 mm.

In contrast to what has been reported for excitatory projections, Kisvarday and Eysel (1993) did not observe significant differences between the iso-oriented, cross-oriented or oblique preferred orientations of boutons contacted by inhibitory cells in area 17 and 18 of the cat. Investigating further, Kisvarday et al. (1994) highlighted some differences: 43% of inhibitory axonic endings reach cortical sites with similar orientations, 35% oblique sites and 22% contact cross-oriented domains, results that were later reproduced (Kisvarday et al., 1997). These authors concluded to a significant difference between excitatory and inhibitory long-distance projections: even though those two

networks strongly overlap, the iso-orientation preference bias of the inhibitory network was found weaker than the excitatory one.

Excitatory lateral connections, more numerous and extended than inhibitory one, are generally thought to be responsible for center-surround responses modulations. However, the role of GABA-related connections cannot be excluded. Their spatial reach could link neighbouring or slightly overlapping RFs. Kisvarday et al. (1994) highlighted that the functional efficiency of basket cells linked by horizontal connections is probably underestimated. According to those authors, despite the smaller number of long-distance connections that basket cells receive, they form more boutons on a given target than excitatory pyramidal cells linked by horizontal connections, those two long-range systems could then interact in a competitive manner. More precisely, long distance inhibitory links can be formed by disynaptic circuits formed of long distance excitatory lateral connections ending up on local short-distance inhibitory ones. This arrangement has been used by modellers to account for the Mexican hat shape of horizontal activity kernel, which might suggest a predominant long-distance suppressive influence. On the other hand, the long-distance network of inhibitory connections described by Kisvarday et al., (1993b) linking basket cells and Parvalbumin-positive GABAergic interneurons might form a network of long range disinhibition.

I-1.2 Functional role

From a functional point of view, since the first characterization of V1 “hypercomplex” cells by Hubel and Wiesel (1965), “end-stopping” and “side-inhibition” phenomena were described in V1 for simple and complex cells (Rose, 1974; Kato et al., 1978; Orban et al., 1979; Gilbert, 1977) and later on in V2 (Allman et al., 1985). Those “End-stopping” and “Side-inhibition” effects reflect specific modulations of a cell response: the activation of a given cell is optimal for a certain bar’s length and beyond that length, the strength of the response decreases. A similar effect is observed for the width of a given bar or in a similar manner, the number of cycles of a grating (Maffei and Fiorentini, 1976; De Valois et al., 1985; Foster et al., 1985, Born and Tootell, 1991; Von der Heydt et al., 1992). Those properties are thought to be linked with inhibitory areas situated outside the excitatory RF along the preferred orientation axis of the cells (“end-zones”) or on its sides (“side-bands”).

The orientation dependency of those effects (specific to a bar or a grating) argues for their cortical origin. Anatomical evidence of iso-binding between cells having the same orientation and retinotopically distributed along their preferred orientation axis or less frequently orthogonally to that axis strengthens the interpretation that long distance horizontal connections *are involved* in those modulatory effects. From a more general point of view, those discoveries led to the notion that the surround of the classical RF could *modulate* the response of its center (Jones et al., 2001), suggesting a more complex picture than the classical rigid filter role attributed to the RF initially described as only sensitive to a spatially restricted area of the visual field.

Although the modulations described above are suppressive, other types of center-surround interactions have been described and from a broader perspective, surround modulations are orientation sensitive (Blakemore and Tobin, 1972; Nelson and Frost, 1978; Allman et al., 1985, Gilbert and Wiesel, 1990, Li and Li, 1994, Sillito et al., 1995; Walker et al., 1999). Data collected in V1 indicate that the size and the selectivity of RF are more dynamic entities that strongly depend on the characteristics of the stimulus used (DeAngelis et al., 1995; Frégnac and Bringuier, 1996; Gilbert, 1998; Wörgötter and Eysel, 2000). Those data indicate that the nature of center-surround modulations can also be facilitatory and that the sign and amplitude of those modulations depend on the relative spatial characteristics between stimuli placed in the surround and in the center of the RF, especially their contrast, orientation, separation and alignment.

I-1.2.1 Role of feature geometry in response modulation

Whether facilitatory or suppressive, it was shown both in cat and monkey that maximal modulations are observed when the central and peripheral stimuli are *iso-oriented and co-aligned* (cat: Nelson and Frost, 1985; Chen et al., 2001, macaque: Knierim and Van Essen, 1992; macaque and human: Kapadia et al., 1995, 2000), strongly advocating for the implication of horizontal connectivity in those modulatory effects. It seems that suppressive modulation is the predominant type when central and peripheral stimuli are iso-oriented and co-aligned but the picture is not that simple and needs to be decomposed. Indeed, it has been shown that iso-oriented and co-aligned surrounding stimuli mostly have a suppressive effect when the contrast of the center stimulus is high. It appears that the contrast of the central stimulus controls the sign of the response modulation: at weak contrast, a similar stimulus presented in the surround can facilitate the responses but suppress it if the contrast of the stimulus in the center is high (Figure 2.2) (Toth et al., 1996; Polat et al., 1998; Sengpiel et al., 1997; Levitt and Lund, 1997a).

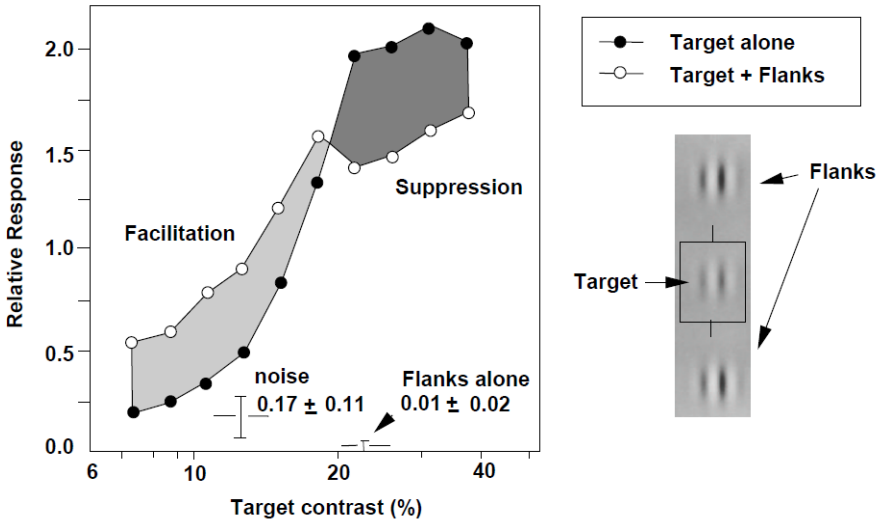

Figure.2.2: ***Effect of collinear surround stimulation on V1 cell contrast response.*** *Example of a contrast response modulation by collinear flankers in a V1 cell recorded in the cat. The presence of iso-oriented and co-aligned high contrast Gabor flankers induces a relative increase of the center response at low contrast. On the other hand, for contrasts above a certain threshold (which may vary from cell to cell), responses are reduced by the co-stimulation of center and flankers when compared to the control response elicited by the center stimulation alone. (Polat et al., 1998).*

Similar results were obtained with bars in the monkey (Kapadia et al., 1995). However, it should be noted that those modulatory effects do not rely on the physical contrast of the stimulus but on the relative contrast of the stimulus regarding the threshold contrast of individual cells (Mizobe et al., 2001). In terms of efficiency, collinear flankers could enhance the detectability of a low contrast center stimulus displaying contiguity in the visual scene. Under the gain control exerted on horizontal activity by feedback connections, horizontal broadcast of contextual information would boost the weak feedforward signal of the center's stimulus (Frégnac et al., 1996), facilitating its detection. On the other hand, high contrast stimuli flanking a high contrast target presented in a cell RF could be interpreted as redundant stimuli, irrelevant to the detection of a contour easily detectable. A plausible interpretation is that horizontal contextual information reduces redundancy by suppressing V1's activity when the contextual information is not especially informative regarding the target (Martin and Von der Heydt, 2015).

From the evidence presented above, iso-orientation and co-alignement of stimuli surrounding a RF stimulated in its center by a strongly contrasted oriented stimulus provoke a suppressive modulation of the response compared to the presentation of the stimulus center alone. Suppressive effects are weaker when the surrounding stimuli are cross-oriented. Occasionally strong facilitatory effects have been reported by Sillito's group: the response is relatively facilitated when compared to the iso-oriented surround configuration. Not only that facilitatory modulation is relative to the iso-oriented surround configuration, but is also absolute, i.e., in some cases it amplifies the response to the center stimulation alone. Those findings were first described by Sillito et al. (1995) in the cat and by Levitt and Lund (1997 a,b) in the monkey. When an optimally oriented stimulus was presented in the RF at high contrast, cross-oriented surrounding stimuli elicited an amplification of the response, superior to the stimulation of the center alone (up to 200% for Sillito et al., 1995). The study of Levitt and Lund in 1997 lowered the strength of those results, adding a contrast dependency of the stimulus used in the center. For low level contrast of the center stimulus, mainly suppressive effects were observed for all surrounding orientations. At high contrast, suppressive effects were limited to the iso-oriented configuration.

I-1.2.2 Overall center-surround contextual modulations

Surprisingly, the results of Sillito et al., (1995) showed that facilitatory modulations were also present for a center stimulation orthogonal to the optimal one, as long as the surrounding annulus grating was orthogonal to the center stimulus. Such cells were termed “orientation contrast” detectors. In the same line of evidence, the tuning of surround modulation in the macaque V1 depends on the stimulus orientation presented to the RF. Compared to the sole stimulation of the center, facilitation even emerges in many cells when both the RF and its surround are non-optimally stimulated, as long as the two stimuli presented are cross oriented (Shushruth et al., 2012), (Figure 2.3), highlighting a real adaptive facilitation based on the relative orientation between center and surround. According to these authors, tuned lateral inhibition (via the surround pathways) of untuned local recurrent connections causes maximal withdrawal of recurrent excitation at the feedforward-input orientation, resulting in the stimulus-dependent tuning of the surround.

Center-surround interactions can be considered as *context-dependent* modulations, relying on dynamic adaption to global statistical changes in the visual environment and the RF surround. They enhance the transmission of relevant information even when the center stimulation is not optimal for a given RF and suppress irrelevant redundant features of a visual scene, conferring to the RFs a status of constantly evolving entity.

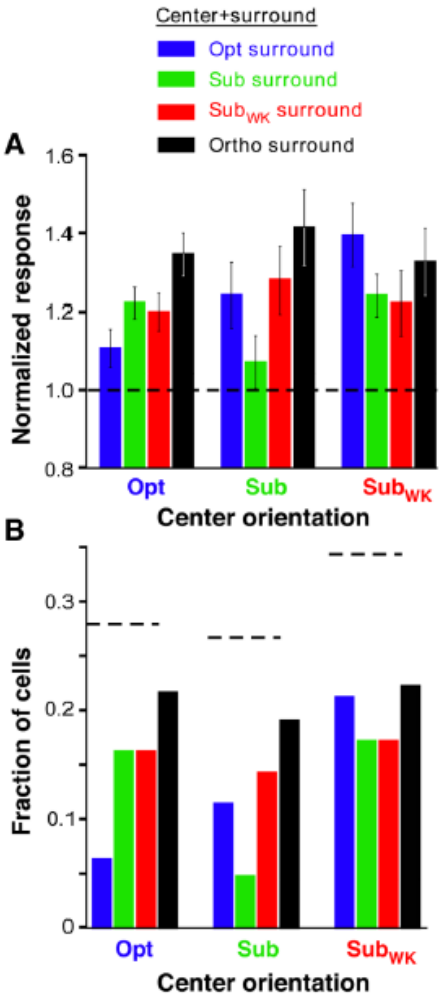

Figure.2.3. ***Orientation tuning of surround facilitation in Macaque V1.*** ***(A)*** *Average normalized population responses for cells showing surround facilitation. Each set of 4 bars indicates the mean normalized response to a given center grating stimulus orientation presented together with a surround grating annulus at each of four different orientations: Opt: optimal orientation eliciting the biggest response in the RF center; Sub: suboptimal orientation; SubWK: suboptimal weak orientation eliciting a response < 50% of the maximum but > 2 SD above spontaneous activity and ortho for orthogonal orientation.* ***(B)*** *Each set of 4 bars indicates, for each center orientation, the fraction of cells showing significant facilitation at each of four different surround orientations. Horizontal dashed lines: total fraction of cells, for each center stimulus orientation, that were facilitated by at least one surround orientation. (Shushruth et al., 2012).*

Though the findings presented above are highly relevant, they are often contradictory. This is probably due to a lack of fixed parametrization across studies and differences between visual stimuli (type: gabor patches or gratings; spatio-temporal characteristics: nearly all of those studies used stimuli flashed in the same position of space, preventing the spatio-temporal dynamic evaluation of the network's stimulation; position regarding the RF: directly concomitant to it or positioned further away and unable to evoke responses if presented alone). Another reason is the

lack of a systematic quantified report of the contrasts of central and surround stimuli in response modulation sign before the studies of Sengpiel et al., 1997, Levitt and Lund, 1997 a,b; and Polat et al., 1998. Inter-species differences (between the cat and the monkey) must also be considered, as well as the type and level of anaesthesia used, which was shown to modulate the variability, orientation selectivity, spatial frequency and contrast of evoked responses (Ikeda and Wright, 1974). More global state-dependent factors should be considered: some authors reported a reduction of RF size when the EEG was in a synchronized state, awake, compared to a desynchronized state reflecting sleep (Hubel and Wiesel, 1974; Wörgötter et al., 1998). Attentional factors also modulate V1 cells responses (Somers et al., 1999; Sengpiel and Hubener, 1999; Roelfsema et al., 1998) and center surround interactions (Ito and Gilbert, 1999).

All in all, in the characterization of receptive fields and of the types of center-surround modulations in V1, clearly identified parameters are involved: the position and spatial spread of stimulation, the level of contrast of the stimuli and the orientation of the local features both in the center and in the periphery. The contribution of the temporal factor in the spatio-temporal stimulation of the network has however been neglected, leading to an oversimplified description of the operations performed by V1. This simplification does not realistically describe the natural statistics of the environment to which the network is continuously confronted. In spite of that, conclusions from the findings brought by those studies allow us to conclude that the orientation dependency of those center-surround modulatory phenomena highlights their cortical origin. The type of observed modulations gives a prevailing role to the relative geometric configuration of oriented stimuli between the center and the periphery of a RF, especially to the iso oriented and co-aligned facilitation by flankers when the center stimulus has a low contrast and suppression when the center's contrast is high. Those specific functional modulations are thought to rely on the propagation of contextual information conveyed by long range horizontal connections (Gilbert and Wiesel, 1979, 1983, 1989; Ts'o et al., 1989). The anatomo-functional description of those modulations rightly matches the architectural requirements to convey such contextual information by linking columns having the same preferred orientation over large distance in the visual field. However, what actual evidence of propagation of information via this connectivity exists and how can it account for peripheral modulatory effects?

I-1.2.3 The depolarizing field hypothesis

The center-surround modulatory effects described above come from extracellular studies. Thanks to the combination of intrinsic imaging and extracellular recordings in the primary visual cortex of the cat, Das and Gilbert (1995) measured the cortical point spread (PS) defined as the cortical area activated by a minimal (focal) visual stimulus. The distribution of the PS measured by optical imaging reflects both the subthreshold and the spiking cortical activation evoked by the

presentation of the stimulus. Comparing the distribution of the PS cortical activation measured by optical intrinsic imaging with the one obtained with extracellular recordings, Das and Gilbert, (1995) found that the spiking PS represented only 5% of the area observed in the optical PS, indicating that 95% of the remaining evoked activity reflected a subthreshold activation diffusing across the laminar plane. Moreover, the pattern of subthreshold activation closely matched the orientation columns distribution, strongly suggesting the implication of horizontal connectivity in the overall observed cortical activation.

In the same study, following binocular retinal lesions, the authors observed an extension of the spiking PS in the corresponding “cortical scotoma” reaching approximately the size of the optical PS observed in normal cortex, suggesting that cortical reorganization following the lesion was mediated by an “unmasking” of normally subthreshold activation to suprathreshold levels (Das and Gilbert, 1995). After five month, the cortical scotoma had diminished; stimulations showed that the cortex had been reorganized: the scotoma had become sensitive to stimulation from RFs lying on the border of the lesion, indicating a reorganization of inputs now driving the insensitive cortical region. Even though the retinotopic inputs had moved to a very different part of visual space representation, the orientation map of the reorganized cortex roughly matched the map in the same region before the lesion and this match was consistent with horizontal connections mediated reorganization (Gilbert and Wiesel, 1992; Darian-Smith and Gilbert, 1994, 1995). The stimulation of overlapping RFs recorded from the reorganized region as well as the adjacent normal cortex, an area covering over 4 mm, revealed by extracellular recordings that this entire region could now be driven to suprathreshold levels by a small visual stimulus positioned in the area of RF overlap. The combination with optical imaging measurement in that area revealed that the previously subthreshold activated area now reaching the suprathreshold level of activation showed a considerable extent and specificity of lateral cortical interactions, mirroring the known extent and orientation specificity of long range horizontal collaterals. The correspondence in the orientation maps of pre-lesion and post-reorganization cortex and the increase in the spiking PS implied that the reorganization process depended on a strengthening of the pre-existing horizontal connections, allowing the change from sub to suprathreshold activation.

In the primary visual cortex of the macaque monkey, using Voltage Sensitive Dye Imaging (VSDI), Grinvald et al. (1994) also found a cortical spread of activity ten times larger than the initial spiking retinotopic site of activation, reflecting the consequent propagation of lateral activity. They showed that the spread of that activity was also anisotropic and modulated by surrounding stimuli. Those results confirm that the anatomical substrate for the lateral spread of activity involved in modulatory effects is likely to come from intrinsic long range horizontal connections with extensive clustered arborisations forming entire “modules” of activation. Large depolarization fields, as Per Roland named them (Per Roland, 2002), have also been observed in auditory, somatosensory, olfactory, parietal and prefrontal cortices (Sawaguchi, 1994; Kleinfeld and Delaney, 1996; Horikawa et al., 1998, Inase et al., 1999). Thus, large depolarization fields are observed experimentally in different species and different cortical areas in layers 1-3. In cat V1 and V2, 10-20 ms after the initial feedforward spiking response, the depolarization field occupies a territory much larger than

the space occupied by several hypercolumns and spreads laterally with a velocity of about 0.3 m/s (Per Roland, 2002), a velocity characteristic of the spread of action potential along horizontal axons (VSDI: Grinvald et al., 1994; Shoham et al., 1999; intracellular: Bringuier et al., 1999).

A cartoon summary of HC activation may be formulated the following way: layer 2-3 pyramidal neurons are interconnected by long-range horizontal connections to their basal dendrites (Gilbert and Wiesel, 1979). When a few, nearby0 layer 3 pyramidal neurons receive nearly identical input from layer 1 (transmitting relevant context signals), their axons respond by firing action potentials that travel almost synchronously along the horizontal layer III axons. These action potentials will rapidly reach the basal dendrites of other layer III pyramidal neurons, entraining their firing. This will repeat at each neuron that receives the similar layer I input. Eventually, this "parallel coincident feedforward computation" will elicit a whole cascade of depolarization and firing of layer III neurons that receive nearly identical layer I input. According to Per Roland (2002), if we assume that the memory associated with a given set of stimuli or "state memory" is encoded by the particular combination of simultaneously activated pyramidal neurons synapses, a subset of the memory storage corresponding to some identical features of a novel set of stimuli will be searched each time a depolarizing field emerges. It is done by the widespread activation of layers 1 and 2, which would tend to maximize the potential available memories for retrieval. A specific part of the searched "state memory", corresponding to the identical part between the two stimuli will be retrieved by firing action potentials. This compulsory search and subsequent retrieval under the form of specific reactivation will stabilize the stored state memories or associations of depolarising fields associated with a given visual scene, for instance. One can then suggest that dynamic depolarization fields act under the form of distinct activated modules and constitute the embodiment of cortical computational entities (Roland, 2002).

I-1.2.4 Intracellular recordings: spatio-temporal subthreshold characterisation of the receptive field silent surround

As previously developed, the cortical area activated by a localized stimulus does not pertain to the feedforward retinotopic imprint of this latter but spread over larger distances via horizontal connections. Intrinsic and voltage sensitive dye imaging reveal the existence of a large depolarising field encompassing several times the size of the spiking response studied extracellularly. Thus, the RF definition, especially its spatial extent, is function of the technique used to characterise it and of the type of stimuli used (Frégnac and Bringuier, 1996; Walker et al., 2000). Different experimental techniques provide different types of information and characterisations of RFs. Contrary to optical imaging techniques and electrophysiological extracellular recordings, intracellular recordings give access to the subthreshold synaptic activity (synaptic bombardment inputs that a given cell receives) as well as the output spiking responses at the single cell level.

The Minimum Discharge Field (MDF) represents the region of space eliciting spiking responses. In accordance with the findings of Das and Gilbert (1995) showing large subthreshold depolarising field with intrinsic optical imaging, Bringuier et al. (1999) showed using intracellular recordings in vivo in the primary visual cortex of the cat that the spatial extent of the depolarising field (DF) is much larger than the MDF and the hyperpolarising field (HF) displays a sparser spatial profile. These authors showed that the spatial sensitivity profile of the DF envelope is co-centered with the MDF (Figure 2.4A). Taken together, the topographical combination of the MDF, the DF and the HF covers on average 5 ± 2.4° of visual angle, an area 4 times larger than the MDF classically defined by extracellular studies. In that study, significant subthreshold depolarizing responses could be evoked by annular flashed gratings surrounding the MDF up to 11.3° without stimulation of this latter, indicating the existence of *excitatory* sensitivity to large surrounding stimuli in the "far periphery" of the classical MDF, much further than originally thought from extracellular studies. The strength of the depolarizing response decreases linearly regarding eccentricity from the MDF center (Figure 2.4A). Moreover, the slope of that linear decrease depends on the spatial summation provided by the test stimulus itself: it is comparable between two-dimensional sparse noise and flashed bars (Figure 2.4B and C). However, the spatial attenuation of depolarising responses was found weaker for annular sinusoidal gratings of larger eccentricity, i.e. the slope of response attenuation over space was much lower when spatial summation was increased (Figure 2.4D). Moreover, the modulations of responses to annular gratings observed in that study were selective to orientation, indicating a cortical origin of interaction mechanisms.

Another source of information on the origin of those center-surround modulations is the onset latency of the responses. Indeed a strong correlation was observed in the study of Bringuier et al., (1999) between the relative eccentricity of the flashed stimuli from the MDF center and the latencies of the evoked depolarizing responses (Figure 2.4 E-G). Taking into account the magnification factor between the visual field and the cortex, the authors converted the visual field distance between stimuli positions into cortical distance. The speed of horizontal propagation of activity was directly derived from the inverse of the slopes obtained from the latency basins distributions. They found a speed of horizontal activity propagation ranging from 0.1 to 0.5 m/s (Figure 2.4 H), a speed matching the velocity of activity spread confirmed by optical imaging techniques (Das and Gilbert, 1995; Grinvald et al., 1994; Shoham et al., 1999; Per Roland, 2002; Jancke et al., 2004; Chavane et al., 2011). Although the propagation of activity responsible for center-surround modulations could come from higher-order cortical areas via top-down feedback connections, it is unlikely. Indeed, the speed of horizontal propagation directly estimated from those spatio-temporal characterizations of receptive fields is consistent with *in vitro* intracellular measurements of horizontal action potential propagation speed in rat and cat visual cortex (Salin and Prince, 1996, Chervin et al., 1988; Komatsu et al., 1988; Hirsch and Gilbert, 1991; Nowak and Bullier, 1998). Feedback connections from higher areas which displays larger MDFs than V1 could explain large synaptic integration fields in the primary visual cortex but there is evidence against that interpretation. Indeed, by opposition to constant speed propagation of cortical wave of activity by horizontal connections, feedback connections do not account for the linear spatio-temporal dependency in visual onset latencies observed here, because of their much higher conduction

speed velocity (superior to HC propagation speed by a factor of 10: Girard et al., 2001; Angelucci and Bullier, 2003; Briggs and Usrey, 2007). Only two milliseconds are needed to convey feedback information from MT to V1. In contradiction with common belief, late visual cortex responses do not necessarily only signal reverberation between cortical areas since the slowest signal propagation, in the order of several tens of milliseconds, may result from unmyelinated propagation along long distance horizontal connections intrinsic to V1.

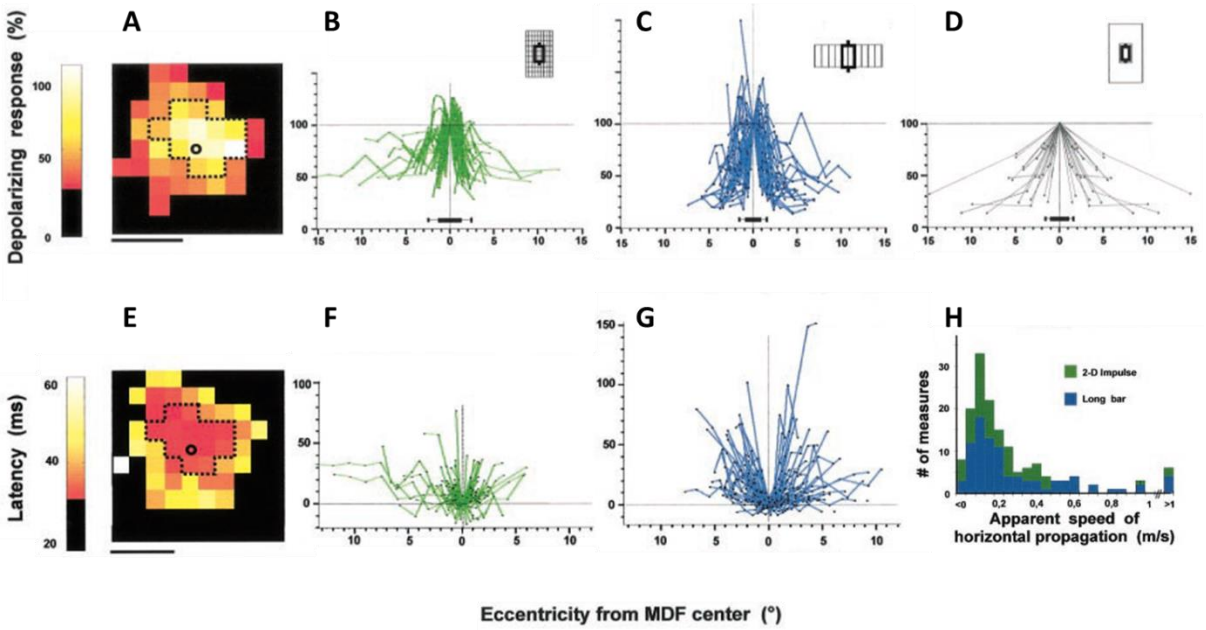

Figure.2.4: ***Spatio-temporal characterisation of subthreshold receptive fields in Cat V1.*** *(A-D) The visually evoked strength of the depolarizing response is normalized relatively to the one observed at the location of the MDF (dotted contour in A) eliciting the maximal discharge (circle). Color-coded map of the response strength of one V1 cell. Black pixels indicate the absence of significant responses. Horizontal scale bar, 2°. (B-D) Each individual profile represents for a given cell the change of response across the width or length of the RF, expressed as a function of the relative eccentricity of the stimulus from the MDF center. B. 2D sparse noise mapping protocol (n = 37). C. Flashed bars (n = 21). D. Flashed (n = 19) or moving (n = 2) sinusoidal luminance gratings. The average MDF extent and its SD are indicated respectively by thick and thin horizontal line segments. (E-H) Latency basins of subthreshold synaptic responses. E. Color-coded map of the absolute latency of depolarizing responses of the same cell than in A. Black pixels indicate the absence of significant change in the onset slope of the postsynaptic response. (F-G) Changes in latency measured across the width or length of the RF and expressed as a function of the eccentricity of the stimulus from the latency basin center, for two mapping protocols (F) sparse noise (n = 37), (G) flashed bars (n = 27). H. Distribution of the apparent speed of horizontal propagation values calculated from the slopes of the latency basins showed in (F) green and (G) blue. (Bringuier et al., 1999).*

Although many electrophysiological intracellular studies addressed contextual influence on V1 RFs (Hirsch et al., 1998; Ferster and Miller, 2000; Douglas and Martin, 2004; Priebe and Ferster, 2012) only a few (Haider et al., 2010), including the Bringuier et al., (1999) study presented above, directly addressed the *synaptic nature* of this influence. VSD imaging experiments confirmed at the mesoscopic level the spatio-temporal properties of the intracortical spread of activity first described at the microscopic level by Bringuier et al., (1999) in different species (cat, monkey) and various brain states (anesthetized and awake) (anesthetized cat: Benucci et al., 2007; anesthetized monkey: Grinvald et al 1994; Jancke et al., 2004; Chavane et al., 2011; Chemla and Chavane, 2016; awake monkey: Slovin et al., 2002, Reynaud et al., 2011, 2012; Muller et al., 2014; Chemla and Chavane, 2016 ; for a review see Sato et al., 2012). Moreover, whereas intracellular studies only allowed an inference (Frégnac, 2012), VSD experiments showed directly that horizontally propagated activity corresponded to a travelling wave. It is evident because the feedforward activation elicited by a localized stimulus appears first in the corresponding retinotopic projection in V1 cortex and progressively spreads to a larger cortical region with an increasing delay of activation function of the distance regarding the initial feedforward site of activation (Sato et al., 2012; Benucci et al., 2007). This dynamic is to distinguish from a standing wave, one that grows in amplitude over time but remains spatially confined to the same cortical area (Destexhe and Contreras, 2006). Those travelling waves, whose velocity is consistent with speed of horizontal activity propagation, are also present when stimuli are weak or absent. They are therefore easily detectable in subthreshold potentials and are thus unarguably affecting spiking responses, strengthening the interpretation that the study of contextual modulations must include the temporal factor, where travelling waves of activity prepare the network by modifying its electrical context (Sato et al., 2012).

I-2. Working Hypothesis

I-2.1 Spread of horizontal activity in V1

In order to develop our working hypothesis, we will detail three different studies characterising distinct functional impacts of horizontal activity propagation on information integration that are involved in perceptual biases. Those functional aspects already exist in the low-level perceptual state of the anesthetized animal. Each of these aspects contributes to the conceptual build-up that horizontal connectivity participates to the propagation of a network-based belief resulting, under specific requirements, in a prediction travelling through the V1 network.

I-2.1.1 Lateral and feedforward activity interact in a spatio-temporal coherent way to shape the overall propagation of cortical activity

The first study highlights the interaction of horizontally propagated activity with the feedforward drive, which bias over space and time the spread of overall activity involved in motion perception in the "line motion illusion" effect (Hikosaka et al., 1993). A certain level of spatio-temporal coherence between those two drives is necessary for their interaction, leading to the progressive emergence of activity propagating across the cortical surface along a spatio-temporal pattern shaped by the preceding horizontal activation and involved in the illusory percept. When a small square is presented slightly before a stationary bar of the same width, partially overlapping with it, subjects perceive a smooth transition between the two stimuli, gradually extending over space and time (Figure 3.1). Combining VSD optical imaging and single-unit recordings, Jancke et al. (2004) compared the cortical activity dynamics evoked in the anaesthetized cat V1 and V2 for five stimuli: a stationary small square and bar flashed independently, a moving square, a progressively extending rectangle and the line motion illusion paradigm: a stationary flashed square preceding the presentation of a stationary flashed bar.

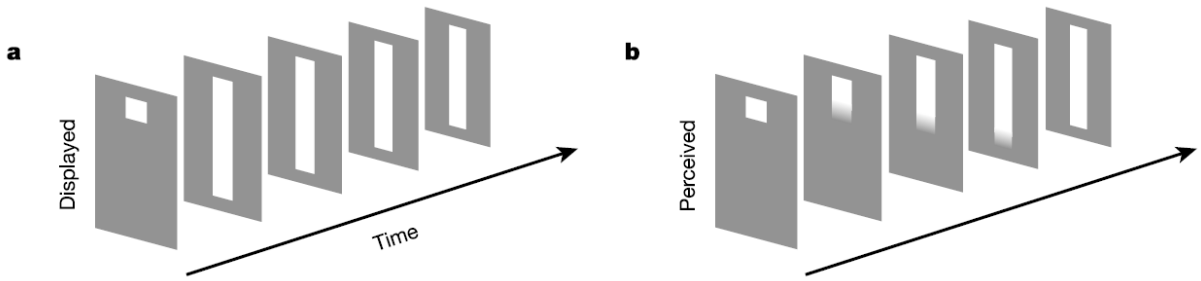

Figure.3.1: ***The line motion illusion****.* ***a****. square ('cue') presented before a bar stimulus.* ***b****. Subjects report an illusory line expanding over space across time. (From Jancke et al., 2004).*

In the cat V1 and V2, the authors found that flashing the bar alone evoked an expected localized, short latency and high amplitude VSD activity uniformly distributed in space over time (Figure 3.2 d).

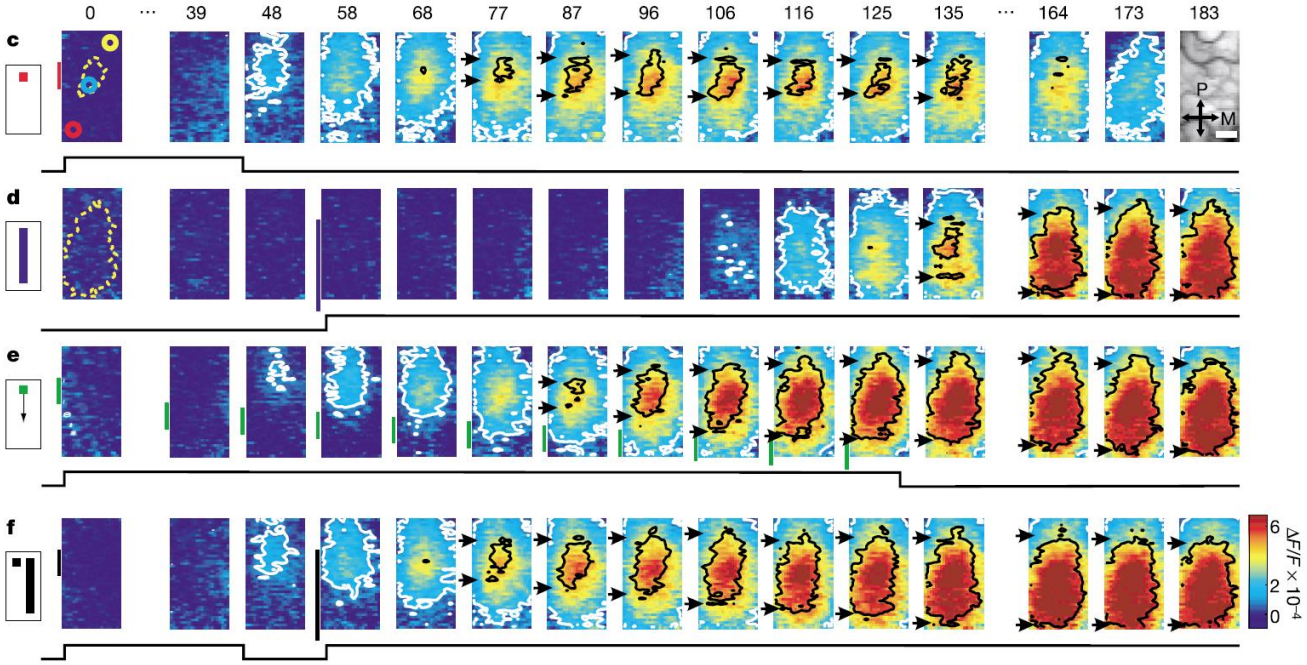

Figure.3.2: ***Cortical activity evoked by stationary, moving and illusory moving stimuli. c-f*** *Patterns of evoked cortical activity as a function of time. Yellow dotted contours approximate retinotopic representation of the stimuli; coloured circles indicate extracellular recording sites. White contours delimit low-amplitude activity (significance level P < 0.05). The cortical area imaged is shown on the upper right. Scale bar, 1 mm; P, posterior, M, medial. Green vertical lines in* ***e*** *indicate estimated position of the stimuli along posterior-anterior axis. Time in milliseconds after stimulus onset is shown at the top. Stimulation time is shown at the bottom of each row. Colour scale indicates averaged fractional changes in fluorescence intensity (ΔF/F). Stimuli:* ***c****, flashed small square.* ***d*** *Flashed bar.* ***e****, Moving small square (32°S^{-1}).* ***f****, Line-motion paradigm. 22 repetitions were averaged. (From Jancke et al., 2004).*

In order to compare VSD measured activity and spiking responses, the authors combined both techniques. The lateral spread of subthreshold activity is known to extend beyond the cortical feedforward retinotopic activation evoked by a localised visual stimulus. On the contrary, spiking responses do not extend beyond the retinotopic feedforward focal activation of the cortex. Because VSD recorded signal is sensitive to synaptic potentials, its relationship with spiking activity is indirect. That is why the authors established a method to delineate spiking responses in the optically recorded signal obtained via VSDI by decomposing the evoked activity recorded optically in high and low amplitude areas whose dynamic were analysed separately. High amplitude areas were

defined as areas of strong activation which did not extend beyond the feedforward imprint of the stimuli.

As we can see in figure 3.2 c, low amplitude activity spreads far beyond the retinotopic representation of the flashed square at a velocity of 0.09 $m.s^{-1}$, speed compatible with conduction velocity of horizontal connections. On the contrary, high amplitude VSD activity (encircled by black contours) showed very small lateral extension (black arrows). The single unit recordings (coloured circles, Figure 3.2 c first frame) confirmed that spiking activity evoked by the square remained enclosed in the high amplitude activity region measured with VSD (Figure 3.3). The flashed bar stimuli elicited the same profile, with a broader spatial activation. The moving square covering the exact same trajectory than the flashed bar (Figure 3.2 e) evoked again a rapid spread of low-amplitude activity but in contrast to the static stimuli presented alone, high amplitude activity propagating anteriorly was observed, reflecting the motion trajectory of the square. Even though the relationship between VSD and spiking activity is not linear, those results suggest that the region of high level VSD activity indeed corresponds to the spiking representation of the evoked response.

The authors compared activity evoked by the flashed square alone + flashed bar alone (Figure 3.2 c+d) to the activity evoked by the line motion illusion paradigm (Figure 3.2 f), by shifting in time the representation of the activity evoked by the flashed bar alone (Figure 3.2d) by the duration of the Inter Stimulus Interval between the presentation of the square and the bar in the line motion illusion paradigm. This time realignment allowed them to directly compare the sum of the activity evoked by the flashed square alone and flashed bar alone to the flashed square and bar composing the illusory paradigm. The activation between the sum (flashed square + flashed bar) and flashed square then flashed bar was undistinguishable. Then, the authors compared the activation pattern of the line motion illusion paradigm to the activity evoked by a moving square covering the exact same trajectory than the bar. The presentation of the line motion illusion paradigm evoked a response profile similar to the moving square, even though in the former the two stimuli used were static: the high activity VSD region representing the “spiking discharge” did not remain stable over space and time but propagated, similarly to activity evoked by the moving square. The combination of those results shows that in the line motion illusion paradigm, the preceding static square created gradually propagating subthreshold cortical activity extending beyond the spiking discharge zone and facilitating the response to the flashed bar, the response to that sequence being undistinguishable from the actual moving stimulus (Figure 3.2 f vs e). It does so by activating maximally the network in a spatially restricted area, with a decreasing level of subthreshold activation further away from the spiking discharge zone evoked by the square, reducing the latency of activation when the flashed bar is presented at the previous loci of subthreshold activation and biasing the propagation of activation in a pattern similar to the real motion, leading to the perception of a gradually extending bar over space and across time.

To verify that assertion, the authors also imaged the response to stimuli mimicking the actual percept of the illusory line motion effect at a speed of $32°s^{-1}$ (a square that progressively extend over space across time to form a line, Figure 3.3, third and fourth rows). The response to that

relatively high speed real motion stimulation exhibited a similar profile than the line motion illusion (Figure 3.3 second vs third row). The link between the actual propagation of a physical object and the subsequent dynamic of cortical activation is shown in figure 3.3 (last row) where the bar was drawn out more slowly (16°s^{-1}). We can see that the cortical pattern of activity shows a much slower propagation of the spiking discharge zone activation, demonstrating that the spiking discharge zone carries information about motion speed.

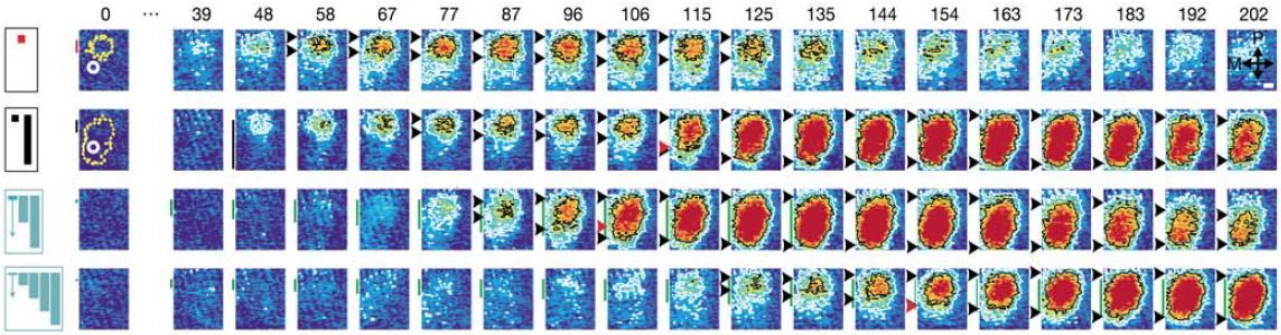

Figure.3.3: ***Both illusory and real motion evokes propagating Spiking Discharge (SD) zones.*** *From top to bottom: VSD images patterns of activity evoked by flashed square, line motion, and drawn-out bar at 32°s^{-1} (third row) and 16°s^{-1} (fourth row). Multi-unit spiking activity was recorded simultaneously at the location marked by the white circle at frame 0; yellow dotted contours at frame 0 approximate sizes of the SD zones representing square and bar (left). (Adapted from Jancke et al., 2004).*

Importantly, to determine whether the characteristics of subthreshold spread account for the illusory motion, the authors determined that the level of activation and speed of propagation of subthreshold activity co-varied: the higher the activation, the slower the propagation speed. This could come from a gradual increase in inhibition or from a gradual decrease in synaptic density/efficacy of horizontal projections at further cortical distances. Most of all, increasing the time between the presentation of the square and the bar from 60 ms to 350 ms prevents the propagation of the spiking discharge zone and no physiological correlates of the line motion effect were found for spatial distances between square and bar beyond 6° of visual field. Those results indicate the existence of a specific range of spatio-temporal coherence necessary for lateral and feedforward activity to interact, inducing even in the low-level perceptual state of the anesthetized animal the propagation of activity participating to the perception of the line motion illusion reported in awake subjects. Those observations are confirmed at the psychophysical level in subjects for which the percept disappears when ISI of the AM sequence is outside of this range.

I-2.1.2 Stimulus-induced cooperativity is necessary for the anisotropic spread of lateral activity

The second study contributing to our working hypothesis investigated more specifically the requirements for the anisotropic spread of lateral activity. To better understand the functional role of lateral interactions, Chavane et al. (2011) combined voltage sensitive dye imaging (done in the lab of Amiram Grinvald, Weizmann) and intracellular recordings (done at UNIC) in area 17 and 18 of the anaesthetized and paralysed cat in vivo. VSD imaging showed that locally oriented stimuli evoked an orientation-selective activity restricted to the cortical feedforward input of the stimulus. Beyond that feedforward imprint of approximately the size of an hypercolumn, the laterally activated area gradually lost its orientation selectivity with a space constant of about 1 mm. Intracellular recordings showed that this loss of orientation preference comes from the orientation preference diversity of converging synaptic input originating from outside the classical RF. However, increasing the stimulus size provoked an extension of the anisotropic spread of cortical activity beyond the feedforward imprint, suggesting that stimulus-induced cooperativity enhances the long-range spread of iso-preference.

First, the authors presented local oriented sinusoidal luminance gratings through a circular aperture whose size was adjusted to the average RF dimensions. Maps evoked by local stimuli were compared to maps of cortical activation obtained from full-field stimulation. Stimuli were presented at four different orientations and normalized by a “blank” stimulus (Figure 3.4 A). The white contours on that figure represent the domain within which each pixel activation was significantly higher, on a trial by trial basis, than the spontaneous level. The time sequence shows an initial local activation at a latency of about 40 ms after stimulus onset before a gradual spread over most of the imaged cortical surface. The speed of this long-range lateral spread was estimated by latency regarding eccentricity and reached a velocity of about 0.09 m/s (a value compatible with that inferred from synaptic echoes: Bringuier et al, 1999). To distinguish feedforward and laterally activated areas, retinotopic mapping was obtained by presenting local stimuli in adjacent visual positions. Local magnification factors were calculated by comparing the cortical distance between the centers of gravity of each visual stimulus cortical activation and the visual distance between the centers of the corresponding stimuli in visual space. These local magnification factors were used to approximate the extent of the retinotopic representation (Figure 3.4 C, black ellipse). The superposition of the stimulus retinotopic representation on the area covered by the spread allow to see that the lateral spread indeed covers large cortical territory extending far beyond the retinotopic activation and covering various orientation domains. (Figure 3.4 D).

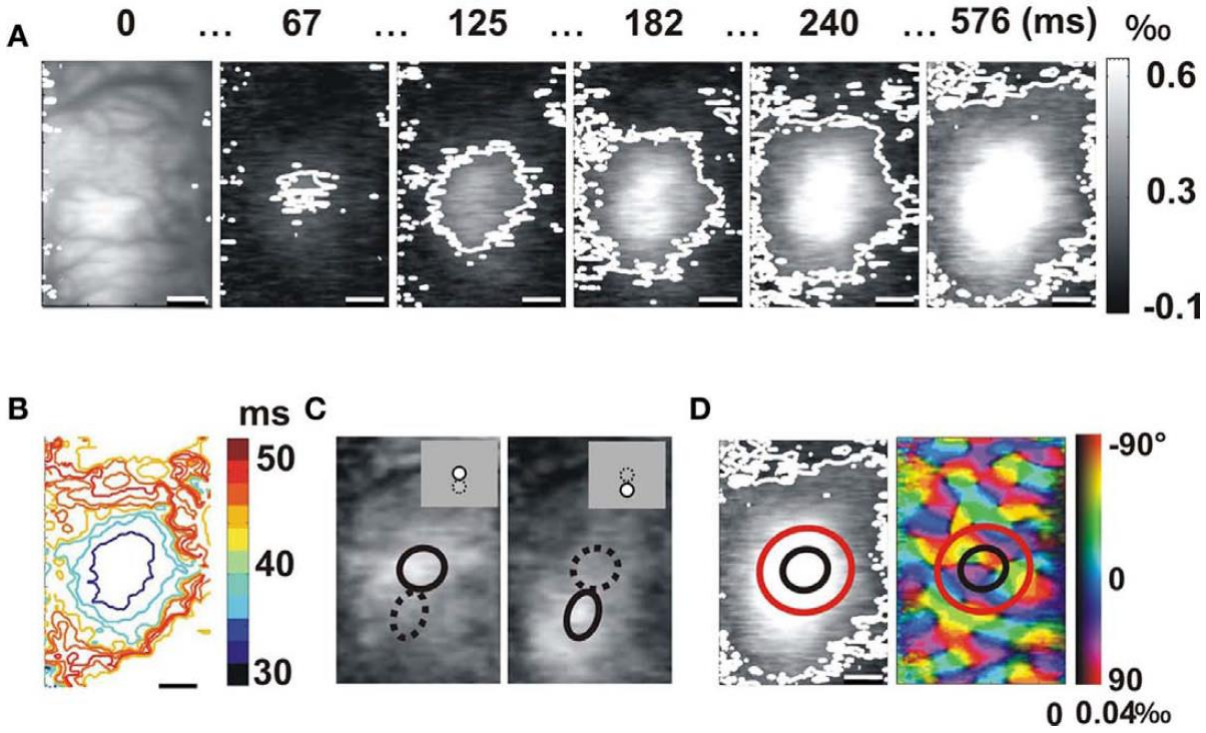

Figure.3.4: ***Voltage-sensitive dye imaging of the lateral spread away from the feedforward imprint. A.*** *Time-series of the cortical response propagation evoked by a local stimulus (averaged over four orientations). The example is from area 17, in response to a stimulus of 2° diameter and eccentricity of 4.1° (average of 28 trials). The white contour delineates the region significantly activated (see article Appendix). Time after stimulus onset is given above each frame. The imaged cortical area is shown in the first frame.* ***B.*** *Latency map. In successive regions of interest delimited by their outer boundary, the colour code indicates the latency of the averaged time-course of the activation spread.* ***C.*** *Retinotopy. The responses to two adjacent positions are shown, averaged over the first time frames. Each averaged cortical response was fitted by a 2D Gaussian function. The size of the retinotopic cortical areas representing the visual stimuli (black ellipses) was inferred from the cortical distance between the two Gaussians centers (stimuli were adjacent and of the same size).* ***D.*** *Left column: retinotopic limit (black ellipse) and feedforward imprint limit (red ellipse) of the stimulus superimposed over the late activation map (576 ms). Right column: orientation map in response to a full-field stimulus. Color hue and brightness code respectively for the preferred orientation and the strength of the orientation tuning. (From Chavane et al., 2011).*

Once the contribution of feedforward evoked activity was measured, the authors studied the impact of spatial summation area by using annular gratings and full field gratings of increasing sizes, which resulted in a significant increase of the lateral spread of iso-preference from a same given cortical locus of retinotopic activation by the feedforward drive. The orientation preference and selectivity of the diffusion domains or target cells were measured using both VSD imaging and intracellular recordings. Two different VSD imaging examples are represented in figure 3.5. In the

first example (Figure 3.5 A), the polar map dynamics of VSD imaging responses to a full field (top row), a local (middle row, 3° of diameter) and an annular grating (bottom row, inner diameter of 6°, outer diameter of 9°) precisely encroaching on the outer border of the local stimulus. As already described, the orientation-selective component activated by the local grating remained spatially restricted to the feedforward imprint (middle row, white contour). However, the annular stimulus evoked an orientation-selective activation filling in the retinotopic representation of its unstimulated inner disk, a region that does not receive direct feedforward input (bottom row).

The inner ring retinotopic representation was inferred from the retinotopic maps shown in Figure 3.5 A (right). The lower position (continuous ellipse) corresponds to the retinotopic activation of the lower stimulus: in the middle row it is activated directly by the local patch; in the lower row, it comes from the ring itself. In this latter case, the contiguous cortical zone activated by the upper position (dotted ellipse) corresponds to the retinotopic representation of the unstimulated inner disk of the annular stimulus. To compare the cortical area over which significant orientation-selective response is observed in the three conditions (cartoons in the left panel), the authors restricted the quantification inside a specific cortical Region Of Interest (ROI) (Figure 3.5 B). This ROI corresponds to a rectangle centered on the representation of the lower stimulus, and aligned to the vertical visual axis representation (antero-posterior cortical axis). Therefore, it allowed them to quantify VSDI responses over a cortical region receiving a same amount of visual stimulation in the local and annular conditions (reddish rectangle superimposed on stimulus cartoon and averaged polar map). Within such ROI, the dynamics of the cortical area becoming significantly orientation selective (delimited by the white contour) is shown in the right column of Figure 3.5 B. Whereas the cortical regions which are significantly activated (gray curve) in the three conditions are comparable, the spatial extent of the orientation-selective cortical area (black curve) is larger for the annular stimulation (bottom row) than the inner disk (middle row).

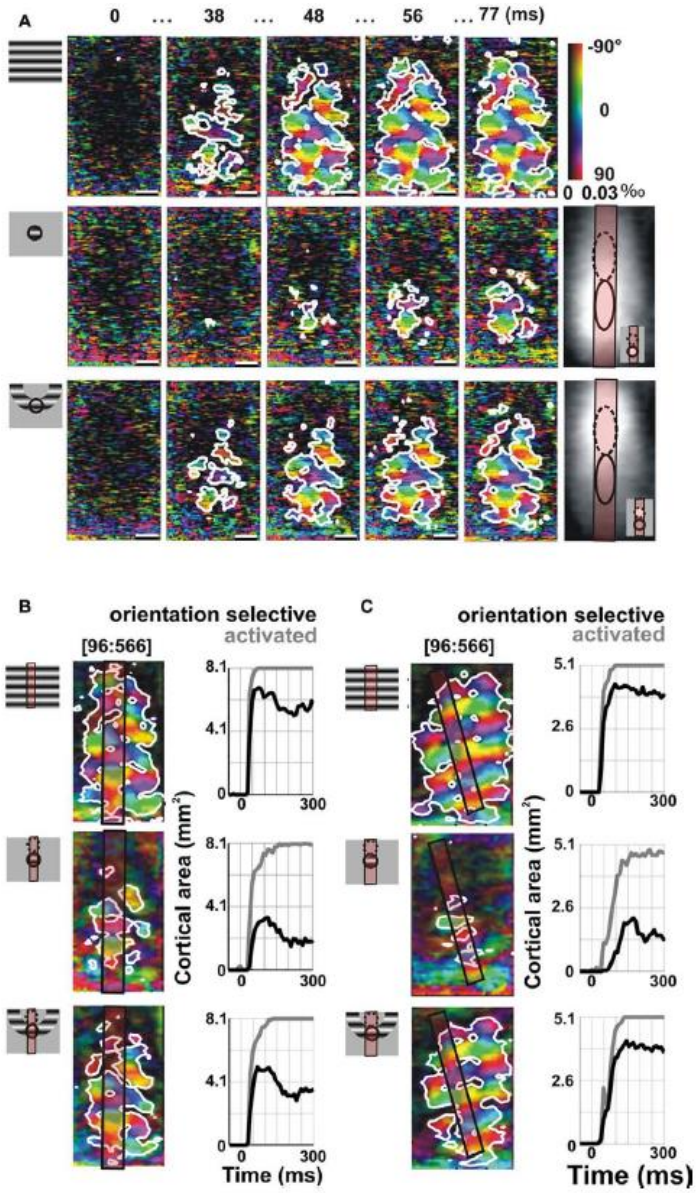

Figure.3.5: ***Propagation of iso-orientation preference emerges from spatial summation (visualized by VSDI). (A)*** *Time-series of polar representation of orientation maps in area 18 in response to full-field (top), local (middle 3° diameter at 5.6° eccentricity), and annular stimuli (bottom, inner diameter 6°, outer diameter 9°) whose position relative to the local stimulus is shown in the stimulus cartoon on the left. White contours delineate the cortical regions significantly selective to orientation. Time from stimulus onset is indicated above each frame. Bottom right: single-condition maps of responses evoked by two adjacent stimuli. Ellipses indicate the estimated cortical limit of the stimulus's retinotopic representation (see paper* ***Figure 1****). Bottom-right inset: stimuli locations in the visual space. Scale bars are 1 mm.* ***(B)*** *Dynamics of the cortical areas significantly activated (gray) or orientation selective (black) in response to the full-field, local disk, and annular stimuli were compared within a cortical region receiving a comparable feedforward drive. This region was defined as an elongated region of interest (ROI) aligned on the representation axis of the upper-to-lower stimuli (reddish rectangle).* ***(C)*** *Another example from area 18 is shown. Stimulus size was 4°*

diameter for the local stimulus (6°, 7° eccentricity), 8° for the inner diameter of the annulus, outer diameter 12°. (From Chavane et al., 2011).

To test for a potential asymmetry of the observed effect, the authors also stimulated the surround of the position alone with annular gratings iso and cross-oriented and they confirmed the lateral spread of orientation selective activity in the central area non retinotopically stimulated. The center and the surround were also stimulated simultaneously but cross-oriented regarding one another. From the expectations described above, the retinotopic representation of the center should receive direct feedforward input and lateral information from the surround, under the form of competitive influences in the case where center and surround stimulation are cross-oriented when both stimuli are presented at high contrast. The cortical representation of the annulus, on the other hand, should only receive direct feedforward input from its stimulation. The authors observed indeed that the response at the locus of the center was nearly abolished whereas the surround retinotopic representation displayed an orientation-selective response. These results confirm that a stimulus configuration recruiting a sufficient level of spatial summation and temporal coherence can initiate a strong iso-orientation selective lateral spread of activity beyond the scale of a hypercolumn.

I-2.1.3 The existence of a synaptic dynamic association field favouring the integration of iso-aligned elements composing a centripetal flow

Another study that is fundamental to the conceptual framework of the work presented in this thesis was made by our laboratory and addresses the synaptic nature of lateral facilitation. Gerard-Mercier et al. (2016), using intracellular recordings in the primary visual cortex of the anaesthetized and paralysed cat in vivo, demonstrated the existence of a synaptic bias intrinsic to V1 for the integration of local and global features composing a visual scene (collinear elements forming a centripetal flow converging onto distinct receptive fields). This synaptic footprint is interpreted as the functional signature, already at the V1 level, of a binding process extending over space and more surprisingly across time. Apart from its dynamic dimension, this synaptic association field mirrors precisely the perceptual association field described in psychophysics (Field et al., 1993; Hess and Field, 1999).

To explore the synaptic integration of locally presented elements embedded in an apparent motion flow in a comparable way across cells, the authors designed a cellulo-centric hexagonal grid referential. It allowed them to study the influence of the pairwise stimulation of two neighboring elements across the surround of the recorded receptive field. The size of the nodes forming the grid was scaled to the size of the subthreshold depolarising field placed in the center, allowing them to distinguish responses evoked from the RF center and from its “silent periphery” (Figure 3.6 A). In order to study the direct impact of the elements geometry and of their congruency within the flow on synaptic integration, pairs of Gabor patches (GP) were flashed at each position of the grid from

neighbour to neighbour, forming all possible spatio-temporal exploration combinations of that grid at six different orientations. The gabors forming the pairs were either co-aligned with the direction of motion (ISO configuration) or orthogonal to it (CROSS configuration) (Figure 3.6 B). Single patches of gabor in the same conditions were also presented (1 stroke, 1S) and interleaved with the apparent motion sequence (2 stroke, 2S) to assess a linear prediction serving as a basis to describe the relationship between static and dynamic association fields (Figure 3.6 A, B). In order to efficiently study the impact of the horizontal connectivity, the patches of Gabor that were presented in the center of the RF had a lower contrast than those in the periphery.

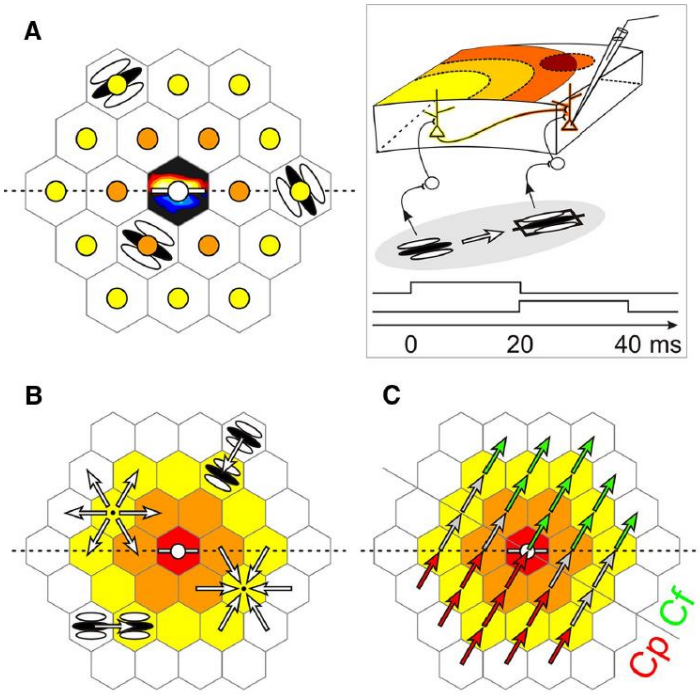

Figure.3.6: ***Probing the synaptic integration field. A-C****. The visual field was paved with an hexagonal lattice centered on the subthreshold RF.* ***A****, the RF is schematized by ON (red) and OFF (blue) subfields overlaid over the central tile (black). The size of the stimuli and of the tiles was chosen to be that of the RF so that stimuli flashed in neighbouring tiles could not overlap and peripheral stimuli could not encroach on the RF center. For each recorded cell, the lattice was positioned with a symmetry axis (dotted line) aligned along the cell's preferred orientation (white bar), represented by convention as the horizontal axis. The "rings" of same relative eccentricity from the RF center are depicted by the colors of nodes or tiles.* ***A-B****, Sparse static (1S) and dynamic (2S) AM Gabor patches were applied in a randomly interleaved fashion to measure the static profile of the synaptic association field (S-AF) and its dynamic associative properties (D-AF), respectively. Each Gabor patch was flashed for 20 ms. The 20 ms interval between stroke onsets was chosen based on previous reports of horizontal propagation speed in cat V1 (Bringuier et al., 1999), to maintain on average in phase the synaptic impact of the horizontal input and that of the feedforward drive (see Box).* ***A,*** *Stimuli of six possible orientations were flashed at each node in the static protocol. Stimuli were presented in isolation, so that the center was not stimulated while peripheral nodes were*

explored. ***B****, Each possible 2S-AM sequence converging onto or originating from each node was presented in the dynamic protocol, and defined a "trajectory" (white arrows). The 2S-AM stimuli could either be in the ISO configuration (illustrated bottom left) or in the CROSS configuration (illustrated top right).* ***C****, A different parametrical reading of the dynamic protocol. Acquisition records are grouped by motion flow direction and relative eccentricity of the AM trajectory, regardless of the original flow retinotopic position and given direction. Trajectories along which relative eccentricity decreases are centripetal (Cp, in red) whereas those along which relative eccentricity increases are centrifugal (Cf, in green).* ***Box inset****, the working hypothesis is that the facilitatory effect of intra-V1 horizontal connectivity is maximal when the feedforward and horizontally mediated synaptic inputs reach in phase the intracellularly recorded cell. (Gerard-Mercier et al. 2016).*

The authors found that stimulation by 1 stroke of the "silent" surround could evoke significant subthreshold synaptic responses even in the far periphery of the RF, up to 10-12 ° away from the RF center. Those peripheral responses were more prominent along the preferred orientation axis of the cells. Strong responses could also be evoked at nodes outside the main axis and for various Gabor patch orientations, mostly at the closest neighbours to the RF center (first ring of relative eccentricity). Moreover, due to spatial summation, spiking responses in some cells could also be elicited as far away as 9° from the subthreshold depolarising field center, along the preferred orientation axis of the cell. However, responses from the far surround remained subthreshold in most cells.

To reveal the structure of functional horizontal interactions, the preferred orientation was estimated for each cell at each node by computing in a first time the circular average of the responses evoked by the six orientations presented at each node in the 1 stroke paradigm. The argument of the resulting average composed the angle of the preferred orientation at each node whereas the modulus of the complex number (|R|) quantified the robustness of the orientation selectivity. Secondly, all preferred orientations were realigned along a common axis before averaging across the population (n = 25) (Figure 3.7 B). Thirdly, the average response was averaged between pairs of nodes by point symmetry whose center was the central node containing the receptive field, to obtain a symmetric version of the structure of preferred orientation in the periphery (Figure 3.7 C). This symmetrized population average revealed functional biases in the form of coherent spatial structure of orientation preference in the "silent" surround. The pattern obtained is highly similar to the perceptual association field bias in contour perception described psychophysically by Field et al. (1993) (Figure 3.7 C).

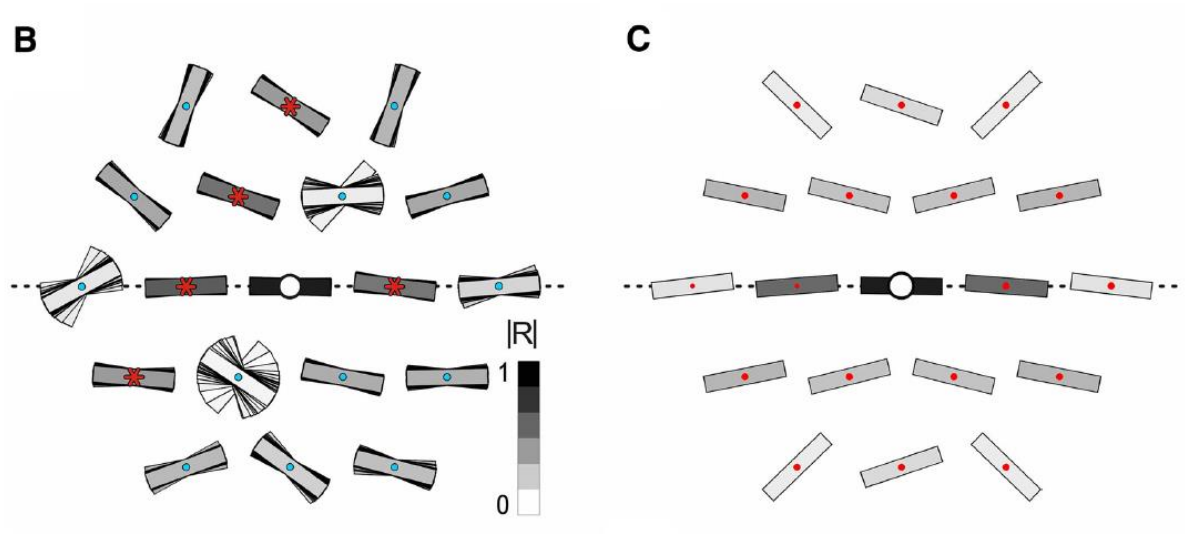

Figure.3.7: ***Synaptic correlate of the perceptual association field in V1. B****, The mean static association field is obtained by performing a circular average over the cell population of the preferred orientations, at each node (n = 25). The |R| value resulting from the average measures the reliability of the result and is represented by the level of gray of each oriented bar. Red asterisks indicate node positions where the |R| value is significantly higher than expected by chance (p < 0.05, one-tailed). To illustrate the reliability of the result, the same computation is performed on all possible sets of 24 cells sampled among the 25 cells in the population. Accordingly, the 25 preferred orientation sample estimates are represented in an overlaid fashion at each node, beneath the estimate for the full population.* ***C****, Symmetrized version of the mean static association field (****B****). Note the similarity in the pattern with the perceptual association field of Hess and Field (Field et al., 1993). (Gerard-Mercier et al., 2016).*

Then, to dissect the dependence of nonlinear interactions on trajectory type (centripetal, centrifugal) and configuration (ISO, CROSS) specific of the dynamic association field, the authors computed all the significant peripheric responses waveforms averaged across all cells. From those average responses, they found that supralinear responses for both centripetal and centrifugal ISO trajectories were around the response peak but that towards the early part of the response, the supralinearity remained strongly significant only for centripetal trajectories, revealing a latency advance of responses specific to elements ISO oriented regarding the motion axis and converging towards the RF center. No sub or supralinear relationship was found for the centripetal and centrifugal CROSS trajectories.

Next, the authors investigated the proportion of significant responses where significant nonlinearities occurred. They found that the average proportion of supralinear interactions was significantly larger than that of sublinear interactions in the ISO configuration and that it was not the case for the CROSS configuration. There were also more supralinear interactions in the ISO configuration than in the CROSS one. This differential ISO versus CROSS effect was specific to centripetal trajectories, as it was absent for centrifugal ones.

Finally, the authors compared the 2 stroke responses to non-central trajectories (discarding responses coming from the first ring or the center where one of the Gabor patch stimulated directly the center of the RF) along the preferred orientation axis of the cell versus along the two non-main axes. They found that the population of cells integrated peripheral 2 strokes stimuli significantly better along their main axis than along other axes, and that it was specific to the ISO configuration.

To conclude, these results suggest that the 2-stroke apparent motion stimulation extends and enhances the responses properties seen for the static (1 stroke stimulation) association field in the temporal domain. The observed responses are most prominent along the preferred orientation axis of the cell and are enhanced through supralinear interactions specifically for centripetal trajectories in the ISO configuration. These two properties suggest that motion at the speed of saccade-induced retinal flow could boost sensory responsiveness by allowing effective temporal interaction between feedforward and horizontally relayed visual activation. More precisely, cells where horizontal inputs preceded or were in phase with the feedforward drive showed shorter response latencies to centripetal than to centrifugal central trajectories and the magnitude of this response latency advance increased with the time lag. This finding supports the interpretation that a minimal integration time is needed to recruit non-linear voltage-dependent mechanisms recruited by horizontal connectivity in order to boost sensory responsiveness evoked by the central feedforward drive.

To summarize, cat VSD experiments (Jancke et al., 2004) showed that the focal activation of a visual cortical area (V1 or V2) can bias the propagation of consecutive feedforward evoked activity via horizontally propagated activity. It does so by creating a cortical wave of activity that progressively spreads beyond the feedforward imprint of a small and spatially localised stimulus at the subthreshold level. The latency of the response to a second stimulus extending beyond the retinotopic representation of the first one and presented after it is reduced at the loci of strongest preceding subthreshold activation. This forms a cascade of consecutive spatiotemporal activation that follows the differential strength of subthreshold activation created by the first small stimulus. The interaction between long-lasting depolarisation to a first stimulus relayed by horizontal connectivity and consecutive feedforward activation to a second stimulus shape and bias the overall propagation of activity on the cortical surface, mimicking the activation observed during real motion and is involved in the illusory perception of motion where two static stimuli (a small square presented before a long bar) are presented i.e the “line motion” illusion. For the interaction to occur, the recruitment of horizontal and feedforward evoked activity must lie within a certain range of spatio-temporal coherence beyond which both physiological and perceptual phenomena disappear.

Secondly, in cat V1 and V2, VSD imaging and intracellular recordings demonstrated that despite the long-range of laterally activated cortical areas, anisotropic activity remains enclosed in the feedforward imprint of cortical activation by a small oriented stimulus, limit beyond which laterally propagated activity becomes isotropic (Chavane et al., 2011). Intracortical mechanisms of spatial summation and cooperativity between activated cortical areas are necessary to shape and amplify

the spatial extent to which laterally propagated activity remains anisotropic. Compared to the presentation of a small localized grating, the presentation of a large annular grating which inner center is not stimulated allows the diffusion of anisotropic activity filling in the unstimulated central zone. Measurements of the speed of propagation of that activity (between 0,07 and 0,16 m/s, Chavane et al., 2011) confirmed that this spread is mediated by horizontal connections (Bringuier et al., 1999).

Thirdly, intracellular experiments in the anesthetized and paralyzed cat V1 highlighted the existence of a synaptic association field extending beyond the subthreshold depolarising field (Gérard-Mercier et al., 2016). That synaptic footprint of a static association field in V1 mirrors the perceptual association field described in psychophysics by Hess and Filed (1993) and is characterized at the physiological level by a bias for elements iso-oriented and collinear to the preferred orientation axis of a cell. The strength of facilitation progressively decreases with eccentricity from the receptive field center and displays a stronger angular tolerance to iso-orientation. Apart from the static characteristics of this synaptic bias, the 2-stroke apparent motion paradigm used by Gérard-Mercier et al., (2016) extended the facilitation to elements iso-oriented and collinear to the RF preferred orientation axis to the temporal domain by expanding the characteristics of synaptic integration facilitation to centripetal flows converging toward the RF center. The integration facilitation to centripetal flows only appeared when horizontally propagated activity reached the cell RF center before its feedforward stimulation, confirming the results of Jancke et al., (2004) by showing that a certain time window is necessary for lateral and feedforward activity to interact.

I-2.2 Exploring in depth the dynamic association field and its implication in the propagation of a prediction travelling through the V1 network

The working hypothesis of the work that motivated this thesis is that at high speed, the successive thalamo-cortical activation of neighbouring Aggregate Receptive Fields creates a subthreshold wave of depolarising activity that is relayed by horizontal connections. At the single cell level, when the periphery of a RF is recruited with a sufficient degree of spatio-temporal coherence by elements iso-oriented and coaligned with the cell's preferred orientation, forming a flow that converges towards the RF, this propagating wave of activity broadcast contextual information that carries a prediction. Horizontally propagated and feedforward activity interact when the RF of a cell is stimulated, which provokes a boosting of the response when compared to the sole feedforward stimulation of the RF center. On the other hand, according to our working hypothesis, without feedforward stimulation of the RF center, the propagating wave of activity relayed by horizontal connections is sufficient to produce filling in/predictive responses.

From the set of experimental findings described above, we designed visual stimuli to extend the functional characterization of the dynamic association field at the single cell level using intracellular recordings in a 6-stroke apparent motion paradigm. Following the work of Gerard-Mercier et al. (2016), in order to test for a differential synaptic integration between local (orientation of the elements regarding the motion axis) and global (spatio temporal coherence of the flows) features of the stimuli, the elements were either collinear to the motion axis or cross oriented to it, composing a flow that was either converging towards the receptive field (centripetal) or diverging from it (centrifugal). Gabor patches were also flashed individually to compute a linear prediction of the response.

By increasing the recruitment of horizontal connectivity, using 5 strokes instead of one in the periphery before stimulating the RF center, we aimed at maximising stimulus cooperativity by inducing the anisotropic spread of a depolarising wave of activity in the far surround of a receptive field to favours the response to the stimulation of its center. This maximisation was not done randomly. Indeed, the recruitment of the periphery was based on a spatio-temporal pattern corresponding at the spatial level to the synaptic imprint of the orientation sensitivity distribution of RFs surround (i.e., the static association field, Gérard-Mercier et al., 2016). At the temporal level, the spatial repartition of orientation sensitivity was progressively recruited according to the characteristics of the dynamic association field, favouring the integration of elements that are iso-aligned to the motion axis of the flow, along the preferred orientation axis of a cell and converging towards it.

By constraining the increase in spatio-temporal summation by a spatio-temporal “template” of stimulation reflecting the synaptic bias for motion integration in V1, we expected a supralinear response reflecting the propagation of a prediction, expressing the "network belief" of what stimulus may be expected on the basis of prior activation and intracortical diffusion. The boosting effect resulting from the internal network lateral broadcasting would translate itself at the physiological level by an amplification of the response and a latency advance of this one compared to the sole feedforward activation of the RF center. Moreover, maximising the lateral connectivity’s recruitment in a spatio-temporal pattern consistent with the dynamic association field synaptic bias would allow us to determine if the putative non-linearity presumably supralinear of the modulatory effect reaches the spiking level in the low-level perceptual state of the anaesthetized cat.

The spatio-temporal “template” of stimulation reflecting the synaptic bias for motion integration in V1 was composed of flows that were presented in different configurations in order to study the influence of several factors on synaptic integration. First of all, the spatial coherence of the stimuli composing the flows was manipulated by stimulating in one configuration the periphery of the RF along the preferred orientation axis of cells (the main one) surrounded by two others forming an angle of 30° with that axis, reflecting the higher angular tolerance from iso-alignment away from the receptive field center. This corresponds to the orientation sensitivity of the surround described by Gérard-Mercier et al., (2016) in the static association field (Figure 3.6 A; 3.7 C). In our experiments, stimuli were presented from both sides of the RF center, composing in total 6 axis of

stimulation; this configuration is referred to as “sector” stimulation. The feature coherence of the elements was also tested. Indeed, the elements were either iso oriented or cross oriented regarding the axis on which they were presented (Figure 3.8 A and B).

Second, because we wanted to study the impact of the periphery’s stimulation on the response to the stimulation of the RF center, this latter was always stimulated by Gabor patches of the optimal orientation. In the sector conditions, in order to avoid a shift of 90° between the GP presented in the periphery and the center, the sector configurations had to be tested by stimulating different retinotopic locations. GP cross oriented regarding the axis on which they were presented could not be presented along the preferred orientation axis of the cell and their neighbours without introducing a shift between the orientation of the elements in the periphery and in the center because this latter was always stimulated by a GP of the optimal orientation (Figure 3.8 A and B). Because those two different “sector” configurations stimulate different retinotopic locations, spatial coherence was also tested by recruiting the entire periphery, stimulating the 12 different axes surrounding the RF center. This latter configuration is referred to as “full” configuration (Figure 3.8 C, D).

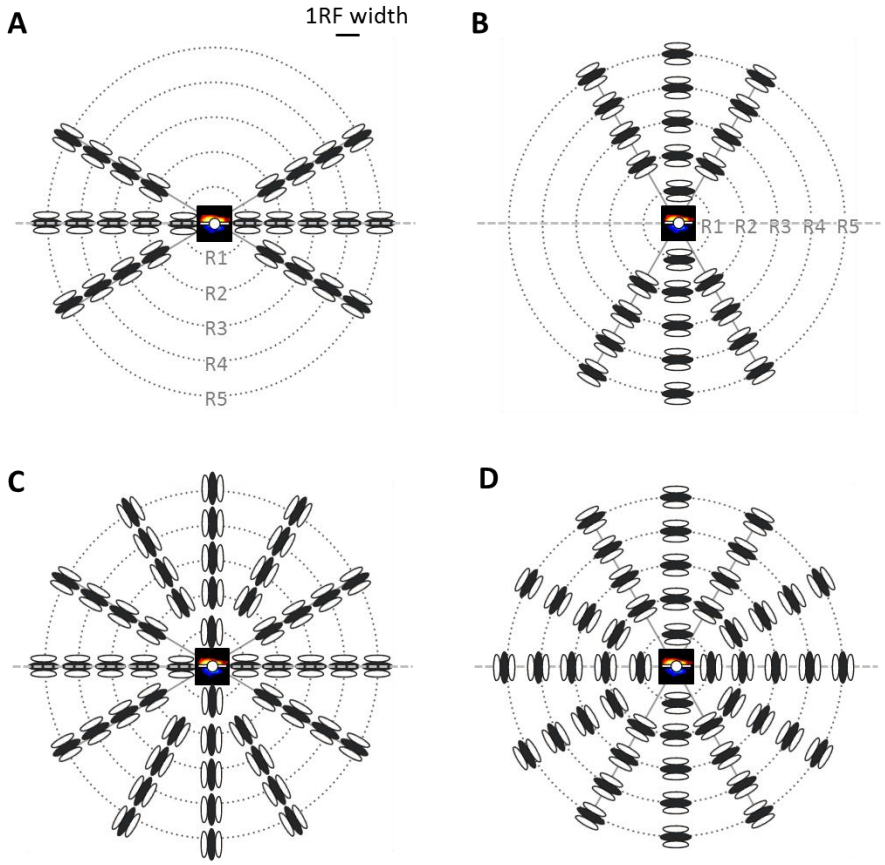

Figure.3.8: ***Temporally frozen representation of the periphery's spatial stimulation.*** *The temporal aspects of presentation of the Gabor patches are not represented here. Only the spatial configuration of the elements recruiting the periphery is shown.* ***A,B.*** *Sector configurations: patches of Gabor are presented along the preferred orientation axis of the cell (**A**) or along an axis orthogonal to it (**B**), surrounded by two neighbouring axis of higher angular tolerance, composing 6 flows presented symmetrically regarding the RF center.* ***C,D.*** *Full configuration: patches of Gabor composing 12 flows are presented symmetrically regarding the RF center, stimulating radially the entire periphery of the receptive field.*

Third, the temporal coherence of the flows was tested. The axis on which the patches of Gabor were presented actually represent motion axis of apparent motion sequences. In sector iso, cross; and full iso, cross configurations, all GP of a given ring were presented simultaneously, preceding the presentation of GP belonging to a neighbouring ring. This formed flows whose temporal coherence was manipulated in order to form centripetal flows where the sequential stimulation of the periphery was done from the 5^{th} ring of eccentricity to the stimulation of the center of the RF. Centrifugal flows, where the sequential presentation of GP started by stimulation of the RF center before extending to rings of increasing eccentricity were also presented. Pseudo-randomised sequences where there was no temporal coherence in the sequential activation of the periphery

were also generated. The set of conditions described above allowed us to study the overall spatio-temporal coherence impact of the periphery's recruitment on the stimulation of the RF center by comparing local (orientation of spatially confined elements) and global (direction of the flows) features of the apparent motion impact on synaptic integration.

At the static level, when the elements are cross-oriented regarding the motion axis, the mismatch between the local orientation feature and the direction of the motion does not engage properly the spatial gradient of orientation sensitivity of the static association field. Only the sector iso configuration recruits the periphery in a way that matches the spatial repartition of orientation sensitivity of the surround described in the static association field (Gerard-Mercier et al., 2016).

However, if we consider both spatial and temporal levels, only the sector centripetal iso sequence, where the elements are iso-aligned regarding the motion axis of the flow and converge towards the receptive field center along its preferred orientation axis correspond to facilitatory effects characteristic of the dynamic association field. Indeed, at the single cell level of the RFs we recorded, centrifugal flows (when the AM sequence diverges from the receptive field center) do not properly engage the V1 network at the temporal level to progressively build a wave of depolarising activity responsible for the boosting effect observed by Gérard-Mercier et al., (2016).

The direct comparison between stimulation of the surround of a cell along its preferred orientation axis and neighbouring ones (sector condition) and the stimulation recruiting the entire periphery (full condition) first allowed us to determine whether the effects observed in one or the other sector configuration (elements iso-oriented or cross-oriented regarding the motion axis) comes from the stimulation of different retinotopic positions or not. More precisely, it allowed us to quantify the dynamic association field sensitivity to anisotropic information carried by the converging flow by revealing or excluding potential competitive information between stimulation of different retinotopic locations. On the other hand, it gave us the opportunity to potentially highlight a more general property: the overall sensitivity of V1 RFs to converging information, Gerard-Mercier et al. (2016) having reported the existence of global motion flow sensors sensitive to centripetal flows, regardless of their retinotopic origin.

From the experiments described previously (Jancke et al., 2004; Chavane et al., 2011; Gérard-Mercier et al., 2016) a certain level of spatio-temporal coherence is necessary to bind lateral and feedforward activity. More precisely, from the characterization of the requirements necessary to induce a latency advance of the responses at the level of the synaptic integration field (Gérard-Mercier et al., 2016), it seems that sensory responsiveness is boosted when and only when laterally propagated activity ride in phase or slightly before the feedforward drive. In order to prove the implication of horizontal connectivity in those non-linear interactions or, in other words, that the recruitment of the periphery must lie within the range of horizontal activity propagation speed to ride in phase with the feedforward drive and induce a supra linear boosting of the response, we manipulated the speed of the apparent motion sequence. By progressively reducing the speed of recruitment of horizontal connectivity, thereby disrupting the synchronicity between the arrivals of the two types of information at the cellular level, we should observe a progressive reduction of the

boosting effect until it is not distinguishable from the stimulation of the center alone. That is why we tested flows whose apparent motion speed ranged on average between 160°/s (which corresponds to 0,16 m/s, speed well in accordance with the 0,1 – 0,3 m/s horizontal connectivity velocity's conduction) and 48°/s (hence 0,048 m/s, a speed well outside this range).

I-2.3 Filling-in and predictive responses

Filling-in is a perceptual phenomenon in which visual features, such as colour, brightness, texture and motion, of a surrounding area are perceived in a certain part of the visual field even though these features are not physically present (Walls, 1954; Gerrits and Vendrick, 1970; Komatsu et al., 1996; Pessoa et al., 1998). It can be regarded as the manifestation of a visual function of interpolation (Komatsu, 2006) and is often assimilated to an active computation of the brain who performs completion when the amount of information is limited, even though another possibility is that no active processing is necessary to induce filling in. This latter possibility is however becoming more and more unlikely as evidence of active neural operations are growing with experimental reports.

There are different types of filling-in, reflected by a large number of psychophysical effects including illusions. Those different types of filling in might have different underlying mechanisms, or there might be a general mechanism. They can roughly be divided in two categories, namely modal and amodal. Modal completion means that an illusory surface is perceived with vivid sensation as if it really exists as part of a certain feature. On the other hand, amodal completion means that the presence of an illusory surface or contour is realized even though it is invisible and it lacks vivid sensation (Komatsu et al., 2006). Several studies have been conducted to identify the neuronal correlates of filling in in the brain and the stages at which those operations are performed. In psychophysics, Murakami et al., (1995) and Shimojo et al., (2001) showed using aftereffect phenomena that filled in motion and real motion share the same neural mechanisms and that this sharing occurs at a relatively early stage where retinotopy is still present.

At the neurophysiological level, several studies have been led using the same strategy by determining whether neurons belonging to the retinotopic area where filling in phenomena happens are activated or not. Extracellular studies led by Fiorani et al., (1992); Matsumoto and Komatsu, (2005) and Komatsu et al., (2000) showed that V1 neurons of cebus and macaque monkeys were sensitive to filling in phenomena. Those studies interestingly highlighted that neural responses related to filling in at the blind spot were only observed in deep layers of V1. On the other hand, studies by Roe et al., (2005) that used the Craik-O'brien-Cornsweet illusion showed that filling in was only observed in V2 and Von der Heydt et al., (2003); who used the Troxler effect did not find any neurons sensitive to filling in phenomena in V1 nor V2, although the recordings of

those latter in V1 were only made in superficial layers. Contrarily, Jancke et al., (2004) and Chavane et al., (2011) found, using VSDI experiments, a spread of activity progressively filling in unstimulated parts of the visual field in both V1 and V2 superficial layers. These differences might be related to differences in the visual stimuli but might also reflect different underlying neural mechanisms.

Processes related to contour formation, such as contextual modulation of contours (Kapadia et al., 1995; Polat et al., 1998) and border assignment, have been shown to be formed in early visual areas, and neural responses related to figure-ground segregation have been observed in both early and late areas (Lamme et al., 1995; Zipser et al., 1996; Zhou et al., 2000; Baylis and Driver, 2001; Qiu and Von der Heydt, 2005; Hupe et al., 1998). This process occurs for any surface, regardless of whether it is modal or amodal. As a result, many representations of surfaces emerge, and they might be maintained through a recurrent feedforward-feedback loop between early and late visual areas (Mumford, 1994; Rao and Ballard, 1999; Mendola, 2003).

In this context, extra classical receptive field contextual modulatory effects such as filling in might be the product of a continuous exchange between early and higher order visual areas in which superficial layers 2/3 neurons that sends axons to higher visual areas are likely candidates as "error-detecting" neurons that signal the difference between an input and its prediction from a higher visual area. Indeed, filling in response might not have been always observed in superficial layers because when the stimulus properties of a neuron's receptive field match the stimulus properties in the surrounding region, little response is evoked from the "error-detecting" neurons because the surround context can predict the center one. Moreover, larger horizontal connections in layers 2/3 facilitate the propagation of information from the surround to the center of a receptive field, favoring the propagation of a rather extended spatial context filling in layer 2/3 neurons RFs under a completion operating mode. On the other hand, when the stimulus is presented in isolation, or is not presented while expected, the difference between visual input and expectation from higher areas is big, and so is the response of the "error-detecting" neuron of superficial layers 2/3 (Rao and Ballard, 1999). By opposition, the larger RFs size of deeper layers would tend to maximize the difference between center and surround of the RF as this latter is already bigger than in superficial layers and already provide more spatially extended information to higher cortical areas. Those latter would tend to modulate more easily differences between surround and center of a large RF as this latter would already cover the size of the stimulus. It would respond more easily to a difference in prediction and signaling filling in responses as well as surround - center differences, being potentially even more sensitive to feedback connections modulatory information because of the smaller spatial extent of horizontal connections in deeper layers. Indeed, in the predictive coding model that Rao and Ballard (1999) developed, the role of "error detecting" neurons of layers 2/3 is based on extraction and according modulation of progressively larger spatial context from early to higher visual areas.

That is why the last aspect that we wanted to tackle aimed at quantifying the functional impact of maximising the lateral broadcast of activity. We wanted to determine whether the recruitment of the periphery alone, without a direct feedforward stimulation of the receptive field center could

induce the propagation of a prediction at the cellular level under the form of a "filling-in" response in the unstimulated center of the receptive field from the periphery. To do so, we also used similar sequences restricted to the stimulation of the periphery, omitting the stimulation of the receptive field center with the experimental expectation that filling in responses would only appear for centripetal flows composed of elements iso-aligned with the motion axis.

I-3. Visual stimuli design

I-3.1 Geometric design of the stimulation and definition of a common cellulo-centric referential

One of the aims of this thesis was to study the impact of the contextual recruitment of the silent periphery on the integration efficiency of feedforward input flashed in the center of the recorded receptive field. The changes in "effective gain" due to surround/center interaction were measured by using an Apparent Motion (AM) paradigm. Our working assumption is that the successive activation of distal regions, hence hypercolumns, along an integration path converging towards the RF center would produce cumulative propagation of lateral activity in V1, which in turn would boost cortical responsiveness when converging on the same target V1 cell in (temporal) phase with the feedforward stimulation of its RF

A main concern was to devise stimulation protocols that could be compared across cells, and still be interpretable in relation with individual RF properties. Intracellular studies have the dual advantage/disadvantage over extracellular studies to amplify the diversity across cells, and we tried in our protocols to make cells more directly comparable to allow meaningful averaging at a further stage of analysis. The easiest way was to scale the integrative view of visual space of each individual cell according to the size of its subthreshold receptive field (sRF) and to quantify eccentricity in the silent surround relative to each individual receptive field center in sRF step units.

Since most recordings were done within 5 degrees of the area centralis, several factors of non-homogeneity were on purpose neglected such as the non-linear distortion of space representation in the retinotopic cortical map, due to eccentricity-dependent changes in magnification factor between the area centralis and the periphery (Tusa et al., 1978). Moreover, at a given retinal eccentricity, the receptive field size and its orientation, phase and spatial frequency preferences are highly variable and depend of the laminar location of the recording. Because of the intrinsic difficulty of intracellular experiments, we could not impose a priori the precise retinotopic position of the cells that we impaled and their recording depth. To simplify the parametric control of our stimuli, for any given cell, we decided to use the same scalable "average" size for the test Gabor stimuli whatever their retinotopic position, which allows to keep the distribution of energy content invariant across the visual scene. This trade-off however prevented us from objectively comparing responses from the periphery to those of the center of the RF, since the size optimisation was done only for the RF center, but was suboptimal for peripheral positions. In practice, the average subthreshold receptive field (sRF) value was in the order of 4-5 degrees of visual angle, which corresponds roughly to the aggregate receptive field size (ARF) of individual functional hypercolumns around the area centralis. Thus, the Gabor stimulus size matched the spatial dispersion envelope of individual RFs recorded in the same hypercolumn, i.e. analysing the same point in visual space.

Two types of visual protocols were used. In a first series of experiments, to which I participated during my training internship (Gerard-Mercier et al, 2016), the visual field paving obeyed both circular and hexagonal symmetry constraints. Once the Gabor template covering the subthreshold RF of the recorded cell was defined, the visual field was paved using an hexagonal lattice (for optimal coverage) of possible stimulation nodes/tiles centered on the RF and the node grid was aligned relative to the preferred orientation axis. The size of each tile (i.e., the distance between neighbouring nodes) was chosen to be the diameter of the Gabor template, so that peripheral stimuli could not overlap nor encroach on the RF center. (Figure 3.4A).

In the second series of experiments (first part of my thesis), we decided to relax the hexagonal symmetry while keeping the circular symmetry constraint alive. The possible AM integration paths were defined as trajectories passing through the RF center. Their possible angles were defined relative to the orientation preference axis (0°) as six possible trajectories discretized by 30° steps. In all cases, the AM paradigm stimulated different loci of the periphery with Gabor patches having the same properties (phase, spatial period and size) than the one eliciting the reference feedforward response of the intracellularly impaled cell. Conversely the eccentricity of the stimulation nodes was simply defined by the intersection points between the AM axis and rings of multiple (1,2,3,4 or 5) sRF step eccentricities relative to the RF center. The resulting cellulo-centric referential and the possible AM sequences are illustrated in Figure 4.5.

The rationale guiding the circular paradigm was to maximise the subthreshold boosting effect observed by Gérard-Mercier et al., (2016) and make its impact detectable at the spiking level. Consequently, to maximize the recruitment of the periphery, we extended the stimulation up to 5 rings of eccentricity before stimulating the RF center. We also aimed at parametrizing more completely the stimulation protocol in order to assess the requirement of spatio-temporal synergy in order to bind feedforward and lateral activity. To do so, the periphery was generally stimulated at an AM speed corresponding to the propagation speed of horizontal connectivity measured in the recorded cell (Bringuier et al, 1999), maintaining at each stimulation location an in-phase relation between the lateral and the feedforward flow (Figure 4.1).

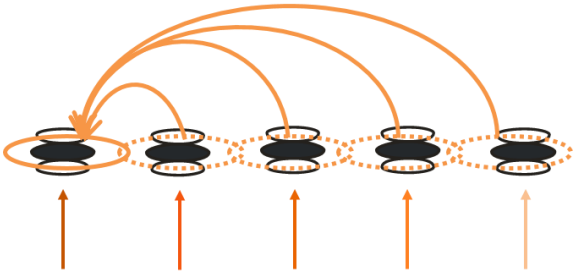

Sequential Feedforward stimulation

Figure.4.1: ***Feedforward stimulation and lateral propagation are kept in phase.*** *This results in an in-phase synchronized arrival at the RF target of multiple lateral synaptic potentials allowing a latency shortening and response boosting of cell's responsiveness when the central target RF of this latter is stimulated. Moreover, lateral connections shared by each aggregate receptive field convey more and more facilitatory influence from neighbour to neighbour, summing up at the RF center stimulation arrival time.*

To maximise the efficiency of laterally propagated activity, the periphery was recruited according to the static "imprint" of orientation sensitivity of the surround found by Gérard-Mercier et al., (2016, Figure 3.5 C). That is why we designed centripetal flows of Gabor converging towards the RF center in a symmetrical way regarding the RF on three adjacent axes. Gabor patches converging towards the RF were flashed along the preferred orientation axis of each cell and two surrounding axes of 30° angular tolerance regarding the preferred orientation axis (Figure 4.2), forming a **centripetal-ISO** sequence. This multi-axis sequence, called sector configuration, matched the orientation sensitivity of subthreshold distal responses in cat V1 RFs described by Gérard-Mercier et al., (2016) and obeyed the collinearity condition corresponding to the perceptual association field described in human psychophysics by Hess and Field (1993, 1999, Figure 1.11A). Additional geometric configurations were designed where the orientation of the local Gabor probe was either co-aligned (ISO-) or cross-oriented (CROSS-) with the AM axis (see below: Manipulating the spatial coherence of the flows, Figures 4.4 and 4.5)

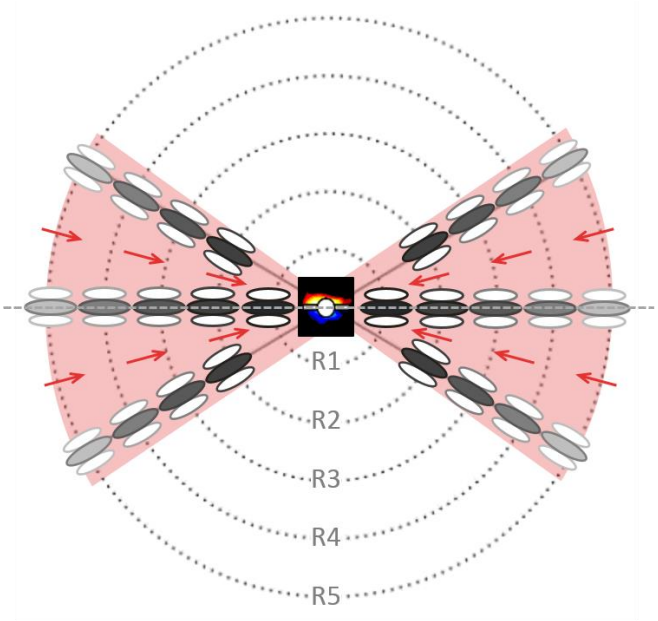

Figure.4.2: ***Spatio-temporal pattern of the Apparent Motion (AM) flow converging towards the RF center in a cellulo-centric referential****. The intersection of the five concentric rings (Ri; from 1 to 5) surrounding the subthreshold depolarising field of the recorded cell and the three co-linear motion axis (-30°, 0°, +30°) define the stimulus locations explored by the AM sequence contracting from the far periphery (R5) to the RF center (central white dot). The distance between each ring, i.e between the center of each neighbouring patch of Gabor is the same and equalized to the sRF size. The illustrated RF is represented by red (ON) and blue (OFF) sub regions. The preferred orientation of the cell is represented by convention as the dotted horizontal line passing through the RF center. The temporal order of each stimulation step is represented by the red arrows, and the recency of each stimulation stroke is coded by the contrast of the Gabor stimulus.*

I-3.2 General Spatio-Temporal design of apparent motion (AM) sequences

Rather than using continuous motion, our protocols are based on apparent motion (AM) where discrete neighbouring locations in the visual field are explored in succession with a specific inter-stimulus delay called inter stroke interval (ISI). The temporal delay and the spacing are low enough to produce in the observer (human or animal) a percept of continuous motion. In the AM sequence, Gabor patches were flashed at each locus for a duration ranging from 14 to 41 ms. In our main stimulation condition, there was no ISI between the presentation of each GP. In other experiments, we introduced ISI of various duration to manipulate the speed of the flow (see below: Probing the implication of horizontal connectivity, Figure 4.3). Flows speed was calculated for each cell by dividing the distance from the outer ring of eccentricity by the overall duration of presentation of

all nodes (5 external rings + 1 central stimulation). The speed of the flows ranged from 72 to 312°/s with an average of 191°/s, corresponding to 0.19 m/s, a speed value well within the 0.1-0.3 m/s range characteristic of lateral activity propagation speed (Bringuier et al., 1999; Chavane et al., 2011; Gerard-Mercier et al, 2016).

Two types of AM sequences were designed: the first aimed at probing the periphery - then - the center stimulation's effect (or in reverse order), and the second type of AM aimed at probing the periphery-only's stimulation while omitting the center. Trials were interspaced with the static stimulation of the center alone (Center-only condition). In this last control condition, recordings were done during a time period equivalent to that of the full AM sequences (omission of 5 rings + center stimulation).

The first type of protocol (Surround-then-Center) was used to quantify the gain control exerted by the contextual periphery's recruitment on the response to the Center-only condition. The second type of protocols (Surround-only) was used to quantify the impact of the periphery's stimulation independently of the ulterior feedforward activation of the RF center. Although all the stimulation points belonged to the "silent" part of the receptive field, their composite stimulation led in certain cells to suprathreshold activation. To assess the predictive nature of this response, the temporal profile of the response to the Surround-only sequence was compared with that expected if the RF center had been stimulated.

I-3.3 Contrast conditions

Most contextual effects of the stimulation of the so-called "silent" surround are quantified here as gain changes relative to the control response to RF center stimulation alone (Center-only condition). The contrast of the patch of Gabor used in the center was adjusted to a subthreshold level (below the depolarization level needed for spike initiation) and thus avoid a saturation of the response by the sole feedforward drive (Kitano et al., 1994; Chavane et al., 2011; Nauhaus et al., 2012; Gerard-Mercier et al, 2016). The contrast of the elements presented in the periphery ranged from 75 % to 100% and was always superior to that of the center (40 to 50%). When the center of the receptive field was stimulated, the orientation of the Gabor stimulus always matched the orientation preference of the cell, regardless of the orientation of the local stimulus flashed in the silent surround (CROSS- oriented or ISO- oriented regarding the motion axis, see below; Manipulating the spatial coherence of the flows, Figures 4.4 and 4.5), by opposition to our previous work (Gérard-Mercier et al., 2016).

I-3.4 Probing filling-in or predictive responses

We also wanted to determine whether the sole recruitment of the periphery could evoke visual responses without any feedforward stimulation of the RF center, omitting on purpose the stimulation of this latter. Our working hypothesis was that that the sole propagation of horizontal activity, under specific spatio-temporal coherence constraints matching the dynamic association field synaptic bias (i.e, centripetal flows composed of elements ISO-aligned regarding the motion axis along the cell's main axis) could result at the single cell level in activity filling in the unstimulated subthreshold receptive field. If filling-in phenomena were specific of flows converging towards the RF center, they could be interpreted as a prediction propagating through the V1 network. That is why for each tested condition (among which controls that we will detail below) a corresponding condition restricted to the stimulation of the periphery was presented without any stimulation of the center.

I-3.5 Probing the implication of horizontal connectivity

From the results of Gérard-Mercier et al., (2016), the bias for the integration of collinear elements along a cell's preferred orientation axis and converging towards the RF center resulted from the interaction of laterally propagated activity arriving slightly *before* the feedforward input at the cellular level. Those facilitatory responses did not occur when the lateral activity arrived after or at the same time than the feedforward drive.

To prove that our effect indeed results from the interaction of laterally propagated activity with the feedforward drive, in another set of recordings, apparent motion speed was also varied for some of the cells, ranging from the average horizontal activity propagation speed to a speed value 3 times lower. The use of apparent motion allowed us to manipulate the speed of the flows without changing the overall energy content of the stimulation by keeping constant the cumulative duration of presentation of the Gabor patches while introducing variable inter-stroke intervals (ISI) between them. This configuration was tested on 12 cells, focusing on our condition of interest where a latency advance and an amplification of the response were generally observed: centripetal flows composed of elements ISO-aligned regarding the motion axis (**centripetal-ISO** sequence).

In practice, we determined during the experiments the smallest duration for which patches of Gabor flashed in the center of the receptive field elicited a clear response distinguishable from the noise. That duration ranged from 14 to 42 ms and, according to the respective size of each subthreshold receptive field, this corresponded to flows speeds ranging from 100 to 214°/s with an average of 160°/s. For each cell, the initial speed defined from the smallest duration of stimulation eliciting a clear response in the RF center and the overall extent of spatial stimulation was set at the "reference speed". Inter stroke intervals were introduced in-between the presentation of two

consecutive spatial unit of stimulation (rings or center) to reduce the speed of the flows to 70%, 50% and 30% of the "reference speed" of each cell (Figure 4.3). The tested speed values were on average 112°, 80° and 50°/s. During those spatio temporal sequences, the center was also stimulated in isolation.

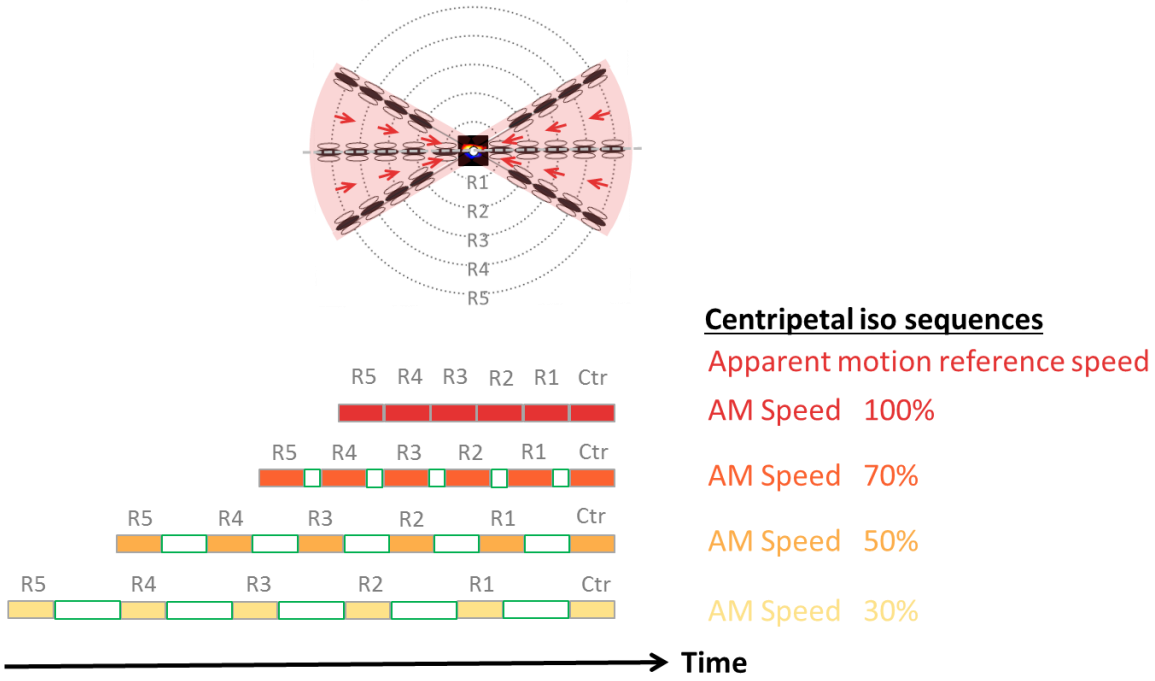

Figure.4.3: ***Manipulating the speed of centripetal-ISO flow.*** *Schematic representation of the variation of flows speeds used to recruit the periphery in an apparent motion paradigm, represented here for the sector configuration. Each filled box represents the duration of stimulation of a spatial unit (rings and the center). Empty boxes delimited by green contours represent the duration of inter stroke interval (ISI) presentation. The use of ISI allowed to manipulate the speed of apparent motion flows without changing the overall energy content of the visual scene by keeping the same duration of stimulation of each spatial unit. The speed of the different flows is colour coded from yellow for lower speed to red for higher speed. Each speed is expressed as a percentage of the reference speed denoted as 100% for which no ISI was presented.*

I-3.6 Manipulating the spatial coherence of the flows

The spatial distribution of local orientation preference biases in the static association field described by Gérard-Mercier et al., (2016) showed that facilitatory effects, characterized at the synaptic level by an amplification and a latency advance of the response, requires a certain level of spatial coherence during the dynamic exploration of the synaptic association field. Indeed, using a two-strokes apparent motion paradigm, Gérard-Mercier et al., (2016) showed that the integration of peripheral information was specific of Gabor patches co-aligned with the motion axis along the preferred orientation of cells. In order to prove that this synaptic bias is specific to a combination of the local feature of the probe stimulus and the global motion of the flow (elements iso-oriented and coaligned with the RF center in visual space), we manipulated the orientation of the elements composing the flows, creating centripetal flows of elements **CROSS-**oriented along the orthogonal axis (width axis) also converging towards the RF center (Figure 4.4).

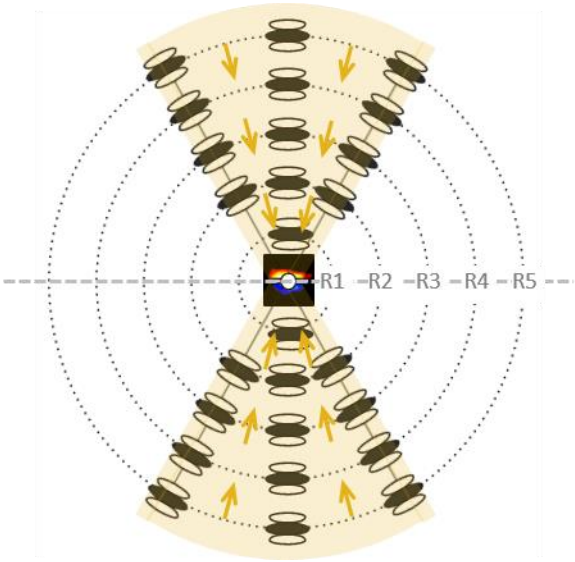

Figure.4.4: ***Centripetal-CROSS AM sequences*** *are composed of individual Gabor elements cross-oriented with the motion path converging towards the RF center, as shown by the yellow arrows. The elements lying on the axis orthogonal (90°; width axis) to the main axis (preferred orientation of the cell) are surrounded by two neighbouring axes of higher angular tolerance (60°, 120°) regarding the central one, resulting in 6 concomitant flows restricted to a specific angular sector of the surround.*

I-3.7 Manipulating the spatial and temporal coherence of the flows

In order to confirm the need of both spatial and temporal coherence in the emergence of our effect and exclude the possibility that the putative supra linear boosting was due to the presentation of more patches of Gabor conferring more energy to the visual scene, we also manipulated the temporal coherence of the flows by presenting AM flows diverging centrifugally from the RF center or presented in a pseudo random fashion (Random condition). Therefore, we interspersed several conditions in long duration protocols, alternating **Centripetal-CROSS**, **Centrifugal-ISO** and **Random-ISO** sequences as controls to the **Centripetal ISO** condition of interest (Figure 4.5).

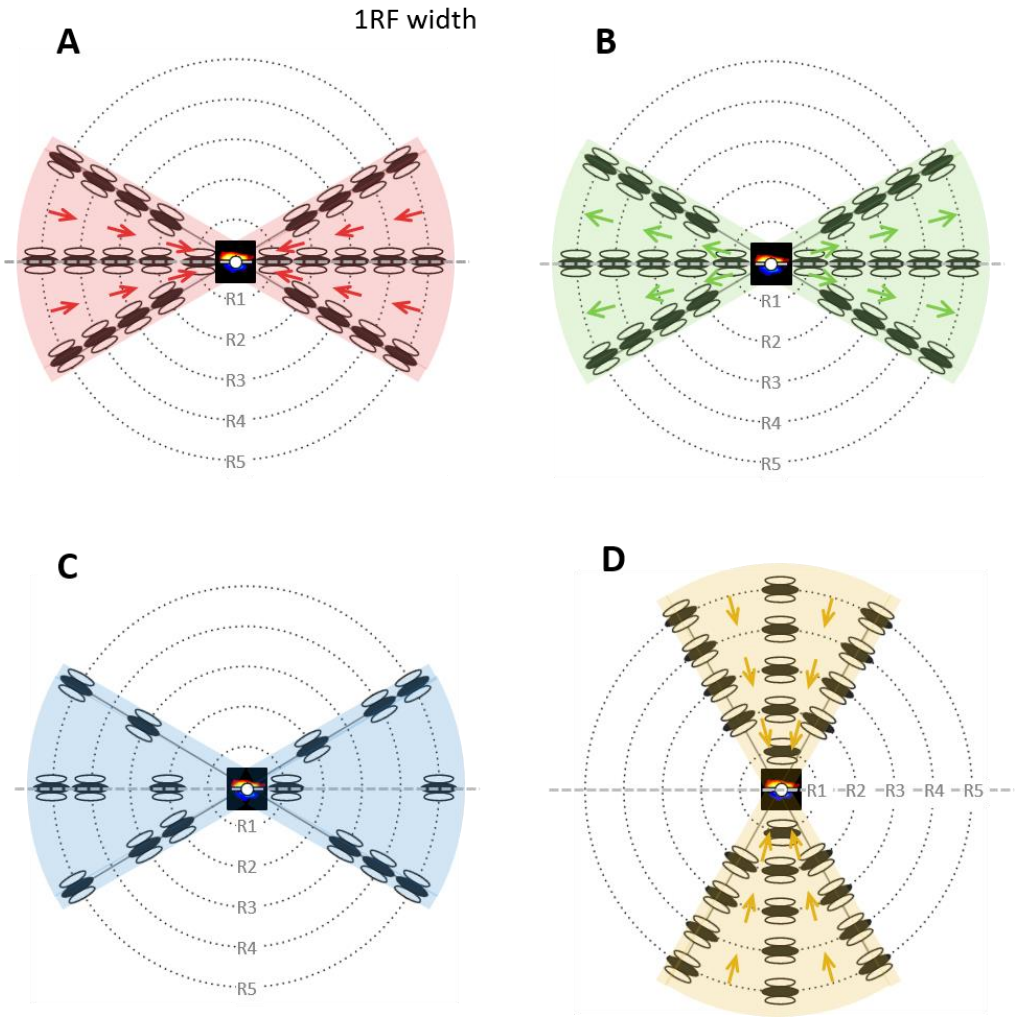

Figure.4.5: ***Spatio-temporal coherence of the flows. A,C.*** *Flows composed of Gabor patches ISO-aligned regarding the motion axis.* ***D.*** *Flows composed of elements CROSS-aligned regarding the motion axis.* ***A,D.*** *Flows converging towards the RF center.* ***B.*** *Flows diverging from the RF center* ***A.***

***Centripetal ISO sequence*. B. *Centrifugal ISO sequence*. C. *Random ISO sequence*. D. *Centripetal CROSS sequence*.** *For each configuration except the random one, patches of Gabor belonging to a given ring were flashed simultaneously before the presentation of Gabor patches belonging to the neighbouring ring in an apparent motion paradigm, in a temporal order following the direction of the flows indicated by the arrows. For the random condition (**C**), at each step of the temporal stimulation the same number of elements were flashed, stimulating all possible positions only once in a trial. Recruitment of the periphery is showed here for the sector configuration.*

For all conditions except the random ones, all Gabor patches of a same ring were presented simultaneously before the presentation of GP of a neighbouring ring, according to the spatio-temporal coherence of a given condition. Temporally, for centripetal flows the RF center was the last spatial position to be stimulated, following the coherent recruitment of successive rings of eccentricity from the 5th to the center. For centrifugal flows, the center was the first position to be stimulated, followed by the successive stimulation of rings of increasing eccentricity.

For the random conditions, Gabor patches of different rings were presented simultaneously, stimulating all possible positions explored in the other conditions without stimulating twice the same location to keep the visual scene overall energy content constant across time.

I-3.8 Probing the existence of local versus global motion flow detectors

We did not restrain our exploration of the periphery to 6 flows converging towards or diverging from the RF center in a symmetrical manner. We also radially stimulated the entire periphery of the receptive field by 12 centripetal, centrifugal and random flows (Figure 4.6 B,D). Indeed, Gérard Mercier and collaborators (2016) already observed the existence of local motion flows detectors only sensitive to the stimulation of the periphery along the preferred orientation axis of cells when the flows were converging towards the RF. In another analysis, they showed that regardless of the retinotopic origin of the flows converging towards the RF, cells were on average more responsive to flows converging towards the RF in a centripetal manner, whether the flows originated from retinotopic position lying along their preferred orientation axis or along an orthogonal axis, highlighting the existence of global motion flows detectors. That is why we designed sequences of AM where each ring contained 12 GP, forming flows where elements were either iso- (Figure 4.6B) or cross-oriented regarding the motion axis (Figure 4.6 D), converging towards or diverging from the RF center as well as presented in a pseudo random fashion.

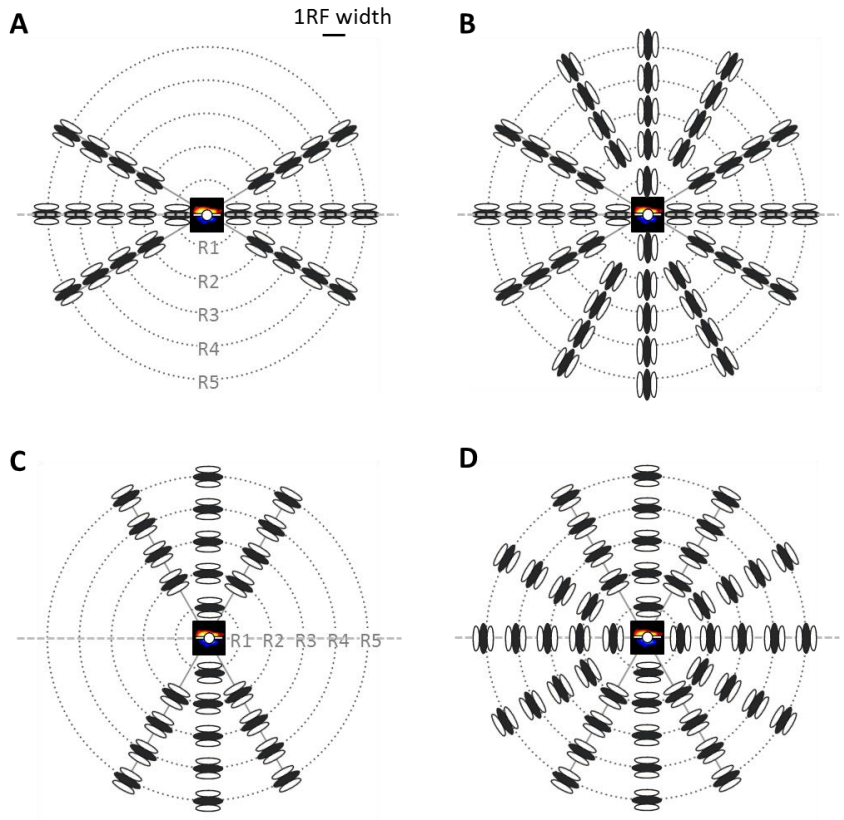

Figure.4.6: ***Sector and Full AM stimulation patterns. A-D.*** *The temporal aspects of presentation of the Gabor patches are not represented here. Only the spatial configuration of the elements recruiting the periphery is shown.* ***A-B.*** *The elements composing the flow are ISO-aligned regarding the motion axis by opposition to (**C-D**) where the elements are CROSS-aligned regarding it (the temporal aspect of the sequences is not shown here; the elements could therefore converge towards or diverge from the RF center.)* ***A,C.*** *Sector configuration: patches of Gabor are presented along the preferred orientation axis of the cell (**A**) or along an axis orthogonal to it (**C**), surrounded by two neighbouring axis of higher angular tolerance, composing 6 flows presented symmetrically regarding the RF center. Only the Sector-ISO stimulation (**A**) match the spatial repartition of orientation sensitivity of the static association field described by Gerard-Mercier et al. (2016).* ***B,D.*** *Full configuration: patches of Gabor composing 12 flows are presented symmetrically regarding the RF center, stimulating radially the entire periphery of the receptive field.*

I-4. Material and methods

All experiments were performed in anesthetized (althesin, 3 mg/kg/h) and paralyzed (pancuronium bromide, 0.2 mg/kg/h) adult cats of either sex, according to the American Physiological Society's Guiding Principles for the Care and Use of Animals. The animals used in the experiments were bred in the Central Centre National de la Recherche Scientifique Animal Care facilities of the Campus of Gif-sur-Yvette (French Agriculture Ministry Authorization: B91-272-105) under required veterinary and National Ethical Committee supervision.

I-4.1 Animal breeding

Cats were hosted in the animal facility of Gif sur Yvette in specific rooms. The facility is composed of free spaces where the animals can move freely. The environment is supplemented with natural and artificial platforms, toys and balls for their well-being. They have access to natural light. Males and females are separated by a metallic grid. For reproduction, the light cycle is fixed at 14 hours of light per day and two females in heat are mated with a male in a separate room. Females and their litter are kept isolated until the new-borns are weaned. A quarantine room allows separating exterior animals arriving to the facility from the rest of the colony until a veterinarian confirm the absence of pathogens. Animals are in contact with humans on a daily basis, their food, water and litter box being changed every day. A veterinarian keeps up to date the vaccination of each animal, visiting the facility every two-months.

I-4.2 Surgical procedure and animal preparation

Thirty-four cats were used during the experiments. The day before the experiment, animals were not fed. The first day of experiment, they were weighted. Initial anaesthesia was done by intramuscular injection of 10mg/ml/kg of Alphaxalone. Animals were then placed on a surgical table over a heating blanket. The neck, top of the head and two hind legs were clipped and an antiseptic composed of Povidone-iodine was applied on the skin. Lidocaine was first percutaneously injected on sites surrounding the saphenous vein and catheters were percutaneously inserted into the two internal saphenous veins and sutured to the surrounding skin to obtain continuous injection routes for perfusions. Continuous injection of Alphaxalone (Alphaxan®; JUROX (UK) Limited) was then set at 2,5 mg/kg/h for the rest of the experiment. After a cutaneous application of povidone-iodine and percutaneous injection of lidocaine at the tracheal level, incision of the skin was made to gain access to the trachea which was detached from surrounding muscles. A lower cartilaginous ring of the trachea was partially incised in order to insert the tracheal tube. Surgical sutures between the

trachea and the tracheal tube ensured the immobility of this latter. An antiseptic cream (CICATRYL®; composed of Allantoïn, Guaiazulene, Para-Chloro-Meta-Cresol and Alpha-Tocopherol Acetate) was used as a disinfectant before closing the wound with staples.

Animals were then placed on an anti-vibrating recording table and their body temperature was continuously maintained between 38 and 38.5 °C during all the time of the experiment by using a rectal probe connected to a homeothermic blanket. Subcutaneous electrodes were placed on both side of the chest to monitor electro cardiogram (EKG) activity as a first indicator of potential nociceptive responses. Lidocaine gel (Xylocaïne®, AstraZeneca Inc.) was placed into the ears and animals were head fixed to the stereotaxic frame using ears, inferior orbital ridges and upper maxilla bars.

A paralysing agent (ESMERON®; 4 mg/kg/h composed of rocuronium bromide) was then injected intravenously to prevent any eye movement during all the experiment. Animals were artificially ventilated with a respiration rate first set to 25 cycles/min and the volume of inhaled air was adjusted to maintain the end tidal CO_2 between 3.5 and 4.5% of the total exhaled gas volume. Control of the level of anaesthesia of the preparation during the intial stages of the surgery was monitored by checking regularly the stability of the pupillary state (slit) before the infusion of atropine (see below) and the absence of retraction reflex to paw pinch. An intravenous bolus of Alphaxalone and a percutaneous injection of lidocaine was then made on the top of the head before incision of the skin with a surgical scalpel. Three holes (coordinates: P=8, L=5; A=8, L=10 and A=16, L=10) were drilled in the skull and Electro Cortico-Gram (ECoG) silver electrodes were placed on the surface of the dura mater to monitor the spectral composition of the brain activity as another measure of anaesthesia depth. Silver electrodes were fixed with silicone gel that rapidly polymerized (Kwik-Cast©, W.P.I. Inc.). Stereotaxic coordinates of the area centralis were determined according to Tusa and Rosenquist (1979) and holes were drilled on the skull surface near those coordinates (between P=2, L=2a and P=5, L=3), following the curvature of the cat primary visual cortex (V1) surface. A chamber was made with dental cement and placed on the skull surface above V1. For each hole, when the dura matter was reached, this latter was incised using an ophthalmic precision scalpel (microsurgical knife, M.S.P.). Recording glass electrodes were then positioned in the hole and progressively lowered in the cortex with a motorized micromanipulator (Luigs Neuman Inc.). The hole was then filled with the silicone gel to prevent the brain form drying, reduce brain movements and stabilize the glass electrode.

Urine density was also monitored using a spectrometer, and the continuous perfusion of hydrating solution of Ringer lactate and glucose adapted accordingly. During the experiment, anaesthetic flow was adjusted to maintain the depth of anaesthesia constant according to the ECoG and EKG spectral composition.

Atropine (1%; Virbac Inc.) and Neosinephrine® (chlorydrate of phenylephrine 10%; Europhta Inc.) were used to dilate pupils, retract nictitating membranes and block accommodation. Scleral contact lenses with 3 mm artificial diameter pupil were used to prevent the corneas from drying. After adapting the animal to darkness, a cold light source coming from a fiberscope was directed into the

eye and the aerial image reflected by the eye tapetum lucidum layer was back-projected on a frontal screen positioned at 57 cm (1 cm = 1 degree of visual angle) and focused with appropriate corrective lenses. The optic nerve position (i.e., the blind spot) defined during the back-projection was used to geometrically determine (according to Tusa, Palmer and Rosenquist; 1978) the position of the Area Centralis on the screen. During experiments, the eyes of the animals were regularly washed with an ophthalmic solution and artificial tears in scleral lenses were renewed.

Experiments usually lasted for three days and two nights. At the end of the experiment, euthanasia was done by intravenous injection of T61 (a mixture of embutramide, mebezonium and tetracaine). Perfusion of the brain was done by intra-cardiac injection of tyrode to evacuate the blood from the vessels, followed by injection of Paraformaldehyde (PFA) that acted as a fixating agent. The skull was opened under terminal anesthesia; a slab of brain containing the visual cortex was taken and placed in PFA for further fixation. The brain was then sliced, mounted and the biocytine revealed for later histological observation (see details below).

I-4.3 Intracellular recordings

Cells were recorded intracellularly *in vivo*, in the primary visual cortex of anesthetized and paralyzed cats. Sharp pipettes were pulled from borosilicate glass capillaries (W.P.I.) using a Sutter instrument P-87 micropipette puller. Micropipettes were filled with an isotonic solution containing potassium methyl sulfate, potassium chloride and of biocytin (1,5%) to stain the recorded cells. PH was adjusted to a physiological range of 7.2-7.4 by addition of potassium hydroxide. Electrodes impedances ranged between 70 and 130 MΩ. Voltage recordings were wade using Axoclamp-2A (Axon Instruments inc.) or sec-05X (Npi electronic) amplifiers in bridge mode. Holding current ranged from 0 to -0.5 nA. Electrophysiological signals were filtered and amplified with a CyberAmp 380 (Axon Instruments inc.) and digitized by an ITC-1600 (InstruTECH®) data acquisition system. The sampling frequency of the ITC-1600 system was set at 10 kHz for the membrane potential; the one of ECoG and cardiac signals at 1 kHz. All data acquisition, processing and visual stimulation were done using an in-house software (Gérard Sadoc, Elphy).

I-4.4 On-line characterization of receptive fields

Stimuli were displayed on a 27 inches LCD monitor with a 1920*1080 pixels resolution and a refresh rate of 144 Hz. For the acquisition of data described in the first section of the Results chapter of the thesis, the screen was placed at 28.5 cm from the vision plane of the cats, where 1° of visual angle corresponds to 0.5 cm in order to maximise the extension of the periphery recruitment up to an eccentricity of 5 time the receptive field size (RF) away from the RF center.

Preceding quantitative RF measurements, ocular dominance, qualitative RF position and size were estimated using manually controlled bars which luminance was 24 cd/m² against a background luminance of 5 cd/m². Once the location and spatial extent of the RF were manually assessed, the ocular dominance was probed and the following stimulation sequences were restricted to the dominant eye only (monocular viewing). The precise position and spatial organization of the RF was measured with sparse binary noise presented in a square matrix encompassing the identified area of interest. This matrix was divided in usually 100 region (10 by 10) positions where visual responses were identified (hence approximately 0,5 by 0,5° of visual angle for a square of 5°). This formed a grid in which bright (40 cd/m²) and dark (1 cd/m²) small squares were sequentially flashed in each position, one position and luminance at a time, in a pseudo random fashion against a uniform background luminance (20 cd/m²). The duration of presentation of each square was of 34 ms, forming an overall trial sequence of 6,8 s (34 ms X 100 positions X 2 tested luminance values). The map of visually evoked responses was obtained using a forward correlation method. Each trial sequence was repeated between 10 and 30 times. Several successive mappings were often necessary to adjust the size and position of the area totally enclosing the subthreshold Depolarising Field (sDF).

After on-line visualization of the results, a square containing the entire subthreshold depolarising field was manually adjusted to set the limits of the responsive region and its immediate silent periphery. To determine the preferred orientation, spatial period and phase of the receptive field, Gabor patches (GP) were obtained by convoluting sinusoidal gratings with a Gaussian envelope. GP that covered the sDF region were flashed for 34 ms at 6 orientations ranging from 0 to 150° by 30° increment steps at 4 phases: 0, 90, 180 and 270° and 5 spatial periods: 0.9, 1.9, 2.9, 3.9 and 4.9 cycles per degree of visual angle, forming a total number of 120 different GPs. The combination of properties eliciting the larger response was retained to compose the optimized Gabor patch presented during the interest protocol. The side size of the square encompassing the sDF ranged from 2.5° to 12° of visual angle with an average of 5± 1,6° SD.

I-4.5 Histology

To characterize the morphology and position of cells intracellularly labelled with biocytin, slices of 80 µM thickness were obtained from the fixated brain tissue using a vibratome (VT1000S Leica®). To reduce the impact of the blood's endogenous peroxidase activity, slices were successively dived during 20 minutes in three alcohol dilutions of respectively 50%, 70 % and 50%. They were then rinsed by three successive baths (5 mn duration) in a phosphate buffer (PS) solution. Slices were then exposed during 90-120 minutes to a detection enzyme: the Horse Radish Peroxidase (HRP) that is labelled by the biotin contained in the biocytin. This biotinylated enzyme forms an avidin-biotin peroxidase complex. After rinsing by three successive baths of 5 mn in PS, the DAB (diaminobenzidine) which is a substrate of the enzymatic complex forms a dark blue precipitate. A

counterstaining by neutral red marking the Nissl body contained in the cytosol colours the cells soma in red. Slices were then mounted on glass slides and observed under microscope.

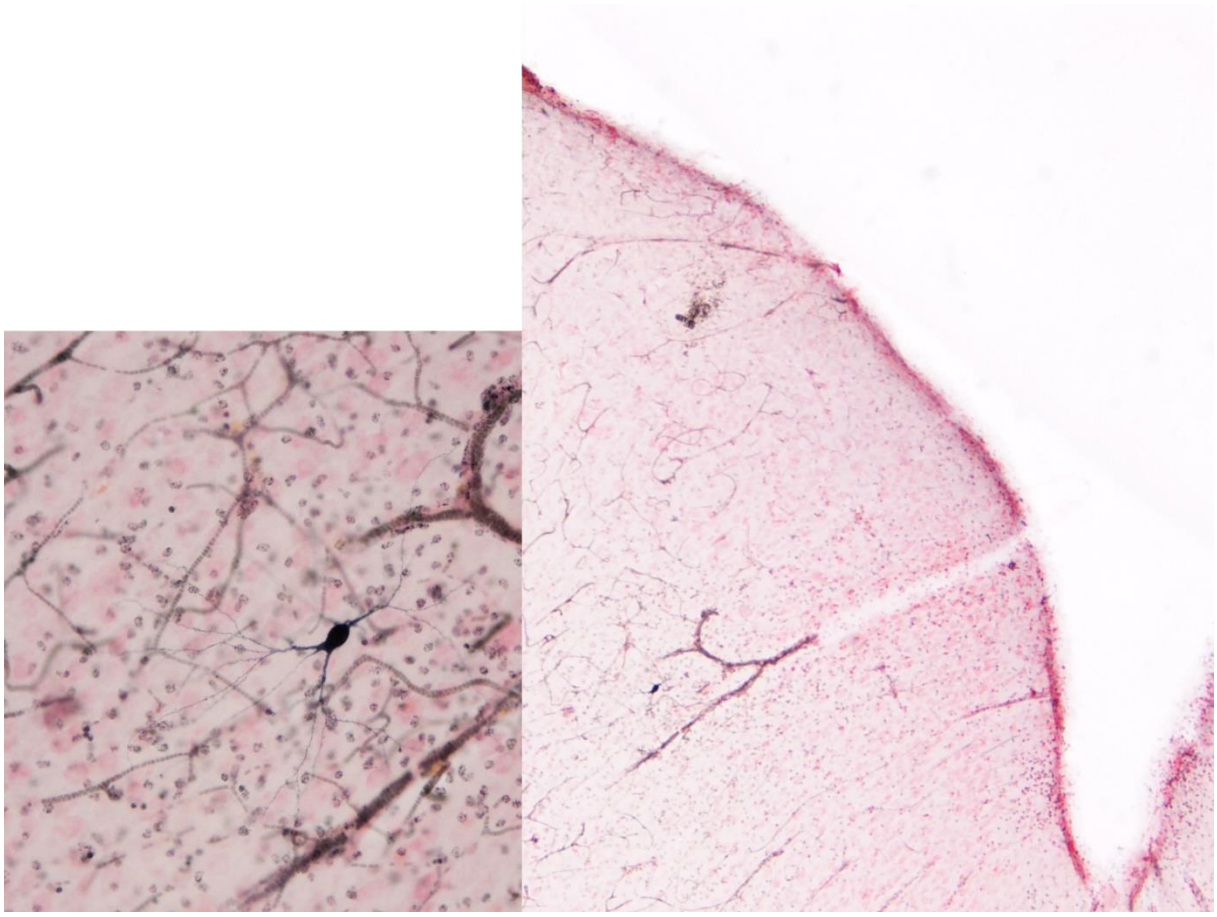

Layer 4 Spiny stellate cell stained by biocytin.

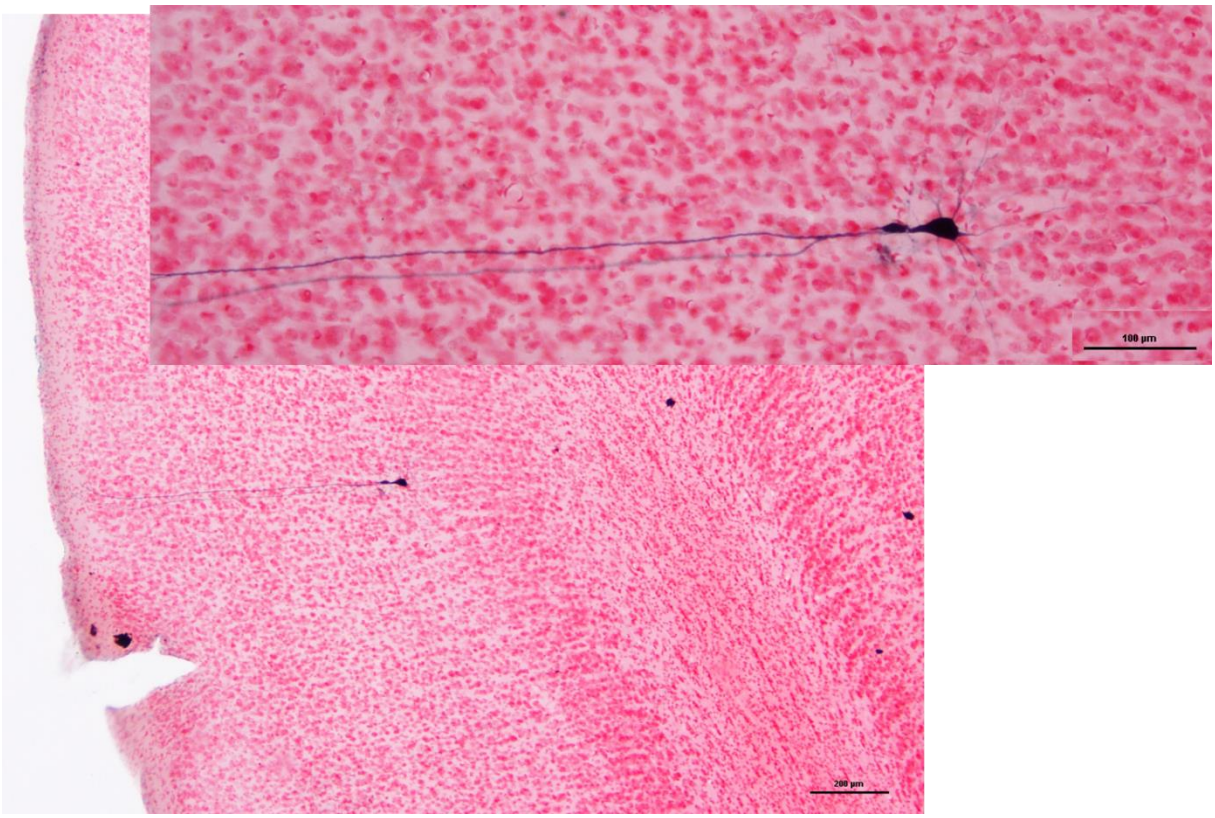

Layer 4 Spiny pyramidal cell. *Top scalebar: 100 µm; Bottom: 200 µm*

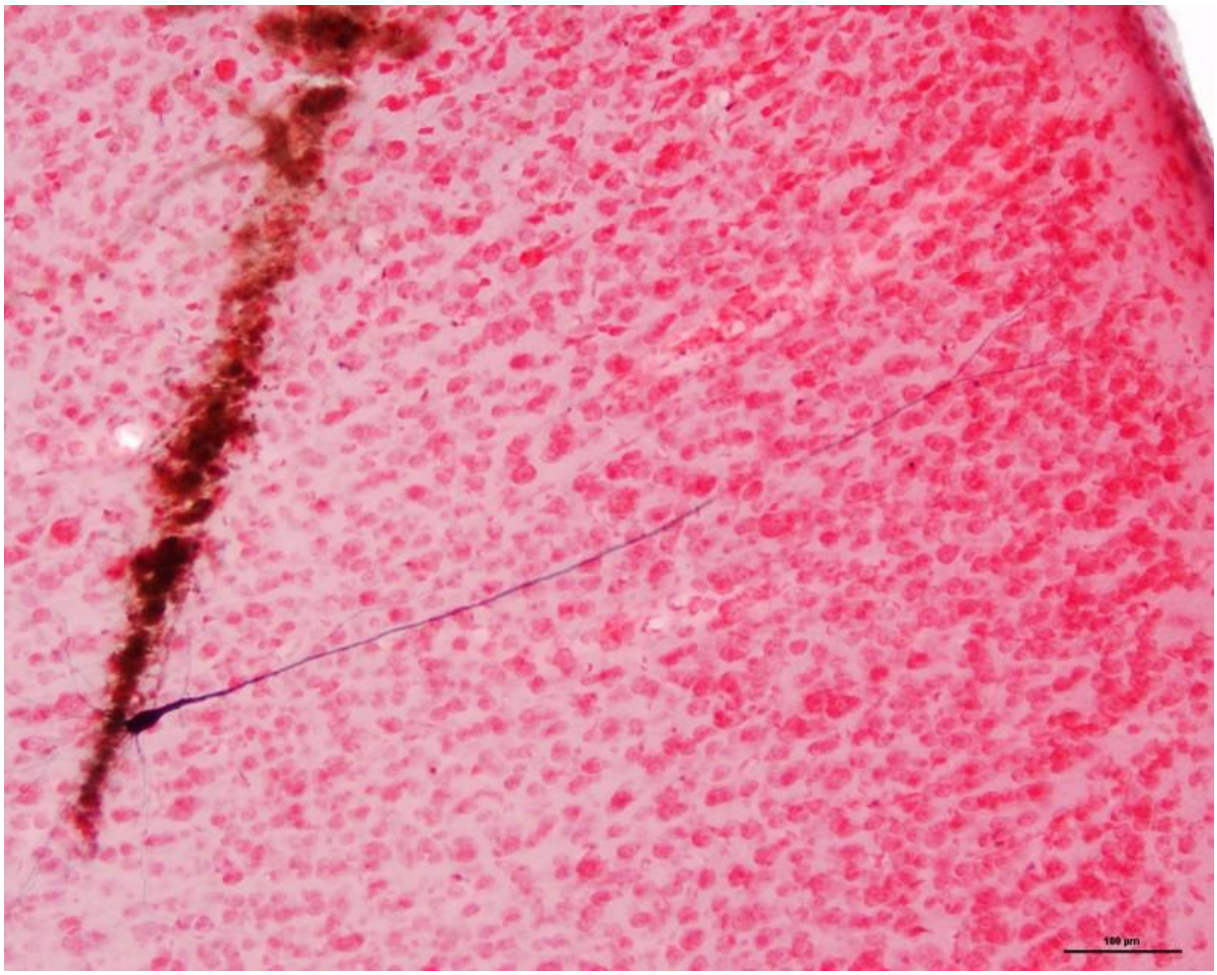

Layer 4 pyramidal cell without spines. *Right scalebar: 100 µm*

I-4.6 – Part I Assessing cells responses linear prediction

The interspersed use of apparent motion sequences with individual location stimulation allowed us to compute a linear prediction of the AM response and disentangle the respective spatial and temporal contribution of the stimulation in the emergence of our effect. To compute this linear prediction, patches of Gabor belonging to a given ring and the center alone were flashed individually at the onset of the recording. This was done during a time window of the same duration than the sequences composed of actual flows because we had no way to determine the temporal window of responses to elements flashed individually, potentially delayed due to the eccentricity of the stimulation.

Each element belonging to a spatial "unit" of stimulation (one ring or the center) was flashed at the onset of the recording and the responses to the stimulation of each of those units were averaged over the number of repetitions. This allowed us to obtain a static referential response for the stimulation of each node of stimulation. The average response for each ring or the center was then shifted in time by the duration of stimulation of a spatial unit and summed to the average responses of the other loci of stimulation. Different linear predictions were computed according to the spatio-temporal coherence of the flows to which we wanted to compare them. To do so, the direction of the shift was done according to the temporal coherence of the flows: starting by the average response to the stimulation of the 5^{th} ring of eccentricity and ending by the average of the response to the stimulation of the center for centripetal flows and in the opposite order for centrifugal ones (Figure 5.1).

The idea behind that calculus is that the recording of a time sequence composed of elements flashed individually allowed us to capture the effect of the stimulation of isolated spatial units (rings or center) and reconstruct it over time to compare it to the actual spatio-temporal sequences. We did so under the hypothesis that responses to stimulation of a given cortical locus are potentially delayed/sustained and can impact the subsequent feedforward stimulation of neighbouring cortical loci stimulated individually. By shifting and summing the average response to the stimulation of a neighbouring node, those delayed/sustained responses would sum up to the average response of the direct feedforward stimulation of a given node, allowing us to extract spatial facilitatory effects between neighbouring hypercolumns receptive field aggregates. This calculus provided us with a basis to estimate the contribution of the temporal factor in the recruitment of the periphery, only introduced during the spatio-temporal sequences.

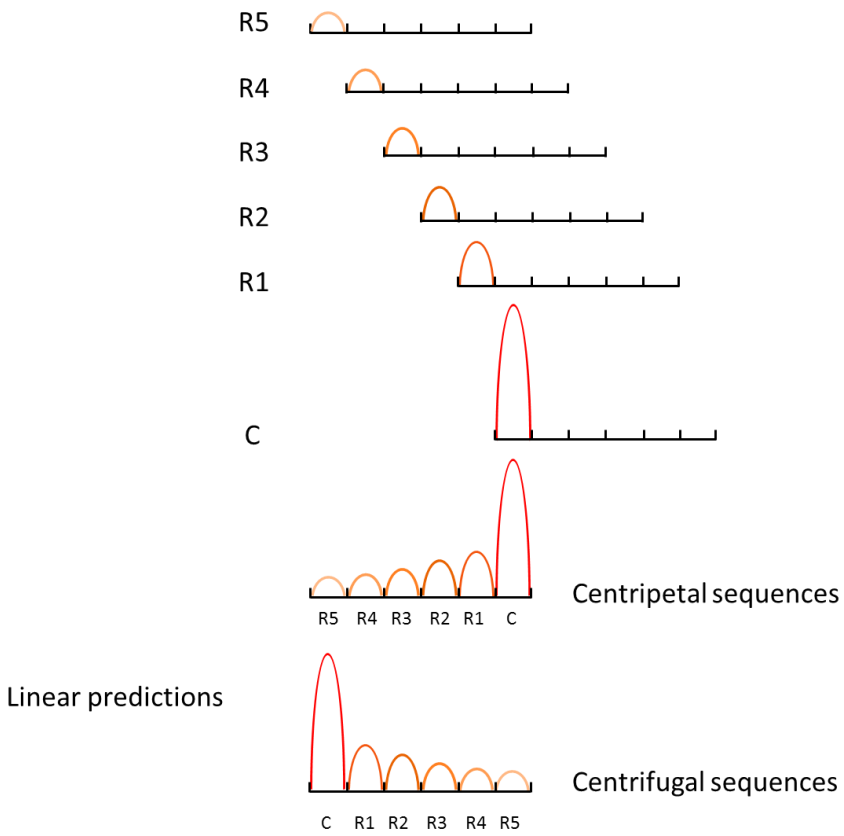

Figure 5.1: ***Scheme of the linear prediction calculus.*** *Linear predictions are calculated from the sum of the averaged responses to the stimulation of each spatial unit (each ring and the center) shifted in time by the duration of stimulation of each unit. The shift is made according to the spatio-temporal coherence of the sequence for which the linear prediction is calculated. This representation assumes that the stimulation of each of the rings (R5, R4, R3, R2 and R1) in the periphery of the receptive field evoked responses, which is not the case. Two ideas underlie the conceptual calculus of the linear prediction: the first is that the strength of the response decrease with eccentricity from the receptive field. The second is that the amplification of the strength of the response to the stimulation of a neighbouring ring comes from a facilitation of the response due to a delayed/sustained response to the stimulation of a preceding ring (R4 vs R5 for example) captured during a large time window and revealed by summation of the shifted averages. This second aspect is however not represented here for clarity purpose.*

List of abbreviations

GP: Gabor patch

AM: apparent motion

CF-ISO: centrifugal AM stimulation with Gabor elements iso-oriented (co-aligned) with the motion axis

CP-ISO: centripetal AM stimulation with Gabor elements iso-oriented (co-aligned) with the motion axis

CP-CROSS: centripetal AM stimulation with Gabor elements cross-oriented with the motion axis

RND-ISO: AM stimulation with co-aligned Gabor elements randomly positioned along the motion axis

HWHH: half-width at half-height

HHP: half-height of peak response

PSTH: post stimulus time histogram

PSTW: post stimulus time waveform

RF: receptive field

sDF: subthreshold depolarizing field

SD: standard deviation

SEM: standard error of the mean

Vm: membrane potential

I-5. Results

I-5.1 Assessing visual response significance

At the beginning of a cell recording, the contrast and flash duration of the Gabor Patch (GP) used to stimulate the RF center were set to values which gave a clear synaptic subthreshold response (above the noise level) and well below spike initiation level. Avoiding saturation allowed to stay in a dynamic range where changes in response latency potentially induced by center-surround interactions could be detected. To that end, in our experimental set, the GP contrast of the element flashed in the center was set around 0.5 ± 0,2 (ranging between 0.25 up to 1 when no visual

response was evoked for a smaller value) while the elements flashed in the surround had an average contrast of 0.9 ± 0,12 (ranging from 0,75 to 1).

Before starting our analyses, we verified that during the main protocol the response to the center-only condition had remained significantly different from the response to a blank field. Using a randomization test (as in Freeman et al. 2013), we determined the 0.5th and 99.5th percentiles of the null distribution expected at each time point due to chance (pink lines in Fig 6.1). Only cells with a response to the center-only condition outside this boundary in the interval 0-to-120 ms were considered for further analysis (response to center-only different from blank, $p<0.01$). 37 cells were retained after this verification.

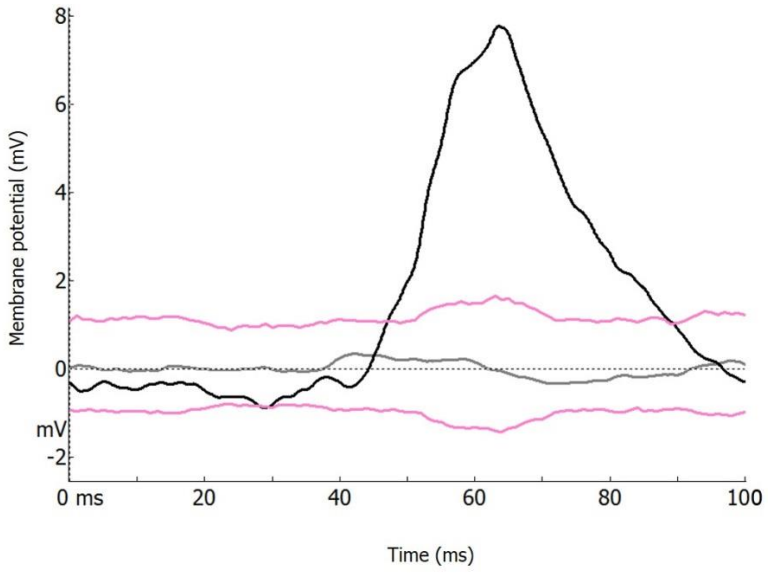

Figure 6.1 ***Statistical test of individual response significance.*** *At t = 0 milliseconds, an optimal GP whose orientation, spatial period and phase elicited the strongest response was flashed on the cell's sDF. The average synaptic potential response (n=50 repetitions) evoked by the sole stimulation of the center ("center only" condition, black trace) was then compared to the "blank response" (grey trace) during which a uniform level of luminance (no stimulation) was displayed on the screen. Lower and upper pink traces indicate the 0.5th and 99th percentiles boundaries of the null distribution difference between the two time series expected at each time by chance (randomization test, 10000 repetitions, p < 0.01).*

The second step of our analysis was to determine for each cell the latency of the response to the stimulation of the RF center alone. Indeed, cells have different latencies of evoked responses, according to the individual propagation speed of the feedforward synaptic input they receive, which may give a clue about the cell's position in the cortical network. Averaging the responses across cells without considering this fact might dilute a potential latency advance effect at the level of the population. That is why, in order to average responses obtained from different cells, we had

to define a temporal reference specific to the latency of each individual cell with respect to their temporal onset. In our hands, this relative time was defined for each individual cell as the first point in time where the synaptic response (Vm) to the sole stimulation of the center (Center-Only) deviated by more than three standard deviations (SD) from the blank condition (Figure 6.2).

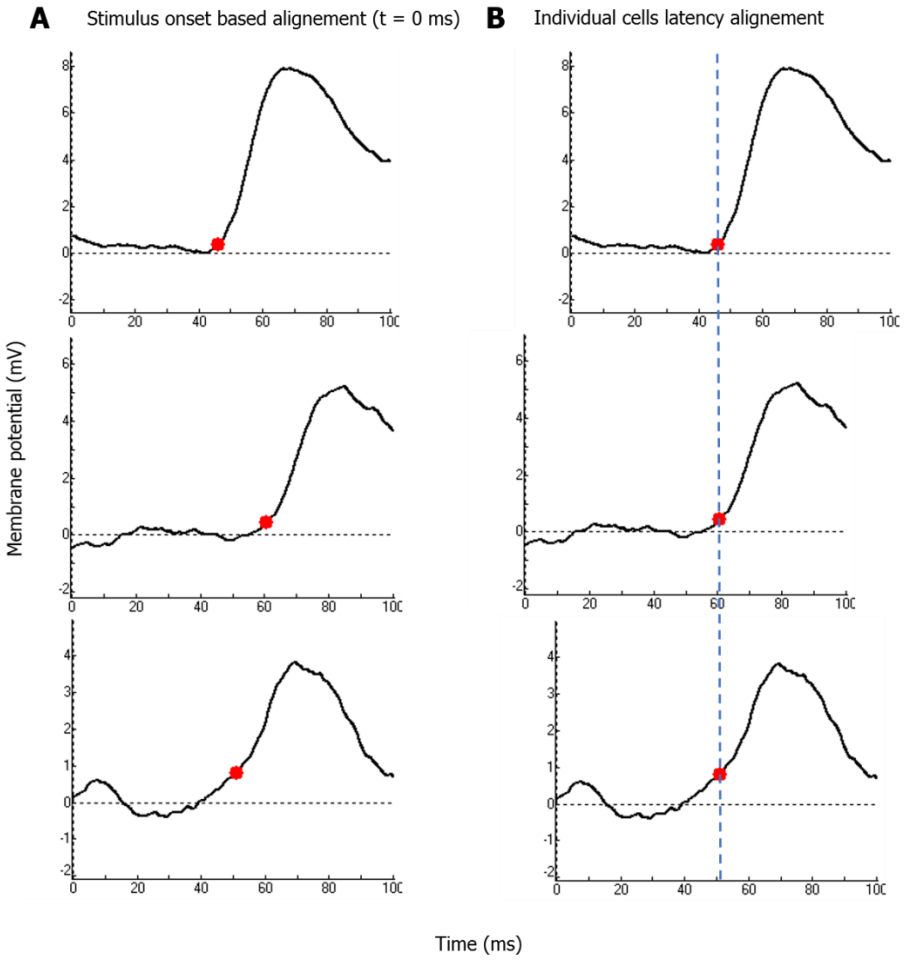

Figure 6.2 ***Determination of individual Center-Only response latencies and realignment across cells. A.*** *A set of cells taken as example for which the average PSTW of the sole stimulation to the RF center (black) is represented. Note that the latency of the center response is variable from cell to cell.* ***B.*** *To compute the population average response from individual cell's average responses and avoid a temporal smoothing, responses were realigned according to their own individual latency (red points) before averaging. The alignment of the responses with the center stimulus onset (t=0; in* ***A****) or with the onset of the Center-Only synaptic response (****B, dotted blue line****) can be compared. The red point in time represents the first point of the Center-Only response above 3 SD from the blank. Individual realignment allowed us to abstract ourselves from individual latency of evoked response although the activation profile of each depolarization remains different.*

To realign Waveforms for the averaging, the temporal reference specific to each individual cell latency was defined differentially for membrane potential (Vm) and spiking responses. On the

population of 37 selected cells, the latency of the feedforward synaptic response to the RF Center stimulation was of 44 ± 10 ms on average.

Finally, the amplitude of the evoked synaptic potential response triggered by the RF center stimulation varied from cell to cell, because of inter-cellular variability and of the GP features chosen for each individual cell. In order to compare cells, the magnitude of the membrane potential depolarizing and spiking responses of each cell was normalized to the maximal amplitude (the peak) of the response to the center stimulation that was set at 1 and average effects were computed on normalized responses.

I-5.2 Input summation during centripetal apparent motion

As detailed in our working hypothesis (chapter Part I.3 Working Hypothesis), our experimental expectation was that the presentation of a sequence of GPs iso-aligned with the motion axis, going towards the receptive field center at high speed along the cell's preferred orientation axis (i.e., CP-ISO sequence) would maximize the recruitment of lateral connectivity and result in a boosting of the recorded cell's synaptic response. This should be translated at the physiological level by a measurable latency advance.

At the level of our population (n=37), an overall boosting of the evoked response to the test center stimulus was indeed observed. Thus, the presentation of a 5 strokes AM sequence of GPs in the surround of a RF progressively recruiting a retinal sector corresponding to the gradient of orientation preference of the synaptic association field found by Gérard-Mercier et al., (2016) led to an amplification of the response compared to the test center stimulus (Figure 6.3). In addition, the membrane potential depolarization produced by the CP-ISO sequence started much earlier than the center only response (from 6 to 28 ms), resulting in a shortening of the spiking response latency. These results are illustrated for a single cell example, for which the boosting effect was seen at the membrane potential level (figure 6.3A) as a progressive build-up of the depolarization preceding the time at which the feedforward drive triggered by the center stimulation would normally occur (figure 6.3A, black trace). This resulted in most of the cells in an overall larger depolarizing response envelope.

At the spiking level, this synaptic boosting also led to a latency advance of the response and a stronger spike discharge (figure 6.3A, bottom graph). Both response boosting and latency shortening are representative of the overall effects observed on our population (Figure 6.3B).

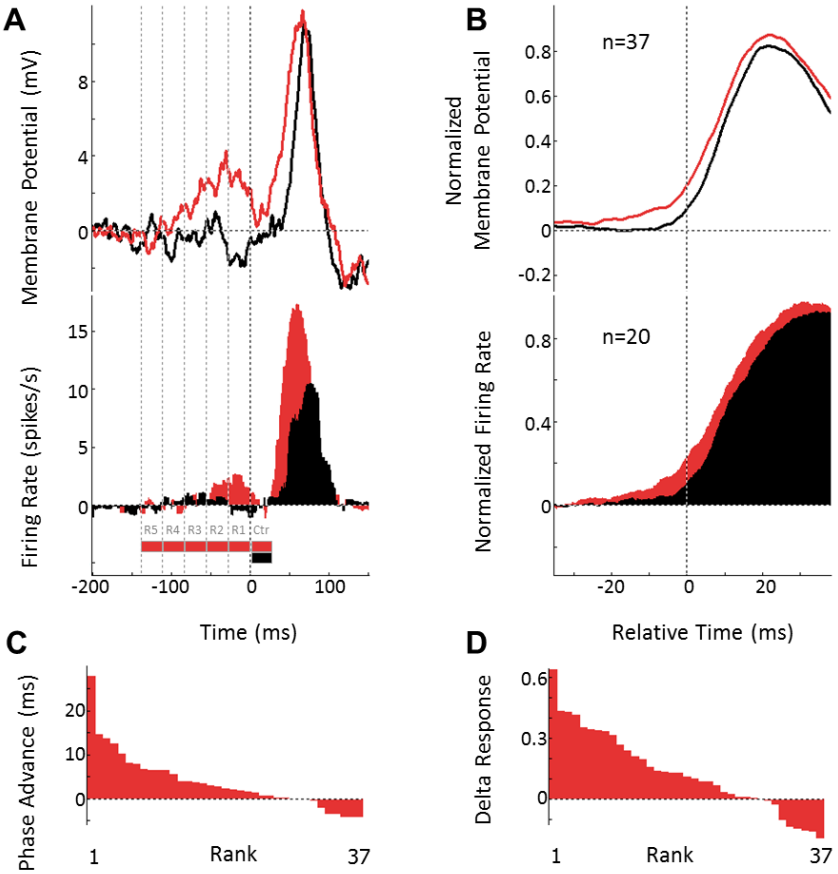

Figure 6.3: ***Boosting of the Center response induced by the CP-ISO AM sequence. A****. Individual example illustrating the boosting effect produced by Centripetal-ISO (CP-ISO) AM sequences (in red) at the level of a cell's membrane potential (top graph) and spiking activity (bottom histogram) when compared to the isolated stimulation of the RF center (black).* ***B****. At the level of the population (n=37), the CP-ISO AM sequence displayed a shortening of the Vm latency and a boosting of the average size of synaptic evoked potentials* ***C.*** *Distribution of the "Phase advance" (CP-ISO AM latency – Center-ONLY latency) of our population measured for each cell at half-height of Center-ONLY Vm peak response.* ***D****. Distribution of "Δ Gain" measured by the Vm response difference between (CP-ISO AM) and Center-ONLY for each cell at the time at which 50 % of the Vm Center-ONLY response peak was reached. In* ***C*** *and* ***D****, distributions of "Phase advance" and "Δ Gain" values measured on individual cells and ranked by decreasing order. Note the strong asymmetry where the peak effect values and the number of cells showing a latency advance and amplification of the response are much larger than those observed for cells showing opposite effects.*

To quantify those effects on individual cells of our population we choose to measure both the latency change (as a "Δ Phase") and the amplitude response variation (as a *"Δ Gain"*) at half-height of the peak (HHP) of the Center-only response. This point in time was set as an objective reference. The rationale behind this choice was to avoid measuring a part of the synaptic response that could be altered by the background synaptic noise the cell receives or by the population of spikes the cell produces, two parameters which varied from cell to cell. The average effect seen for the CP-ISO AM

condition on the population (Figure 6.3B), was seen individually for three quarters of the cells composing the population (n=37). At the population level, the latency change was on average a phase advance of 3,7 ± 0,2ms (ranging from -4 ms up to 28 ms, Figure 6.3C) and the gain change in amplitude was an amplification by 13 ± 1% (ranging from -19 to +64 %, Figure 6.3D). Note that the averaging assumes that all the cells were affected in a similar way, which clearly was not the case, as we will detail during the evaluation of individual cell significance for each of our tested conditions (CP-ISO one and controls, Figure 6.7 and 6.8).

I-5.3 Spatio-temporal coherence is necessary for binding lateral and horizontal waves

In order to demonstrate whether (or not) the spatio-temporal organization of the CP-ISO AM sequence is indeed necessary to induce a facilitatory effect on the center response, we presented visual stimulations in which the spatio-temporal structure of the GPs AM sequence was altered although keeping unchanged the stimulus energy distribution (for details see Visual stimuli design in chapter I.3). Thus, the complete experimental protocol contained three other conditions of visual stimulation used as controls that were interleaved with the coherent AM sequences in a pseudo random fashion. In a first control condition, namely the CF-ISO AM sequence (Figure 6.4, green waveform), the spatial distribution of the GPs along the preferred orientation axis of the cell was kept, but the temporal order during their presentation was reversed, resulting in centrifugal AM flow. For that condition, no effect was induced on the population average (n=37), as the rising phase of the CF-induced response was undistinguishable from the center-only response. This demonstrates that the iso-alignment of GPs is not enough in itself to induce the observed boosting effect and that some kind of anticipatory flow from the periphery is necessary to induce the effect. In a second control condition, the same retinal sector space was stimulated with the same GPs (i.e., with the same number, features, and energy distribution) but the spatio-temporal coherence of the flows was pseudo randomized. This RND-ISO condition induced an average synaptic waveform (Figure 6.4; in blue) presenting a slight facilitatory effect, but the effect was smaller than the CP-ISO facilitation (figure 6.4, Red vs Blue) and was found significant in a smaller number of cells (Figure 6.7, 6.8). In a third control condition, the 5 GPs were cross-oriented with respect to the AM axis and were presented in a surrounding region of the RF covering a retinal sector corresponding to an axis orthogonal to the preferred orientation of the cell. In that condition, GPs converged towards the RF and ended up, as in all the stimulating conditions, by an optimally oriented GP flashed on the RF center. On average, we did observe neither any latency advance nor any amplification of the response in that condition in which the visual elements are cross aligned regarding their motion axis and converge towards the RF center (figure 6.4; CP-CROSS sequence in yellow).

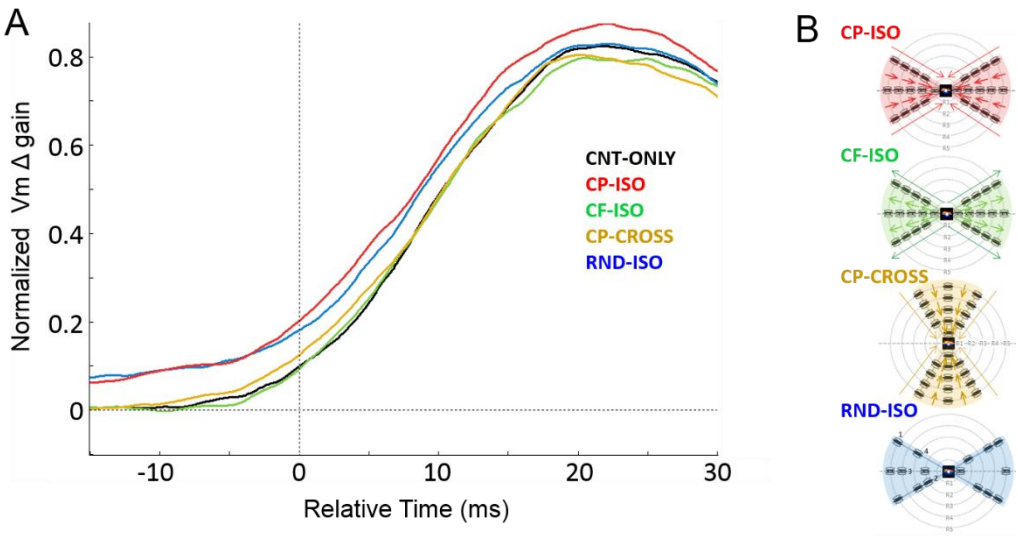

Figure 6.4: ***The boosting effect is specific to the centripetal iso-oriented apparent motion sequence.*** *To demonstrate the specificity of the synaptic boosting induced by the centripetal iso-oriented (CP-ISO, red) sequence, the entire experimental protocol contained the presentation of three other sequences used as controls. Those controls were composed of centrifugal (CF-ISO, in green) or random (RND-ISO, in blue) AM sequences or as centripetal AM of GPs cross-oriented relative to their motion axis (CP-CROSS, in yellow).* ***A.*** *Average population responses computed from the individual average Vm responses of all cells (n=37) obtained for the different conditions of stimulation.* ***B.*** *Snapshot of the different types of stimulation. Note that for all the stimulation modes, the GP flashed on the RF center was always at the preferred orientation and of low contrast. In addition, it was always flashed at the end of the sequence except for the CF-ISO sequence where it was flashed first.*

The results presented above show that, at the level of our population, there is a relative increased sensitivity to centripetal flows composed of elements iso-oriented and converging towards the RF center, presented on retinal sectors on both RF sides along the cell's preferred orientation axis. It also shows that both the spatial (local orientation of the elements) and global (direction of the motion) features of the flow's coherence interact synergistically to induce a latency advance and amplification of the response amplitude, compared to the sole stimulation of the RF center. When those conditions are gathered, a clear contextual gain control of the feed-forward response by horizontal connectivity can be seen. However, two legitimate questions remain while detailing our observations. The first one concerns the residual facilitatory effect seen on the RND-ISO response. For that case, a possible confound is the degree of pseudo randomization in the RND-ISO stimulation, mathematically limited by the small number of nodes (i.e. GP presented on each ring of retinal eccentricity) concerned in this restricted angular stimulation. Indeed, there is a small number of potential combinations letting too little place for an extensive randomization. We cannot exclude that the slight facilitation seen on average could reflect the fact that in some RND-ISO trials of the protocols, GPs were presented from time to time by chance at the R1, or even R2 eccentricity, just before the RF center stimulation, mimicking elementary CP-ISO AM-like effects. In other words, the level of pseudo randomization of our RND-ISO stimulation was probably not

sufficient and often engaged the orientation preference distribution of the RF surround described by Gérard-Mercier et al. (2016). To discard the hypothesis of remnant proximal-to-center interactions in the RND case, we set up a stimulation configuration in which the probability to find such R1 (or R2) GP followed by the RF center stimulation during the full stimulation protocol was lowered, i.e., the level of pseudo randomization was much higher. To do this, we built a "FULL" stimulation configuration in which the RND-ISO stimulation was not restricted to retinal sectors on both side of the RF but was extended isotopically to the full surround of the RF, thereby reducing the probability to obtain such random proximal-to-center interactions. It greatly increased the possible number of nodes exploration and combination across pseudo randomization trials (Figure 6.5, 6.6A). As a matter of fact, we did find that the responses induced by the FULL ISO-RND stimulation was much reduced, closer to the responses of the sole stimulation of the center (Figure 6.5, 6.6A), confirming that in the angular sector stimulating configuration, the level of pseudo-randomization was insufficient.

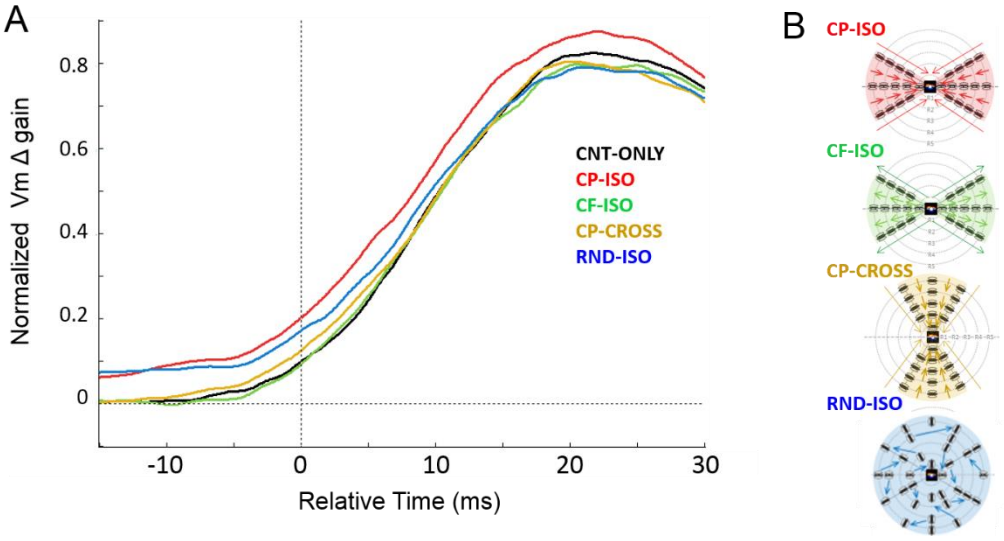

Figure 6.5: ***Comparison with random control condition with a proper degree of randomization.*** *Same Figure than 6.4, except that the trace in blue corresponds to the response evoked on average in our pool of 37 cells in the Full configuration, where the pseudo-randomization was larger. First, we can see that this blue trace is indeed much closer to the black and control ones than to the CP-ISO one in red. Second, it serves as a basis to compare responses evoked by our interest condition in the Sector and Full configurations, see the similarity of the profiles in Figure 6.6 A and B.*

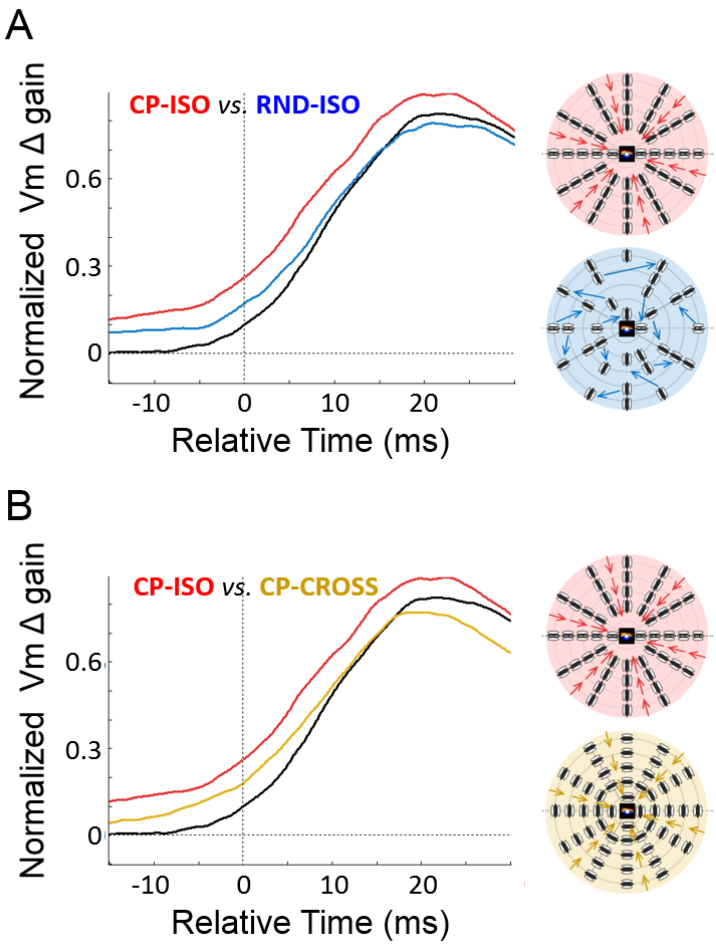

Figure 6.6: ***Isotropic stimulation of the visual field surrounding the RF.*** *As additional controls, experimental protocols also included the presentation of the different stimulation modes (i.e., CP-ISO, CF-ISO, RND-ISO and CP-CROSS) generalized in a "FULL" isotropic configuration. In these trials, the stimulation of the visual field by the GPs AM sequences were not restricted to a "SECTOR", i.e., the preferred orientation axis of the cell and its two ±30° flanking axes but were isotropically presented in the visual field surrounding the cell's RF.* ***A.*** *Comparison of the average population responses obtained from the same pool of 37 cells when presenting the FULL CP-ISO (red) and FULL RND-ISO (blue) modes with the Center-ONLY response (black).* ***B.*** *Similar comparison but for the FULL CP-ISO (red), FULL CP-CROSS (yellow) and Center-ONLY responses (black). Snap-shot on the right of the graphs are static reminders of the stimuli sequences in "FULL configuration". In all those stimulating sequences the number of stimuli and their distribution in time was kept even.*

The second question that remains concerns the result obtained in the CP-CROSS stimulation. One could indeed legitimately wonder whether our boosting effect observed in the CP-ISO stimulation and not in the CP-CROSS stimulation comes from the fact that different retinotopic locations were stimulated (Figure 6.4B, 6.5B red vs yellow). If this were the case, then we would not observe a differential effect between those latter conditions in the FULL configuration where both retinal angular sectors are simultaneously stimulated. However, we do see that the FULL CP-CROSS

condition is much closer to the response of the Center-only stimulation than to the FULL CP-ISO one (Figure 6.6B), meaning that the differential effect seen between CP-ISO and CP-CROSS AM conditions in the SECTOR configuration was not due to the stimulation of different retinotopic locations.

One may add that the effect seen with the CP-ISO stimulation is comparable between SECTOR (Figure 6.5A) and FULL configurations (Figure 6.6 A and B), since there is neither drastic amplification of the latency advance nor increase of the amplitude gain of the CP-ISO response between those configurations, despite the use of more patches of Gabors conferring more energy to the visual scene in the FULL configuration. This argues in favor for an exclusive contribution of facilitatory retinotopic regions covering the preferred orientation axis of the cell. From that result, we also conclude to the absence of excitatory-inhibitory competition between effects induced by the Gabor elements converging towards the RF center both along the preferred orientation axis and the cross-oriented (width) axis. Finally, this result emphasizes the requirement of iso-orientation of the elementary visual elements along the AM axis presented along the cell's main axis to induce the synaptic response boosting.

We already mentioned that the averaging assumes that all the cells were affected in a similar way, which is not the case. The significance of the population effect could be measured by comparing the same type of ranked distributions as in figure 6.3 C,D for CP-ISO vs CP-Cross AM sequences, or, using paired statistics, by comparing paired CP-ISO and CP-Cross value distribution (cell by cell). To that end, cells individual significance was assessed by using the same randomization test described previously ($p < 0.01$) by evaluating for each condition (CP-ISO and control ones) the proportion of cells displaying a significant latency advance or amplitude gain regarding the center only response (Figure 6.7 and 6.8). The proportion of individual cells presenting a significant latency advance and amplitude gain was always the highest for our tested condition in red (Figure 6.7), for which latency advance was on average of 11,5 ± 2 ms in the sector condition vs 16,2 ± 4 ms for the FULL configuration. On the other hand, the amplitude gain of our condition of interest is of 38 ± 3 % against 35 ± 4 % in those configurations, respectively (see Figure 6.7 and 6.8). Moreover, the significance of individual cell response to the CP-ISO condition was evaluated regarding each control condition (data not shown).

In our pool of 37 cells, for the CP-ISO condition in the sector configuration, a significant latency advance was found in 24% of our cells regarding the CF-ISO condition, 22% regarding the CP-Cross condition and 11 % in the Random condition. For the amplitude difference, results were qualitatively similar since response to the CP-ISO stimulation was significantly larger than to the CF-ISO or CP-Cross condition in 22% of cells. This proportion decreased to 8 % regarding the sector Random condition. For the remaining of the cells, no significant change was found across conditions

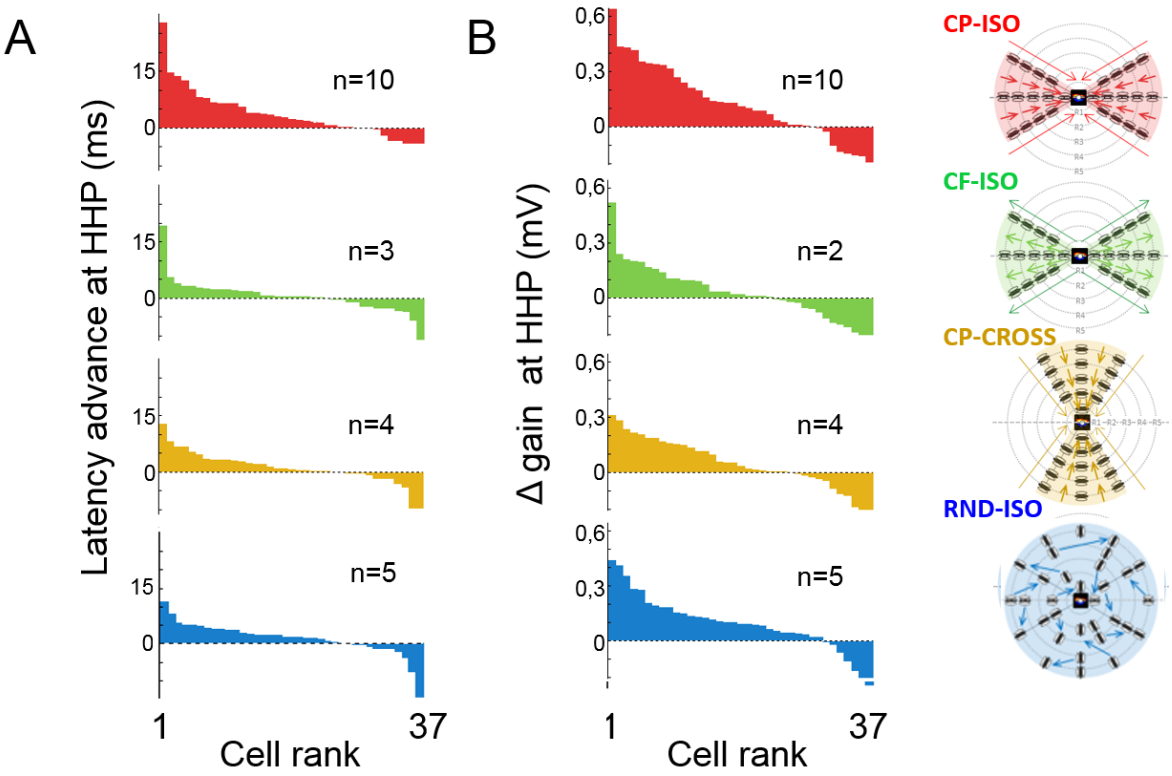

Figure 6.7 ***Ranked distributions of Latency advances and "Δ Gain". A and B*** *respectively show the distribution of latency advances and delta responses measured at the time point corresponding to half height of the peak (HHP) of the center-only response. From top to bottom the graphs correspond to individual cells differentially ranked across conditions according to their responses in the CP-ISO, (red) CF-ISO (green), CROSS-ISO (yellow) and RND-ISO (blue) AM sequences. For all the conditions, the number given in inset on the graph indicates the number of cases showing a significant phase advance (left column) or gain increase (right column) of the response of the Center-only stimulation.*

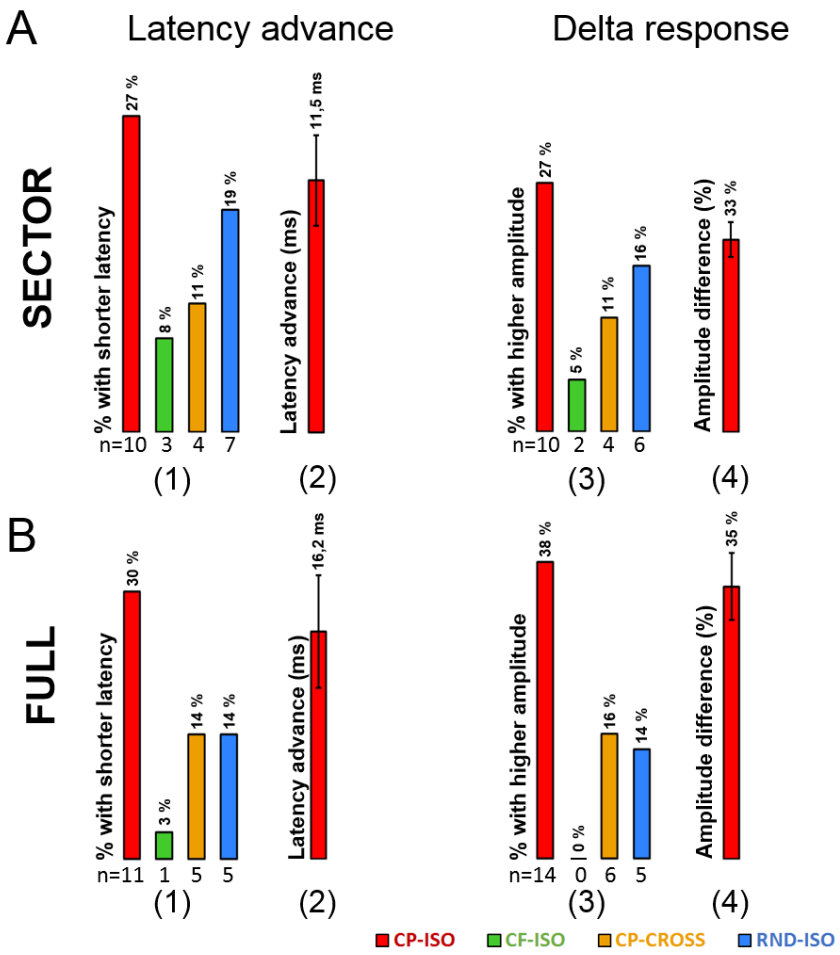

Figure 6.8: ***Statistics evaluating the significance of the amplitude and latency changes measured on the individual synaptic responses in the different stimulation conditions. A.*** *Histograms concern the measurements made on the responses obtained when the CP-ISO (in red), CF-ISO (in green), CP-CROSS (in yellow) and RND-ISO (in blue) stimulations were presented. All the statistics are expressed with respect to the Center-Only response. Four Histograms represents the proportion of cells displaying a significant latency advance (left, number 1) and the amplitude gain (right, number 3) of our different stimulations and are given for the "SECTOR" configuration (A, upper part) and the "FULL" one (B, lower part). The absolute number (n) of significant cells is indicated for each condition below each bar of the histograms. On the right of each histogram, the average latency advance (left, number 2) and response amplitude gain (right, number 4) of the subpopulation displaying significant responses are represented for our CP-ISO condition of interest (red) and expressed in milliseconds and %, respectively while error bars indicate +/- SEM.*

At the spiking level, the overall effects are quite similar although the non-linearity between sub and suprathreshold responses only allowed us to readily observe a clear latency advance and boosting of the response in the population average of the FULL configuration (Figure 6.9). In contrast with the membrane potential analysis, for which the sample population is composed of 37 cells, only 20 cells displayed significant spiking responses (with a minimum discharge rate of 5

spikes/s). This sample size is probably too small to clearly extract significant effects at the population level in the SECTOR configuration, which implies that we should increase the number of cells recorded in that condition. The “Full” stimulation condition is composed of elements ISO-aligned along the RF main axis combined with elements CROSS-aligned along an axis orthogonal to it. One could argue that the contextual gain that we visualize for the FULL configuration could come from a facilitatory effect of the retinal flows composed of elements ISO-aligned regarding the motion axis but presented on the retinal sector along an axis orthogonal to the main axis of individual receptive fields. Although we did not test separately all sector configurations to exclude that possibility, it is unlikely that the contextual gain effect stems from the particular orientation of the elements added in the retinal sector stimulated during the FULL configuration compared to the SECTOR one.

Several arguments support this interpretation:

1) The contextual gain increases already seen at the subthreshold level was found only for the CP-ISO condition presented in the angular sector corresponding to the main axis of RFs.

2) Previous results from the lab specifically showed that the static spatial sensitivity along an axis orthogonal to the main one is weakly orientation biased, compared to the main axis (Figure 3C in Gerard-Mercier et al, 2016).

3) Using 2 stroke-AM in the RF surround, Gerard-Mercier and colleagues tested the sensitivity of motion integration along an axis orthogonal to the main one and specifically showed that at high speed, there was no specificity for centripetal flow integration along that axis, whatever the orientation of the Gabor elements (ISO- or CROSS-) relative to the motion path.

Consequently, latency advance and response amplification seen at the spiking level for our CP-ISO condition in the FULL configuration most likely comes from an overall increase in the visual scene energy content where more Gabor Patches converging towards the RF facilitated the preferential integration of the converging flows along the main axis of individual RFs. Additionally, the analysis of individual cells in the sector configuration revealed that there is indeed a larger proportion of individual cells displaying both a significant latency advance and amplitude gain for the CP-ISO condition (red) than for control ones (Figure 6.10), although the corresponding average latency advance and boosting response are slightly smaller than for the FULL configuration (see below).

At the spiking level, individual case significance was assessed using the same randomization test described previously ($p < 0.01$): we evaluated for each condition (CP-ISO and control ones) the proportion of cells displaying a significant latency advance or amplitude gain regarding the Center-Only response (Figure 6.10). The proportion of individual cells presenting a significant latency advance and amplitude gain was always the highest for the CP-ISO condition (in red in Figure 6.10), for which latency advance was on average of 13,8 ± 3,3 ms in the SECTOR condition vs 16,1 ± 2,47 ms for the FULL configuration. On the other hand, the amplitude gain in the CP-ISO condition of

interest is of 47,4 ± 12,4 % for the SECTOR condition and reaches a much larger value of 61,7 ± 15,9 % in the FULL configuration, respectively (see Figure 6.10). In a second step, the significance of individual cell response to the CP-ISO condition was evaluated regarding each control condition (data not shown). In our pool of 20 cells, for the FULL configuration, 10 % of the CP-ISO condition showed a significant spiking latency advance regarding the CF-ISO one, 10% regarding the CP-Cross one and 15 % when compared to the Random sequence. For the amplitude difference, results were, as for the Vm, also qualitatively similar since 10 % of our cells showed a significantly larger response to the CP-ISO stimulation than to the CF-ISO one, against 5 % for the CP-CROSS and 20 % regarding the Random condition. No opposite sign changes were found significant.

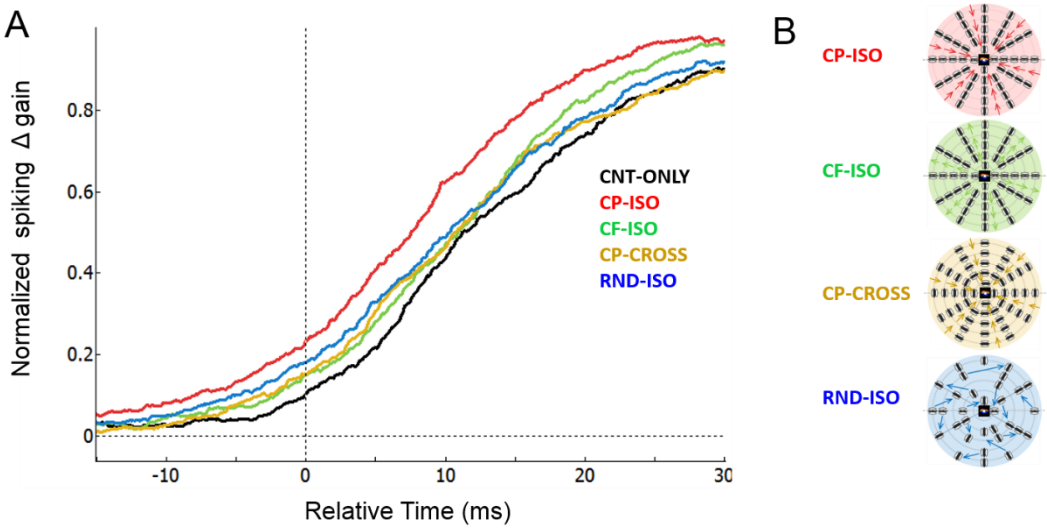

Figure 6.9: ***The spiking boosting effect reaches significance for FULL sequences of centripetal iso-oriented sequences of apparent motion.*** *Same convention as in figure 6.4, for spiking responses.* ***A.*** *Average population responses computed from the individual average spiking responses of all cells (n=20) obtained for the different conditions of stimulation. Only cells having a minimal spiking discharge rate of 5 spk/s were retained for this analysis. Latency advance and response amplification are clearly visible in the population average for our CP-ISO condition when compared to control conditions that are much closer to the response of the sole center stimulation.* ***B.*** *Snapshot of the different types of stimulation in the FULL configuration. Note that for all the tested stimulation configurations, the GP in the RF center was always flashed at the preferred orientation and of low contrast. In addition, it was always flashed at the end of the sequence except for the CF-ISO sequence where it was flashed first.*

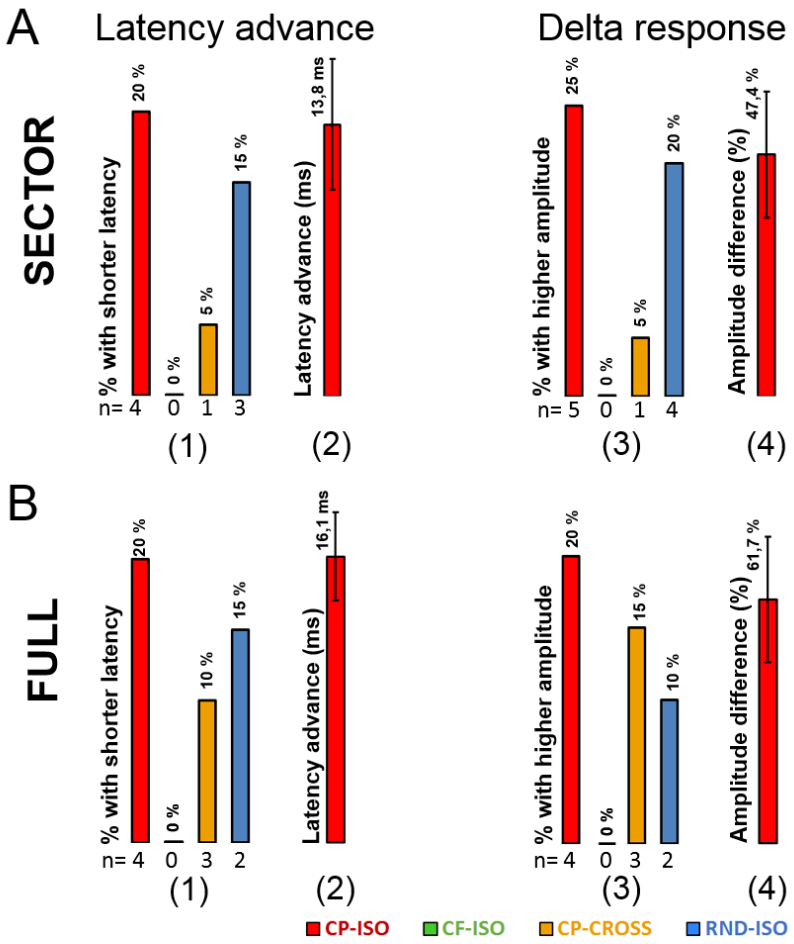

Figure 6.10: ***Statistics evaluating the significance of the amplitude and latency changes measured on the individual Spiking discharge responses to the different stimulation conditions.*** *Same convention as in figure 6.8.* ***A.*** *Histograms concern the measurements made on the responses obtained when the CP-ISO (in red), CF-ISO (in green), CP-CROSS (in yellow) and RND-ISO (in blue) stimulations were presented. All the statistics (randomization test, $p < 0.01$) are expressed with respect to the Center-Only response. Four Histograms represents the proportion of cells displaying a significant latency advance (left, number 1) and the amplitude gain (right, number 3) of our different stimulations and are given for the "SECTOR" configuration (A, upper part) and the "FULL" one (B, lower part). The absolute number (n) of significant cells is indicated for each condition below each bar of the histograms. On the right of each histogram, the average latency advance (left, number 2) and response amplitude gain (right, number 4) of the subpopulation displaying significant responses are represented for our CP-ISO condition of interest (red) and expressed in milliseconds and %, respectively while error bars indicate +/- SEM.*

The position of the recorded cell in the cortical network, its laminar location, the features of the GPs used to set the stimulation and the speed chosen for the AM sequence are as many parameters which could explain the inter-individual diversity of the observed effects. Finally, one can also note that in our hands we did not find any clear correlation neither between the latency advance nor

amplitude gain and the orientation tuning of the cells which was evaluated by 2 methods: circular variance and HHHW (half height half width of a Gaussian Fit). However, in spite of the inter-cellular variability, it appears that both the spatial (local orientation of the elements) and temporal (direction of the flow) features of the apparent motion matter, since only the combination of elements iso-oriented composing a flow converging towards the cell RF along its main axis results in a significant latency advance an amplitude gain of the response. Spatio-temporal coherence is therefore needed to bind feedforward and horizontal wave of activity in V1 where anticipatory stimulation of the far surround is the likely mechanism involved in the observed gain control and latency advance of the responses.

I-5.4 Apparent motion speed needs to match the cortical horizontal propagation speed

In additional experiments, our objective was to assess the effects of temporal interactions between visual elements presented inside and in the surround of the RF of cortical cells. The results described above, obtained with AM of GPs presented under various conditions, allowed us to define a type of AM sequence, namely the CP-ISO sequence, which was able to induce, at the cell level, a specific form of phase and gain control. The functional boosting induced by the cumulative effects of a sequence of five strokes of GPs in the surround illustrates a center-surround temporal binding process.

The presentation of an elementary visual stimulus on the retina triggers a feedforward synaptic activity in cells positioned in the corresponding retinotopic cortical area, which afterwards spreads laterally inside the cortex through intra-cortical axonal horizontal connections. It has been established (by our own lab, Bringuier et al., 1999; Gerard-Mercier et al., 2016) that the latency of the synaptic potentials recorded intracellularly increases with the relative eccentricity of the stimulus position with respect to the RF center.

Taking this into account, it is clear that the temporal characteristic of the visual GPs presentation during the CP-ISO sequence is a crucial parameter in the induction and modulation of the cell's response boosting which directly depends on the temporal interplay between the activity spreading in the V1 cortex and the feed-forward activity. Our working assumption assumes optimal boosting when the monosynaptic effects of the different surround input sources impinge on the same target cell at the same time. In our main experimental set described above (Figure 6.3 – 6.10), the speed of the AM sequence was adjusted to the characteristics of each individual cell since the response latency and strength both depends on the stroke duration (which is itself dependent on the GP contrast value) and the distance between strokes, two parameters which were specific of each cell. On average, in our pool of cells (n=37) the subthreshold RF size (s-DF), was of the order of 5° (5,07 ± 1,64°), the stroke duration was of 27 ± 9ms and the visual stimulation speed was of 189 ± 47°/sec (ranging from 100° to 312 °/s). These values fit the apparent propagation speed (ASHP) estimate

derived from the latency basin of synaptic responses (Bringuier et al, 1999; Gérard-Mercier et al., 2016). Such high velocity values, in the range of fast saccadic eye-movements in the cat, are necessary to bind in phase the various information sources recruited sequentially by our centripetal CP-AM protocols. In a subset of cells (n = 12, Figure 6.11) we were able to reduce the speed of the AM for the ISO-CP condition by several folds, and results show that the AM speed must lie within the range of conduction velocity of horizontal connectivity to bind effectively feedforward and horizontally propagated activity.

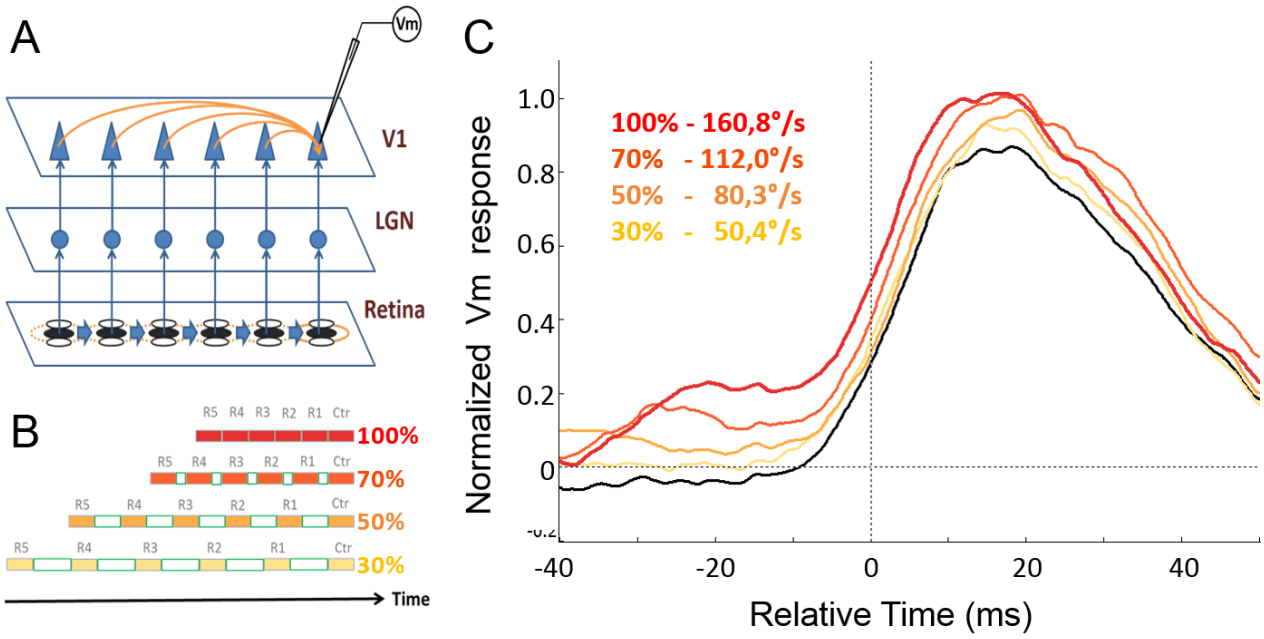

Figure 6.11: ***The boosting effect depends on the apparent motion speed of the CP-ISO sequence. A.*** *From our hypothesis the boosting effect is due to the temporal interaction between the intra-cortical horizontal spread of activity and the feed-forward synaptic input.* ***B.*** *To test this hypothesis the CP-ISO AM speed was reduced by adding a temporal delay (green boxes) introduced between presentations of individual GPs in sequences. Four delays have been tested, allowing the reduction of the test speed to 70%, 50% and 30% of the optimal speed (100%) defined for each cell.* ***C.*** *While still presenting each AM speed in a pseudo random fashion, in our population sample average (n=12) where speed was varied for the CP-ISO condition, the reduction of the AM speed from 100%, to 70%, to 50% then to 30% (respectively in red, dark orange, light orange and light yellow) led to a progressive decrease of the boosting effect on the Vm. At 30% speed there is almost no difference between CP-ISO response and the CNT-ONLY response (black).*

In order to reduce the speed of lateral connectivity's recruitment, we chose to alter the AM stimulation of the CP-ISO sequences by introducing a temporal delay between GPs strokes (Figure 6.11B). Our hypothesis predicts that facilitatory effects comes from the recruitment of lateral connectivity and are only seen when this latter is recruited in phase with its velocity conduction. Accordingly, the progressive reduction of the AM speed should gradually reduce the boosting

effect. To test for this, four speed ranges were tested on a subset of twelve cells. The speed used in our main protocol was taken as the 100% reference speed, and was lowered to 70%, 50% and 30% in a pseudo random fashion. When we compare the synaptic responses waveforms obtained for each of these speed conditions, there is a clear reduction of the CP-ISO facilitatory effect correlated with speed's reduction. The amplitude of the boosting induced with the reference speed (Figure 6.11C, red trace) co-evolves with the strength of speed reduction to disappear for test speeds lower or equal to 30% of the optimal speed (compare light yellow and black traces in Figure 6.11.C). For the particular group of cells on which the effect of AM speed was quantified, the range of optimal speed explored extended on average from 160°/s down to 50°/s. Note that in our experiments, it was not possible to test for higher stimulation speed since, an increase of the reference speed would lead to a change in the number of GPs displayed at the same time on the stimulation screen, thereby changing the peak of maximal visual stimulus energy. Taken together the results demonstrate that the speed of the retinal visual stimulation has to match the propagation speed of the horizontal connectivity in the cortex (Figure 6.11 A) to induce detectable gain and phase control of sensory responsiveness.

I-5.5 Predictive/filling-in responses

Our results suggest that the cortical activity triggered by 5 strokes GPs successively flashed outside the RF, under certain conditions, produce a build-up of anticipatory activity, leading to gain and phase control of the feed-forward response targeting the RF Center. This functional boosting is expressed by a latency shortening and amplification of the synaptic response to the Center-only stimulus. Therefore, the next step of this work has been to demonstrate that the lateral spread of intra-cortical activity induced by the AM sequence restricted to the surround does prepare the integration of the next stimulus stroke to be flashed in the RF center.

To do so, we included, in each of the stimulation conditions (CP-ISO, CF-ISO, RND-ISO and CP-CROSS), an additional protocol in which the final GP which was expected to be flashed on the RF center, was omitted. Thus, by limiting the AM sequences to 5 strokes in the surround, we could record the sole synaptic contribution of lateral influence coming from visual regions outside the sDF. Protocols containing such AM stimulation restricted to the RF surround were presented to all our cells (n=37). For about one-third of the cells (n = 12), the CP-ISO Surround-Only stimulation triggered a synaptic wave riding clearly above the noise level, indicating a process of filling-in or anticipation in the cortical retinotopic region for which the expected visual feed-forward synaptic volley was missing. For the single cell example given in Figure 6.12A, a clear membrane depolarization was seen in response to the 5 GPs sequence presentation in the Surround-Only condition (Figure 6.12A, red trace). In this case, the interaction of that lateral wave with the Center-Only response (Figure 6.12A, grey trace) led to a clear facilitation of the Center-Only response as demonstrated by the complete CP-ISO sequence where both Surround and Center were stimulated in the appropriate order (Figure 6.12A, light red trace). Nevertheless, the algebraic summation of

the two traces (Surround Only (red) + Center-Only (light grey) gives a larger expected waveform amplitude than that observed for the “full” AM sequence “Center-then-Surround” (light red trace).

To certify the existence of a substantial lateral synaptic influence in the case of each 37 cells, we looked at the significance of the Surround-Only synaptic wave using the same statistical approach than the one used to determine the individual significance of our cell’s response (randomization test, 10000 repetitions; alpha = 0.05). Due to the noisy nature of the weak amplitude “predictive” responses, we retained only waveforms for which the statistical significance threshold was trespassed for at least 15 consecutive milliseconds. 12 cells (about a third of the recorded population) showed a CP-ISO Surround-Only response significantly larger than the noise (Figure 6.12B). The average result from that population indicates that CP-ISO Surround-Only response reaches its maximum peak amplitude precisely at the predicted time of onset of the Center-Only response (had the Center-stimulus been presented). This suggests that some form of subthreshold prediction is generated within the proper temporal window to interact with the feed-forward synaptic volley (Figure 6.12B, red trace). The almost homothetic similarity in the temporal profiles of the Surround-Only and the hypothetical expected signal fully justifies the use of the term “predictive” to better characterize the “anticipatory” facilitation (Figure 6.12C). Once more, this result underlines the crucial role of the AM speed of the GPs strokes and of the concomitant corresponding recruitment and propagation of horizontal activity during the CP-ISO stimulation in the building process of the Center-response boosting.

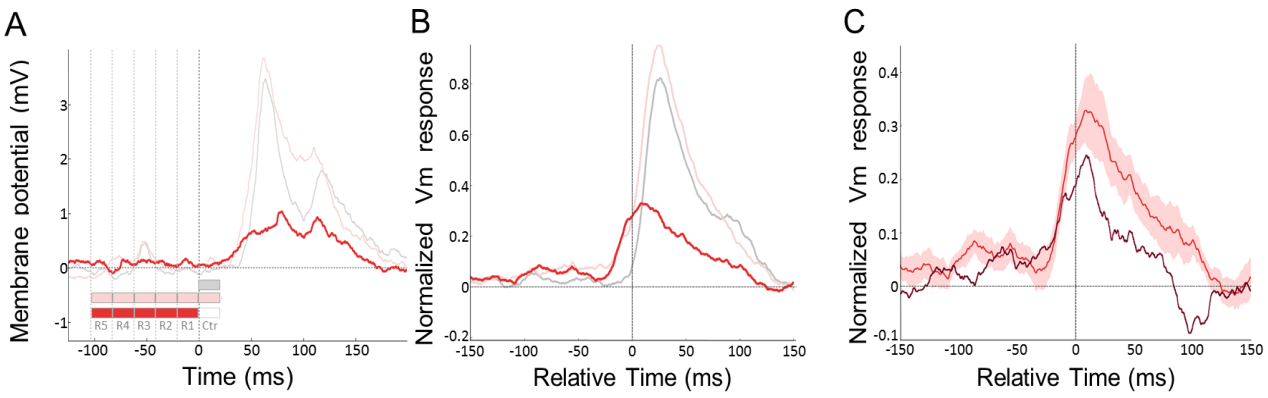

*Figure 6.12: “**Expectation” response results from the lateral spread of the horizontal intra-cortical synaptic wave. A.** Case-example, where the CP-ISO AM 5-stroke sequence restricted to the "silent surround", evokes a significant anticipatory wave (red trace). When the CP-ISO AM sequence included a 6th stroke in the RF center (shaded light red trace) a boosting of the response was observed when compared to the response given by the RF Center-Only stimulation (shaded grey trace). The relative timing of the stroke sequence composed by GPs flashed at different eccentricities (R5 to R1) in the surround or in the RF center (Ctr) is indicated by a series of horizontal filled boxes (above the absolute time axis). Color code: grey for Center-only; light shaded red for Surround-then-center and bold red for Surround-only AM sequences. **B.** Mean anticipatory response profile averaged on a subset of cells (n=12) for which the lateral synaptic wave was significant. **C.** This*

"expectation" signal can be compared with the prediction (brown waveform) given by the substraction of the Center-Only response (grey trace in B) from the complete CP-ISO AM sequence (pink trace in B). The red trace is the averaged CP-ISO Surround-Only response already shown in B (plotted with a different scale axis), with its SEM indicated by the pink area. See text for an interpretation of the down-regulation of the predictive wave during surround-center interaction.

In order to further study the complex interaction between each of the strokes in the silent Surround and, possibly, the existence of critical non-linearities between Surround and Center, we computed a series of incremental additions of elementary waves elicited by the static presentation of each individual GP. This allowed us to characterize the supra-linear nature of the build-up of the observed anticipatory wave. The comparison between the response evoked by the CP-ISO AM Surround-Only sequence (R5-to-R1) and the linear predictor (LP) obtained by summing the responses to each individual stroke gives two indications: 1) the LP incremental waveforms, hence the linear predictor based on static responses, reach rarely significance at the time where the expected stimulus (R0 GP) should be observed; In contrast, the combined dynamic recruitment of the same input sources along the AM motion axis shows a progressive build-up signal which anticipates by a few milliseconds the appearance of the feedforwad signal evoked by the Center-stimulus. 2) the AM sequence puts into play a non-linear amplification process of subliminal sources, attesting for a need of synergy in triggering an efficient horizontal propagation.

A second calculation characterizes the non-linear interaction between the Surround-Only horizontal wave and the feedforward input triggered by the last GP element of the AM sequence flashed in the RF Center. When compared with the Surround-Only response (Figure 6.12C, red), the subtraction of the Center-only response from the full AM sequence response (Figure 6.12C, brown) shows a down-regulation of the prediction given by an additive model, since this hypothetical waveform has a similar temporal profile than the Surround-only response, but with a scaling down in amplitude of 25 %.

In order to further clarify the terminology used in the interpretation of our results, we define and quantify here the "predictive" term propagated by the horizontal connectivity by the result of the subtraction between the observed response in the dynamic Surround-Only sequence and the sum of the individual static Surround-Only GP responses. This latter term, the sum of the static individual stroke responses in the periphery corresponds to the net additional feedforward input from the surround, *had there been no lateral interactions recruited by the AM dynamic sequence within the Surround*. The horizontal "prediction" due to the dynamic interaction in the AM sequence grows with the spatial synergy and temporal coherence with which the Surround is recruited. Conversely, we will define the "expectation" given by a linear Center-Surround model as the sum of the Surround-Only AM and the Center-Only responses, *had there been no proximal lateral interactions between the surround and the Center.*

We interpret these different results as supporting the hypothesis that horizontal connectivity carries a prediction about the future presence of an object in motion in the visual space. The horizontal wave input can be seen as a form of “Surround” belief broadcasted to the rest of the unstimulated cortical network. The dynamic stimulation of the Surround provides a predictive input, which, according to the predictive coding theory, can be compared with the true Centre-Only signal (had it not been omitted). If similarities between the two waveforms in their temporal profiles are found, predictive coding schema assumes in addition a down-scaling of the full AM sequence response, indicative of a redundancy reduction process (Mumford et al., 1992; Rao and Ballard; 1999). In our case, an "active" down-regulation of the expectation based on the comparison between the full AM sequence “Periphery-then-center” response that is inferior to the sum of the Surround-Only and Center-only inputs is observed when the last stroke of the dynamic AM sequence actually flashed in the RF-Center has the same features (space, time occurrence and orientation) as those propagated by the Surround-Only AM sequence. It is however crucial to precise that in our terminology and calculus, the interpretation of the down regulation is not expressed through the summation of the responses to the “Surround-only + Center-only” compared to the “Surround-then-center” responses. To the opposite, the down regulation effect is expressed through the subtraction of the “Center only” response to the “Surround-then-center” one, represented by the brown predictor in Figure 6.12 C. Because the brown hypothetical waveform is inferior to the actual “Surround only” response (red trace in figure 6.12 C), we conclude to a down regulation of the response to the full AM sequence when the RF center was stimulated. Those comparison are mathematically identical and are simply expressed in that way for representation purpose. Future studies should test the condition where the 6th stroke does not have the expected orientation, which could lead, to the opposite, to a "surprise" signal and an up-regulation of the full AM sequence response.

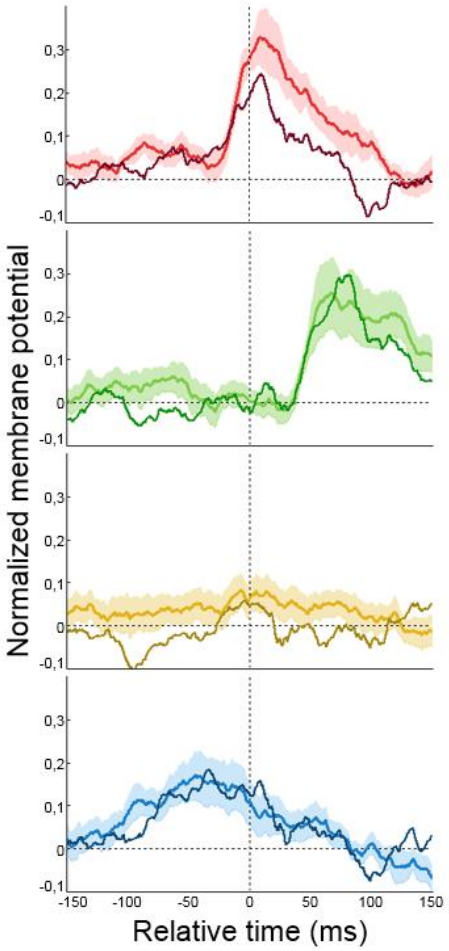

Figure 6.13: ***The predictive response is specific to the CP-ISO stimulation.*** *From the top row to the bottom row, the four graphs show the respective average of the responses induced by the Surround-Only stimulation in the CP-ISO (red), the CF-ISO (green), CP-CROSS (yellow) and RND-ISO (blue) conditions with their respective standard error of the mean (shaded color area). For each graph, the dark (red, green, yellow or blue) traces are the respective "expectation" signals computed by subtracting the "Center-only" response from the "Surround-then-Center" one. Note that the CP-ISO condition is the only one showing a noticeable non-linearity.*

As additional controls, we realized identical computations for the CF-ISO, RND-ISO and CP-CROSS conditions (Figure 6.13). When the results of these computations are compared with the Surround-only responses in all the conditions, it is clear that the down-regulation non-linearity is only readily observed in the CP-ISO condition (Figure 6.13, top graph) which further puts the emphasis on the specificity of the CP-ISO condition in producing non-linear integration of the combined horizontal and feedforward input signals. From that result, one concludes that all these cortical cells can thus be seen as able to generate filling-in or predictive responses in conditions of dynamic vision. In spite of the fact that the population sample is small, such cells did not show laminar specificity (as could be expected from predictive schema à la Rao-Ballard) and were recorded through layer 3 to 5-6.

I-5.6 Reversal of V1 neuron axial sensitivity as a function of the retinal flow speed

Since early 60's and the discovery of the orientation and direction sensitivity of the cortical V1 neurons in both carnivores and non-human primates (Hubel and Wiesel, 1965, 1968), it is well established that neurons are sensitive to elongated oriented stimuli, corresponding to the optimal orientation preference axis of the RF, and displaced at a moderate speed (0.2°/sec to 10°/sec in area 17, 5-15°/sec in area 18 (Hubel and Wiesel, 1962; Sanseverino et al., 1973; Duysens et al., 1982; Orban et al., 1981) across the width axis. Orientation and directional sensitivity axis correspond each to orthogonal axis (main axis for preferred orientation and width axis for direction preference). More recently, a new form kind of global motion sensitivity has been described for a much higher range of speed (about 180 to 350 °/s, Gérard-Mercier et al. 2016). This type of sensitivity of the cells, compatible with the detection of fast moving stimuli or with visual scene displacements during ocular movements, exists in a retinal area along the preferred orientation axis of the V1 cortical cells on one (Baudot thesis, 2006; Gerard-Mercier et al, 2016) or, more rarely, both sides of their RF.

In the present experiment, we did record few cells in order to demonstrate that both types of sensitivity to high and low speed motion could be observed in the same single V1 cell, along cross-oriented axis of its RFs: low speed preference across the width axis and high-speed preference across the orientation preference axis. We then ran a stimulating protocol in which the cell was submitted to the CP-ISO and CP-CROSS stimulations presented in both motion conditions. This allowed us to assess in the same protocol the sensitivity to high motion speed along the preferred orientation axis as well as to low motion speed perpendicular to it. As shown in Figure 6.14, we demonstrate that both types of sensitivity cohabitate in the same cell for different stimulus speeds. Consistent with the results described previously, when the motion was set to a high speed (180°/sec) the CP-ISO stimulation led to a larger spiking response than the CP-CROSS stimulation, which often was non-existent (Figure 6.14B, top row PSTH). Conversely, for slow motion speed condition (5°/sec), the spiking response triggered by the CP-ISO (Figure 6.14B, bottom row PSTH) was weaker than for CP-CROSS stimulation (the most efficient way to activate V1 cells (Hubel and Wiesel, 1962)). These observations have an important functional implication, since they suggest that V1 cells could change the orientation of their synaptic integration field as a function of the instantaneous speed of the retinal flow to which they are submitted (Frégnac, 2012). When the input spectrum contains high spatial and low temporal frequency components, V1 cells are best described as Hubel and Wiesel edge detectors. When the input contains low spatial and high temporal frequency features (for instance during blur by fast eye-movements), the synaptic integration field becomes dominated by horizontal/lateral input and V1 cells integrate motion flow along their orientation preference axis. Such a 90° flip has been observed using imaging techniques by Wei Wang and his colleagues when switching the speed from 15 to 100 °/sec (cat and monkey V1: An et al., 2014, Geisler et al., 2001 - see discussion).

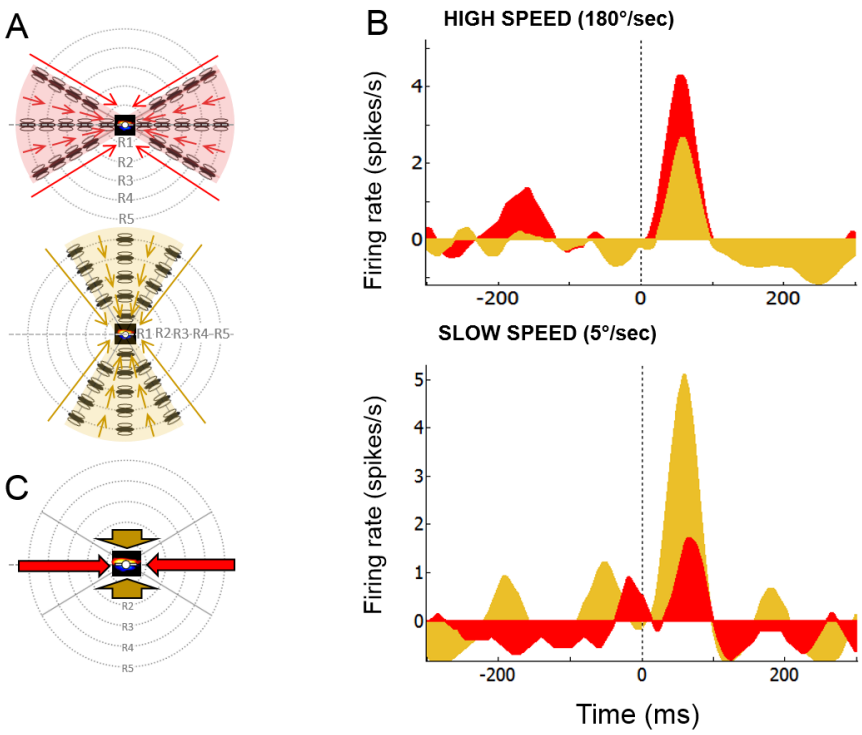

Figure 6.14: ***The same cortical V1 neuron can detect contrasted oriented edges at slow speed and co-linear motion at high speed.*** *To examine the sensitivity of a cortical neuron to various motion speeds of a visual object, the effects of the CP-ISO (red) and CP-CROSS (yellow) presented at high and very low speed were compared (**A**). **(B)** At high speed (180°/sec) the CP-ISO condition gave a larger spiking response than the CP-CROSS one. At low speed (5°/sec) the result was the opposite, i.e., the CP-CROSS was the more efficient. Note that in slow motion condition, the GP was slowly continuously displaced (5°/sec) in the surround and then flashed in the center of the RF and this, in order to prevent differential effects which could be related to the anisotropic organization of the ON and OFF sub-regions of the RF.* ***C.*** *This summary cartoon illustrates the differential spatio-temporal sensitivity of V1 neurons to local (orientation) and global (motion) features, respectively at slow (<20°) speed across the width axis (short yellow arrows) and high (>150°/sec) speeds along the preferred orientation axis (long red arrows).*

I-6. Discussion

I-6.1. General context of the findings

One of the most striking feature of horizontal connectivity's functional architecture is the spatial regularity of its patchy motifs that has been linked to the periodicity of hypercolumns at the cortical level. It is best expressed in visual cortical areas of higher mammals where geometric features (orientation, direction, spatial phase) other than retinotopy are continuously mapped on the same target structure to the contrary of rodents where visual features are organized in a "salt and pepper fashion". Most remarkably, it has been studied across various brain states spanning behavioural methods in behaving non-human primates and man combined to multiscale electrophysiological techniques ranging from intrinsic and extrinsic imaging down to synaptic studies in the anesthetized primary visual cortex of mammals.

In contrast with rodents where such long-distance binding architecture is lacking, higher mammals (tree shrew, tupaia glis, ferret, cat as well as non-human primates including the lissencephalic marmosets) appear as ideal experimental models to study the structuro-functional specificity of "horizontal connectivity" intrinsic to V1. Many reconstructed axons of pyramidal cells remaining within the grey matter have been shown to extend over several hypercolumns (up to 6-8 mms in the ferret: Bosking et al, 1997; in the cat: Kisvarday et al, 1997; Callaway and Katz, 1990; Gilbert and Wiesel, 1983; Gilbert and Li, 2012; Buszas et al, 2006; but see Martin, 2014).

Electrophysiological studies have reported that at the cortical stage, interactions between the center and the surround of receptive fields are orientation selective (Blakemore and Tobin, 1972; Nelson and Frost, 1978; Allman et al., 1985, Gilbert and Wiesel, 1990, Li and Li, 1994, Silito et al., 1995; Walker et al., 1999). Experimental evidence has refined the rigid viewpoint of spatially restricted sensitivity of receptive fields by extending stimulation of V1's RF to encroach surrounding regions having substantial modulatory effects on visual cell responsiveness whether the RF center is stimulated or not. This modulatory region has been called the Integration Field (IF; Li and Li., 1994). However, the biological substrate and functional role of those interactions cannot be simply disentangled since both suppressive and facilitatory modulatory effects of the IF have been described (cat: Jones, 1970; Blackemore and Tobin, 1972, Bishop et al., 1973; Creutzfeld et al., 1974; Maffei and Fiorentini, 1973; Nelson and Frost, 1978; 1985; Rizzolatti and Camarda, 1977; Hammond & Mackay, 1981; De Valois et al*.,* 1985; Gilbert and Wiesel, 1990; DeAngelis et al., 1994; Sillito et al., 1995; monkey: Miezin et al., 1982; Allman et al., 1985; De Valois et al*.,* 1985; Gulyas et al., 1987; Sillito et al., 1995; Levitt and Lund, 1997a,b, 2002).

Because of its reported anisotropic patchy aspect spanning several hypercolumns (but see discussion in Chavane et al, 2011), horizontal connectivity has long been presented as the biological substrate of iso-preference binding in the electrophysiological and psychophysical cortical

literature. At the neuronal level, this view is supported by the peculiar anatomy bias of long-distance horizontal connections sent by supragranular pyramidal cells found consistently in higher mammals (but see Martin et al, 2014). This principle has been derived from a developmental canonical rule which posits that "who fires together (or is alike) tend to wire together" (Callaway and Katz, 1990). From a functional point of view, the preferential iso-binding of lateral connections has been associated with center-surround facilitatory effects between elements iso-aligned in the visual field. At the psychophysical level, this view corresponds to the perceptual "association field" concept, developed by Field, Hess and their colleagues in the nineties (Field et al, 1993). This concept assumes the facilitation of collinear and, to a lesser extent, co-circular spatial integration of oriented contrast edges. This elegant psychophysical hypothesis accounts in humans for the "pop-out" perception of smooth contiguous path integration even when immersed in a sea of randomly oriented edge elements (Field et al, 1993) and the facilitation of target detection by high contrast co-aligned flankers (Polat and Sagi, 1995).

In spite of some pioneer attempts (Kasamatsu et al., 2010; Mizobe et al, 2001), still limited physiological data concern the synaptic contribution of the "silent" surround of the classical V1 receptive field. To a large degree, the role of long distance horizontal connectivity in influencing the response gain within the classical receptive field, and in particular in boosting it for specific center-surround stimulus conditions (Jones et al, 2010; Sillito et al, 1995; Sillito and Jones, 1996), remains an issue of debate. However, Walker et al., (1999) precisely emphasized that surround facilitation is more narrowly tuned and extensive along the preferred orientation axis of cells than surround suppression, providing the first electrophysiological description of collinear facilitation compatible with the psychophysical association field (Field et al., 1993; Hess et al., 1997). This differential sensitivity is consistent with reports that V1 surround suppression is less orientation tuned than surround facilitation in the cat (Bishop et al., 1973; Maffei and Forentini, 1976; Polat et al., 1998; Walker et al., 1999), in the alert (Knierim and Van Essen, 1992) and anaesthetized macaque (Nothdurft et al., 1999).

In the cat, Mizobe et al., (2001) found that concomitant stimulation of some V1 RF with neighboring flankers of the same orientation along their main axis could evoke facilitatory effect up to 12-15° in the periphery. Studies of the same group (Chen and Kasamatsu, 1998; Chen et al., 2001) confirmed and largely extended those findings by describing similar facilitatory effects at high central target and collinear flanker contrast, phenomenon that they termed expansive facilitation. Those findings concord with more recent studies in the cat V1 reporting that the low contrast rate of expansion for the suppressive space is substantially lower than for the excitatory space (Chen et al., 2013; Wang et al., 2009). Moreover, primate studies in the macaque had already highlighted the existence of expansive facilitation: Kapadia et al., (1995) showed in the awake monkey that in many cells of V1, presenting a high-contrast single bar of optimal orientation in the Classical Receptive Field (CRF) resulted in facilitation when a second collinear bar at high contrast was presented outside the receptive field.

Switching from the anesthetized to the awake behaving preparation, the same group provided a definitive electrophysiological demonstration of a "neural facilitation field" (Kapadia et al., 2000; review in Gilbert and Li, 2012). These latter experiments, realized in the attentive behaving monkey, demonstrated an impressive boosting of the response gain to an optimally oriented contrast edge within the classical RF when flankers were simultaneously flashed in the "silent surround" and co-aligned along the preferred orientation axis of the recorded cells. Most remarkably, Charles Gilbert and his colleagues, showed that, in order to be expressed, the co-linearity binding rule required the existence of top-down signals, present during target-attending tasks. This gain control effect was weakened by diverted attention (Li et al, 2006) and the ability to learn contour integration was suppressed by anesthesia (Li et al, 2008).

These remarkable studies gave nevertheless limited answers in terms of cortical mechanisms that could implement some form of canonical computation since they addressed only the modulatory nature of the center-surround effects, without probing the existence of a subthreshold influence. This issue has been addressed intracellularly in the anesthetized mammal by our lab over the last 30 years, and we were able to demonstrate, in the context of various stimulation protocols, the existence of long-distance propagation of visually evoked activity through lateral (and possibly feedback) connectivity outside the classical receptive field (Frégnac and Bringuier, 1996; Bringuier et al, 1999; Frégnac, 2012; Gerard-Mercier et al, 2016; Troncoso et al, 2015; Le Bec et al, present work). This propagation, initially hypothesized by Amiram Grinvald (Grinvald et al, 1994) and inferred from the synaptic echoes we recorded intracellularly (Bringuier et al, 1999), has been since confirmed in the same species by voltage sensitive dye (VSD) imaging techniques (Benucci et al, 2007; Chavane et al, 2011), which provides a direct visualization of the horizontal propagation pattern at the mesoscopic level of the V1 retinotopic map. Most remarkably, the VSD waves were found to travel at the same speed as that inferred from our intracellular recordings (0.3 m/s).

In a recent intracellular study (Gérard-Mercier et al, 2016; Frégnac et al., 2015), we demonstrated the existence of a structuro-functional bias detectable at the subthreshold level, even in the absence of attention-related signals. By averaging synaptic response properties across several tens of cells in a unified "cellulo-centric" reference frame centered on the discharge field center (i.e. realigning each cell subthreshold receptive field with a common spike-based orientation preference), we found a coherent spatial organization of visual synaptic responses, reflecting the grouping bias of the "perceptual association field" for collinear contours (Hess and Field, 1993). This result, apparently contradictory to Gilbert and Li's failure to find the "facilitatory neural field" under anesthesia, was only seen at the population level by summation across cells. Its expression is revealed (or facilitated) here by the use of oriented Gabor stimuli, large enough to recruit by spatial summation the whole extent of the aggregate receptive field of an hypercolumn in the cat. A previous study of our lab combining VSD imaging and intracellular recordings done in collaboration with the lab of Amiram Grinvald (Chavane et al, 2011) showed that a critical threshold of spatial synergy and temporal summation has to be trespassed in order to make the weak functional impact of these long-range interactions (in the mV range) detectable. The most likely interpretation of

these recent results is that a mean-field effect (in the sense of physics) is needed to enhance a slight bias in the subthreshold impact of the synaptic connectivity intrinsic to V1.

I-6.2. Summary of the main findings

We have investigated the role of long-distance intracortical connections in form and motion processing by measuring, with intracellular recordings, their synaptic impact on neurons in area 17 (V1) of the anesthetized cat. Our study had two impacts, one confirmatory which consolidates previous findings and one more exploratory which points to a functional role of horizontal connectivity.

Indeed, by systematically mapping synaptic responses to stimuli presented in the "silent" surround of V1 receptive fields, we confirm the results of two previous studies from our lab and other authors: first, visual evoked latencies of subthreshold synaptic responses of the silent surround increase monotonously with the relative eccentricity of the test stimulus regarding the spiking discharge field center. The linear slope (delay vs eccentricity change) estimates of evoked synaptic responses is in the exact range of apparent propagation speed (ASHP) derived from the latency basin of subthreshold synaptic responses conveyed by proximal monosynaptic horizontal connections (Bringuier et al., 1999). Second, our results confirm that the linear increase in latency regarding eccentricity - corresponding to synaptic modulatory influence conveyed by lateral connections - extend beyond the proximal monosynaptic extent of this latter (Gérard-Mercier et al., 2016) by recruiting very long-distance horizontal connections extending up to 15-20° of visual angle in the periphery of V1 receptive fields.

The dominant view is that modulatory influence of a receptive field surround cannot be accounted for by horizontal connections beyond their monosynaptic extent but likely comes from more spatially extended feedback connections (macaque V1 and human: Angelucci et al., 2002 a,b; Shushruth et al., 2009, 2012, 2013; Nurminen and Angelucci, 2014). In this context, our results argue for a significant contribution and detectability of lateral influence of the “far” surround, in accordance with the findings that laterally-mediated activity extend up to 12-15°, especially along the main axis of receptive fields (cat: Mizobe et al., 2001) where expansive facilitation phenomena occur (cat: Chen and Kasamatsu, 1998; Chen et al., 2001, 2013 2014; Wang et al., 2009; macaque: Kapadia et al., 1995). Those functional effects are supported by intracellular anatomo-functional evidence of facilitatory extra-classical receptive field cells of the cat V1, displaying long distance horizontal connections. These observations are in contrast with the description of suppressive extra-classical receptive fields that do not present long-distance axonic arborization plexus (Song et al., 2010, for an extensive review, see General introduction).

Third, we also confirm the previous report of Walker et al., (1999) of influences originating from particular end-zones of the RF. However, in contrast to the predominance of suppressive interactions in Freeman’s group studies (Walker et al, 1999; 2000), our work and that of Gerard-

Mercier et al., (2016), refine the notion that depolarizing facilitatory subthreshold responses to oriented stimuli flashed in isolation in the non-spiking surround exhibit a geometrical organization around the preferred orientation axis mirroring the psychophysical “association field” for collinear contour perception.

The novel part of our study concerns the dependency of the gain control effect exerted by horizontal connectivity on spatial and temporal synergy built within the surround: by increasing the number of elementary strokes in the AM sequence, we increased the postsynaptic efficiency of the delayed association protocol initially designed by Gerard-Mercier, i.e leading to a predictive control of the spiking discharge. This finding is important since the two-stroke apparent motion of Gerrard-Mercier and colleagues provided evidence for subthreshold amplification of an existing synaptic response. We organized our stimulation designs to delineate the protocol potentially the most efficient to trigger a significant discharge increase. This protocol corresponded to centripetal apparent motion stimulus sequences, originating from the far periphery and converging towards the RF center along its preferred orientation axis. This axis is precisely the one reported by Gerard-Mercier et al., (2016), for which horizontal and feedforward synaptic inputs summed in-phase, resulting dominantly in facilitatory non-linear interactions at saccadic-like speeds.

Finally, the strongest impact of our study introduces the notion that perceptual filling-in, whose neuronal correlate is generally described in the electrophysiological literature as a completion phenomenon of static stimuli inducing the propagation of activity invading a retinotopically unstructured area (review in De Weerd, 2006), can be extended to the propagation over cortical space and time of a prediction signal travelling through the V1 network (“network belief” in Frégnac, 2012). When the local features (orientation of the elements regarding the motion axis) of a visual scene compose a flow whose global (spatio-temporal coherence) dynamic converges towards a V1 RF target cell along its “dynamic association field”, predictive filling-in responses are observed in the absence of direct feedforward stimulation. By maximizing the recruitment of the periphery in an apparent motion paradigm, our results shade a new light on a potential generalization of the progressive build-up and diffusion over space and time of predictable information. More precisely, in the context of the Hierarchical Predictive Coding hypothesis, we show that the anisotropic congruency of individual elements embedded in a coherent motion flow is crucial to diffuse a prediction, suggesting that V1 possesses its own mechanism to solve the motion extrapolation problem.

I-6.3 Gain control during centripetal apparent motion

The working assumption of our group is that the implementation of Gestalt’s psychological laws of perceptual binding requires an intra-V1 stimulus-driven bottom-up process combined to lateral diffusion of information, which operates *even in the absence of attentional modulation.* The results of Gerard-Mercier et al., (2016) in the anaesthetized cat V1 first provided a detailed description of

the orientation sensitivity distribution of the surround by using static stimuli flashed in isolation at different orientation in the surround of receptive fields. This paradigm first confirmed that the synaptic description of the surround orientation sensitivity mirrors the perceptual association field described in psychophysics (Hess, Hayes and Field, 1993).

Second, it showed that the geometric organization of orientation sensitivity forms a gradient of decreasing strength as eccentricity increases relative to the RF center. Using a 2-stroke apparent motion paradigm, the results of Gerard-Mercier and colleagues also highlighted the existence of a cooperative mechanism between feedforward and lateral connectivity favouring the integration of flows composed of elements iso-oriented regarding the motion axis and converging towards the RF center along its main axis.

In the present study, our results highlight that the conduction properties and the anatomical specificity of V1 intra-cortical horizontal connectivity allow to infer precise spatiotemporal constraints on cell responsiveness. Maximizing the recruitment of horizontal connections by using 5 strokes in the surround before stimulating the RF center induced a detectable latency advance and response boosting that depended on the relative timing (imposed by the visual input pattern) of feedforward and horizontal inputs to the same V1 neuron. The implication of horizontal connectivity in our results is translated both through the anatomical specificity and conduction properties of lateral connections.

First, the boosting and latency shortening of cell's response was restricted to AM flows composed of elements iso-aligned regarding the motion axis and converging towards the cell's RF center, not only along its main axis but along the entire peripheral sector reflecting the synaptic association field described by Gérard Mercier et al., (2016). Indeed, at the anatomical level, horizontal connections axonic arborizations are elongated along the preferred orientation axis of a given cell's RF where they spread over larger distance and make more connections than along the width axis (cat: Gilbert and Wiesel, 1983, 1989; Schmidt et al., 1997a; tupaia: Fitzpatrick, 1996; Bosking et al., 1997; macaque: McGuire et al., 1991; Malach et al., 1993; Grinvald et al., 1994, squirrel monkey: Sincish and Blasdel, 2001).

Second, both response amplification and latency advance were maximum for each individual cell optimal velocity of lateral spread and progressively decreased as that reference speed was lowered to 70, 50 and 30 %, for which it was almost indistinguishable from the sole feedforward stimulation of the center. Taken together, our results reveal a clear contextual gain of sensory responsiveness where the convergence of relevant information matching the underlying spatio-temporal characteristics of V1's anatomo-functionnal architecture results in lateral broadcast of activity progressively building an anticipatory response in V1.

I-6.4 Non-linear Center-Surround spatio-temporal integration during apparent motion: the roles of spatial synergy and temporal coherence and their implication in the predictive coding hypothesis

The need to maintain an in-phase relationship between the diffusion of lateral activity and the feedforward increase in the recruitment of multiple lateral afferents to maximize synchronized horizontal inputs summation at the RF level is already highlighted by our experiments where the speed was lowered. There is a clear relationship between the AM recruitment velocity of lateral connectivity and the amplitude of boosting and latency advance effects: both decreased as recruitment departed from the optimal speed of lateral inputs propagation speed. We quantified the differential impact of the cumulative responses evoked by each ring of eccentricity flashed in isolation to the actual spatio-temporal sequences by computing a linear prediction that allowed us to directly compare the summed static spatial influence of the stimulation of the periphery to the actual spatio-temporal effect of dynamic sequences.

Our results show that the latency advance and boosting of the responses observed in actual spatio-temporal sequences recruiting the periphery before stimulating the center are large and cannot be predicted by the summed linear prediction of the elements flashed in isolation. The supra-linearity of the latency advance and boosting of cells responsiveness during dynamic sequences was only found for centripetal flows composed of elements iso-aligned regarding the motion axis and converging towards cells RFs along their main angular axis.

Altogether, those findings indicate that local (position and orientation) and global (direction) features of the AM flows interact synergistically in a supralinear fashion to generate and broadcast in the periphery of a receptive field a progressive build-up of anticipatory activity propagating along unmyelinated horizontal axons. This build-up and lateral diffusion of activity prepare the network to an expected stimulus seen when the center of the RF is stimulated. Moreover, the stimulus dependency of the effect argues for the existence, as early as V1 of a natural property of the network that facilitates the binding of form and motion when extended collinear contours are explored at high saccadic-like speed.

Our findings however go beyond the sole lateral broadcast of anticipatory response in the periphery resulting in a contextual gain when the RF center is stimulated. Indeed, in a third of our cells, the same spatio-temporal coherent stimulation pattern - restricted to the periphery (Surround-Only) and omitting the stimulation of the center - resulted in the invasion of activity filling-in the unstimulated subthreshold depolarizing field. In our search of surround-center non-linear integration of the anticipatory response, we computed a linear prediction between both dynamic sequences by subtracting Surround-Only filling responses to Surround-then-Center sequences. This calculus revealed that filling-in responses restricted to the periphery were larger in amplitude than the linear predictor. Interestingly, this result could be interpreted in two different ways: an up-regulation of filling-in responses or a down-regulation of the final impact of full AM

sequences when an additional (last) Gabor patch is flashed in the receptive field. This latter interpretation of down-regulation is in accordance with the Hierarchical Predictive Coding framework (Rao and Ballard, 1999). According to this principle, repetition of a given stimulus leads to the emergence of a prediction in higher cortical areas which in turn suppress responses to the presentation of the same stimulus via inhibitory feedback connections in order to reduce redundancy. As contextual information increases, so do the accuracy and the strength of the inhibitory modulation of the prediction on lower areas.

I-6.5 Experimental evidence of prediction influence throughout the cortical hierarchy

The predictive power of those core notions of mutual modulations lying at the heart of the model of Rao and Ballard (1999) has proven itself extremely efficient in explaining empirical electrophysiological findings that feedback connections can both facilitate and suppress firing in lower hierarchical areas depending on the content of the classical and extraclassical receptive field. In the literature of visual electrophysiology, inactivation of feedback connections at the cortical level prevents the inhibitory influence of the prediction generated in higher areas on lower ones, leading to disinhibition of responses in earlier areas when – and only when – stimuli can be predicted over multiple Classical Receptive Fields (CRF) (Bullier et al., 1996, 2001; Hupé et al., 1998, 2001 a,b)

This putative computational mechanism is illustrated in monkey experiences where cooling of area V5/MT increased single unit activity in earlier areas only when a stimulus extending beyond the Classical Receptive Field (CRF) was presented, preventing redundancy reduction. By opposition, increased activity was observed when a stimulus was only presented in the CRF (Hupé et al., 1998, 2001 a,b; Bullier et al., 2001). Similar center-surround modulations by back projections were obtained in V1 when V2 was cooled (Bullier et al., 1996). In addition, response suppression to repeated stimuli have been observed in the macaque inferior temporal cortex (Desimone et al., 1984). Neuronal activity in the same area and in superior temporal sulcus is also significantly reduced during the presentation of a learned predicted sequence of natural images, compared to unpredicted sequences (Perrett et al., 2009; Meyer and Olson, 2011).

In human, fMRI (Summerfield et al., 2008; Yi et al., 2008) and EEG recordings (Summerfield et al., 2011) have shown a reduction of activation in face-sensitive regions of extrastriate visual cortex (fusiform face area FFA) when the same face is presented in a coherent manner over time, to the contrary of angular twist, new faces or other objects that led to increased activation. fMRI activity in V1 also decreased when elements formed coherent shapes like 3-D squares when compared to separated line segments or randomly moving dots, suggesting that activity in early visual area is reduced as a result of grouping processes performed in higher areas (Murray et al., 2002; review in

Murray et al., 2004). This is crucial since this suppression in V1 activity cannot result from local adaptation because the primary visual cortex does not encode such a complex level of binding.

I-6.6 Human experimental evidence of predictive influence in coherent motion integration

The studies afore mentioned provide ample evidence for the modulatory influence via feedback connections of relatively higher cortical areas on earlier ones where contextual information (both in the spatial and temporal domain) allows to generate a prediction that is corrected and updated by the residual error messages forwarded by direct FF connections. Those experimental results are as many evidences generalizing the initial prediction/residual error mutual exchange of modulatory information (Mumford, 1992; Rao and Ballard, 1999) between distinct areas as a more general principle of information treatment spanning the overall cortical hierarchy. This computational principle has been validated for vision as well as for the auditory modality (mismatch negativity: Garrido et al., 2007, 2009; Wacongne et al., 2011).

Nevertheless, such studies do not specifically address the nature of modulatory effects in the integration of coherent motion in V1. Precisely, using fMRI, the work of Harrison et al., (2007) showed in human a relative suppression of V1 and MT responses combined to an increase in other visual areas activity to coherent motion of compound dots stimuli regarding incoherent motion. According to Harrison and colleagues, this suppression is most likely mediated by feedback connections. Similarly, relative suppression in human V1, V2, V3 and MT to coherent motion when compared to incoherent was reported (McKeefry et al., 1997; Bartels et al., 2008). In the same line of evidence, using a higher compound stimulus density, Braddick et al., (2001) found a relative decrease in V1 activity to coherent motion regarding incoherent with a relative increase throughout V2, V3 and, contrarily to Harrison et al., (2007), also in MT. Rees et al., (2001) nuanced those results by highlighting a positive linear relationship between the coherence percentage of moving dots and responses of human V2 and MT. Consequently, Harrison et al., (2007) concluded that the characterization of MT's activity relative suppression to coherent motion is not as clear cut as in V1. More recently, using fMRI and BOLD measures, Alink et al. (2010) showed a decrease in V1 activity when motion direction of stimuli can be predicted from the dynamics of surrounding illusory motion.

Those human studies enlarge the extent of the predictive coding hypothesis interpretation since they suggest that the residual error correction by low area - high area generation of a prediction down regulating expected stimuli - are not restricted to the sequential presentation of local or global full field static stimuli. To the contrary, they suggest that sequential presentation of static stimuli over several positions in space over time generalize the predictive coding framework of mutual exchange of information, as early as V1, between low and high visual cortical areas to a progressive spatio-temporal build-up of coherent motion prediction. They specifically confirm our results interpretation in the cat that only visual flows of information forming a coherent and expected motion matching the association field of V1 RFs results in a relative suppression or down-

regulation of activity, an effect that we visualize at the level of single cells receptive fields when those latter are stimulated. Moreover, our results point out to a striking similarity between human and cat integration of coherent motion flows in V1.

Interestingly, Harrison et al., (2007) highlighted that cooling inactivation of MT – such as done in Hupé et al., (1998) macaque study - reduced surround suppression in V1 to low salience stimuli, an effect that was much less pronounced for middle and high salience ones. The initial interpretation of Hupé et al., (1998, 2001 a,b) and Bullier et al., (2001) was that the relative loss in retinotopic precision of feedback projections on lower areas, say V1, compared to feedforward connections, confers a "loose" retinotopic character to feedback connections. This loss of specificity led Hupé et al., (1998) and Bullier et al., (2001 c) to suggest that feedback connections control the modulatory influence of the RF surround on the response elicited by the stimulation of the RF center.

In our results, this heterogeneity between the far and immediate periphery of a RF suggests that the higher areas down-regulation that we observe could specifically target the lateral connections in the immediate vicinity of the RF center. Thus, it is plausible that when this latter is stimulated, down-regulation partially inhibits the anticipatory activity built in the far periphery, which still results in a contextual gain when compared to the sole feedforward drive but does not reach its full potential activation because the response was predictable and therefore redundant. This latter point is important since it nuances the interpretation of coherent motion flows integration in human V1 where only a *relative* decrease to coherent motion is observed in the overall activation of the striate cortex when compared to incoherent motion. Human imaging studies did not specifically distinguish population of cells specifically sensitive to the features of coherent motion, potentially drowning the supra-linear latency advance and boosting of V1 RFs responses that we still observe, in spite of the sub-linear surround-center down regulation of predictable information.

Interestingly, in the human fMRI and especially BOLD part of the study of Alink et al., (2010), there was no differential down regulation of V1 activity at the retinotopic location of the first AM stimulus between predictable coherent apparent motion regarding incoherent one. This suggests that the predictability response down-regulation is only retinotopically located to the V1 representation of the test stimulus along the coherent apparent-motion path (Alink et al., 2010). This is consistent with the down-regulation that we observed in our findings when the center of the RF is stimulated, only once a progressive anticipatory build-up arose in the periphery and in parallel, in higher areas. However, Alink and colleagues used an apparent motion composed of bars that were orthogonal to their motion axis, which may be compared to our control condition of Gabor patches CROSS-oriented regarding their motion axis and converging towards the cell's RF. In our findings, the response to such stimulation was similar to the sole feedforward stimulation of the RF center.

Thus, the overall boosting effect that we observe in our results is probably an intrinsic and exclusive property of V1 whose small receptive fields allows the collection of multiple clues whose individual spatial and orientation features, when forming a global coherent motion flow, allows an efficient recruitment of lateral connections. This results in a supra-linear integration of motion along the

coherent path. Finally, beyond differences in motion speeds, a likely factor explaining differences between the findings of Alink et al., (2010) and ours are the presence of attentional processes in awake behaving human subjects.

Indeed, the same group than Alink and colleagues reproduced the same experimental apparent motion paradigm and asked subjects to saccade towards the expected target stimulus according to its predicted spatio-temporal location in the AM (Vetter et al., 2012). They found that in-time coherent targets presented in the right spatial position over time according to the AM clues were more often detected than out-of-time incoherent targets. They interpreted the relative decrease in detectability of incoherent targets as top-down expectation modulations that overwrote the prediction. This interpretation is in line with evidence that motion induced blindness in which static stimuli that do not fit the motion percept are overwritten by top-down motion prediction, even though the unexpected stimulus induce a stronger V1 signal (Schölvinck and Rees, 2010). In addition, the findings of Hidaka et al., (2009) where three blinking bars triggered a strong apparent motion prime that was followed by a test stimulus of two blinking bars (either consistently continuing the AM direction or blinking in the opposite one) resulted in both case in perception of coherent motion. This strongly suggests that high area attentional motion prediction may overwrite the feedforward signal which does not fit with the global apparent motion component.

In the search of the down-regulation origin of center-surround interactions in V1, Harrison et al., (2007) proposed an alternative solution to V1 down-regulation: extrastiate influence other than MT. Harrison and colleagues argue that down-regulation of V1 does not come from MT since they found relative decreased activity of both during coherent motion. Harrison and colleagues discussed that the combined results of Hupé et al., (1998, 2001 a,b), Bullier et al., (2001) in the macaque and their own findings of concomitant decrease in V1 and MT activity in human would suggest reduced center-surround effects in V1 associated with decreased MT activity. According to their view, V1 and MT have similar response profiles consistent with a low-level position in cortical hierarchy. They argue that, although MT is usually considered as a relatively high-level area, about 10% of direct LGN inputs in the macaque monkey (Sincich et al., 2004) bypass V1, leading to similar or earlier latency activation of V5 than V1 (Raiguel et al., 1989; Schmolesky et al., 1998). In this context, one might expect MT and V1 to respond similarly in some contexts where MT activity decrease might first represent a residual error suppression by supra-ordinate regions during a predictable stimulus.

In addition, given that MT receptive fields are larger than V1 (macaque: Mikami et al., 1986; Raiguel et al., 1995; 1997), the large residual error correction corresponding to a decrease in MT activity could also come from the fact that even a sparse stimulus array of coherent motion that does not activate V1 lateral connections would activate the ones of MT, leading to response suppression. On the other hand, the response enhancement that they observed in other extrastriate areas would be responsible for down-regulation of V1 activity. This view is not incompatible with observations that inactivation of V1 induces a loss of visual responses in practically all V2 neurons (Girard and Bullier, 1989) despite the presence of a strong residual activity in MT (Girard et al., 1992). According to

Bullier et al., (2001), this residual activity in MT should be able to drive V2 neurons if feedforward and feedback connections combined in a linear fashion. Moreover, this is consistent with the interpretation that larger receptive field in areas superior to V1 allow to determine the trajectory of long-range apparent motion (Angelucci and Bullier, 2003; Angelucci and Bressloff, 2006, Ichida et al., 2007). This fact, taken together with the observation that during long-range apparent motion, MT sends feedback signal to V1 (Muckli et al., 2005; Sterzer et al., 2006; Ahmed et al., 2008; Wibral et al., 2008), can be considered as a strong indication that differential activation in MT could partially drive the predictability down-regulation effect of V1 (Alink et al., 2010).

I-6.7 Filling-in as a prediction

Filling-in is often described, both in the psychophysical and electrophysiological literature, as an interpolation function of the visual brain that completes the information content of a retinotopic area devoid of any direct feedforward stimulation accordingly to the surrounding contextual information. From the studies reported in the previous section, we saw that generation of a prediction in a relatively high cortical area is not restricted to the sequential presentation of local or global static full field stimuli. To the contrary, it extends to the spatio-temporal domain, especially during the build-up of coherent motion prediction whose predictive impact targets specific retinotopic locations in human V1, according to the expected spatial position of a target stimulus presented in an apparent motion paradigm. In this context, the filling-in responses that we only observed when coherent motion flows converged towards the receptive field along its angular association field without stimulating the RF center can be regarded as an extrapolation of the V1 network under the form of lateral diffusion of predictive information.

Other experimental findings already linked temporal filling-in and predictive response: Hunt and Cavanagh (2009) showed that subjects, who followed the arms of a fast-moving clock with peripheral vision, preceded fixation of the clock by several tens of milliseconds. This process might be described as a temporal filling-in diffusion of predictive information to avoid discontinuities introduced by saccades. Other motion illusions are related to this temporal filling-in: movement into the blind spot is extrapolated in its expected retinotopic location even though this latter does not receive any feedforward information (Maus and Nijhawan, 2008). Those predictions are described as being adjusted forward in time (Vetter et al., 2012) and a classical demonstration of this forward prediction adjustment is the flash lag illusion (Nijhawan, 2008).

Our results nuance the findings of Liu et al., (2004) who concluded that apparent-motion-induced filling in activity does not occur in V1 but only in area MT of human. Using fMRI in an apparent motion paradigm composed of two annuli flashed in adjacent spatial positions, Liu and colleagues found that the activity evoked in the retinotopically unstimulated central annular position of their paradigm evoked very reduced activity in V1. In their study, the level of V1 activation was undistinguishable from responses to the two annuli flashed simultaneously, in opposition to MT

where large activity was evoked. To the contrary, smooth continuous motion evoked stronger activity in V1 than the two annuli flashed simultaneously. The authors claimed to have “conducted the definitive test of the filling in hypothesis in lower retinotopic area”, highlighting that it does not occur in V1 but in MT.

First of all, the latency of activation seen in their results, due to the Bold signal features range from 2-17 seconds and cannot be related to our electrophysiological measurements. They cannot account for the speed of an actual propagating wave of activity carrying apparent-motion-related filling-in activity but resemble more to a delayed-and-sustained activation of cortical area that is probably linked to the long duration of the flashed stimuli (200 ms each) and the types of signals used to quantify cortical activity. Second, the speed of their apparent motion paradigm was on average of 40°/s, a speed well below the minimal speed required to induced long range peripheral apparent motion (60-240°/s: Jung and Spillmann, 1970) and largely inferior to the one that we used in our cat intracellular experiments. Third, they only used two compound stimuli, which, according to our 5-peripheral strokes paradigm, is not sufficient to maximize the recruitment of laterally-conveyed filling in activity. Fourth, the most crucial parameter of their work explaining that they failed to see filling-in in V1 is the lack of any anisotropic information in their annular stimuli.

In our work, the spread and efficient transmission of activity filling-in in the unstimulated receptive field requires a synergistic cooperative mechanism between the local orientation/ spatial position of the elements and their congruency within the flows direction, along the angular association field of individual cells RF. Indeed, the binding between local and global features of the AM flows must match the underlying anatomo-functional properties of V1 horizontal connections in order to visualize an effective build-up of anticipatory response diffusing as a prediction in the unstimulated retinotopic area. Without those requirements, we did not observe any filling-in responses in none of our control conditions. Especially, our control condition that resemble the most to the one of Liu et al., (2004) is the presentation of Gabor patches CROSS-oriented regarding their motion axis on rings of decreasing eccentricity forming flows that converged towards the RF throughout the entire periphery, condition for which we did not observe any filling-in response.

It therefore appears that the emergence and diffusion of filling-in predictive responses obeys very strict conditions in V1 that probably do not apply to higher visual cortical areas. It seems compatible with the hierarchical predictive coding scheme of Rao and Ballard (1999) where the effective generation of “relevant” predictions are based on learned statistical regularities of natural scenes. It is therefore plausible that different forms of predictions are generated according to the functional specialization of each cortical area. This is what our results point towards since, beyond the classical feedforward/feedback inter-area mutual exchange of information, it seems that V1 generates its own parallel prediction upon which the classical inter-area modulation intervenes. Crucially, even though we cannot exclude feedforward/feedback modulatory influence on each step of the AM sequence, our reason to believe that this prediction diffusion is exclusively intrinsic to V1 is the temporal profile of our filling-in responses that match exactly the temporal profile of the cortical synaptic activation waveform produced by “full” AM sequences terminating in the RF Center. This

strongly advocates for a common mechanism of diffusion along lateral connections and, from a broader perspective, adds a temporal dependency to the maximization of spatial anisotropic diffusion of lateral activity that is not restricted to the sole spatial domain (Chavane et al., 2011; Jancke et al., 2004).

Given our interpretation that the sublinear nature of the actual sequence stimulating the periphery before the center reflects an active-down regulation of an expected stimulus, we interpret our filling-in responses as a passive lack of inhibition from higher areas on proximal lateral connections carrying the overall anticipatory activity built in the periphery. We do not see this passive lack of down-regulation of an expected stimulus that was omitted as a residual error signaled in a feedforward fashion but as a simple reaction of the visual system that allows the prediction built in the periphery to invade the RF center, maintaining an expectation.

Our results interpretation finds some legitimacy in the theoretical modelling approach of Kaplan et al., (2013). Kaplan and colleagues first expressed the difficulty of tracking a moving object while adapting the eyes trajectory to stabilize the image on the retina. In natural circumstances, a moving object may be blurred or occluded by another one. In addition, its detectability might even be harder while a subject blink. Kaplan et al., (2013) therefore pointed out the advantage of the ability to predict the position and speed of a moving object in spite of this "blank" period reflecting the temporal loss in feedforward input updating information about the object's position in time, a phenomenon known as motion extrapolation. In their paper, they first reviewed neurophysiological evidence and modelling results of such motion extrapolation.

In the literature of motion extrapolation modelling, in spite of the use of Bayesian probabilistic inference that specifically allows the representation of uncertainty, models using such approach did not provide any neuronal substrate (Bogadhi et al., 2011; Weiss et al., 2002; Stocker and Simoncelli, 2006; Hedges et al., 2011). Other models using spiking population encoding (Beck et al., 2008); a functional principle of energy cost reduction to derive the architecture of a hierarchical predictive network (Friston, 2009; Adams et al., 2012) or a more general mean firing rate neural field (Spratling et al., 2010; Tlapale et al., 2010) successfully captured some extra-classical receptive fields effects. Notably, some of them explained some motion extrapolation related phenomena (Lim and Chloe, 2008; Nijhawan, 2008; Baldo and Caticha, 2005; Liu And Wang, 2008; Jancke and Erlhagen, 2010). However, they did not take advantage of the interest to compute neuronal spiking activity in order to both integrate the input and detect synchrony over both space and time.

Kaplan and colleagues underlined the fact that the shared property between these models is the use of a diffusive mechanism implemented by the connectivity to propagate predictive information from a local to a global scale. However, they also pointed out that even though those models accounted for some motion extrapolation phenomena, they all assume an isotropic diffusion of information in all directions. They specifically challenged this viewpoint by introducing anisotropic connections in a new model under the assumption that it is a key mechanism in the diffusion of coherent motion information.

To that end, basing themselves on the work of Laurent Perrinet (Perrinet and Masson, 2012; Voges and Perrinet, 2012), Kaplan and colleagues generated classic spiking recurrent neural networks using conductance-based integrate and fire neurons. They built an hexagonal grid model of a 100 cells inspired from primates retinotopic cortical area V1 and MT and studied the responses of their model to the disappearance of a dot in a coherent motion paradigm under three connectivity profile: random, isotropic and anisotropic. More specifically, they studied their network's response to a moving dot stimulus and assessed the network's ability to predict the trajectory of the dot when it disappeared behind an obstacle producing a blank gap in the input signal.

The rationale was that introducing anisotropic connectivity is sufficient and constitutes one of the simplest way to successfully explain motion extrapolation, in addition to be biologically plausible. Interestingly, their interpretation is that the explicit dependence of local motion signal between neighboring times and positions knowing the current speed along a smooth trajectory would cancel out incoherent features while coherent information would be enhanced. This is probably more relevant than our targeted experimental conditions as it reflects a larger statistical heterogeneity retrieved in the visual exploration of natural scenes. To the opposite, in our experiments we directly tested the local AM features anisotropic requirement in coherent versus incoherent motion trajectories and evaluated their differential functional impact on single V1 RF sensors.

The main findings of the simulations of Kaplan et al., (2013) is that, to the contrary of an isotropic connectivity network, anisotropic connections provide an efficient structural property that allows the diffusion of motion information and more importantly, solves the motion extrapolation problem when a stimulus disappears. In theirs results, this is expressed by a high performance of the anisotropic networks to maintain an activity and a high probability distribution of speed along the cortical space corresponding to the trajectory of the dot that disappeared, maintaining a prediction in spite of the lack of feedforward input. More precisely, at stimulus onset the dot is displaced over cortical space over time and the network activity increases instantaneously while the probability distribution of both space and velocity changes into a meaningful representation of motion information. When the moving dot disappears, the network activity drops immediately but the probability distribution of activity in both spatial and velocity domains decrease less dramatically, conferring a higher predictive power to the remaining activity despite its overall decrease. When the stimulus reappears, the network activity grows again until it is counterbalanced by inhibitory feedback, which can be seen as a down-regulation of predictive information diffusing a redundant and predictable information.

In our experimental design, we could not test the stimulation of a new locus in the continuity of the motion path trajectory because both sides of the receptive fields were symmetrically stimulated by centripetal flows and because we were testing the integration sensitivity of a single sensor whose spatial position was unchangeable. However, the decrease in activity preserving a relatively high probability distribution about the spatial position and velocity of the stimulus (had it not been omitted) found by Kaplan and colleagues matches in first approximation our experimental findings of activity filling-in the unstimulated RF when anticipatory build-up of activity in the periphery was

sufficiently high. Furthermore, it reinforces our interpretation that this filling-in invasion of a prediction corresponds to a natural process of information diffusion intrinsic to V1 that does not imply modulatory feedback.

On a more conjectural note, the authors specifically restrained the anisotropy of their network to recurrent excitatory connections. As themselves stated, their network is unrealistic in several ways as their primary interest was to provide a proof of concept that anisotropic connections could efficiently solve the motion extrapolation problem. Because of computational costs, their network was of a relatively small size. As they pointed out, in larger networks, similar results could be obtained with recurrent excitation working on a more local scale while long-range connections would convey an expectation signal, potentially at the subthreshold level, which is what we observed in our data. It is worth noting that one of the main limitation of their model is the use of long interconnection delays necessary in the current state of their model. While considering that anisotropic diffusion acts in motion processing networks, other neuronal mechanisms shortening the interconnection delays that they use in their model would be required to effectively perform the predictive function that they highlight. They successfully reduced the interconnection delay of their network by rendering recurrent connection spatial scale even more local.

What is interesting here is that both long interconnection delays and relatively shorter ones both allowed to capture the anisotropic resolution of the extrapolation problem, a fact that Kaplan et al., (2013) highlighted as a hint regarding the potential generalization of anisotropic spread of predictive information in motion integration. Even though the differential order of magnitude of their results is not comparable, this is not incompatible with our results where lateral connections recruitment lies in a relatively wide range from 0.05 to 0.5 m/s in our study. In addition, the values that we report here corresponds to the optimal recruitment of lateral connectivity's individual cells maximal sensitivity. The experiments in which we reduced those individual cells optimal speed showed that latency advance and boosting of the responses were still observed, although to a smaller extent, while this speed recruitment was reduced to 70 and 50 % in the same cells. Even though we did not test different speeds in individual cells filling-in responses, our experimental results provide a biological cornerstone compatible to a certain extent with the differential interconnection delays successful resolution of the motion extrapolation problem described by Kaplan et al., (2013).

Additionally, our main results of contextual gain responses resulting in a boosting and latency advance are consistent with the modelling findings of Khoei, Masson, and Perrinet., (2013) that motion-based prediction acts on a global scale as a gain control mechanism. Moreover, our findings interpretation of progressive build-up of anticipatory activity when numerous peripheral sources are recruited concord with Khoei and colleagues results that motion-based prediction only leads to the emergence of a tracking behavior when a certain amount of information has been accumulated along the motion path. Although our study is unrelated to observable behavior, it is relevant in our experimental context since latency shortening and response amplification sublinear profile suggest a down-regulation effect of higher areas when the RF center is stimulated, only once substantial

anticipatory activity was built in the periphery. Although we could not test for a potential down-regulation of other receptive fields in the periphery, the down-regulation observed when the RF center was stimulated was absent when the last GP stroke was omitted. It can be conjectured that past a certain threshold, the progressive inflation of response enhancement and prediction diffusion that we observed might facilitate the emergence of a specific behavioral tracking response following the coherent motion path in awake behaving subjects. However, as discussed before, our motion flows did not integrate any form of "noise" level. They were coherent or not, and this coherency extended to the local features of the AM. Therefore, we cannot directly compare our results to the latency of noise-perturbated temporal convergence of spatial position and velocity estimation via the eye-tracking behavioral performances of Khoei et al., (2013) simulations.

I-6.8 V1's latency advance as a neuronal correlate of psychophysical speed overestimation of co-aligned elements apparent motion

From the findings reported in this work and modelling evidence discussed in the previous section, beyond the motion extrapolation problem, the effective integration of apparent motion relies on the global coherence of this latter but also on the congruence of the elements within the flows. A simple question arises from our observation: to which extent does the orientation of the features composing an apparent motion flow influences motion perception? Up to now, we have presented arguments justifying the necessity to maintain the orientation of single Gabor patches consistent with the global flow direction. This interpretation is based on the small size of V1 receptive fields and on the peculiar organization of laterally-mediated propagation of activity between distinct Aggregate Receptive Fields (ARF), particularly well suited to the binding of form and motion as early as in the primary visual cortex. The relatively simpler and most of all, more documented properties of V1 regarding other areas, especially regarding its position in the "cortical hierarchy" argues for a relatively primitive but extended role of "primary filter" allowing to sketch a first perceptual skeleton. Prior to our work, electrophysiological studies already reported that some V1 cells respond to motion along an axis collinear to their preferred orientation (Crook et al., 1994; Geisler et al., 2001; Wörgotter and Eysel, 1989), as in MT (Albright, 1984).

At the psychophysical level, a number of studies also reported that the detectability of motion is enhanced along its direction (Alais and Lorenceau, 2002; Anstis and Rachamadran, 1987; Verghese et al., 2000; Watamaniuk et al., 1995; Werkhoven et al., 1990). Specifically, psychophysical (Löffer and Orbach, 2001; Lorenceau et al., 1993), behavioral (Masson et al., 2000) and physiological (Pack and Born, 2001) studies showed that perceived direction of moving lines depends on their relative inclination regarding the motion path. Neurons selective to the same orientation that interact through long-range horizontal connections are often co-aligned in the visuotopic cortical representation of space (Gilbert and Wiesel, 1989; Sincich and Blasdel, 2001; Ts'o et al., 1986). Under certain circumstances, horizontal connections facilitate the response of cells with similar orientation preference while they reduce their response otherwise (Gérard-Mercier et al., 2016;

Kapadia et al., 1995, 2000; Nelson and Frost, 1985). Knowing that the influence of lateral connections monotonously increases regarding eccentricity from the receptive field spiking discharge field center (Bringuier et al., 1999), those combined evidence called for the evaluation of a potential latency modulation of coherent motion integration by lateral connections.

This is what we tested in our experiments. When, and only when, the orientation of the Gabor patches is iso-aligned along the motion axis, a latency shortening and supra-linear response boosting is observed. Our results thus constitute a possible correlate, as early as V1 of the human psychophysical speed-up bias in motion flow integration: results from our lab showed that collinear sequences composed of elements iso-aligned regarding their motion axis are perceived as moving faster than cross-oriented elements AM sequences (Georges et al., 2002; modeled by Series et al, 2002; review in Series et al, 2003). The speed bias decreased as the angle between the motion axis and the Gabor patches orientation increased but was still present for curvilinear path reflecting a higher tolerance of iso-binding.

The authors already pointed out that the fine orientation tuning of the effect more likely involves V1 than MT, for which cells show some orientation tuning but with a much broader dispersion than in V1 (Albright, 1984). In addition, the anisotropic sensitivity of the speed-up effect resembles the association field (Field, Hayes and Hess, 1993) that likely reflects the perceptual counterpart of long-distance horizontal connections linking neighboring orientation preference in V1 (Gilbert and Wiesel, 1989; Kisvarday et al., 1986; Ts'o et al., 1986). As already mentioned, this binding is moreover preferentially made along cells aligned in the cortical representation of visual space (cat: Schmidt et al., 1997; Tree shrew: Bosking et al., 1997; monkey: Sincich and Blasdel, 2001). The functional impact of those connections in V1 has already been identified as facilitating the processing of static collinear aligned visual stimulations (Kapadia et al., 1995, 2000; Polat et al., 1998; Sillito et al., 1995) and dynamic ones (Gérard-Mercier et al., 2016). To the contrary, horizontal connections have been showed to reduce facilitation or even inhibit responses to elements cross-oriented regarding their adjacent distribution axis in V1 (Knierim and Van Essen, 1992; Levitt and Lund; 1997; Li and Li, 1994; Polat et al., 1998).

Crucially, the speed for which the speed-up effect was the strongest ranged from 40 to 96 °/s, while peaking at 64 °/s. If we take the magnification factor of human as superior by a factor of 3 than the cat's in parafoveal regions of V1 (cat: 1mm/1° of visual angle: Tusa et al., 1978; monkey: 2,5-3,5mm/° at an eccentricity of 2-4 ° from the area centralis: Dow et al., 1981), the speed up optimal range speed of 40-96 °/s seen in human corresponds to 120 – 198°/s in the cat. That speed lies exactly in the 100° – 300°/s that we report in the present cat study and the 64°/s optimal velocity eliciting the strongest differential speed-up effect between iso aligned and cross-aligned elements in human corresponds to 192 °/s in the cat, hence a speed of 0.19 m/s lying strikingly well in the 0.1 m/s – 0.3 m/s of horizontal connections velocity that we report here. From a broader perspective, it is consistent with previous report of in vivo horizontal connection speed measurements from our lab (cat: 0.1-0.4 m/s, Bringuier et al., 1999; monkey: 0.05 – 0.5 m/s, Grinvald et al., 1994). These speed estimates strongly emphasize the implication of lateral connections in the speed-up effect

and legitimate our findings interpretation that the latency shortening and response boosting that we observe in the cat constitute a plausible correlate in the anesthetized cat V1 of the effect seen in the awake human. This once again pinpoint a remarkable similarity between the two species under two different brain states and argues for a “pop-out” characteristic of coherent motion integration that does not require attentional processes.

Interestingly, in addition to the relative increased perceived speed of elements iso-aligned regarding their motion compared to cross-aligned ones, Georges et al., (2002) also tested for an over- and under-estimation of the two types of stimuli regarding elements devoid of any anisotropic information, serving as a basis to exclude the role of anisotropy in modulation of perceived motion latencies. Using circular isotropic Gabor blobs presented in the same apparent motion paradigm, Georges and colleagues found that the increase in perceived speed was not simply a differential effect when compared to cross-oriented elements but was also an absolute over-estimation when compared to isotropic blobs. Complementarily, cross-oriented sequences perceived speed was under-estimated. While our electrophysiological results are compatible with an over-estimation of collinear elements motion speed at high velocities, we did not find any latency lag for centripetal flows composed by Gabor cross-aligned elements. The latency response to that latter stimulation was undistinguishable from the sole stimulation of the center. This finding argues for a potential extra-striate origin of motion speed under-estimation and/or for a potential attentional modulatory process possibly mediated by feedback from higher-areas in the awake behaving condition.

Most remarkably, the boosting mechanism revealed in the present intracellular cat study confirms the computational prediction of an earlier model of our lab (Series et al., 2002). Series and colleagues provided a conceptual framework where a simple cooperative mechanism of summation between feedforward and lateral inputs corresponding to the AM stimulation of iso-aligned and collinear elements of Georges et al., (2002) results in a latency advance in V1 spiking responses while using 2 and 4 patches in the periphery (Figure 6.15). In that model, if lateral inputs arrive “too late” i.e, while the suprathreshold level elicited by the Gabor patch flashed in the center has already been crossed, there is no latency advance, something that we have already found experimentally (Gerard-Mercier et al., 2016). The same goes for lateral inputs arriving “too early” when it does not facilitate the subsequent response elicited by the feedforward stimulation of the RF center. The model of Series et al., (2002) also predicted that latency shortening could be accompanied by a response amplification, at the subliminal and potentially spiking level when the RF center is stimulated. In addition, it was expected that increasing the inter-stimulus interval between the presentation of the elements composing the flows should decrease the latency advance, which is what we observed, together with a reduced response amplification in experiments where speed was lowered by introducing longer inter-stroke intervals.

However, the intracellular study goes one step beyond spike-based modeling. In Series et al., (2002) model, the composite synaptic summation is linear at the membrane potential level. It is the change in rising phase in the composite PSP which elicits the spiking response advance. The non-

linearity of the functional effect is simply due to that of spike initiation. Experimentally, the origin of the non-linearity can be probed with more acuity. The use of intracellular recordings shows a latency shortening at the subthreshold level, and some form of non-linearity can emerge from the synaptic interaction process between FF and horizontal input. In Gerard-Mercier et al., (2016) pioneering study, the subthreshold process is linear when horizontal input just precedes FF input (within a window of 5.5 ms). Interestingly, the interaction becomes supra-linear when FF input lagged by more than 5.5 ms the horizontal contextual signal (Fig. 7 C in Gerard-Mercier et al, 2016). This observation suggested that a minimal integration time is needed to recruit non-linear voltage-dependent mechanisms recruited by horizontal connectivity, such as the persistent sodium current or NMDA receptor activation (Hirsch and Gilbert, 1991; Fregnac et al., 1996). Our own finding supports this scenario of phase advance both at the spiking and subthreshold levels, and confirms latency shortening up to several tens of ms. Such sizeable impact at the synaptic integration level should be taken into account in realistic conductance-based models of V1.

In addition, although the model of Series et al., (2002) predicts that increasing the number of GP elements in the periphery increases the latency advance, it also predicts that for a larger (> 3) number of elements the latency modulation saturates and reaches a plateau. In our experiments, increasing the number of surround strokes to 5 resulted, among the pool of cells that showed a significant latency advance, to a latency shortening reaching a maximal value of 47 ms. Although it might first seem at odds with the model's prediction, a potential explanation is that the model also predicted that extending the spatial recruitment of the periphery in the far surround should result in an increase of the range of misjudged speed and optimal speed. This is what we performed in our experiments where the periphery's recruitment extended up to 25° of visual angle. In addition, the range of modulatory effects did increase since in experiments where speed was lowered to 70% (112°/s on average) and 50% (80°/s on average) of each individual cell optimal speed, a latency advance and boosting of the response was still observed. It was although smaller than at the optimal reference speed (160°/s), that ranged between 100 and 312 °/s in our main experiments where speed was not varied (189°/s on average).

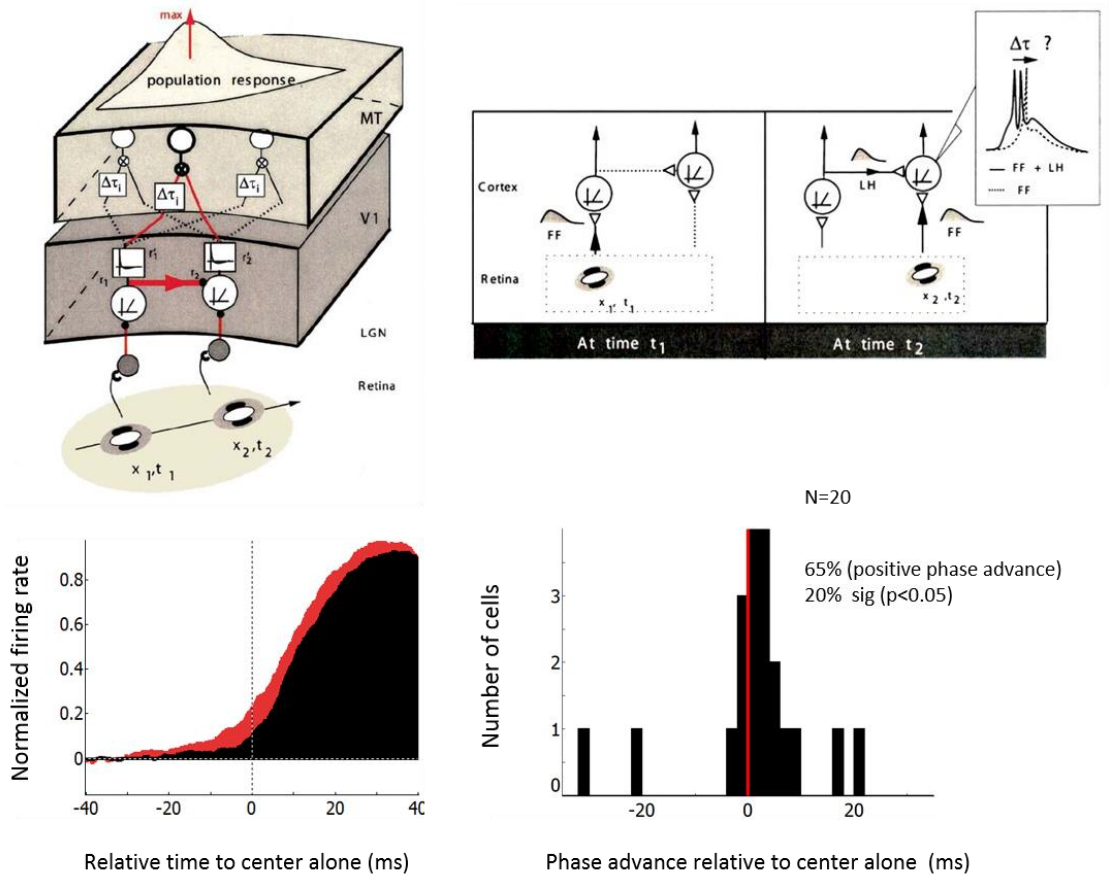

Figure 6.15: ***Model prediction and experimental confirmation that in-phase summation of feedforward and lateral inputs results in latency advance to collinear apparent motion along the preferred orientation axis of V1 cells. Upper left****: full model of Series et al., (2002) where inputs are visual sequences of varying speeds. Each element of the AM sequence is first processed in V1 by a RC circuit followed by a rectification and high-pass filter ("sandwich model"). V1 outputs then converge to MT, which consists of a large population of Reichardt correlators. The AM speed of the sequence is given by the maximally active correlator read-out. Latency advance resulting from in-phase summation of feedforward and lateral inputs in V1 biases the spatio-temporal correlation read-out of MT towards a speed overestimation.* ***Upper right****: cartoon of the model where two V1 units having the same preferred orientation and non-overlapping RFs coaligned in the retinotopic representation of visual space interact via lateral connections. The model's prediction is that the spatio-temporal coherent recruitment of a first V1 unit evokes a subthreshold wave of activity propagating along horizontal connections that lead to a latency shortening of the response to the concomitant stimulation of an adjacent RF.* ***Lower left****: population average of the spiking responses to the sole stimulation of the center (black) and to the centripetal stimulation of a V1 RF periphery-then-center by elements ISO-aligned regarding their motion axis (red) presented along the preferred angular association field of each cell.* ***Lower right****: Distribution of each individual cell latency advance of spiking responses regarding responses to the stimulation of the RF center (Adapted from Series et al, 2002).*

I-6.9 Functional shift of the synaptic integration field anisotropy as a function of the speed of the global motion flow

The pioneer work of Hubel and Wiesel (1959, 1962) highlighted the organization of receptive fields and their "edge detector" role. The maximum responses that the authors reported consisted of a strong spiking discharge of receptive fields (several tens of spikes/sec) when a bar of a given orientation was swept slowly (1-2 °/sec in area 17) from the excitatory to the inhibitory sub-zones of the recorded receptive field. The directional preference corresponded to a motion orthogonal to the preferred orientation axis of cells, i.e. to a trajectory sweeping the width axis. The orientation preference was defined by the geometric distribution of on and off sub-regions of the RF. Both observations of dynamic and static responses led the authors to conclude that the receptive fields of V1 indeed detected contrasted edges. The initial speed reported by the authors in the cat V1 RFs was cell-dependent and ranged from 1 to 10°/s. This low speed sensitivity was later confirmed by other authors: (cat: maximum response at 1 °/s: Hubel and Wiesel, 1962; 0.25 – 25°/s: Pettigrew et al., 1968; 3-10 °/s: Sanseverino et al., 1973; 0.3 -4 °/s: Duysens et al., 1982; 0.18-41°: Orban et al., 1981; monkey: 0.12-10°/s: Dow et al., 1974; 0.3 – 30 °/s: Priebe et al., 2006; 0.2- 49°/s: Orban et al., 1986).

However, Duysens et al. (1982) and Orban et al., (1981) highlighted that in the primary visual cortex of the cat, velocity sensitivity changes with eccentricity: the proportion of low-pass cell decrease as eccentricity increases while the proportion of broad-band-pass cells increases. While dividing their cat V1 cells in 3 eccentricity ranges, 0-5 °; 5-15° and 15-45°, Orban et al., (1981) found that the median optimal velocity of velocity-tuned cells in the lower eccentricity class 0-5° was 8°/s compared to 41°/s in the 15-45° eccentricity class. Nevertheless, cell still responded, although weakly, to speed up to 900°/s, with a more pronounced response at larger eccentricities. Although the very large majority of V1 cells sensitivity profile was found for very low speeds, residual responses were still observed at very high ones, for which cell proportion and response relative strength increased with eccentricity. The lowest range speed that Orban and colleagues tested (0.18°/s) closely correspond to the velocity of eye drift during fixation in the alert cat (Winterson and Robinson, 1975) while the fastest velocities tested (700°/s – 900°/s) correspond to the fastest saccades observed in the awake cat (Crommelinck and Roucoux, 1976).

Our results show that two distinct regimes of information processing occur in the cat primary visual cortex where, depending of the spectrum of the input, both the edge detector sensitivity to slow (5°/s) speed and the preferential sensitivity to fast (180°/s) motion flows composed of elements ISO-aligned converging towards and along the preferred orientation axis of cells cohabitate in the same cell. One obvious functional prediction from our findings, repeated in 37 cells, is that increasing speed motion to the saccadic range flip by 90° the motion-axial-sensitivity of V1 RFs from the classical edge detector preference for slow motion of optimal local stimuli along the RF width axis towards fast global motion of collinear stimuli along the main RF axis. It has been occasionally observed by Orban, (1984) Wörgotter and Eysel (1989, 1991) that the preferred orientation axis for

motion of a long bar and a spot is identical at slow velocities but orthogonal at high velocities where motion along the preferred orientation axis causes greater temporal summation than motion along the classical RF width axis.

Crook et al., (1994) indeed found in cat V1 that motion of a long bar evoked stronger responses along an axis orthogonal to the preferred orientation axis, while moving dots evoked stronger responses while displaced along the preferred orientation axis of cells for all velocities that they tested. This led Crook and colleagues to posit the existence of a separate mechanism between orientation and motion direction sensitivities. Our results suggest a reinterpretation of those results, since, in our experiments, the orientation of the elementary Gabor patches was crucial in the induction of latency advance and response boosting. Nonetheless, orientation tuning for the spot became sharper as velocity was increased above 25°/s up to 53 °/s, maximal speed that Crook and colleagues tested.

Geisler et al., (2001) reproduced and extended those findings by testing responses evoked by dots and gratings moving either along the preferred orientation axis of cells ("parallel" motion) or along the width axis ("perpendicular" motion), at different velocities. They found that parallel motion sensitivity dominates above 25°/s, in both cat and monkey V1. They also found that for oriented objects such as plaids, the temporal frequency tuning was similar for "parallel" and "perpendicular" motion, with a strong decrease of firing response above 5-10 Hz. The difference was the sensitivity in spatial frequency, displacing towards values below 0.5-1.0 c/deg for "parallel" motion (Figure 6.16). Geisler et al., (2001, 1999) interpreted this differential integration sensitivity as the product of a motion "streak" effect. According to their view, when an isotropic dot feature moves fast enough, it becomes smearer in space since the blurring of the fast displacement creates a spatial signal oriented in the direction of motion. To the contrary, a plaid pattern covering the entire visual field would not create such a motion-streak effect. Geisler et al., (2001) therefore concluded that "the oriented spatial motion signals" … (devoid of any anisotropy) … "in natural images produce oriented spatial motion streak signals in the population response of striate cortex neurons". However, the switch effect as a function of speed is seen for non-oriented stimuli only and does not explain our findings with oriented elements since low spatial frequency plaid responses to temporal frequencies drop sharply for values above 5-10 Hz.

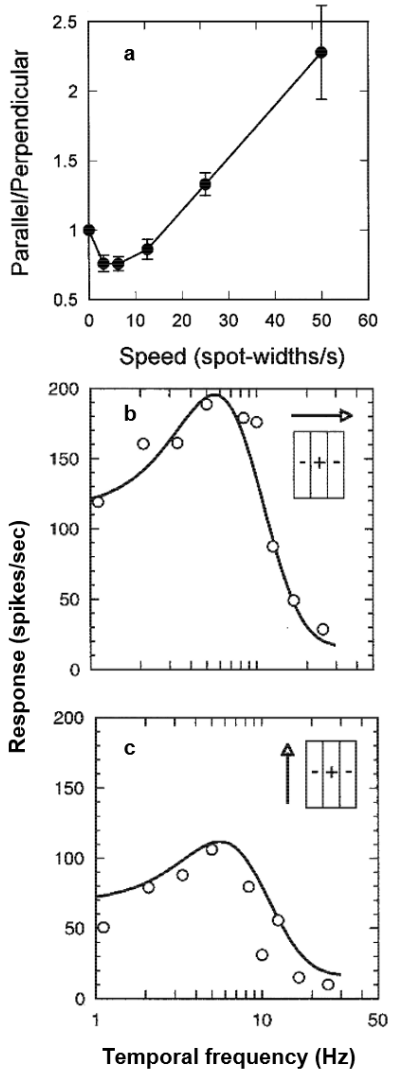

Figure 6.16: ***Response of a representative neuron in the monkey visual cortex to a moving spot and to orthogonal contrast modulated gratings.*** **a.** The vertical axis plots the response amplitude for parallel motion divided by the response amplitude for perpendicular motion. The horizontal axis plots the spot speed in spot-widths /s. The spot width was set to the preferred spatial period of the receptive field (i.e. one over the preferred spatial frequency). Responses for perpendicular motion (**b**) and for parallel motion (**c**) as a function of temporal frequency. The solid curve in each panel shows the prediction from the standard model of striate cortex neurons. (Adapted from Geisler et al., 2001).

Other descriptions of functional shift according to stimuli speed have been reported. Using extracellular recordings (Jancke, 2000) and VSDI (Jancke and Grinvald, 2007) in the anesthetized cat, 90 ° shift in orientation preference was found using random square and moving dots at high speeds. In the macaque, An et al., (2012) studied regional changes in cortical activation simultaneously in V1 and V2 with intrinsic optical imaging. Using a full field noise stimulus where the motion direction of individual pixels was controlled, the authors found that the cortical domains activated by dots moving at a speed of 1°/s were the same than those activated by drifting gratings moving orthogonally to the direction of the dots (i.e. having the same orientation than the direction of the moving dots). However, when noise pixel motion was increased to 2°/s and above (up to 7°/s), the activity domains in the orientation maps of both V1 and V2 were completely switched by a 90° change in preference. This flip in preference showed that, for faster motion, noise motion preferentially activated orientation preference domains corresponding to their motion axis, in V1 as in V2. However, the threshold speed that they reported was much lower (2°/s) than in any other studies and much lower than the initial 25°/s reported in the macaque V1 by Geisler et al., (2001).

Pursuing their work, using single cell-recording and intrinsic optical imaging in V1 and V2 of the cat, An et al., (2014 a) extended the 90° functional shift in orientation preference at high speed to a 90° functional shift in direction preference in direction-selective neurons. Using an apparent motion paradigm of moving dots, they found that motion trajectory at low speed was encoded primarily by groups of neurons preferring that motion direction, with an orientation preference cross-oriented with the motion axis. They found a 90° change in orientation domain recruitment when the motion speed trespassed a critical threshold speed, with a respective value of 15°/s in V1 and 31°/s in V2. Note that this value is higher than in their previous macaque imaging study (An et al., 2012). For speed above this threshold (up to 100°/sec, the highest speed they tested), the motion noise activated direction-selective neurons whose orientation preference was now collinear with the global motion (the “parallel” condition of Geisler et al., 1999, 2001). In contrast with V2, direction-selective neurons in V1 rapidly lost their direction-sensitivity as speed was increased, but this was due to the much higher direction selectivity of V1 neurons than the ones of V2. This however suggest that at high speed (75 – 100°/s), in V1 and V2, only the orientation component corresponding to the motion axis is relevant and allow to encode the motion axis.

Although those studies provide solid electrophysiological ground advocating for the existence of a dual mechanism operating differentially at low and high speed, because of the isotropy of the compound stimuli used, their interpretation remains confounded with a possible motion streak effect. There are only few studies that directly tested the use of actual anisotropic stimuli at high speed. One example can however be found in the work of White, Basole and Fitzpatrick. Using optical imaging, White et al., (2001) and Basole et al., (2003) showed in the ferret V1 that the functional regime of oriented cells in V1 shifts with motion speed, breaking around 20 – 30°/s, such that orientation preference domains activated by a moving field of small (2°) parallel bars and moving dots switched by 90° when these composite full-field patterns moved above this critical speed range. However, the angular shift was smaller for longer bars (57° shift for 40° bars and 22° shift for 10° bars). The findings of White et al., (2001) and Basole et al., (2003) were successfully

modelled by Mante and Carandini, (2005) and Baker and Issa, (2005). At first view, there is little difference between the use of small (2°) anisotropic bars and isotropic dots: both types of motion activate orientation domains parallel to the motion axis at comparable high speeds above 20 and 30°/s. However, our results and the ones of Georges et al., (2002) suggest a dependency on local feature anisotropy in the magnitude of the effect.

Crucially, the findings of Georges et al., (2002) showed that motion streak is not the only phenomenon that switches orientation preference to the axis of motion at high speed. Indeed, in Georges and colleague's psychophysical experiments, the orientation of each Gabor patch needed to be collinear to the next element of the same orientation in order to produce an effective over-estimation of speed in their apparent motion paradigm. More importantly, Georges et al., (2002) showed that collinear elements (ISO configuration) led to AM sequences perceived as faster than isotropic Gabor blobs presented in the same condition. In addition, the isotropic Gabor blobs used by Georges et al., (2002) were themselves perceived as moving slightly faster than their actual physical speed, which probably reflect the motion streak effect. Finally, the range for which the maximal speed-up effect was reported in human (40 – 96°/s, Georges et al., 2002) is close to the upper bound speed of horizontal connectivity conduction in primate (Series et al, 2002; 167°/s). Consequently, the fine sensitivity to orientation of the speed-up effect and its functional impact regarding motion streak are maximized at high speeds, since the overestimation of collinear and coaligned oriented Gabor patches AM speed regarding isotropic Gabor blobs is maximum at those high velocities.

The anisotropic lateral diffusion of facilitatory activity that we report in the present work argues for a finer mechanism than motion streak extrapolation since our findings strongly depends on the orientation of the local Gabor elements forming the motion flow. In our results, latency advance, response boosting and predictive filling-in responses impose strong anisotropic constraints on the integration and extrapolation of coherent motion in the cat V1. Such effects were not present when the orientation of the local features of the AM flow converging towards the RF along its preferred orientation did not match the flow's direction. Even though motion streak and the lateral broadcast of facilitatory activity that we found might cohabitate and their speed range partially overlap, the former cannot account for our findings. Crucially, the anisotropic dependency of our results indicates an additional intracortical computation linking local form extraction to global motion in order to facilitate binding and induce a perceptual bias. In that regard, we nuance the dominant view that only an elementary type of binding between form and motion occurs in early cortical areas due to the motion streak effect. Furthermore, we challenge the hypothesis that higher visual areas specify the separation of orientation and stimulus position computation (Burr and Morgan, 1997) by showing that V1 already performs those operations, probably subserving a refined mechanism of form and motion binding in higher areas like MT.

I-6.10 Reconfiguration of retinal flow integration by lateral connectivity during oculomotor exploration

Insights on the possible dynamics of natural retinal flow can be obtained from the study of relatively simpler models than higher mammals like the fly, where body motion predominates and fast neural speed estimation mechanisms during flight are needed to avoid a possible crash (Haag and Borst, 2004). In the visual system of the blowfly, optic flow information is encoded by a set of about 60 large-field motion-sensitive neurons called tangential cells (Weber et al., 2008). Among those latter, a subgroup of three neurons form the so-called Horizontal System (HS), that most strongly reacts to horizontal motion whereas the 10 vertical cells preferentially respond to vertical motion (VS) (Hengstenberg, 1982).

Crucially, each VS cell is electrically coupled to its neighbors (Cuntz et al., 2007; Haag and Borst, 2004; Farrow et al., 2005) and receives direct information from them, which broadens its tuning for downward motion along the horizontal tuning of the visual field (Haag and Borst, 2004). Outside the part of the visual field where a VS cell responds most strongly, responses exhibit different local preferred directions whose global arrangement resembles a directional flow (Krapp et al., 1998; Krapp and Hengstenberg, 1996). Particularly, it was proposed that the axis of rotation induced by self-motion should be encoded by the VS cell which responds the most strongly in a kind of winner-takes all, i.e., by the cell whose local RF field response preference best matches the rotational flow field (Krapp and Hengstenberg, 1996).

In short, the receptive field of those cells consists of two components: one that they receive from the local motion detectors in their immediate vicinity and a second from longer distance interaction with other VS cells, weighting the overall gradient distribution of activation profile of each VS cell tuned to distinct rotational flows (Haag and Borst, 2004). The description of this seemingly “simpler” elegant system is strikingly reminiscent of the modular specialization of each Aggregate Receptive Fields in higher mammals, that best integrate translational or rotational coherent motion flows according to the spatio-temporal profile activation of distant ARF possessing similar tuning properties.

In this context, the 90° functional shift in cortical territory activation along the motion axis seen for the motion-streak effect in higher mammals might reflect an overall simplification regime of visual information extraction during brisk and uncertain changes in visual statistics inherited from simpler models of visual flows extraction. Particularly, alignment of cortical activation along the motion axis at high speed may represent a form of primary grid pavement strategy, as suggested by the natural image decomposition of Bartels, Zeki and Logothetis (2008).

The functional effect reported here goes beyond this primary functional facilitation of fast retinal flow integration matching the ocular behavior since it specifically selects the extended collinear contours emerging above the noise level. Consequently, the +/- 30° tolerance in iso-orientation preference binding of lateral connections seen in higher mammals may stem for the ability to

detect relatively coherent and salient continuous features serving as “reference landmarks” in the face of uncertainty. In other words, the binding tolerance subserves a maximization of relatively persistent features in the environment that could have been preserved throughout evolution. This might have been derived not only for the exploration of heterogeneity in natural contours but might also have been inherited from abrupt behavioral responses like translation and rotation during brisk eye and head movements in the face of danger.

Since a visual flow – in cat V1 – on the order of 100-300°/s in retinal space is needed to maintain an in-phase relationship between intra-V1 lateral diffusion of activity and the feedforward drive, the amplification and latency advance of visual responses of our findings likely reflects the integration of edges collinear to the motion path during specific brisk phases of eye-movements corresponding to saccadic exploration. In contrast, these speeds are hardly ever experienced with passive motion, corresponding to fast displacement of objects in our natural environment. This mechanism could participate to the transient discharge responses only observed for centripetal contours coaligned with the receptive field axis of behaving macaque V1 at very high saccadic speed (900°/s, Judge et al., 1980; see discussion in Frégnac, 2002). A possible functional impact could be to produce an anticipatory signal predicting the future orientation of the target, when co-aligned with the saccade elicited to foveate the target. This boosting could participate to the rescaling mechanisms of LIP neurons described by Duhamel and Goldberg (Duhamel et al., 1992; Colby et al., 1995, 1996). It could also provide a functional correlate to the perceptual oculomotor skeleton of Yarbus, where fast saccades could signal the outline of the skeleton of the face that the human observer explores dynamically by successive changes of fixation. Similar oculomotor skeleton strategy has been described in the cat and non-human primate (review in Martinez-Conde, Otero-Millan and Macknik; 2013).

However, the visual flow speeds reported in the present cat study are inferior by a factor of 3 in the macaque because of the differential magnification factor between the two species, corresponding to 33-100°/s in primate. Nevertheless, that speed correspond exactly to the range of the maximal speed-up effect (64°/sec) reported in human psychophysics by Georges et al., (2002, 40° - 96°/s). Although the overall extent of horizontal connection conduction velocity covers the range of eye movements saccadic speeds in the cat, this is not the case in non-human primate and human. That is why caution must be taken when comparing cat and primate. In non-human primates (Angelucci et al., 2002 a,b; Shusruth et al., 2013, Nurminen and Angeluci, 2014), cortico-cortical feedback have taken a more prominent role than long-range horizontal connections intrinsic to a given primary cortical area, e.g V1 for vision in ferret, cat or tree shrew (Fregnac, 2002; Gérard-Mercier et al., 2016).

In the cat, monosynaptic horizontal connections extend over larger regions than in NHP, spanning up to 8-10 mm of cortex, which correspond to 8-10° of visual angle (Gilbert and Wiesel, 1989; Callaway and Katz, 1990; Kisvarday et al., 1997). In primates, on the other hand, the reach of long-distance axons only represents a few degrees in foveal vision: between 4-6 mm, corresponding to 1-3° in the visual field (Angelucci et al., 2002 a,b; Angelucci and Bressloff, 2006). That distance is

closer to the psychophysical results of collinear facilitation obtained in humans (up to 3°: Polat and Sagi, 1993, 1994 a,b, 1998) where cortico-cortical loops of feedback connections from higher cortical areas are more likely involved than horizontal connectivity in the transmission of far-surround modulation beyond the limit of monosynaptic lateral connections.

This change in spatial scale comes from the refined grain of the retinotopic map in NHP (resulting in an increase in retino-cortical magnification factor) and from the relative size increase of cortical areas that are the product of evolutive pressure. Very long-range horizontal connections may have become insufficient in primate (potentially too slow, too diluted or too expensive) to mediate long distance center-surround interactions in the visual field (Frégnac and Bathellier, 2015). Therefore, the control of feedback projections on V1 lateral connections is very likely much more important in primate than in the cat, ferret or tree shrew. Despite the difference in spatial scale, horizontal connectivity remains similar between cat and monkey in its functional essence and essential as it was preserved through evolution.

In summary, horizontal propagation of activity could embody an elementary form of collective predictive belief broadcast to distant parts of the network, reminiscent of the psychophysical Gestalt principles of common fate and axial collinearity (review in Wagemans et al., 2012). When this predictive belief matches the evidence, strong responses would occur, which could provide landmarks for visual stability across saccades and/or facilitate anticipatory responses (described at the spiking level in higher visual cortical areas in Duhamel et al., 1992) when acquiring a new target along a saccadic trajectory collinear to the orientation preference of the recorded cell (Judge et al., 1980). As a whole, our study thus supports the new concept of a “Dynamic synaptic Association Field” in V1 neurons, whose spatial extent and anisotropy passively adapt to the retinal flow changes during natural visuomotor exploration.

Psychophysical experiments (Georges et al., 2002), modelling evidence (Series et al., 2002) and intracellular studies (Gerard-Mercier et al., 2016; present work) strongly advocate for the implication of lateral connections of the primary visual cortex in the functional emergence of this Dynamic association field, in cat and potentially, to a smaller extent in primate. The only differences between the two species is the spatial extent of laterally-mediated anisotropic spread of activity and, by extension, the relative contribution of feedback and lateral influence in the emergence of this dynamic facilitation of motion integration in V1.

From a broader perspective, the type of stimuli that we use are not representative of visual statistics scenes but use compound stimuli that optimally match the RF properties of the V1 network in order to probe potential general mechanism subserving functional extraction of information in a natural environment. The saccadic exploration of elongated contours is a realistic application of our visual stimuli design and of our results interpretation. Our visual stimulations comprised centripetal flows of Gabor Patches converging towards the RF along its mains axis from both sides. This experimental choice aimed at maximizing the recruitment of lateral connections. Nonetheless, this is not a naturalistic configuration as flows rapidly converging towards a receptive field from both sides would correspond to a very fast contracting motion like during a rapid fall.

Fast centripetal motion can be found in natural environment such as a prey rapidly escaping an animal but the speed encountered in such situation are nevertheless much slower than the “optimal” ones used in our experiments.

Because flows converged towards the RF from both sides, we cannot exclude that this unnatural configuration resulted in a potential competitive influence between each hemifield flow converging symmetrically towards the RF center. More precisely, hints on our interpretation relevancy can be obtained from the blowfly, in which the receptive fields of the Vertical System are retinotopically arranged in a sequential manner covering in each hemisphere one half of the visual field surround (Weber et al., 2008). More specifically, there exist many connections between the two Horizontal Systems of each hemisphere, that project from the so called Lobula plate between the two parts of the brain (Borst and Haag, 2007).

In our results, it is possible that the main functional effect corresponds to the invasion of the RF by the lateral wave elicited by "horizontal" flow originating from the far periphery in the contralateral hemifield and that inputs from the ipsilateral part of the visual field may be less important. Recruiting the periphery from both sides of the RF, as we did in our protocols, might have masked a potentially more powerful effect, notably in the sub to suprathreshold integration of synaptic inputs. This should be tested in future work where the sensitivity to the directional flow origin of individual cells would be determined while targeting retinotopic locations precisely crossing the vertical meridian. Visual stimulations will then be composed of flows collinear to the RF axis and converging towards it from only one direction before escaping away from the target, as in natural saccadic exploration or head movements.

I-6.11 Binding in-phase versus rolling wave

The overall framework of our work, expressed in our visual stimuli paradigm and subtending the interpretation of our results is that the discrete consecutive stimulation of Aggregate Receptive Fields in adjacent cortical position over time by Gabor Patches co-aligned with the motion axis allows to recruit an increasing number of monosynaptic lateral inputs. When each input target is recruited in phase with the speed of horizontal connection conduction, a wide range of short- to long-distance lateral monosynaptic inputs converges towards the Receptive field center of the cell recorded intracellularly. Their nearly simultaneous arrival ("in-phase" temporal convergence) results in the contextual gain that we observe in our findings.

We should also note that the functional impact of remote eccentricity (25° from the RF center) cannot be accounted for by the sole very long-distance monosynaptic horizontal propagation of activity beyond their maximal 10° spatial reach in the cat. Thus, we cannot exclude the recruitment of a neighbor to neighbor rolling wave of facilitatory activity between adjacent ARF, involving shorter range monosynaptic lateral connections, at least in the far periphery. This hypothesis is biologically plausible since density of horizontal connections have been reported to be sparser in

the far periphery than in parafoveal regions (Stettler et al., 2002). Indeed, at the anatomical level, horizontal connections axonic arborizations are elongated along the preferred orientation axis of a given cell's RF where they spread over larger distance and make more connections than along the width axis (cat: Gilbert and Wiesel, 1983, 1989; Schmidt et al., 1997a; tupaia: Fitzpatrick, 1996; Bosking et al., 1997; macaque: McGuire et al., 1991; Malach et al., 1993; Grinvald et al., 1994, squirrel monkey: Sincish and Blasdel, 2001). It is therefore likely that distinct ARF share a substantial proportion of horizontal connections, finding nested synaptic relays along the integration of extended collinear contours during saccadic exploration.

Nevertheless, this neighbor to neighbor ARF facilitatory activity cannot explain the differences found between the spatial extent of the subthreshold association field and the minimal discharge field. Let us imagine a rolling wave composed of a chain (size: N) of non-overlapping collinear RFs spatially offset along their orientation preference axis. Let us consider an effective spike-based transmission until the N-1 the neuron. The consequence of this firing chain implies that the discharge field size of the $(N-1)^{th}$ presynaptic neuron is of the same order as the subthreshold RF of the last neuron (that is the topological union of all the active elements of the chain).

However, the propagation of activity between neighboring ARF is necessary to generate a refined prediction downstream in the cortical hierarchy. According to the predictive coding scheme and experimental evidence in human, down-regulation of a predictable input requires a certain accumulation of coherent information over both space and time. The mean field spatial summation and transmission of coherent spatio-temporal information cannot be accounted for by each elementary monosynaptic horizontal connections whose individual functional impact cannot generate by itself a feedforward input to higher areas but rather sum up in ARFs. In other words, the build-up and transmission to higher areas of predictive information inputs in V1 require a spatially segregated summation process transmitted by feedforward connections downstream in the cortical hierarchy. This inter-area transmission of information requires a physiological entity that is able to generate such feedforward input. Series of spatio-temporal inputs information subserving the emergence of refined predictions downstream in the cortical hierarchy are therefore probably sequentially integrated in and transmitted by distinct hypercolumns units. In that scenario, the recruitment of each ARF relay provide a slightly higher facilitatory baseline at each synaptic relay of horizontal connection recruitment that partially counterbalance the reduction of activity as this latter propagates along unmyelinated axons.

In contrast, in the non-human primate, Angelucci et al., (2002) argued that center-surround lateral facilitatory influence comes from overlapping connectional fields of neighboring Adjacent ARF. According to their view, polysynaptic chains of horizontal axons are unlikely to generate far surround modulation because their conduction velocity is too slow (0.1 – 0.3 m/s) to account for the fast onset of far-surround modulation in V1 cells (Angelucci et al., 2017). However, this argument only relies on center-surround facilitatory effects observed for *static stimuli flashed simultaneously*, not for the progressive dynamic recruitment of the periphery corresponding to our experimental paradigm. Numerous studies have confirmed the range of both monosynaptic and

polysynaptic horizontal connections speed conduction initially reported in intracellular studies by Bringuier et al., (cat: 0.05-0.5 m/s; 1999) and by Grinvald et al., (monkey VSDI: 0.2 m/s; 1994), cat VSDI: 0.09 m/s (Jancke et al., 2004); 0.2 – 0.5 m/s (Benucci et al., 2007); cat and monkey LFP: 0,2 – 0,3 m/s (Nauhaus et al., 2009), monkey VSDI: 0.4 m/s (Sit et al., 2009).

This lateral diffusion of activity is described in the cortical space as travelling waves, and as standing waves in the orientation domain. However, the column to column propagation of activity (0.1 – 0.3 m/s) emphasized by Angelucci et al., (2002, 2017) must critically be distinguished from slower horizontal waves, namely "rolling waves" (Frégnac, 2012) described in vitro by VSD imaging of primary visual cortex slices of the rat (Tanifuji et al., 1994). By electrically stimulating the white matter of rat primary visual cortex, Tanifuji and colleagues observed that activity propagated in a vertical direction towards the cortical surface as it first emerged in layer 6, then layer 4 and layers 2-3. The vertical propagation was followed by an horizontal spread in sub and supragranular layers, travelling at a speed of 0,025-0,094 m/s, velocity below the lowest estimate of horizontal propagation speed reported previously. This led the authors to conclude that lateral diffusion was not only mediated by horizontal connections but also by a vertical diffusion component. Indeed, the authors did not see horizontal propagations mediated by the "usual" 0,05-0.5 m/s conduction velocity specific to horizontal clustered connections, potentially because their subthreshold effect was drowned in the strong electrical drive that they applied.

To test the impact of this vertical diffusion on the lateral one, the authors lesioned their slices from layer 1 to layer 4, under the assumption that lateral propagation would be disrupted and would not cross the lesion site. Contrarily to their expectation, vertical lesion did not interrupt lateral propagation on the other side of the cut in either supra or infragranular layers. When the lateral activity reached the lesion site, it spread vertically towards infragranular layers and bypassed the cut before propagating again laterally on the other side of the cut. Similar activation profile was observed for a lesion of infragranular layers, where activity this time spread vertically upward towards supragranular layers and bypassed the cut before spreading again laterally. To the contrary, horizontal lesion in layer 4 abolished lateral propagation, advocating for a prominent role of vertical diffusion on lateral one.

Those observation led Tanifuji et al., (1994) to conclude that strong reciprocal connections between distinct layers, notably between supra and infragranular ones (Martin and Whitteridge, 1984; Toyama and Tanifuji, 1991; Komatsu et al., 1988) provide close-loop circuits that enhance purely lateral diffusion. Although we cannot exclude such rolling waves, their slow (0,025 – 0,094 m/s) velocity is way too low to account for the 0.1 – 0.3 m/s speed range characteristic of our results latency advance, response boosting and filling-in predictions, that are best accounted for by purely laterally-mediated diffusion of activity and feedback modulatory influence.

However, the overall timing of the activation profile subtending rolling waves account strikingly well for the effects reported recently by the group of Chavane (Benvenuti et al., 2015). Benvenuti and colleagues specifically addressed the predictive impact of a bar displaced in the periphery of V1 awake macaque receptive field from distinct eccentricities ranging from 1.5° to 6 ° from the RF

center at low speeds (6,7 – 10°/s corresponding to 0.016 – 0.02 m/s in the cortex). Their first paradigm was composed of bars moving orthogonally to the motion axis and converging towards the RF center, not only along an axis orthogonal to the preferred orientation of the cell, but from 12 different directions separated by 30 ° angular steps. Remarkably, they observed in their experimental results an anticipatory spiking response of the RFs recorded extracellularly that started several hundreds of milliseconds before the bar actually entered the RF discharge field center. Response where the bar trajectory started at 1.5° of eccentricity from the RF center was similar to the one elicited by the sole stimulation of this latter, while responses to bars presented from 3 and 6° of eccentricity presented a progressive ramp-like increase of the discharge field firing rate at 327 and 397 ms, respectively, for half of their cells. The peak response was however almost similar to the sole stimulation of the RF

One remarkable feature in their results is that even though they did observe stronger anticipatory spiking responses for bars cross-oriented relative to the motion axis (i.e, the classical stimulation mode for revealing “edge detector” properties of V1 neurons), weaker anticipatory responses were still observed for all motions directions. Later on, they confirmed their results using LFP recordings obtained from two electrode arrays implanted in two monkeys where anticipatory responses were obtained once again for the longest 3 and 6° trajectory lengths at a retinal speed of 6.6°/s (hence, 0.015 m/s propagation at the cortical level), which was confirmed in a fourth monkey in VSDI experiments.

Specifically, their VSDI experiments showed that response onset latencies for pixels that were close (< 1.5°) from the bar motion starting point increased very slowly, indicating a relatively fast horizontal conduction (0.08 m/s) of anticipatory response in the immediate vicinity of the feedforward thalamic input. To the contrary, for responses of pixels located more than 1.5° away from the starting retinotopic position of the stimulus, latencies increased much faster (corresponding to a cortical spread speed of 0.02 m/s). Their results suggest that anticipatory responses seen for the longest trajectories of the bars come from a sequential activation of horizontal network having a limited spatial extent. In that situation, local anticipatory responses are rolled over larger distances as a new retinotopic location is stimulated by a new feedforward input, following retinal image speed. Nevertheless, the cortical speed of activation that Benvenuti and colleagues observed for pixels extending beyond 1.5° of eccentricity remains faster than the retinal image speed (10°/s vs 6.7°/s), which advocates for a potential implication of feedback loops of predictive facilitatory activity.

The activation profile of the VSD imaging of Benvenuti et al., (2015) is consistent with subthreshold depolarizing influence conveyed at a speed compatible with lateral connections but over a spatial range that does not reach the RF center immediately. However, the progressive spatio-temporal progression of the bar *de novo* recruits those horizontal connections, leading to a progressive displacement and accumulation of subthreshold depolarizing influence that displace itself in a nested way. This convergence of lateral connections, combined with the faster and longer-range facilitatory influence of feedback connections reflecting a coherent motion prediction leads to an

overall convergence of synaptic inputs targeting the RF center, building-up a progressively growing anticipatory activity up until it becomes detectable at the spiking level. Benvenutti et al., (2015) conclude that low speed anticipatory response in V1 can be explained by a composite horizontal-feedback information propagated, crucially, at an apparent speed slightly faster than the actual feedforward retino-thalamo-cortical inputs encoding the retinal image position.

The synaptic scenario and the speed of laterally propagated activity (speed: 0.016 – 0.02 m/s) that Benvenuti and colleagues describe in the awake monkey V1 is reminiscent of the findings of Tanifuji et al., (1994) (speed: 0.025-0.094 m/s; 1994) in slices of primary visual cortex of the rat. In this context, the rolling wave effect observed in the awake monkey at low speed likely comes from spatially restricted immediate diffusion of lateral activity, amplified by local recurrent connections but also enhanced throughout the entire hypercolumn by inter-layers reciprocal connections, and combined to an increase of feedback modulatory influence in the awake animal.

We are then faced with two striking complementary functions of lateral connections in the diffusion of anticipatory activity (Figure 6.17). At saccadic speed, the anisotropic congruency of elementary Gabor patches embedded in a retinal flow converging towards single RFs is crucial in the effective build-up and broadcast of contextual anticipatory responses allowing the integration of coherent and salient features riding above the noise level of the motion streak effect. This lateral broadcast, combined to feedback influence also reveals that V1 is able to generate its own prediction about the future position of an object in time by diffusing predictive activity filling-in an unstimulated retinotopic area, sustaining information enabling V1 to solve the motion extrapolation problem in the face of transient uncertainty. Those mechanism are already revealed in the low level perceptual state of the anesthetized cat.

Complementarily, the results of Benvenuti et al., (2015) show that in the awake monkey V1, slow retinal flows (below 10°/s) engage a diffusion of spatially restricted horizontal activity whose *de novo* recruitment by the slow retinal flow induce a progressive accumulation of isotropically diffusing activity converging towards single RFs in a nested way. This horizontal isotropic diffusion, combined with the continuous feedforward input, and facilitated by the coherent motion prediction influence of feedback connections lead to the progressive build-up of sub and suprathreshold anticipatory activity along a coherent motion path.

To which extent the two mechanisms (rolling wave and monosynaptic propagation) are shared and cohabitate within the two species remains to be determined although preliminary MUA and LFP recordings in our lab suggest that the low speed anticipatory mechanism described in the macaque by Benvenuti et al., (2015) is observable in the anesthetized cat V1.

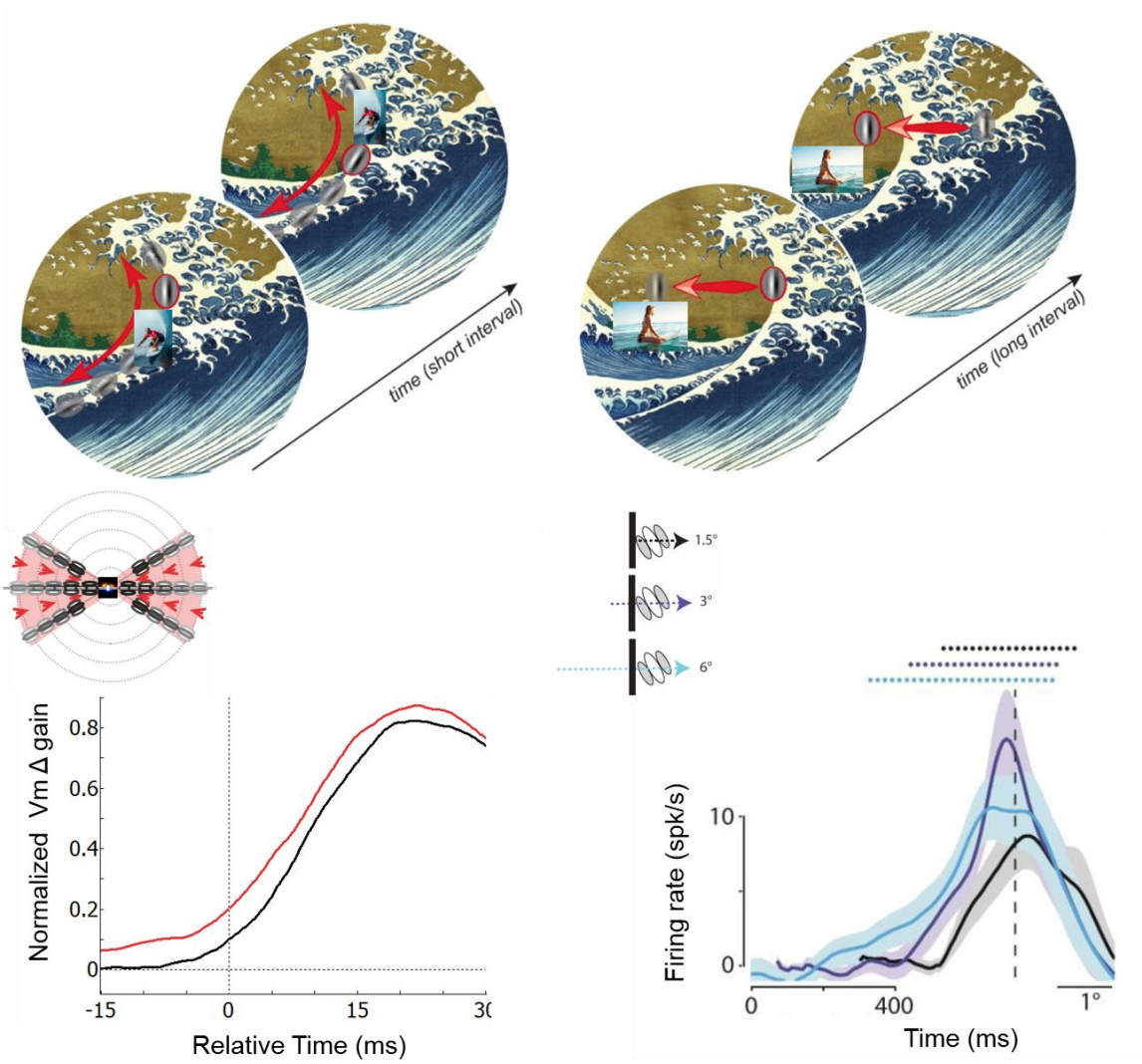

Figure 6.17: ***Complementary functional roles of horizontal connectivity: saccadic speed broadcast of predictive information and low speed vs isotropic diffusion of anticipatory activity. Upper left****: cartoon of collinear facilitation along contour integration at high speed where the feedforward recruitment of lateral connections rides in phase with the horizontal wavefront.* ***Upper right****: cartoon depiction of slow anticipatory build-up of activity where nested displacement of horizontal recruitment by a slow feedforward input generates anticipatory activity allowing to read the wave forward in time.* ***Lower left****: Anesthetized cat intracellular measurement of contextual gain of single V1 RFs responses realigned according to their individual latencies and averaged over 37 cells. Responses are obtained from a 6 strokes apparent motion paradigm composed of elements iso-aligned regarding the motion axis and converging towards the RF center along its preferred orientation from up to 25° of retinal eccentricity at saccadic speed (100 – 300°/s) (red) regarding the sole feedforward stimulation of the RF center (black).* ***Lower right****: Average response profile of single unit anticipatory activity recorded from 29 V1 RFs neurons of an awake monkey in a continuous slow (6.7 °/s) motion paradigm composed of bars presented from 12 different direction at 6, 3 and 1.5 ° of eccentricity (blue, purple and black, respectively) regarding the classical discharge field center, indicated by a dotted line (Adapted from Benvenuti, 2015).*

I-6.12 Future work and bottleneck

If our protocols proved to be well adapted to study changes in gain and latencies, similar analysis on spiking discharges require either dense discharges or larger number of repetitions. In the case of surround stimulation, spiking probability remains low and the difficulty of maintaining intracellular recordings for several hours (in order to explore parametrically all the possible conditions) bears a strong limitation. It is not thus surprising that the sole protocol where we could reveal a clear contextual gain control/phase, both in the average response profile as well as in individual cell analysis, was when the entire periphery was radially stimulated. This situation, which ensures maximal peripheral input summation, allows the characterization of the full integration process leading to spike output and propagation across the V1 network. One should note from our SECTOR protocol and from the two-stroke AM protocols between neighboring positions (Gerard-Mercier et al, 2016) that these situations led to similar effects at the subthreshold level, without effectively producing a significant evoked discharge. This requirement for summation may explain why facilitatory effects from Surround modifications are so difficult to observe in the literature. Furthermore, the present experiments show, that independently of spatial summation, the anisotropic sensitivity of cat V1 RFs is almost null along axes orthogonal to the main one at high speed (Gérard-Mercier et al., 2016). In that context, for most of the cases, addition of spatio-temporally coherent elements converging towards the RF center along the width axis facilitated the passage of facilitatory subthreshold depolarizing activity conveyed by elements flashed along the main one up to the spiking level for our condition of interest.

Asymmetry in Surround organization

New protocols could explore the possibility that some of the effects reported here present some form of spatial and retinotopic asymmetry along the dynamic association field of each individual RF. The asymmetry hypothesis fits with some of our recordings (Gerrard-Mercier et al, 2016) and the extracellular reports of Walker, Ohzawa and Freeman (Walker et al., 2000). It was not explored in our actual visual paradigm where contraction motion flow was centered on the RF center of the recorded cell. Consequently, the stimulation pattern originated from both axial sides or obeyed a radial symmetry.

Hemifield selective stimulations of the Surround of strictly foveal discharge fields should enable us to determine whether surround summation is more effective when the centripetal flow originates from the contralateral field rather than when it recruits simultaneously homotopic sites in the ipsilateral field. Such experiments require delineating with high precision the eccentricity coordinates of the recorded receptive field (from the gaze axis, i.e the area centralis location) as well as the position of the vertical meridian (partitioning the visual field in two hemifields – contra and ipsi). One should remember however that there is a twilight uncertainty zone, corresponding to an anatomical band of 600 µm, where contralateral responses can still be evoked, even for RFs in the ipsilateral field. For instance, for vertically oriented RFs centred on the vertical meridian, the

radial protocol, which would recruit in that case both contralateral and ipsilateral input sources, is not appropriate to predict the impact of retinal flow crossing the vertical meridian following horizontal head and/or eye-movements. In contrast, the potentially competitive influence of non-naturalistic flows both converging symmetrically towards the RF center, could reduce latency advance, response boosting and amplitude of filling-in responses produced by homogenous hemifield "parallel" flow.

Laminar analysis

Another point that should be explored is the laminar dependency of the emergence of our functional effect. In the contextual framework of their Hierarchical Predictive Coding schema, Rao and Ballard (1999) emphasized the anatomo-functional view that residual error messages sent by lower cortical areas to higher ones via feedforward connections should originate from layer 3 cells having numerous and spatially extended lateral connections. From a functional point of view, cells having long distance horizontal connections are indeed ideal candidates to provide such residual error feedforward inputs. During the time course of lateral diffusion, mutual exchange of feedforward-feedback information allows to generate multiple predictions/residual errors that update and refine the prediction of the new stimulus that is expected and compared to the actual contextual information obtained when lateral inputs are integrated. Providing experimental evidence that filling-in diffusion of activity sustaining a prediction in the face of transient uncertainty is more pronounced in layer 2/3 than in granular and infragranular layers would constitute an important step in the identification and characterisation of the striate cortex functional specialisation.

The histological revelation of the cell bodies that were stained during our intracellular recordings did not allow us to correlate our effects strength to any layer or cell type. Highlighting a potential laminar dependency could be done by using Multiple Electrode Arrays inserted perpendicularly to the cortical surface. Receptive fields of all layers of an hypercolumn would roughly have the same retinotopic position and the current source density spatial profile of the recordings would allow to segregate infra and supragranular layers, together with the histological reconstruction of the electrode penetration. However, there are several difficulties pondering the interpretation of such experimental framework. First, the LFP mapping of the spiking discharge field and of its lateral subthreshold influence would not be as precise than in our intracellular recordings, implying that the Gabor patch size of the Aggregate Receptive Field chosen for the visual stimulations could partially encroach on the subthreshold Depolarising Field of some RFs. Second, because multiple receptive fields would be recorded, the individual spatial extent of each of them would be different, forcing the stimulation choice of the Gabor patch size to encompass the largest extent of the cumulated retinal eccentricities covered within the hypercolumn, under the assumption of a mean-field effect.

Dependency on spatial input recruitment

Other experimental sets could be proposed to certify the existence of a cooperative mechanism operating between V1 and other areas downstream in the cortical hierarchy that generates a prediction whose effective impact by feedback connections target specific retinotopic locations in space and time. To test whether the amount of coherent information is relevant in the prediction's functional impact, we should progressively reduce the number of Gabor Patches presented in the periphery before stimulating the center and without stimulating it. If a qualitative and/or quantitative change between the down-regulation observed when the RF center is stimulated is observed when fewer elements progressively build a predictive peripheral response, it should allow us to correlate and quantify the functional impact of our peripheral recruitment up to 25° of retinal eccentricity. Alternatively, it may be that there exist two spatial surround contributions which can be distinguished depending on the far/near eccentricity of the Surround components. Our data show clearly some form of subthreshold supra-linear summation in the far periphery and, in contrast a down-regulation when the last proximal stroke is followed by the test stimulus in the RF center. The hypothesis of a critical non-linearity in the near periphery can be found in Sillito's studies.

Dependency on Center-Surround orientation congruence

Another possible development would be to test whether the peripheral progressive build-up of predictive activity is boosted by feedback connections when the stimulus flashed in the RF center largely deviates from the prediction by presenting a Gabor Patch cross-oriented to the cell's preferred orientation and motion path. This could lead to a supra-linear "surprise response" where V1 signal a strong prediction-based residual error to higher areas. This interpretative schema has been proposed in awake human imaging experiments in which static stimuli that do not fit the motion percept are overwritten by top-down motion prediction even though the unexpected stimulus induced a stronger V1 signal (Schölvinck and Rees, 2010). Whether an attentional modulation process by higher areas overwrites the non-fitting elements contradicting the unified coherent percept is not within the reach of our anesthetized animal experimental framework. Nevertheless, the existence of a similar underlying physiological process should be tested for in the low-level perceptual state of the anaesthetized cat V1.

Differential recruitment of lateral diffusion by repeated static vs AM stimulation

In the anesthetized visual cortex of the rat, Han et al., (2008) showed, using VSDI that repetition of a same stimulus resulted in the emergence in spontaneous cortical activity of reverberating patterns similar to the ones elicited during the visual stimulation, phenomena persisting for several minutes. In addition, repetition facilitated the activation of the retinotopic area initially activated and strengthened the direction spread of activity. A similar line of evidence has been provided by Shang et al., (2011) using whole patch clamp in the anesthetized rat. These authors showed that repeated periodic presentation of a square flashed outside the subthreshold depolarizing field rendered a region initially insensitive responsive to visual stimulations. Additionally, Response

amplitude strength was correlated to the number of repetitions. Those findings confirmed the previous cat report of Eysel et al., (1998) showing that cortical cells expanded their RF into unresponsive regions within minutes and changed their functional receptive field structure for hours after associative co-stimulation by adjacent bars presented in the RF center and in a concomitant region primarily unresponsive.

In such context where Hebbian rules guides synaptic plasticity according to the statistics of visual stimulation exposure, determining to which extent the wiring of an adult subject can be modified to learn new expectancies is of paramount importance. More precisely, we should test whether the plasticity of the visual system extend to the integration of uncoherent elements along a coherent path by presenting consecutively the same sequence of stimulation where the last Gabor patch presented in the RF center is Cross-oriented regarding the motion axis. The comparison between the putative high residual error responses of the first dozens/ hundreds of trials should be compared to the last block of trials to see if the residual error's magnitude has been reduced by the conditioning visual stimulation, providing a quantitative measurement of a functional change in a rather elaborated extraction function of the striate cortex.

Part II – Lateral connectivity and hallucinatory-like states in V1

II-1. Background

II-1.1 On the origins of Geometric hallucinations in the brain

In human, stereotyped geometric hallucinations, often triggered by migraine, drug intoxications, and empty-field flicker are thought to share similarities with autonomous activity in visual cortex as they can occur without any visual stimulation, in total darkness (Siegel, 1977) and in enucleated subjects (Krill et al., 1963). Similar hallucinatory patterns occur during binocular eye-ball pressure and following electrical stimulation of the temporal cortex (Penfield and Perot, 1963). Consequently, it seems that paroxysmal external influence diverging from the classical activation of the visual system (physical pressure, propagation of activity through the brain) can modulate the internal activity of visual areas to generate hallucinatory percepts.

Geometric hallucinatory percepts are planforms. These planforms patterns take their neural origin at the cortical level. They are however defined at the retinal sensory level where the resulting read-out of the cortical activation domains can be linked to visual percepts. They are highly specific and possess a peculiar geometry that has been used to model the transition of cortical states of activity using reaction diffusion equations (Ermentrout & Cowan, 1979). Such models take into account the inverse application of the nonlinear mapping existing between the retina and the visual cortex in higher mammals. Experimental quantification of log-polar transformations between retina and cortex were first obtained in the macaque V1 (Tootell et al., 1982) and later on in human (Tootell et al., 1998; Figure 7.3). This transform accounts for the correspondence between the different classes of geometrical hallucinatory planforms of the visual field that Klüver first classified in 1966 (Figure 7.1) and matching domains of neural activity. Those domains of neural activity have a laminar lay-out that corresponds to periodic stripes of specific spatial orientation in primary cortical visual areas (Humans and NHP: Ermentrout & Cowan, 1979; Bressloff et al., 2001; Figure 7.2.).

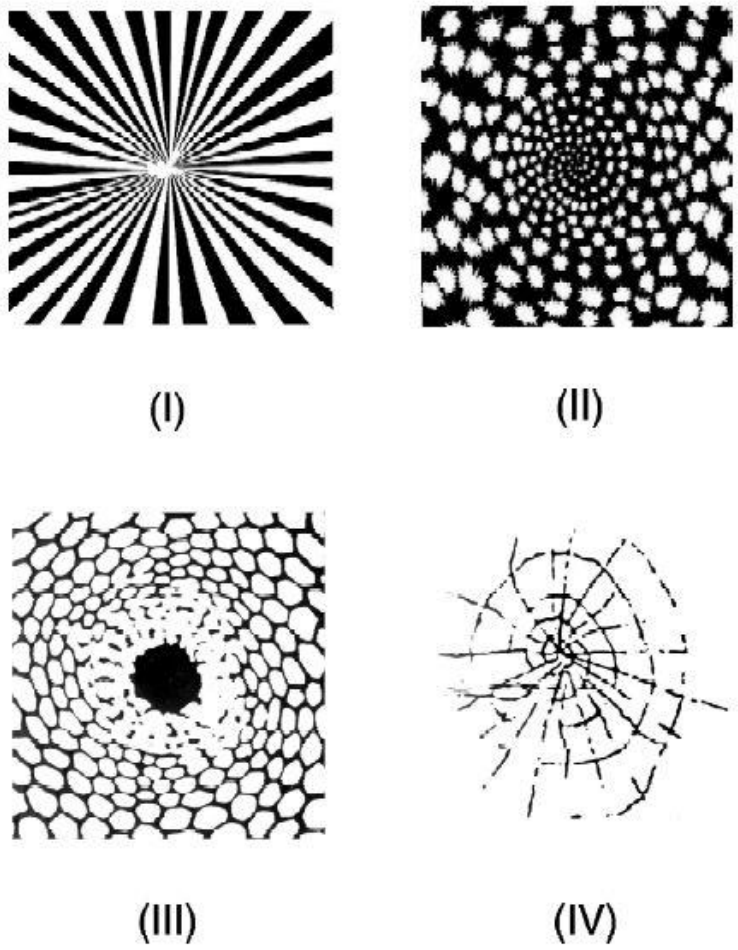

Figure.7.1: ***Hallucinatory form constants described by human subjects following drug ingestions and classified by Klüver (1966)***

(I). *Funnel and* ***(II)*** *spiral images seen following ingestion of LSD or mescaline (redrawn in Siegel and Jarvik (1975). (****III****).* ***Honeycomb*** *generated by marijuana (redrawn in Siegel and Jarvik, 1975), and (****IV****) cobweb petroglyph (redrawn in Patterson, 1992). Those ground breakings observations were made across many subjects, over multiple sessions and have been regarded for more than fifty years as a strange mystery of human visual perception, a seemingly unexplainable common sensory experience, despite the lack of structured physical visual stimulation.*

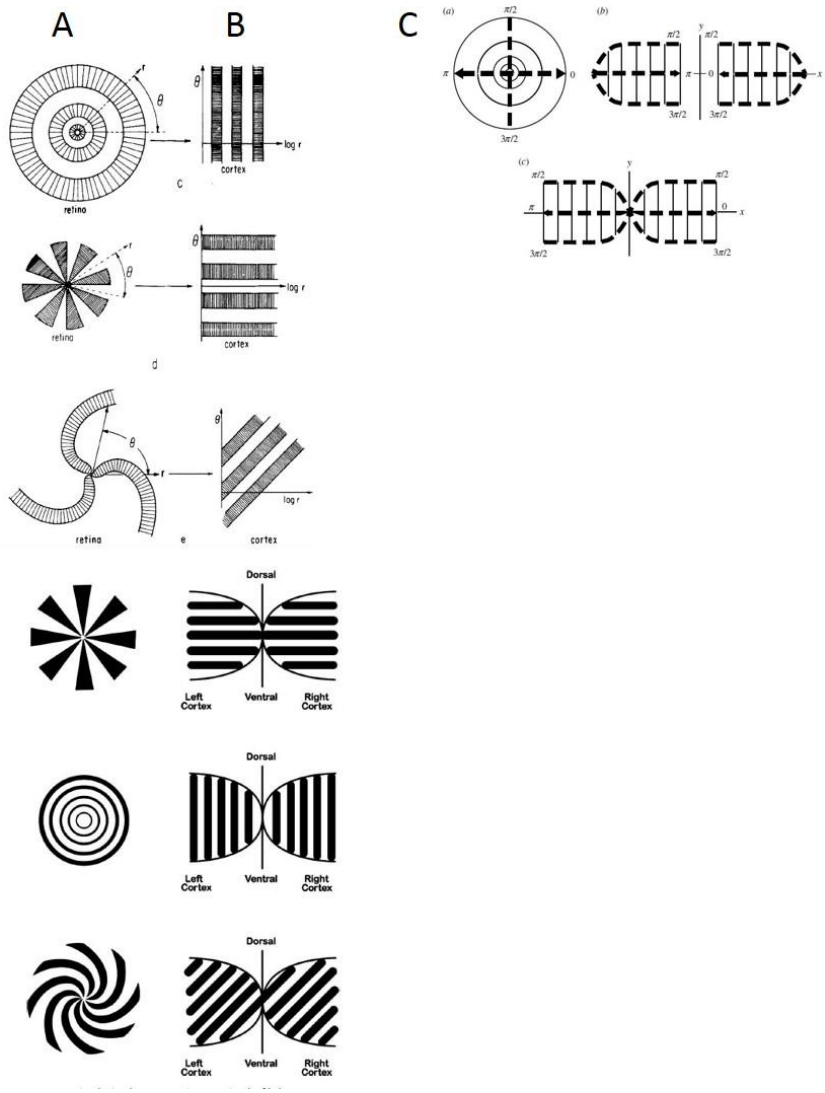

Figure.7.2: ***Log polar transformation between retinal geometrical planforms and stripes of activity on V1.***

A, left: *Radial symmetrical planforms at the retina,* ***(c)*** *annuli,* ***(d)****, radial concentric lattice,* ***(e)*** *spiral constant.* ***B****: corresponding stripes of neural activity on V1 surface. (Upper part adapted from Ermentrout and Cowan, 1979, lower part, simplification representation adapted from Billock and Tsou, 2007).* ***C****: V1 transforms by the log-polar transform in the laminar plane of V1.* ***(a)****: visual field;* ***(b):*** *reconstruction of cortical left and right hemispheres from the visual field content.* ***(c):*** *actual cortical map, comprising right and left hemisphere transforms in which the two transforms are realigned so that both foveal regions correspond to x = 0. (Adapted from Bressloff et al., 2001).*

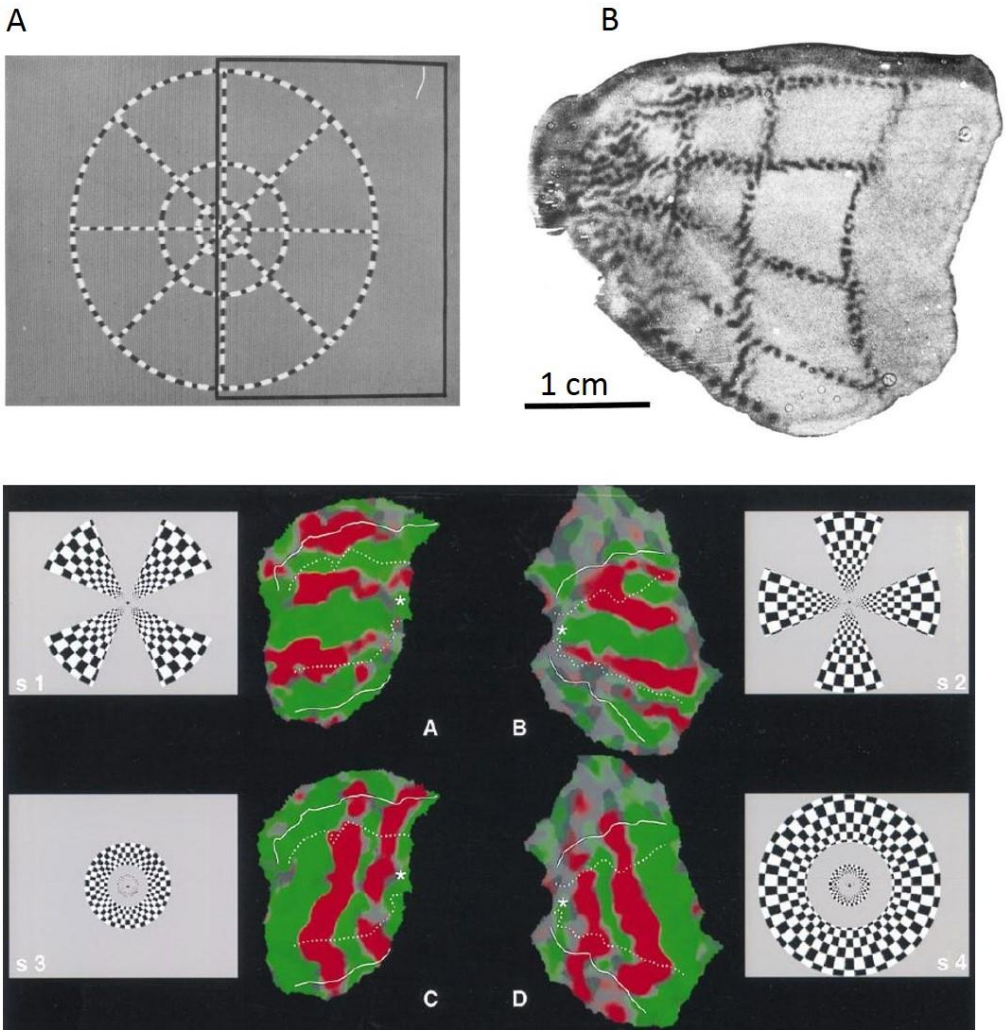

Figure.7.3: ***Imaging of cortical stripes and their perceptual correlates***

The log-polar transformation between retina and V1 introduced in figure 7.2 can be visualized using imaging techniques. ***A-B, upper pannel.*** *The most compelling evidence of the non-linear mapping between retina and cortex was obtained by Tootell et al., 1982 where the polar web pattern representing the visual field (**A**) was used to stimulate the visual system of an anesthetized macaque perfused with the 2-Deoxy-d-Glucose marker. After sufficient time to accumulate the marker in the most active cells, the autoradiography (**B**) of the animal's primary visual cortical slices was made (after histological flattening). The log polar transforms of the radial and concentric stimulation grid were visualized as a rectilinear grid in V1.* ***Lower panel.*** *Tootel et al., (1998) reproduced this observation in humans using non-invasive fMRI. Dynamic reversal of checkerboard pattern contrast at the retina (**A**) was used to activate both on and off cells with both sustained and transient temporal responses properties to respond nearly continuously, rendering possible the visualisation of the continuous strong blood oxygen level-dependent response. (**A-B**) Radial patterns on the retina (s1, s2) evoke horizontal stripes on V1 while (**C-D**) concentric patterns (s3, s4) evoke orthogonal vertical stripes on V1). (From Tootell et al., 1982 and Tootell et al., 1998).*

Many of these hallucinations arise from self-organized autonomous activity in visual areas, composing subsets of cortical dynamics that very often fall into a small number of perceptual geometries (The Klüver form constants, 1966). The perception of these form constants has been reported by humans across distinct and isolated ethnicities all over the world, as attested by similar geometrical shape found in paintings and carvings in prehistorical caves. Those observations date from up to tens of thousands of years (Clottes and Lewis-Williams, 1998) in Africa, Europe and other caves across the world and were also found as scratchings on petroglyphs (Patterson, 1992). The similarity across patterns appears as a structural or mechanistic invariant. Indeed, as we already saw in figures 7.1, 7.2 and 7.3, although the hallucinatory percepts appear diversified, the neural mechanisms at their origin seems of the same nature. In each case, the patterns of cortical activity correspond to a periodic unidimensional band cortical pattern, only differing in cortical location and orientation in the laminar plane. These arguments indicate that geometric hallucinations are not a panel of disparate curiosities whose study has more to do with an obscure esoteric mystical quest than a scientifically relevant approach of an archetype: the common functional architecture of the brain in Humans and potentially Non-Human Primates. The theoretical field derived from the mathematics of pattern genesis has been called Neurogeometry (Frégnac, 2003). It is based on reaction-diffusion differential equations applied to excitable media where the spatio-temporal formation of patterns of activity in the brain is generated by weighted integral functions of spatial and temporal excitatory and inhibitory influence. It represents in a schematic fashion the architectural (connectivity) and functional (modular) properties of primary visual areas.

One of the many difficulties met in the study of hallucinations is that the brain behaves in a rather stable manner, prerequisite to the stability of our cognitive functions: how would we be able to efficiently adapt ourselves to our environment and respond accordingly if we were “disconnected” from the physical reality and hallucinating all the time? This means that if we want to understand the brain as a complex non-linear dynamic system, we must push it out of its ordinary regime. Indeed, even though stereotyped geometric hallucinations arise from autonomous activity, this latter must lie within a certain range as we do not continuously experience geometric hallucinations when we close our eyes, although more frequently when we press our eyeballs or are subject to migraines. It means that geometric hallucinatory percepts emerge from a disequilibrium leading to a paroxysmal regime of activity in the brain. Perceptual departure and dissociation from physical reality of our environment then becomes a tool to identify the “limits” of our brain as a system, allowing us to pinpoint and unravel its intrinsic functioning.

Moreover, geometric hallucinations are the manifestation of an important principle in cognitive science. It is now acknowledged that complex systems such as the human brain exhibit collective properties referred to as emergent properties of the collective system that no individual neural element possesses on its own. This statement if often associated with analogies with better understood systems in physics. In that context, elementary hallucinations, especially geometric

hallucinations provide particularly relevant examples of neural emergent behavior, the self-organized spatio-temporal formation of patterns corresponding to specific percepts. Those phenomena are even better suited to focus scientific investigations on early visual areas where geometric properties, spatial and temporal scales as well as connectivity and functions are rather well documented.

On top of that, it has been shown for centuries that geometric hallucinations can also be induced via purely visual contextual stimulation, using an homogeneous flickering field (Purkinje, 1819-1823; Brewster, 1834; Fechner, 1838; Helmholtz, 1925; Brown and Gebhard, 1948; Mundy-Castle, 1953; Walter and Walter, 1949; Walter, 1956; Smythies, 1959 a, b, 1960; Freedman and Marks, 1965; Remole, 1971, 1973) or a flickering field combined with and/or composed of a geometric planform initially perceived as an hallucination (Fechner, 1838; MacKay, 1957 a,b, 1965; Billock and Tsou, 2007). Not only does geometric hallucinations can emerge from intracortical autonomous activity, but also from the cortical interaction between intrinsic and physically evoked neural activity by a visual stimulus. This topic is a crucial one in neuroscience and takes to a whole different level the interest of studying geometric hallucinations pattern formation.

It addresses very complex interactions: on one hand, the behavior of self-generated autonomous activity, reflecting the principles of functional architecture construction of the visual system, guided by Hebbian mechanisms of plasticity and exposure to the external visual world. On the other hand, the rules of modulation of that ongoing activity by an actual external visual input. More simply, it raises the question of how the activity of the brain, initially constrained both at the architectural and functional level by exposure to the visual environment, does react to actual exposition to that environment. If geometric hallucinations can be induced by visual stimulation from an actual physical stimulus, it means that somehow, visually evoked activity can control / constrain the organization of self-generated ongoing activity by perturbing this latter. To be fair, this is more the result of a mutual modulation between the two, as the structuration of self-organized ongoing activity by the visually evoked one will depend on the initial state of ongoing activity before any interaction and, once interacting, neither of them can really be considered as independent.

As introduced above, a key notion to stress out is that, in addition to emerge via homogeneous physical stimulation like flickering fields, geometric hallucinatory percepts can also be induced by visual stimuli that are composed of geometric planforms corresponding to actual hallucinatory percepts or, more precisely, to orthogonal planforms. This is crucial because it means that the specificity of retinal geometric planforms visual stimuli can entrain the visual cortex activity into states that already emerge in ongoing activity. This strengthens the interpretation that sensory-driven activity, when corresponding to hallucinatory visual states present in ongoing activity, can force this latter into specific paroxysmal regimes of orientation exploration dynamic characteristic of the visual cortex spatial and temporal properties. Control theory englobes both experimental and theoretical conceptual framework that convergence of sensory driven modulation of ongoing

activity and self-organization of this latter alone into specific, paroxysmal regimes of orientation exploration is useful. It provides an innovative access to the inner organization of the mesoscopic functional architecture of early visual areas. This is particularly relevant for the primary visual cortex (V1 in humans and Non-Human Primates, areas 17 and 18 of the cat). Hallucinations are then, as Wilkinson (2004) said, “windows on the visual brain”.

In order to extend the conceptual framework of the work presented here, we must first precise what is the correspondence between geometric hallucinations induced by visual planforms, that are themselves perceived as geometric hallucinations, and actual induced hallucinatory percepts. Geometric hallucination induced by a physical geometric planform embedded or not in a flickering field does not generate perception of a similar geometric hallucination. It would then be difficult to call it an hallucinatory-like percept since the physical stimulus is actually presented, but adaptation mechanisms will instead generate opponent geometric percepts orthogonal to the geometrical physical inducer. Fans shape and concentric circles are two of the most commonly found and described hallucinatory percepts. They are, as described in figure 7.2 and 7.3, opponent planforms that generate orthogonal stripes of activity on the visual cortex of macaque (tootell et al., 1982) and humans (Tootell et al., 1998) (Upper panel: A, lower panel s1,s2 vs s3,s4). What actual psychophysical evidence do we have concerning that large-scale form of cortical opponency? What potential underlying mechanisms could be responsible for the spatial features of this opponency?

II-1.2 Beyond Mackay’s after-effect: sequential and simultaneous contrast adaptation and spatial opponency

Donald MacKay (1957 a,b, 1965, 1978) was the first to describe a series of perceptual phenomena that were named after him. The large majority of those phenomena involves an opposition between geometric spatial forms. MacKay described those forms as complementary: when a pattern of static, concentric circles is steadily stared at for many seconds, observers report the perception of faint noisy fan-like shape as an afterimage for a few seconds, when the concentric circles inducer is suddenly replaced by a white uniform field. By opposition, when steadily fixating static fans shape patterns for a few seconds, subjects report as an after effect the perception of faint concentric circles for a few seconds. In addition, if subjects do not steadily fixate concentric circles but are allowed to displace their gaze along the visual scene containing the static physical inducer, they report perceiving rotating fans shapes superimposed over the static concentric circles physical inducer and vice versa for fans-shape physical inducer (Figure 7.4, upper and lower pictures). This effect disappears under retinal image stabilization.

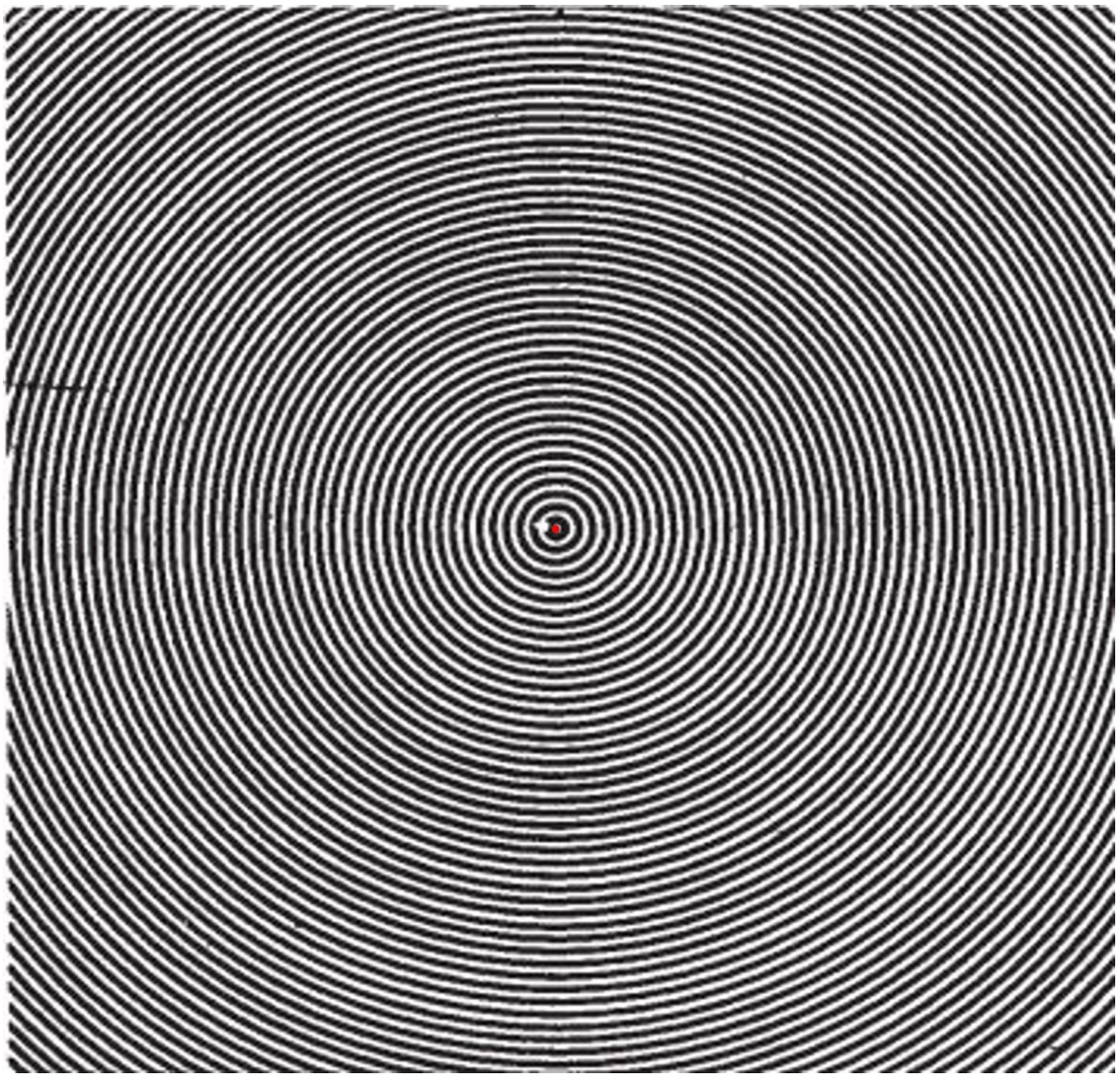

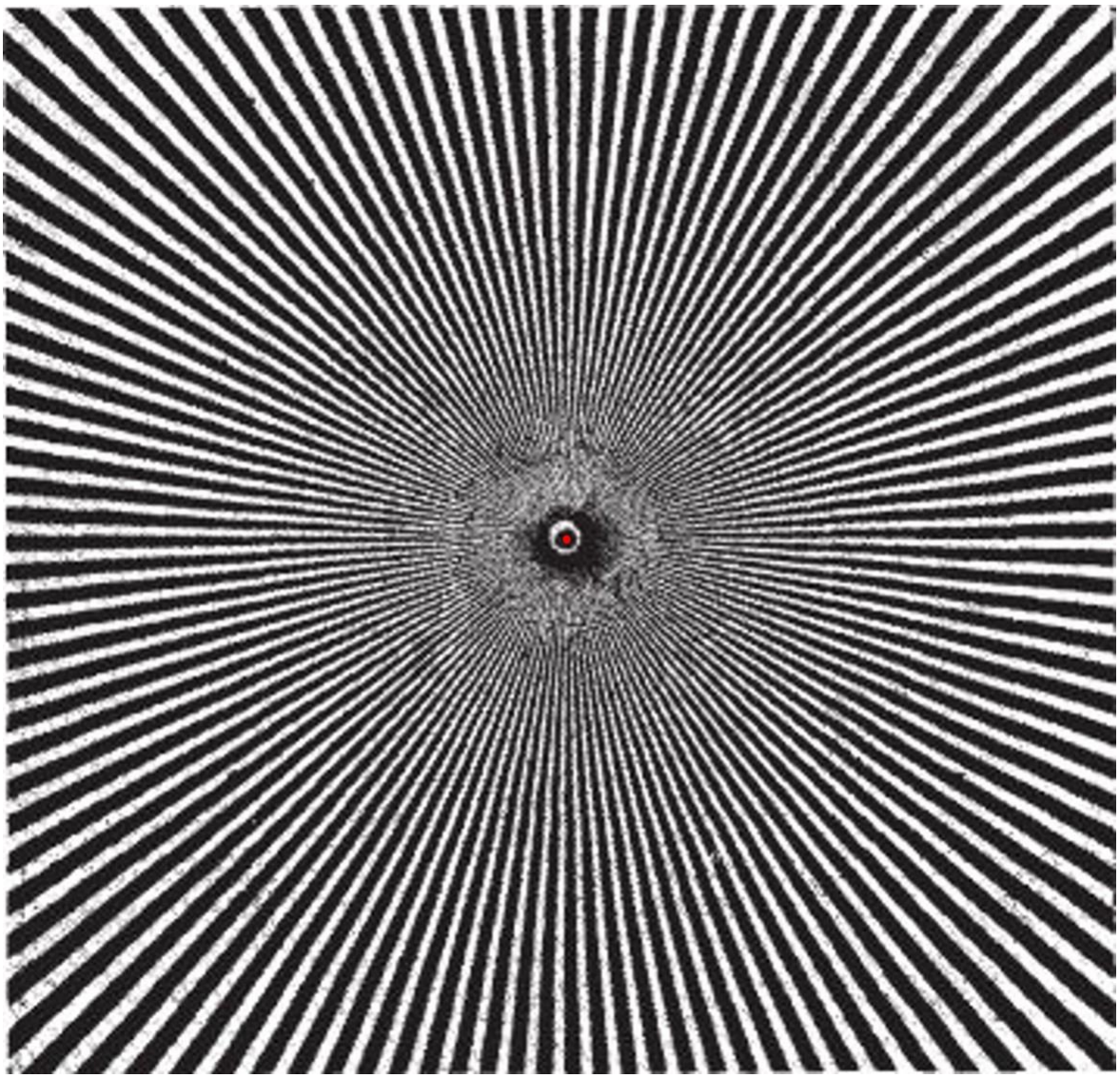

Figure.7.4: ***MacKay's sequential contrast aftereffect and superimposed simultaneous contrast eye movement opposition effect***

Upper image. *After steadily fixating the red point at the center of the concentric circles geometric inducer for a few seconds, perception of radially rotating fans shape is reported for a few seconds when all geometry disappears and is replaced by a uniform level of white or when subjects close their eye. Alternatively, when rapidly moving the gaze across the figure, or more efficiently, when the image is rapidly displaced, subjects report in the* ***Upper image*** *rotating radial fans shape superimposed over the concentric circles physical inducer and in the* ***Lower image****, subjects report pulsating and contracting circles overlaid on the Fans shape physical inducer. Effects are the strongest when visualized on a computer or any device where the luminance of the background is higher than in ordinary vision on paper. These effects advocate for the necessity of a high contrast between geometric inducer and background. See MacKay D. M. (1957 a) Moving visual images produced by regular stationary patterns. Nature, 180, 849 – 850.*

Similarly, if the same geometric inducers patterns are seen while flickering, opponent planforms overlaying the geometric physical inducer will be perceived: rotating fans shape for concentric circles inducer and pulsating circles for fans shape geometric inducer. MacKay interpreted these effects as two phases of perception superimposed on one another: physical concentric circles are seen during the illumination flash period while opponent rotating fans shape are seen during the dark phase (MacKay, 1957 a,b). This extends the notion of opposition from the spatial domain between two orthogonal geometric shapes to the temporal domain where one opponent form is perceived out of phase with the other. While the subject reports seeing both illusions simultaneously when the flicker's frequency is sufficiently high (15-30 Hz) to induce flicker-fusion, the alternation of bright and dark phases is undistinguishable by subjects observing the scene without blinking rapidly. Another variation of the MacKay effect was observed when the physical geometric patterns were printed, cut and superimposed over a TV's static (noise) channel (MacKay, 1965). The same percepts were observed, where noise pixels seemed to aggregate in a spatio-temporal coherent manner corresponding to rotating fans shape and pulsating circles for concentric circles and fans shape physical inducers, respectively. The strength of the percepts was actually different across different channels of static, strengthening the interpretation that the statistics of the noise itself were of importance in the emergence and evolution of the perceived effect. Interestingly, interleaving frames of noise with frames of uniform luminance, strengthened the percepts when viewed binocularly. In contrast, the hallucinatory-like percept disappeared when noise and mask were seen by one eye and blank and mask frames by the other, proving that the phenomena could not take place before the cortical stage where binocular interaction is generated. In 2007, Billock and Tsou strengthened the MacKay noise effect using fractal $1/f^{\alpha}$ noise, whose properties and functional implications will be discussed later.

In the same study, Billock and Tsou (2007) also tested whether structuring only a part of a uniformly flickering field via fans shape and concentric circles geometric inducers placed in the center or the surround of the visual field could extend the hallucinatory-like perception of the physical inducer in the geometrically unstructured part of the visual field. Interestingly, when a geometric inducer was presented in the center of the visual field at flickering frequencies between 10-20 Hz with an optimum at 15 Hz, subject reported opponent planforms in the surround of the physical inducer (pulsating circles for radial fans shape inducer and rotating fans shape for concentric circles inducer). Vice versa, when physical geometric inducers where presented and flickering in the surround of the visual field (Figure 7.5). If surround and center areas were both flickering in phase, the hallucinatory-like percepts were perceived over the entire visual field. It means that it overlaid the physical geometric inducer while the percept of opponent planforms remained confined in the geometrically unstructured area when the geometric inducer area was not flickering or out of phase with the concomitant unstructured region.

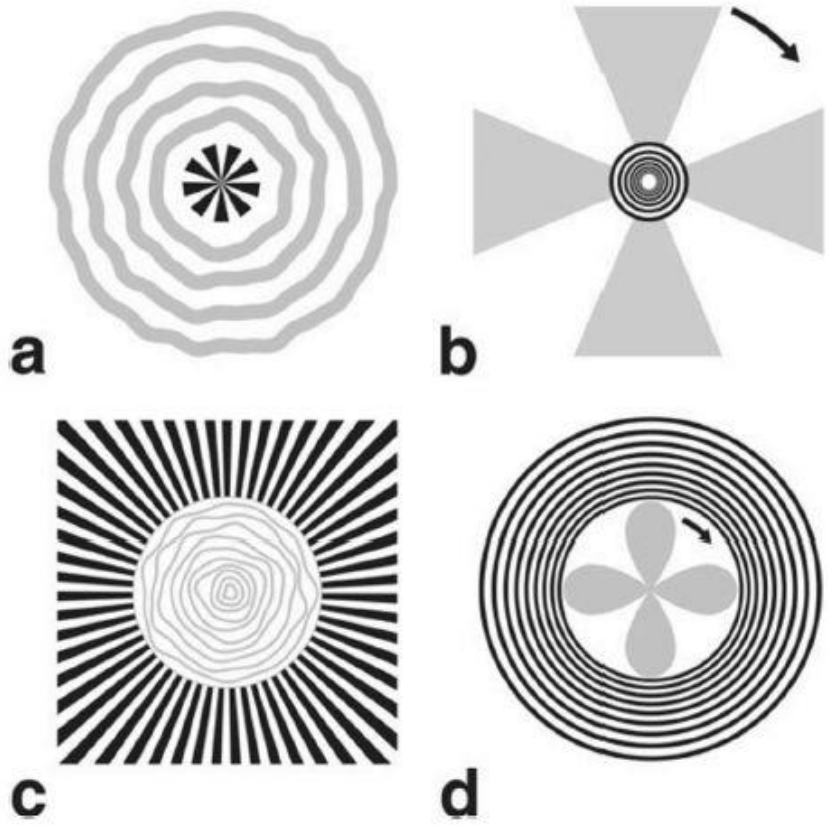

Figure.7.5: ***Flickering induces the propagation of opponent hallucinatory-like percept in unstructured areas of the visual field***

*Billock and Tsou (2007) described their results as a way to bias hallucinatory-like perception of unstructured areas of the visual field. When physical geometric inducers (bold figures) are placed within a flickering field, the hallucinatory-like percept induced by the flicker (gray figures) is orthogonal to the physical geometric inducer. Hallucinatory rotating fans shape or petals are perceived at the borders (**b**) or at the center (**d**) of the visual field when concentric circles are used as a physical inducer while pulsating or wobbling circular patterns are perceived in the surround (**a**) or the center (**c**) of fans shape physical geometric inducer. When center and surround are flickering out of phase, the hallucinatory-like percept remains enclosed in the geometrically unstructured area while it invades the overall visual field and is perceived overlaying the geometric physical inducer when center and surround flicker in phase.*

The findings of Billock and Tsou (2007) strengthen the evidence of a long distance spatial opposition between complementary planforms and their corresponding patterns of activity at the level of the primary visual cortex. More specifically, they introduce the idea that this long distance spatial opposition extends beyond the retinotopic feedforward imprint of a geometric planform inducer, in a concomitant area geometrically unstructured, and that even in those geometrically unstructured parts of the visual field, mechanisms of spatial opposition are sufficient to reach the conscious perceptual level. However, some nuances must be opposed to that interpretation. In

their study, these authors reported that out of 7 subjects, 7 reported perceiving rotating fans shape in the surround of the flickering central area composed of concentric circles physical inducer and pulsating circles in the surround of flickering physical fans shape inducer (Billock and Tsou, 2007).

However, when we take a closer look at the description of their findings in the supplementary information section of their paper, the authors pointed out that: “rotating fans were seen in all experiments” (flickering field, apparent motion and fractal noise induced geometric hallucinations). While in their flickering field experiments: “pulsating rings were occasionally seen”, “but were always seen in experiment 3”: in this experiment, they used fractal noise combined to a stationary geometric inducer and did not test for the invasion of geometrically unstructured area by induced hallucinatory percepts. Firstly, this puts into question the perceptual saliency and reproducibility of the induced hallucinatory pulsating circles percepts in their flickering field experiments. Secondly, this advocates for the confinement of induced hallucinatory percepts into geometrically structured areas, and not beyond, a phenomenon that MacKay had already described (MacKay, 1965, 1978).

This reading of their original report is also in accordance with our own findings: we were not able to replicate the observations of Billock and Tsou (2007). We could not distinguish pulsating rings percepts in flickering field experiments using fans shape physical inducer while we were able to distinguish rotating fans shape, but this latter remained confined in the central region containing the concentric rings geometric inducer. On the other hand, we also observed both rotating fans shape and pulsating circles in visual stimulations combining fractal noise and geometric inducers.

Confining the scope of our investigation to the case mentioned above: appearance of opponent complementary geometric planforms only perceived in geometrically structured areas, the most likely anatomical candidate for a long distance spatial opposition is the anisotropic lateral connectivity of early visual areas. More specifically, the horizontal connectivity intrinsic to V1 (see Chapter "General features of horizontal connectivity, Part I Background”). Indeed, it has been shown that orientation preference of neurons is altered by exposure to oriented stimuli where adaptation produces a “repulsive shift in orientation perception” (Del Mar Quiroga et al., 2016) (human: Clifford et al., 2001; macaque: Carandini et al., 1997; Müller et al., 1999; Wissig and Kohn, 2012; Patterson et al., 2013; 2014; cat: Dragoi et al., 2000b; Sanchez-Vives et al., 2000; Felsen et al., 2002). Moreover, neural adaptation can be observed for stimulus presentation as short as a few hundreds of milliseconds (Müller et al., 1999; Felsen et al., 2002). In this context, this is very likely that ensemble of neurons sharing similar orientation properties and coaligned in visual space become adapted to geometric inducers and can no longer convey facilitatory influence via long distance horizontal connections under the form of excitation. This creates an asymmetry of excitability between populations of cells of orthogonal orientations, where, relatively to the adapted population, cells orthogonal to the ones adapted to the physical inducer are the most excitable. In the MacKay’s after effect, disappearance of the physical stimulus can create a perturbation of the state already in disequilibrium. Non-adapted cells orthogonal to the geometric

inducer would share a similar degree of relative increase in excitability. The neighbor to neighbor binding of facilitatory activity via long distance horizontal connections preferentially linking iso-oriented patch would, under the influence of that perturbation, bring up to the perceptual threshold level waves of activity. Their geometric distribution in the visual field corresponds to opponent planforms orthogonal to the geometric inducer.

Similarly, in flickering field experiments, the flicker would evoke an homogeneous perturbation of cortical activity mainly influencing non-adapted cells. By opposition, cells adapted to the geometric inducer would be rather insensitive to the homogeneous perturbation and would not facilitate via horizontal connections the neighbor to neighbor activation of iso-oriented patches. The confinement of hallucinatory-like opponent planforms to geometrically structured areas, and not beyond, suggests that each contrasted feature of the geometric planform (each fan and each ring) acts as a spatial relay of relative inhibition. On the other hand, each population of cells locally orthogonal to the geometric inducer would still be relatively more excitable because they are not adapted. That "opponent" population would not be adapted both in areas directly stimulated by the geometric inducer but also between the features composing it. This would explain why the homogeneous perturbation elicited by the flicker would only bring to perceptual threshold the preferential neighbor to neighbor binding activity of the non-adapted population locally orthogonal to the geometric inducer. Under the influence of the homogeneous perturbation providing excitation, cells sharing similar orientation properties locally orthogonal to the features of the geometric inducer would propagate facilitatory activity both in between features of the physical inducer and overlaying this latter. At the perceptual level, this corresponds to the effects described by MacKay in his flickering field and noise experiments, as well as the results of Billock and Tsou (2007) in their flickering field and noise experiments.

The conceptual framework of the MacKay's after-effect and flickering field simultaneous effect presented in the last paragraph provides a rather extended and plausible view of physiological correlates of those perceptual phenomena. The notion of adaptation to a geometric planform was already introduced by MacKay himself, as well as others after him. For instance, Georgeson (1976) explained MacKay's rotating fan shapes percepts by proposing the existence of a mutual antagonism between pattern and movement channels within the same orientation column. In addition, Vidyasagar et al., (1999) found that opponent after-effects are stronger when opponent geometric planforms are seen successively, interleaved by a blank screen (Figure 7.6 a). They also found that presentation of dynamic geometric planforms (rotating fans-shape in a clockwise then anticlockwise and pulsating then wobbling concentric circles) induced much stronger perception of opponent planforms when the temporal dynamic of presentation of the geometric inducers was raised, while remaining in a slow regime (from 0.2 to 2 Hz). According to them, the slow temporal dynamic that they used is a requirement to induce the percept, indicating that the sustained stimulation of patterns channels is crucial to the hallucinatory-like percept, advocating once again for an adaptation phenomenon. They proposed that the synaptic trace of exposure to a geometric

pattern lasts for about half a minute, but also that this trace is brought back to perception (and stronger) by a rebound of inhibition caused by orthogonal orientations. In other words, the synaptic trace of the first geometric inducer would be amplified and reach the perceptual threshold by a rebound of inhibition caused by a strong adaptation to the second geometric inducer orthogonal to the first one. According to them, this effect would come from an antagonism not only existing within an orientation column (Georgeson, 1976), but between orthogonal orientation columns.

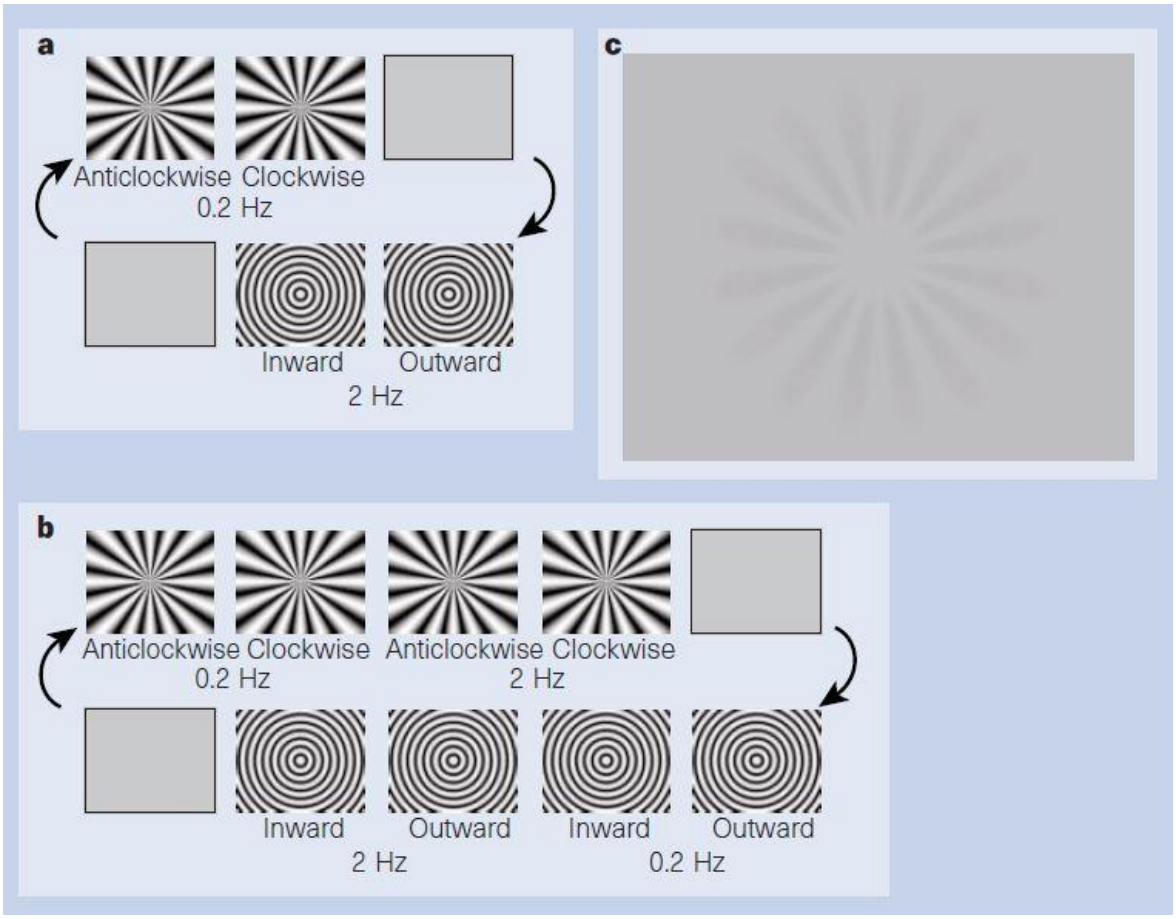

Figure 7.6: ***Inhibition rebound from release of adaptation to a geometric inducer reinforces opponent geometric planform perception: evidence for cross-orientation intercolumnar interaction.*** *Two different sequences of image were presented in* ***a*** *and* ***b*** *to test for the after-effect. The screen was placed at a distance of 85 cm from the observers.* ***a****. Anticlockwise and clockwise rotation of fans at an angular frequency of 0.2 Hz were sequentially presented on a uniform blank screen of the same average luminance (31.3 cd.m²) before pulsating and wobbling circles presented at a frequency of 2 Hz. The presentation of that sequence greatly strengthened the perception of opponent fan planform for a few seconds when switching to a blank screen at the end of the sequence (lower left gray panel).* ***c****. Enlargement of the fans shape pattern perceived at the end of the sequence in the lower left blank panel. The perceived fans shape represented reproduce with*

fidelity the contrast of the reported percept. ***b.*** *In another set of experiments, increasing the angular speed of rotation of fans shape presented in anticlockwise then clockwise fashion from 0.2 to 2 Hz greatly increase the perceptual saliency of opponent concentric circles when a gray blank field is presented at the end of the sequence. The same phenomenon is observed for concentric circles physical geometric inducer (From Vidyasagar et al., 1999).*

Other arguments in favour of the implication of lateral connectivity in the anisotropic modulation of activity of V1 between distinct hypercolumns exist. The notion that an homogeneous perturbation or destabilization process of the intracortical state is part of a larger theoretical framework explaining spatio-temporal pattern formation in V1.

II-1.3 Theoretical models of selection and stabilisation of spatio-temporal stable states intrinsic to V1's functional architecture

Ermentrout and Cowan (1979) were the first to introduce a model of hallucinatory pattern formation during migraines, basing themselves on Turing (1952) differential equations of reaction-diffusion. These equations describe interactions between an activator and an inhibitor where both have a mutual effect on each other (inhibition of activation and activation of inhibition) via a coupling constant and depend on different spatial and temporal diffusing processes and concentrations. In Turing's initial model of reaction-diffusion system (1952), those different parameters accounted for the formation of different periodic patterns of stripes and spots coloration off some animal's fur. Later on, Tass (1997) decomposed the dynamic of transition of Ermentrout and Cowan (1979) initial model of pattern formation which initially only accounted for the emergence of purely static patterns of activity on V1 (Figure 7.2 A). His work also studied how specific patterns could emerge and compete with each other according to the initial conditions of spontaneous activity. In 2001 and 2002, Bressloff et al., (2001, 2002) extended the initial model of Ermentrout and Cowan (1979) by introducing anisotropies between iso-orientation preference domains connected by long-distance horizontal connections. They funded the mathematical prerequisite to the emergence of specific patterns of activity by defining the relative weight and spatial extent of excitatory and inhibitory influence between orientation patch belonging to distinct hypercolumns. Assuming symmetries between hypercolumns lateral connections, Bressloff and his colleagues established that the basic pattern of connection between hypercolumns is invariant under shift in spatial position and twist in angular representation of orientation under the action of the Euclidean group E(2). Using this symmetry, they showed that the various patterns of activity that spontaneously emerge when V1's spatially uniform resting state becomes unstable actually correspond to the form constants defined by Klüver (1966) when transformed to the visual field using the retino-cortical map. Their results suggest that cortical mechanisms that generate geometric hallucinations are closely related to those used to process edges, contours, surfaces and

textures. This work has been extensively reviewed by Jean Petitot, Giovanna Citti and Alessandro Sarti (Citti and Petitot, 2007, 2009).

Let us introduce key notions of their work.

Each location in the visual field is approximately represented in V1 by a hypercolumn-sized region containing all orientations, i.e, an Aggregate Receptive Field. Therefore, each point of space $\mathbf{r}$ and orientation $\boldsymbol{\phi}$ are considered as independent variables, so that all possible orientation preferences exist at each corresponding position $\mathbf{r}_R$ in the visual field. This describes a continuum approximation that allow to mathematically tract V1's surface as a lattice of hypercolumns.

Within that continuum framework, let $\mathcal{W}(\mathbf{r}, \boldsymbol{\phi} \mid \mathbf{r'}, \boldsymbol{\phi'})$ be the strength or weight of connections from the iso-orientation patch at $\{x', y'\} = \mathbf{r'}$ in V1 with orientation preference $\boldsymbol{\phi'}$ to the patch at $\{x, y\} = \mathbf{r}$ with preference $\boldsymbol{\phi}$. $\mathcal{W}$ can then be decomposed in terms of local connections from elements within the same hypercolumn and patchy lateral connections from elements in other hypercolumns, that is,

$$\mathcal{W}(\mathbf{r}, \boldsymbol{\phi} \mid \mathbf{r'}, \boldsymbol{\phi'}) = \mathcal{W}_{LOC}(\boldsymbol{\phi} - \boldsymbol{\phi'})\, \delta(\mathbf{r} - \mathbf{r'})$$

$$+ \beta\, \mathcal{W}_{LAT}(s)\, \delta(\mathbf{r} - \mathbf{r'} - s\mathbf{e}_{\boldsymbol{\phi}})\, \delta(\boldsymbol{\phi} - \boldsymbol{\phi'}), \qquad (1.1)$$

where $\delta(.)$ is the Dirac delta function, $\mathbf{e}_{\boldsymbol{\phi}}$ is a unit vector in the $\boldsymbol{\phi}$ direction, β is a parameter that measures the weight of lateral relative to local connections and $\mathcal{W}_{LAT}(s)$ is the weight of lateral connections between iso-orientation patches separated by a cortical distance s along a visuotopic axis parallel to their orientation preference. Figure 7.7 illustrates the different parameters of equation (1.1).

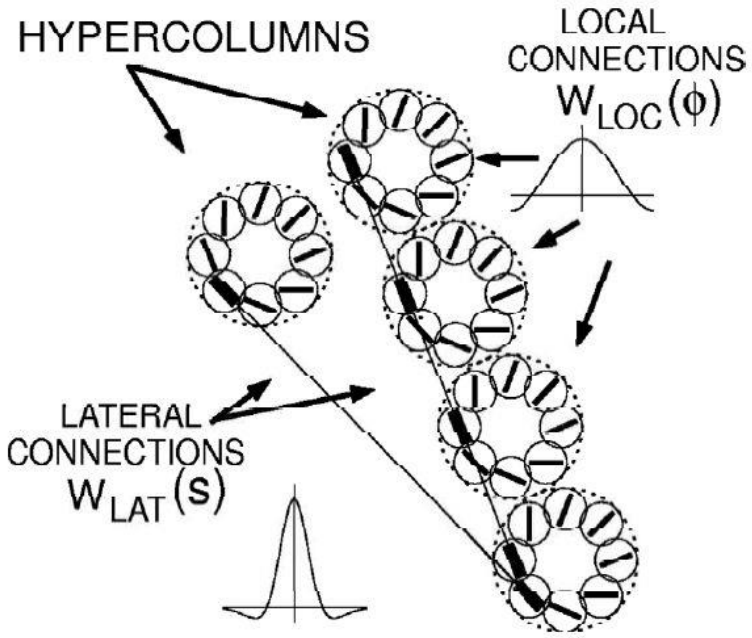

Figure.7.7: ***Parameters of equation (1.1) illustrated at the cortical level***

Here, local connections correspond to connections between orientation columns within an hypercolumn and are isotropic, as opposed to long distance lateral connections linking iso-orientation patches of distinct hypercolumns that are anisotropic. (From Bressloff et al., 2002).

The influence of horizontal connectivity is generally considered as modulatory rather than strong enough to drive V1 activity (Hirsch and Gilbert, 1991), that is why β is small. It has been shown (Wiener, 1994; Cowan, 1997; Bressloff et al., 2001) that the weighting function described in equation (1.1) has a well-defined symmetry: this connectivity pattern is invariant to certain operations in the plane of V1 such as

translation $\{\mathbf{r}, \boldsymbol{\phi}\} \rightarrow \{\mathbf{r} + \mathbf{u}, \boldsymbol{\phi}\}$,

reflection $\{x, y, \boldsymbol{\phi}\} \rightarrow \{x, -y, -\boldsymbol{\phi}\}$,

rotation $\{\mathbf{r}, \boldsymbol{\phi}\} \rightarrow \{R_\theta[\mathbf{r}], \boldsymbol{\phi} + \theta\}$,

where $R_\theta[\mathbf{r}]$ is the vector $\mathbf{r}$ rotated by the angle θ. This form of the rotation operation comes from the anisotropy of the lateral weighting function. It comprises a translation or shift of the orientation preference label $\boldsymbol{\phi}$ to $\boldsymbol{\phi} + \theta$, together with a rotation or twist of the position vector $\mathbf{r}$ by the angle θ. The fact that the weighting function (1.1) is invariant to such shift-twist operations in the Euclidean plane E(2) is extremely important for any model of the dynamics of pattern formation and propagation of V1. Specifically, the equivariant branching lemma of Golubitsky and Schaeffer, (1985) assures that when a homogeneous state becomes unstable, new states

possessing the symmetry of certain subgroups of the Euclidean plane can arise. These new states are combinations of cortical planforms.

Let us dive deeper in the formulation of the dynamic of V1 activity over time, taking as a starting point the weighting function defined in (1.1). By incorporating the continuum of the weighting function, let the activity variable $a(\mathbf{r}, \boldsymbol{\phi}, t)$ be the average membrane potential or spiking response in an iso-orientation patch at the point $\mathbf{r}$ with orientation preference $\boldsymbol{\phi}$. Its evolution over time is given by:

$$\frac{\partial a(\mathbf{r}, \boldsymbol{\phi}, t)}{\partial t} = -\alpha\, a(\mathbf{r}, \boldsymbol{\phi}, t) + \frac{\mu}{\pi} \int_0^{\pi} W_{LOC}\,(\boldsymbol{\phi} - \boldsymbol{\phi}')\ \sigma\,[a(\mathbf{r}, \boldsymbol{\phi}, t)]\, d\,\boldsymbol{\phi}'$$

$$+ \nu \int_{-\infty}^{\infty} W_{LAT}\,(s)\ \sigma\,[a(\mathbf{r} + s\mathbf{e}\,, \boldsymbol{\phi}, t)]\, ds, \qquad (1.2)$$

Where α is a time constant, $\boldsymbol{\mu}$ and $\nu = \boldsymbol{\mu}\beta$ are coupling constant weighting the relative strength of local and lateral connectivity and where the distribution over π of local connectivity denotes its isotropy. $\sigma\,[a]$ is a smooth sigmoidal function of the activity a. In that single population model, excitatory and inhibitory neurons are not distinguished. The form of the functions $\mathcal{W}_{LOC}(\boldsymbol{\phi})$ and $\mathcal{W}_{LAT}(s)$ are therefore assumed to be "Mexican hats" of the generic form:

$$\sigma_1^{-1} \exp(-x^2 / 2\,\sigma_1^{\,2}) - \sigma_2^{-1} \exp(-x^2 / 2\,\sigma_2^{\,2}) \qquad (1.3)$$

$(\sigma_1 < \sigma_2)$, such that iso-orientation patches at nearby locations mutually excite if they have similar orientation preferences while inhibit otherwise and similar iso-orientation patches at locations at least $\mathbf{r_0}$ mm apart, when reaching the inhibitory sides of the Difference of Gaussians, mutually inhibit. From the application of the shift-twist action on the Euclidean symmetry of the weighting function $\mathcal{W}(\mathbf{r}, \boldsymbol{\phi} \mid \mathbf{r}', \boldsymbol{\phi}')$, it follows that the evolution of the weighting function from 1.2 is equivariant regarding the shift-twist operation. Not only does the strength of connections between iso orientation patches is left invariant under shift in spatial position and twist in angular representation, but the activity carried by this connectivity pattern also remains unchanged. It is extremely important for the dynamic of V1 activity as we understand that both the connectivity template between different iso-orientation patches and the activity carried by that connectivity pattern are left unchanged under displacement in space and rotation in the plane, provided that

the orientation label is changed. This reminds us of the pulsating/wobbling and rotation characteristics of the hallucinatory-like concentric circles and fans-shapes, respectively, that reflect a displacement of cortical activity. If the excitability of V1 is increased by the action of hallucinogens, migraines or by a uniform perturbation of the visual field like a flickering field the homogeneous stationary state becomes unstable. New states develop that can be approximated by finite linear combinations of the eigenfunctions of the linearized version of equation 1.2 where the equivariant branching lemma (Golubitisky and Schaeffer, 1985) guarantees the existence of new states that possess the symmetry of certain subgroups of the Euclidean group (E2). Using mathematical decomposition methods, the authors obtained the actual patterns of cortical activity corresponding to the cortical planforms that are left invariant under the shift-twist action. The most stable planforms are then generated by plotting at each point $\mathbf{r}$ a contour element at the orientation $\boldsymbol{\phi}$ most strongly signaled at that point (Figure 7.8).

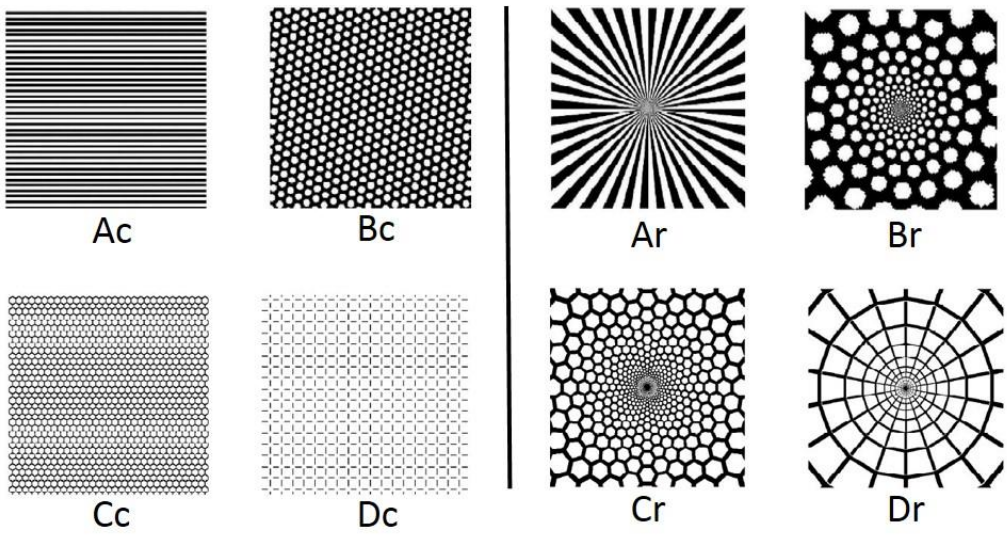

Figure.7.8: ***V1 and Visual field corresponding stable planforms***

Left panel: *V1 planforms corresponding to some axial subgroups. Second letter c for cortex. Ac, Bc: Roll and hexagonal patterns generated in V1 when this latter is in the Hubel-Wiesel operating mode. Cc, Dc: Honeycomb and square patterns generated when V1 is in the coupled-ring (coupled hypercolumns) operating mode.* ***Right panel:*** *Same planforms as in* ***Left panel*** *in visual field coordinates. Second letter r for retina. (From Bressloff et al., 2002).*

Figure 7.8 depicts the cortical and matching retinotopic representation of some of the most stable planforms that can emerge under increase of excitability of V1. We must emphasize that those planforms are not stable: once selected, one planform pattern or state of activity won't remain stable over all time but can evolve into other planforms. In other words, rotating fans shape can emerge, before transforming themselves into rotating spirals that themselves turn into pulsating circles (Billock and Tsou, 2007, 2012). This corresponds to the temporal instability of the transition dynamic characteristic of hallucinations, happening both in spontaneous activity when subjects have migraines or under drug influence and in flicker-induced reported percepts.

In all those cases, subjects report an apparently random transition and alternation between different planforms, something that complicates tremendously a parametrized study of geometrical hallucinations in the visual brain, of their neuronal correlates and of the underlying dynamic of population interaction. This cortical instability of transition between planforms has been described as multistables states because the shapes and duration of perceived hallucinations evolve and their transition seem random. This is analogous to empty-field flicker induced hallucinations which may take as long as 30s of visual stimulation before appearing and then change unpredictably (Billock and Tsou, 2007). According to Billock and Tsou (2007), empty-field flicker stimulation elicits a succession of perceptual states where a subject may fleetingly perceive a fan shape before a hexagonal lattice appears which in turn gives way to a spiral. However, the same authors (2012) pointed out that the results of an anisotropic model like the one of Bressloff et al., (2001, 2002) is in accordance with their observations that fans and concentric circles hallucinatory percepts are more salient and appear more often than spirals, what the initial theoretical model of Ermentrout and Cowan, (1979) didn't account for. Moreover, in empty-field flicker experiments, Billock and Tsou (2007, 2012) argue that each temporal modulation is both a stimulus to pattern formation by providing increased excitation to the network, but also a perturbation disturbing the previously elicited state. Such perturbation or changes in the fragile guidance of the pattern in formation could also happen in spontaneous activity, when no visual stimulation is present, explaining the seemingly random duration and transition of perceived planforms.

The planforms obtained by Bressloff et al., (2002) are said to be either contoured or non-contoured and correspond closely to Klüver's form constants. According to Bressloff et al., (2002), in what they call the Hubel-Wiesel mode, interactions between orientation patches within a single hypercolumn are weak and purely excitatory. However, stronger inhibition via long range lateral interactions allow distinct hypercolumns to amplify certain orientations, resulting in plane waves of cortical activity with no label for orientation preference. The resulting planforms are called non-contoured (Figure 7.8 Ac, Bc) and correspond to type I and II form constants (Figure 7.1 I, II). On the other hand, coupled-ring mode interactions (interaction between coupled hypercolumns) between neighbouring iso-orientation patches of distinct hypercolumns may be strong. If they are strong enough, so that even weakly biased activity can trigger a sharply tuned response, then, under the combined action of many interacting hypercolumns, plane waves labeled for orientation preference can emerge. Resulting planforms (Figure 7.8 Cc, Dc) correspond to types III and IV form constants (Figure 7.1 III, IV). Although this interpretation is interesting, it must however be nuanced because

the authors themselves explained that even non-contoured planforms (type I and II) can emerge if the strength of lateral connections is sufficiently high. It however becomes apparent that the circuits in V1 that are normally involved in detection of oriented edges and contours formation are also responsible for the generation of the form constants. The reason to think so is that form constants which are seen as hallucinations in the visual field correspond to the most stable planforms obtained by Bressloff et al., (2001, 2002) in a mathematical model framework that directly implements specific aspects of V1's wiring architecture.

II-2. Working Hypothesis

As described in the previous chapter, homogeneous perturbation during empty-field flicker stimulation evokes activity that provides isotropic excitation. At the functional level, that visual stimulation physically presented is the analogue of the increase in ongoing activity of V1 under the influence of drugs or migraines. This increase in activity results at the psychophysical level in the perception of multistables states during which distinct geometric planforms alternate between one another in a seemingly random fashion. The set of described geometric planforms is however relatively restricted since human subjects depict and report similar percepts through time and all over the world. Mathematically, the relative invariance of these sets of planforms, as defined by Paul Bressloff, are predictable in a theoretical framework. They correspond to the Klüver form constants and are the most stable planforms of V1 obtained under the shift-twist action of the Euclidean group on the patterns of connections between distinct hypercolumns linking iso-orientation patches via anisotropic lateral connections (Bressloff et al., 2002). The similarity between the geometry of planforms, the hallucinatory-like retinal patterns reported in psychophysics and the cortical activation patterns evoked by stimulation of specific classes of physical stimuli is compelling. It strongly suggests the implication of V1 and of its anisotropic lateral connectivity in the emergence, selection and propagation of activity leading to hallucinatory-like percepts.

In order to develop our working hypothesis, we propose a model of plausible physiological interactions between hypercolumns, based on electrophysiological, psychophysical and modelling evidence. In the models of hallucinatory planforms formation of Ermentrout and Cowan., (1979); Tass., (1995, 1997); Bressloff et al., (2001, 2002), the log-polar transform between retina and cortex imply that cortical stripes of activity correspond to neighboring orientations smoothly distributed in adjacent loci on V1's surface. However, in those models, there is no description of potential mechanistic interactions between neighboring hypercolumns that explains how a smooth distribution of neighboring orientations on the cortical surface can emerge as a stable state. We approach the problem from a phenomenological point of view as we seek to explain how hypercolumns interactions are at the origin of geometric planforms formation and selection in V1. By introducing our model, we will first distinguish how can those interactions account for the emergence of static, spatially uniformly distributed hallucinatory-like percept and justify their implication into dynamic, progressively propagating ones. Then, we will explain how physical stimulation by a geometric planform can account for the passage between seemingly random alternations of multistables geometric planforms to directly inducible and stable over time ones, necessary condition to a parametrized study. We will then detail the necessary conditions of activity dynamic in V1 and justify the use of the cat as an adequate model. This will allow us to build-up the conceptual framework that interaction between evoked and ongoing activity results in

propagating waves of activity whose geometric distribution over time corresponds to hallucinatory-like percepts, rendering them detectable at the single cell level of V1.

II-2.1 Geometric pattern formation results from a repulsive shift in orientation within and between hypercolumns: link between experimental data and theoretical models

II-2.1.1 Neural Stripes of activity in V1 results in a smooth spatial gradient of orientation preference shifts

We saw, from figure 7.2 A, B and C and 7.3 upper panel: A, B and lower panel that the log polar transformation of retinal planforms corresponding to fans shapes and concentric circles results at the cortical level in horizontal and vertical stripes of activity, respectively. Although it is evident from a neurogeometric point of view, it is important for our model to precise that a retinal circle presented in a visual hemifield corresponds to a cortical stripe of activity along which orientations present a smooth transition between adjacent loci of the cortical stripe, ranging from -π/2 to + π/2, as illustrated on Figure 8.1.

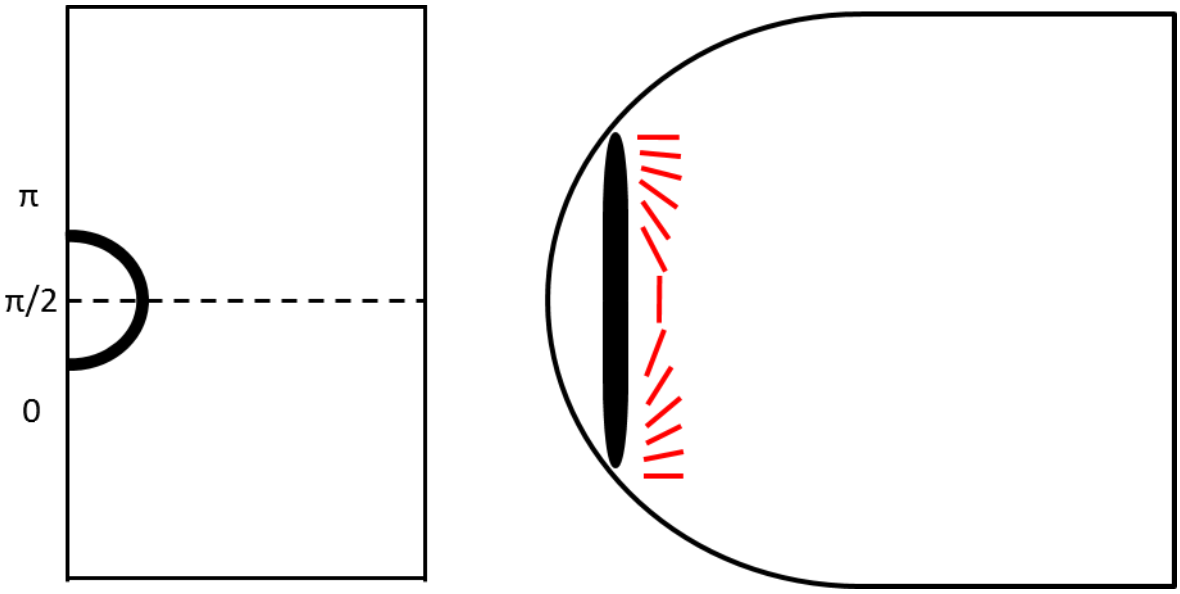

Figure.8.1: ***Neural stripes of activity correspond to smooth transition of orientation preference representation in adjacent loci on V1. Left****; visual hemifield representation where half of a circle is*

represented in bold black. ***Right****; bold black: cortical mapping of a neural stripe of activity on V1's surface corresponding to the log polar mapping of the half circle of the visual field on the left. In red is depicted a cartoon of the smooth orientation transition representation along the cortical stripe of activity. If the circle is physically presented as a visual stimulus, then the corresponding stripe of activity is evoked. Conversely, if the neural stripe of activity forms in V1 as an hallucinatory state, then the circle is perceived under the retino-cortical transformation of visual space.*

When a physical stimulus is presented (several circles), the smooth transition of orientation representation on V1, manifesting itself under parallel neural stripes of activity, is a direct consequence of the log-polar transformation of visual space. The same goes for a fans shape planform. If, without any visual stimulation, concentric circles are perceived as hallucinations, it means that this peculiar distribution of orientation representation emerges at the cortical level as a stable state and therefore represents an intrinsic property of the functional architecture of V1. This is the case as we saw that fans-shape, which only differ from concentric circles by the orientation of the corresponding cortical stripes of activity (horizontal instead of vertical), is one of the most stable planforms of V1. As Bressloff et al., (2002) demonstrated, (Figure 7.8 Ac and Ar) the pattern of connections between iso-oriented patches of distinct hypercolulmns is left invariant under the shift-twist action of the Euclidean group, resulting in some of the most stable states in horizontal stripes of activity (Figure 7.8 Ac). This corresponds at the perceptual level to fans shape (Figure 7.8 Ar). From a systemic approach, how can the smooth transition of orientation representation across cortical space be one of the most stable states of V1? What potential mechanisms could underlie this physiological reality and what experimental evidence can possibly explain that observation?

II-2.1.2 Psychophysical evidence of repulsive shift in orientation

To answer those questions, we need to dive into evidence of repulsive shifts (or attractive ones) in orientation distribution of activity both at the psychophysical and electrophysiological level, as well as model predictions of such phenomena. Pioneer psychophysical study showed that the orientation discrimination threshold of a target line segment becomes increased when a line is presented in superposition to a second line segment tilted about 10-20° from the target (Westheimer et al., 1976). Blakemore et al., (1970) were the first to introduce the idea that summation of mexican-hat-like profiles of activity evoked by lines of different orientations presented in concomitant regions of space result in a repulsive shift of orientation. It does so because the peak of the two populations of activity is displaced from one another, due to mutual inhibition coming from the lateral inhibitory sides of the activity profile distribution. By measuring the perceived orientation of a line segment, studies reported that human observers perceive the angular distance between the target and a simultaneously presented line or mask grating as larger than physically presented (orientation repulsion or tilt illusion; Blakemore et al., 1970; Mitchell and

Muir, 1976; O'Toole and Wenderoth, 1977; Wenderoth and Johnstone, 1988, Westheimer, 1989, 1990). The repulsion effect was reported to be maximal for angular differences of about 20° and to be tightly tuned for spatial position (Westheimer, 1989, 1990). It is accepted by most authors that repulsion can be explained by inhibitory interactions between orientation-tuned neurons in V1, which was successfully modelled with such assumptions (Bednar and Mikkulainen, 2000; Jin et al., 2005). Paradiso (1988) argued that such repulsion-attraction interactions can be explained by inhibitory interactions within a neuronal population of a V1 hypercolumn (Figure 8.2).

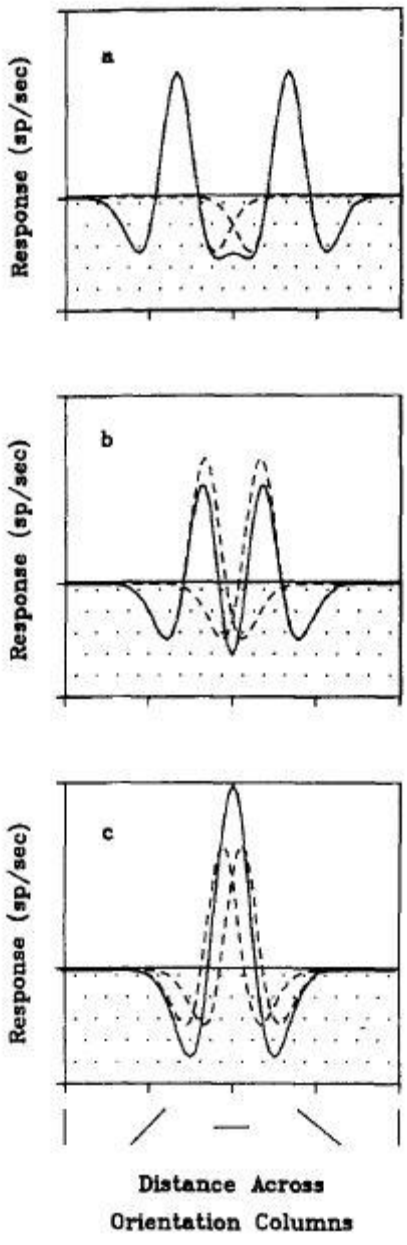

Figure.8.2: ***Orientation estimation errors in a V1 hypercolumn.*** *Tilted lines at the bottom of the figure represent optimal orientations for cells in the hypercolumn.* ***a****; When two lines differ significantly in orientation, lateral inhibition via local connections between orientation patches have little impact: the total activity profile (solid lines) does not differ from the peaks from isolated lines (dashed lines).* ***b****; On the other hand, if the inhibitory tails of the mexican hat produced by the activation of neighbouring orientation patches are significantly overlapping with the excitation provided by the other orientation source, the peaks of the activity profile of each orientation is reduced and displaced from each other (angular expansion or orientation repulsion)* ***c****. If the two test orientations are close to each other, the total activity profile can have peaks (or a single peak) displaced towards each other (angular compression or orientation attraction). (From Paradiso, 1988).*

II-2.1.3 Electrophysiological evidence of repulsive shift in orientation

At the physiological level, several studies have shown that the orientation preference of single neurons is altered by exposure to oriented stimuli (Clifford et al., 2001; Dragoi et al., 2000b, 2002; Felsen et al., 2002; Muller et al., 1999; Patterson et al., 2013, 2014; Wissig and Kohn, 2012). These alterations in neuronal response have been linked to the tilt-after effect, where adaptation extends the repulsive shift in orientation in the temporal domain as neurons shift their preferred orientation after exposure to an oriented stimulus. These fast adaptation mechanisms can be observed even when the adapting stimulus is presented for only a few tens of milliseconds (Felsen et al., 2002; Müller et al., 1999). Felsen et al., (2002) measured in cat V1 tuning curves during sequences of very brief (17-25 ms) oriented stimuli. They reported that neurons showed repulsive effects on tuning curves, as the preferred orientation of neurons shifted *away* from that of the preceding stimulus and the effect was greater for adaptor orientation values on the flanks of the tuning curve. These two facts enlarge the spectrum of simple shift in orientation to real, continuous exploration of neighboring orientation domains over time. Patterson et al., (2013) found the same phenomenon in the macaque V1 but found larger and longer lasting repulsive shifts (about 200 ms), potentially because they used longer adaptation and test stimuli (400 ms each).

II-2.1.4 Lateral connectivity as a self-organizing engine for the spatial propagation of fast repulsive orientation shift adaptation

Del Mar Quiroga et al., (2016) modelled a network of recurrent connections specifically adapted to reproduce the findings of Felsen et al., (2002) in the cat and of Patterson et al., (2013) in the macaque V1. Their model of a function hypercolumn (all receptive fields are co-registered to the

same location in space) is in the line of well-documented models of biologically plausible recurrent connections (Carandini and Ringach, 1997; Somers et al., 1995; Teich and Qian; 2003). The hypercolumn model consists of a bank of V1 filters, each with a different stimulus orientation preference inherited from a weakly tuned feedforward input from thalamus. Lateral connectivity for each neuron was modelled as the difference of two von Mises functions, representing excitatory and inhibitory connections. The appropriate choices of the parameters resulted in a typical Mexican hat profile in the orientation domain, as initially posited by Swindale. Those parameters of the model were fixed over time and did not implement any long-lasting form of plasticity (associative change in synaptic weight or response gain). The free parameters of the model were however constrained by general knowledge about V1 neuron properties and by experimental data obtained by Felsen et al., (2002). The experimental results constraining the model were the following: repulsive effect on tuning curves with a shift away from the orientation of the preceding visual stimulus and greatest effect for adaptor orientation stimuli on the flanks of the tuning curves, i.e, near the neuron's preferred orientation. More precisely, the model had to satisfy two criteria: first, to produce V1-like responses to oriented stimuli presented in isolation (plausible peak firing rate, tuning bandwidth, time-to-peak). Second, the responses to sequential pairs of oriented stimuli had to reproduce as closely as possible the cat V1 adaptation pattern and dynamics of Felsen et al., (2002), which resulted in their C-Model (C for Cat). Their model captured very well the direction, magnitude and time course of the tuning curve shifts found experimentally in cat V1, without assuming any form of synaptic plasticity. By modulating the duration of stimulation, their model also captured very well the adaptation effects found in the macaque V1 by Patterson et al., (2013).

In summary, the important result was to show a form of adaptation which did not require neural plasticity, but emerged naturally from the dynamics of a recurrently connected network of neurons within a single hypercolumn. The "adaptation engine" is assumed to be the recurrence added by lateral connectivity since simulations showed that lateral connectivity strength was a significant contributing factor to the magnitude and decay time course of the functional adaptation dynamics. Note that lateral connectivity is restricted here to local intercolumnar interactions within the hypercolumn.

Their extensive simulations showed that the recurrent nature of the intracortical architecture was the key factor generating large (10°) and long-lasting (1 s) tuning curve shifts while maintaining basic tuning properties for isolated stimuli consistent with recordings in V1. However, this 10° shift amplitude was lower than the 20° observed in psychophysics experiment. Interestingly, comparison between simulations suggested that the strength of lateral connectivity titrated decay time course of the adaptation dynamics. For instance, models in which tuning curve shifts decayed rapidly had relatively weak lateral interactions, whereas both large and long-lasting shifts in orientation tuning curve required strong lateral connections. This makes sense, knowing that the weak interaction model (C-model) was based on experimental findings where the authors (Felsen et al., 2002) used pairs of stimuli flashed for 17-25 m. In such conditions, the slow velocity of activity propagation along unmyelinated lateral projections had reduced time opportunity to impact the model, contrarily to long decay of tuning curve shift for several hundreds of ms. Interestingly recurrent

inhibition and excitation has opposite effects: an increase in the relative strength of inhibition regarding excitation decreased the size of tuning curve shifts. This must be pondered since, according to the level of activation, the spatial extents of excitation and inhibition both vary with a broad dispersion for weak activation and much narrower distributions for higher levels of activation.

To understand why tuning curves shift after exposure to an oriented stimulus, the authors then examined single unit and population responses to sequential pairs of gratings. The first grating (the adaptor) was presented until the network converged. What is really of key importance here is what happened to the network when the stimulus was then switched to a new orientation (the test). Interestingly, the authors found that the network dynamics of convergence largely depended on the orientation difference between the two successive gratings. Importantly, for pairs or neighboring orientation (-20°/0°) exactly in the range of stronger angular repulsion reported in psychophysics, population activity resembled a traveling wave in the orientation domain of increasing amplitude as it displaced itself towards the 0° test stimulus and away from the preceding -20° adaptor stimulus. For larger angular distance (90°), it no longer resembled a travelling wave as activity collapsed around 90° and resurfaced around 0° (Figure 8.3 D). Moreover, the dynamic of transition was much faster for small angular distance as the neuron reached a steady state more quickly (40 ms for a 0-10 ° pair against 60 ms for a 0-90° pair). While this model simulates the response of an entire hypercolumn, using VSD imaging, Benucci et al., (2009) found, throughout several hypercolumns in cat V1, spatial shifts across distinct orientation domains whose transition dynamic is compatible with the results of Del Mar Quiroga et al., (2016).

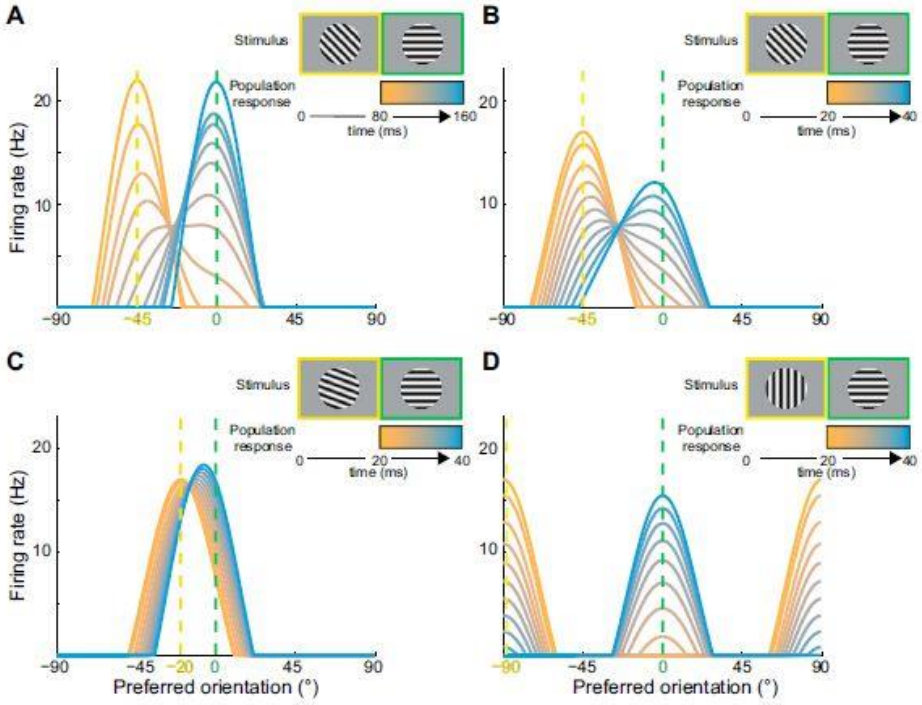

Figure.8.3: ***Transition dynamic of the population response of the hypercolumn network during an orientation adaptation paradigm.*** *In each panel, the response to an horizontal grating that was preceded by an adaptor orientation (color represents time after the onset of the horizontal grating).* ***A****. Response to an 80 ms presentation of a stimulus with orientation 0°, preceded by an 80 ms grating oriented at -45° (-45°/0°) pair. The final population response peaks at the neuron with preferred orientation 0°.* ***B****. Response to a -45°/0° pair with each grating presented for 20 ms.* ***C****. Response to a 20 ms -20°/0° pair.* ***D****. Response to a 20 ms -90°/0° pair. The short stimulus presentations were reduced on purpose and interrupted the dynamic of transition to a state whose proximity to the test orientation stimulus is function of the orientation difference between adaptor and test stimuli (****B****-****D****). However, the short stimulus presentations bias the population response for some of the pairs (****B*** *<* ***C****) with a response increase for the -20°/0° pair, according to the distance in orientation between stimuli, but not for the orthogonal pair (****D****). (From Del Mar Quiroga et al., 2016).*

This analysis shows that the responses of neurons in the recurrent network were not only determined by the immediate sensory input, but also influenced by the preceding temporal context of activation. To summarize, the key notions of those results are first, that a travelling wave of activity is only found for an angular distance of 20°, corresponding exactly to the angular distance where repulsive shifts reported in psychophysics experiments are maximal. Second, that an increase in the amplitude of the propagating wave of activity is only found for the same small angular distance (20°) while the profile of activation is examined for a similar duration between adaptor and test stimulus, (0-20 ms, clearest yellow vs 20-40 ms, darker blue; Figure 8.3,C). This last point is of tremendous importance for our model and must be kept in mind.

To be able to directly compare experimental results (which typically report tuning curves of individual neurons rather than population responses) to their model, the authors extended their simulations. They first simulated neural responses in a standard orientation tuning protocol (test stimuli in isolation) and in an adaptation protocol where the test stimulus was preceded by an adaptor 20° away from horizontal. In both cases, they measured the orientation tuning curve of the neuron whose preferred orientation was 0°. As, expected, the tuning curve in the standard protocol had a peak at the 0° orientation (Figure 8.4 B, gray curve). The authors however did not expect in the adaptation paradigm that the presence of a hill of activity generated by the adaptor would result in a shift of the tuning curve *away* from the adaptor orientation (Figure 8.4 B, black curve). Those result are consistent with prior experimental observations of Dragoi et al., (2000 b). Using single unit recordings and intrinsic imaging, Dragoi and colleagues showed that the shift in the adapted tuning curve is dominated by an increase response to orientations in the non-adapted flank.

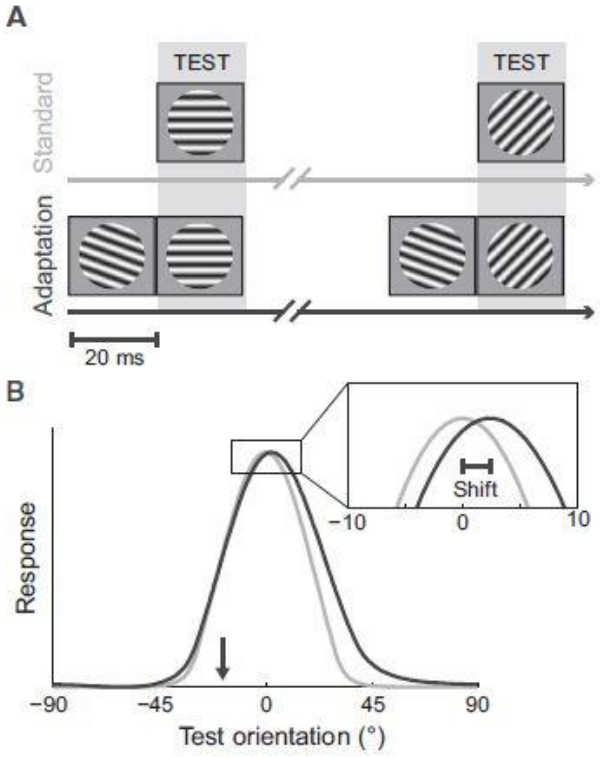

Figure.8.4: ***Hills of activation generate a repulsive shift in orientation representation in an adaptation protocol.*** ***A****. Standard and adaptation orientation tuning protocols.* ***B****. Peak normalized tuning curves for a neuron that prefers horizontal gratings obtained under the standard (gray) and adaptation (black) protocol. In the adaptation protocol, the tuning curve peaked at 3°, meaning that the -20° adaptor (arrow) induced a lasting repulsive shift. (From Del Mar Quiroga et al., 2016).*

At the level of a single hypercolumn, we interpret this phenomenon as a wave rotating on an attractor ring. This wave displace itself in the orientation domain because of a repulsive shift due to

the long-lasting activation of the adaptor stimulus. Indeed, at the time when the transitional wave of activity reaches the orientation of the test stimulus, the hill of activity evoked by the adaptor stimulus is still present, even though weaker in amplitude (Figure 8.3 C, clearest yellow). This hill of activity still interacts with the transitional wave of activity and pushes it further than the 0° target orientation of the test stimulus (because of its Mexican hat inhibitory flanks profile, Figure 8.2 b). Therefore, still in a single hypercolumn, the propagating wave initially defined in the orientation domain follows the gradient of transitional activation and moves in the physical network from less to more excitable neighboring adjacent loci in the continuous representation of orientation domains.

II-2.1.5 Model of coupled hypercolumns under global repulsive shift

Let us project the findings that we have gathered onto a more global model of coupled interacting hypercolumns covering several degrees of visual angle. In one previous model, Paradiso (1988), adaptive dynamics resulted from interactions between different orientation preference domains within a single hypercolumn. However, the spatial scale of angular repulsion reported in psychophysics studies suggests that the spatial scope of repulsive shift in orientation extends further than a single hypercolumn. In a first time, let us imagine in Figure 8.5.1 a single hypercolumn, under continuous physical stimulation by empty field flicker or increase in cortical instability due to migraines. The hypercolumn is represented by a ring assembly of orientation selective channels (since orientation preference is defined modulo 2pi). The distance between the bumps represents the angular difference between the functional preference of each activated domain on the ring. In such conditions, we can make the reasonable assumption that at t0, all orientation domains θ are simultaneously explored, although the amplitude of activation of each patch of orientation is weak due to the lack of orientation bias in the stimulation drive (Figure 8.5.1 A). Functionally, this cartoon stands for the isotropic mutual excitation between orientation patches within a single hypercolumn described by Bressloff et al., (2002).

The consequences of such a configuration is that each hill of activity corresponding to the activation of an orientation patch exerts a mutual repulsive shift on each neighboring hill of activation (i.e, from both sides of each orientation patch, Figure 8.5.1, blue arrows), creating a tension that is, in a first time, restricted to our single hypercolumn. Then, at t1, one hill of orientation activity suddenly inflates and directly forms a transitional propagating wave restricted to the hypecolumn, which is represented by a rotation step per time unit in our cartoon (Figure 8.5.1 B, dotted patch b). This is analogous to Tass (1997) model of selection of hallucinatory percepts between competing

populations of planforms where a winner takes all selection of a state dictates the consecutive pattern that will be formed.

The sense of propagation in the orientation space of that wave is dictated by the strongest repulsive shift exerted by one or the other of its side (i.e., by which surrounding hill is higher at t1, provoking the strongest repulsive shift, Figure 8.5.1 B, black dotted patch a vs dotted patch c). The reason why the inflated hill of activity (patch b) is the one to propagate, is that because of its higher activation, the inhibitory sides of its Mexican hat profile are more narrowly distributed than the one of its neighbors. On the contrary, its neighboring patches a and c have a broader distribution of inhibitory sides. However, even if patch a is more activated than patch c, its activation lies in the same range than this latter and it exerts a stronger repulsive shift on patch b than patch c because the angular distance between patches a-b and patches b-c is initially the same. As it is the one to initiate the propagation, the wave of activity of patch b gains in amplitude as it displaces itself away from the inhibitory influence of the patch a on patch b, which is stronger than the one of patch c on patch b. However, the profile of inhibition of the inflated hill b becomes narrower and narrower and its relative gain in amplitude is temporarily compensated by an increase of the lateral inhibitory side of patch c as the wave displace itself towards this latter. Nevertheless, when the propagating wave of inflated activity reaches the side of patch c, the steeper but stronger inhibitory influence of its lateral Mexican hat profile suddenly repels the hill of activation of patch c by exerting a strong repulsive influence on this latter. The hill of activity of patch c is therefore pushed away in neighboring orientation domains much faster than the speed of the hill of activity of patch a that pursues the propagating wave of activity of patch b, explaining why this latter abruptly increases.

Contrarily to Del Mar Quiroga et al., (2016), there is no anisotropic stimulation (i.e; test stimulus) that dictates towards which preferred orientation attractor the wave should move to. The travelling wave of activity must then rotate along the ring until it reaches a new equilibrium corresponding to the maximum stability between neighboring hills of activation. The principle is that the wave will stop itself around an orientation preference representation that obeys a new equilibrium state, where the repulsive influences of the newly activated neighboring patches of orientations both exert a repulsive influence that stabilize the inflated hill of activity that has now stopped. This leads to a new balanced state of orientation activation under mutual repulsive influence of neighboring patches of orientation (Figure 8.5.1 C).

One may argue that the increase in activity only found for small angular distances (0-20 °) by Del Mar Quiroga et al., (2016; figure 8.3 C) only comes from the fact that the test stimulus following the adaptor corresponds to the preferred orientation of the neuron (i.e., the attractor). We argue that, in our model, the attractor within a single hypercolumn is the new balanced state of orientation reached when the hill of activity has stopped and is stabilized by neighboring patches of orientation that exerts a repulsive influence. As we detailed above, it results, as the transitional wave propagates, in a progressive increase of this latter. The increase of activity of the transitional wave of activity of patch b is the key assumption of our model for several reasons: first, because it allows the emergence of a single dominant orientation representation in a single hypercolumn.

We propose for visual representation purpose that once the propagating wave has reached half the distance that separated the initial position of activity of the patch b and patch c (Figure 8.5.1 A), the overall distribution of hills of activity in the hypercolumn has been twisted by the angular distance that the wave has travelled (Figure 8.5.1 B vs C). That angular distance is arbitrarily given. However, the angular distance to consider is much smaller than in our cartoon (up to 20° for its maximal).

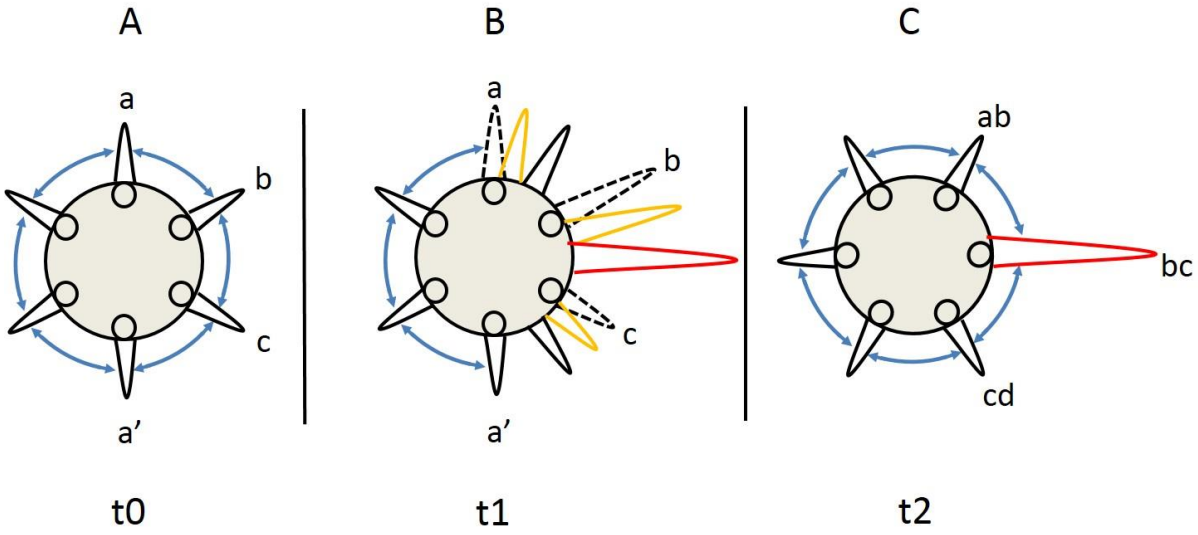

Figure.8.5.1: ***Mutual repulsive shift in orientation gives rise to the selection of a single dominant orientation state within an hypercolumn****. A single hypercolumn is represented at three different times: A,B,C by a black circle. Activated orientation patches are represented by small black circles. The activation of each orientation patch is represented by black bumps. Dotted black patches indicate the initial profile of activation of different orientation patches while yellow and red bumps indicate the progressive temporal evolution of each orientation patch activation rotating in a clockwise manner. Blue arrows represent mutual repulsive influence from neighbouring orientation preference patches within the hypercolumn.* ***A****. One hypercolumn at t0 where no orientation state dominates.* ***B****. At t1, the hill of activation of one orientation patch inflates (dotted patch b). This immediately forms a travelling wave of activity (in the orientation domain) whose sense of rotation is determined by which of the neighbouring orientation patch exerts the strongest repulsive shift (i.e., is the more activated), (upper panel, dotted patch a is more activated than dotted patch c). The propagating wave of activity originating from patch b progressively gains in amplitude as it is the one to initiate the propagation and to distance itself from inhibitory influence of the dotted patch a. The dotted patch a however almost instantaneously pursues the propagating wave of activity initiated by patch b and creates a new propagating wave of activity by filling a void of repulsive influence, still under the influence of the repulsive shift of its neighboring activated patches on the left. Simultaneously, the propagating wave of activity initiated by the patch b repels the hill of activation of patch c by exerting a stronger and stronger repulsive influence as it grows in amplitude*

and gets closer, displacing its activity. ***C.*** *At t2, only one orientation dominates in the hypercolumn ans is stabilized by neighbouring mutual repulsive influence.*

Let us imagine in figure 8.5.2 a second hypercolumn spatially adjactent to the one described in figure 8.5.1. This second hypercolumn is in the exact same initial conditions than the first one at t0, i.e. no orientation state predominates. The only difference with the first hypercolumn is that at t1, no hill of activity inflated. The hill of activity of patch b remains constricted in the first hypercolumn. However, as it increases, the excitatory influence that its horizontal connections convey to the second hypercolumn is stronger and stronger. This is however not the only transitional wave that convey lateral excitatory influence as patch a that pursues patch b and patch c that flees patch b also convey excitatory influence to the second hypercolumn. Note that here, lateral connections are not anymore restricted to a single hypercolumn but are long-distance horizontal connections linking spatially distant hypercolumns. When the activity of patch b reaches its maximum and is stabilized, its horizontal influence is also maximal and allows to jump from the first hypercolumn to the second one, starting a cascadic activation that now extends across space. At the level of the second hypercolumn, the activity of patch b is the strongest between patches b' and c'. Moreover, the patch a of the first hypercolumn exerts its lateral influence between patches a' and b' on the second hypercolumn and this influence is superior to the lateral activity exerted by patch c on the second hypercolumn on the left of patch c', which is represented by the size of the positive signs on figure 8.5.2.

Because the second hypercolumn is exactly in the same initial conditions than the first one, the lateral influence of the first hypercolumn on the second one is the only soucr of modulatory influence that triggers the emergence of a novel inflation of activity that follows the gradient strength of lateral activitation provided by the first hypercolumn. This results in the inflation of activity of patch c' that end up, at t2, in the selection of a dominant orientation state slightly different than the one dominating in the first hypercolumn (figure 8.5.2, C: patch bc vs patch cd'). This "guided influence" under the form of a self-organizing process is only possible because of the increase in the activity of one orientation that becomes predominant in a single hypercolumn. This increased activity reaches a threshold above which the influence conveyed by strong reciprocal horizontal connections is sufficiently high to guide, between spatially neighboring hypercolumns, the emergence of a smooth transition of orientation representation. This results in the spatial diffusion of an intracortical wave that progressively recruits slightly different orientations as it travels across the cortical surface (Figure 8.5.3).

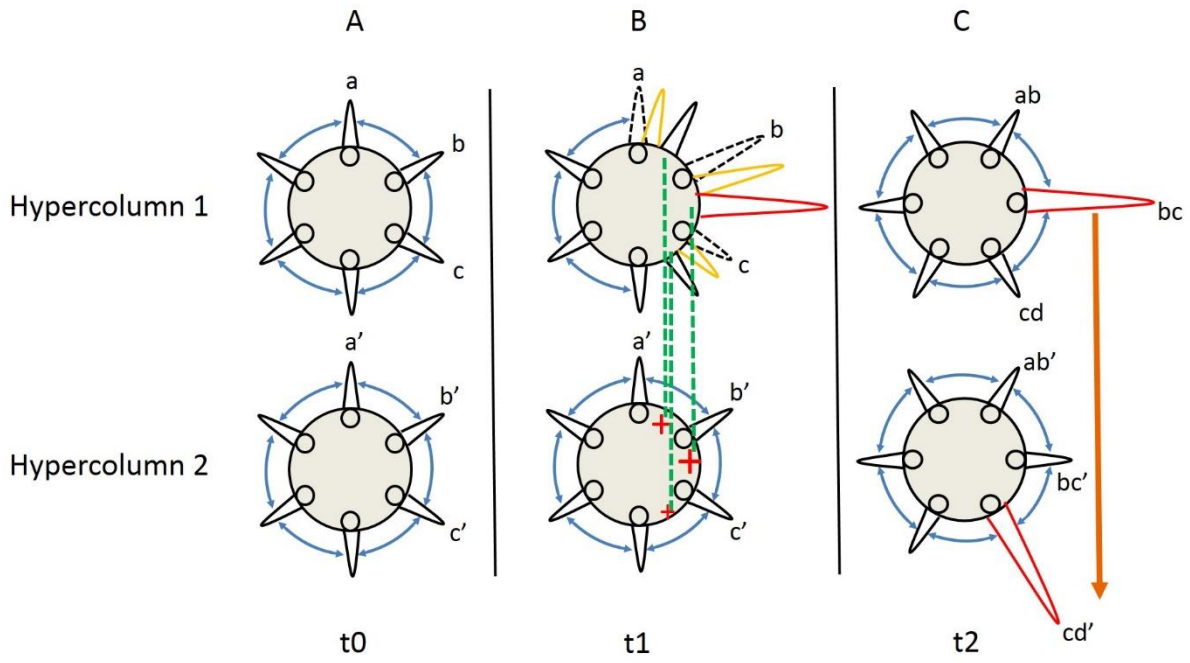

Figure.8.5.2: ***Coupled ring model of interacting hypercolumns gives rise to neighboring orientation states between spatially adjacent loci.*** *Same convention and color code that in figure 8.5.1. A second hypercolumn (second row) spatially adjacent to the first one is represented here. In the first hypercolumn, the transitional wave of activity of patch b progressively inflates. Simultaneously, horizontal connections (represented by dotted green lines) convey excitatory influence from the first hypercolumn to the second. The strength of modulatory influence conveyed by horizontal connections follows the gradient of activation of the different waves of propagating activity in the first hypercolumn. This progressively displace a continuum of modulatory influence. From hypercolumn 1 to hypercolumn 2, excitatory influence conveyed by horizontal connections is the strongest between patches b' and c' (**B**, **lower panel**) but relatively, the excitatory influence arriving between patches a' and b' is stronger than the one arriving on the left of the c' patch. This gradient of activation dictates the sense of rotation of activity where the repulsive force coming from patch b' on c' is stronger than the one coming from c' towards b'. Therefore, the hill of activation of the patch c' forms a propagating wave of activity that progressively inflates, following the direction of rotation initiated by the first hypercolumn and resulting at t2 in the dominance of activation of the patch cd' (**C, lower panel**). At t2, the orange arrow represents the slight shift in orientation between spatially distant neighbouring hypercolumns.*

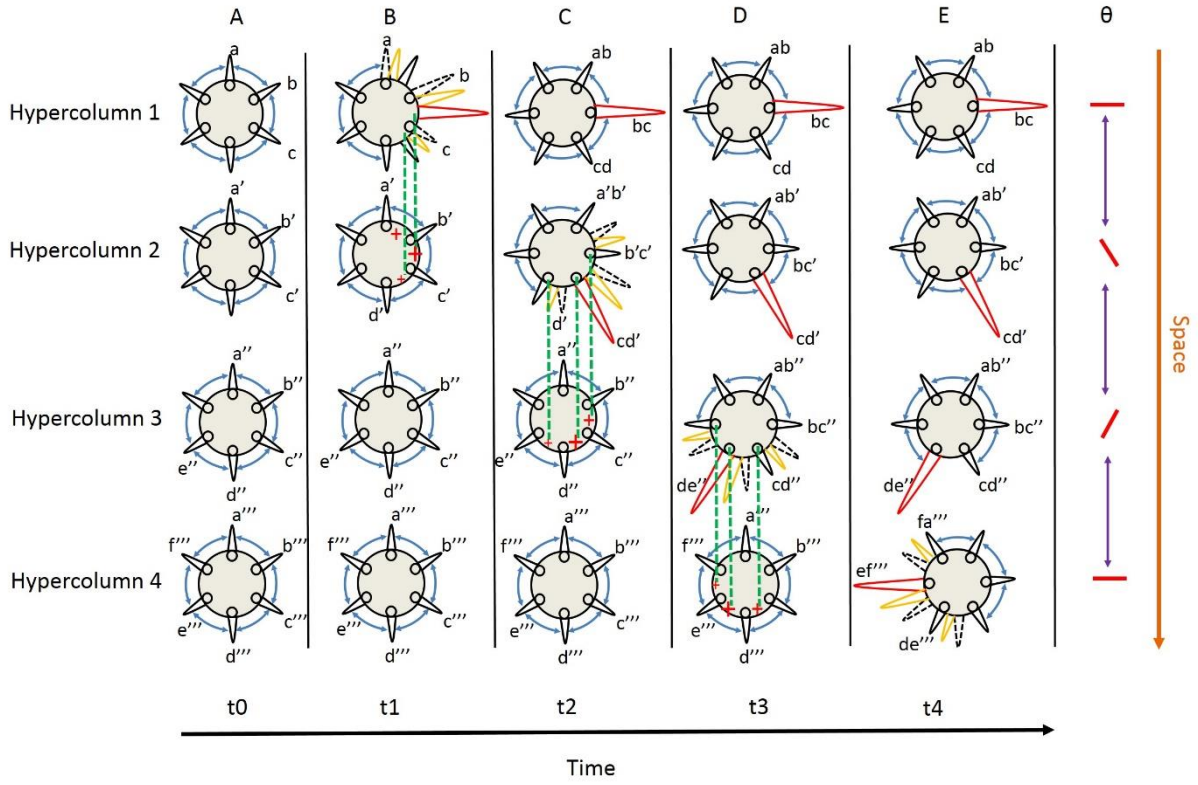

Figure.8.5.3: ***Series of coupled ring models results in an intracortical wave of activity recruiting neighbouring orientations in adjacent loci of V1.*** *Same convention and color code that in figure 8.5.1 and 8.5.2. Four hypercolumns are represented here. The anisotropic dominance state of each hypercolumn is represented as a function of time (from A to E, five columns). Because each hypercolumn is in the same initial state than the first one at t0, where no orientation state dominates, the selection of the predominant orientation in the first hypercolumn at t1 result in a step by step cascadic emergence of slightly neighbouring orientation states across space and time, hypercolumn by hypercolumn. The theta column on the right indicate the predominant orientation of each hypercolumn at t4. Purple double arrows represent the mutual self-stabilizing repulsive influence exerted by each hypercolumn on its neighbouring ones via strong reciprocal long-distance horizontal connections. Note that the angular step between each hypercolumn is of 60° for visual purpose representation, in order to cover the overall angular distribution represented in figure 8.1 along a cortical stripe of activity. To represent with fidelity the strongest angular repulsive shift in orientation reported in psychophysics, the number of angular steps should be multiplied by 3 to obtain a minimum angular step of 20° between each neighbouring hypercolumn.*

To summarize our model, recurrent isotropic connectivity in an hypercolumn generates a dynamic adaptive process, an idea shared by Kevan Martin (Martin and Schröder; 2013; Martin et al., 2014; Keller and Martin; 2015) but not by Sonja Hofer (Iacaruso et al., 2017; Ho et al., 2011) nor by Clay Reid (Ohki et al., 2005; Glickfeld et al., 2013). This process may be described by a progressive change of activation in the orientation domain, best described by a rotating polar wave in the ring model. Therefore, the continuous evolution of the adaptation mechanism can be described by a propagation in a virtual orientation space localized to the spatial location of a single hypercolumn. Paroxysmal conditions of isotropic activation lead to an increase in cortical activity, for instance during migraines / drug ingestion or physical visual stimulation by an empty field flicker or noise in the visual field. During this increase in cortical activation, this phase transition extends to neighbouring spatial locations via a step by step biased reverberation between distant hypercolumns. This reverberation recruits iso-orientation-preference reciprocal links and the orientation wave initially constrained in a single hypercolumn gives birth to a spatial intracortical wave propagation linking in a nested way neighbouring but slightly repulsive orientation preference domains. This neighbour to neighbour slight repulsive shift exerts a self-stabilizing influence that locally maintains an equilibrium within the network. One may describe from this step by step amplification in repulsive shift the typical profile of sub-Riemanian geodesics forming the co-circular orbits of the association field of Hayes, Hess and Field (Field, Hess and Hayes, 1993). As a matter of fact, Jean Petitot built an initial model where horizontal cortico-cortical connections of V1 implement in the brain the anatomo-functional contact structure of a continuous fibration where the concept of association fields, to the plural, reflects the progressive propagation of local orientations in V1 (Petitot, 2003). Later on, this model was pursued by Giovanna Citti and Allessandro Sarti (Citti and Sarti, 2006; for a detailed description, see Duits et al., 2013). At the psychophysical level, evidence of such association field has been obtained (Georges et al., 2002) and modelled (Series et al., 2003). Electrophysiological evidence of association fields in V1 has also recently been obtained by our group (Gerard-Mercier et al, 2016). In this context, the application of geodesics to several models of visual geometric hallucinations and models of curved modal illusory contour takes all its meaning. From an experimental point of view, the curvature constraint of these association orbits follows the psychophysical findings that lateral binding between neighbouring orientation detectors has a tolerance of +/-20°.

In our model, horizontal connections can also be inhibitory. In that case, only the direction of propagation of the travelling orientation wave is changed. It yields some similarities with Bressloff et al., (2002) model where the authors precise that instead of their long-range inhibition, it is possible to obtain similar planforms using inverted Mexican hat functions that incorporate short-range inhibition and long-range excitation, which may provide a better fit to anatomical data. The displacement of activity under repulsive influence between neighbouring hills of activation and the simultaneous displacement of modulatory activity via horizontal connections resembles other population models. It is for instance reminiscent of the link between Ermentrout and Cowan's model of hallucinations (1979) and the behaviour observed in models of predator-prey pursuit-

evasion (Murray, 1989; Segel and Jackson, 1972; Segel and Levin, 1976), derived from Turing's initial diffusion model of periodic coloration spots and stripes (1952).

II-2.1.6 Formation of static vs dynamic hallucinatory planforms

The model that we propose explains from a mechanistic point of view how the smooth transition between neighbouring orientations representation can emerge along a single stripe in adjacent loci of V1, which is one of the most stable state of this later under certain paroxysmal regimes of activity. In this thesis, we restrict the scope of our investigations to fan-shapes and concentric circles that respectively map as horizontal and vertical stripes of activity on V1, we do not consider more complex type II and III contoured planforms (Klüver, figure 7.1). We propose that horizontal connections help to synchronize the dynamic exploration of orientation domains both between hypercolumns belonging to a single neural stripe of activity (Figure 8.1) but also between different neural stripes of activity. During the perception of simultaneous, static geometric planforms such as fans shape and circles (Klüver, 1967; Siegel and West, 1975; Siegel, 1977), the concomitant exploration of neighbouring orientation domains can occur simultaneously between different neural stripes of activity. Neighbouring stripes of activity can even mutually synchronize each other via longer-range horizontal connections and converge towards the same continuous representation of neighbouring orientations in adjacent loci of V1 (Figure 7.2 A, B, C and 7.3 upper panel: A, B and lower panel).

However, perception of dynamic, propagating hallucinations is more commonly reported (Wilkinson, 2004; Richards, 1971; Siegel and Jarvik, 1975; Siegel, 1977; Tyler, 1978; Sacks, 1995; Crotogino et al., 2001; Hadjikhani et al., 2001; Billock and Tsou, 2007). During the perception of dynamic concentric circles, we believe that the first neural stripe of activity to form is the one at the smallest retinal eccentricity, closer to the area centralis (Figure 8.1, right panel). An explanation is that the distance that horizontally propagated activity has to cover in order to synchronize hypercolumns in neighbouring states of orientation is smaller than at larger eccentricities. This first stripe of activity forms and then propagates as a travelling wave away from the area centralis retinotopic position, towards the periphery. This explains why hallucinatory circles are most often reported to pulsate, rather than wobble (Billock and Tsou, 2007; Wilkinson, 2004). This pulsation is, to us, an oscillatory signature of the refractory period of the single stripe formation that, after propagation, forms again in the same cortical location after sufficient time. The propagating wave of activity is composed by an excitatory wave front followed by a neuronal depression before another similar stripe of activity emerges when the refractory period of that depression has passed. Indeed, in the movement of fortification arcs in humans, Wilkinson (2004) suggested that "a wavefront of neural excitation operating on intrinsic cortical networks is presumed to underlie the positive hallucinations and the subsequent neuronal depression".

The first stripe of activity partially conserves its initial geometric distribution under the shift-twist invariance of the Euclidian group provided by the expansion in cortical territories where the magnification factor is different, but not only. As Bressloff et al., (2002) proposed, type I and II noncontoured planforms (including fans shape and concentric circles) could arise from a filling-in process. We interpret this as the possibility that the initial sites of activation of the first stripe have changed in position and orientation as they progress onto V1 surface under the shift-twist invariance of the Euclidean group provided by the change in magnification factor. Under such conditions, activity filling-in between neighbouring hypercolumns via horizontal connections would allow completion, thereby preserving the initial geometry of the first stripe of activity at larger retinal eccentricities. On the other hand, for fans-shape percept, which correspond to vertical stripes of neural activity on V1, the formation of each fan is made along different axes of increasing eccentricity. Therefore, laterally propagated activity does not cover shorter distances to form each stripe, which might explain why rotating fans-shape are most often reported as multistables as they rotate in both clockwise and anti-clockwise directions (Billock and Tsou, 2007). This suggests that for each visual hemifield, the corresponding neural stripes of activity on each hemisphere could propagate both anteriorly and posteriorly, leading at the cortical level to colliding waves of activity. This might lead to the perception of a dominant direction of rotation for a few seconds, before alternating with the opposite direction, or even the superposition of clockwise and anticlockwise perception of fans shape rotation.

Through our model, we believe that fan shapes and concentric circles planforms emerge as some of the most stable states of the network because from a dynamic point of view of interacting systems, it reaches minimum angular repulsion between distinct neighbouring hypercolumns, thereby maintaining the network in an equilibrium. That is why our interpretation is that the system converges towards those states both under continuous visual stimulation by empty field flicker and increase in cortical excitability during migraines or drug ingestion. The mechanism that we propose do not account for immediate selection of such planforms, as emergence of different orientation domains can arise in neighbouring hypercolumns and interrupt the domino's cascade of activation of neighbouring orientation state in adjacent cortical loci. This is analogous to the observations of Billock and Tsou (2012) who argued that the temporal instability of many induced hallucinations can be due to empty field flicker stimulation where "each temporal modulation is both a stimulus to pattern formation and a perturbation, disturbing the previously elicited state". This might account for the long duration of flicker-induced geometric patterns, which may take as long as 30s (Billock and Tsou, 2007). However, we do believe that the mechanism that we propose explains how the system self-organizes itself and converges towards such stable states under many attempts. The long-lasting effects of orientation repulsion found by Patterson et al., (2013) in the macaque V1 and successfully modelled by Del Mar Quiroga et al., (2016) could maintain selected orientation while neighbouring ones are progressively stabilized. The more neighbouring orientations are activated in adjacent loci of V1, the harder it is to disturb that state since each slightly different orientation is stabilized by surrounding repulsive influence from neighbouring hypercolumns. This is consistent with the interpretation of Jack Cowan who stated that, compared to fluctuation-dependent pattern formation, the most robust pattern formation is a mean-field

effect as “if this were not the case most people would see geometric visual hallucinations most of the time, and normal vision would not be possible”. Thus, it is reasonable to assume that growing and growing mean-field influence of minimum angular repulsion exert a stabilizing influence explaining the stability of those form constants.

II-2.2 Geometric physical inducers constrain orientation domains exploration: towards a directly inducible and temporally stable percept

II-2.2.1 Experimental evidence of smooth spontaneous orientation transition between neighbouring hypercolumns

In addition to provide a plausible mechanism of interactions between neighbouring hypercolumns, our model is consistent with experimental evidence of smooth exploration of neighbouring orientation domains within and between hypercolumns in ongoing activity of the anesthetised cat V1 (Kenet et al., 2003, Figure 8.7). Many hallucinations can be explained by models based on the primary theoretical proposal of Ermentrout and Cowan (1979) (Tass et al., 1995; Tass, 1997; Bressloff et al., 2001, 2002). However, perhaps the greater significance of those models is that they suggest that spontaneous pattern formation arise in visual cortex, conferring a perceptually meaningful and useful status to ongoing activity. Kenet et al., (2003) used voltage sensitive dye imaging to capture the ongoing neural activity in the visual cortex of anesthetized and visually unstimulated cats. They found that autonomous ongoing cortical activity is highly structured and matches cortical activity induced in the same animals by viewing oriented grating patterns (Figure 8.6), which greatly reinforce the plausibility of the initial assumptions of our model. They also found that some orientation states (cardinal orientations) occurs more often (about 20%) than oblique orientations state. This might represent a relative facilitation or spark of activity initiation that occurs more often, inflates and dictate the transition of neighbouring orientation domains in adjacent hypercolumns. However, the results of Kenet et al., (2003) must be pondered as the result largely depends on the detection algorithms used to attributed a given recorded cortical orientation response to an orientation response template, which is a totally artificial stimulus. The dynamic of orientation exploration of ongoing activity is certainly much richer, as the “replayed” stored memories, direct consequence of the exposition to a rich and complex natural environment are probably much more complicated. Moreover, the effect of anaesthesia, a significant and still poorly understood factor must be taken into account.

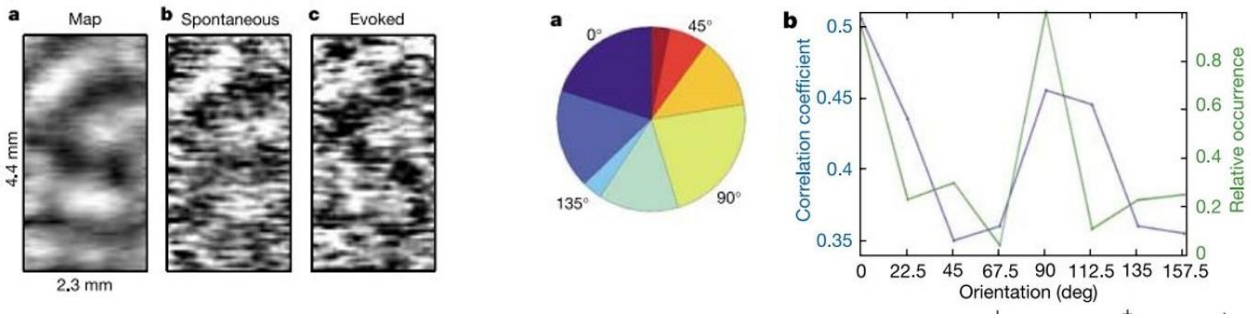

Figure.8.6: ***Spontaneous cortical pattern formation in cats. Left****: similarity of spontaneous states arising in sensory-deprived cats to the activity evoked by oriented stimuli.* ***Left, a****. Cortical activity evoked by presentation of vertical gratings, averaged over 160 frames.* ***Left, b****. Single frame of spontaneous activity resembling the activity pattern in* ***a****.* ***Left, c****. Single frame of imaged neural activity evoked by vertical grating, shown for comparison.* ***Right, a****. Example of the distribution of occurrence of the different orientation states. Spontaneous activity is correlated with cardinal orientation maps that appear 20% more often than the oblique orientation state.* ***Right, b****. The relationship between orientation and number of spontaneous occurrences of that orientation state (blue), or maximal coefficient (green) (averaged from three hemispheres). (Kenet et al., 2003).*

These autonomously formed patterns are elementary bricks reminiscent of and providing solid experimental ground to Ermentrout and Cowan, (1979) patterns. Indeed Goldberg et al., (2004) treated both Kenet et al., (2003) and Ermentrout-Cowan patterns as subsets of attractors (Billock and Tsou, 2012), interpretation reinforced by more recent theoretical work (Ghosh et al., 2008; Luczak et al., 2009; Ringach, 2009). However, the interpretation of Billock and Tsou's, (2007, 2012) on the neural attractor dynamic based on the findings of Kenet et al., (2003) is different than ours. Indeed, Billock and Tsou (2012) stated that in Kenet et al., (2003) results: "The spontaneous neural activity continually and unpredictably switched between states describing different grating orientations". This might be true to a certain extent, but this certainly does not highlight the subtlety of the main findings of Kenet et al., (2003). We believe, as Kenet et al., (2003), that the spontaneous activity visiting neighbouring orientation states that they found may vary unpredictably but that this unpredictability is limited as their results show a remarkable smooth transition between neighbouring orientation domains over time (Figure 8.7).

Our position is strengthened by the results of Fiser et al., (2004) who found in the awake ferret that the correspondence between evoked activity and the structure of the visual input signal was weak in young animals but improved with age. This improvement was linked to a change in the dynamics of spontaneous activity. However, their results suggested that in both developing and mature visual cortex, what we measure as evoked activity in fact represents more the modulation of ongoing activity by a visual input rather than the structure of the visual stimulation itself. Growing evidence gives a prominent role to ongoing activity (Luczak et al., 2007). Luczak and colleagues found in ongoing activity of both anesthetized and awake rats UP states associated with a progressive, stereotypically organized sequential spread of activation. Moreover, they found that in both awake

and anesthetized animals, propagating spontaneous activity initiated similar local sequences of activation in each direction they travelled towards and that those local patterns of activation were predictable from the latencies of individual neurons during UP states. Their results suggest a high reproducibility where the stereotyped pattern of activity formation that they observed during ongoing activity arise from the interplay between the intrinsic properties of the cells they examined (conductance) and the local circuit properties. Luczak and colleagues (Luczak et al., 2009) extended their findings to the auditory and somatosensory cortices of rats. They showed that although neurons displayed variability across trials, both ongoing and evoked population activity preserved a sequential activation. More importantly, they observed that response evoked by individual stimuli occupied a portion of the larger, but still constrained subset of potential activation displayed by ongoing activity. In their terms, "population spike patterns are drawn from a limited vocabulary sampled widely by spontaneous events but more narrowly by sensory responses".

Back to the visual cortex, our interpretation of the results of kenet et al., (2003) in the anesthetized cat is still very different than the one of Billock and Tsou., (2007). Indeed, Billock and Tsou went even further in their description of kenet et al., (2003) results by stating that "A subject may fleetingly perceive a fan shape before a hexagonal lattice appears, which in turn gives way to a spiral. Theoretically, no spontaneous state is predominant, and, experimentally none are stable, perhaps because each flicker can disturb the previously elicited state. This is analogous to the random succession of spontaneous orientation states in cat cortex found by Kenet et al., 2003". While Kenet et al., (2003) described their own results in that way "Long epochs of smooth transitions between neighbouring templates (of orientation) were clearly present in the data" (Figure 8.7).

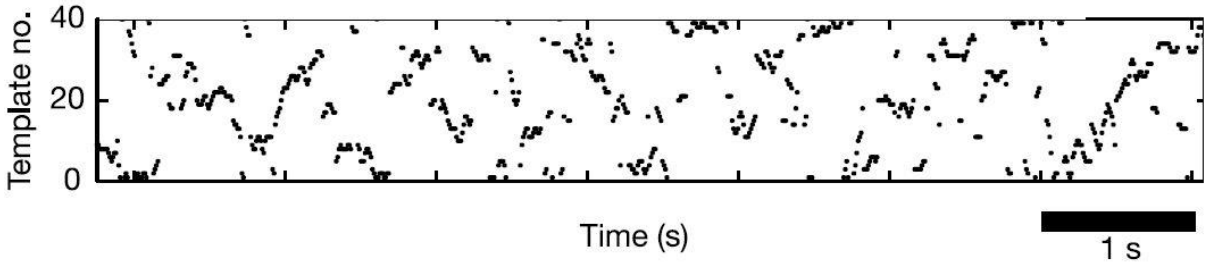

Figure.8.7: ***Transition of spontaneous cortical states of orientation in anesthetized cat V1.*** *Spontaneous states revealed using a Kohonen map algorithm. Position of a best-matching Kohonen template as a function of time. (Adapted from Kenet et al., 2003).*

It indeed appears from the results of Kenet et al., (2003) that ongoing activity smoothly visits neighbouring orientation states. This cannot result from a random sampling process, even though some abrupt jumps appear in between some epochs of smooth transition. Moreover, the dynamic

of transition is slow, of the same order of magnitude than the findings of Del Mar Quiroga et al., (2016), in the order of several hundreds of ms, up to 1s.

Regardless of the interpretation of Billock and Tsou (2007, 2012) on the dynamics of orientation transition in cat V1, we agree with their remark that if similar patterns than the ones of Kenet et al., (2003) are present in awake human, they must be subliminal, since we do not perceive hallucinatory oriented gratings wherever we look. Ringach, (2009) suggested that sensory-deprived hallucinations may stem from these patterns crossing the perceptual threshold. However, even subthreshold neural patterns could alter perception by interacting with activity evoked by visual stimulation. This raises the question of how to render those patterns visible and leads us to the conceptual idea that introducing a geometric planform inducer, that can emerge as one of the most hallucinatory stable state of V1, can modulate the activity of the visual cortex that already explores similar or complementary orientation domains in ongoing activity.

II-2.2.2 Biasing ongoing activity's orientation exploration by the physical presentation of a geometric planform inducer combined with a perturbation

Now that we have introduced our conceptual framework of interacting hypercolumns that stabilize the distribution of neighbouring states of orientation in adjacent loci of V1, it is easier to understand how the physical presentation of one of those planforms can lead to the emergence of the opponent one. Concentric circles and fans shape form vertical and horizontal stripes of activity on V1's surface, respectively. According to our working hypothesis, the feedforward drive provided by the continuous physical presentation of a fans shape inducer (or concentric circles) provokes an adaptation phenomenon where every orientation signalled at each locus along the horizontal stripes of activity locally provoke a repulsive shift away from that orientation. The consequence is that each orientation locally orthogonal to the one signalled by the physical inducer acts as an attractor, where the repulsive shift is minimal. The interaction between the feedforward drive and ongoing activity, which already visits neighbouring states of orientation across time and cortical space locally converges towards those orientation states where repulsion is the weakest and is constrained towards the opponent planform state that becomes the most possible stable state. The network doesn't have to self-synchronize itself via horizontal connections, where hallucinatory fans shape and concentric circles may take as long as 30 s for to appear under empty field flicker stimulation (Billock and Tsou, 2007) as the initial conditions are already dictated. Each orientation falls into its spatially localized attractor orthogonal to the physical inducer, inducing immediately the perception of an opponent planform, i.e., rotating fans shape for concentric circles physical inducer and hallucinatory-like pulsating circles for a fans shape inducer (Billock and Tsou, 2007, Figure 8.8).

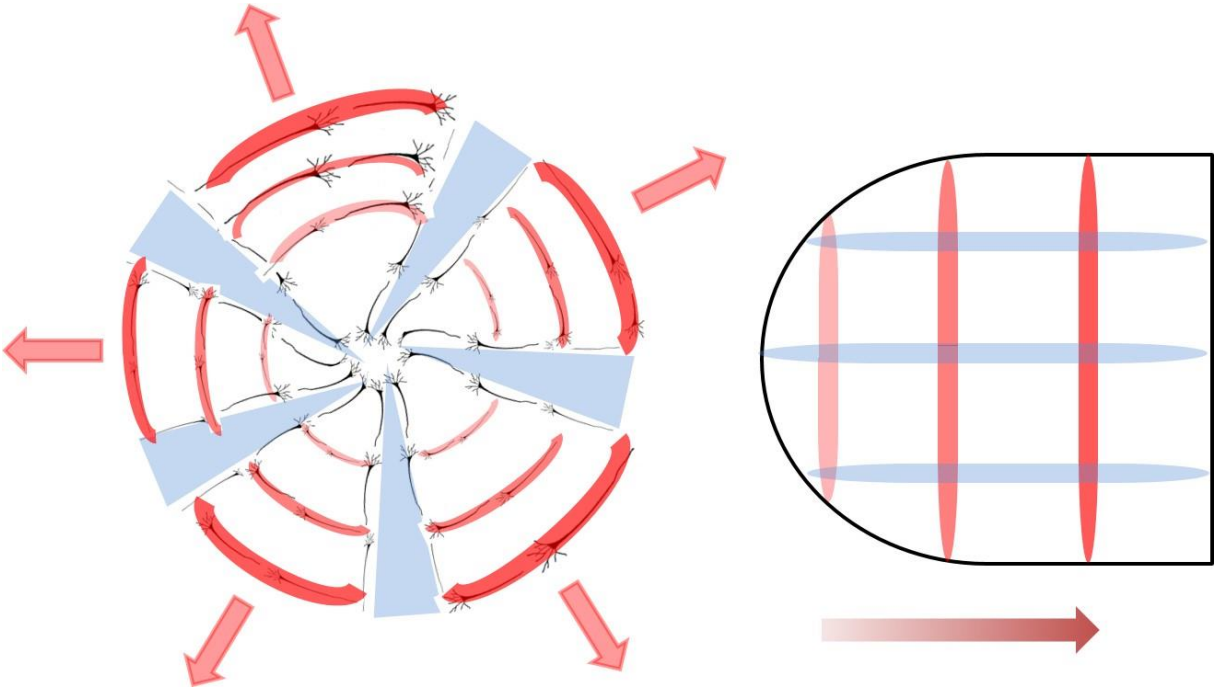

Figure.8.8: ***Adaptation to the activity evoked by the continuous feedforward drive of a geometric planform inducer constrains activity's exploration into an opponent geometric planform state under perturbation.*** *In blue, a fan shape geometric inducer presented in the visual field (left) evoke horizontal stripes of activity onto V1's surface (right). This feedforward drive provokes an adaptation phenomenon that result in every locus of activation on the cortical surface into a repulsive shift in orientation, forcing the resulting activity into locally orthogonal orientation attractors where repulsive shift is minimal. A first stripe of vertical activity first forms on V1's surface near the area centralis retinotopic position (right, lighter red), where horizontally propagated activity has a shorter distance to travel to bind neighbouring orientation columns and induces activity filling in between geometrically unstructured areas. This first stripe then propagates from the area centralis towards the periphery. At the perceptual level (left), this results in the perception of hallucinatory-like pulsating rings of increasing eccentricity (from lighter to darker red).*

However, as we already saw through the description of the experimental results of MacKay, (1957, a,b, 1965); Billock and Tsou (2007), and through the models of hallucinatory pattern formation of Ermentrout and Cowan, (1979); Bressloff et al., (2001, 2002), the presentation of a given geometric planform in isolation is not sufficient to bring its opponent planform to the perceptual threshold. A perturbation, under the form of an increase in cortical excitability is necessary. This perturbation can take the form of the disappearance of the geometric planform (Mackay; 1957 a,b), of the combination of a geometric planform flickering in phase with the background (Billock and Tsou, 2007) or combined with noise (MacKay, 1965; Billock and Tsou, 2007). This latter combination seems to give the more salient percepts of opponent planforms as only in that condition the subjects of Billock and Tsou., (2007) always reported perception of both pulsating circles and rotating fans shape under the physical presentation of the opponent planform. Moreover, as MacKay already highlighted (1965), the statistics of the noise seem to be of importance, findings than Billock and Tsou, (2007) confirmed by the use of $1/f^{\alpha}$ filtered noise,

whose characteristics were the most efficient in triggering salient percepts for spatial and temporal exponents corresponding to natural image statistics (Figure 8.9).

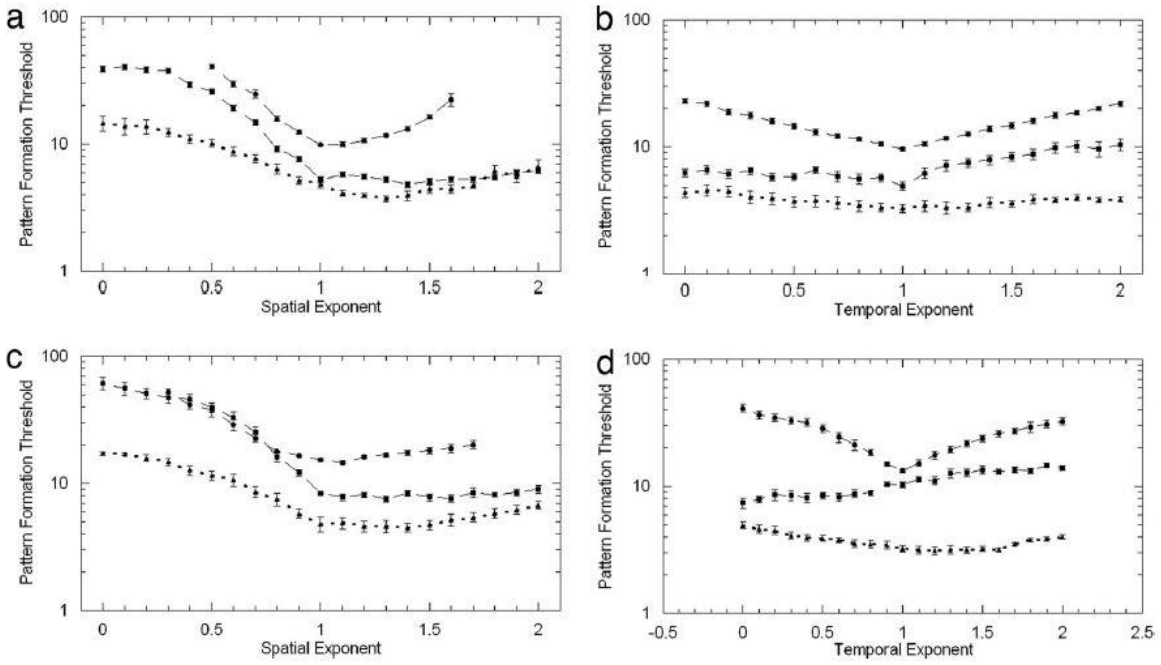

Figure.8.9: ***Effect of 1/f$^{\alpha}$ filtered noise on hallucinatory pattern formation.*** *The rms contrast of the spatiotemporally filtered noise needed to induce hallucinatory-like pattern formation is plotted as a function of the spatial (α), left; and temporal (β), right; exponent of the noise when this latter is viewed through a geometric mask pattern. The spatial and temporal exponents were varied independently between experiments. The data of three subjects are shown. Each line is the average of nine runs (9h in total) while error bars are +/- SE.* ***(a)*** *Circular mask: detection of hallucinatory-like fans shape as a function of spatial spectra exponent (β fixed at 1).* ***(c)*** *Fan-shaped mask: detection of hallucinatory pulsating rings as a function of spatial frequency exponent (β fixed at 1).* ***(b)*** *Circular mask: detection of hallucinatory-like fan shapes as a function of temporal frequency spectra exponent (α fixed at 1.0).* ***(d)*** *Fan-shaped mask: detection of hallucinatory rings as a function of temporal spectra exponent (α fixed at 1.0). (From Billock and Tsou, 2007).*

In the experiments of Billock and Tsou (2007), all observers reported that for low spatial exponents (whiter Fourier spectra), the classic MacKay effect often occurs: subjects reported noise streaming orthogonally to the black-and transparent geometric mask. As the spatial exponent increased (becoming ‘‘pink noise’’), actual pattern formation occurred; subjects reported shadowy illusory fan shapes overlying both the physical circles and the noise and hallucinatory-like circles overlying the physical fan shapes and the noise. Subjects reported that hallucinatory fan shapes rotate while hallucinatory circles pulsate. Noise contrast affected the time required for pattern formation: at suprathreshold contrast levels, the hallucinatory patterns appeared within a few

seconds or were immediately visible, whereas at threshold the pattern could take 10–45 s to appear. The hallucination disappeared if the biasing mask was reduced in contrast (i.e., by raising the luminance of the opaque sections). For all of their subjects, the noise contrast required for pattern formation dropped dramatically as the spatial exponent was increased from 0 to 1.0–1.4 (Figure a,c);. These exponents are typical of the statistics of natural images (Billock et al., 2001 a,b). Similar tuning for temporal frequency exponents is not evident (Figure 8.9 b,d), but illusory fans/circles appeared to rotate/pulsate slightly faster for lower temporal exponents.

II-2.2.3 Oscillatory activity accompanies dynamic, propagating percepts: implications of $1/f^{\alpha}$ filtered noise in pattern formation and propagation

Interestingly, Billock and Tsou found that in geometric planform combined to $1/f^{\alpha}$ filtered noise experiments, the most effective statistics of the noise in pattern perception induction were similar to natural images statistics spatial exponents (1,4 -1,8: Knill et al., 1990; 1.09 – 1.35: Billock, 2000; Billock et al., 2001 a,b). This effect is somehow similar to the predictions of Busch and Kaiser, (2003) and Carillo et al., (2003).

The ability of noise to induce temporal coherence in nonlinear systems is a well-documented fact. In Stochastic resonance, random fluctuations enhance the response to weak periodic driving, as observed in many different physical, chemical and biological scenarios (Wiesenfeld and Moss, 1995; Wang et al., 1999; Alonso et al., 2001; Kadar et al., 1998; biological system: Jung et al., 1998). Even systems showing no implicit time scale exhibits an enhancement of temporal coherence due to noise (Hu et al., 1993; Rappel and Strogatz., 1994). This autonomous stochastic resonance, where noise extracts a hidden, intrinsic time scale of the system's dynamics, has been termed coherence resonance and has been predicted theoretically in a wide variety of models (Lindner et al., 2004) and observed experimentally in many fields, including neuroscience (Gu et al., 2002). In addition to the temporal extraction of hidden, intrinsic property of the system dynamics, Carillo et al., (2003) showed that a spatial coherence resonance also exists close to pattern-forming instabilities, mimicking the standard temporal coherence resonance. More precisely, they showed that this second, less studied mechanism takes place near the onset of dynamical instabilities, which give rise to periodic behaviour where noise excites precursors of the bifurcation. Such noisy precursors exhibit an optimal spatial coherence resonance at intermediate noise strength. Busch and Kaiser (2003) found similar results as they showed that noise-induced spatiotemporal pattern formation, known as spatiotemporal stochastic resonance, is a phenomenon wherein spatial excitation patterns are induced by fluctuations acting upon the system that show an optimal coherence at intermediate noise intensity.

Interestingly, all of the above experimental findings are reported to occur in subexcitable media, i.e., waves travelling through the system are not supported without any external (deterministic or

stochastic) driving. The main findings of Busch and Kaiser (2003) is that coloured noise (also called pink noise, fractal noise) yields a closer approximation of the actual fluctuations present than white noise, especially in biological systems. Busch and Kaiser (2003) found that spatiotemporal stochastic resonance behaviour is affected by both the spatial and temporal correlations of the noise and that this is due to an interplay with the length scales of the deterministic network, in our case, of V1. Increasing the spatiotemporal noise correlation shifts the occurrence of spatiotemporal stochastic resonance to smaller values of the noise variance, which strongly remind us of the findings of Billock and Tsou, (2007) reported in the previous section. On the other hand, if the spatial correlation of the noise exceeds that of the network, the excitation patterns disappear in favour of cloudy structures.

In light of those findings, our interpretation is that when the spatio-temporal statistics of the pink noise that is presented to V1 rightly overlap the spatiotemporal characteristics of the deterministic V1 network with spatiotemporal exponents corresponding to its tuning properties (characteristic of natural images (1,4 -1,8: Knill et al., 1990; 1.09 – 1.35: Billock, 2000; Billock et al., 2001 a,b), addition of pink noise amplifies the subjacent excitatory patterns of opposition and bring them to the perceptual threshold. By continuously providing an external visual input (geometric inducer), pink noise with natural statistic exponents sparsely activate the V1 network without providing any anisotropic information susceptible to perturb the subthreshold subjacent opponent planform attracting the resulting activity. Moreover, pink noise with a $1/f^{\alpha}$ power spectral law allows the binding of the population of cells falling into the attractor orientation locally orthogonal to the physical inducer by its scale invariance, covering both distinct spatial scales and temporal refractory periods. Combination of interplay between natural statistics of the noise interacting with V1 and the imposed subset of possible activated orientation states attractors provided by the physical geometric inducer pushes V1 in a paroxysmal regime of activity. It forces V1 to reveal its hidden underlying functional architecture, resulting in hallucinatory-like travelling waves of activity whose geometric distribution generate perception of a planform opponent to the physical inducer.

Complementarily, Peter Tass (1995) had already predicted in his model of hallucinatory pattern formation in V1 that addition of noise can result in pulsating circles and rotating fan shapes. However, the previous models of Ermentrout and Cowan, (1979) and Tass (1995) specifically modelled and only accounted for static hallucinatory percepts. In his model of dynamic hallucinatory pattern formation, selection and propagation, Tass (1997) demonstrated that an oscillatory instability results in periodic dynamic propagating waves of activity including pulsating circles and rotating fan shapes. To us, this oscillatory instability is an intrinsic property of V1 that reflects the signature of hallucinatory travelling waves of activity and the refractory period of neural stripes formation.

Indeed, this oscillatory activity is not present in the physical stimulus of Billock and Tsou's noise experiments but only in the perception of the dynamic hallucinatory-like induced percepts. Our experimental working hypothesis is that such an oscillatory signature of hallucinatory propagating waves is detectable at the single cell level. Moreover, given the geometric nature of the travelling

waves of activity, we believe that those latter can only be detected at the single cell level when their wavefront is locally parallel to the preferred orientation of the individual impaled cell.

II-2.3 The cat as a model of geometric hallucinations in the brain

It is legitimate to wonder whether or not the cat is a good model for the study of hallucinations in the brain. Indeed, cats, Non-human primates and humans do not have the same size of visual cortical areas nor the same magnification factor. In the context of the psychophysical results of Billock and Tsou., (2007), we can then interrogate ourselves by raising the question: do the cat perceive the same hallucinatory-like percept than we do? This interrogation is even more legitimate in the anesthetized state of the animal under which we realize our experiments. There is however evidence of similarities between cat, human and NHP low-level perception. First, as we already described in the first part of the thesis, VSDI experiments showed that the activation of cat's V1 is compatible with the description of the line motion illusory effect (Jancke et al., 2004) demonstrated psychophysically in humans (Hikosaka et al., 1993). In this illusion of motion-induction by a pair of static stimuli, the interaction between consecutive waves of activity evoked by each of the asynchronous stimuli results in the propagation of a global activity pattern that is undistinguishable from actual motion of a related physical stimulus. The dynamic of interaction of those waves (evoked by a first flashed square cue followed by a flashed bar) is consistent with the dynamic of perception reported by human in psychophysics. If the delay between the square and the bar is increased from 60 ms to 350 ms, the initial wave of subthreshold depolarising activity evoked by the square no longer facilitates the consecutive propagation of the second wave evoked by the presentation of the bar. The same increase in the interval between the presentation of square and bar leads to the disappearance of the illusory percept of a line gradually extending over space and time in humans. This is a first indication that even in the anesthetized state of the animal, the anatomo-functional properties of the cat V1 seem to match the requirements for perception of low-level illusions in human. The spatio-temporal range of time constants of lateral connectivity measured in cat electrophysiological experiments have been used previously to account for illusory percepts in humans.

For instance, the results of the first section of this thesis are taken as the functional implementation in V1 of the speed-up illusory effect observed in human psychophysics (Georges et al, 2002; Series et al, 2003; Gerard-Mercier et al, 2016). In the first and second studies, human observers report perception of collinear elements successively presented in an apparent motion paradigm and parallel to their motion axis as faster than parallel elements orthogonal to their motion axis.

There are other examples of similarity between cat and human perception and there is evidence that awake cats see subjective contours (Bravo et al., 1988). Using a conditioning paradigm, Bravo and colleagues showed that cats are able to perceive, as humans, the subjective motion of illusory

squares in an apparent motion paradigm (Figure 8.10). In addition, cats fail on that task under stimulus conditions where humans also fail.

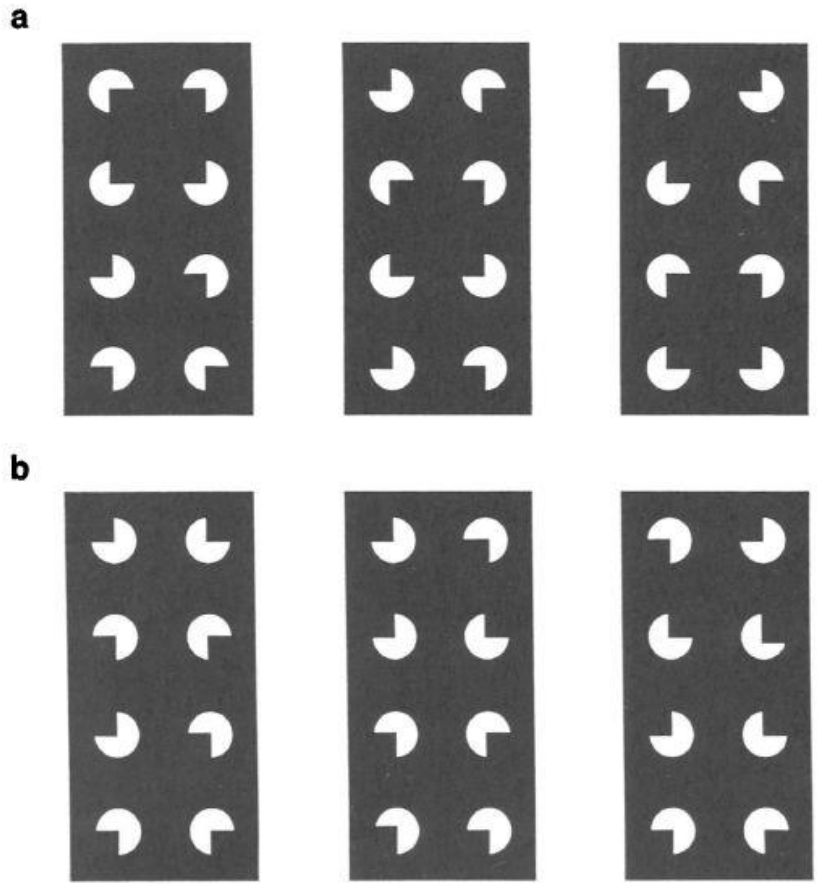

Figure.8.10: ***Continuous motion of an illusory contour in an apparent motion paradigm. (a)*** *Three frames from a movie of a subjective square undergoing apparent motion. Perception of the square is vivid over a range of frame durations***.** ***(b)*** *Three frames from the control movie in which a given configuration of sectored disks is displaced over frames. This configuration occupies the same position as that occupied by the subjective square in* ***a****. With the configuration illustrated in* ***b****, neither apparent motion, a subjective figure nor the configuration itself are perceived at any movie speed. (From Bravo et al., 1988).*

An additional point strengthening the resemblance of perception between humans and cats is that the necessary increase in cortical excitability to induce entoptic hallucinations (Ermentrout and Cowan, 1979; Tass, 1995, 1997; Bressloff et al., 2001, 2002) was confirmed experimentally in both Human and cat. During hallucinations, the EEG's profile of humans where intermittent hypersynchrony superimposed over the usual low voltage fast activity patterns has been observed (Winters and Wallach, 1970). After injection of LSD, similar EEG patterns are seen in awake cats, concomitant with bizarre postures and inappropriate behaviors (Adey et al., 1962).

All the elements reported in that section are for us clues strengthening our opinion that perception of cat and human are sufficiently similar to use the cat as a model of geometric hallucinatory pattern formation, propagation and detection under the form of travelling waves of activity whose oscillatory nature matches the dynamic of the propagating percept induced in human. Up to now, geometric hallucinatory pattern formation has mainly been studied psychophysically or with non-invasive electrophysiological techniques. The perceptual effects should be observable at the subconscious level in anesthetized animals since they do not require attention and are described as a "pop-out" feature of low-level perception. To provide experimental evidence that such waves of activity indeed emerge and propagate in V1, we reproduced and adapted the stimuli of Billock and Tsou, (2007) composed of a geometric planform inducer combined with $1/f^{\alpha}$ noise possessing natural image statistics and presented it to anesthetized and paralyzed cats *in vivo.* The use of this type of pattern in sensory electrophysiology, to our knowledge, has never been done before. We took advantage of the main characteristics of the findings of Billock and Tsou, (2007): the direct induction of such percepts and their stability over time. Such properties maximized our chances to detect neural correlates of such phenomena and are necessary conditions to a parametrized study of neural activity without any subjective reports.

In our hand, this visual stimulation paradigm indeed induced the perception of a dynamic opponent planform to the one presented: when static fans shapes were physically presented, we observed pulsating concentric circles and when concentric circles were presented, rotating fans shapes were perceived. To address more specifically the synaptic and neural nature of the emergence of waves of hallucinatory-like activity in V1, we used intracellular recordings to enhance the scope of their detectability down to the subthreshold level. We did so in the hope that the synaptic echoes recorded intracellularly would reflect the oscillations corresponding to the observed dynamic of the percept as a signature of the waves of activity travelling through V1. Moreover, to prove that such oscillations would be the signature of the hallucinatory-like percepts, we aimed at probing their geometric nature. To do so, we manipulated the spatial position of the center of the geometric physical inducers to obtain a wavefront of the percept locally parallel to the preferred orientation of the impaled cell. We did so under the assumption that travelling waves of activity would only be detectable at the single cell level in that condition (Figure 8.11).

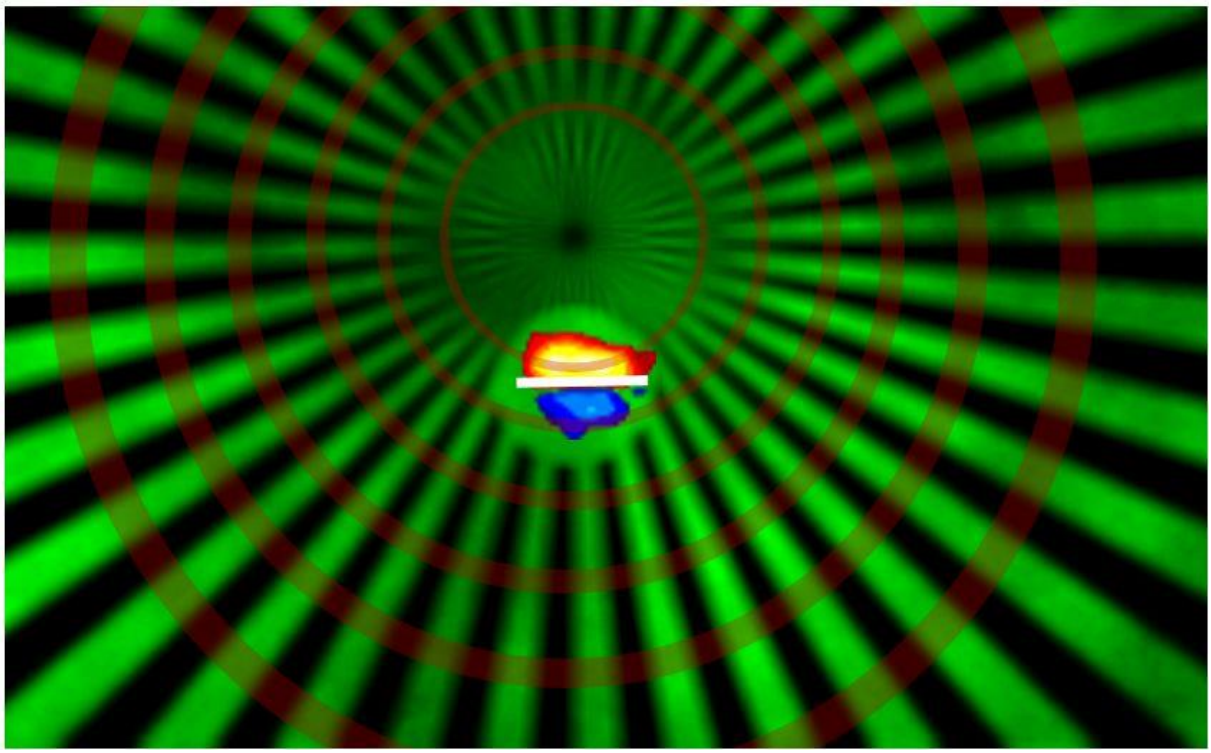

Figure.8.11: ***Conceptual framework of our working paradigm: the wavefront's local geometry of induced hallucinatory-like pulsating circles when geometric fan shapes inducer is combined with 1/f $^{\alpha}$ noise is detectable at the single cell level.*** *The preferred orientation of the cell is indicated by the white bar superimposed over its receptive field with ON (red) and OFF (blue) regions. The receptive field is placed in a geometrically unstructured area to avoid completion phenomenon and adaptation to the physical fans shape inducer (black). The center of the fans shape inducer has been displaced in the visual field so that the combination with 1/f $^{\alpha}$ noise (green levels) seen in between the features of the geometric inducer induce pulsating circles (shadowy red) whose wavefront should be locally parallel to the preferred orientation of the impaled cell. The induced pulsating circles are here shaded in red for representation purpose but are perceived as shadowy dynamic black shapes.*

II-3. Visual stimuli design

II-3.1 Probing the geometric nature of hallucinatory-like propagating waves of activity and maximizing their detectability at the single cell level

The aim of the second part of this thesis was to highlight the existence of neuronal correlates of the propagation of geometric hallucinatory-like waves of activity in the primary visual cortex of the anaesthetized cat. Our working assumption is that the induced percepts of pulsating circles and rotating fan shapes described by Billock and Tsou (2007) in their noise experiment are sufficiently stable over time and directly inducible to be detected at the single cell level during the time course of a trial but also in between trials. Indeed, Billock and Tsou (2007) reported in their noise experiment that the biased hallucination appeared to be induced by the physical pattern interacting with the noise. They described the appearance of the percepts as "stimulus locked" as those latter were directly induced at the onset of the visual stimulation presentation. However, we do not know if during the time course of the stimulation, the phase relationship between oscillations is preserved as the first percept can appear immediately but present a dephasing over the time course of a trial but also in between trials. Our working hypothesis is that travelling waves of hallucinatory-like activity visually induced by the presentation of a geometric planform combined with $1/f^{\alpha}$ noise correspond to the induced percepts. At the electrophysiological level, our experimental expectation is that first: those waves of activity are sufficiently stable over time to be detectable at the single cell level under the form of oscillations of the membrane potential matching the perceived dynamic of the propagating hallucinatory-like percepts. Second that the percept's stability over time preserves the phase of the periodic oscillations corresponding to the travelling waves of activity is in between trials.

One of our working assumption was that the oscillatory signature of the propagating waves of hallucinatory-like activity would only be detectable when the wavefront of this latter was parallel to the preferred orientation axis of the cell recorded intracellularly, probing the geometric nature of the effect. This was a necessary prerequisite to confirm that the observed oscillations indeed reflect the propagation of the cortical travelling waves of activity, resulting in a set of locally distributed orientations in the visual field, hence the geometric nature of the percept. That is why we could not place the receptive field of the impaled cell at the center of the geometric inducer where all orientations are perceived. The center of the geometric inducers (i.e., static concentric circles and fan shapes) was consequently displaced in order to induce wavefronts either locally parallel or orthogonal to the cell's preferred orientation (Figure 9.1). To facilitate the comparability between our cells, as in the first experimental protocols of the thesis, we scaled the distance between the RF of each cell and the center of the geometric inducers proportionally to the subthreshold Receptive Field (sRF) of each individual cell. To do so, we placed the center of the geometric inducers 1,5 sRF away from the center of this latter, which avoided the sRF to encroach on the center of the

geometric inducers and maintained the visibility of the latter to preserve the strength of the percept.

In order to maximize the inference of potential oscillatory responses, we placed the sRF in a circular opening that did not contain any features of the geometric inducers but in which only noise was continuously presented. This circular opening in the geometry was attenuated on the borders to progressively fade in the surround. To that effect, the features of the geometric inducers were also attenuated to avoid any figure/ground segregation phenomenon. This experimental choice was done in order to attribute any potential oscillatory response only to the synergy between geometric inducer, its position and noise in the detectability of propagating waves of activity. Moreover, this avoided any potential adaptation or completion phenomenon to geometric inducers physically presented in a feedforward manner to the sRF of our cells. We did so under the hypothesis that the percept was detectable even in an unstructured geometric area, as long as this one was sufficiently surrounded by geometric features that acts as spatial relays of adaptation, allowing the displacement and invasion of the wave of activity in the aperture encompassing the sRF. Therefore, the interactions that we studied aimed again at probing how the surround of a RF, composed of a geometrically structured area combined to $1/f^{\alpha}$ noise, can generate propagating waves of activity that invade a geometrically unstructured area containing the sRF by activity filling-in this latter. This is analogous to the proposition of Bressloff et al., (2002) who suggested that type I and II noncontoured planforms (including fan shapes and concentric circles) could arise from a filling-in process. As proposed in our working hypothesis, activity filling in between spatially distant activated hypercolumns via horizontal connections could allow completion of a geometric shape displacing itself on the cortical surface. It would preserve its initial geometry under the shift-twist invariance of the Euclidean group provided by the differential magnification factor, as the wave travels on the cortical surface.

To avoid an abrupt “rupture” between the circular opening containing the subthreshold depolarizing field as well as to facilitate filling-in of the propagating waves of activity in the geometrically unstructured opening when both geometry and noise were presented in the surround, $1/f^{\alpha}$ noise was continuously presented in the opening in all experimental conditions (Figure 9.1). The noise perturbation in the opening also locally maintained the increase in cortical excitability necessary to the formation and propagation of hallucinatory-like percepts (Ermentrout and Cowan, 1979; Tass, 1995, 1997, Bressloff et al., 2001, 2002). It maximized our chances to detect propagating waves of activity corresponding to the induced hallucinatory-like percepts at the level of a single cell. During the time course of the experiments, our experimental paradigm evolved and we introduced the presentation of a last control condition where the visual field had a uniform level of luminance, only condition where the sRF was not stimulated by noise in a feedforward manner. Therefore, the “absolute blank” condition was not presented to all of our cells but only to 3.

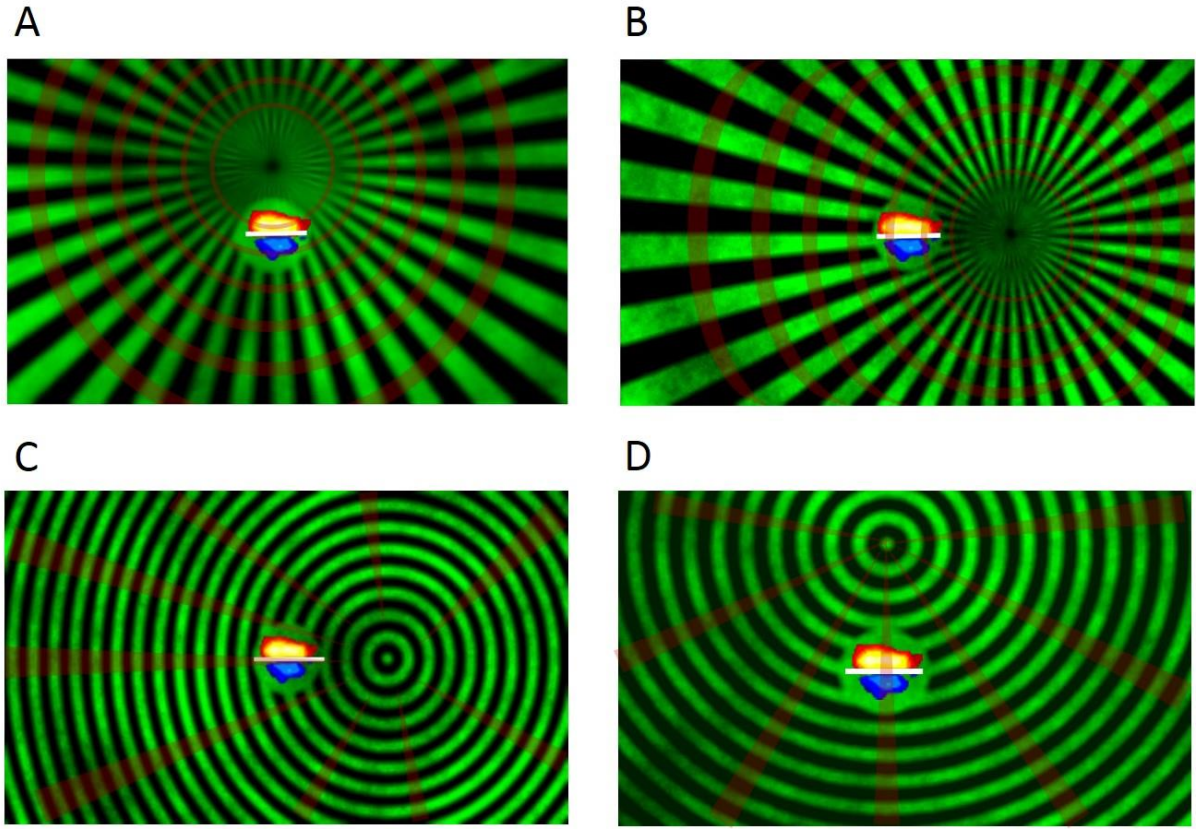

Figure.9.1: ***Probing the geometric nature of hallucinatory-like induced waves of activity. A-D****. The subthreshold depolarizing field (sDF) mapped intracellularly and defined by ON (red) and OFF (blue) sub regions is placed into a circular opening drawn into the geometric inducers to avoid adaptation and completion phenomena to those latter. The preferred orientation of the cell is represented by convention as the horizontal white line superimposed over the sDF. $1/f^{\alpha}$ filtered noise is continuously presented in the opening containing the sDF and in between the features of the geometric inducers (levels of green).* ***A-B.*** *The presentation of fan-shapes geometric inducer (black) induces the perception of pulsating circles (shadowy red).* ***C-D****. The presentation of concentric circles geometric inducers induces the perception of fan shapes rotating both in a clockwise and anticlockwise fashion.* ***A****. The center of the geometric fan shape inducer is positioned on an axis orthogonal to the preferred orientation axis of the impaled cell, at a distance of 1,5 sDF away from its receptive field center. This results in propagation of pulsating circles that, when reaching the sDF of the cell have a wavefront that is locally parallel to the sDF preferred orientation.* ***B****. By opposition to* ***A****, the center of the fan shapes inducer lies along the axis of the cell's preferred orientation, which results in pulsating circles whose wavefront is locally orthogonal to the preferred orientation of the sDF.* ***C****. The center of the geometric concentric circles inducer is positioned on the preferred orientation axis of the sDF, by opposition to* ***D*** *where it lies along an axis orthogonal to it. In* ***C****, this results in rotating fan shapes whose wavefront is locally parallel to the cell's preferred orientation, in contrast to* ***D*** *where the wavefront of rotating fan shapes is locally orthogonal to that axis.*

II-3.2 Probing the need of a synergistic interaction between geometric inducer and 1/f$^{\alpha}$ noise in the emergence of hallucinatory-like waves of activity

In order to test our working hypothesis, for each condition presented in Figure 9.1, a corresponding condition where a uniform luminance replacing the noise in the surround was also presented. This allowed us to compare the interacting effects of geometric inducer + noise versus geometric inducer + uniform luminance in the surround of the subthreshold receptive field. Moreover, for a given position of the geometric inducer in the surround, there was a corresponding condition where the same retinotopic locations were stimulated by the geometric inducer whether noise or uniform luminance was presented (Figure 9.1 A vs B and C vs D against Figure 9.2 A vs B and C vs D). This provided us with control conditions potentially highlighting the existence of a range of both local and global perturbations statistics beyond which the V1 network is not optimally perturbated. At the perceptual level, this is the case as presentation of geometric inducers combined with uniform luminance did not induce perception of pulsating circles nor rotating fan shapes.

In addition, to exclude the sole contribution of noise and of uniform luminance presented in the surround of the receptive field in the emergence of pulsating circles and rotating fan shapes waves of activity, we designed control conditions where only noise and only a field of uniform luminance were presented in the surround of the opening containing the sDF (Figure 9.3). In those conditions, the opening containing the sDF was still continuously stimulated by 1/f$^{\alpha}$ noise.

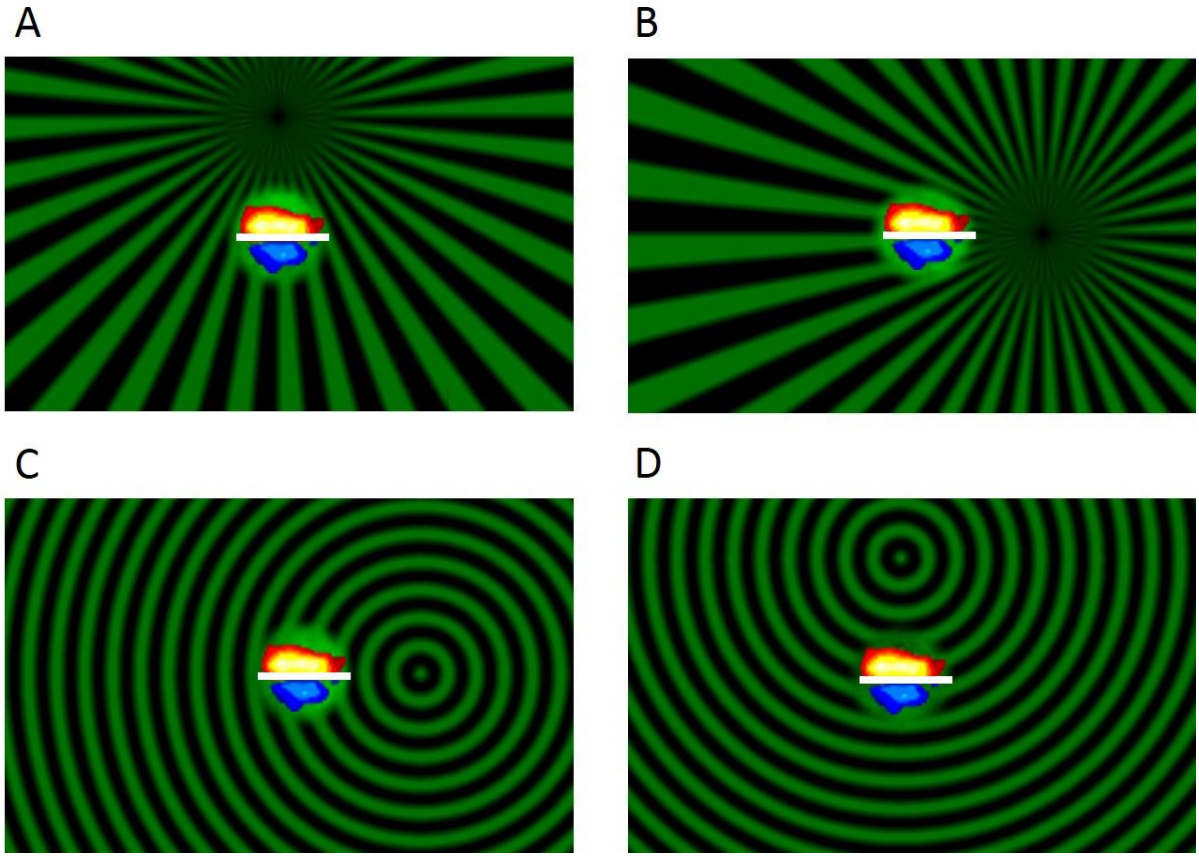

Figure.9.2: ***Excluding the presentation of geometric inducers combined with a uniform level of luminance in the induction of hallucinatory-like waves of activity.*** *Same convention as in Figure 9.1 for the opening containing the subthreshold depolarising field in which $1/f^{\alpha}$ noise is continuously presented.* ***A-B****. The center of fan shapes inducers is presented either along the preferred orientation axis of the cell (**B**) or along an axis orthogonal to it (**A**).* ***C-D****. The center of concentric circles inducers is presented along the preferred orientation axis of the cell (**C**) or along an axis orthogonal to it (**D**).* ***A-D****. A uniform level of luminance of the same value than the average luminance of the surrounding noise in Figure 9.1 is presented in between the features of the geometric inducers. No hallucinatory-like percepts (pulsating circles or rotating fan shapes) are induced in those configurations.*

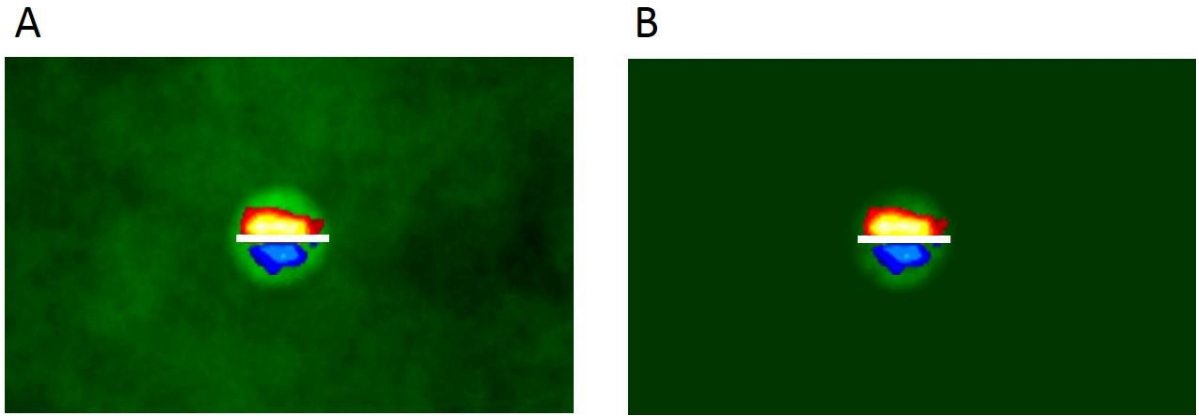

Figure.9.3: ***Excluding the presentation of noise alone and uniform level of luminance alone in the induction of hallucinatory-like waves of activity.*** *Same convention as in Figure 9.1 for the opening containing the subthreshold depolarising field in which 1/f$^{\alpha}$ noise is continuously presented.* ***A****. In the surround of the opening containing the sDF, only 1/f$^{\alpha}$ noise is presented. The mean luminance of the noise in the surround is equal to the average luminance of the surround in Figure 9.1, composed of noise and of geometric inducers. This is why the noise in the surround appears darker than in the central opening.* ***B****. Uniform background with the same luminance level as the average value of the surrounding noise in* ***A****. No hallucinatory-like percepts (pulsating circles or rotating fan shapes) are induced in those configurations.*

II-3.3 Geometry's position and luminance equalization across conditions

In all conditions where hallucinatory-like percepts were induced (Figure 9.1), because we wanted to maximize potential responses filling-in from the surround of the receptive field, the noise that was presented in the opening and in the surround (between the geometry's features) had the same luminance whose average value was set at 18 cd/m². This value is very close to the one used by Billock and Tsou (18,8 cd/m²). This formed our test conditions (Figure 9.1 A and C) where the wavefront of the induced percept was parallel to the preferred orientation axis of the cell. This had on one side the advantage of facilitating the transition between the noise in the surround and the one in the opening, maximizing the potential invasion of hallucinatory-like percepts in the geometrically unstructured opening containing the sDF. On the other side, this had the disadvantage of creating a disequilibrium between average luminance in the opening and average luminance in the surround where geometric inducers were also presented at a luminance of 1 cd/m² to maintain a necessary high contrast between noise and geometric inducer to induce the percept. However, between each condition, the average luminance was kept constant by only manipulating the features of the surround, as the luminance of 1/f$^{\alpha}$ noise and uniform background

in the surround were always equal in each test and control condition. In the rest of this section, we will detail how luminance was equalized between conditions.

Because of the geometric nature of the inducers physically presented on a screen that possess its own rectangular shape, it was not possible to present different types of inducers at different positions without adjusting some parameters of the geometry to preserve the overall average luminance equal across conditions. Moreover, due to the difficulty of intracellular experiments, we could not impose a priori the preferred orientation or position of the cells receptive fields that were impaled intracellularly. Once the subthreshold depolarising field was mapped and its preferred orientation determined (see section Material and methods), the sDF was placed into an opening whose size was proportional to it. The opening was attenuated on the borders by a Gaussian function whose standard deviation was equal to a quarter of the sDF radius. Past the radius of the sRF center, the attenuation of the aperture was obtained using that Gaussian function by increasing the transparency (alpha parameter) of the noise pixels presented in the opening. It resulted in a smooth transition between aperture's noise and the content of the surround (noise and geometry: figure 9.1, uniform luminance and geometry: figure 9.2, darker noise and uniform luminance: figure 9.3). Therefore, the opening encompassing the sDF and containing noise was presented above the surround content in a layer disposition of the elements composing the visual scene. In the surround, in order to attenuate border effects, the geometric inducers were themselves presented above the noise or the uniform luminance presented and a transparency alpha value was differentially attributed to geometry's pixels.

In practice, the X and Y cardinal axes intercepted at the center of the screen. According to the size of the sDF, the center of the geometry was placed 1,5 sDF away from the center of this latter, along its preferred orientation axis or along and axis orthogonal to it. The center of the geometric inducer was positioned on the side where there was maximum place for the geometry, (on the right of the sDF for geometric inducers placed along the preferred orientation axis of 0°, Figure 9.1 B and C and above the sDF for geometric inducers placed on an axis orthogonal to the 0° preferred orientation axis of the cell, Figure 9.1 A and D). The luminance of the fans and rings was set at 1 cd/m². The number of fans and rings was fixed at 36, even though we do not see 36 rings on the screen, this simply mean that the bitmap that was generated was larger than the screen and that an optimization calculus was made, but only on the rectangular region that the screen occupied on the bitmap. To obtain the same average luminance of the surround between fans whose center was placed along the preferred orientation axis of the cell or along an axis orthogonal to it (Figure 9.1 B on the right VS 9.1 A above the sDF), an optimization calculus was made on only one free parameter. The angle between the edges of the fans was calculated to obtain a difference of surface covered by the geometry in the surround of the opening (Figure 9.1 A vs B) inferior to 2% between the two conditions. This operation created templates of the fan geometry. For the concentric circles inducers, the radius of the first ring as well as the distance between each ring was fixed at 2° of visual angle. However, the width of each ring was optimized to obtain a difference of

surface between rings placed along the preferred orientation axis of the cell or on an axis orthogonal to it (Figure 9.1 C VS D), but also between the surface occupied by the rings geometry and the fans geometry (Figure 9.1 A and B) inferior to 2%. This created templates for the rings geometry. Those templates allowed attenuating the luminance values of the geometry by increasing differentially the transparency of the pixels composing it. For each pixel occupied by the templates of geometry, a transparency or alpha value ranging from 0 to 1 was calculated as a function of the average luminance of the neighbouring 25 pixels, forming a square of 5 by 5 pixels surrounding each pixel. This explains why pixels at the center of the geometric features (fans or circles) are dark at their center where the density is maximal and progressively more transparent on the edges, as the number of neighbouring pixels where noise is present is higher and higher. This smoothing of the geometry avoided aliasing phenomena and avoided figure/ground segregation as the geometric inducers display a progressive transition towards the noise.

Once the optimization calculus done, the stimulation area occupied by the geometry was nearly the same in between types of inducers and in between their position regarding the sDF. The geometry occupied an area that was very close to half of the surround's extent, given the 2% maximum limit of difference between the conditions where geometry was presented. This means than when uniform luminance replaced noise in between the geometry's feature in the surround (Figure 9.2), the luminance of that uniform field was set at 18 cd/m², the same average luminance of the noise's in Figure 9.1. However, for the noise only and blank conditions (Figure 9.3 A and B, respectively), because no geometry was presented, the average luminance of the noise in the surround of the noise only condition (Figure 9.3 A) was set at 9 cd/m², give or take the 2% upper limit of differences in between conditions where geometry was presented. The same luminance value was applied to the uniform level of luminance of the surround in the blank condition (Figure 9.3 B).

II-3.4 Temporal display of the stimuli

Figure.9.4: ***Pictograms of the visual stimulations.*** *Each pictogram corresponds to a visual stimulation described in Figures 9.1, 9.2 and 9.3. Hallucinatory percepts are only induced in the 4*

upper conditions where both noise and geometry are present in the surround of the opening containing the sDF. However, the conditions for which oscillations reflecting the dynamic of the hallucinatory-like waves of activity are expected are the ***Fans iso noise*** *and* ***Rings iso-Noise*** *conditions, where the wavefront of the hallucinatory-like induced waves of activity is parallel to the preferred orientation axis of the cell. Each condition containing geometry (first eight panels) is named as following: the first word describe the type of geometric inducer, the second word the orientation of the hallucinatory-like wavefront of induced activity regarding the preferred orientation axis of the cell and the third word the type of background presented in the surround of the opening. Note that for the four conditions where geometry and a uniform level of luminance are presented in the background (last letter: grey), no percepts of pulsating circles or rotating fans-shape are induced. iso and cross labels are only present to facilitate the comparison of the geometric inducer's position in the visual stimulation to the four conditions where noise and geometry are presented in the surround of the opening and where actual pulsating circles and rotating fans shapes are perceived. The last condition where a uniform level of luminance was presented on the entire screen was called "absolute blank". This is the only condition where the opening containing the sDF was not stimulated by noise. This figure represents the order of presentation of each stimulation response in the results section.*

We initially set the duration of each tested condition at 3.5 seconds. During the evolution of our experimental paradigm, we increased that duration up to 4 seconds. Therefore, our recordings do not all have the same duration. Each condition tested was preceded by the presentation of the blank condition presented for only 500 ms (Figure 9.5). The blank condition was also tested for 4s in the batch of conditions. We decided to present the blank stimulation for 500 ms before every tested stimulation in order to capture the sole contribution of the stimuli presented in the surround while the opening containing the subthreshold depolarising field was continuously stimulated by $1/f^{\alpha}$ noise, even before the appearance of a given tested condition.

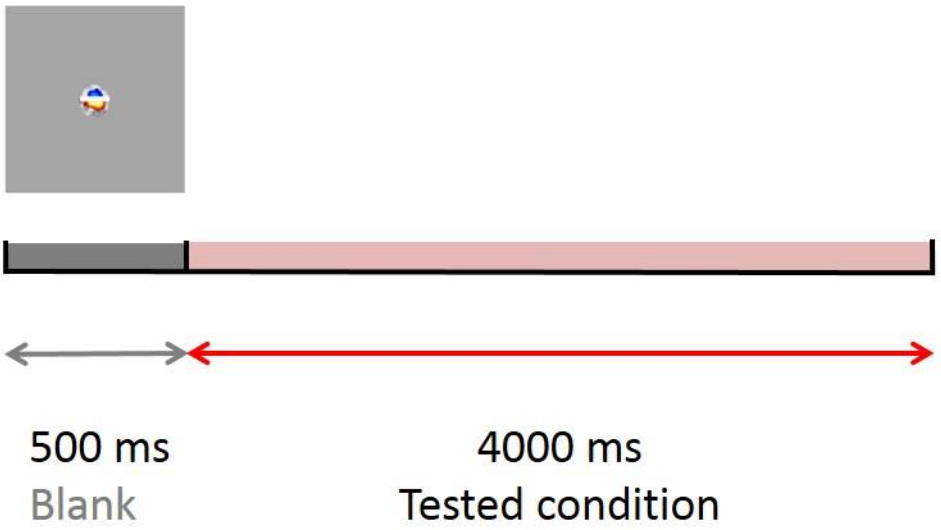

Figure.9.5: ***Composition of a stimulation.*** *Each visual stimulation previously described was preceded by the presentation during 500 ms of the blank condition to adapt the subthreshold depolarising receptive field to 1/f$^{\alpha}$noise. At t = 500 ms, a given condition was presented, which allowed to study the impact of the content of the surround of the receptive field which was the only parameter that changed across stimulation as 1/f$^{\alpha}$noise was continuously presented in the opening.*

Figure 9.5 only represents the time course of the stimulation of one condition. All conditions were presented consecutively in a batch or episode. In all of our experiments, including the ones of the first part of the thesis, conditions were pseudo randomized across trials. This is even more important here as we wanted to study the potential oscillatory nature induced by our conditions of interest. Therefore, we had to eliminate any intrinsic periodicity in our stimulations. That is why the order of presentation of each stimulation was pseudo randomized as each condition had to appear only once in an episode and the order of presentation of each condition was changed across episodes (Figure 9.6). We made an exception for the absolute blank condition that was always presented at the end of each episode to avoid any perturbation at the level of the sDF. Indeed, this latter was continuously stimulated with noise to only study the impact of the change in the surround of the receptive field, and not of the emergence of noise in addition. That is why, when the absolute blank condition was presented, it was always at the end of each episode.

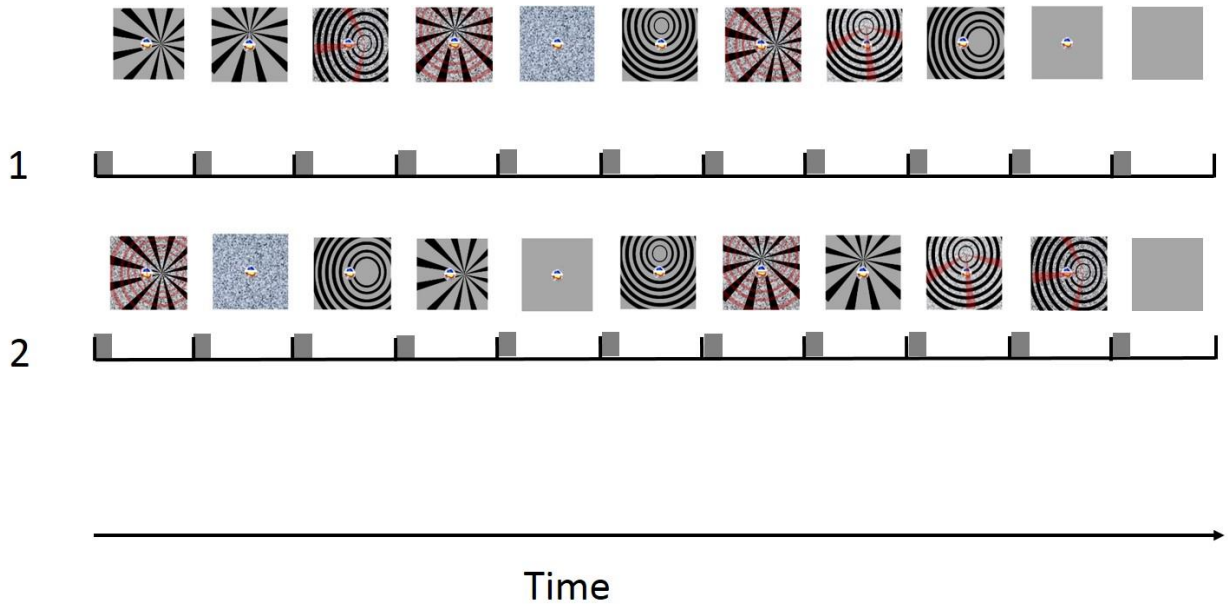

Figure.9.6: ***Pseudo randomization of the conditions presentation across trials.*** *Each condition was only presented once in a trial (episode) and the position of each condition in the trial was pseudo randomized. Upper pictograms indicate the successive conditions that were presented while the timeline below is cut into segments delimited by vertical small black lines that indicate the beginning of each stimulation. The shaded grey region on the right of each vertical line indicate the presentation of the blank condition for only 500 ms while each condition, including the blank condition, was tested for 4000 ms (against 3500 ms for some cells).*

II-3.5 Generation of 1/f$^{\alpha}$ spatiotemporally filtered noise

II-3.5.1 Spatial filtering of the noise

For each frame of noise, we first generated 1024 by 1024 pixels matrices of Gaussian white noise centred on 0 with a standard deviation of 1. We then generated a spatial filter matrix of 512 by 512 pixels in the Fourier space which obeyed a power law of 1/f$^{\alpha}$ with a spatial filtering value of α set at 1.4.

Each pixel of the spatial filter matrix has coordinates (x,y) expressed in terms of indices (i,j). The modulus R, or distance at the origin of each pixel is given by $\sqrt{(i^2 + j^2)}$. In order to obtain Gaussian white noise that obeyed a power spectral law of 1/f$^{\alpha}$, we applied the following formula:

$$\forall i, f(i) = R(i)^{-\alpha}$$

Where i represent a given pixel. The matrix of 512 by 512 pixels that we obtained was then symmetrized regarding a vertical axis and an horizontal one to obtain a 1024 by 1024 pixels spatial

filter matrix of the same size than the Gaussian white noise matrices that we generated (Figure 9.7, right). The quadrants were not reorganized so as to place the DC (frequency 0) in the center of the image. This spatial filter gave us pondering coefficients in the spectral domain that we applied to the 2D Fourier transform of each frame of noise. This ponderation was obtained by applying a point by point multiplication of each matrix (Figure 9.7). We then performed the inverse Fourier transform of the resulting matrix to obtain a single matrix (Figure 9.7, bottom). We evaluated the quality of our parametrisation by calculating in the Fourier space, for each pixel in a single quadrant the average modulus (Z) of the complex number between 10 frames that we represented as a function of its distance to the origin (modulus of each pixel, figure 9.8, left). We then plotted for each pixel the log value of the estimated average modulus as a function of its distance to the origin, also expressed in log scale and performed a linear regression which slope was evaluated (Figure 9.8, right). The average luminance of each noise matrix was then set at 18 cd/m² and the standard deviation at 4.5 cd/m². For experimental and storage purpose, the noise and geometry's parameters optimization were calculated online. Two hundred frames of noise were calculated to converge towards the desired statistics and 3 noise frames were stored in the graphic card's memory buffer. Because of computation difficulties, it was not possible to generate noise frames larger than 1024 pixels. However, our screen had a resolution of 1920 by 1080 pixels. Therefore, the generated noise frames were smaller than the screen. In order to avoid a distortion of our power spectral law, we decided not to use a linear interpolation to solve that problem but increased the matrices dimensions by a nearest neighbour interpolation method. Therefore, each noise pixel occupied four pixels on the screen, which implies that only a portion of each noise matrix was displayed on the screen.

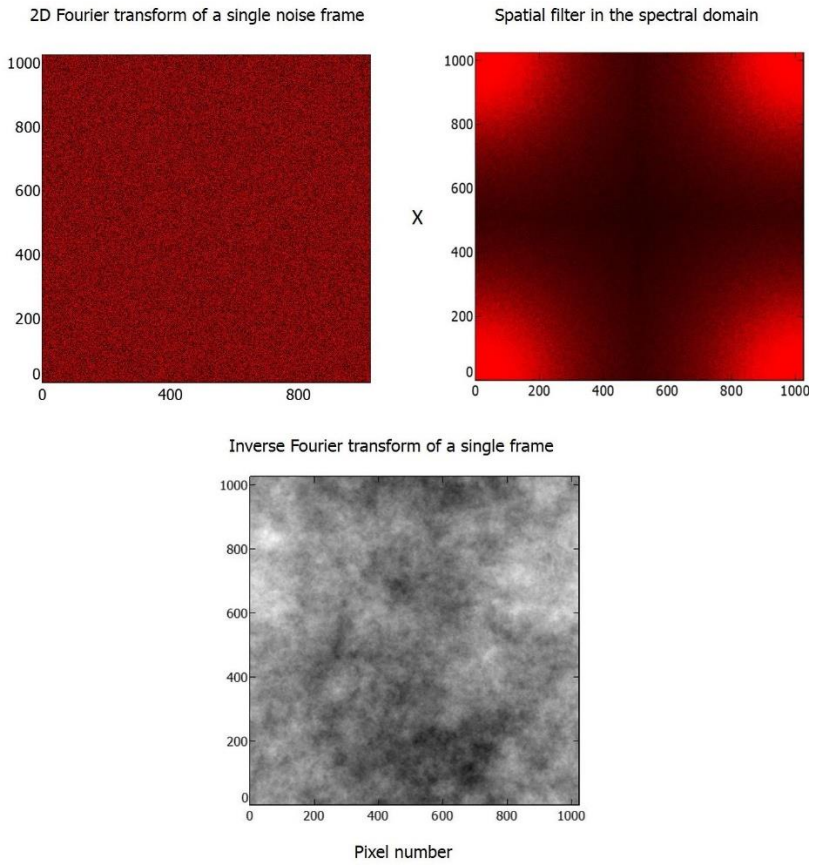

Figure 9.7: ***Spatial filtering of the noise.*** *The 2D Fourier transform of a single frame of Gaussian white noise is represented on the left. The profile of the spatial filter coefficients in the spectral domain are represented on the right. The point by point product of the two is shown below in grayscale, after inverse Fourier transform.*

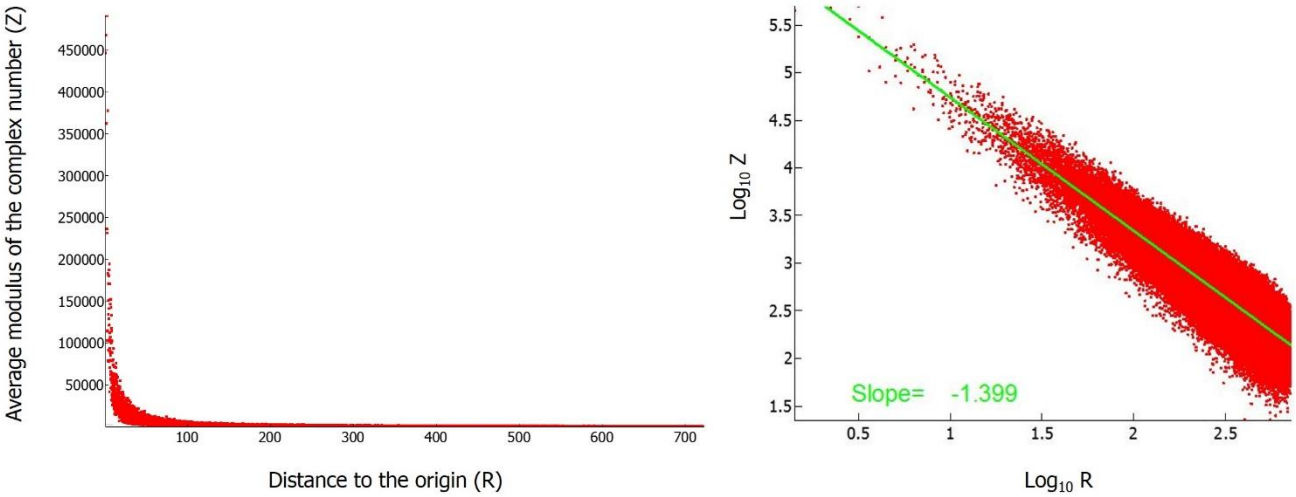

Figure.9.8: ***Spatial filtering evaluation of the noise.*** *We can clearly see on the left that the spatial filtering of our noise obeys a power spectral law that decreases in $1/f^{\alpha}$. On the right, the linear regression of the log-log representation has a slope of -1.399 for a spatial filtering value of 1.4. (n = 10 matrices).*

II-3.5.2 Temporal filtering of the noise

The temporal filtering of our noise was obtained by combinations of first-order digital filters (Mingesz et al., 2004). For a discrete data sequence x_i, the output of a digital filter is given by:

$$y_i = D_1 . x_i + D_0 . x_{i-1} - C_0 . y_{i-1} \quad (1)$$

Where the parameters of a first-order digital filter with a cut-off frequency f_0 and amplitude A_0 are:

$$C_0 = \frac{1-l}{1+l}, D_0 = D_1 = \frac{A0}{1+l} \quad (2)$$

where: $l = ctg\frac{\pi}{\Omega S}$, $\Omega S = \frac{fs}{f0}$ (3)

where ΩS is a normalized sampling frequency fs that only depends on the ratio between the sampling frequency (or refresh rate in our case) and the cut off frequency of the filter. Now that we introduced all the parameters of equation (1), we can precise that y_i is the luminance value of pixel i that depends on the input value x_i given to the filter, the previous input value x_{i-1} at the preceding frame and of the output value y_{i-1} returned by the filter for the preceding frame. The coefficients D_1, D_0 and C_0 were calculated and applied to each pixel i. We must however precise that equation (1) only gives the output value of a single filter. As Mingesz et al., (2003) noted, as long as we consider digital signals, the sampling frequency plays no role: only the ratio of the frequencies is important. We used a combination of 16 filters that were equally spaced on a logarithmic scale by a factor of 2. An example of the filter configuration that we used is shown in figure 9.9. A $1/f^{\alpha}$ decreasing spectral profile of the luminance value in the temporal domain was obtained by setting the amplitude of each filter proportionally to $1/f^{\alpha/2,}$ which gave us, when squared, a power spectral content obeying a decreasing power law of $1/f^{\alpha}$. (From Mingesz et al., 2003).

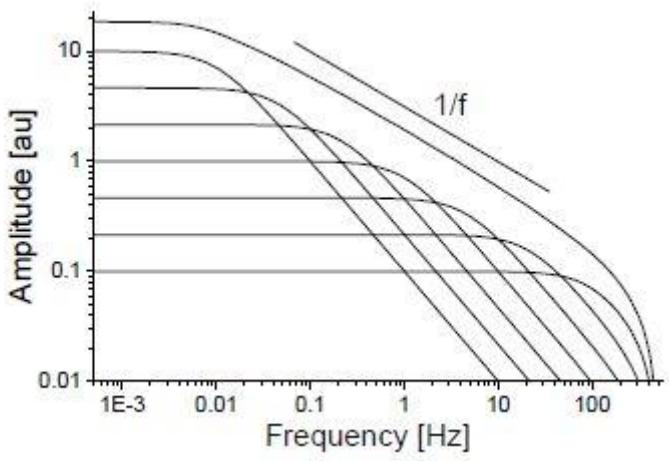

Figure.9.9: ***A filter with a transfer function of 1/f power rule.*** *In our case, we used 16 filters regularly spaced on a logarithmic scale, as shown in the figure. However, our filters were not distributed over the same bandwidth.*

We did not use quite the same conditions as figure 9.9, as we can see that the serie of filters obeys a 1/f spectral law. Moreover, the filter with the highest cut-off frequency does not have the same relative amplitude on a logarithmic scale than the other filters. We followed the same distribution as Mingesz et al., (2003) by setting the amplitude A(f), of each of our 16 filters at $1/f^{\alpha/2}$where f represents the cut-off frequency of each filter and α the desired exponent. Therefore, the amplitude of each filter was

A1 = a1

A2 = a1 + a2

….

A16 = a1 + a2 + … + a16,

Which corresponds to an homogeneous distribution on a logarithmic scale. During our experiments, the refreshing rate of our screen was set to 28 Hz, the closest of our 144 Hz LCD screen to the 30 Hz value used by Billock and Tsou (2007) on their 60 Hz CRT monitor. Therefore, the coefficients C_0 and $D1$ of equation (1) were obtained by summing the different coefficients C_0 and $D1$ obtained for each filter who had a different amplitude A_0 and cut-off frequency f_0.

In order to evaluate the parametrization of our temporal filtering, we generated a very large number of very small (4 by 4 pixels) matrices. We then picked a pixel and evaluated the evolution of

its luminance across matrices until we reached 1.10^6 values. In order to meaningfully evaluate the power spectral distribution of our luminance values, we set a dx of 1/28 seconds (our refreshing rate) between each point of our signal representing the evolution of luminance values of a single pixel across matrices. We then performed the power spectral analysis of our signal (Figure 9.10, left). We also plotted our signal in a log-log scale and performed a linear regression whose slope was evaluated (Figure 9.10, right). The maximum cut off frequency of the highest filter cannot be superior to fs/2. Hence, our power spectral was restricted to values up to 14 Hz (Figure 9.10), the filter with the highest cut-off frequency.

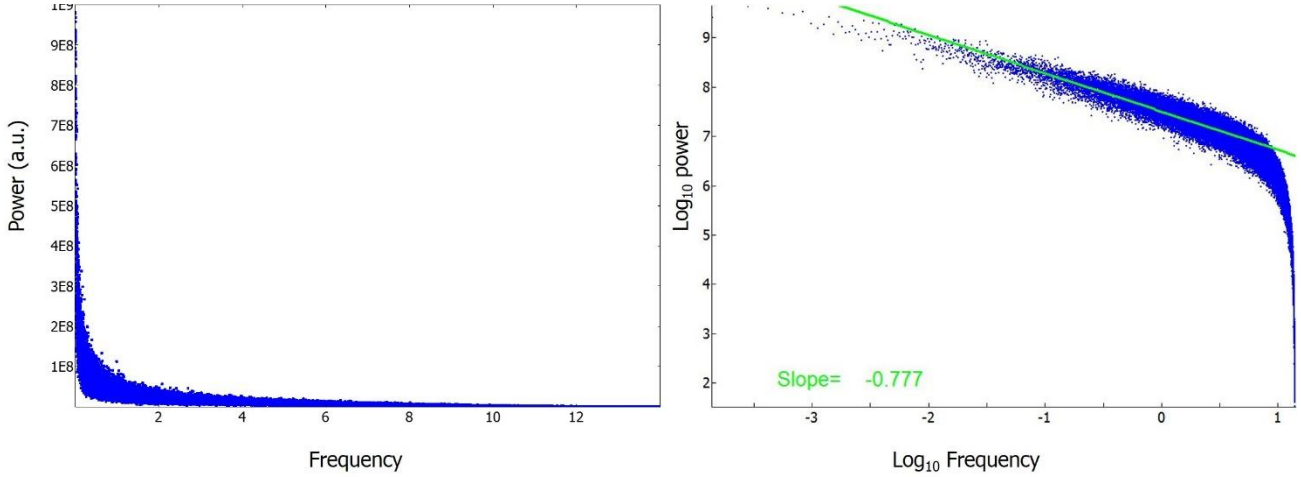

Figure.9.10: ***Temporal filtering of the noise.*** *We can clearly see on the left that the temporal filtering of our noise obeys a power spectral law that decrease in $1/f^{\alpha}$. On the right, the linear regression of the log-log representation has a slope of -0.77 for a temporal filtering value of 0.8 (n = 1.10^6 points).*

II-4. Results

We analysed our intracellular recordings under the working hypothesis that travelling waves of hallucinatory-like activity could be detected at the single cell level under the form of oscillations of the membrane potential matching the dynamic of perceived propagation of pulsating circles and rotating fan shapes when both geometric inducer and noise are present in the surround of the RF. We worked under the assumption that those waves of activity would only be detectable at the single cell level when the wavefront of the geometric percept is parallel to the preferred orientation axis of the recorded cell in an attempt to locally confirm the geometrc distribution of the propagating waves of activity in the visual field. We also simultaneously recorded ongoing and visual electrocorticograms (ECoG) and investigated the oscillatory characteristics of our recordings by performing frequency and time-frequency analysis.

II-4.1 Detecting oscillatory activity

In order to detect oscillatory activities, two components in the intracellular fluctuations were looked for: first, stimulus-onset synchronized oscillations, that may constitute the bulk of stimulus-locked responses obtained by averaging Vm across trials. Second, stimulus-induced oscillations where frequency analysis is performed on each trial. This latter method preserves oscillations that would be evoked at each trial at variable latency and does not affect the mean membrane potential or visual ECoG (For a review, see Tallon-Baudry and Bertrand, 1999; Figure 10.1 and 10.2). In addition, in order to characterize their specificity, we compared oscillatory frequency distribution across visual stimulus conditions.

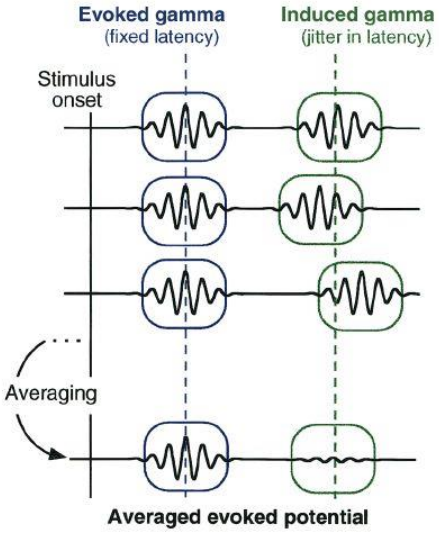

Figure.10.1: ***Schematic representation of evoked and induced oscillatory responses.*** *In this case, the cartoon represents oscillatory activity in the gamma band. The principle is that an evoked response (Blue boxes) appears at the same latency and phase in each trial can be detected during the summation process of the averaging. To the contrary, an induced response (green boxes) appears with a jitter in latency (a dephasing) from trial to trial, centred around a given latency (green dotted line) while preserving the same frequency. According to the level of dephasing between trials, it tends to cancel out in the averaged evoked potential. That is why specific methods must be used in order to characterize induced activities. (From Tallon-Baudry and Bertrand, 1999).*

Before any analysis, all traces were filtered with a Bessel high pass filter with a cut off frequency of 1 Hz to eliminate very low frequencies. This filter was applied in a forward then backward fashion to avoid any distortion of the signal. We then applied on this filtered signal a classical wavelet decomposition method to estimate the time course of the instantaneous spectrum (time-frequency analysis). The methods are described in detail in the annex of Baudot et al, (2013).

In this time-frequency analysis, uncertainty is related to the Heisenberg inequality and only depends in this representation on the frequency σ^2. $f = cste \geq 1$. The frequency uncertainty increases as the frequency grows and the temporal uncertainty decreases as the frequency grows, because of smaller and smaller time windows. Because we wanted to maximise the temporal precision of our analysis, we first used classical Gabor wavelets. This tradeoff between frequency and time resolution in favor of the time resolution allowed us to estimate the temporal extent of potential transient responses synchronized to the stimulus onset. As a matter of fact, changing the overall content of the RF surround at the same time between each trial for each condition provides a sudden time dependent modulation of the energy content in the visual scene, which is likely to be reflected by evoked oscillations locked to the onset of the stimulus and therefore visible in the average PSTW of the trials. Stimulus-locked transient responses were studied by convoluting each average PSTW with a bank of complex-valued Gabors (Figure 10.2) of the form

$(\Psi_{t,f}(\tau))$:

$$\Psi_{t,f}(\tau) = \sqrt{f}.\exp(-2.\pi.i.\ f(\tau - t)).\exp\left(-\frac{\tau - t}{\sigma^2}\right)^2$$

The bank of Gabor filters used is non-orthogonal with frequency ranging from 1 to 30 Hz with 1 Hz value change steps while the temporal sampling of the membrane potential was of 0.1 ms. To obtain a good temporal resolution, the Gabor function used in this analysis had a Gaussian standard deviation of two gabor period $(\sigma^2. = 3)$ and was normalized to an energy unit (Figure 10.2).

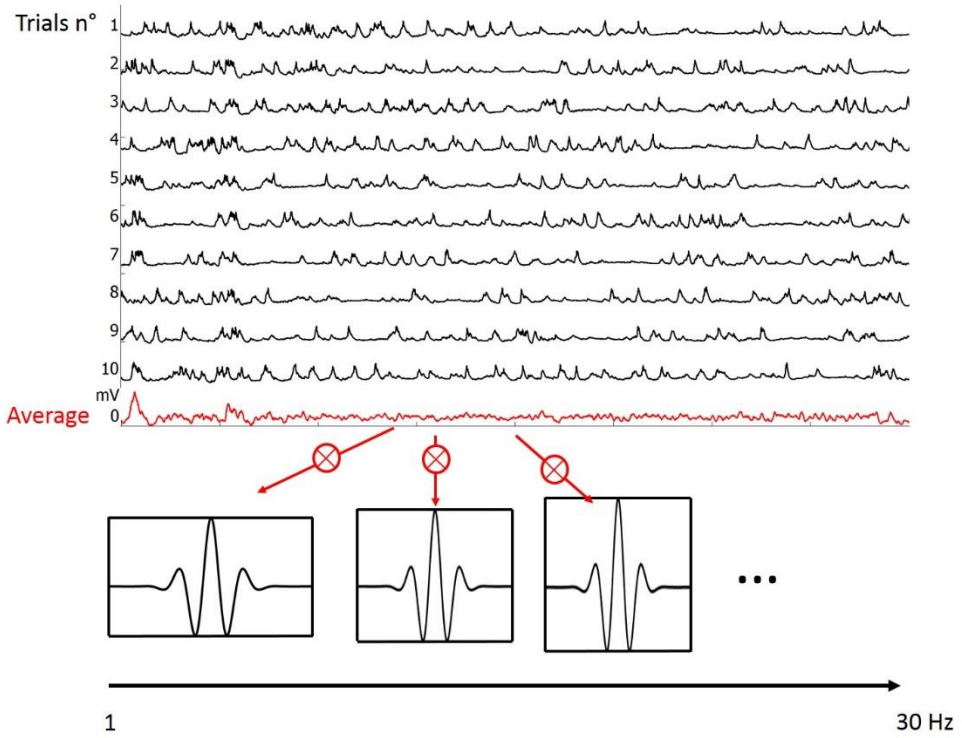

Figure.10.2: ***Convolution of the average PSTW with a bank of Gabor filters.*** *Single cell example where each individual trial to a given condition is indicated in black with its number on the left. Only 10 trials are represented, among the 29 repetitions obtained for that cell. The average of the PSTW is represented in red, below the trials. To estimate the temporal duration of the transient response, each average PSTW was convolved with Gabor wavelet functions of increasing frequency from 1 to 30 Hz by 1 Hz steps.*

However, from figure 10.1 we saw that the overall characterization of oscillatory responses must be clearly distinguished between stimulus-locked responses that can be retrieved in the average PSTW, to the contrary of induced oscillatory responses that might cancel out in the average evoked responses due to a trial to trial temporal jitter between oscillations. That is why the overall spectro-temporal content of individual trials must be evaluated separately (Figure 10.3).

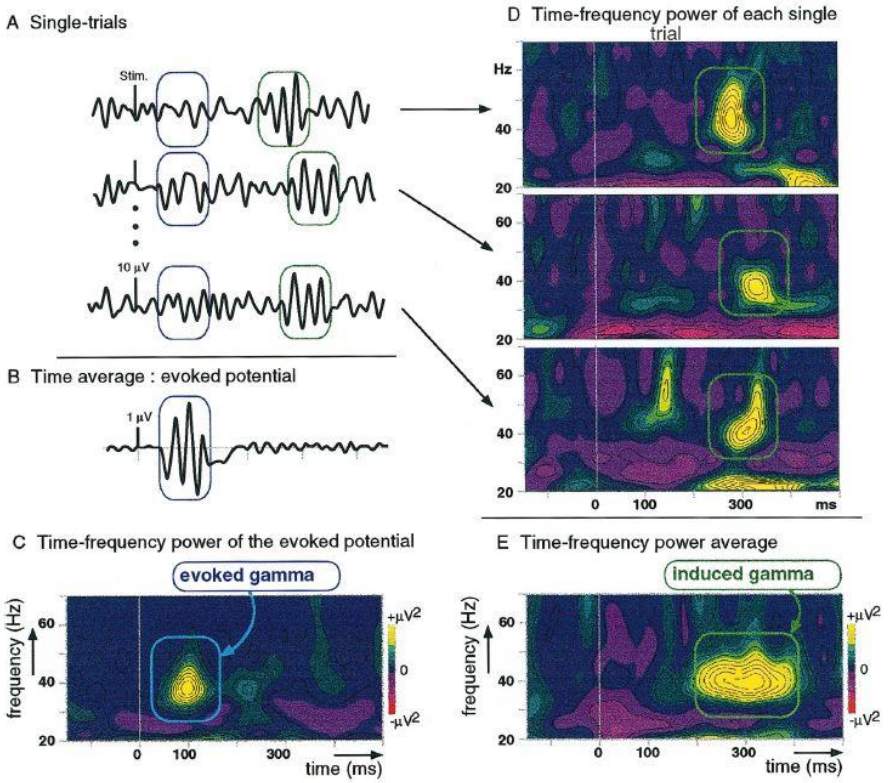

Figure.10.3: ***Principle of time-frequency analysis revealing induced oscillations. A.*** *Successive EEG trials with a small amplitude gamma response phase-locked to the stimulus onset (blue boxes) and a gamma burst jittering in latency (green boxes).* ***B.*** *Averaging across single trials leads to the conventional evoked potential.* ***C.*** *Time-frequency power representation of the evoked gamma response by convolution of the evoked potential (average) with Morlet wavelets. The abscissa represents time and the ordinate frequency. The non-phased locked activity is cancelled out. When the time-frequency power is computed for each single trial (**D**), and then averaged across trials (**E**),* *the induced gamma response is revealed, if the temporal jitter between trials is sufficiently small. (From Tallon-Baudry and Bertrand, 1999).*

We used a method similar in its essence to the one presented in Figure 10.3, although we did not directly average the time-frequency results of each trial but instead, we used time-frequency convolution of each trial with a bank of Morlet wavelets to evaluate the signal, noise, total power of the signal and the Signal to Noise Ratio (SNR) distribution over time. To that end, we used the wavelet decomposition method introduced by Baudot et al., (2013). This method can be understood as an extension in the time-frequency domain of the signal and noise estimation proposed by Croner et al., (2003) and Baudot et al., (2013).

For a given frequency and a given time, we define $S_i\ (t,\ f)$ as the complex result at time t and frequency f of the response and wavelet convolution for the trial i. The signal power S_{est} of the stimulus-locked waveforms is then measured as the squared modulus of the trials average vector of the wavelet transform in the complex domain (Figure 10.14) and is given by:

$S_{est}(t, f) = \left| \langle S_i(t, f) \rangle_i \right|$

where angular brackets $\langle\ \rangle$ indicate the average across all trials and straight brackets || indicate the modulus. The Noise power N (t, f) is measured as the average distance between the trial vector and the trials average vector of the wavelet transform in the complex domain and is given by:

$$N(t, f) = \langle | S_i(t, f) - S_i(t, f) \rangle_i | \rangle_i$$

The total signal power $S_{tot}(t, f)$ is measured as the average modulus of the trials vector:

$$S_{tot}(t, f) = \langle | S_i(t, f) | \rangle_i$$

Signal to Noise Ratio $SNR(t, f)$ is measured as:

$$SNR(t, f) = \frac{Sest(t,f)}{N(t,f)}$$

In practice, Signal to Noise Ratio $SNR(t, f)$ is obtained by dividing the S matrix term by the N matrix term for identical time and frequency values, an example is illustrated in Figure 10.14 where the principle of Signal, Noise and Total signal power measure is decomposed.

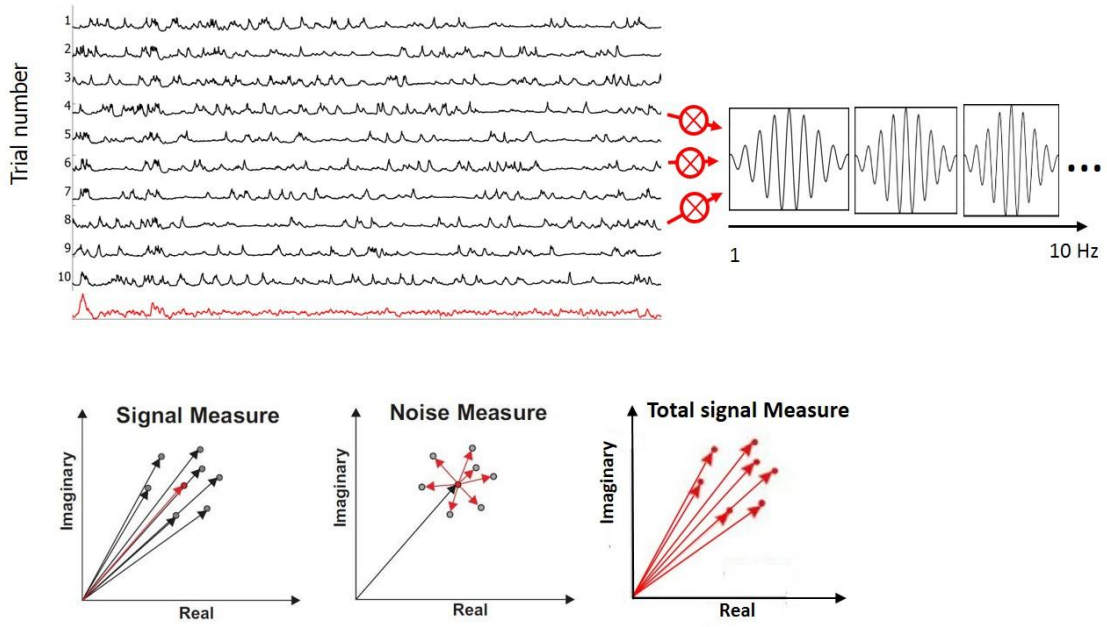

Figure.10.4: ***Signal, Noise and Total Signal measurements.*** Upper left panel: single cell individual trials. Upper right panel: schematic representation of the Morlet Wavelets used for the convolution with each trial. Bottom: Signal measure, the black points represent the trials result of the wavelet

convolution in the complex plane for one particular time and frequency. The red point indicates the average trials vector which modulus gives the estimated signal. Noise: the black point indicates the average trials vector while red points the individual trials result of the wavelet convolution in the complex plane. Noise is measured as the average dispersion distance of trials to this mean. Total Signal Measure, each red point represents the trials result of the wavelet convolution in the complex plane, the Total Signal is measured as the average modulus between each trial vector in the complex plane. (From Baudot et al., 2013).

Signal, noise and total signal average power spectra can be obtained by averaging the function over time, Figure 10.15. The different power spectra are then defined by:

$$F_{Signal}(f) = \int_{tstart}^{tend} (Sest(t,f))^2 / (tend - tstart)\, dt,$$

$$F_{Noise}(f) = \int_{tstart}^{tend} (N(t,f))^2 / (tend - tstart)\, dt,$$

$$F_{Tot}(f) = \int_{tstart}^{tend} (Tot(t,f))^2 / (tend - tstart)\, dt,$$

$$F_{SNR}(f) = \int_{tstart}^{tend} (SNR(t,f))^2 / (tend - tstart)\, dt,$$ (Figure 10.16).

Those measures represent the average energy of the signal, noise and SNR over time at a given frequency. We propose a mutual-information upper bound based on the classical Shannonian channels. To that end, we consider that neuronal response and neuronal noise have Gaussian probability distributions in the frequency domain for each time and that neuronal noise is additive. Potentially, there is however a redundancy between the various times, which implies that the integral over time of this measure only gives an upper bound estimate of the mutual information. The information rate is given by the Shannon-Hartley theorem (Shannon, 1948). The average information rate over time for each frequency f is given by:

$$I_m(f) = \int_{tstart}^{tend} Log_2(1 + (SNR(t,f))^2)\, df / (tend - tstart)\, dt,$$ (Figure 10.16)

For the study of oscillations locked to the onset of the stimulus, we used original Gabor wavelets filters because of their high temporal resolution that allowed us to evaluate the instantaneous spectrum energy distribution at the onset of the stimulus (Figure 10.2). To the contrary, to characterize induced oscillations we chose to use Morlet wavelets because of their higher frequency resolution, at the expanse of the temporal one (Tallon-Baudry and Bertrand., 1999; Figure 10.3). This tradeoff between temporal and frequency resolution is inevitable in time-frequency analysis and is inherent to the uncertainty principle of Heisenberg. The Morlet wavelet is composed of a complex exponential (carrier) multiplied by a Gaussian window (envelope), whose

standard deviation σ allows trade between time and frequency resolution. The wavelet exists as a complex version or a purely real-valued version. Some distinguish between the "real Morlet" vs the "complex Morlet". Others consider the complex version to be the "Gabor wavelet", while the real-valued version is the "Morlet wavelet". In any case, the Morlet wavelet is not a replacement of the Fourier transform but an additional information that allows a qualitative access to time related changes in frequency component and are therefore well suited to the time-frequency analysis of non-stationary signals. This wavelet has been reported to be closely related with human perception, notably in vision (Daugman, 1985). Historically, Jean Morlet modified the initial definition of Gabor wavelet to keep the same wavelet shape over equal octave intervals, resulting in the first formalization of the continuous wavelet transform (Goupillaud, Grossman and Morlet, 1984).

In order to improve the readability of the time-frequency representation, the Morlet wavelet decomposition presented here was largely oversampled by using 0.1 Hz linear steps to increase the frequency resolution, testing for the presence of very close frequencies during the convolution with the trials. Morlet wavelets were obtained by the convolution of four lobes windowed sinusoids with a Gaussian window of the same length and 2 sigma period for each frequency (Figure 10.4). Morlet wavelets were normalized to a unit energy value.

Finally, we aimed to examine the oscillatory behavior of our responses and its stability over time, in the search of sustained induced and evoked oscillations reflecting the pulsating circles and rotating fan shapes percept's stability and reproducibility that we found during our preliminary psychophysical observations. To that end, we performed normalized AutoCorrelation Functions (ACF) on each individual recorded trial, on the average of those trials (stimulus-locked oscillations) and we also averaged the individual ACF of each trial (induced oscillations). In addition, we performed normalized CrossCorrelation Function (CCF), a generalization of the ACF, between each pair of trials and averaged them. To characterize the profiles of our ACF, we inspired ourselves from Bringuier et al., 1997. To assess the rhythmicity of their intracellular recordings where bars of the optimal orientation were presented at an optimal velocity in a periodic manner, Bringuier and colleagues used classical ACF from which they extracted 2 parameters. Because they used classical (i.e. non-normalized) ACF, their analysis showed an alternance of peaks regularly distributed over time s and decreasing exponentially. The first parameter that they extracted was the "contrast" of their first peak, defined as the Michelson contrast: the ratio of the local maxima of the first peak minus the average of its two surround minima over the sum of maxima and minima. Their second parameter was derived from an exponential decreasing fit applied to the first 3 peaks of their ACF and represented a dumping constant tau corresponding to a decrease of 50 % of the first peak amplitude. From those two parameters, Bringuier and colleagues plotted the first parameter as a function of the second and delimited ACF showing oscillations from non-oscillatory one by a linear separation obtained thanks to a pocket algorithm running on a perceptron. The detail of their analysis can be found in the Methods section of their paper. To the contrary of Bringuier et al., (1993), we used normalized ACF, which means that there wasn't any exponential decrease in our analysis profile because at each time t for which the signal was displaced regarding itself, the

correlation coefficients were calculated on the number of points that overlapped. By definition, the correlation coefficients that we found ranged between -1 and 1. To characterize oscillations found in our analysis, we did not classify ACF as oscillatory or non-oscillatory but provided a gradual evaluation of the oscillatory components. To explain the rationale of of our analysis, let's start by introducing the result of a single sinusoid of a given frequency. The ACF profile of such trace will be a sinusoid where peaks are homogeneously distributed at the period characterizing the signal. However, apart the exception of periodic stimulations like bars or gratings, electrophysiological recordings generally show a mixture of frequency components which result in a distribution of peaks of different amplitudes heterogeneously distributed in an ACF, which means that the spectral density of the signal is not centered on a signal frequency. It follows that the maxima and minima (higher and lower coefficients values) reflect the low frequency carrier of the signal over which higher frequencies display smaller correlation peaks. In order to provide both a qualitatively loyal and quantitatively based evaluation of the power spectral density of our ACF, we detected local minima and maxima reflecting higher spectral components superimposed over the carrier by setting a threshold detection value down to 10 % of the maximal peak correlation amplitude (that was equal to 1 at t0). This allowed us to obtain local minima and maxima for each peak of the ACF between +/- 50% of the signal, boundary that we set to preserve relevant coefficients values as beyond 50% of temporal jitter, less than half of the signal overlap with itself. We then calculated the average period of oscillation between each local minima-maxima and maxima-minima and the standard deviation of that average. From those measures, we calculated the Coefficient of Variation (CV) of the average oscillatory period found for each ACF and compared it across conditions.

II-4.2 Stimulus-locked analysis

By computing the average of our trials, we obtained average Post-Stimulus Time Waveform (PSTW) reflecting the membrane potential and visual ECoG responses of our cells recorded intracellularly synchronized to the stimulus onset. We observed that at the very beginning of the recording sequence, when only noise is presented in the opening containing the RF and a uniform level of grey in the surround, phase locked oscillations appeared in almost all conditions. This surround-onset evoked response was due to the sudden change in the content of the surround that preceded the trial for a given condition (Figure 9.6) and was found in nearly all conditions for 3 out of the 5 cells (where complete protocols were performed). Those responses were observed in the membrane potential (Figure 10.5 A) as well as in the visual ECoG. A second surround-change evoked oscillation was found for all conditions in the average of the PSTW, showed in Figure 10.5 A for a single cell example, starting at 500 ms, when the content of the surround was suddenly changed, marking the beginning of a new stimulation condition. This was the case for all stimulations, excepted for the blank condition where there was no difference between the content of the surround in the adapting pre- condition and the tested condition (between 0-500 and 500 – 3500 ms).

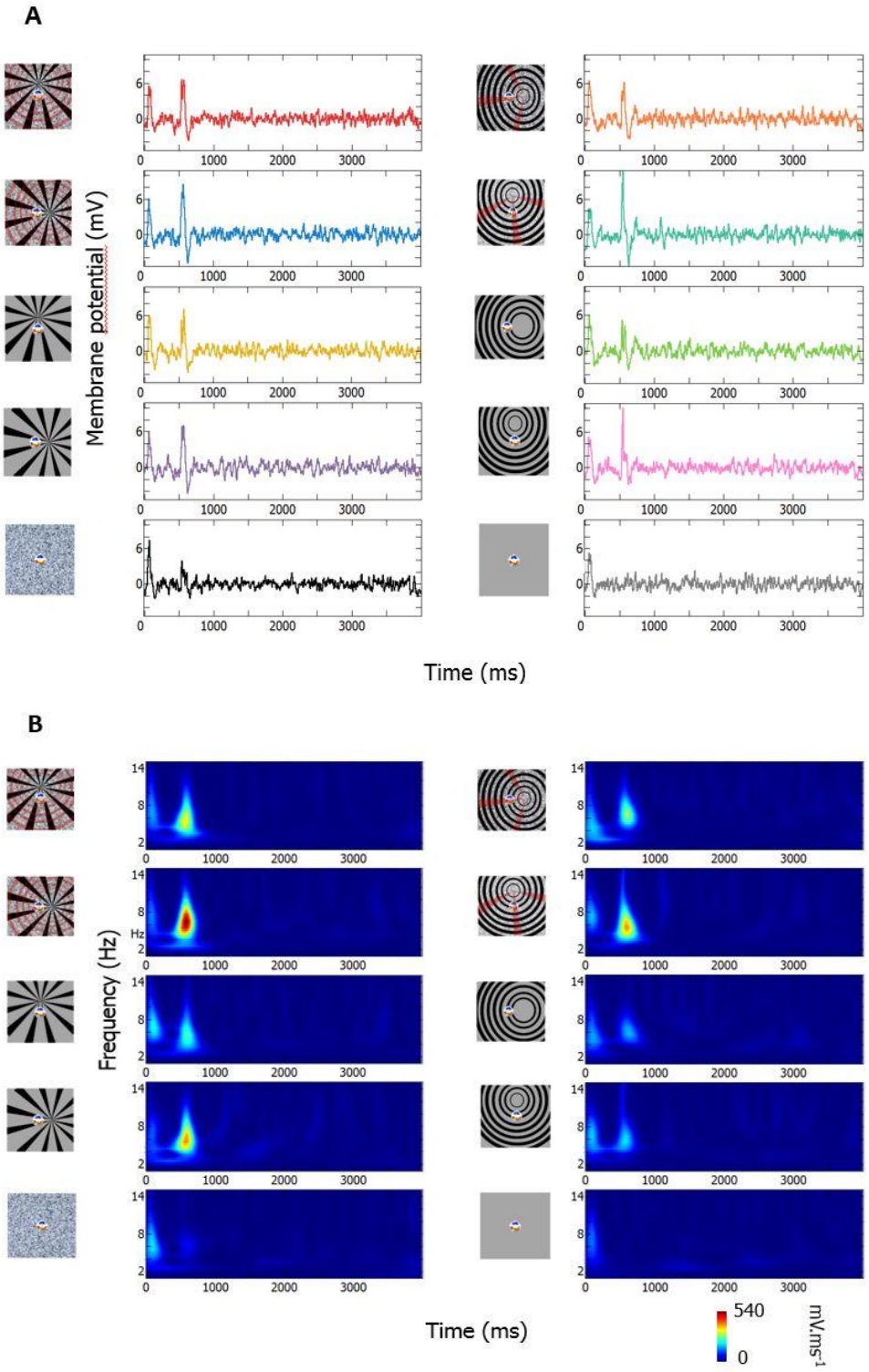

Figure.10.5: ***Frequency-time analysis of stimulus-locked oscillations. A.*** *The average PSTW of each condition of an individual cell is represented on the right of each pictogram describing the corresponding visual stimulation.* ***B.*** *Representation of the time-frequency convolution of each condition average PSTW with the bank of Gabor filters described in Figure 10.2. The first transient responses starting at T0 is easily visible in all conditions whereas the second transient response at t = 500 ms appear for all conditions except the last one corresponding to the blank.*

We can already clearly see that at T0, a transient depolarising event reflected in the average of the PSTW appear (Figure 10.5 A). It is linked to the change from the previous stimulation of the content in the surround of the RF and is a non-specific full field effect. A second transient response, starting at t = 500 ms can be seen for all conditions except the last one representing the blank, where the content of the surround did not change between the pre-stimulation and tested stimulation. The Eiffel tower profile of time-frequency energy distribution seen in Figure 10.5 B reflects the uncertainty principle and the width of the Gabor wavelet window gives some spectral energy before and after the peak. From the time-frequency analysis reported in Figure 10.5, we found the energy distribution of the second transient response to be precisely centred at a short latency after the 500 ms transition ranging between 575 and 615 ms while the frequency centre peak ranged between 5,8 and 6,3 Hz across conditions and spread in the frequency domain from 4 to 8 Hz. We also estimated the temporal spread of energy distribution around that peak to reach a maximal value of 250 ms after stimulus onset at t = 500 ms, although that duration was slightly different across conditions, it remained relatively stable, ranging from 220 up to 250 milliseconds (Figure 10.5 B). We must take care in the evaluation of oscillatory responses as stimulus locked component often last about 200 ms while unlocked dephased oscillation following the stimulus-locked ones can last up to 400 milliseconds after stimulus onset (Tallon Baudry and Bertrand, 1999). However, those longer lasting oscillations are not stimulus-locked and must be taken into account as part of the induced visual responses.

In our data, the duration of the second stimulus-locked response was consistent across cells showing transient responses both at the membrane potential and visual ECoG level. However, interestingly enough, we observed a stimulus-dependency in the strength of the transient energy, which was dependent on the stimulus in the surround (compare second left row where maximal amplitude is obtained when the RF is physically locally surrounded by a fan almost having the preferred orientation of the cell combined with noise and the third row with the cross-oriented fan combined with grey). Similarly, compare the right second row where the ring inducer is locally parallel to the cell's preferred orientation to the right first raw where the inducer is locally cross oriented, displaying a smaller energetic distribution of the transient response. In contrast, the transient response was reduced when significant areas of the immediate surround were stimulated with lower energy stimuli (right 3rd and 4th row from the top, ring of different orientations combined with homogeneous grey luminance level configuration). Note also in the PSTW average a different profile of transient responses where a significant hyperpolarisation could follow a strong depolarization in some conditions and not in others (dark green VS pink condition, Figure 10.5 A). In all cases, the stimulus-locked response was so transient that no sustained oscillatory pattern was evoked which could constitute a possible correlate of the expected percept's electrophysiological signature. Even if all conditions in all cells did not show a stimulus-locked transient response starting at t = 500 ms, because we were only interested in sustained frequency components specific to each condition, we decided to discard the first 250 ms of the tested conditions in order to compare our analyses between conditions and between cells in a conservative manner. Therefore, all our analysis started at t = 750 ms up to the end of the recording.

II-4.3 Sustained nature of the oscillations and autocorrelation measures

We first investigated whether we could find a structure in the temporal distribution of the oscillations of our tested conditions. We wanted to determine whether oscillations of the membrane potential and of the visual ECoG were sustained over the time course of the interest conditions, in the hope that despite the use of a different noise between trials and conditions, the induced percept were sufficiently stable over time and directly inducible to be captured as continuous phase locked oscillations. To that end we calculated the average normalized CCF between each pair of trials (induced-oscillations), the average ACF between trials (induced oscillations) and the ACF of the trials average (stimulus-locked oscillations) between -50 and +50 % of the signal duration. Those calculus are represented in Figure 10.6 for the Vm of a single cell example and the simultaneously recorded visual ECoG for one of our condition of interest where induced pulsating circles had a predicted wavefront parallel to the cell's preferred orientation.

In the average CCF and ACF, we did not find any particular structure of induced oscillations as the correlation coefficients are low (between -0.04 and 0.04) and do not peak regularly both at the Vm and at the visual ECoG level. Individual ACFs did not display any particular profile as correlation coefficients were higher than in the average but peaks were heterogeneously distributed over time and did not show sustained oscillations except for one Vm trial, where oscillations were peaking regularly at a single frequency for our condition of interest. However, when we performed the normalized autocorrelation of the average PSTW (stimulus locked oscillations), we found a strikingly well-organized structure quite resembling a sinusoid, peaking regularly at a single frequency of 3 Hz at the Vm level (Figure 10.6; B: left third row). This frequency corresponds exactly to our preliminary estimations (3 – 3.5 Hz) of the dynamic of the hallucinatory-like induced percept of pulsating circles when a geometric fan shapes inducer is combined with $1/f^{\alpha}$ spatiotemporally filtered noise. This last analysis gave us two types of information. First, it indicated a very high power spectral density centred on 3Hz. Second, it extended the spectral analysis to the temporal domain by indicating that 3Hz oscillations were not concentrated in a single portion of the signal but were distributed across all the duration of the tested condition of interest, the signal resembling itself every 333 ms, signature of continuous oscillations that we were looking for. If it was the case, we would expect to find the same profile in the average of the ACFs, unless each trial does not display sustained oscillations over its entire time course but only at key moments where it is not dominated by noise unspecific to each trial, which would explain that we only retrieve sustained oscillations during the summation process of the averaging and the poor profile of the average ACF composed of heterogeneous individual ACFs. Surprisingly, we found the same profile for visual ECoG recordings as neither the average of the normalized cross correlation between each pair of trials nor the average ACF displayed any particular profile and where correlation coefficients were pretty similar (from -0.04 to 0.04, Figure 10.6; B: right 1st and 2nd row). In contrast, similarly to the Vm, the normalized autocorrelation of the trials average displayed a relatively high power spectral density and peaked at approximately 3 Hz (Figure 10.6; B: right third row), as if in that

condition, the fluctuations of both the membrane potential and the visual ECoG were entrained towards a single oscillatory frequency that we only to retrieve as stimulus locked oscillations in the average of the trials. We must however take care in the interpretation of those results as one possibility is that stochastic resonance occurs at the dominant noise frequency, which follows a $1/f^{\sigma}$ power spectral law and is therefore the most important in the 2-3 Hz frequency bandwidth after our filtering. However, we do not believe that this is the case as those 3 Hz oscillations are only found for our condition of interest where the predicted wavefront of induced pulsating circles is locally parallel to the cell's preferred orientation and no other condition including controls showed such an ACF profile of the average PSTWs (Figure 10.7 and 10.8).

The ACF of the average Vm PSTW and average visual ECoG PSTW are shown for comparison between each condition in figure 10.7A and 10.8A, respectively, together with the results of our detection of local minima and maxima that allowed us to evaluate the Coefficient of Variation (CV) of the estimated period of oscillations in each condition ACF (Figure 10.7 B and 10.8 B). As described in the first section of the results chapter, ACF local minima and maxima were detected by setting the threshold detecting value down to 10 % of the maximal correlation coefficient of 1 obtained at t=0. At the membrane potential level (Figure 10.7), we can clearly see that among all our conditions, the ACF of the average pstw of our condition of interest in red (upper right part) present the largest, most stable and sustained oscillations at a single frequency of 3 Hz compatible with our experimental expectations. Contrarily, other conditions mainly display higher frequency content reflected by lower correlation coefficients riding on a carrier of different frequencies. This stable behaviour therefore appears to be proper to our condition of interest. The second most stable ACF is obtained for the condition where induced rotating fan shapes have a predicted wavefront locally orthogonal to the cell's preferred orientation (dark green, right second row). However, that condition oscillate at a lower frequency of 2.4 Hz and present peaks transition less smoothly distributed than for our condition of interest in red while having smaller correlation coefficients, reaching a maximal value of 0.32 against 0.39 for our condition of interest. From the detection of local minima and maxima, we estimated the oscillatory period of our condition of interest to be of 313 ms and the CV of that condition is the lowest among all conditions, reaching a value of 0.27, although closely followed by the condition in dark green reaching a CV of 0.29 (Figure 10.7 B). For the visual ECoG, (Figure 10.8 A and B), the profile is sensibly the same as for the Vm for our condition of interest in red as it displays a smooth ACF oscillating at about 3Hz, reaching a maximal correlation coefficient of 0.49, highest value found between conditions. Its oscillatory period is of 304 ms and that period CV is the second lowest among conditions, reaching a value of 0.22, only superior to our second condition of interest in orange where predicted induced rotating fan shapes are locally parallel to the cell's preferred orientation. That last condition has a period CV of 0.2, although its correlation coefficients are lower than in our first condition of interest. Between Vm and ECoG, the only reproducible constant is the 3Hz sustained oscillations found in the average PSTW ACF of our first condition of interest.

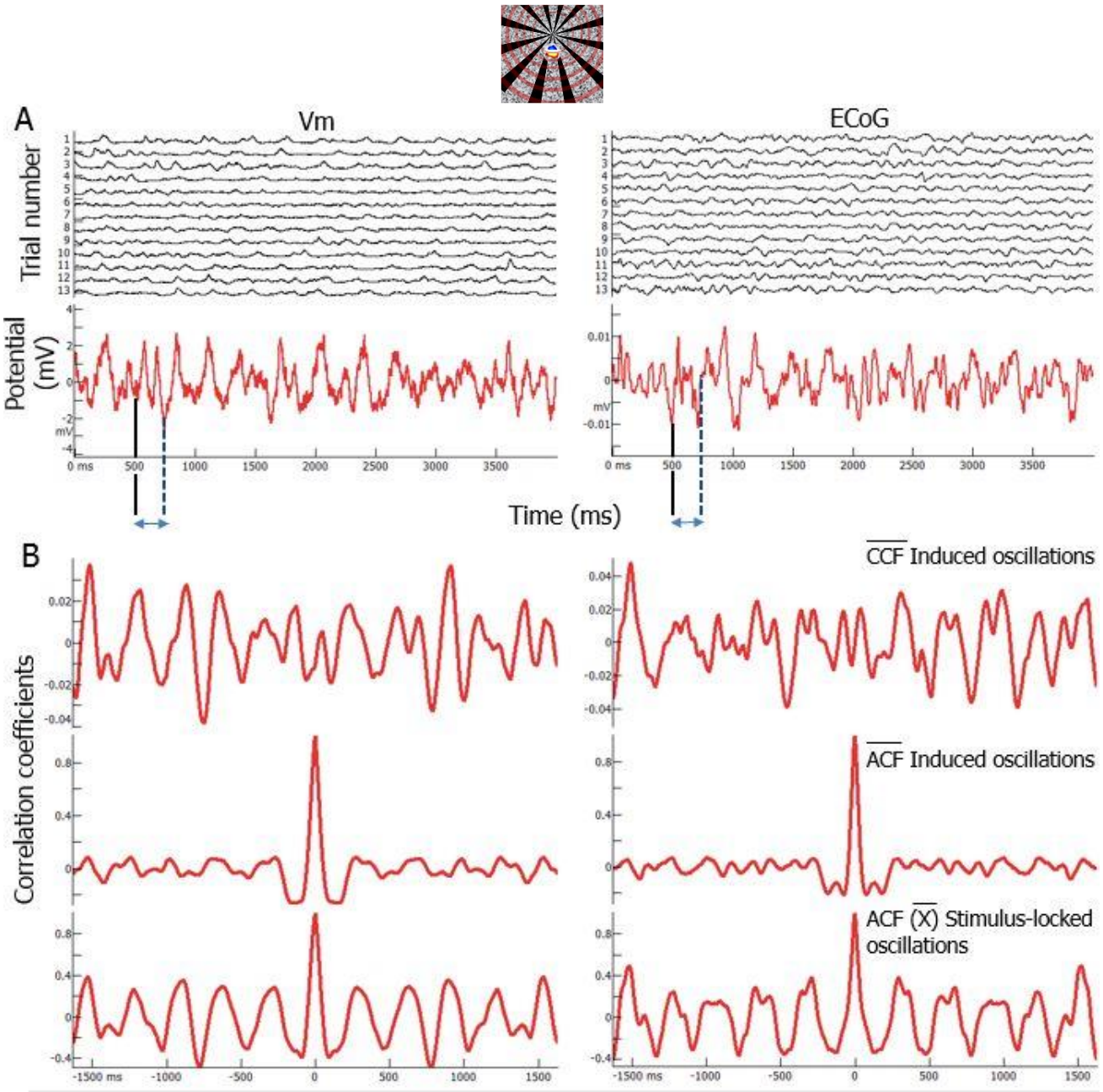

Figure.10.6: ***Periodic oscillations are found in the average PSTW of the trials.*** *Single cell example (n= 13 repetitions). Left: membrane potential analysis, Right: Visual ECoG.* ***A.*** *Individual trials are represented in black in the first row while the average PSTW of the trials is represented in the second row. Black solid line represents the onset of the stimulus, when the RF surround content was changed and dotted blue line delimits the end of the transient response. For those recordings, in that condition, the transient response starting at t=500 ms is reflected by an hyperpolarisation that is more visible in the average PSTW of the visual ECoG (A, second right row). The following analysis where then performed from t= 750 ms up to the end of the recordings. The average normalized cross-correlation (CCF) between each pair of trials is shown in the first row of panel B. It did not display any particular structure over time as peaks are irregularly distributed and correlations coefficients are low (between -0.04 and 0.04) for both Vm and visual ECoG. The average autocorrelation (B, second row) does not display any particular temporal structure, with low*

correlation coefficients (-0.02 -0.01). However, the normalized autocorrelation (ACF) of the trials in the third-row present regular oscillations over time where the signal presents a high power spectral density at only 3Hz and resembles itself at that frequency.

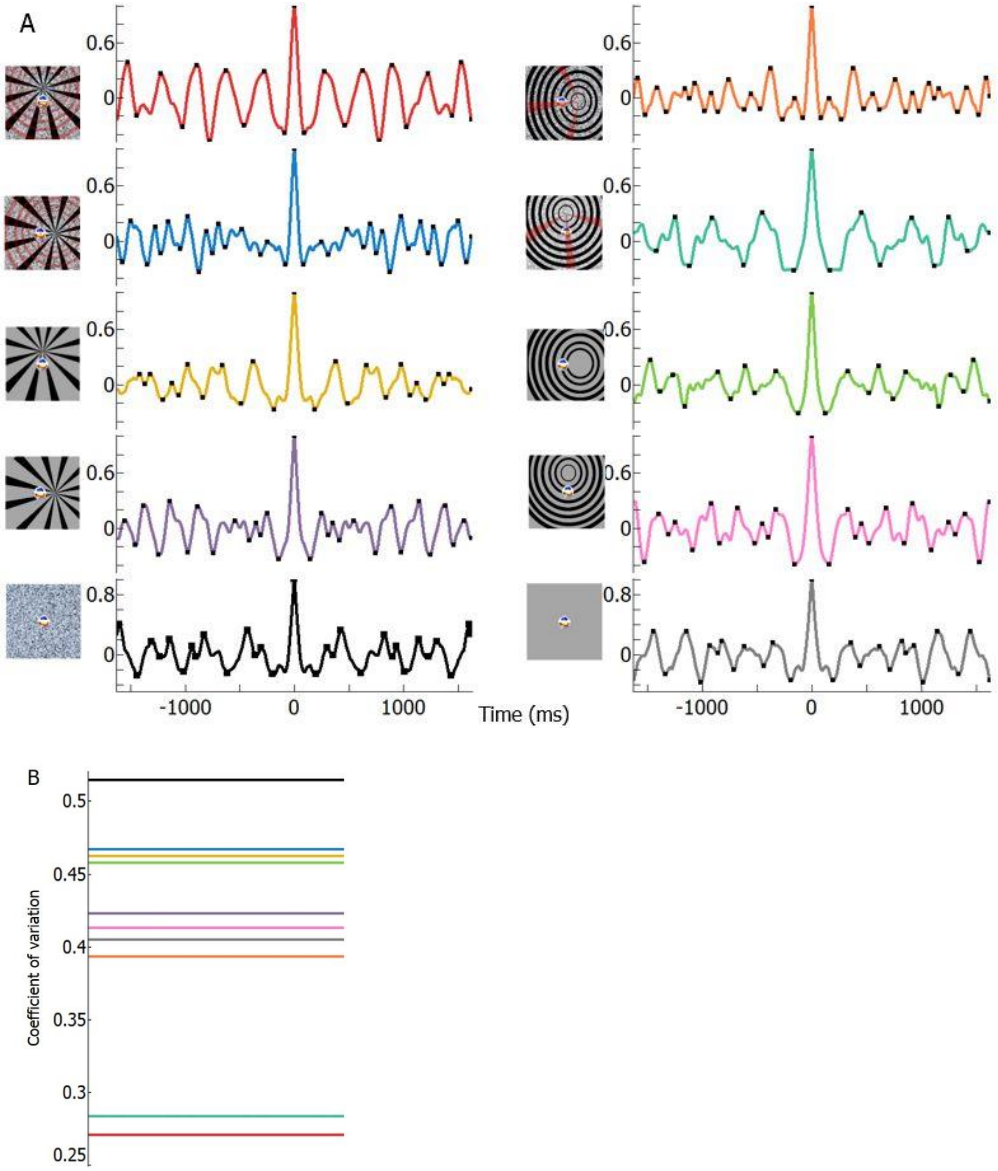

Figure.10.7: ***Periodic oscillations of the membrane potential trials average only appear when the predicted induced pulsating circles are parallel to the cell's preferred orientation.*** *Same cell as in figure 10.6, n=13 repetitions. The normalized autocorrelation of the trials average PSTW is represented for all conditions. Oscillations matching the perceived dynamic of the induced percept of pulsating circles are only found in our condition of interest when the predicted wavefront of the percept is locally parallel to the preferred orientation axis of the cell (upper left condition in red). On the other hand, no such phased locked oscillations resembling a sinusoid of a single frequency are found in other conditions, including our other condition of interest where induced rotating fan shapes are locally parallel to the cell's preferred orientation (upper right condition in orange).*

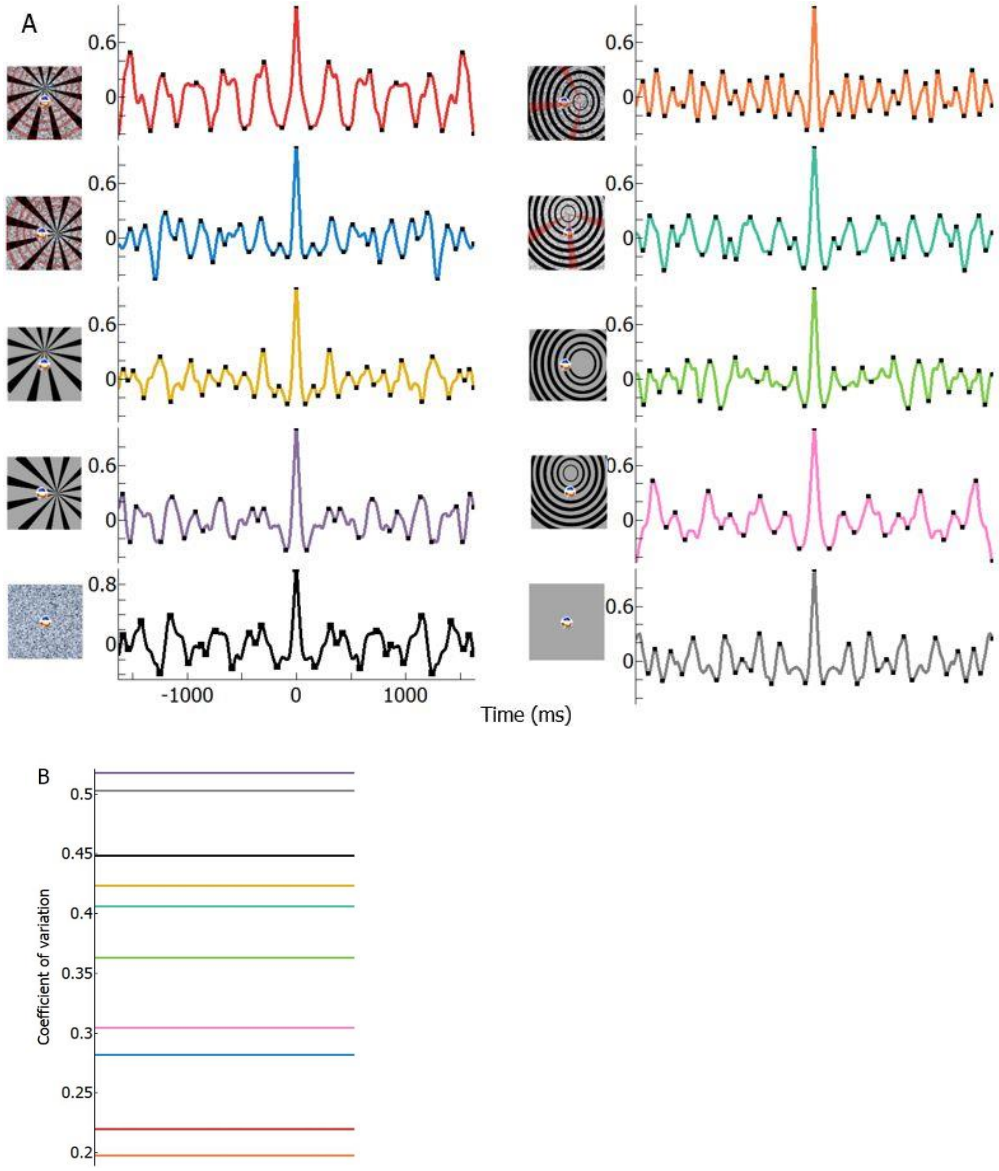

Figure.10.8: ***Periodic oscillations of the visual ECoG trials average only appear when predicted induced pulsating circles are parallel to the cell's preferred orientation.*** *Same Visual ECoG as in figure 10.6, n=13 repetitions. Same convention as in figure 10.7. The normalized autocorrelation of the trials average PSTW is represented for all conditions. Oscillations matching the perceived dynamic of the induced percept of pulsating circles are only found in our condition of interest when the wavefront of the percept is locally parallel to the preferred orientation axis of the cell (upper left condition in red). However, the autocorrelation of that condition has a slightly smaller amplitude than for the Vm as peaks are not as neat and sometimes present several lobes. Similarly, as for the Vm, no such phased locked oscillations resembling a sinusoid close to a single frequency are found in other conditions, excepted for our second condition of interest in orange where predicted induced rotating fan shape are parallel to the cell's preferred orientation. The ACF correlation coefficients of that condition are however lower than for our first condition of interest in red, whose CV is lower than all conditions except the orange one (panel B). Note that we do not retrieve the low CV value obtained in the Vm for the dark green condition.*

Logically, we should retrieve in the time-frequency analysis of the average PSTW of our condition of interest a dominant bandwidth of 3Hz spreading over the entire time course of the average PSTW and synchronized on the onset of the stimulation both at the Vm and ECoG level. This is indeed what we find (Figure 10.9). At the Vm level, 3Hz oscillations are already present during the pre-stimulus first period of 0-500 ms but with a much smaller amplitude. We see that 250 ms after stimulus onset (at t=500 ms), the 3Hz bandwidth amplitude progressively increases and is sustained for almost all the stimulus duration as it progressively decreases after 3000 ms. The visual ECoG also displays progressively increasing 3 Hz oscillations starting 250 ms after stimulus onset. It reaches its maximal amplitude faster than the VM and is sustained until the end of the stimulus, although its amplitude also decreases. It seems that 3Hz oscillations captured in the ACF of the average PSTW indeed correspond to a sustained phenomenon, which is in accordance with our experimental expectation that 3Hz oscillations matching the perceived dynamic of pulsating circles is sufficiently stable over time to be detected at the Vm and ECoG level. However, those sustained oscillations are not maintained throughout the overall time course of stimulation and are non-stationary as their amplitude varies over time but the duration where maximal amplitude is found (between 1 and 1.3 seconds) is largely sufficient to account for a possible correlate of the expected percept. In addition, we must precise that the duration of the transient response found at 7-8 Hz for the Vm and 5.5-8Hz for the visual ECoG is superior to our previous analysis (500-750 ms). This temporal spread of the transient response duration estimation results from a loss of temporal resolution by using Morlet wavelets when compared to classical Gabor decomposition and applies to all frequencies.

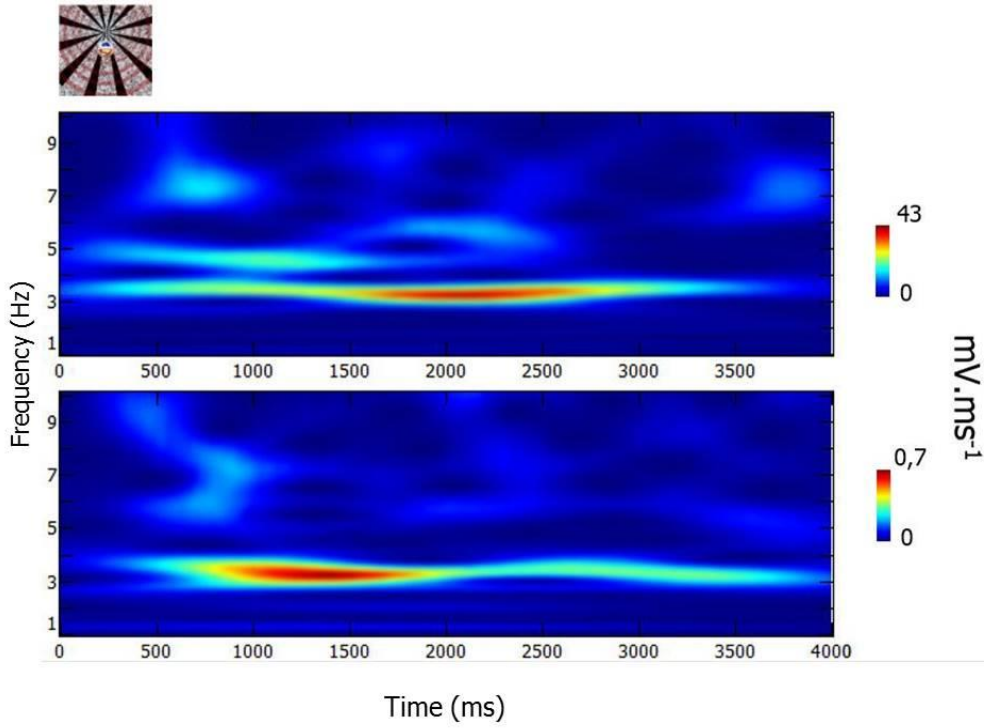

Figure.10.9: ***Sustained oscillations are non-stationary.*** *Same recordings as in figure 10.6-10.8, n=13 repetitions. Top: Vm; bottom: visual ECoG. The average PSTW was convolved with a bank of Morlet wavelet from 1 to 10 Hz. For both recordings, 3 Hz oscillations dominates and progressively gains in amplitude slightly after stimulus onset (about 750 ms). Vm reaches its maximal amplitude at t = 2125 ms while the strongest oscillations are sustained from 1500 to 2750 ms. Visual ECoG reaches its maximal amplitude faster at t = 1420 ms and strongest oscillations are maintained from 800 to 1900 ms.*

II-4.4 Comparison between the Power spectral content of stimulus locked and stimulus-induced response components

From the temporal analysis provided by the average CCF and ACF (induced oscillations), we saw that 3 Hz oscillations are not sustained during the time course of single trials as almost no single trial resemble itself, resulting in a relatively flat profile during the averaging process of their individual ACF. We posited earlier that 3Hz oscillations are not present during the overall time course of single trials but that when they appear, it would be at key locations in time that are sensibly the same across trials, dominated by the noise otherwise. This would explain why we only

retrieve sustained oscillations locked to the stimulus onset after the averaging process of individual trials in the average PSTW. This is a strong hypothesis as if it is real; it means that the visual stimulus generates a stimulus-locked 3 Hz oscillatory pattern on which on certain cycles summation (but not all of them) the local characteristics of the noise stimulus amplify the signal via stochastic resonance. This is not surprising and expected, since we used a different noise in between each trial. Therefore, in between trials, even though the overall spatio-temporal statistics of the noise are preserved, the luminance of the noise locally varies, giving birth from time to time to shapeless dark spots in the opening encompassing the subthreshold depolarizing field, which prevents filling in phenomena of the surrounding propagating wave of activity.

To our opinion, the use of different noise between trials allowed to eliminate the spatio-temporal characteristics specific of each particular noise sequence in order to reveal the subjacent hidden dynamic of propagating waves of activity characteristic of the 3 Hz rezoning frequency of V1. We believe that this dynamic reflects the refractory period of neural stripes formation in V1. As detailed in our model (for details, see Chapter Part II Working hypothesis), when a fan shapes inducer is presented in combination with noise, the first stripe of activity to form is the closest to the area centralis, where horizontal connections have a smaller distance to cover. This first stripe of activity, corresponding to an hemi circle then propagates towards the periphery (pulsating circles) under the continuous global excitation provided by the noise stimulus. This forms an excitatory wavefront followed by a neuronal depression, an idea already introduced by Wilkinson et al., (2004) in the movement of fortification arcs hallucinations in humans. To us, the 3Hz dynamic that we observed in our preliminary psychophysical observations and retrieved here at the neuronal level reflects the formation of other stripes of activity that emerge after sufficient time when the refractory period of the depression has passed. We believe that this 3 Hz dynamic starts at the stimulus onset and corresponds to a stimulus-locked clock that generates a periodic input pattern to the Vm of our single cells and ECoG population on which the noise stimulus intermittently produces a facilitatory effect. One may consider that this would only be plausible if the same stimulus-locked frozen noise pattern stimulus was added at the same phase for each trial but this is unlikely as we would need a single noise sequence that facilitate filling-in phenomena at each cycle summation of the system's clock. However, by definition, during a noise sequence, there is no periodicity as this latter constantly evolves. We believe that only the use of a different noise stimulus between trials provides enough richness to intermittently facilitate the intrinsic 3 Hz clock of the V1 network by providing more and more temporal windows where the local characteristics of the noise in the opening allows filling-in phenomena at the level of a single cell. In addition, because of this richness where no single noise sequence is similar, the spatio temporal variability of the different noise sequences used in between trials and locally detected by our sensor would cancel each other in the averaging process, both in temporal and frequency domains. According to our hypothesis, this would allow to locally extract the only temporal constant, the dynamic of the V1 clock.

If our hypothesis is true, we should observe three things. First, we should retrieve in the frequency domain, as Tallon-Baudry and Bertrand (Figure 10.3), 3 Hz induced oscillations in single trials by estimating the frequency spectrum of each trial before averaging them. Those 3 Hz induced

oscillations could be stronger than for other conditions than the one of interest but not necessarily as what matters for each single condition is the relative dispersion of spectral oscillations. This means that a single condition could have a stronger power in the 3-4 Hz bandwidth than our condition of interest, but it should show other frequency peaks that reduce the relative power spectral density in the 3 Hz frequency when compared to our condition of interest. This would result during the summation of the averaging process in a larger heterogeneity of frequency distribution over time, explaining why other conditions do not display an ACF of the PSTW oscillating at a single frequency. Second, for our condition of interest where induced pulsating circles have a predicted wavefront locally parallel to the cell's preferred orientation, we should observe that the power of the average cross spectrum between each pair of trial is larger at 3 Hz than for any other frequency and control conditions. Otherwise it would mean that one or several other frequencies are shared between each pair of trials in a proportion superior to the single dominant frequency that we retrieve in the ACF of the average PSTW for our condition of interest. Here, the power shared between each pair of trials in our interest condition should be stronger for 3 Hz than other conditions. This leads us to our key requirement: if the noise dominates the signal in single trials but is unspecific, then the power of the average cross spectrum would extract the in-phase or close to in-phase oscillations corresponding to the signal while cancelling out the noise and the argument of the average cross spectrum should show a relative reduction of the temporal jitter for 3 Hz oscillations in our condition of interest across trials, tending towards 0. This is a necessary condition to obtain the stimulus-locked oscillatory profile that we obtained in the average PSTW. In the frequency domain, this temporal jitter is measured for each frequency as the phase between two signals, which corresponds to the argument between two vectors in the complex plane. The argument of the average cross spectrum should tend towards 0 in the the average cross spectrum of our interest condition for 3Hz oscillations, indicating the phase-locked relationship of the signal's oscillations. This reduction in the temporal jitter for the 3-4 Hz bin does not necessarily need to be lower than for all frequencies but need to be low in the 3-4 Hz bandwidth.

Now that we set in place the combination of requirements that we should retrieve to explain the ACF profile of both induced and stimulus-locked oscillations, to test those requirements, we abstracted ourselves from the temporal domain and skipped to the frequency one. We estimated in a first time the frequency spectrum of the average PSTW (stimulus locked component) as well as the spectral content of each single trial before averaging them (stimulus induced component) by performing a Discrete Fourier Transform (DFT) on those signals. Because the duration of the tested conditions was different between cells as we refined the protocol parameters exploration (3500 ms after the pre-stimulus duration of 500 ms in some cells vs 4000 ms in others), we resampled our spectral analysis. During that step, we largely oversampled our spectral analysis by using a 0.01 Hz new dx step in order to really capture with fidelity the initial spectral distribution because resampling methods use a linear interpolation on the initial spectrum, which often resulted in a significant reduction of some peaks when we used a larger dx step. We first tested if our power spectrums had a normal distribution and rejected that hypothesis (D'Agostino's test, (D'Agostino., 1970); $p < alpha = 0.01$). Then, in order to compare our different conditions between them we sliced

our spectral distributions in 1 Hz bandwidth and performed Wilcoxon paired tests on the membrane potential (Vm) (Figure 10.11, 10.12 and on the visual ECoG recordings (Figure 10.13 and 10.14).

By performing pure spectral analysis, we indeed did retrieve a 3-4 Hz dominant induced oscillation in the average of the individual trials power spectra both at the Vm and visual ECoG level (Figure 10.10, upper panel). Moreover, that 3-4 Hz bandwidth dominance for our condition of interest is actually significantly higher than for all conditions but one for the Vm (Figure 10.11) and larger than 7 conditions out of 9 at the visual ECoG level (Figure 10.13). As expected from stimulus-locked ACF measurements, for our condition of interest in red, the Vm power energy of the stimulus-locked response (average PSTW) in the 3-4 Hz bandwidth (Figure 10.10, lower panel) is significantly higher than 8 conditions out of 9 while no different than one (Figure 10.12). At the visual ECoG level, in the same frequency bin, our condition of interest where induced pulsating circles have a predicted wavefront locally parallel to the cell's preferred orientation is significantly larger to 7 out of 9 conditions and no different than 2 other conditions (Figure 10.14). However, we do note that for our EcoG recordings of our interest condition, the relative difference between the average power spectrum of the trials and the power spectrum of the average in the 3-4 Hz frequency bin is less clear than at the Vm level when compared to control conditions. On the other hand, it seems that the noise cancels out to reveal the signal in the power spectrum of the trials average, by opposition to the average power spectrum of each trial where the noise dominates and is sensibly the same in between conditions.

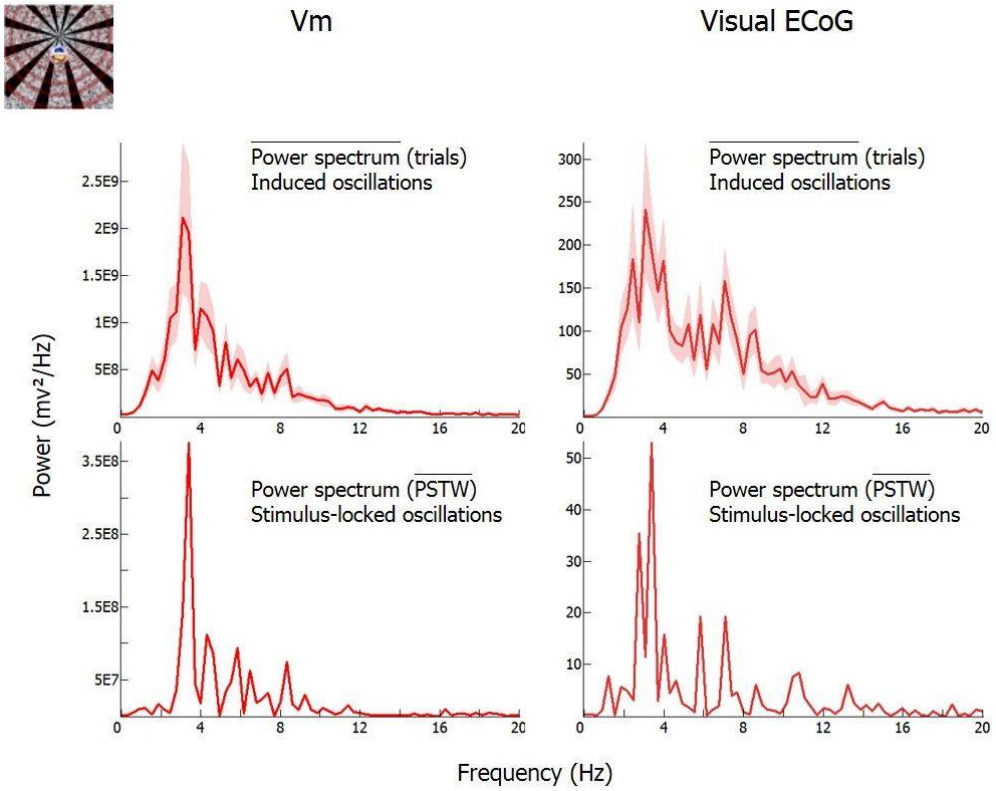

Figure.10.10: ***Single cell membrane potential and visual ECoG spectral analysis of the trials and average PSTW.*** *Same recordings than in figure 10.6 – 10.9 with 13 repetitions. Those recordings were obtained during the presentation of one of our interest condition, when fan shapes geometric inducers are presented in combination with $1/f^{\alpha}$ spatiotemporally filtered noise in the surround of the receptive field, inducing hallucinatory-like pulsating circles whose predicted wavefront is parallel to the preferred orientation axis of the cell. Analysis was performed from t = 750 ms up to the end of the recordings to eliminate transient response linked to the sudden change of the surround content at t = 500 ms. The average of the power spectrum obtained by summing all individual trial spectrum together is represented in the upper panel (Vm: left, ECoG: right). Bold red traces indicate the mean and shaded red areas indicate +/- SEM. The lower panel indicates the power spectral distribution of the PSTW average. Those latter Spectrums respectively peak at 3.25 and 3.35 Hz.*

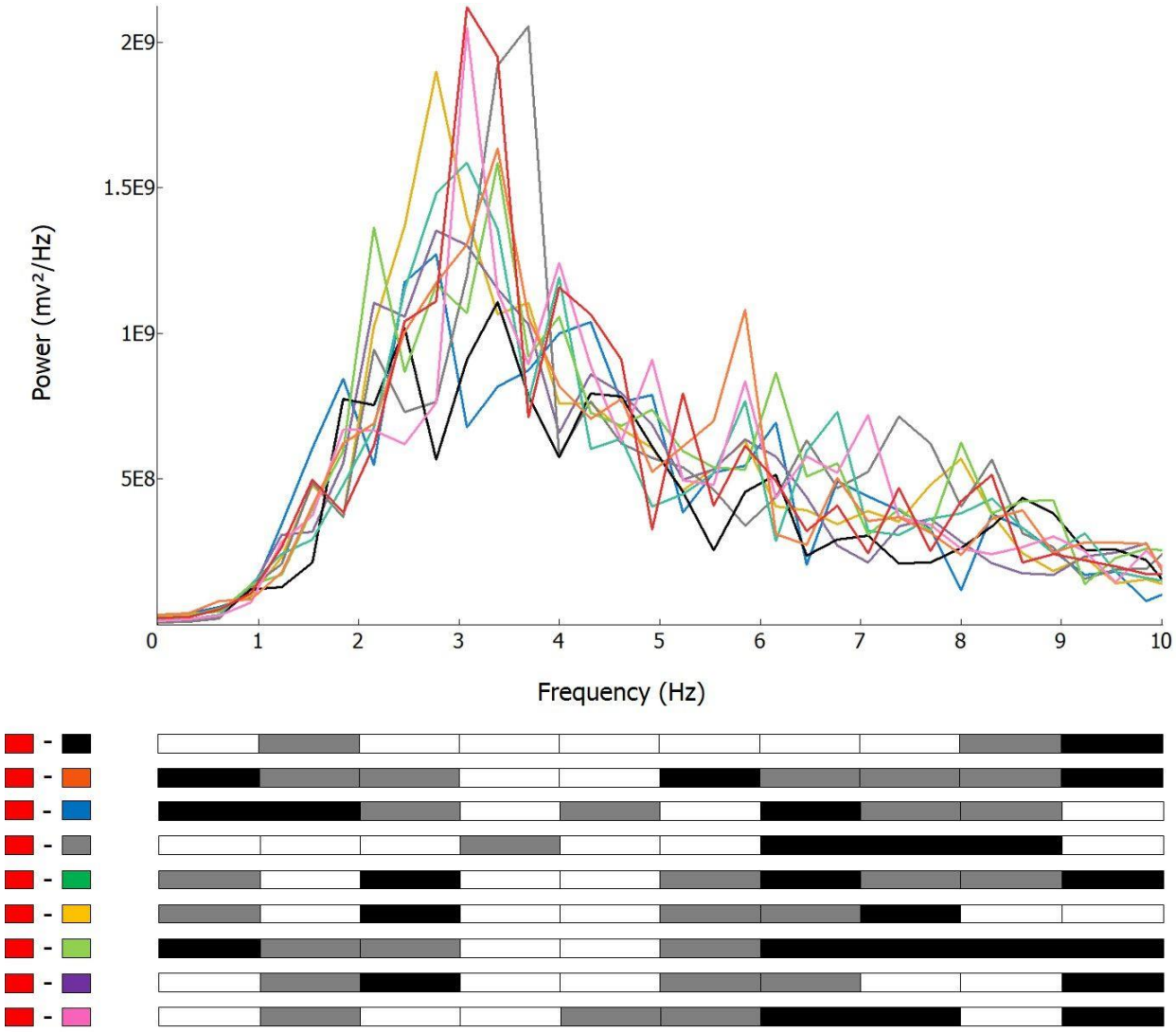

Figure.10.11: ***Comparison of stimulus-induced oscillatory response component across conditions.*** *The power spectrum of each trial of the same cell Vm than figure 10.10 was calculated and averaged for each condition and is represented between 0 and 10 Hz where more than 95% of the power is concentrated for clarity purpose. Each box plot below expresses the result of a Wilcoxon paired test when comparing the condition of interest (in red) to each other condition for 1Hz frequency bins. The color code for "red" minus "condition X" is white: "red" significantly higher than X; grey: "red" not significantly different than "X"; black: "red" significantly lower than "X", with p<0.01).*

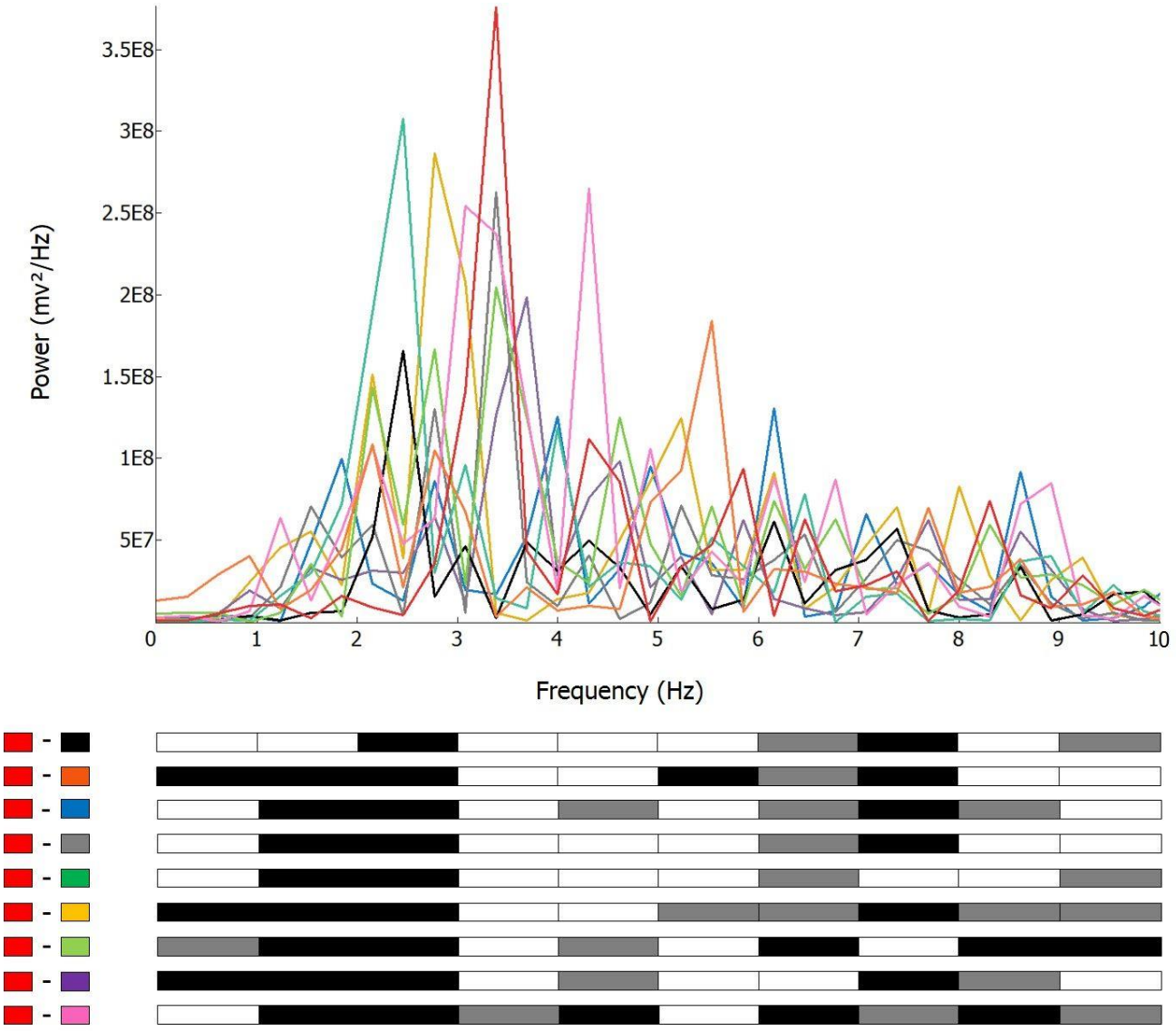

Figure.10.12: ***Comparison between a single cell membrane potential power spectrum of the average PSTW across conditions.*** *Same cell as in figure 10.6 - 10.11. The power spectrum of the average PSTW was calculated for each condition and is represented here between 0 and 10 Hz. As in figure 10.11, each box plot represents the result of a paired Wilcoxon test between our condition of interest in red and each other condition for 1Hz bins with the same color code: white: "red" significantly higher than X; grey: "red" not significantly different than "X"; black: "red" significantly lower than "X", with p<0.01).*

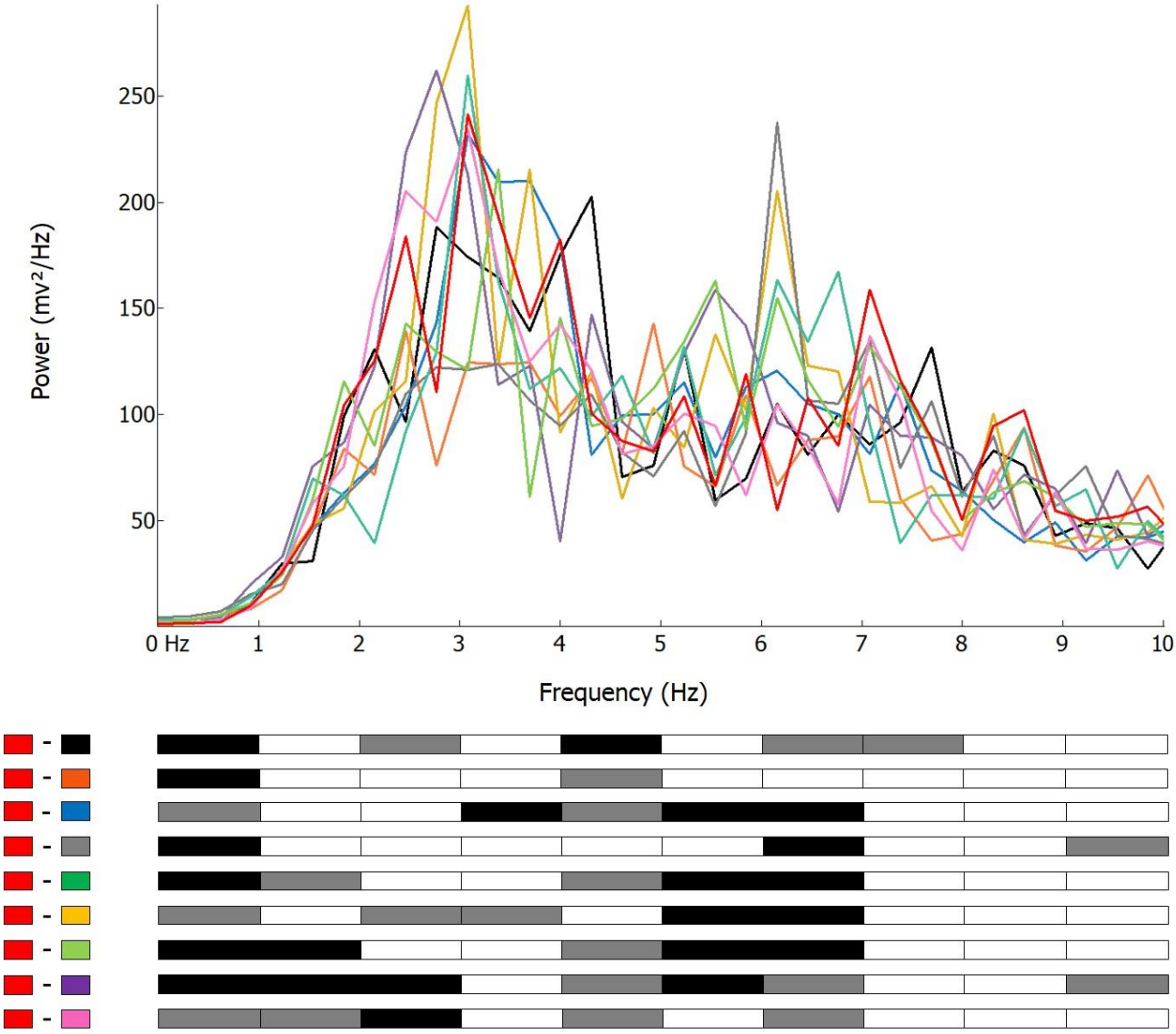

Figure.10.13: ***Comparison between the visual ECoG average power spectrum of each trial PSTW across conditions.*** *Same visual ECoG and convention as in figure 10.11 – 10.12, but for the average power spectrum of each trial of the Visual ECoG recordings. Each box below abscissa plot represents the result of a paired Wilcoxon test between our condition of interest in red and each other condition for 1Hz bins with the same color code as in figure 10.11 and 10.12: white: "red" significantly higher than X; grey: "red" not significantly different than "X"; black: "red" significantly lower than "X", with p<0.01).*

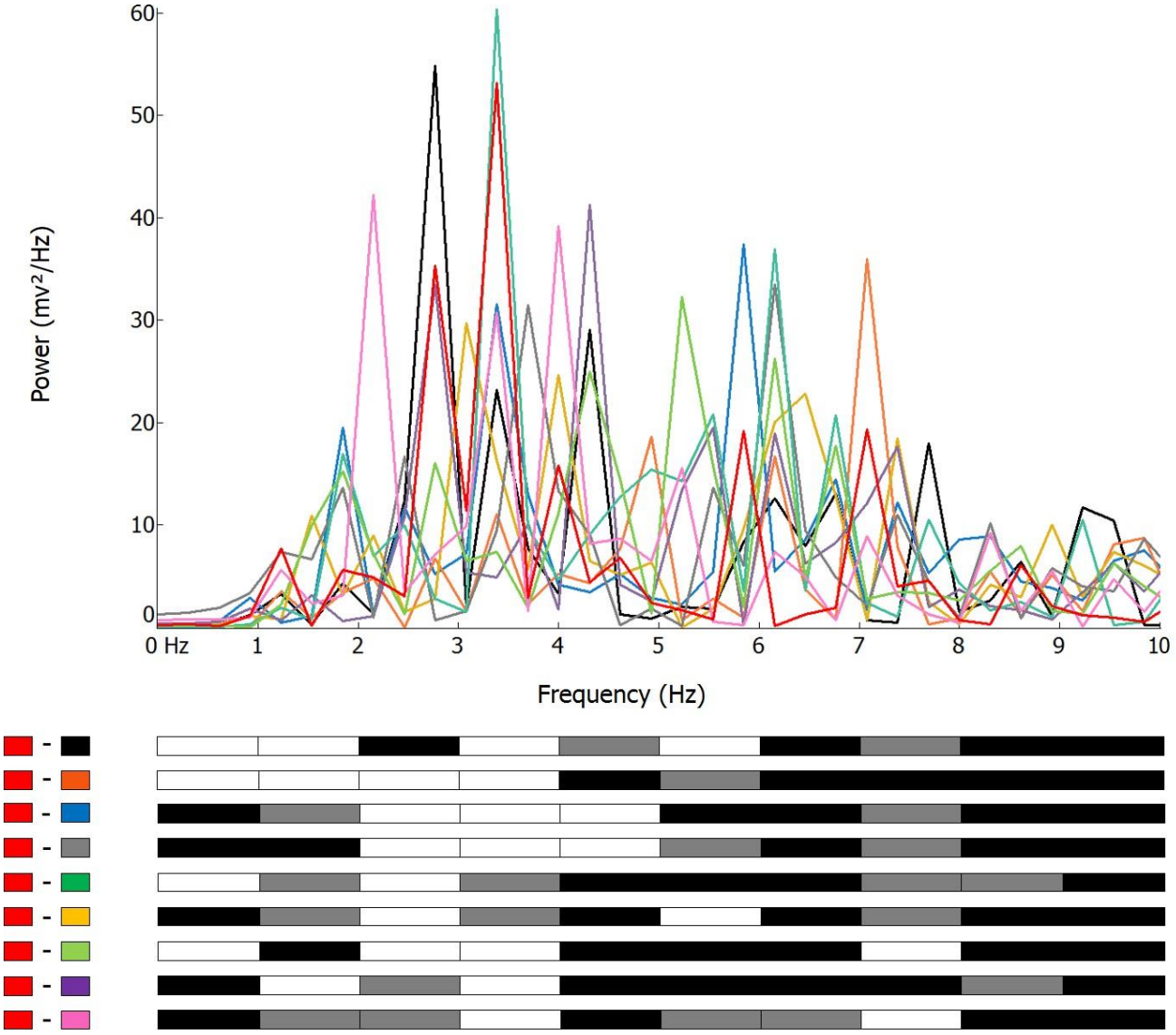

Figure.10.14: ***Comparison between the visual ECoG power spectrum of the average PSTW across conditions.*** *Same visual ECoG as in figure 10.6 – 10.10. The power spectrum of the average PSTW of the visual ECoG was calculated for each condition and is represented here between 0 and 10 Hz. As in figure 10.11 – 10.13, each box plot represents the result of a paired Wilcoxon test between our condition of interest in red and each other condition for 1Hz bins with the same color code: white: "red" significantly higher than X; grey: "red" not significantly different than "X"; black: "red" significantly lower than "X", with p<0.01).*

II-4.4.1 Average cross spectrum between each pair of trials and dephasing

We pursued the exploration of our condition of interest where our prediction would be that induced pulsating circles propagate locally tangentially to the cell's preferred orientation resulting in the trials average in a dynamic that we believe to reflect V1's intrinsic clock. We already determined that 3-4 Hz oscillations are present in the individual trials of our condition of interest for both Vm and visual ECoG, and in a larger proportion than a vast majority of control conditions (Figure 10.10, upper panel, 10.11, 10.13). We already provided an estimation of the variability by presenting the SEM of our spectral analysis in figure 10.10. However, we still haven't showed that for our condition of interest the actual signal, dominated by the noise in individual trials is actually extracted during the summation process of the averaging because of its phase-locked nature, by opposition to the noise that has no unique spectral content nor phase relationship and therefore cancel out. To that end, we calculated the average Cross Spectrum Density (CSD) between each pair of trials for each frequency in order to test if our condition of interest's 3-4 Hz oscillatory signal is larger in this bandwidth than in any other frequency bin (relative power spectral density) and control conditions. For real temporal series

$x(t)$, $y(t)$, the cross spectral density between those signals is given by

$A_k = A_{-k}$ and $B_k = -B_{-k}$ so that

$Fx(k)\ Fy^*(k) = Fx(-k)\ Fy^*(-k)$ so that

$$Fx(k)\ Fy^*(k) = 0.25\ \{(Axk\ Ayk + Bxk\ Byk + i(Axk\ Byk - Ayk\ Bxk)\}$$

Where $Fx(k)$ denotes the Discrete Fourier Transform of x at wave k and $Fy^*(k)$ the conjugate of the DFT of y and $Fx(k)\ Fy^*(k)$ is the cross-spectrum of x and y for wave k where the real part (the cospectrum) = $x'y'$ is the in-phase signal and the quadrature spectrum (the complex part) is the out of phase signal.

That calculus was done for each pair of trials and then averaged. We then took the squared modulus of the resulting complex vector as the power of in-phase oscillations shared on average between each pair of trials. As stated above, individual trials might present oscillations at key locations in time but not during the overall time course of the visual stimulation, drown into the noise component. If our hypothesis is true, in order to obtain the high power spectral density found in the stimulus-locked analysis of the average PSTW for our condition of interest, both in the temporal (ACF, Figure 10.7, 10.8) and in the frequency domain (Figure 10.10, lower panel, 10.12,

10.14), we should logically find a reduction of the temporal jitter between trials for that frequency. In the frequency domain, this temporal jitter reduction would translate itself under the form of a phase of the average cross spectrum tending towards 0 for the 3-4 Hz frequency bandwidth of our condition of interest. The dephasing of in-phase oscillations was measured as the argument of the average cross-spectrum between each pair of trials in the complex plane. This latter was distributed between +/- π. For visual purpose representation, we normalized the average dephasing between 0 and 1, 1 representing maximal dephasing (+/- π) and superimposed it over the average CPSD for our condition of interest (Figure 10.15).

In the same recordings than the ones presented above, for our condition of interest where induced pulsating circles had a predicted wavefront locally parallel to the cell's preferred orientation, we found that the power of the average CSD between each pair of Vm trials peaked at 3.4 Hz and that the average dephasing at that frequency indeed tended towards 0 since it was equal to 17 % of the maximal dephasing (between 0 and 1, +/- π), (Figure 10.15, left panel). For the visual ECoG, it peaked at the same frequency although 3-4 Hz oscillations were slightly more out of phase as the average dephasing was equal to 27 % of the maximal dephasing (Figure 10.15, right panel). We then compared the average CPSD between our different conditions. In the membrane potential of the impaled cell, we indeed found that the power of the average CSD is larger in the 3-4 Hz frequency bin than in any other frequency bandwidth and second, that it is also larger than for all other conditions in the same bin of interest. Moreover, this it is the only frequency bandwidth for which it is the case (Figure 10.16). However, at the visual ECoG level, the average CSD of our interest condition was only significantly larger than 7 out of 9 conditions, smaller than one and no different from another (Figure 10.17). The profile that we found in the ACF of the average PSTW results from complex continuous interactions between the power shared between each pair of trials and their relatively weak dephasing. For instance, for the visual ECoG in Figure 10.17, the condition in dark green where induced rotating fan shapes have a predicted wavefront locally orthogonal to the cell's preferred orientation presents a larger average CSD than our condition of interest in the 3-4 Hz bandwidth. We already found that this condition indeed displays power in that frequency bandwidth both in our spectral analysis of induced oscillations (performed on each trial before averaging, Figure 10.13) and in phase locked oscillations (performed on the average PSTW, Figure 10.14). If we look closely, this condition also presented a dominant oscillation at 3 Hz in the temporal domain as we can see on the ACF of its average PSTW (Figure 10.8, dark green Vs red). However, those oscillations have a larger coefficient of variation and smaller correlation peaks. This is because this condition also displayed a relative decrease in the dephasing of the average cross spectrum for 3-4 Hz oscillations but this decrease in dephasing of the average also extended to other frequencies that, although weaker in power magnitude, contributed to the distortion of the signal during the averaging process. This led to a greater high frequency content distribution than for our condition of interest in the ACF of the average PSTW (stimulus-locked oscillations, Figure 10.8). The extraction of single oscillatory components therefore results from a complex balance between the relative power magnitude of distinct frequencies (spectral density) and their corresponding dephasing throughout trials.

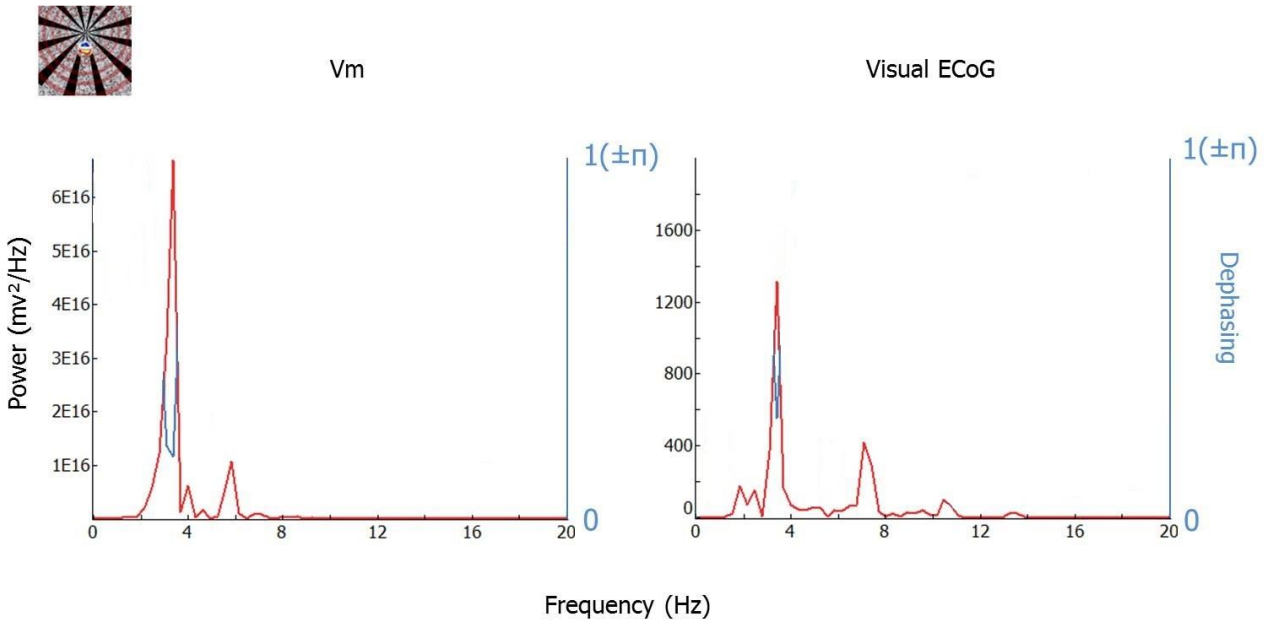

Figure.10.15: ***Power spectral density of the average cross spectrum between each pair of trials.*** *Same cell and visual ECoG as in figure 10.6 – figure 10.14 for our interest condition, n=13 repetition; 78 combinations. Left: membrane potential analysis, Right: Visual ECoG. Both the membrane potential and visual ECoG peak at 3.38Hz. The dephasing of the Vm average CSD is lower than for the visual ECoG, reaching 17% of the maximal dephasing set at 1 (+/- π) against 27 % for the Visual ECoG.*

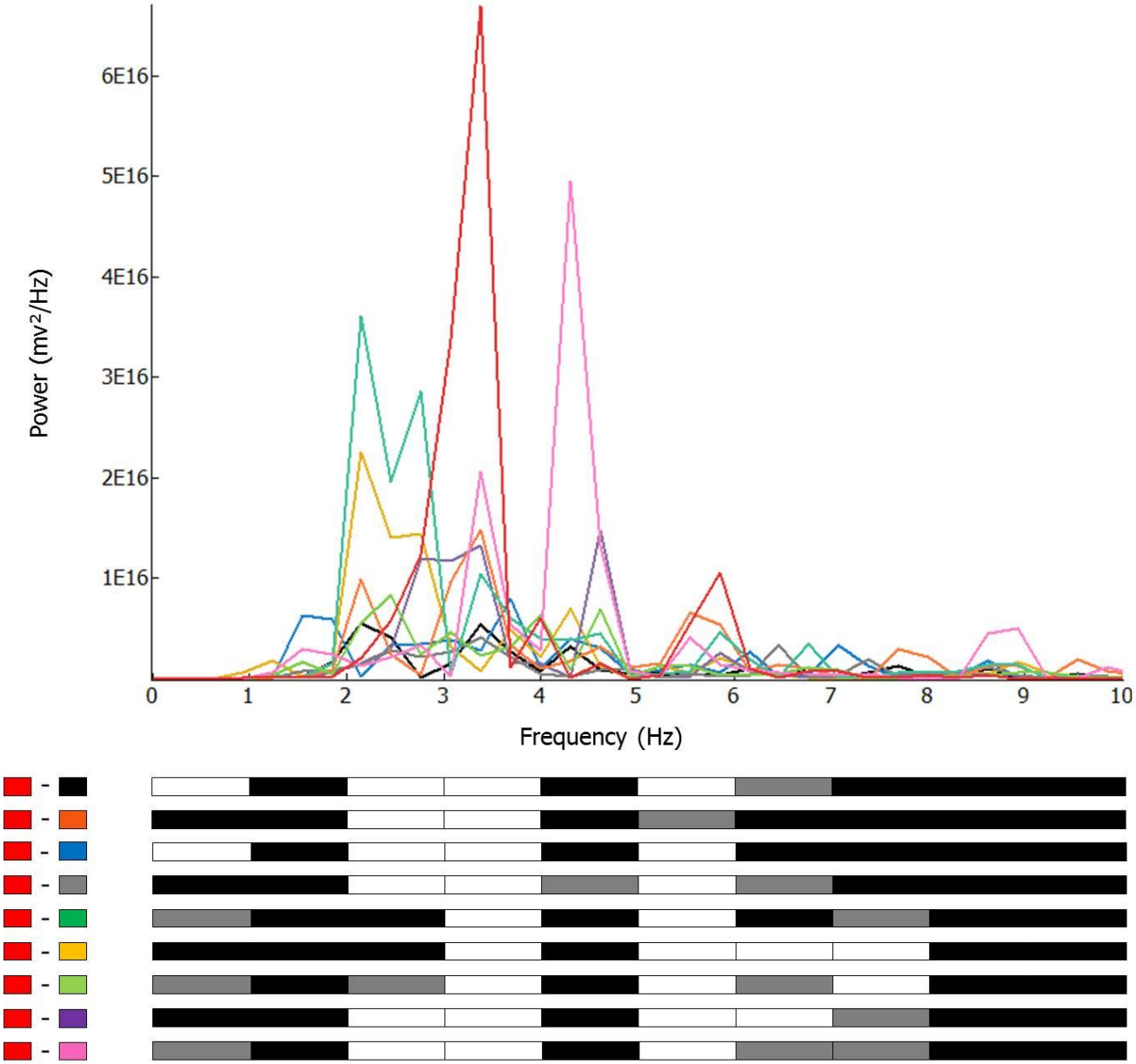

Figure.10.16: ***Comparison between the average CSD of the membrane potential across conditions.*** *Same cell as in figure 10.3 –10.11, n = 13 repetitions. The cross spectrum of the membrane potential was calculated between each pair of trials, averaged and its squared modulus is represented here for each condition between 0 and 10 Hz. As in figure 10.4- 10.7, Box plots: paired Wilcoxon test, color code: white: "red" significantly higher than "X"; grey: "red" not significantly different than "X"; black: "red" significantly lower than "X", with p<0.01).*

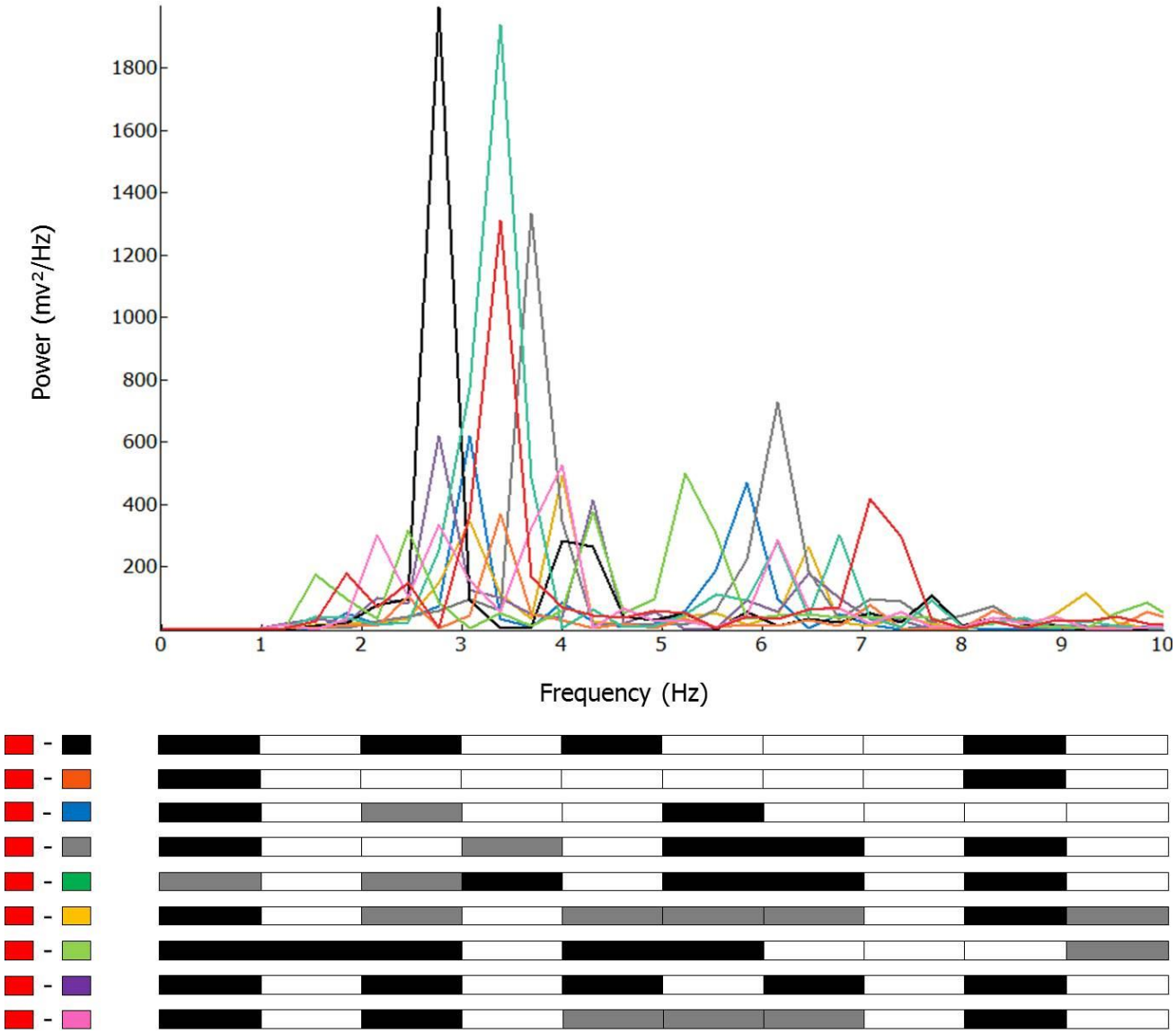

Figure.10.17: ***Comparison between the average CSD of the visual ECoG across conditions.*** *Same Visual ECoG as in figure 10.3 –10.12, n= 13 repetitions. The cross spectrum of the visual ECoG was calculated between each pair of trials, averaged and its squared modulus is represented here for each condition between 0 and 10 Hz. Box plots: paired Wilcoxon test, color code: white: "red" significantly higher than "X"; grey: "red" not significantly different than "X"; black: "red" significantly lower than "X", with p<0.01).*

We posited earlier that the 3-4 Hz oscillations that we observed in the stimulus-locked ACF of our condition of interest trials average correspond to a stimulus-locked clock intrinsic to V1 that generates a periodic input pattern to the Vm and ECoG of our recordings on which the use of a different noise between each trial intermittently produces a facilitatory effect. Those intermittent facilitations occur during different time windows across trials, depending on the characteristics of each noise sequence. However, because of the richness of different noise sequences, the noise-related oscillations evoked by each sequence cancel out during the averaging process, allowing us to extract the hidden dynamic of V1's intrinsic clock. That hypothesis explains why we didn't retrieve 3 Hz oscillations during the stimulus-induced summation of each individual trial ACF as individual trials do not resemble themselves over time and averaging individual ACF results in a relatively flat profile. From those observations, we derived expectations that should logically be found. First, from the pure spectral analyses presented above, we did retrieve 3-4 Hz induced oscillations in the individual trials of our condition of interest in a larger proportion than almost all other conditions for the Vm (Figure 10.11) and larger than 7 out of 9 conditions for the ECoG (Figure 10.13). Second, we also found in the average cross spectrum that the 3-4 Hz frequency bandwidth is the one where individual trials of our condition of interest share the more power between each pair of trials and because those oscillations are more-in phase in between each trial than in control conditions. The power of this average cross spectrum is larger in the 3-4 Hz bin of our condition of interest than in all conditions for the Vm (Figure 10.16), and than 7 out of 9 for the visual ECoG (Figure 10.17). This analysis proves that the out-of phase oscillations corresponding to the noise cancelled out during the summation process of the averaging, to the opposite of the in-phase oscillations of our signal in our condition of interest, for which power is maximal and larger than in any other condition and frequency bandwidth in the 3-4 Hz, indicating an in-phase relationship between the signal's oscillation in between trials. Finally, the signal's in-phase 3-4 Hz oscillations of our condition of interest sum up during the averaging process while the noise cancel out and the phase of the average cross spectrum naturally tends towards 0 (Vm: 0.17; ECoG: 0.27) for those oscillations in our condition of interest, indicating that the signal's ocillations are more in phase in between trials than for control conditions (Figure 10.15), only for that bandwidth. To summarize, more 3-4 Hz power in individual trials that dominates other frequencies across trials combined to a relative decrease in temporal jitter under the form of a weaker dephasing for that frequency bin explains the stimulus-locked profile of our interest condition ACF of the average PSTW during the summation process of the averaging. Those summation gives rise to a temporally homogeneous distribution of 3 Hz oscillations over the time course of the average PSTW for both membrane and visual ECoG. If this was artefactual or a random profile only related to noise, we would expect to retrieve the same time-frequency combination in control conditions. This is not the case as, despite a great number of control conditions (8), none of them displays a similar oscillatory profile that not only just emerges in our condition of interest where the predicted wavefront of induced pulsating circles is parallel to the cell's preferred orientation but also happens to match the dynamic of the induced percept of our preliminary psychophysical estimations.

II-4.4.2 Signal, Noise, total signal power and Signal to Noise Ratio evaluation

In view of the similarity between the spectrum of noise and signal, we searched for a more quantitative study of the SNR, which, by definition, should be the measure the most correlated with filling-in phenomenon of the hallucinatory propagating waves of activity. To that end, we performed a time-frequency decomposition from which we determined several time-frequency dependent measures: signal power, noise power, total signal power and Signal to Noise Ratio (SNR). To that end, we used the wavelet decomposition method introduced by Baudot et al., (2013) that is must suited to non-stationary signals than the Fourier transform by taking advantage of the higher frequency resolution of Morlet wavelets while focusing on frequencies ranging from 1 to 10 Hz.

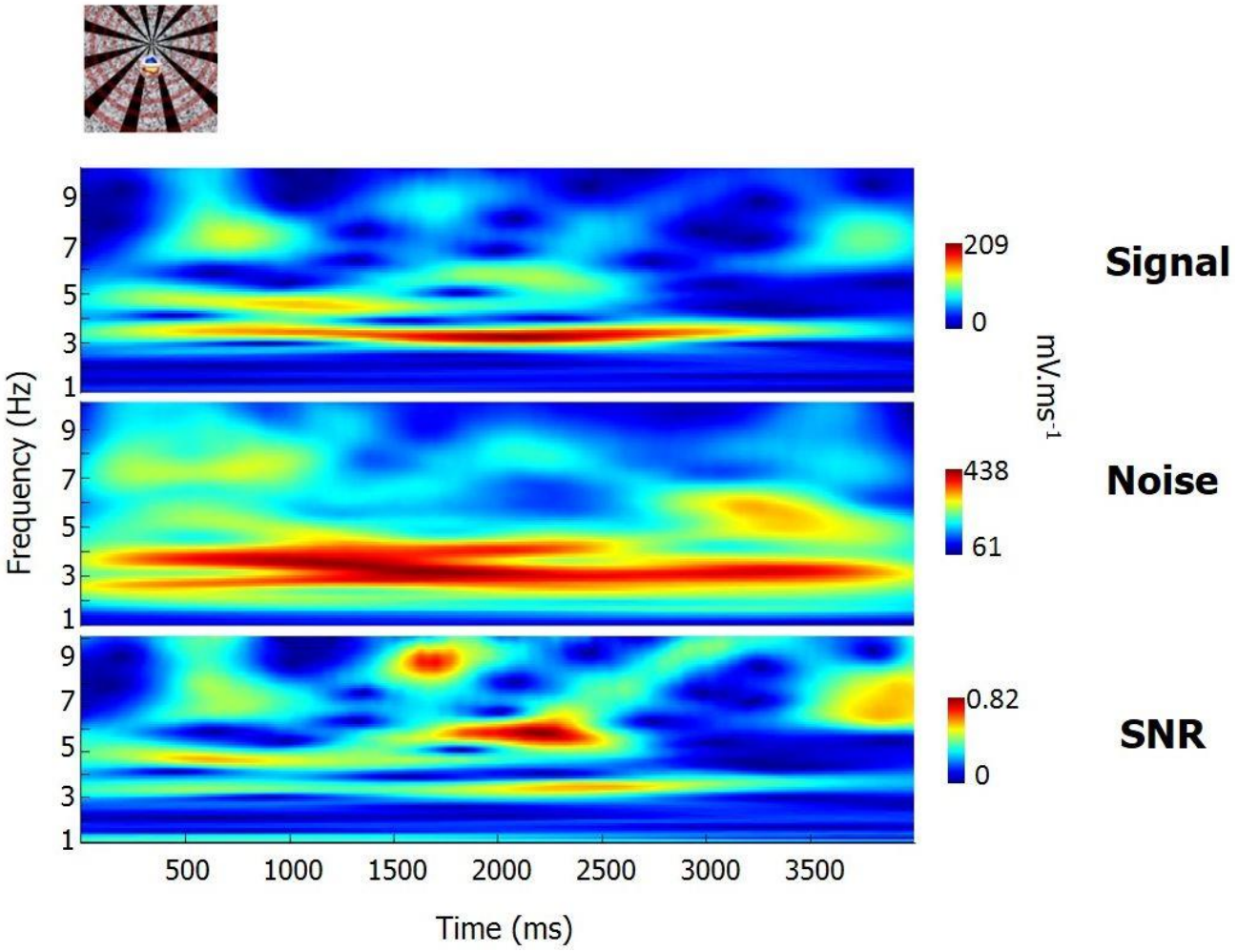

Figure.10.18: ***Intracellular measures of Signal, noise and SNR time-frequency matrices.*** *Same cell as in figure 10.6 –10.17 for our condition of interest. Note that in this figure, results are presented from t0 up to the end of the stimulation, including the 0-500 ms pre-stimulus where only noise is presented in the SDF, surrounded by a uniform level of luminance. In this example, as in the convolution with the average PSTW, Figure 10.9, we retrieve the transient response starting a little*

before 500 ms and ending up after 750 ms in the 6.5-7.5 Hz bandwidth of the signal (first row) and in the SNR (third row). The strongest SNR value is found for 5-6.5 Hz frequency range but the most consistent one over time is found at 3-4 Hz (lower row).

The comparison of Signal, Noise and SNR matrix shows the overlap between the signal spectrum and the noise dominance in the 3 Hz bandwidth. In an unexpected way, SNR reaches its maximum value outside the 3 Hz band, around 5.7 Hz in this example. Note that this increase in SNR does not extend throughout the stimulation presentation but is present for a more restricted window, between 1750 and 2500 ms. This persistency is still long enough to be correlated with the duration of a percept but does not corresponds to our preliminary psychophysical observations nor to the 3Hz dominance observed both in frequency and temporal analysis of our electrophysiological signals. One can only speculate on the origin of this latency improvement of the SNR that is probably specific to each cell. Indeed, using single unit recordings in the anesthetized and paralyzed cat V1, Funke et al., (2007) characterized the SNR of several dozens of cells according to the level of noise that was presented. In their experiments, noise was not of the same kind as ours but consisted in jitter of bars of optimal orientation or brightness modulation where the standard deviation of the jitter covered the overall extent of eye-movements (micro tremors, tremors saccades). Their main findings were that Stochastic Resonance (SR) like phenomena induced by noise (image jitter sigma) that they applied amplified response strength and SNR that were initially weak improved on 85 % of the cells they recorded over a wide range of noise. However, even if SNR improvement was locked on the stimulus onset, latency response improvement varied largely from cell to cell and, interestingly, the noise level range required to reach maximal SNR was also the one inducing the largest inter spike interval distribution (Figure 6B and 7 of their paper).

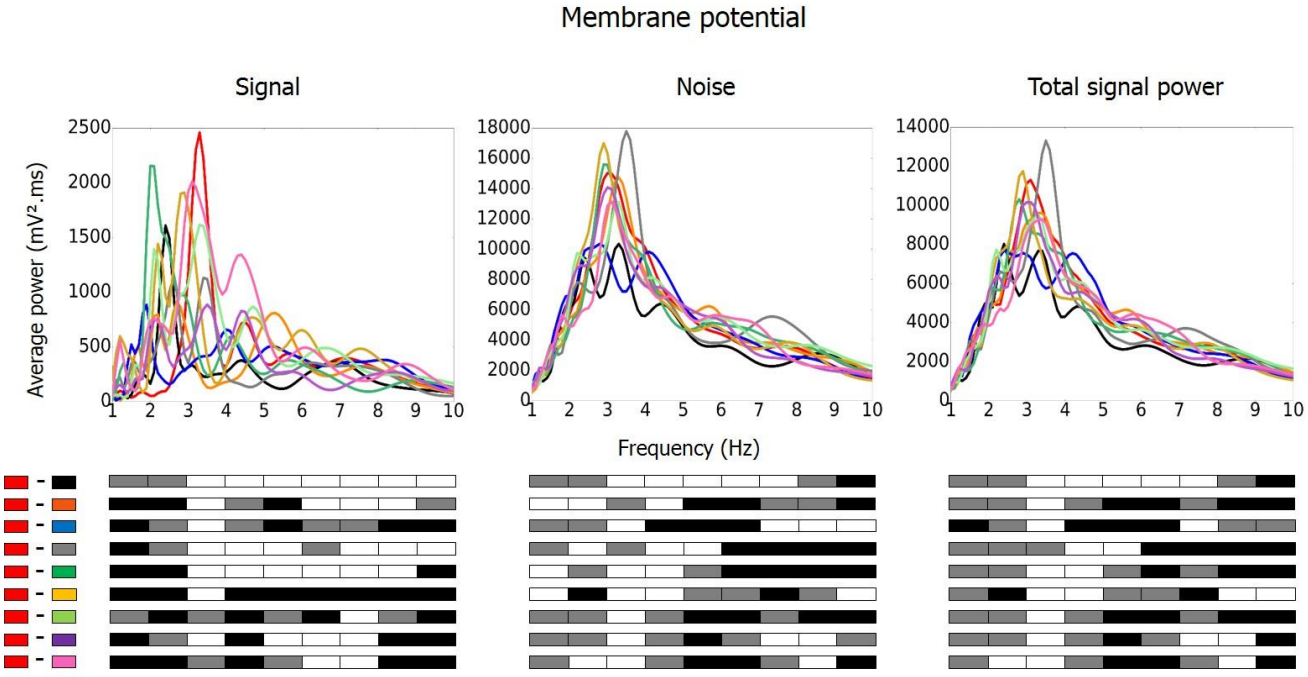

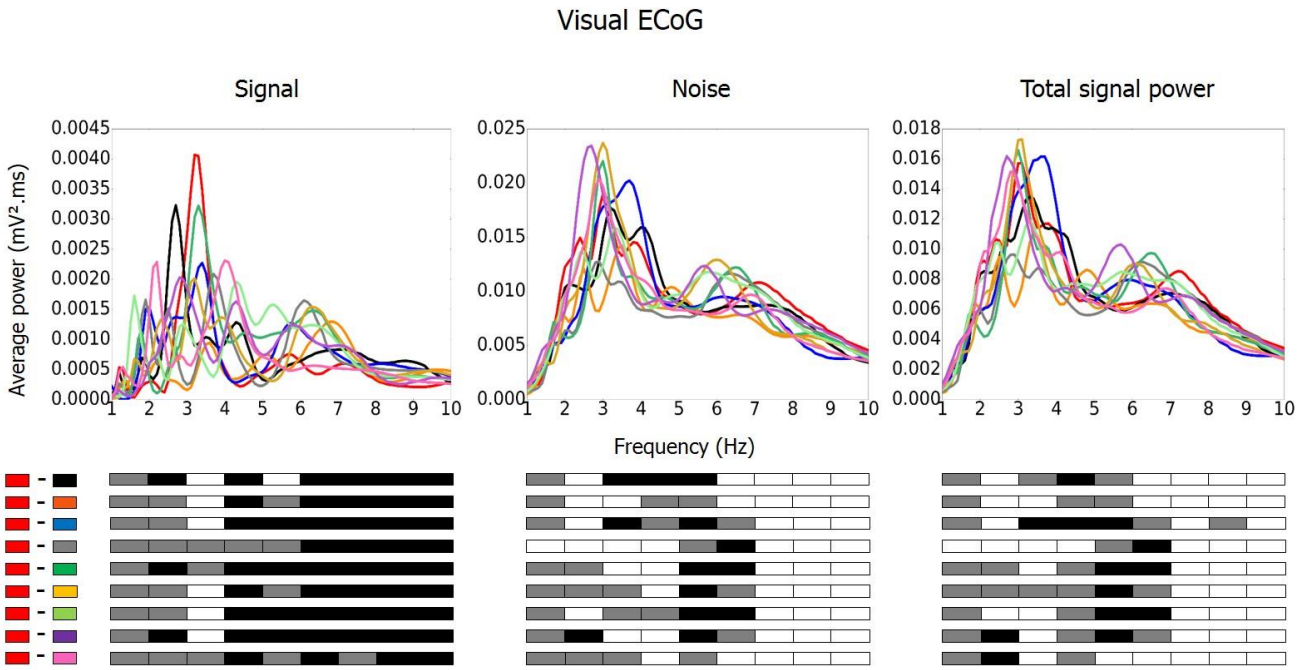

Figure.10.19: ***Average Power spectrum of signal and noise.*** *Same cell and visual ECoG as in figure 10.6-10.18, n = 13 repetitions. Upper part: membrane potential of the cell. Lower part: simultaneously recorded visual ECoG. Left: signal; middle: noise; right: total signal power. The average signal, noise and total power over time were calculated and are represented here for each condition between 1 and 10 Hz. Box plots: paired Wilcoxon test with color code: white: "red" significantly higher than "X"; grey: "red" not significantly different than "X"; black: "red" significantly lower than "X", with p<0.05).*

From figure 10.19, we retrieve at the membrane potential level an increase in the signal for our condition of interest in red as this latter is larger than 7 conditions and no different from 2 others in the 3-4 Hz bin (upper part, left). In accordance with previous analyses, this is the only frequency bandwidth for which it is the case. This signal increase does not seem to come from a reduction of the noise as this latter was also found to surpass 7 out of 9 conditions in the same bandwidth (upper part, middle). That signal increase seems to come from an amplification of the total power that is significantly larger than 8 conditions out of 9 and no different from the blank (upper right part). However, in the blank condition, the noise is more important (although not significantly) than in our condition of interest at 3-4 Hz (grey vs red, upper part, middle), which explains why we retrieve more signal in our interest condition (upper left part).

At the visual ECoG level, the picture seems quite similar as the evaluated signal for our condition of interest significantly prevails over 6 out of 9 conditions and is no different from 3 others (figure 10.19, lower part, left). However, the evaluated noise is "only" greater than 4 conditions out of 9 while no different than 3 and smaller than 2 (lower part, middle). It seems that in the visual ECoG, similarly as in the Vm, the 3-4 Hz signal increase in the test condition also comes from an amplification of the total signal power which dominates 6 conditions out of 9, is no different from 2 and smaller than another (lower part, right). The conditions where total power is either greater or

no different than in our condition of interest for the same frequency bin (black, blue and gold conditions) were among the ones that either displayed an amplification or no difference in the noise level (lower part, middle). That explains why our evaluated signal is more important than in those conditions (lower panel, left).

At the Vm and ECoG level, we can see that the SNR for all conditions is low (inferior to 1, Figure 10.20, top left). This is not surprising, since we used a different noise between all trials. For both Vm and visual ECoG, we are not interested in higher values of both SNR and information rate in the 1-2 Hz frequency bin as those frequencies were the most affected by the 1 Hz cut off frequency of the Bessel high pass filter applied on our traces, which artificially rendered the power content more reliable across trials in those frequencies.

However, the Vm 3-4 Hz SNR of our primary condition dominates 6 controls out of 9, is no different than 2 conditions and lower than the pink one where no percept is induced (Figure 10.20, upper panel, left). However, this latter condition displays several SNR peaks, indicating a more heterogeneous SNR distribution over the frequency domain. As the information rate is function of the squared SNR, we logically found that it was above the same 6 conditions than this latter, no significantly different than 2 other conditions and also surpassed by the pink condition (Figure 10.20, top right).

The 3-4 Hz SNR of the visual ECoG is higher than the Vm one in the red trace, (0.53 vs 0.41) (Figure 10.20, bottom left). This is the highest SNR value in that frequency bin, although it only significantly outmatches four conditions and is no different from 5 others (Figure 10.20 bottom left; Wilcoxon paired test, $p < 0.05$). Similarly, the information rate is the highest for our interest condition in the 3-4 Hz frequency bin, reaching a value of 369 bits/s against 230 bits/s for the Vm (Figure 10.20, upper right vs bottom right).

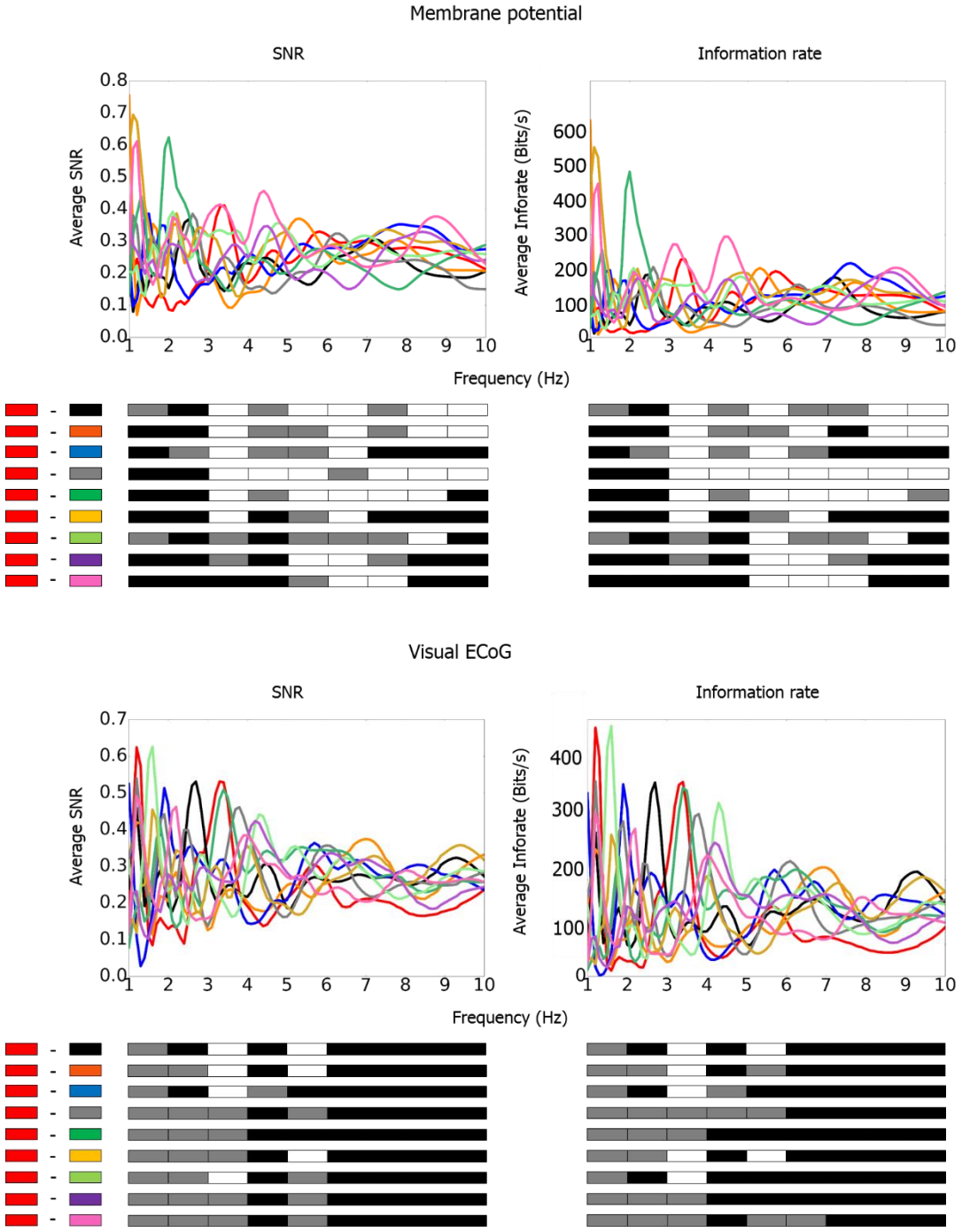

Figure.10.20: ***Average SNR and information rate over time of a single cell membrane potential and visual ECoG recordings across conditions.*** *Same cell and visual ECoG as in figure 10.6 -10.19, n = 13 repetitions. Upper part: membrane potential of the cell. Lower part: visual ECoG simultaneously recorded. Left: SNR; right: Information rate. Box plots: paired Wilcoxon test; color code: white: "red" significantly higher than "X"; grey: "red" not significantly different than "X"; black: "red" significantly lower than "X", with p<0.05).*

II-4.5 Population analysis

At the psychophysical level, different human subjects reported the same hallucinatory-like percepts of pulsating circles and rotating fan shapes in the presence of opponent planforms combined with $1/f^{\alpha}$ spatio-temporally filtered noise (Billock and Tsou, 2007). Those observations are consistent with what several persons reported with our set of visual stimuli during preliminary psychophysical observations. It therefore seems that those hallucinatory-like percepts reflect common anatomo-functional properties of the brain. As detailed in our working hypothesis, we believe that the cat is a relevant model for the study of hallucinatory-like percepts as first, behavioural evidence showed the ability of this model to perceive illusory contours (Bravo et al., 1988). Second, electrophysiological recordings demonstrated that the cat V1' machinery possesses the anatomo-functionnal requirements that account for the propagation of activity linked with the perception of an illusory line extending over space and time, activity dynamic lying in the same range than the spatio-temporal characteristics necessary to induce the illusion in humans (cat: Jancke et al., 2004; human: Hikosaka et al., 1993). If perception of hallucinatory-like geometric shapes reflect a global common principle of wiring in the brain, we should be able to observe and compare our recordings across several animals. Before describing our results at the population level, obtained with the same analysis, we must first precise that intracellular studies show a high level of diversity, amplifying the well-known heterogeneity of V1's cells properties. However, in spite of this variability, Funke et al., (2007) found by single unit recordings in anesthetized and paralysed cats primary visual cortex that 85 % of the cells that they recorded showed stochastic resonance like amplification of initially weak responses due to the presentation of noise (image jitter). We therefore believe that the comparison between our cells is relevant, although all cells did not show sustained stimulus locked oscillations like the one observed for our condition of interest described previously, another one displayed a similar profile in protocols with all control conditions (Figure 10.27 -10.29) and a third one in a pre-protocol (Figure 10.30). Consequently, the spectral content of each individual cell is of interest to us. Because of the cellular variability that we mentioned, cells have different magnitudes of depolarising and hyperpolarizing events. Averaging spectral analysis between cells without taking this fact into account might lead to an overrepresentation or underrepresentation of some cells in the population average. In order to make the spectral analysis comparable across cells, we expressed the result of each spectral analysis of a given condition as a function of a common reference, the blank condition. To that end, we expressed each point of the spectral analysis of each condition as a percentage of the total power of the blank condition in the same analysis in the 0-30 Hz bandwidth for pure spectral analysis and between 1-10 Hz for time-frequency ones. We did not use a frequency by frequency normalization to avoid spectral distortion during the averaging process and preserve initial spectral distribution. For every condition, each point of each spectral analysis was therefore normalized by the entire power of the blank condition.

II-4.5.1 Power spectral content of the trials

As we can see on Figure 10.21, at the membrane potential population level, induced oscillations (average power spectrum of the trials) expressed as a percentage of the power of the blank in the 0-30 Hz frequency bandwidth and averaged across our 5 cells significantly dominates 8 out 10 conditions and are no different than 2 others in the 3-4 Hz bin for our condition of interest in red (Figure 10.21, top left). It was the case for 7 out 10 conditions for the raw average that was not expressed as a percentage of the blank. When we look at the power shared on average between each pair of trials cross spectrum, our condition displays the highest cross spectral density in the 3-4 Hz bin (larger than 10 out of 10 conditions, against 9 out of 10 for the raw average, Wilcoxon paired test, $p< 0.05$) and this is the only bin for which it is the case (Figure 10.21, top right). At the level of the visual ECoG (Figure 10.21, bottom left), induced oscillations are stronger than for all conditions in the 3-4 Hz bin of our condition of interest (against 8 out of 10 for the raw average). However, for our condition of interest the power of the average cross spectrum shared between each pair of trials only surpass 4 out of 10 conditions, is no different than 4 others and smaller than 2. Therefore, it seems that for visual ECoG recordings at the population level, the power content of our interest condition shared by each trial in the 3-4 Hz bin is much less reproducible than at the Vm level. However, it presents a rather strong peak at 3.6 Hz that seems stronger than all conditions but one (Figure 10.21 bottom right, red vs pink) but that peak does not cover the overall extent of the 3-4 Hz bin, to the opposite of the Vm (Figure 10.21, top right).

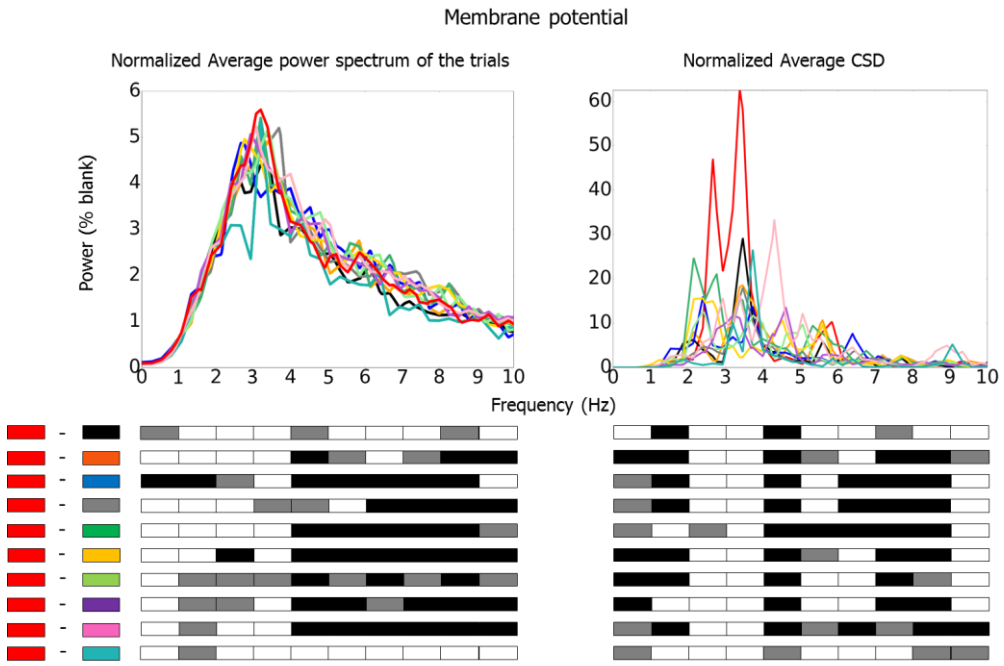

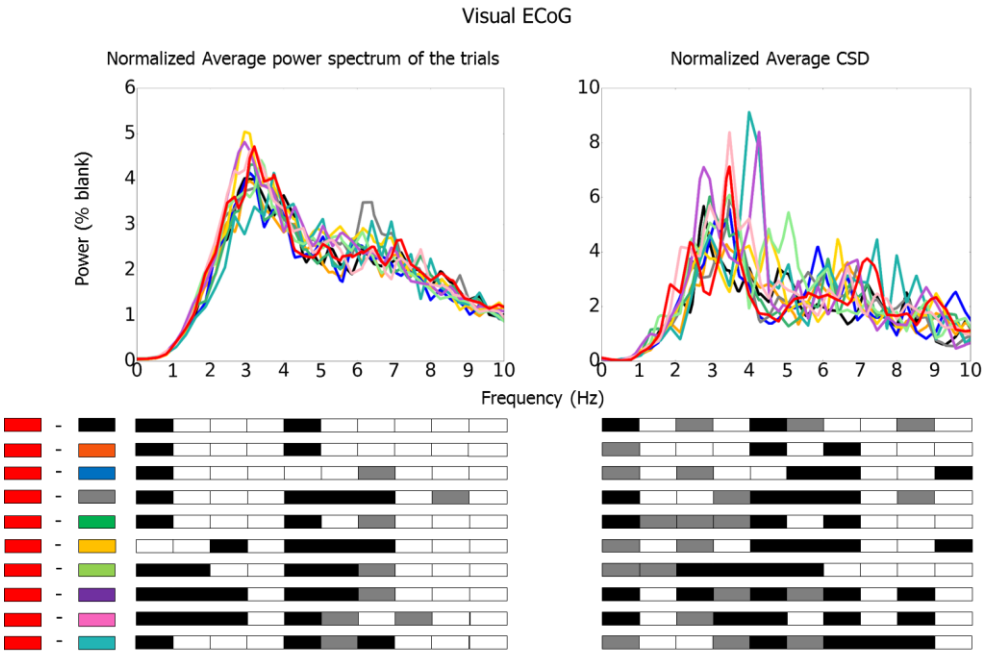

Figure.10.21: ***Comparison of membrane potential and visual ECoG induced oscillations and in-phase oscillations power shared between trials.*** *Top: membrane potential, n = 5; bottom: visual ECoG, n = 5. Left: average power spectrum of each trial for the population expressed as a percentage of the blank condition between 0-30 Hz. Right: power of the average cross spectral density between each pair of trials, between cells. Box plots below abscissa: paired Wilcoxon test with color code: white: "red" significantly higher than X; grey: "red" not significantly different than "X"; black: "red" significantly lower than "X", p<0.05).*

II-4.5.2 Dephasing of the cross spectrum average and power spectral content of stimulus-locked oscillations

The average dephasing is the difference of phase between two signals in the complex plane. In our average cross spectrum, we took it as the argument of the resulting complex numbers representing the average dephasing of the signal's in-phase oscillations that sumed up during the averaging process. We calculated it for each cell and condition between each pair of trials and then averaged across our population (Figure 10.22, left). The power spectral content of the average PSTW (stimulus-locked oscillations) was also calculated for each recording and averaged across our population (Figure 10.21, right). For the Vm we can clearly see that the lowest dephasing in the 3-4 Hz bandwidth is obtained for our condition of interest for which it is inferior to all other conditions (Wilcoxon paired test, $p<0.05$) as it tends towards 0, reaching a minimal value of 0.22 (Figure 10.21, left upper part). It therefore seems to be a characteristic shared by the cells of our population in that tested condition. The normalized average CSD of our condition of interest also prevails over all other conditions in the 3-4 Hz bin at the population level (Figure 10.21, top right). It means that when 3 Hz oscillations appear in our condition of interest, it is in a larger proportion than for other

conditions and that these oscillations are relatively more phase locked than in control conditions. For our main condition of interest condition, 3-4 Hz oscillations are not necessarily present during the overall time course of a trial, sometimes drown out in the noise but when they appear, it is at key temporal moments that are sensibly the same across trials. We are convinced that it is not an artefactual effect as it only appears for that particular condition where the predicted wavefront of the propagating wave of activity corresponding to the percept locally propagate tangentially to the cell's preferred orientation. Moreover, 3-4 Hz oscillations are in accordance with our preliminary psychophysical estimations (3-3.5 Hz). The combination of a relative power increase shared in a single frequency bin between trials (stimulus-induced oscillations) and presenting a smaller temporal jitter from trial to trial naturally results in a power increase in the average of the trials (stimulus-locked oscillations) during the summation process of the averaging. That power increase is moreover superior in our tested condition than in all other conditions in normalized as well as raw averaging, Figure 10.21, top right). For the Vm, that observation is an extension at the population level of the stimulus locked oscillations found in the autocorrelation of the single cell average PSTW presented in Figure 10.6 -10.20.

Indeed, for that cell the stimulus locked oscillations found in the ACF of its average PSTW displayed a high power spectral density as it resembled a sinusoid of a single frequency of 3 Hz. However, its average cross correlation between each pair of trials in the temporal domain did not display any particular similarity over time as peaks were not regularly distributed nor equivalent in amplitude, confirming that oscillations did not systematically appear every 333 milliseconds in each trial (Figure 10.6 B, upper left row). Among our pool of 5 cells where all control conditions were presented, as well as in parallel recordings where only noise was presented, we did not observe a similar oscillatory profile except for one. In that cell, our other condition of interest (orange) - corresponding to the case of hallucinatory rotating fans with a predicted wavefront parallel to the cell's preferred orientation - had a PSTW average ACF presenting a high power spectral density centred on 3.5 Hz. Still for the same cell, one control condition corresponding to the case where induced pulsating circles had a predicted wavefront tangentially orthogonal to the cell's preferred orientation displayed a similar profile, although less clear (Supplementary Figure 10.27, 10.28). Among our 5 cells, 2 others presented stimulus-locked ACF of the average PSTW, still in our condition of interest, during pre-protocols where all control conditions were not present (Supplementary Figure 10.29, 10.30).

At the visual ECoG level however, the difference with the Vm at the population level seems to confirm itself: we did not find across our 5 cells the results of the individual recordings presented in the previous section. Indeed, in the 3-4 Hz frequency bin, the argument of the average cross spectrum for our first condition of interest in red was above 4 out of 10 conditions, no different than one and only smaller than 5 conditions (Figure 10.22, bottom left). In average PSTW (Figure 10.22, bottom right), this results in a spectral composition where the power in the 3-4 Hz bin of our first condition of interest in red only surpass 6 conditions out of 10, is no different than 2 and dominated by 2 other conditions.

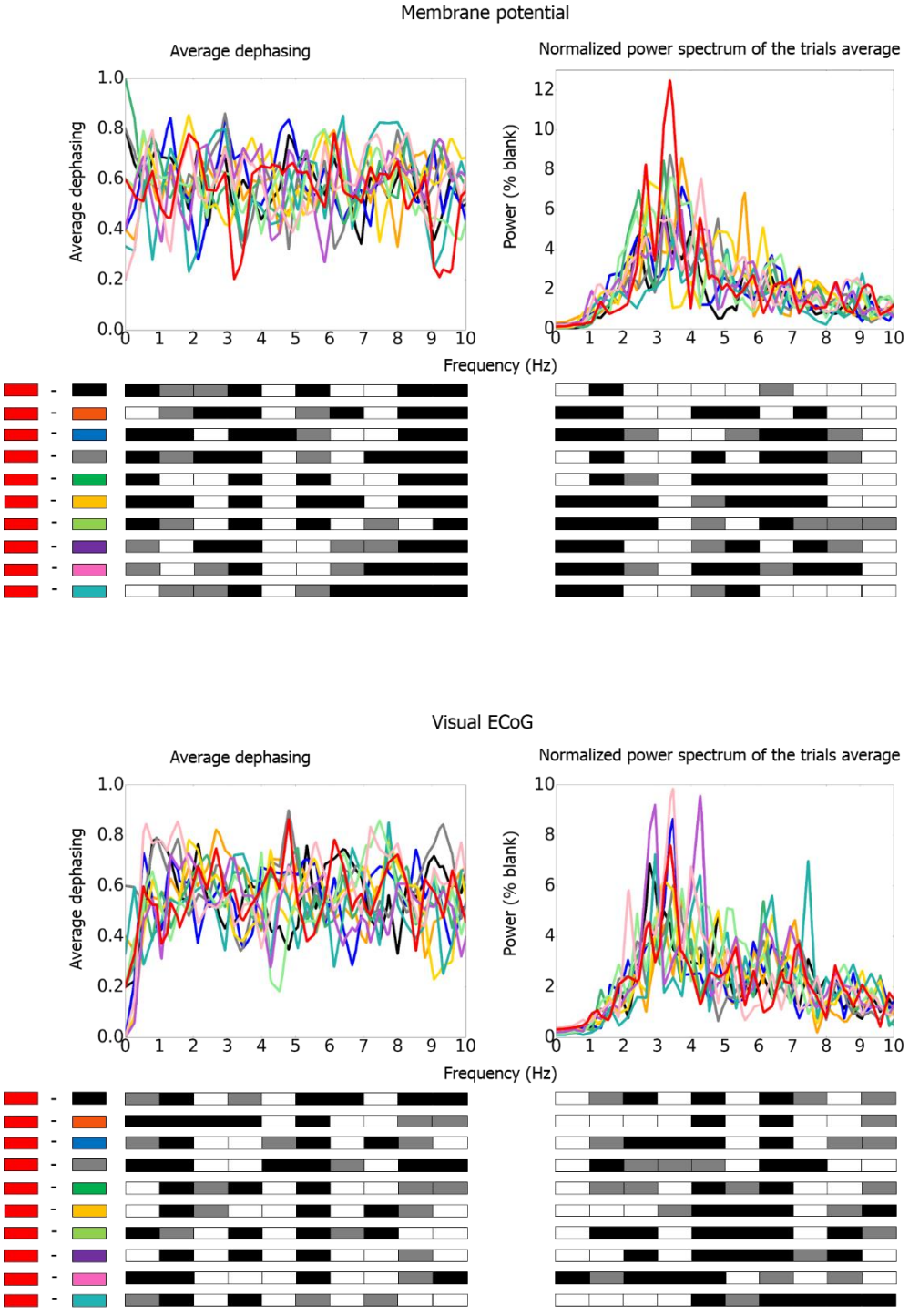

Figure.10.22: ***Population level comparison between membrane potential and visual ECoG of the average dephasing and power spectrum of stimulus-locked in-phase oscillations*** *Top: membrane potential, n = 5; bottom: visual ECoG, n = 5. Left: dephasing averaged acrosseach recording. Right: the power spectrum of the average PSTW was expressed as a percentage of the blank condition power before averaging across cells. Box plots: paired Wilcoxon test with color code: white: "red" significantly higher than X; grey: "red" not significantly different than "X"; black: "red" significantly lower than "X", with p<0.05).*

II-4.5.3 Signal, noise, and total signal power spectral estimation

Signal, noise and total signal power were evaluated thanks to the convolution by Morlet wavelets presented in section II-4.1. As previously, spectral analyses were normalized by the blank power, focusing between 1 and 10 Hz. For the Vm, unsurprisingly our condition of interest presents a signal increase in the 3-4 Hz band that significantly prevails over 8 conditions out of 10 and is similar to two others (Figure 10.23, top left panel). Without normalization, the signal dominates 9 out of 10 conditions, (Figure 10.23, bottom left). This signal power increase comes from an increase in the total signal power, something clearly more visible without normalization than after (Figure 10.23, bottom right vs upper right). This is where we start to see the limit of our normalization process that, up to now, represented with fidelity the raw averaging. Indeed, in this latter, the increase in the total signal power in the 3-4 Hz bandwidth of our condition of interest is clearly more visible as it is not inferior to any condition (Figure 10.23, bottom right), to the opposite of the normalized averaging (Figure 10.23, top right). Similarly, the increase in the total signal power is accompanied by an increase in the noise, which is not that evident in the normalized averaging when compared to the raw one (Figure 10.23, top middle vs bottom middle). The fact that the noise power surpasses the total power of the signal is inherent to our estimation method when applied to our data where the signal to noise ratio is low. Indeed, as presented in Figure 10.4, the signal (represented on the left by the red arrow) is of the same magnitude than the noise. This is not our case as we saw that the signal of our condition of interest is about forty percent of the noise (Figure 10.20, red trace). The total signal power is measured as the average modulus of the trials vectors. It therefore does not take into account the dephasing between said vectors. Even if the dephasing is lower in the 3-4 Hz frequency bandwidth of our condition of interest, it is still not equal to 0. The noise is measured as the average distance between each trial vector and the signal one and therefore do take into account the dephasing. When there is dephasing and when the signal is low, the evaluated noise is slightly superior to the total power, a difference that is amplified during the squaring step of the power spectral analysis of those measures.

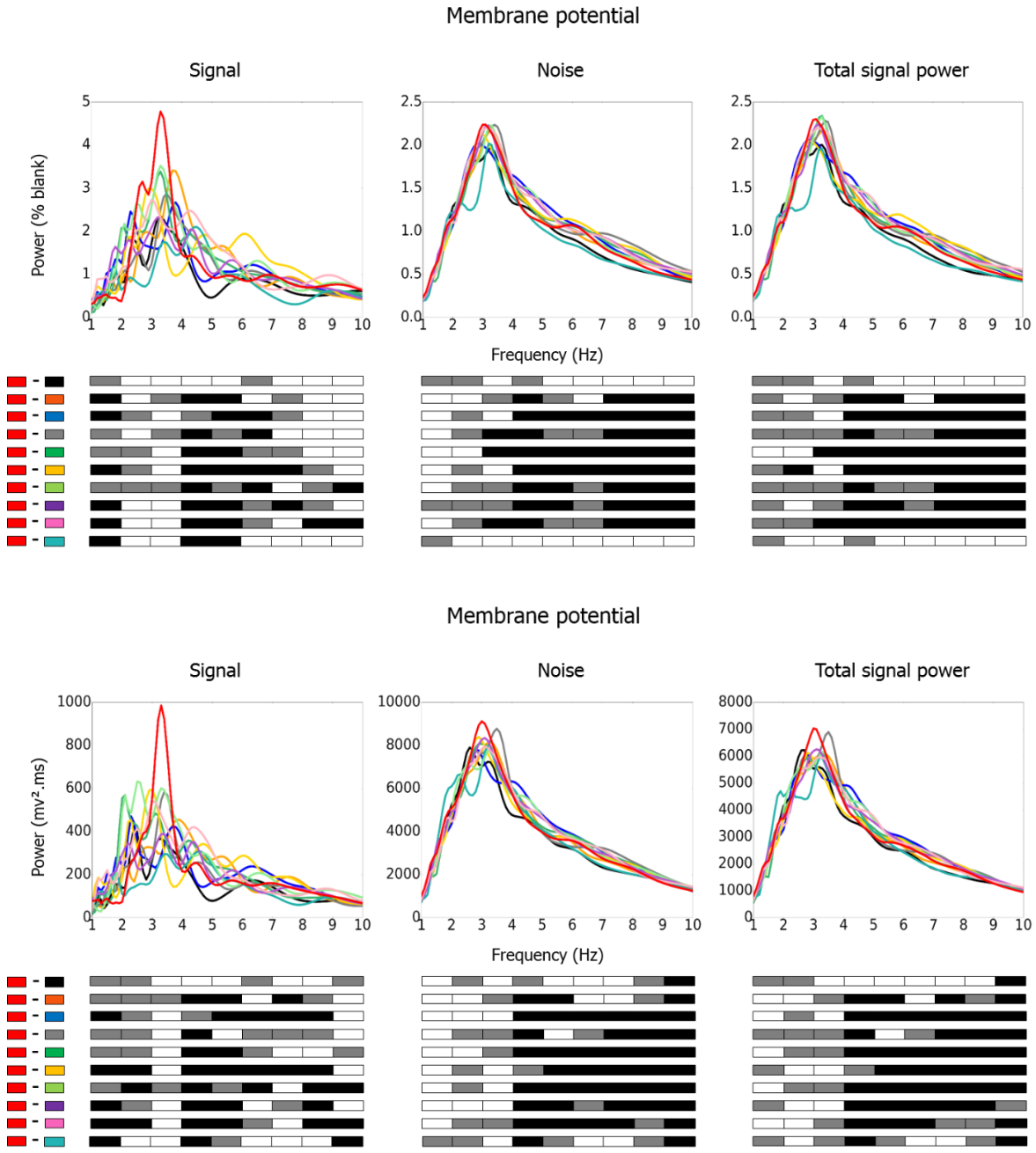

Figure.10.23: ***Comparison between raw and normalized averaging of Vm signal and noise power.*** *Upper and lower raw: membrane potential, n = 5; Top: calculus for each cell expressed as a percentage of the blank condition total power in the 1-10 Hz frequency bandwidth before averaging across cells; bottom: same, except that the spectra were not normalized by the blank power and were directly averaged across cells. Left: signal, middle: noise, right: total power. Box plots: paired Wilcoxon test with the same color code as previously: white: "red" significantly higher than X; grey: "red" not significantly different than "X"; black: "red" significantly lower than "X", with p<0.05).*

At the visual ECoG level, our first condition of interest in the 3-4 Hz bin does not distinguish itself from other conditions as we did not find evidence of a relative increase in its signal (Figure 10.24,

left panels). However, we do note in both normalized and raw averaging a relative signal increase in the 3-4 Hz bandwidth of our second condition of interest in orange corresponding to the second percept of rotating fans locally tangent to the cell's main axis. In the same frequency bin, the condition where induced pulsating circles are orthogonal to the cell's main axis (blue), the signal presents a relative increase in power (Figure 10.24 top and bottom left). In the first case (orange trace), the relative 3-4Hz signal increase comes from an amplification of the total power (Figure 10.24, top and bottom right). This latter is accompanied by an increase of the noise in the same frequency bin (Figure 10.24, top vs bottom middle).

Normalized averaging has the dual advantage/disadvantage of expressing each condition as a percentage of the blank condition power in a given analysis, which renders the comparison between different analyses more delicate as the initial referential is not the same. However, it is also an advantage as it frees each analysis of its initial absolute value and allows comparison of relative changes between different analyses. Indeed, if we look carefully, for our second condition of interest (orange trace), the 3-4 Hz total power increase is slightly larger than the relative increase of the noise in the same frequency bin, which explains the relative signal increase (Figure 10.24, top left and bottom left). To the opposite, for our condition in blue, the relative signal increase comes from a reduction of the noise that presents a negative deflection right in the middle of the 3-4 Hz frequency bin (Figure 10.20 middle top and bottom), deflection that is absent in the total power. Because the magnitude of the signal power is inferior to the noise and total power by a factor of ten, such small relative changes between noise and total signal power lead to important modifications in the evaluated signal.

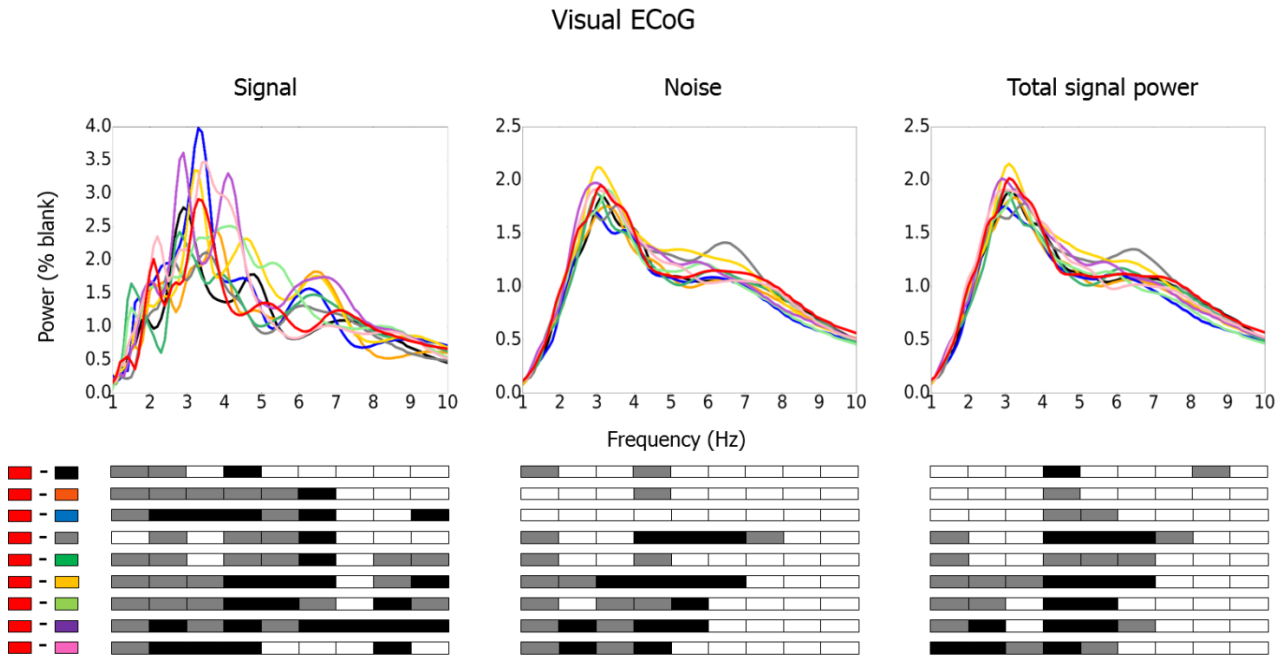

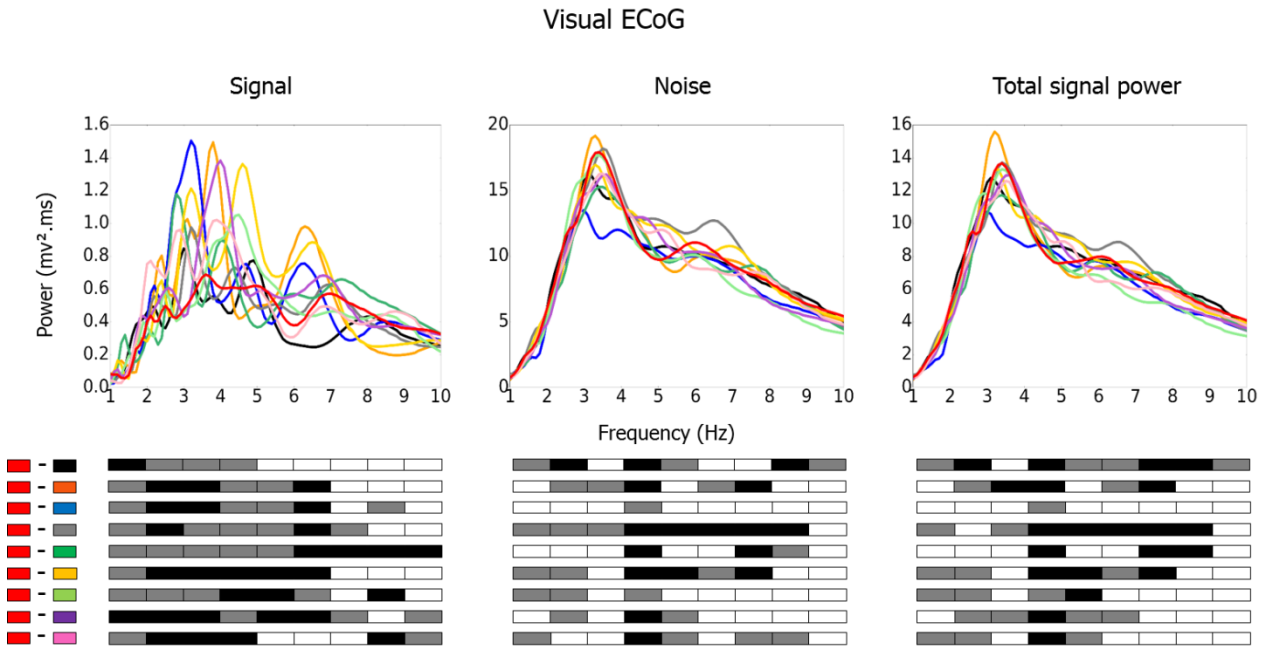

Figure.10.24: ***Population level comparison between raw and normalized averaging of visual ECoG signal.*** *Upper and lower raw: visual ECoG, n = 5; Top: calculus for each recording expressed as a percentage of the total power of the blank condition in the 1-10 Hz frequency bin before averaging; bottom: same, except that the spectra were not normalized by the blank power and were directly averaged. Left: signal, middle: noise, right: total power. Box plots below abscissa: paired Wilcoxon test. Color code: white: "red" significantly higher than X; grey: "red" not significantly different than "X"; black: "red" significantly lower than "X", p<0.05).*

II-4.5.4 Signal to noise ratio and information rate

From the estimation of the signal, noise and total signal obtained using Morlet wavelets as described in section II-4.1, for each frequency, we calculated the average Signal to Noise Ratio (SNR) and derived the average information rate over time before averaging. We must recall that those measures were not obtained via the power of the signal, noise and total signal presented in previous section II-4.3.3. The SNR is a dimensionless measure that is not function of the absolute value of the signal or the noise but of their ratio. That is why we did not need to normalize it by the power of the blank condition and directly averaged it across recordings. This was also the case for the information rate as this latter is function of the squared SNR.

For the membrane potential, we found that the SNR is the highest for our first condition of interest in the same bin (Figure 10.25, top left), reaching a value of 0.3 significantly stronger than 7 conditions and similar to 3 others. For that bin, the information rate is also the highest for our condition of interest, reaching a value of 153 bits per second. At the visual ECoG level, our condition of interest reaches the third position with an SNR value of 0.27 in the 3-4 Hz frequency bandwidth.

Interestingly, the condition in blue presents the highest SNR and information rate values in the 3-4 Hz bin (Figure 10.25, bottom left and right). This is coherent with the relative signal power increase found for that condition in the previous section. However, our second condition of interest (orange) does not present a relative increase in the average SNR nor in the information rate in the same frequency bin at the population level.

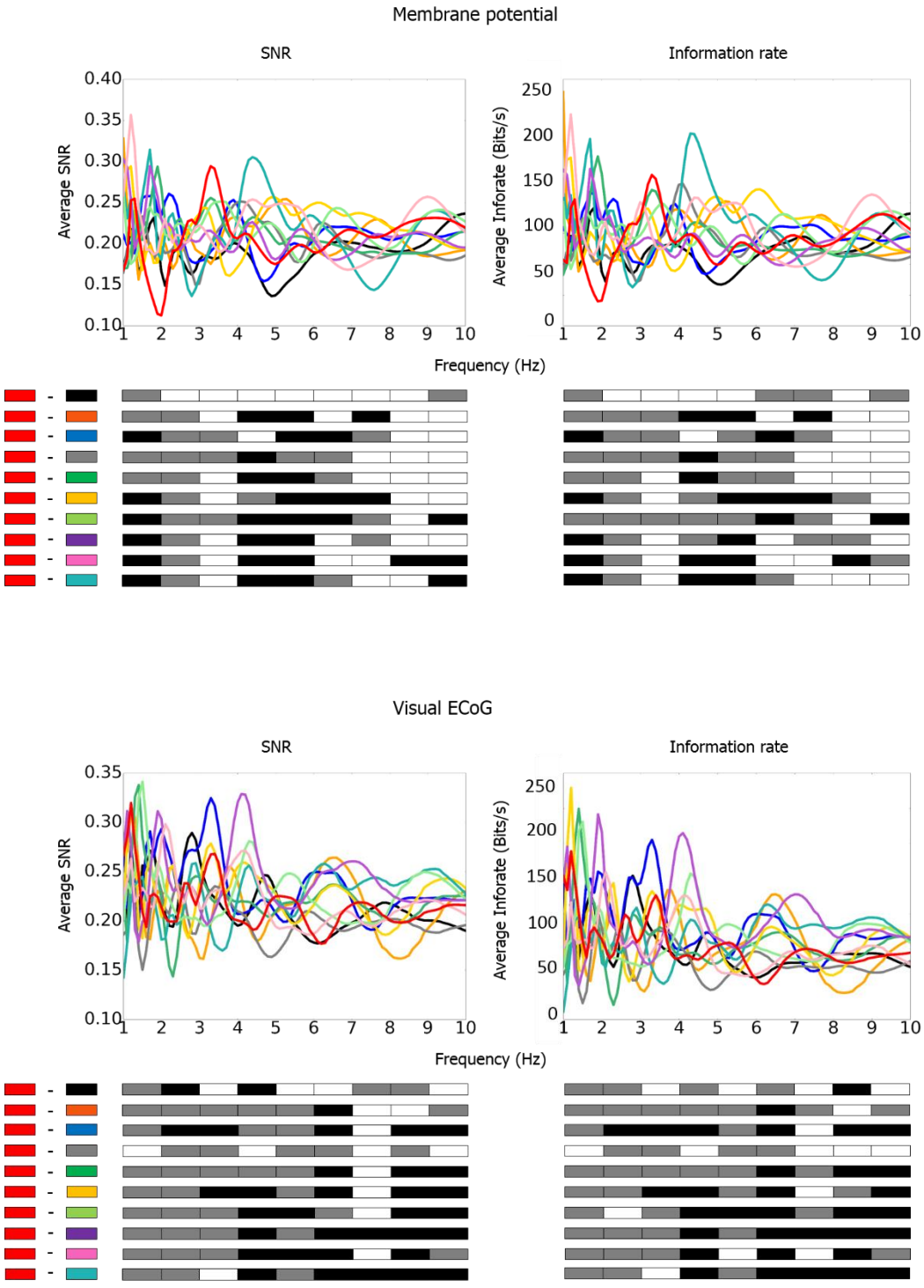

Figure.10.25: ***Vm and visual ECoG comparison of the average SNR and information rate over time.*** *Upper raw: membrane potential, n = 5; lower raw: visual ECoG, n= 5. Left: SNR average across recordings; right: same for the information rate. Box plots: paired Wilcoxon test. Color code: white: "red" significantly higher than "X"; grey: "red" not significantly different than "X"; black: "red" significantly lower than "X", with p<0.05).*

We then searched for a more precise evaluation of the SNR as we saw from Figure 10.18 that this latter is not stationary over time. To that end, for each cell and visual ECoG traces, we defined temporal windows sufficiently large to correspond to a potential correlate of the percept, ranging from 1 to 2 seconds by steps of 0,25 seconds. For conservative purpose, within a given set of conditions the time window duration was the same but it was displaced over time to capture the highest time-frequency combination giving the overall strongest SNR value for each condition, without any a priori on the frequency content. For the Vm, the results appear immediately as the SNR value of our condition of interest is the highest of all in the 3-4 Hz bandwidth and this is the only frequency bin for which this is the case (Figure 10.27, upper left). Even if the absolute value of the SNR of our condition of interest does not change much from the integration over the entire time course of stimulation (0.3 VS 0.37), the relative distribution does change a lot as the SNR value of our test condition emerges from the surrounding noise that was more homogeneously distributed over frequencies in the previous analyses (Figure 10.26). Because the squaring procedure amplifies differences in the information rate evaluation, for the channel's capacity, the averaging process of our small sample did not tame variability across cells as well as in the SNR (Figure 10.27, upper right). The information rate of our interest condition does not display such a clear dominance as the SNR although it is higher than all other conditions in the 3-4 Hz bin, only competed by the pink trace.

For the visual ECoG, population recordings do not show any improvement of the 3-4 Hz SNR for our condition of interest nor for other tested conditions where percepts are induced as control conditions (blue, dark green). Conditions where no hallucinatory-like percept is induced (gold, light green, grey, black, purple and pink) present higher SNR value in 1-2 and 4-5 Hz bandwidth than our tested conditions in the 3-4 Hz one (Figure 10.26, lower left). However, in the 3-4 Hz bandwidth, the highest SNR and information rate values are observed for the blue trace - corresponding to pulsating circles tangentially orthogonal to the cell's main axis - findings that we already obtained in the previous analyses (Figure 10.25, lower left and right panels).

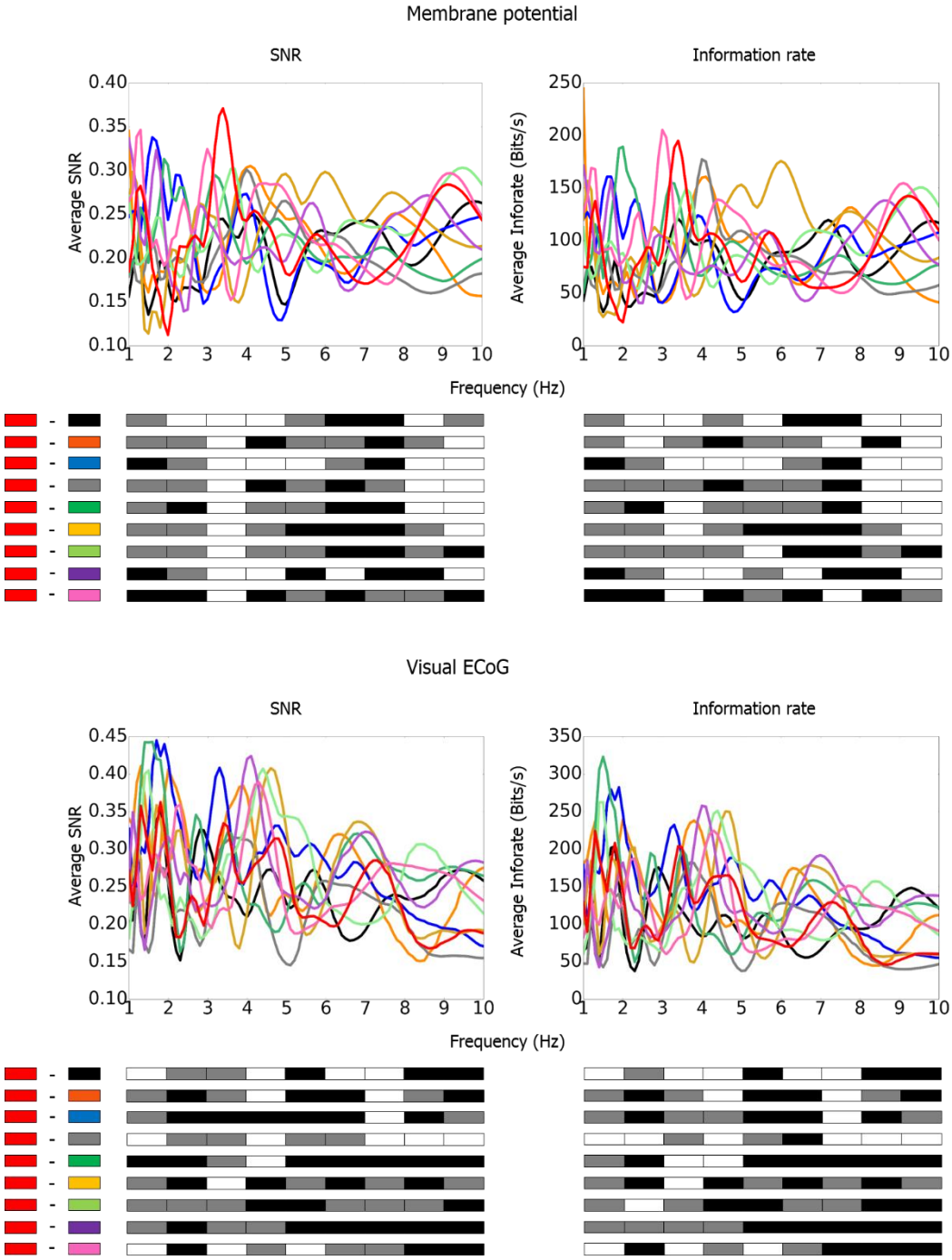

Figure.10.26: ***Temporally localized comparison of highest SNR and information rate.*** *Upper raw: membrane potential, n = 5; lower raw: visual ECoG, n= 5. Left: SNR average across recordings; right: same for the information rate. Contrarily to Figure 10.25, the SNR was not averaged over the entire time of stimulation but in temporal windows where it was the highest. Those temporal windows were of the same duration for a given recording but evaluated individually for each condition. Their duration ranged between 1 and 2 seconds. Box plots: paired Wilcoxon test. Color code: white: "red" significantly higher than "X"; grey: "red" not significantly different than "X"; black: "red" significantly lower than "X", with p<0.05).*

II-4.6 Supplementary figures

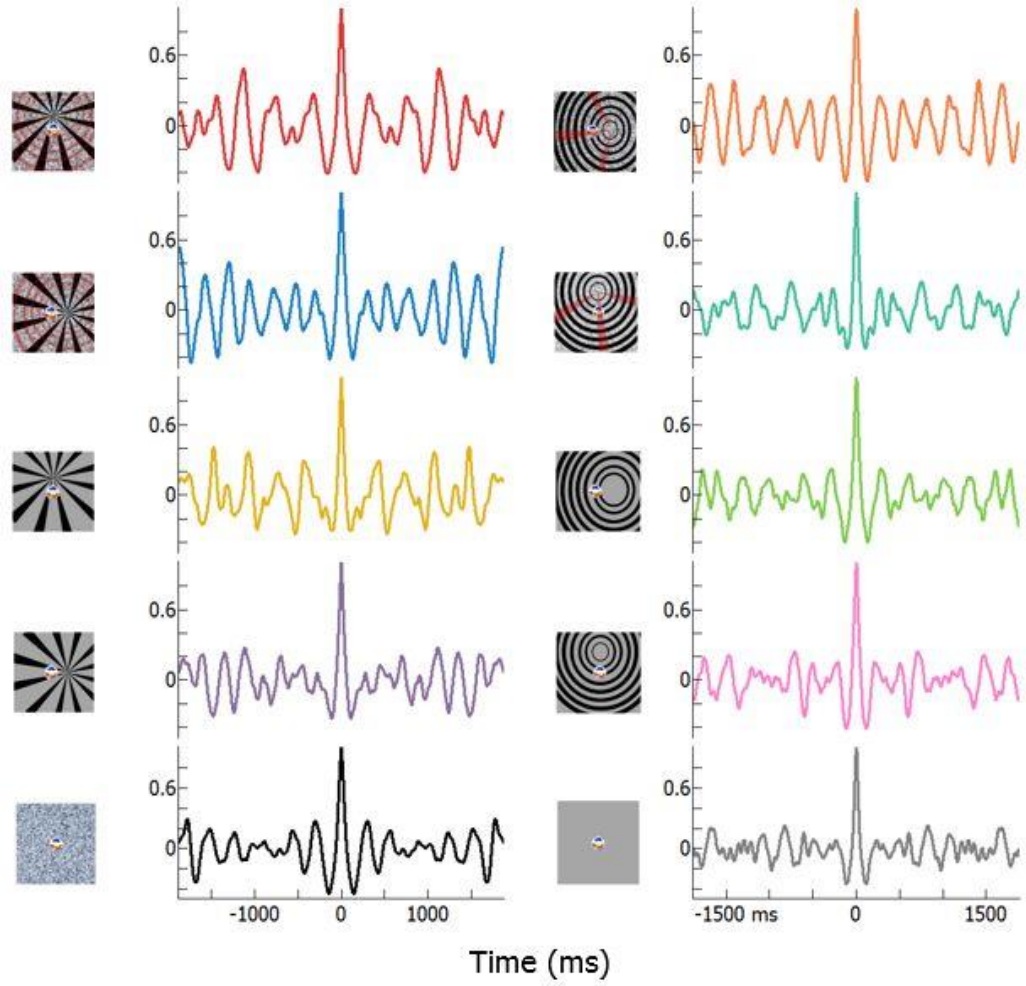

Figure.10.27: ***Single cell autocorrelation of the average PSTW.*** *Another example cell than the one presented before, n= 30 repetitions. The autocorrelation was performed on +/- 50 % of the signal, starting at t = 750 ms to discard the unspecific transient response starting at t = 500 ms and lasting 250 ms, due to the sudden change in the RF surround content. First row: Our first condition of interest in red (top left column) does not display any remarkable behaviour. Our second condition of interest in orange (top right) however displays a clear oscillatory power spectral density, peaking with periodic side-peaks at 3.5 Hz. The condition where induced pulsating circles have a predicted wavefront orthogonal to the cell's preferred orientation (second row, blue) also displays a quite striking power spectral density around 3.7 Hz but the side-peaks are more irregular. No other condition (including the 6 lower control ones where no percept is induced) presents oscillatory behaviour sustained over time.*

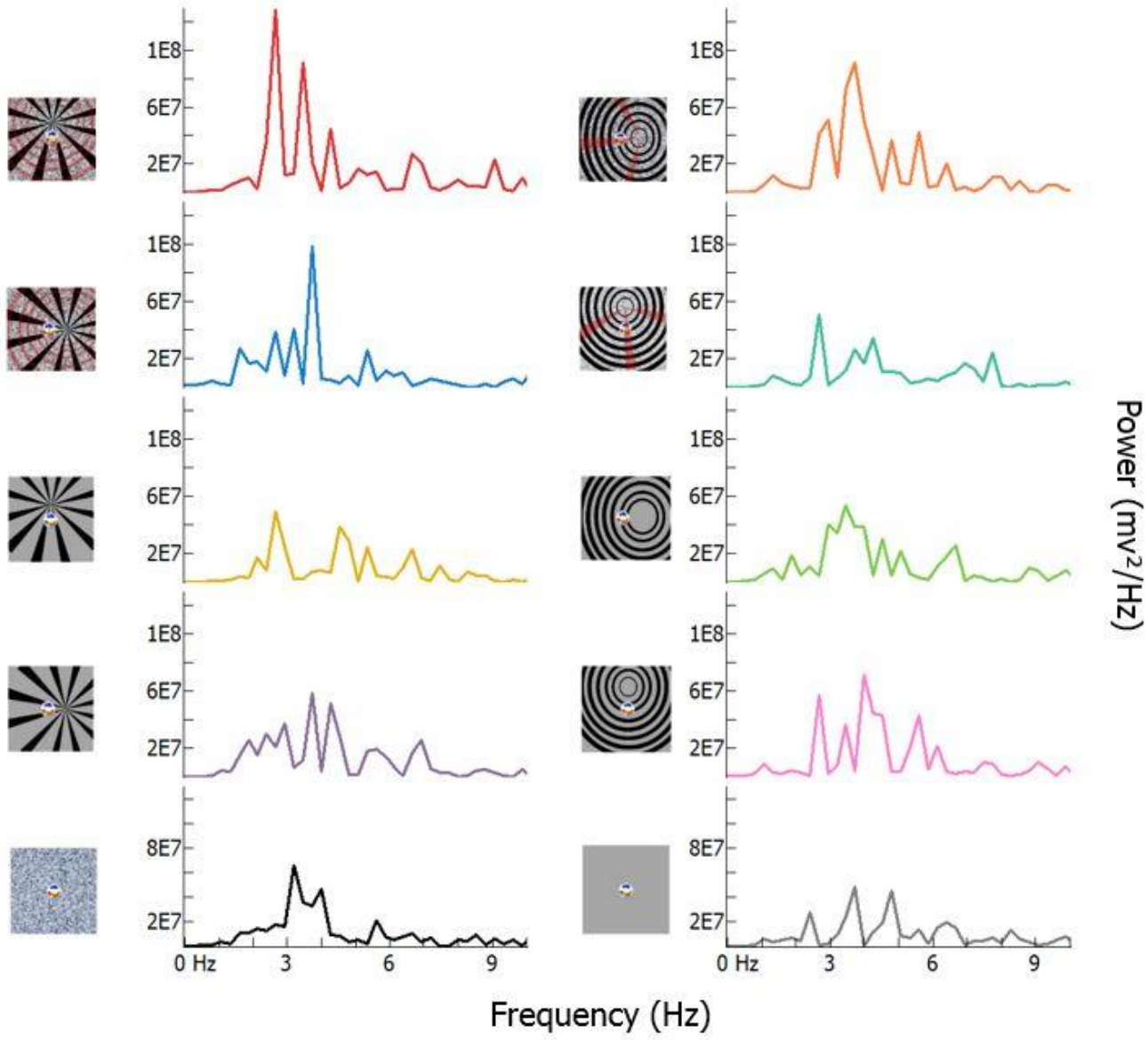

Figure.10.28: ***Single cell power spectrum of the average PSTW.*** *Same cell than in figure 10.27, n= 30 repetitions. The power spectrum of the average pstw was calculated from t = 750 ms to the end of the signal. In parallel of figure 10.27, we can see that our first condition of interest in red indeed displays a peak at 3.45 Hz whose amplitude is comparable to the one of the orange condition but also another one at 2.7 Hz. This explains why the stimulus locked ACF of the average PSTW do not present oscillations at a single frequency over time for our condition of interest in figure 10.27 but a carrier at a lower frequency. On the other hand, our second condition of interest in orange present a single dominant peak at 3.75 Hz, which relative amplitude reflects a single dominant oscillatory frequency homogeneously distributed over time (figure 10.27). The blue condition also presents a single dominant peak at 3.75 H, although sharper than for the orange condition. This explains its ACF of the average PSTW profile (Figure 10.27. No other condition displays a peak of such amplitude in the 3-4 Hz nor in any other bandwidth. Other conditions display relatively lower peaks more homogeneously distributed between 0 and 10 Hz, which explains why their autocorrelation doesn't present any particular structure over time.*

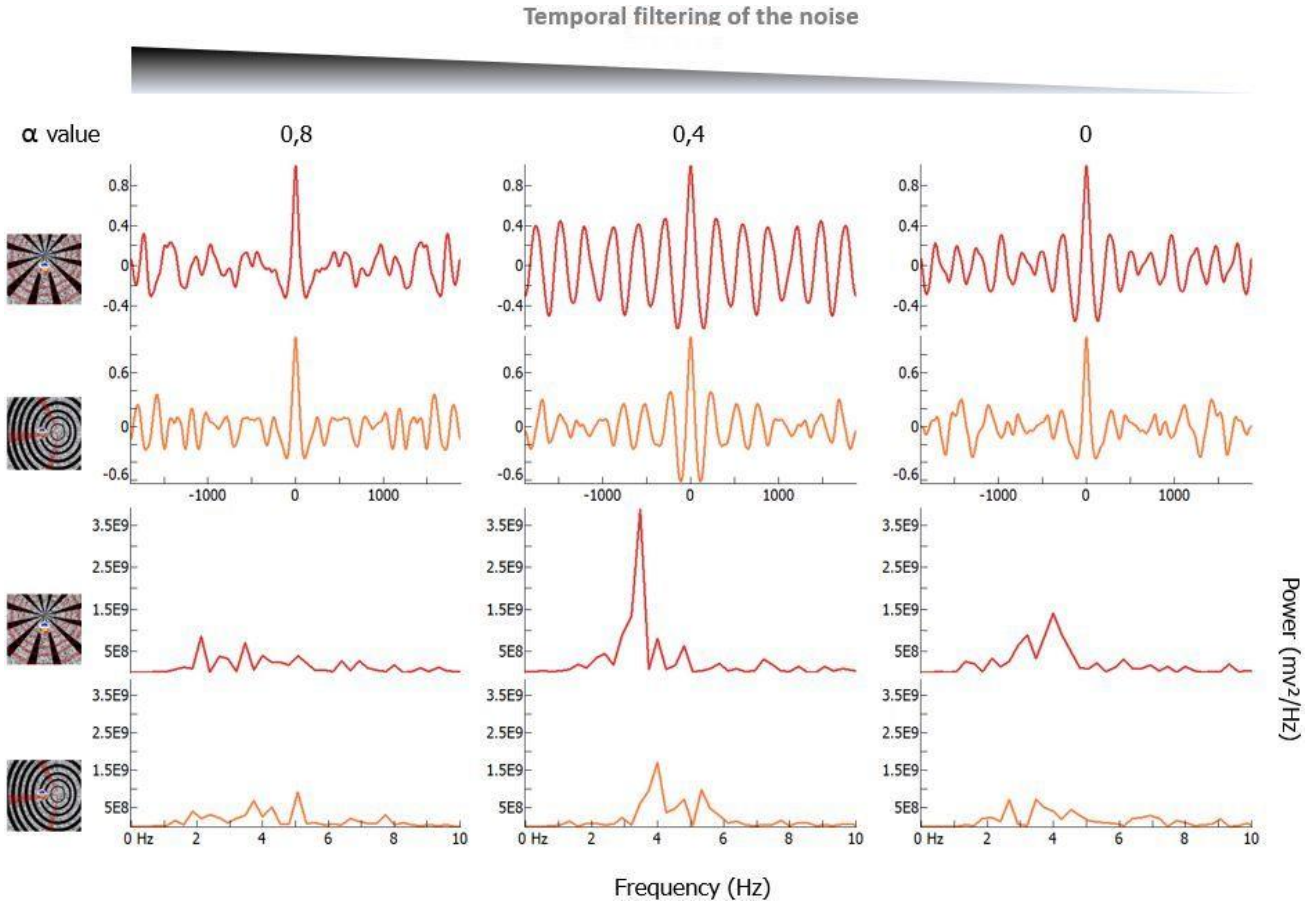

Figure.10.29: ***Single cell power spectrum and normalized autocorrelation of the average PSTW.*** *Same cell than in figure 10.27 - 10.28, n= 10 repetitions. Our 2 conditions of interest at the Vm level were tested in a pre-protocol where the temporal filtering of the noise was tested for 3 different values: left column, αt = 0.8; middle column: αt = 0.4; right column: αt = 0. The spatial filtering of the noise was left unchanged: αs = 1.4. First two rows: autocorrelation of the average PSTW calculated from t = 750 ms up to the end of the signal for +/- 50 % of the signal duration. Last two rows: corresponding power spectra. We can see in the pre-protocol that for a temporal filtering value of 0.4, our first condition of interest in red indeed presents a very high oscillatory power spectral density centred on 3.45 Hz, peak that we retrieved in the same condition of interest while the control conditions were presented (Figure 10.28). However, in contrast to the recordings where control conditions were displayed, in the pre-protocol, this was the only dominant frequency. For our second condition of interest in orange, we do find the second highest peak at 4 Hz (vs 3.75 Hz in figure 10.23) in the power spectrum of the average PSTW for a temporal filtering value of 0.4 (fourth row, middle panel). This peak is the only one, which explains why the autocorrelation for that condition also presents a temporal structure peaking regularly, especially in the initial part (0-1000 ms) of the autocorrelation. The value of the temporal filtering of the noise chosen for the interest protocol (Figure 10.27) was 0.4.*

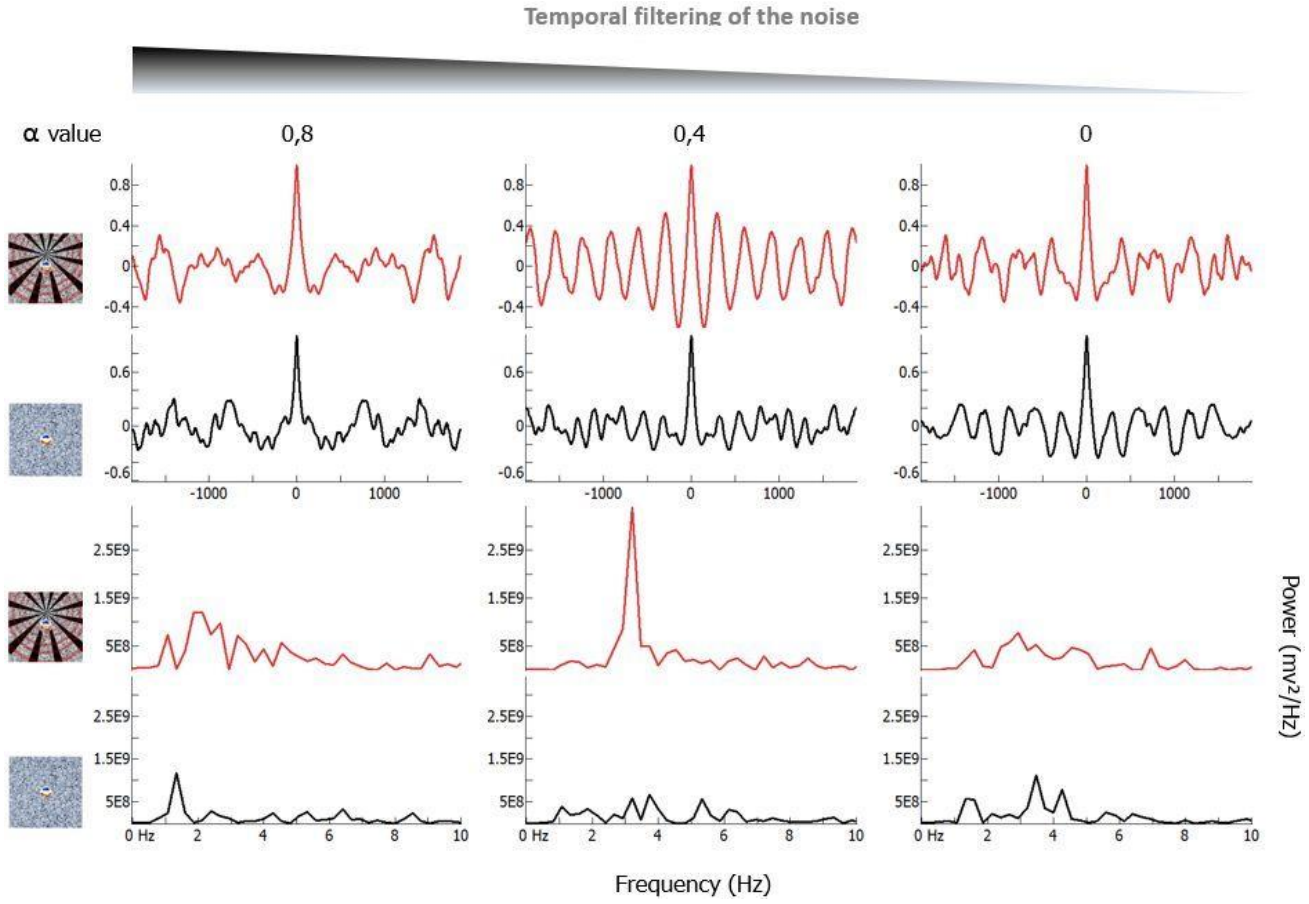

Figure.10.30: ***Single cell power spectrum and normalized ACF of the average PSTW.*** *Another example cell, n= 6 repetitions. This time, we chose to present in the pre-protocol only our first condition of interest (in red) and a control condition where there was only noise in the surround of the receptive field (in black). The temporal filtering of the noise was tested for the same 3 different values: left column, αt = 0.8; middle column: αt = 0.4; right column: αt = 0 while the spatial filtering of the noise was left unchanged: αs = 1.4. First two rows: autocorrelation of the average PSTW calculated from t = 750 ms up to the end of the signal for +/- 50 % of the signal duration. Last two rows: corresponding power spectra. We can clearly see that only our condition of interest presents a single peak at 3.2 Hz (third row, middle panel) for the same value of temporal filtering (0.4) than the cell in figures 10.22, 23 and 24. This is the only condition where it is the case as other conditions (more importantly, control conditions in black) do not present a particular peak only distributed in the 3-4 Hz frequency bin. While the number of trials is small (n = 6), it is sufficient to retrieve four our condition of interest a regular distribution of 3.2 Hz oscillations over time (first row, middle panel). The value of the temporal filtering of the noise chosen for the interest protocol with control conditions was also of 0.4 for that cell.*

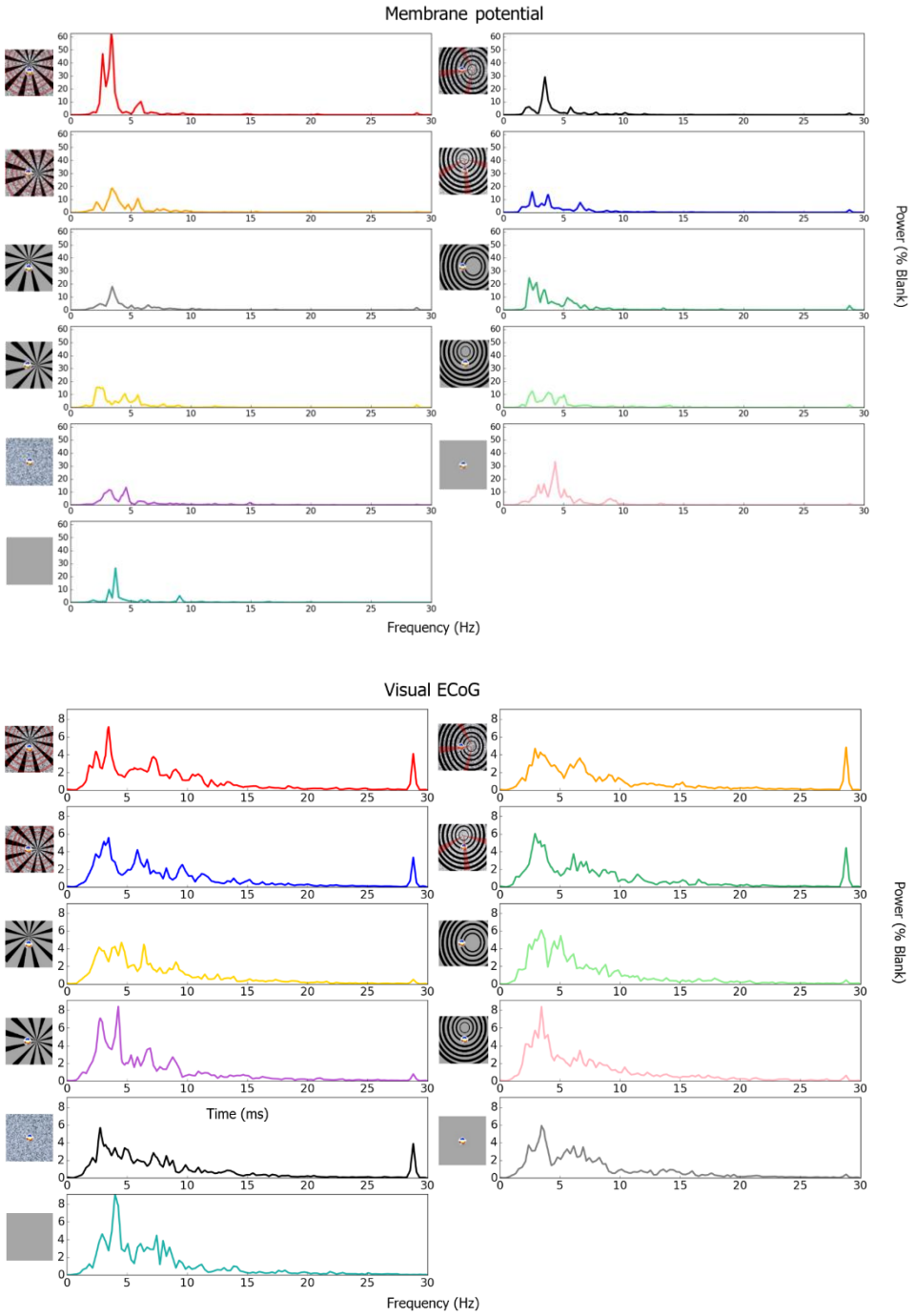

Figure.10.31: ***Population Vm and visual ECoG normalized average cross spectral density between 0 and 30 Hz.*** *Same figure as figure 10.21 but represented differentially for each condition between 0 and 30 Hz for visual purpose representation. We can see at the Vm level (top panel) a peak at 28 Hz, the refreshing rate of our screen. The magnitude of that peak is comparable across all conditions where noise was presented in the RF but not to the last one (turquoise) where there was no stimulation. At the visual ECoG level (lower panel), we can also see a peak at 28 Hz, supplementary indicator that our recordings correspond to visual responses. However, contrarily to the Vm, the visual ECoG displays much larger peaks at 28 Hz in conditions where noise was presented in the surround, to the contrary of conditions where this latter was absent (yellow, light green, purple,*

pink, grey and turquoise). This is one of the reason why we chose to do our normalization by the total power of the blank in the 0-30 Hz bin for pure frequency analysis.

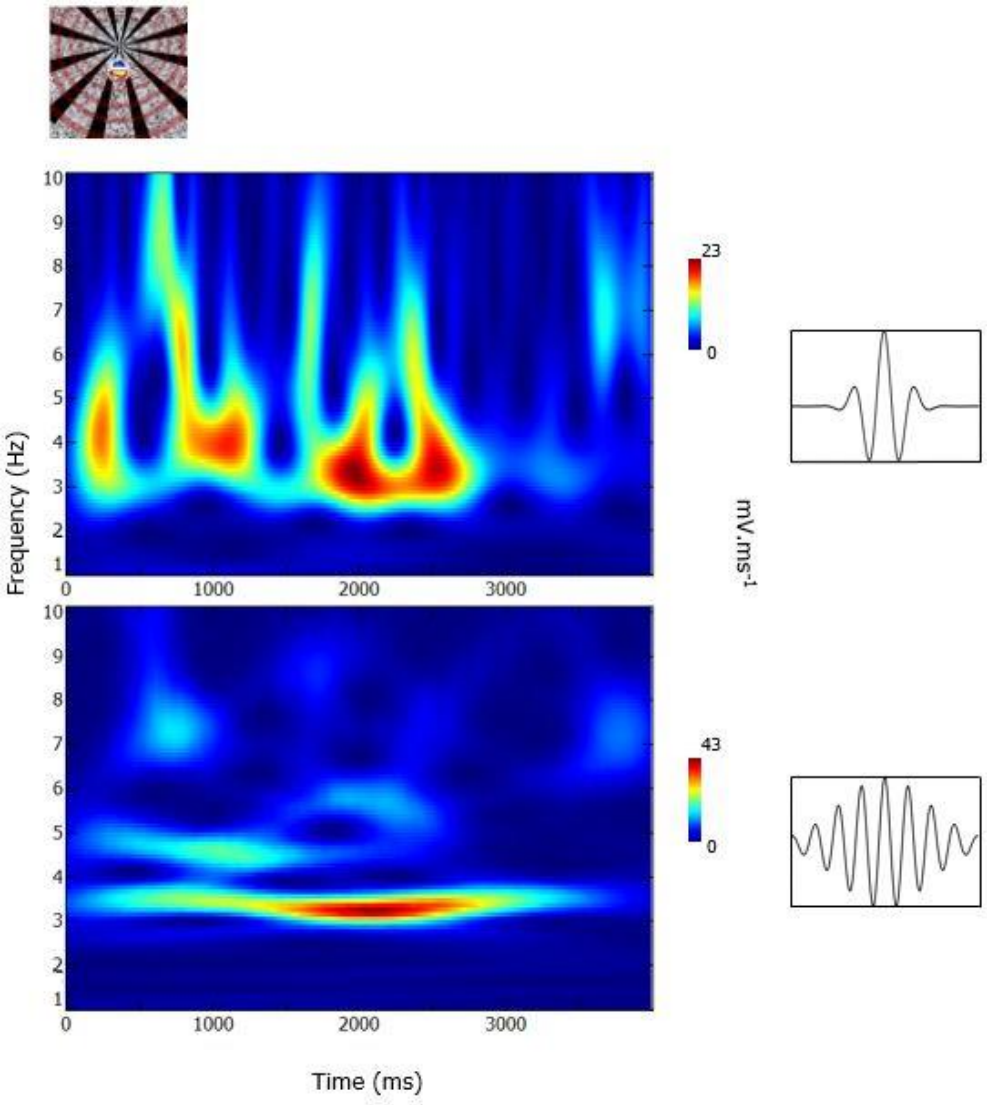

Figure.10.32: ***Comparison between Morlet and Gabor time-frequency analysis.*** *Same individual cell as the one detailed in the first part of the results section. The convolution of the average PSTW by a bank of original Gabor filters (top) and by Morlet filters (bottom) is represented for our condition of interest. Note the poor frequency resolution of the convolution with Gabor wavelets where activity peaks spread over several Hertz, to the contrary of results obtained with Morlet wavelets where the frequency content is much more narrowly distributed. By opposition, the impulse-like shape of Gabor filters allows a precise temporal localisation of energy distribution, by opposition to Morlet wavelets where energy spreads over larger temporal windows in the abscissa dimension.*

II-5. Discussion

II-5.1. From subjectivity to an Archetype

We committed ourselves during the second part of this thesis to the construction of a conceptual framework allowing an experimental test of predictions of Neurogeometry principles. This scientific field is still a young one as difficulties encountered in its development are the same that applies to Neuroscience in general. Studying the brain is a fascinating enterprise whose potential benefits are perhaps only equalled by its tremendous complexity. The brain may be the most complex non-linear system that we know or at least, that we believe to be aware of. Everyone experiences science, as science is also an experiment: sampling the environment that surrounds us, making correlations, attributing causality and evolving by adapting our behaviour according to the conclusions that we drew are at the heart of life and scientific investigations. Nevertheless, the scope of scientific investigations has to be bounded in order to eliminate any subjectivity, allowing the comparison of objective and parametrized measures that must be reproducible.

This last notion is the core difficulty of the study of neurogeometry since the idea that the brain might implement geometry via its wiring emerged from clinical reports of subjects reporting perception of static or dynamic geometric shapes under the influence of mescaline, LSD or during migraines. The cognitive bias arising from the judgement of those persons lifestyle decreased the credibility of their reports that were judged untrustworthy or as the product of confabulation. Despite this common belief, pioneer scientists started to show interest in geometric hallucinations and founded the first parametrization of their study by proving via psychophysical experiments that they could be evoked in any human subject by visual stimulation, using an empty flickering field (Purkinje, 1819-1823; Brewster, 1834; Fechner, 1838; Helmholtz, 1925; Brown and Gebhard, 1948; Mundy-Castle, 1953; Walter and Walter, 1949; Walter, 1956; Smythies, 1959 a, b, 1960; Freedman and Marks, 1965; Remole, 1971, 1973).

However, those type of stimulation, evoke percepts that remains unstable and are described as multistable states because geometric shapes like rotating fans can turn into spirals that themselves gives birth to pulsating circles without any time constant nor possible generalisation. This was nevertheless a first step that brought credibility to the existence and interest of studying geometric hallucinations, setting in motion a common ground upon which the existence of an archetype reflecting the universality of those phenomena could not be questioned anymore. However, those studies still relied on psychophysical observations because the experimental tools that now allow us to study the brain's activity were still out of reach at the time. Moreover, identification, description and quantification of hallucinatory-like induced percepts still relied on subjectivity because of the instability and unpredictability afore mentioned.

In 1909, Hermann von Helmholtz provided the first description of reproducible constant geometric percepts by physically presenting one of the most often reported one: concentric circles, which resulted in perception of opponent form of radial fans shapes. In 1957, the physicist Donald MacKay extended those findings by using both fans shape and concentric circles inducers (MacKay, 1957a,b). While viewing those patterns on ordinary paper during a dozen of seconds, subjects reported as a sequential after effect the perception of an opponent planform for a few seconds when the physical inducer was suddenly removed (Figure 7.4). Those percepts could also be seen by rapidly displacing the gaze throughout the visual scene. Moreover, in stroboscopic light at rates of few flashes per second, subjects reported similar opponent planform overlaying the geometric inducer physically presented. Finally, during exposure to TV's empty channels noise seen through geometric transparent masks, subjects reported vivid and continuous perception of pixels aggregate streaming orthogonally to the geometric inducer, forming dynamic and stable over time opponent planforms whose strength varied across empty TV's channels noise.

That last experiment was crucial: it first suggested that the noise statistics were of importance in geometric hallucinatory-like pattern perception and second, it extended those perceptual phenomena to invariant and stable events over time, necessary requirement to a parametrized study finally abstracting itself from subjectivity. Pursuing his work, advances in psychophysical discoveries allowed MacKay to introduce the notion that adaptation mechanisms to a geometric planform resulted in perception of its opponent one (MacKay, 1964). In parallel, since the 20's, a physiological psychologist, Heinrich Klüver, gathered for years reports of geometric hallucinatory percepts and led experiments on subjects under mescaline, marijuana and LSD. His work led to the publication of a book in 1966 that would become the reference of hallucinatory geometric percepts classification that was divided in 4 groups: the Klüver form (or "planforms") constants (Figure 7.1). More than a decade later, thanks to the electrophysiological ground-breaking findings of Hubel and Wiesel highlighting the orientation detector properties of the primary visual cortex receptive fields of the cat (1962, 1965) and of the monkey (1968), Bard Ermentrout and Jack Cowan (1979) proposed the first mathematical model of hallucinatory geometric pattern formation in the primary visual cortex. By translating the physiological parameters specific of the primary visual cortex (the orientation selectivity organization of V1, its anisotropic lateral connectivity bias) into mathematical equations, Ermentrout and Cowan demonstrated that under paroxysmal regimes of activation, V1's activity gives rise to relatively stable subsets of orientation states that results in planforms corresponding exactly to the Klüver form constants.

This *a posteriori* narration of parallel discoveries obtained in several fields simply aims to describe how, from often untrusted reports of hallucinatory geometric shapes, parametrized psychophysical studies managed to abstract themselves from subjectivity, describing phenomena that started to talk to brain physiologists. Hand in hand, the two sides of this dice inspired mathematician whose model results converged towards what was initially described as subjective: the Klüver form constants. The initial model of Ermentrout and Cowan (1979) predicted that the activity pattern that should be observed when circles and fans shapes are perceived respectively correspond to vertical and horizontal stripes of activity on the primary visual cortex (Figure 7.2). The

interdisciplinary loop that we described extended to physiological experimental results as, using perfusion by 2-Deoxy-d-Glucose marker of anesthetized macaques visually stimulated by concentric circles and radially extending lines, Tootel et al., (1982, Figure 7.3 upper panel) showed that stained cells indeed formed vertical and horizontal stripes on V1 slices after histological flattening revelation. Those findings were confirmed and extended to humans 16 years later by the same authors by the use of non-invasive fMRI (Tootel et al., 1998, Figure 7.3, lower panel).

Perhaps the most inspired part of Ermentrout and Cowan's initial work (1979) was their focus on the emergence of purely hallucinatory geometric percepts, reflecting the "autonomous activity" of the brain that we now more commonly call "ongoing activity". Indeed, by letting aside hallucinatory-like geometric percepts induced by physical visual stimulation by a uniform flickering field or by a geometric inducer combined with noise, the spirit tainting their work not only showed that some Klüver form constants emerged as some of the most stable states of V1 under paroxysmal activation but emphasized the prominent self-organization property of ongoing activity. Finally, the experimental work of Billock and Tsou (2007) amplified the potential electrophysiological detectability of hallucinatory-like geometric planform waves of activity as their major contribution was to combine a geometric inducer with spatiotemporally filtered pink noise whose power law decreases in $1/f^{\alpha}$. Their deep exploration of noise statistics up to spatio-temporal exponents characteristics of natural images greatly improved the strength of induced percepts of pulsating circles and rotating fans shapes when compared to the initial observations of MacKay (1957 a,b). Moreover, their tremendous effort of correlation between psychophysical evidence of hallucinatory-like percepts and more recent theoretical models of hallucinatory pattern formation in V1 reinforced the involvement of this latter in geometric hallucinations by providing clues potentially extending the scope of their detectability at the electrophysiological level (Billock and Tsou, 2012).

Peter Tass (1995) deepened the mathematical implications of Ermentrout and Cowan's initial model (1979) and developed a mathematical framework accounting for the evolution of V1 activity during geometric pattern formation, leading to the first formalization of dynamic and propagating waves of activity corresponding to geometric percepts in V1 (1997). Paul Bressloff worked in collaboration with several persons, including his mentor Jack Cowan to extend the initial model of hallucinatory pattern formation to static and dynamic ones. This work resulted in a new model covering not only type I and II Klüver form constants (corresponding to non-contoured planforms on V1's surface, including fans shapes and concentric circles) but also type III and IV contoured planforms (Bressloff et al., 2001, 2002; Figure 7.8). In particular, under the equivariant branching lemma (Golubitsky and Schaeffer, 1985), Bressloff and colleagues showed that both the pattern of lateral connections between orientation patches and the activity conveyed by those connections were left unchanged under shift in cortical spatial position and rotation in orientation label. The implications of those findings jump to the mind while thinking to pulsating circles and rotating fans shapes. However, none of those models aimed at describing the emergence of geometric pattern under visual stimulation by an opponent planform because they focused on the self-organization of V1 ongoing

activity and on its physiological consequences, i.e, the formation of stripes or spots on the primary visual cortex surface.

II-5.2. Lateral diffusion of repulsive shift in orientation between neighbouring hypercolumns as a potential mechanism of neural stripe formation on V1

Because we were first interested in the immediate and stable over time experimental induction of hallucinatory-like geometric planforms, we had to develop a physiologically plausible conceptual framework explaining how, from a mechanistic point of view can presentation of a geometric inducer results in the emergence of its opponent planform in V1. That is why, at the theoretical level, we developed a rather elementary phenomenological model of interacting hypercolumns that first explains how a single active orientation state emerges in an hypercolumn. In a second time, our model details how this initial selection leads to a neighbour to neighbour spatial propagation of repulsive shift in orientation via long-distance horizontal connections. Our model implements biologically plausible anatomical substrates and physiological processes subtending the self-organization of ongoing activity, which results in the smooth transition of orientation distribution found along a cortical neural stripe of activity in the primary visual cortex. In a second time, we detailed how the physical presentation of a geometric inducer constrains the activity subset of potential orientation state activation and how it modulates the dynamic of interaction between feedforward and ongoing activity self-organization.

To our knowledge, no one proposed an explanation detailing the agents (active patches of orientation within a single hypercolulmn) that compete (their behaviour) via mutual repulsive shift in orientation (the mechanism) to select a single dominant active orientation state within a V1 Hubel and Wiesel original “unit”. There lies the novelty of our model: the extension to an entire hypercolumn of mutual repulsive shift between neighbouring activated patches of orientation. That extension to an entire hypercolumn results from our assumption that global cortical increase in excitability provides a weak homogeneous isotropic activation of each orientation domains in a single hypercolumn. Functionally, this is analogous to Bressloff et al., (2001, 2002) assumption that within a V1 unit, orientation patches mutually excite each other in an isotropic fashion. At some point, within an hypercolumn the activity within an orientation domain inflates, which can be seen as the “random” initial conditions dictating the overall behaviour of pattern formation of Tass model (1997). According to which surrounding orientation patch exerts the strongest repulsive shift, this inflated hill of activity initiates a transitional propagating wave of activity rotating on the polar ring, locally leaving a void of repulsive shift pursued by its neighbour while exerting a repulsive shift on the orientation domains towards which it converges, creating an overall rotational displacement of activity across the hypercolumn domain (Figure 8.5.1).

The key assumption of our model is the increase in activity of the strongest transitional wave of activity as it rotates on the ring and, to a smaller extent, of its neighbouring ones. It first allows the

selection of a single dominant orientation in an hypercolumn, when mutual repulsive shift exerted by active surrounding orientation patches have absorbed the initial compression exerted by the strongest transitional wave of activity, generating an opposite extension force that stabilizes the travelling wave by stopping it. In parallel, the combination of activity rotating on the ring to the increase of this latter provides a rotational imprint gradient of increasing strength on similar orientation patches of an adjacent hypercolumn in the same initial conditions than the first one via strong long-distance lateral connections. During this increase in cortical activation, the rotational gradient imprint of activity conveyed by long distance lateral connections allows a step by step spatial jump between neighbouring hypercolumns that undergo the same transitional rotating phenomenon but starting from a slightly different orientation that follows the orientation gradient imprint of each spatial location (Figure 8.5.2).

This reverberation recruits iso-orientation preference reciprocal lateral connections and the transitional orientation wave initially constrained in a single hypercolumn gives birth to an intracortical wave propagating over space and time, linking in a nested way neighbouring but slightly repulsive orientation domains across hypercolumns (Figure 8.5.3). While the wave propagates in the cortex, the more progressive the shift across orientations is in adjacent units, the more stable this state becomes because the neighbour to neighbour stabilizing influence exerted by each unit grows as the number of hypercolumns stabilized in neighbouring orientation states increases, maintaining and diffusing a mean field equilibrium regime of activity (Figure 8.5.3). Because of the dynamic nature of the phenomenon that we describe, one might see a parallel between the phase transition of orientation distribution explained by our model and the phase diffusion reported by Peter Tass in his model of dynamic propagation of hallucinatory geometric pattern (Tass, 1997).

During visual stimulation, presentation of a geometric inducer provokes an adaptation phenomenon where the local orientation of each feature of the inducer creates a repulsive shift whose influence is minimal at orthogonal orientations. Addition of noise provides a continuous isotropic perturbation guiding cortical activity into each local attractor orientation orthogonal to the geometric inducer. MacKay (1957a) initially described fans-shapes and concentric circles as highly redundant stimuli where, in order to profit from such redundancy, the system must reduce the number of degrees of freedom of the signalling system to increase informational efficiency. It is conceivable that the number of degrees of freedom of the V1 network signalling is indeed highly reduced by the presentation of a redundant geometric inducer down to the signalling of an opponent planform. From a systemic point of view, complementary planform propagation can be seen as a reaction of the V1 network signalling a saturation response to the geometric inducer orientation. During after-effects, opponent planforms diffuse for a few seconds antagonist information resetting balance to the previously adapted population by maximising detectability of the most relevant contextual information that was missing while the geometric inducer was present. However, when the geometric inducer is continuously presented, under global excitation this antagonistic diffusion maximizing non-redundant relevant information is continuously generated.

II-5.3. Multiscale evidence of repulsive shift in orientation as the substrate of our model

Our model takes its roots in psychophysical, electrophysiological and modelling evidence of repulsive shift in orientation and simply extends their scope to a set of hypercolumns linked by strong reciprocal lateral connections. Up to now, repulsive shift in orientation has been successfully modelled between only two neighbouring patches of orientation within a single hypercolumn (Paradiso, 1988; Figure 8.2; Bednar and Mikkulainen 2000; Jin et al., 2005). This repulsive shift in orientation originally comes from psychophysical studies reporting an angular extension of 10-20° between two lines segments presented concomitantly to human observers, phenomenon also known as the tilt illusion (Blakemore et al., 1970; Westheimer et al., 1976; Mitchell and Muir, 1976; O'Toole and Wenderoth, 1977; Wenderoth and Johnstone, 1988, Westheimer, 1989, 1990). Modelling of such phenomena has been inspired by the proposition of Blackemore et al., (1970), who were the first to introduce the idea that summation of Mexican Hat like profiles of activity evoked by two spatially adjacent lines would lead to a displacement of the orientation peak of activity away from each other.

However, the spatial scale of those psychophysical findings indicates that not only one, but several hypercolumns are involved in this phenomenon, a notion incorporated in our model. Electrophysiological evidence of repulsive shift in orientations has also been obtained in the cat and Non-Human Primate: orientation preference of neurons shift away from the orientation of the preceding stimulus (Clifford et al., 2001; Dragoi et al., 2000b, 2002; Felsen et al., 2002; Muller et al., 1999; Patterson et al., 2013, 2014; Wissig and Kohn, 2012). From electrophysiological data, Del Mar Quiroga et al., (2016) proposed a model that captured very well the amplitude and temporal dynamics of repulsive shifts in orientation found in the cat (Felsen et al., 2002) and in the macaque V1 (Patterson et al., 2013). By implementing a model of recurrent connections within a single hypercolumn, the simulations of Del Mar Quiroga and colleagues showed that repulsive shift in orientation likely results from an adaptation mechanism that does not require any form of plasticity but emerges as a natural behavior of the V1 network, a notion that confers plausibility to our model.

Importantly, their simulations showed that only in the small range of orientation repulsion reported in psychophysics (20°), activity's profile between two oriented stimuli sequentially presented to a neuron corresponds to a transitional wave of activity travelling in a virtual orientation space that progressively gains in amplitude, which corresponds to our model key assumption. Throughout several hypercolumns, using VSDI Benucci et al., (2009) found in the cat V1 spatial shifts across distinct orientation domains with a dynamic compatible with the results of Del Mar Quiroga et al., (2016). Moreover, the long-lasting (1 second) adaptation mechanism reported by Del Mar Quiroga and colleagues is compatible with the dynamic of smooth transition between neighboring orientation domains found in the cat V1 ongoing activity by Kenet et al., (2003).

II-5.4. Potential implications and parametrization

In their experiments, Kenet et al., (2003) first used VSDI to map the orientation preference of neurons in area 17 and 18 of the anesthetized cat using a large number of gratings of different orientations, which allowed them to obtain forty templates of orientation activation. The correlation of those templates with the temporal dynamic of ongoing activity of their data revealed spontaneous transition between approximately 5° neighbouring states of orientation spanning 180° over a time course with a slowest dynamic of approximately 1 second. This transition profile of activity is in accordance with our model prediction of slow diffusion of very slight repulsive shift in orientation. Moreover, the slow temporal dynamic of orientation transition described by Kenet and colleagues matches the 1 second long-lasting repulsive shift obtained in Del Mar Quiroga et al., (2016) simulations.

In parallel, Kenet and colleagues observed that some orientation states (cardinal orientations) occur more often than oblique orientations (about 20%). We wonder whether this differential distribution of orientation might reflect the initial spark of orientation activation corresponding to the emergence of our transitional wave of activity. Determining whether or not this differential distribution is locally heterogeneous across distinct cortical loci along a neural stripe of activity (i.e, for a same given retinal eccentricity, along the antero-posterior axis of the brain) would allow us to evaluate if the activation emergence of a specific orientation can occur at any cortical location along a stripe or not. Additionally, the smooth orientation transition described by Kenet et al., (2003) does not correspond to any particular increase in cortical excitability, prerequisite to the formation of hallucinatory pattern formation. We suspect that homogeneous global activation of V1 by electric stimulation or homogeneous visual isotropic stimulation might greatly strengthen the orientation transition dynamic that they observed.

We do not claim that the findings of Kenet et al., (2003) reflects the organization of ongoing activity as this latter has a much richer dynamic and cannot be reduced to the exploration of neighbouring orientations. Moreover, the detection of neighbouring orientation pattern activation strongly depends on the algorithm used to match templates of orientation activity to actual data. Nevertheless, those findings do provide a fertile terrain implying that ongoing activity spontaneously visit neighbouring orientation states, a solid experimental ground for any model of geometric activity pattern formation in the primary visual cortex. In addition, the report of Kenet et al (2003) inscribe itself in a more global experimental framework suggesting that ongoing activity presents a progressive and remarkably well organized stereotypic sequential activation (Luczak et al., 2007).

Those findings extend from the anesthetized to the awake state of rats in auditory as well as somatosensory cortices (Luczak et al., 2009) and support the notion that selection of activity emerges from the interaction of sensory evoked activity that acts as an attractor to guide the larger subset of possible ongoing activation states (awake and anesthetized rat: Luczak et al., 2009; awake and anesthetized ferret: Fiser et al., 2004). The combination of those results builds a context that

confers plausibility to our model's assumption that presentation of a geometric inducer combined with noise constrains the organisation of the primary visual cortex activity that self-organizes itself to converge towards the strongest attractors domains of orientation locally orthogonals to a geometric inducer's features.

Even if our model provides plausible conditions of physiological interactions allowing the emergence of a neural stripe of activity on the primary visual cortex surface, it still needs parametrization. We see several parameters that should be incorporated in view of future simulations: the number of orientations to consider within a single hypercolumn, the mexican hat amplitude and spatial spread distribution of each orientation patch according to its level of activation, the number of hypercolumns along a single stripe, their spacing as well as the relative strength of strong reciprocal lateral connections regarding local ones. The incorporation of biologically plausible values of those parameters and of their interplay in distinct species should allow us to determine if our model's results remain within a physiologically and psychophysically plausible range compatible with the dynamic of activity emergence and diffusion of purely hallucinatory and hallucinatory-like visually induced geometric patterns. More specifically, it should allow us to determine if the relatively low speed of horizontal connectivity (0.05 - 0.5 m/s) can account for the stabilization of an entire stripe of activity while still remaining in the long-lasting range of repulsive shift adaptation (1 second), something that seems plausible but should especially be tested during global perturbation devoid of anistropic content.

Finally, our model only accounts for the formation of stripes of neural activity on V1's surface where the step by step transmission of repulsive shift may correspond to the typical profile of sub-Riemannian geodesics forming the co-circular orbits of the association field of Hayes, Hess and Field (Field, Hess and Hayes, 1993) modelled by Jean Petitot (2003, Figure 11.1 A,a). At the anatomical level, horizontal connections axonic arborizations spread over large distance and are elongated along the preferred orientation axis of a given cell's RF (cat: Gilbert and Wiesel, 1983, 1989; Schmidt et al., 1997a; macaque: McGuire et al., 1991; Malach et al., 1993; Grinvald et al., 1994, squirrel monkey: Sincish and Blasdel, 2001). Along that particular axis, lateral connections extend over larger distances and make more connections (superior by a factor of 4 on average) regarding the width axis (tupaia: Fitzpatrick, 1996; Bosking et al., 1997). The functional impact of this anisotropic bias of horizontal connections has already been described by our lab (Gérard-Mercier et al., 2016). Moreover, in the first part of this thesis, our results indicate that iso-aligned elements forming flows that converge towards the RF center of a target cell at high speed results in a fibration of activity along the main axis of a cell resulting in a latency advance and boosting of the response.

Our model's implications however extend beyond the particular case of neural stripes formation on V1 as from an experimental point of view, the curvature constraint of these association fields follows the psychophysical and anatomical findings that lateral binding between neighbouring detectors has a tolerance of +/- 20°. We believe that this tolerance upper limit should be implemented as a constraint bias of horizontal connections anisotropy in mathematical equations

of geometric pattern formation. The geodesics study of neighbour to neighbour propagation of lateral activity does not necessarily follow a straight path on the cortical surface nor on the visual field (Figure 11.1 A, b). This can lead to sets of curved hallucinatory patterns corresponding to more complex type III and IV Klüver form constants corresponding to contoured planforms (Figure 11.1 B; Frégnac, 2003; Duits et al., 2014).

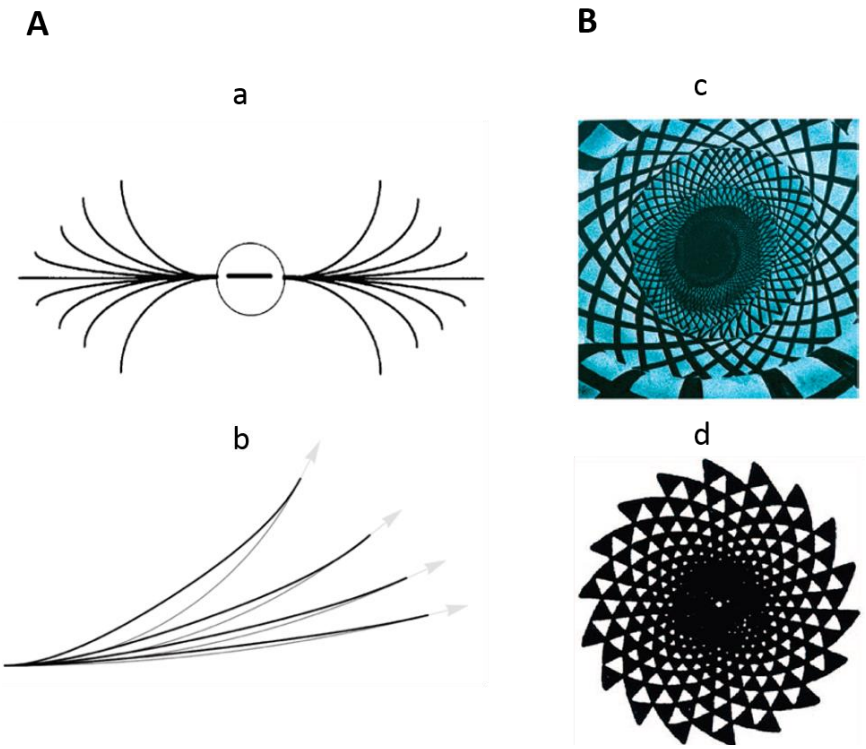

Figure.11.1: ***Geodesics of association fields and complex contoured planforms. A.*** *Modelling the association field with sub-Riemannian geodesics and exponential curves.* ***(a)*** *The association field originally described by Field, Hess and Hayes., (1993).* ***(b)*** *Comparison of sub-Riemannian geodesics with exponential curves with the same (co-circularity) ending conditions (grey arrows; from Duits et al., 2014).* ***B.*** *Examples of complex contoured planforms in the visual field.* ***(c)*** *Complicated lattice-like patterns produced by THC intoxication (Siegel and Jarvik, 1975) and by binocular eye pressure* ***(d)*** *(Tyler, 1978).*

II-5.5. Experimental framework: subthreshold detectability of hallucinatory-like propagating waves of activity by intracellular recordings in the cat V1

At the experimental level, we developed a set of visual stimuli reproducing the findings of Billock and Tsou (2007). In our hands the combination of fans shapes and concentric circles physical inducers to spatiotemporally filtered noise following a power spectral law of $1/f^{\alpha}$ possessing natural image statistics (αs = 1.4; 1,4 -1,8: Knill et al., 1990; 1.1-1.35: Billock, 2000; Billock et al., 2001 a,b) also immediately induced the continuous perception of opponent planforms of pulsating circles and rotating fans shapes, respectively.

We adapted and modified those stimuli to probe in vivo, at the single cell level of the anaesthetized and paralyzed cat, the existence and the detectability of hallucinatory-like propagating waves of activity corresponding to the induced geometric percepts. We did so under the assumption that the perceptual effects should be observable at the subconscious level of anaesthetized animals since they do not require attention and emerge as a "pop-out" feature of perception. We also worked under the assumption that perception between human/non-human primates and cat is sufficiently similar to capture such effects.

Several studies addressing perceptual similarities and physiological correlates led us to those assumptions. First, the awake behaving cat is able to perceive illusory squares contours in an apparent motion paradigm in the same conditions and with performances comparable to human (Bravo et al., 1988). Second, even in the low level perceptual state of the anesthetized cat, interaction of feedforward and lateral activity of the primary visual cortex results in a spatio-temporal diffusion of activity that lies exactly in the range of induction of the line motion illusion effect in human (cat: Jancke et al., human: 2004; Hikosaka et al., 1993). The distribution of orientation preference of the surround of a cat receptive field (Gérard-Mercier et al., 2016) displays a striking resemblance with the perceptual association field described in psychophysics by Hayes, Hess and Field (1993). Moreover, perceptual correlates of the speed-up effect reported in psychophysics (Georges et al., 2002) are detectable at the single cell level of the anesthetized cat (results of the first part of this thesis) and match the modelling predictions of such phenomenon in human (Series et al., 2003).

Those arguments are to us as many clues strengthening our interpretation that perception of cat and human is sufficiently similar to test for the sensitivity of cat individual cells to hallucinatory-like waves of activity, since numerous physiological correlates of human illusory percepts have been successfully obtained down to the single cell level of anesthetized cats. Moreover, this similarity extends to the low-level perceptual state of the anesthetised animal in primary areas such as the primary visual cortex, which advocates for the legitimacy of our approach.

To test for the detectability of hallucinatory-like propagating waves of activity corresponding to induced percepts at the single cell level, we designed a series of control conditions to prove the need of a synergistic interaction between noise and geometric inducer in the emergence of the

percepts, something that is necessary at the psychophysical level (Billock and Tsou, 2007). Moreover, to prove the geometric distribution of the propagating waves of activity, we took advantage of the orientation detector properties of V1 receptive fields and manipulated the position of the geometric inducer center so that, at the psychophysical level, the predicted wavefront of the propagating waves was locally parallel to the cell's preferred orientation. We did so under the assumption that propagating waves of activity would only be detectable at the single cell level under that condition. Moreover, working at the level of single cells, we had to avoid potential adaptation and completion phenomenon due to the presentation of geometric inducers. To that end, the subthreshold Depolarising Field of our recorded cells was placed in an opening that was smoothly attenuated to progressively resemble the content of the receptive field surround.

We therefore did not only test for the single detectability of propagating waves of activity but for filling-in of this latter in the opening encompassing the sDF. The plausibility of this expectation derives from the description of type I and II noncontoured planforms (including fans shapes and concentric circles) by Bressloff et al., (2001,2002). Bressloff and colleagues hypothesized that type I and II non-contoured planforms could arise from a filling-in process, an assumption according to which we envision that the differential magnification factor modifies the activity of a neural stripe ofactivity that locally change in position and orientation label as it travels on the cortical surface. Under such conditions, our hypothesis is that activity filling-in between neighbouring hypercolumns via horizontal connections allows completion, thereby preserving the initial geometry of the stripe of activity.

At the experimental level, to facilitate filling-in phenomena, the opening encompassing the sDF was continuously filled with spatiotemporally filtered noise similar to the one of the surround, decreasing in that way contrast between surrounding noise where pixels aggregates form the percepts and the opening. The experimental choice of presenting noise in the opening also pertained to the theoretical prediction that an increase in cortical activity is necessary to the formation of hallucinatory pattern by locally maintaining a continuous excitation, necessary condition to the invasion of hallucinatory-like waves of activity in a geometrically unstructured area. To our Knowledge, an experimental attempt intended to prove the existence of hallucinatory-like waves of activity and their geometric nature in the primary visual cortex has never been done in any species, neither by using non-invasive electrophysiological techniques nor by the use of invasive ones.

II-5.6. Neural stripe formation and propagation refractory period as a signature of an intrinsic clock of the primary visual cortex

Contrarily to Billock and Tsou, we were not primarily interested in the description of the induced percepts stability and reproducibility over time at the psychophysical level but to their electrophysiological signature detectability at the single cell under the form of oscillations

corresponding to propagating waves of activity whose oscillatory dynamic would match the perceived dynamic of the induced percepts. That is why, contrarily to them, we did not use the same single noise sequence across trials but used different noise sequences across trials and conditions. At the psychophysical level, the use of a single noise sequence across repetitions is indeed sufficient to detect and report continuous perception of pulsating circles and rotating fans-shapes as the overall binding process occurs at a global scale encompassing the entire visual scene where the local characteristics of the noise has little impact on the overall extraction of the percept's coherence. Locally, at the level of a single cell receptive field, the picture is different. Even though intracellular recordings allow to capture the "synaptic rumour" (Fregnac, 2004) that reflects the synaptic bombardment that a single cell receives, the overall spatial extent of information integration of a single cell is by definition restricted since the monosynaptic extent of proximal lateral connections defining the subthreshold depolarizing field covers about 2.5° from each side of the sDF center in the cat V1 (Bringuier et al., 1999).

In psychophysics, pulsating circles and rotating fans shapes percepts were described as faint shadowy dark shapes overlaying noise and geometric inducers (Billock and Tsou, 2007). The use of a single noise sequence does not contain by definition any periodicity as the luminance of the noise locally varies over time, giving birth from time to time to shapeless dark spots in the opening encompassing the sDF, which prevents filling phenomena of the surrounding propagating wave of activity. That is why we used different noise sequences across trials, in the hope that the spatio-temporal characteristics of each noise sequence feedforward input that might compete with lateral filling-in phenomena would cancel out across trials, allowing the extraction of the subjacent resonance frequency of V1 characteristic of the percepts dynamic.

The notion of resonance frequency of the system is no stranger to us as Billock and Tsou initially reported in their study (2007) that perception of induced pulsating circles and rotating fans-shapes was locked to the stimulus onset and that perceived speed was constant for a given spatio-temporal filtering of the noise. Our observations concur with the ones of Billock and Tsou (2007) since in our hands induced pulsating circles and rotating fans shapes were immediately perceived at the stimulus onset and their speed did not vary over time although we used different noise sequences across trials. This advocates in favour of the importance of the global statistics of the noise sequences in the emergence of the percept, that must be preserved across distinct noise sequences used in distinct trials. According to the conceptual framework of our model, the combination of pink noise with a $1/f^{\alpha}$ power spectral law corresponding to natural statistics to which the V1 network is tuned to allows the binding of cells falling into the attractor orientation locally orthogonal to the physical inducer by its scale invariance. This scale invariance covers both distinct spatial scales and temporal refractory periods. The dynamic of activity's convergence towards opponent planforms is therefore reduced as each orientation locally orthogonal to the geometric inducer simultaneously acts as local attractors.

Additionally, the resonance frequency of the network as a signature of the percepts dynamic periodicity is reminiscent of the mathematical model of hallucinatory pattern formation, selection

and propagation of Peter Tass (1997) who demonstrated that an oscillatory instability gives rises to dynamic propagating percepts (including travelling waves of pulsating circles and rotating fans shapes). This strongly strengthen our interpretation that oscillatory instability occurring during perception of dynamic hallucinatory-like percepts is the signature of travelling waves of activity. To us, this periodicity corresponds to an intrinsic clock of the V1 network that reflects the refractory period of neural stripes formation under specific continuous dense stimulation by $1/f^{\alpha}$ noise.

Our preliminary results suggest that hallucinatory-like induced travelling waves of activity do emerge in the primary visual cortex and that their geometric nature is detectable at the level of single cells. Our findings do not extend to our two conditions of interest but only to the first one where induced pulsating circles have a predicted wavefront locally tangent to the cell's preferred orientation. For that condition, a particular oscillatory activity corresponding to 3-4 Hz oscillations emerged at the individual cell and population level. This oscillatory behaviour lies exactly in the 3-3.5 Hz range of our preliminary psychophysical observations on the perceived dynamic of the induced percept. To our opinion, this oscillatory behaviour is not artefactual because we did not retrieve it for control conditions where no percept is induced, in spite of their large number (8), nor in conditions where the percept is locally orthogonal to the cell's preferred orientation.

In our population, 3-4 Hz induced oscillations of our primary condition of interest were present in individual trials in a larger proportion than in any other frequency bin, surpassing all other conditions. The average cross power spectral density revealed that those oscillations frequency taken as the signal was shared and consistent over time across trials in a greater proportion than for control conditions. Moreover, the phase of the average cross spectrum between each pair of trials for that frequency displayed a relative decrease regarding other ones, tending towards zero. In our condition of interest, the combination of coherent induced oscillations having a similar phase between each trial to the contrary of any other frequency and control conditions naturally resulted in an increase of stimulus locked oscillations retrieved in the average PSTWS. Those results were obtained in spite of the use of different noise sequences in between trials and conditions. This strongly advocates for the extraction of a coherent oscillatory signal emerging during the summation of the averaging process because of its phase-locked relationship preserved across trials while trial to trial unspecific noise component mutually cancel out.

In one cell where all control conditions were presented, the summation of 3Hz oscillations during the averaging process resulted in sustained phase locked oscillations of the average PSTW only resembling itself at that single frequency. It probably reflects an extreme case of summation of a single frequency across trials during the averaging process. The autocorrelation function of the individual trials for that cell's condition of interest did not show any resemblance over time, indicating that 3 Hz oscillations were not sustained over the entire time course of individual trials, drown by the unspecific noise dominating in individual trials as showed by our signal-to-noise ratio analysis.

Nevertheless, the fact that we retrieve those oscillations in the frequency domain of individual trials combined to the relatively weak dephasing of the signal oscillatory behaviour across repetitions

resulting in stimulus-locked oscillations in the average PSTW indicates reproducibility over time. We attribute this reproducibility to a stimulus-locked clock of the primary visual cortex that generates periodic input pattern to the Vm on which the noise intermittently produces facilitatory effect on certain cycle summation, depending on its local contrast regarding the surrounding noise, allowing or preventing filling-in phenomena during certain temporal windows. This intermittent facilitation explains why the ACF of single trials is not sustained over time. Second, the reproducibility of 3-4 Hz oscillations resulting in stimulus-locked oscillations of the average PSTW indicate intermittent facilitation that are homogeneously distributed over time across trials. We interpret this temporal homogeneity as the detection at the single cell level of travalling waves of activity corresponding to the percept's propagation and to its reproducibility over time, when the local luminance of the noise in the opening encompassing the sDF had a weak contrast regarding the surrounding noise, allowing the propagating wave of activity to fill-in the geometrically unstructured area.

This reading of our results is compatible with our interpretation that the use of a single noise sequence does not allow completion phenomena of the surrounding propagating waves of activity during the entire time course of a single trial as a single noise sequence constantly evolves. Consequently, the local characteristics of each noise sequence at a given time prevents filling in phenomena of the subjacent periodic input pattern, resulting in a dominance of the noise. On the other hand, the richness of different noise sequences provides an increasing number of temporal windows where the local characteristics of the noise in the opening encompassing the sDF allows filling phenomena. During the summation process of the averaging, the spatiotemporal characteristics specific to each noise sequence and representing the actual noise in our cells responses cancel out as it is never repeated twice.

In two other cells of our pool, during pre-protocols where the number of control conditions was reduced, we did find a similar stimulus-locked oscillatory behaviour only for our primary condition of interest but not for control conditions. Interestingly, this suggests that the temporal dynamic of stimulation might play an important role in the entrainment of the network towards a single oscillatory frequency since the delay between the presentation of conditions where the percepts were induced was reduced.

In another cell where all control conditions were presented, we did find a similar stimulus locked oscillatory behaviour of the same frequency in the autocorrelation of the average PSTWS, but only for conditions where geometric percepts were induced. Those conditions correspond to our second condition of interest – where induced rotating fans have a wavefront locally tangent to the cell's preferred orientation – and to the condition where induced pulsating circles predicted wavefront is locally orthogonal to the cell's preferred orientation. This might reflect a broader orientation tuning sensitivity of that cell to induced percepts as we also found in the frequency domain a peak at 3.5 Hz for our primary condition of interest that was not present for control conditions where no percept is induced.

Three hertz oscillatory behaviour was only retrieved at the population level for our primary condition of interest. First, it argues for the importance of the geometric nature of the percept in its

detectability at the single cell level and second, for a greater saliency and reproducibility of induced pulsating circles regarding induced rotating fans-shapes. At the psychophysical level, rotating-fans shapes are indeed reported as rotating both in clockwise and anticlockwise fashion while pulsating circles are much more often reported as pulsating from the center towards the periphery rather than wobble (Billock and Tsou, 2007; Wilkinson, 2004). According to the framework of our model, during the perception of dynamic concentric circles, the first stripe of activity to form is the closest one to the area centralis (Figure 8.1, right panel). A likely explanation is that the distance that horizontally propagated activity has to cover in order to synchronize hypercolumns in neighbouring states of orientation is smaller than at larger eccentricities, explaining why the first stripe to form is the closest to the area centralis. This hypothesis explains how this first stripe forms and then propagates towards the periphery and why it appears at the same initial spatial position at each trial, necessary condition to capture phase locked oscillations.

On the other hand, each horizontal stripe of neural activity on V1 - corresponding to fans-shapes percept - form along different axes of increasing eccentricity. Therefore, laterally propagated activity does not cover shorter distances to form each stripe. From a dynamic point of view, this suggest that for each visual hemifield, each vertical stripe could propagate both anteriorly and posteriorly, leading at the cortical level to colliding waves of activity. This might result in perception of a dominant rotation for a few seconds before alternating with the opposite direction or their superposition, phenomenon that we do observe in our visual stimuli. In addition, even at the small distance at which we placed our receptive field regarding the geometric inducer center position (1,5 sDF away), the spatial period of induced rotating fans shapes is superior to the one of pulsating circles, which might reduce the detectability of their geometric impact regarding the fine orientation sensitivity and relatively high spatial period tuning of V1 cells.

The signal to noise ratio of our cells responses at the population level of our primary condition of interest was the greatest of all conditions in the 3-4 Hz frequency bin. That value dominated all other conditions and frequencies when we did not integrate it over the entire time course of the stimulation but focused for each cell and condition to temporal periods giving the highest SNR value, all frequencies considered. Nevertheless, this value is weak (0.3 -0.37). We do no find this surprising, considering that we used a different noise across each trial, that we aimed at probing filling-in phenomena and that the perceptual saliency of induced pulsating circles is weak and cannot be compared to the physical feedforward presentation of actual pulsating circles.

The single cell example that we presented in the Part II – Results section showed a weak SNR value that was not stationary but that remained nevertheless the most stable one over time for our condition of interest in the 3-4 Hz bandwidth. This was not the case for all our cells where the 3-4 Hz bandwidth SNR value was often restricted to 1-2 seconds, in temporal windows that varied across cells but that were still long-enough to be considered as a perceptual correlate. Interestingly, Funke et al., (2007) obtained results that can be linked to ours. Using single unit recordings in the anesthetized and paralyzed cat V1, Funke and colleagues characterized the SNR response of several dozens of cells according to the noise level that they presented. In their experiments, they did not

use pink noise as we did but jitter of bars of optimal orientation or brightness modulation. In their experiments, the noise level was characterized as the standard deviation of the jitter or luminance modulation that they applied.

They found that stochastic resonance phenomena induced by noise amplified the strength of initially weak responses eliciting sub-threshold or slightly suprathreshold responses. At supra-threshold level, noise did not induce a stochastic resonance increase of the response SNR and only intermediate noise levels amplified the SNR of the initially subthreshold responses. The findings of Funke and colleagues are in accordance with previous reports describing a facilitatory effect of initially weak responses by noise-induced stochastic resonance, notably in visual perception (Simonotto et al., 1997; Ditzinger et al., 2000; Mori and Kai, 2002). Nevertheless, the comparison of Funke and colleagues results with ours is particularly relevant because it was the first report of visual cortex increase of SNR via stochastic resonance. In their data, they found an increase in the SNR of cell's responses that was correlated with a modulation of the Inter spike interval distribution and the mean firing rate of cells, two parameters that varied a lot from cell to cell. Those results precisely highlight the inter-cellular temporal heterogeneity of stochastic resonance amplification of SNR responses across cells, something that we do observe in our sample where maximal SNR values did not emerge in the same temporal window across cells.

Second, they found that in spite of the heterogeneity of their cells, 85 % presented a noise induced stochastic resonance amplification of the SNR. Third, even cells having an initially weak SNR value (0 - 0.5) displayed an SNR amplification under the presentation of noise. Finally, in their recordings they found cells displaying an heterogeneity of behaviour as some of them showed an increase in SNR up to a certain level of noise and then a decline while others showed a continuous decrease in SNR at increasing noise level. In our experiments, the input noise "level" can be measured as two different parameters: the temporal filtering of the noise and the standard deviation of the luminance of this latter. As in the recordings of Funke et al., (2007), among our pool, it is conceivable that the noise that we applied was not "optimal" for each cell. Some of them indeed showed a temporally localized SNR increase in the 3-4 Hz bandwidth of our condition of interest that was not maintained throughout the overall time course of stimulation.

This behaviour may stem from the individual sensitivity of each cell to the spatio-temporal characteristics of the noise. This interpretation is compatible with the view of Wenning and Obermayer (2003) who proposed that an "activity-driven stochastic resonance" adaptation phenomena could happen at the level of a single cortical neuron. According to them, this adaptative mechanism would take place via an intrinsic feedback mechanism where a powerful source of active noise response suppression may evolve from the cortical pattern of connectivity with long-range lateral projections. At the level of our population, cells having long-distance horizontal connections might indeed be more sensitive to surrounding filling-in activity but we could not make that correlation because of the small size of our sample and of the difficulty to systematically stain cells.

Finally, taking into account the distance between our receptive field and the geometric inducer center, diffusion of 3 Hz oscillations correspond to propagating waves travelling at a speed of 0.02 m/s, a speed below the lower limit of lateral connections conduction velocity (0.05 -0.5 m/s) that further suggests rolling waves of activity (see Discussion part I). However, the faster conduction velocity of lateral connections (0.05 -0.5 m/s) can very well account for the transmission of activity filling in between neighbouring activated hypercolumns as the hallucinatory-like rolling waves of activity travel on the cortical surface.

II-5.7. Future work and potential implications

In order to determine if the 3-4 Hz oscillatory signature that we observed in our condition of interest is present in a significant proportion of cells of the primary visual cortex, we should first increase the size of our sample. Second, to infer the oscillatory signature of our electrophysiological recordings as a neuronal correlate of induced pulsating circles in V1, we must conduct a proper psychophysical study in naïve subjects unaware of our preliminary observations to precisely quantify the perceived dynamic of the induced hallucinatory-like percepts. This will allow us to confirm that this latter lies within the 3-3.5 Hz of our preliminary observations. We envision in a first step an experimental paradigm where noise should be combined to a geometric inducer positioned at the center of the screen. In a second step, we would introduce an opening as in our electrophysiological experiments to test and quantify reports of percepts invading the geometrically unstructured area for long temporal periods. This would enable us to test for the evolution of the percepts strength over time via long duration recordings, a factor that is a major limitation in intracellular assessment. In spite of this limit, intracellular recordings greatly amplified the detectability of the relatively weak oscillatory behaviour of our effect down to the subthreshold level and provided us a with a first characterization of the magnitude of hallucinatory-like related oscillations in single cells of the anesthetized cat.

Nevertheless, if pulsating circles and rotating fans shapes reach the perceptual threshold and are described by subjects in psychophysical study (Billock and Tsou, 2007), they should be detectable in the awake human and non-human primate. In spite of its great sensitivity, intracellular assessment only allows to infer the dynamic of the effective input network in cortical space (Brunel et al., 2003; Fregnac, 2011, 2012). Cells recorded intracellularly are spatially localized activity sensors that serves as a basis to generalize the detected periodic activity as a wave travelling on the cortical surface. In order to demonstrate that induced percepts actually correspond to propagating waves of activity in V1, we are convinced that psychophysical studies should be combined with electroencephalogram recordings in human subjects. To the contrary of our experiments where we only used a single ECoG probe, we believe that the combination of multiple sensors distributed over the scalp surface would enhance spatial detectability of activity over time in order to reconstruct the spatiotemporal dynamic of the induced propagating waves corresponding to the percepts. Moreover, in the behaving subject, the spatial distribution of electrophysiological probes having a great temporal

sensitivity might allow the detection of periodic unintentional modulations of attentional signals linked to the perception of the induced geometric shapes in awake subjects.

More specifically, it has been shown that the direction of pulsation/rotation of many geometric and non-geometric hallucinatory-like percepts can be reversed by mental effort (Billock and Tsou, 2007; Pearson et al., 2016). The trackability of those modulatory signals origin and the nature of their influence on lower-level cortical areas targets might provide extremely interesting information on inter-area communication and specialisation in the awake subject.

At an intermediate level, VSDI experiments on awake non-human primates could allow to partially reconstruct the geometric distribution of activity on the cortical surface over time. Because of the relatively slow dynamic of the induced percepts, this experimental technique is particularly relevant in the search of neuronal correlates of hallucinatory-like induced waves of activity. The superposition of the three-dimensional map of activity obtained via voltage sensitive dye imaging on the orientation map of each area recorded on each animal might allow to detect a local adaptation to the features of a geometric inducer concomitant to the sequential activation of a set of hypercolumns corresponding to orientations locally orthogonal to the inducer's features that displace itself over space and time.

The set of experiments that we propose is rather ambitious and certainly requires further parametrization, according to each experimental expectation. However, it might allow to link the activity of individual cells in the anesthetized cat up to the conscious perception in human while detailing the spatio-temporal activation profile of orientation domains in the awake non-human primate. This multi-dimensional scale experimental framework might enable to characterize, between different species and brain states, an archetypal interaction structure between evoked and ongoing activity in higher mammals. We trust that the effort gathering psychophysical, electrophysiological, mathematical and modelling evidence of orientation interaction between ongoing and evoked activity that allowed us to construct a plausible phenomenological model will contribute to unravel the puzzling field of Neurogeometry. The set of visual stimuli that we developed as well as the underlying experimental expectations and the encouraging preliminary results of the second part of this thesis are to us a first step that we hope will help to blur the fringe between distinct fields and inspire future experiments and models.

"And who are you, the proud lord said
That I must bow so low?
Only a cat of a different coat,
That's all the truth I know.
In a coat of gold or a coat of red,
A lion still has claws,
And mine are long and sharp, my lord,
As long and sharp as yours."

Georges R. R. Martin, The rains of Castamere, A song of Ice and Fire

"Qui que je sois au fond de moi, je ne suis jugé que par mes actes."

Batman, Batman begins

"All the world's a stage,
And all the men and women merely players;
They have their exits and their entrances,
And one man in his time plays many parts,
His acts being seven ages."

William Shakespeare, As You Like It

"What we do in life echoes in Eternity."

Maximus Decimus Meridius, Gladiator

- What was real to you Daniel?
- The time in between the seconds. And my books. And my friend.

Daniel Holden, Rectify

“Nature doesn’t recognize good and evil Philip.
Nature only recognizes balance and imbalance.”

Walternate Bishop, Fringe

“The quieter you become, the more you can hear.”

Ram Dass

“Just because my path is different doesn’t mean I’m lost.”

Gerard Abrams

“Tell me and I will forget. Show me and I will remember. Involve me and I will understand.”

Confucius

“As Black Rolf had once shown me, much discomfort was based on human expectations. As a man, I expected to be warm and dry when I chose to be. Animals did not harbour any such beliefs. So it was raining. That part of me that was wolf could accept that. Rain meant being cold and wet. Once I acknowledged that and stopped comparing it to what I wished it to be, the conditions were far more tolerable. I set out. Leave the pain behind and let your life be your own again. There is a place where all time is now, and the choices are simple and always your own. Wolves have no kings.”

FitzChivalry Farseer, Robin Hobb

Bibliography

Adams, R. A., Perrinet, L. U., Friston, K. (2012). Smooth pursuit and visual occlusion: active inference and oculomotor control in schizophrenia. PLoS ONE: e47502.10.1371/journal.pone.0047502.

Adey, W. R., Bell, F. R., & Dennis, B. J. (1962). Effects of LSD-25, psilocybin and psilocin on temporal lobe EEG patterns & learned behavior in the cat. Neurology 12, 591-602.

Ahmed, B., Hanazaw, A., Undeman, C., Eriksson, D., Valentiniene, S., Roland, P.E. (2008). Cortical dynamics subserving visual apparent motion. Cereb Cortex;18(12):2796–2810.

Alais, D., Lorenceau, J. (2002). Perceptual grouping in the ternus display: evidence for an "association field". Vision Research, 42, pp. 1005-1016.

Albrecht, D.G, Hamilton, D.B. (1982). Striate cortex of monkey and cat: contrast response function. J Neurophysiol; 48:217–237.

Albright, T.D. (1984). Direction and orientation selectivity of neurons in visual area MT of the macaque. Journal of Neurophysiology, 52, pp. 1106-1130.

Albright T.D., Desimone R. (1987). Local precision of visuotopic organization in the middle temporal area (MT) of the macaque. Exp Brain Res. 1987; 65:582–592.

Albus, K., Wahle, P., Lubke, J. and Matute, C. (1991). The contribution of GABA-ergic neurons to horizontal intrinsic connections in upper layers of the cat's striate cortex, Exp Brain Res 85(1): 235–9.

Alfonso, S., Sendina-Nadal, I., Perez-Munuzuri V., Sancho J.M., and Sague F., Phys. Rev. Lett. 87, 078302 2001.

Alink, A., Schwiedrzik, C. M., Kohler, A., Singer, W., and Muckli, L. (2010). Stimulus predictability reduces responses in primary visual cortex. J. Neurosci. 30, 2960–2966.

Alitto, H.J., Usrey, W.M. (2008). Origin and dynamics of extraclassical suppression in the lateral geniculate nucleus of the macaque monkey. Neuron; 57:135–146.

Alitto, HJ., Usrey, W.M. (2015). Surround suppression and temporal processing of visual signals. J Neurophysiol; 113: 2605-2617.

Allman, J., Mierzon, F., McGuinness, E. (1985). Stimulus specific responses from beyond the classical receptive field: neurophysiological mechanisms for global-local comparisons in visual neurons, Ann. Rev. Neurosci. 8: 407–430.

An, X., Gong, H., Qian, L., Wang, X., Pan, Y., Zhang, X., Yang, Y., Wei Wang. (2012). Distinct Functional Organizations for Processing Different Motion Signals in V1, V2, and V4 of Macaque. The Journal of Neuroscience: The Official Journal of the Society for Neuroscience 32(39):13363-79.

An, X., Gong, H., Yin, J., Wang, x., Pan, y., Zhang, X., Lu, Y., Yang, y., Toth, Z., Schiess, I., McLoughlin, N., Wang, W. (2014). Orientation-Cue Invariant Population Responses to Contrast-Modulated and Phase-Reversed Contour Stimuli in Macaque V1 and V2. Journal.pone.0106753.

Anderson JC., Martin K.A., Whitteridge, D. (1993) Form, function, and intracortical projections of neurons in the striate cortex of the monkey Macacus nemestrinus. Cereb Cortex 3:412– 420.

Anderson, J.C., Martin, K.A. (2009). The synaptic connections between cortical areas V1 and V2 in macaque monkey. J Neurosci; 29:11283–11293

Angelucci, A., Bijanzadeh, M., Nurminen, L., Federer, F., Merlin, S., Bressloff, P.C. (2017). Circuits and Mechanisms for Surround Modulation in Visual Cortex. Annual Review of Neuroscience. Vol. 40:425-451.

Angelucci A, Bressloff P. C. (2006). The contribution of feedforward, lateral and feedback connections to the classical receptive field center and extra-classical receptive field surround of primate V1 neurons. Prog Brain Res; 154:93–121.

Angelucci, A., Bullier, J. (2003). Reaching beyond the classical receptive field of V1 neurons: horizontal or feedback axons? J. physiol. (Paris), 97(2-3), 141-154.

Angelucci, A., Levitt, J. B., Lund, J. S. (2002a). Anatomical origins of the classical receptive field and modulatory surround field of single neurons in macaque visual cortical area V1, Prog Brain Res 136: 373–88.

Angelucci, A., Levitt, J.B., Walton, E.J., Hupe, J.M., Bullier, J., Lund, J.S. (2002b). Circuits for local and global signal integration in primary visual cortex. J Neurosci; 22:8633–8646.

Angelucci, A., Sainsbury, K. (2006). Contribution of feedforward thalamic afferents and corticogeniculate feedback to the spatial summation area of macaque V1 and LGN. J Comp Neurol; 498:330–351.

Anstis, S.M., Ramachandran, V.S. (1987). Visual inertia in apparent motion. Vision Research, 27, pp. 755-764.

Bair, W., Cavanaugh, J.R., Movshon, J.A. (2003). Time Course and Time–Distance Relationships for Surround Suppression in Macaque V1 Neurons. J Neurosci; 23:7690–7701.

Baker, T.I., Issa, N.P (2005). Cortical maps of separable tuning properties predict population responses to complex visual stimuli. J Neurophysiol 94:775–787

Baldo, M. V. C., Caticha, N. (2005). Computational neurobiology of the flash-lag effect. Vision Res. 45, 2620–2630.

Barlow, H.B. (1953). Summation and inhibition in the frog's retina. J.Physiol.119, 69-88.

Barlow, H.B., Hill, R.M., Levick, W.R. (1964). Retinal ganglion cells responding selectively to direction and speed of image motion in the rabbit. J.Physiol.173, 377-407.

Bartels, A., Zeki, S., Logothetis, N.S. (2008). Natural Vision Reveals Regional Specialization to Local Motion and to Contrast-Invariant, Global Flow in the Human Brain. Cerebral Cortex, Volume 18, Issue 3, Pages 705–717.

Basole, A., White, L.E., Fitzpatrick, D. (2003). Mapping multiple stimulus features in the population response of visual cortical neurons. Nature, 423, pp. 986-990.

Bastos, A.M., Vezoli, J., Bosman, C.A., Schoffelen, Jan-Mathijs, Oostenveld, R., Dowdall, J.R., De Weerd, P., Kennedy, H., Fries, P. (2015). Visual Areas Exert Feedforward and Feedback Influences through Distinct Frequency Channels. Neuron. 85(2) :390-401.

Baudot, P., (2006). Natural computation, much ado about nothing? Thesis manuscript.

Baudot, P., Levy, M., Marre, O., Monier, C., Pananceau, M., Fregnac, Y. (2013). Animation of natural scene by virtual eye-movements evokes high precision and low noise in V1 neurons. Frontiers in Neural Circuits 7: 206.

Baylis, G. C., Driver, J. (2001). Shape-coding in IT cells generalizes over contrast and mirror reversal, but not figure–ground reversal. Nature Neurosci. 4, 937–942.

Beck, J.M., Ma, W.J., Kiani, R., Hanks, T., Churchland, A.K., Roitman, J., Shadlen, M.N., Latham, P.E., Pouget A. (2008). Probabilistic population codes for Bayesian decision making. Neuron;60(6):1142–52.

Bednar, J. A., Miikkulainen, R. (2000). Tilt aftereffect in a self-organizing model of the primary visual cortex. Neural computation, 12, 1721–1740.

Benardete E.A, Kaplan E. (1999a). The dynamics of primate M retinal ganglion cells. Vis Neurosci.; 16: 355-368.

Benardete E.A, Kaplan E. (1999b). Dynamics of primate P retinal ganglion cells: responses to chromatic and achromatic stimuli. J Physiol. 519: 775-790.

Benucci A., Frazor R.A., Carandini M. (2007). Standing waves and traveling waves distinguish two circuits in visual cortex, Neuron, 55, 103-117.

Benucci, A., Ringach, D.L., and Carandini, M. (2009). Coding of stimulus sequences by population responses in visual cortex. Nat. Neurosci. 12, 1317–1324.

Benvenuti, G. (2014). Anticipation of a bar by neuronal populations in awake monkey V1. Thesis manuscript.

Benvenuti, G., Chemla, s., Boonman, A. Masson, G., Chavane, F. (2015). Anticipation of an approaching bar by neuronal populations in awake monkey V1. Journal of vision 15 (12), 479-479.

Billock, V.A. (2000). Neural acclimation to 1 ⁄ f spatial frequency spectra in natural images transduced by the human visual system. Physica D, 137(3):379—391.

Billock, V.A, Cunningham, D.W, Havig, P.R., Tsou, H.P. (2001a). Perception of forbidden colors in retinally stabilized equiluminant images: an indication of softwired cortical color opponency? J. Opt. Soc. Am. A 18(10), 2404-2413.

Billock, V. A. de Guzman, G. C., Kelso, J. A. S. (2001b). Fractal time and 1⁄f spectra in dynamic images and human vision. Physica D, 148, 136–146.

Billock, V. A., Tsou, B. H. (2007). Neural interactions between flicker induced self-organized visual hallucinations and physical stimuli. PNAS, USA, 104, 8490– 8495.

Billock, V. A., Tsou, B. H. (2012). Elementary visual hallucinations and their relationships to neural pattern-forming mechanisms. Psychological Bulletin, 138(4), 744-774

Bishop, P. 0. Coombs, J. S. & Henry, G. H. (1973). Receptive fields of simple cells in the cat striate cortex. Journal of Physiology, London, 231, 31-60.

Blakemore, C., Carpenter, R. H. S., & Georgeson, M. (1970). Lateral inhibition between orientation detectors in the human visual system. Nature, 228, 37–39.

Blakemore, C., Tobin, E. A. (1972). Lateral inhibition between orientation detectors in the cat's visual cortex. Exp Brain Res; 15(4):439–440.

Blasdel, G. G., Campbell, D. (2001) Functional retinotopy of monkey visual cortex. J. Neurosci., 21: 8286-8301.

Blasdel, G. G., Fitzpatrick, D. (1984) Physiological organization of layer 4 in macaque striate cortex. 1 Neurosci., 4: 880-895.

Blasdel, G. G., Lund, J.S. (1983) Termination of afferent axons in macaque striate cortex. J. Neurosci., 3: 1389-1413.

Bogadhi, A., Montagnini, A. and Masson, G.S. (2011). Dynamical interaction between retinal and extra-retinal signals in motion integration for smooth pursuit. Journal of vision. 4;13(13):5

Bonin, V., Mante, V., Carandini, M. (2005). The suppressive field of neurons in lateral geniculate nucleus. J Neurosci; 25:10844–10856.

Born, R. T., Tootell, R. B. (1991). Single-unit and 2-deoxyglucose studies of side inhibition in macaque striate cortex, Proc Natl Acad Sci U S A 88(16): 7071–5.

Borst, A., Haag, J. (2007). Optic flow processing in the cockpit of the fly. In: Invertebrate neurobiology (North G, Greenspan RJ, eds), pp 101–122. New York: Cold Spring Harbor

Bosking, W. H, Fitzpatrick, D. (1995) Physiological correlates of anisotropy in horizontal connections: length summation properties of neurons in layers 2 and 3 of tree shrew striate cortex. Soc. Neurosci. Abstr. 21:1751.

Bosking, W. H, Zhang, Y., Schofield, B., Fitzpatrick, D. (1997) Orientation selectivity and the arrangement of horizontal connections in tree shrew striate cortex. J Neurosci 17:2112–2127.

Braddick, O. J., O'Brien, J.M., Wattam-Bell, J., Atkinson, J., Hartley, T., Turner, R. (2001). Brain areas sensitive to coherent visual motion. Perception, 30 (1), pp. 61-72.

Bravo, M., Blake, R., & Morrison, S. (1988). Cats see subjective contours. Vision Research, 28(8), 861-865.

Bressloff, P. C., Cowan, J. D., Golubitsky, M., Thomas, P.J., Wiener, M.C. (2001). Geometric visual hallucinations, Euclidean symmetry and the functional architecture of striate cortex. Phil. Trans. R. Soc. Lond. B, vol. 306, no. 1407, pages 299–330.

Bressloff, P. C., Cowan, J. D., Golubitsky, M., Thomas, P. J., Wiener, M. C. (2002). What geometric hallucinations tell us about the visual cortex? Neural Computation, 14, 473– 491.

Brewster, D. (1834). On the influence of successive impulses of light upon the retina. London Edinburgh Philosophical Magazine Journal of Science, 4, 241–245.

Briggs, F., Usrey, W. M. (2007). A fast Reciprocal pathway between the lateral geniculate nucleus and visual cortex in the macaque monkey. J Neurosci; 27:5431–5436.

Briggs F., Usrey W. M. (2008). Emerging views of corticothalamic function. Curr Opin Neurobiol; 18:403–407.

Bringuier, V., Chavane, F., Glaeser, L., Fregnac, Y. (1999). Horizontal propagation of visual activity in the synaptic integration field of area 17 neurons. Science; 283:695–699.

Brown, C. R., Gebhard, J. W. (1948). Visual field articulation in the absence of spatial stimulus gradients. Journal of Experimental Psychology, 38, 188–200.

Bullier, J. (2001). Integrated model of visual processing, Brain Res Brain Res Rev 36(2-3): 96–107.

Bullier, J., Henry, G.H. (1980). Ordinal position and afferent input of neurons in monkey striate cortex. J Comp Neurol 193:913–935.

Bullier, J., Hupe, J. M., James, A. C., Girard, P. (1996). Functional interactions between areas V1 and V2 in the monkey. Journal of Physiology-Paris. Volume 90, Issues 3–4, 1996, Pages 217-220.

Bullier, J., Hupe, J. M., James, A. C., Girard, P. (2001). The role of feedback connections in shaping the responses of visual cortical neurons, Prog Brain Res 134: 193–204.

Bullier. J., McCourt. M. E., Henry, G. H. (1988). Physiological studies on the feedback connection to the striate cortex from cortical areas 18 and 19 of the cat. Exp Brain Res 70:90-98.

Burr, D.C., Morgan, M. J. (1997). Motion deblurring in human vision. Proc. R. Soc. B. 1997; 264:431–436.

Busch, H., Kaiser, F. (2003). Influence of spatiotemporally correlated noise on structure formation in excitable media, Phys. Rev. E 67 041105.

Buzas, P., Eysel, U. T., Adorjan, P., Kisvarday, Z. F. (2001). Axonal topog- raphy of cortical basket cells in relation to orientation, direction, and ocular dominance maps. J. Comp. Neurol. 437, 259–285.

Buzas, P., Kovacs, K., Ferecsko, A. S., Budd, J. M., Eysel, U. T., Kisvarday, Z. F. (2006). Model-based analysis of exci- tatory lateral connections in the visual cortex. J. Comp. Neurol. 499, 861–881.

Callaway, E. M. (1998). Local circuits in primary visual cortex of the macaque monkey, Annu Rev Neurosci 21: 47–74.

Callaway, E.M, Katz, L. C. (1990). Emergence and refinement of clustered horizontal connections in cat striate cortex. J Neurosci 10:1134 –1153.

Cannon, M.W., Fullenkamp, S. C. (1991). Spatial interactions in apparent contrast: Inhibitory effects among grating patterns of different spatial frequencies, spatial positions and orientations. Vision Research, 31, pp. 1985-1998.

Carandini M, Heeger, D. J. (2012). Normalization as a canonical neural computation. Nat Rev Neurosci; 13:51–62.

Carandini, M., Ringach, D. L. (1997). Predictions of a recurrent model of orientation selectivity. Vision Res. 37, 3061–3071.

Carrillo O., Santos M. A., Garcia-Ojalvo J., Sancho J. M. (2003). Spatial coherence resonance near pattern-forming stabilities Europhysics Letters 65, 452-458.

Chang, L., Tsao, D. Y. (2017). The code for facial identity in the primate brain. Cell; 169(6): 1013–1028

Chavane, F., Sharon, D., Jancke, D., Marre, O., Fregnac, Y., Grinvald, A. (2011) Lateral spread of orientation selectivity in V1 is controlled by intracortical cooperativity. Front Syst Neurosci 5:4–24.

Chemla, S., Chavane F. (2016). Effects of GABA kinetics on cortical population activity: computational studies and physiological confirmations. Journal of Neurophysiology, 115: 2867-2879.

Chen, C. C. & Kasamatsu, T. (1998). A sensitivity modulation model for lateral interactions among striate cells in cat visual cortex. Society for Neuroscience Abstracts 24, 1979.

Chen, C. C., Kasamatsu, T., Polat, U., Norcia, A.M. (2001). Contrast response characteristics of long-range lateral interactions in cat striate cortex. NeuroReport 12, 655–661.

Chen, K., Song, X. M., Dai, Z. Q., Yin, J. J., Xu, X. Z., & Li, C. Y. (2014). The spatial summation characteristics of three categories of V1 neurons differing in non-classical receptive field modulation properties. Vision Research, 96C, 87–95.

Chen, K., Song, X. M., Li, C. Y. (2013). Contrast-dependent variations in the excitatory classical receptive field and suppressive nonclassical receptive field of cat primary visual cortex. Cerebral Cortex, 23, 283–292.

Chervin, R. D., Pierce, P. A., Connors, B. W. (1988). Periodicity and directionality in the propagation of epileptiform discharges across neocortex. J. Neurophysiol. 60, 1695–1713.

Citti, G., Sarti, A. (2006). A cortical based model of perceptual completion in the roto-translation space. J. Math. Imaging Vis,24, 307–326.

Cleland, B. G., Dubin, M. W. & Levick, W. R. (1971). Sustained and transient neurons in the cat's retina and lateral geniculate nucleus. Journal of Physiology (London) 217, 473-496.

Cleland, B. G., Lee, B.B., Vidyasagar, T. R. (1983) Response of neurons in the cat's lateral geniculate nucleus to moving bars of different length. J Neurosci 3:108–116

Clifford, C. W., Wyatt, A. M., Arnold, D. H., Smith, S. T., Wenderoth, P. (2001). Orthogonal adaptation improves orientation discrimination. Vision Res. 41, 151–159.

Clottes, J., Lewis-Williams, D. (1998). The shamans of prehistory: Trance and magic in the painted caves. New York: Abrams.

Coen-Cagli, R., Dayan, P., Schwartz, O. (2012). Cortical Surround Interactions and Perceptual Salience via Natural Scene Statistics. PLoS Comput Biol. 2012; 8: e1002405.

Colby, C. L., Duhamel J. R., Goldberg M.E. (1995). Oculocentric spatial representation in parietal cortex. Cereb. Cortex.5(5):470-81.

Colby, C. L., Duhamel, J.R., Goldberg, M. E. (1996). Visual, presaccadic, and cognitive activation of single neurons in monkey intraparietal area. J. Neurophysiol. 76, 2841-2852

Cook, G. (1965). Control system study of the saccadic eye-movement mechanism. SC. D. Thesis. Dept. Electrical Engineering, M.I.T., Cambridge, Mass.

Cowan, J. D. (1997). Neurodynamics and brain mechanisms. In M. Ito, Y. Miyashita, & E. T. Rolls (Eds.), Cognition, computation, and consciousness (pp. 205–233).

Creutzfeld, O.D., Garey, L., Kuroda, R. and Wolff, J.-R. (1977). The distribution of degenerating axons after small lesions in the intact and isolated visual cortex of the cat, Exp Brain Res 27: 419–440.

Creutzfeldt, O. D., Kuhnt, U. & Beneveto, L. A. (1974). An intracellular analysis of visual cortical neurones to moving stimuli: Responses in a cooperative neuronal network. Experimental Brain Research, 21, 251-274.

Crommelinck, M., Roucoux, A. (1976). Characteristics of cat's eye saccades in different states of alertness. Brain Research, 103(3), 574-578.

Croner, L. J, Purpura, K., Kaplan, E. (1993). Response variability in retinal ganglion cells of primates. Proc Natl Acad Sci U S A. 90(17):8128-30.

Crook, J. M., Eysel, U. T. (1992). GABA-induced inactivation of functionally characterized sites in cat visual cortex (area 18): effects on orientation tuning. J. Neurosci. 12, 1816–1825.

Crook, J. M., Kisvárday, Z. F., Eysel, U. T. (1998). Evidence for a contribution of lateral inhibition to orientation tuning and direction selectivity in cat visual cortex: reversible inactivation of functionally characterized sites combined with neuroanatomical tracing techniques. Eur. J. Neurosci. 10, 2056–2075.

Crook, J.M., Worgötter, F., Eysel, U. T. (1994). Velocity invariance of preferred axis of motion for single spot stimuli in simple cells of cat striate cortex. Experimental Brain Research, 102, pp. 175-180.

Crotogino, J., Feindel, A. F., & Wilkinson, F. (2001). Perceived scintillation rate of migraine aura. Headache, 41, 40–48.

Cuntz, H., Haag, J., Forstner, F., Segev, I., Borst, A. (2007). Robust coding of flow-field parameters by axo-axonal gap junctions between fly visual interneurons. Proc Natl Acad Sci U S A.; 104(24):10229-33.

Da Costa, N. M., and Martin, K. A. C. (2010). Whose cortical column would that be? Front. Neuroanat. 4:16.

D'Agostino R. B. Transformation to normality of the null distribution of g_1. Biometrika *;* 1970; 57 (3): 679–681.

Dalva, M. B., Weliky, M., Katz, L. C. (1997). Relationships between local synaptic connections and orientation domains in primary visual cortex. Neuron, 19:871—880.

Dantzker, J., Callaway, E. M. (2000). Laminar sources of synaptic input to cortical inhibitory interneurons and pyramidal neurons, Nature Neurosci 3(7): 701–707.

Darian-Smith, C., Gilbert C. D. (1994). Axonal sprouting accompanies functional reorganization in adult cat striate cortex. Nature. *1994*;368(6473):737-40.

Darian-Smith, C., Gilbert, C. D. (1995). Topographic reorganization in the striate cortex of the adult cat and monkey is cortically mediated J. Neurosci., 15, pp. 1631-1647

Das, A. and Gilbert, C. D. (1999). Topography of contextual modulations mediated by short-range interactions in primary visual cortex, Nature 399(6737): 655–61.

Daugman J. G. Uncertainty relation for resolution in space, spatial frequency, and orientation optimized by two-dimensional visual cortical filters. Journal of the Optical Society of America, 2(7):1160–1169.

Dawis, S., Shapley, R., Kaplan, E., Tranchina, D. (1984). The receptive field organization of X-cells in the cat: spatiotemporal coupling and asymmetry; Vision Research Vol. 24. No. 6. pp 549-564.

DeAngelis, G. C., Anzai, A., Ohzawa, I. and Freeman, R. D. (1995). Receptive field structure in the visual cortex: does selective stimulation induce plasticity? Proc Natl Acad Sci USA 92(21): 9682–6.

DeAngelis, G. C., Freeman, R. D., Ohzawa, I. (1994). Length and width tuning of neurons in the cat's primary visual cortex. J. Neurophysiol., 71: 347-374.

Derrington, A. M., Fuchs, A. F. (1979). Spatial and temporal properties of X and Y cells in the cat lateral geniculate nucleus. J. Physiol. 293, 347–364.

Destexhe, A. Contreras, D. (2006). Neuronal computations with stochastic network states. Science, 314, pp. 85-90.

De Valois, R. L., Thorell L. G., Albrecht, D. G. (1985). Periodicity of striate-cortex-cell receptive fields. Journal of the Optical Society of America A, 2, 1115-1122.

De Weerd, P. (2006). Perceptual filling-in: More than the eye can see. Prog Brain Res ;154 :227-45.

Dong, D. W., Atick, J. J. (1995). Statistics of natural time-varying images. Pages 345-358.

Douglas, R. J., Martin, K. A. C. (1991). A functional microcircuit for cat visual cortex. J. Physiol. 440, 735–769.

Douglas, R. J., Martin, K. A. C. (2004). Neuronal circuits of the neocortex. Annu. Rev. Neurosci., 27:419–451.

Dow, B. M (1974). Functional classes of cells and their laminar distribution in monkey visual cortex. J Neurophysiol 37:927–946.

Dow, R. C., Hill, A. G., McQueen, J. K. (1974). Proceedings: Effects of some dopamine receptor stimulants on cobalt-induced epilepsy in the rat. Br J Pharmacol;52(1):135P–135P.

Dräger, U. C. (1975). Receptive fields of single cells and topography in mouse visual cortex. J Comp Neurol ;160 : 269–290.

Dragoi, V., Sharma, J., Miller, E. K., Sur, M. (2002). Dynamics of neuronal sensitivity in visual cortex and local feature discrimination. Nat. Neurosci. 5, 883–891.

Dragoi, V., Sur, M. (2000a). Dynamic properties of recurrent inhibition in primary visual cortex: Contrast and orientation dependence of contextual effects, J Neurophysiol 83: 1019–1030.

Dragoi, V., Sharma, J., Sur, M. (2000b). Adaptation-induced plasticity of orientation tuning in adult visual cortex. Neuron 28, 287–298.

Duhamel, J. R., Colby C. L., Goldberg, M. E. (1992). The updating of the representation of visual space in parietal cortex by intended eye movements. Science 255: 90–92.

Duits R., Boscain U., Rossi F., Sachkov Y. (2014). Association Fields via Cuspless Sub-Riemannian Geodesics in SE (2) J Math Imaging Vis; 49:384–417.

Duysens, J., Orban, G. A., van der Glas, H. W., de Zegher, F. E. (1982). Functional properties of area 19 as compared to area 17 of the cat, Brain Res. 231, 279–291.

Enroth-Cugell, C., Robson, J. G. (1966). The contrast sensitivity of retinal ganglion cells of the cat. J Physiol. 187: 517-552.

Ermentrout, G. B. (1998). Neural networks as spatial pattern forming systems. Rep. Prog. Phys., 61, 353–430.

Ermentrout, G. B., Cowan, J. D. (1979). A mathematical theory of visual hallucination patterns. Biological Cybernetics, vol. 34, no. 3, pages 137–150.

Eysel, U. T., Eyding, D., Schweigart, G. (1998). Repetitive optical stimulation elicits fast receptive field changes in mature visual cortex, NeuroReport, 9, 949–954.

Farrow, K., Borst, A., Haag, J. (2005). Sharing receptive fields with your neighbors: tuning the vertical system cells to wide field motion. J Neurosci; 25(15):3985-93.

Fechner, G. T. (1838). Über eine Scheibe zur Erzeungung subjectiver Farben [Via a disk for generating subjective colors]. Poggendorff's Annalen der Physik und Chemie, 45, 227–232.

Felisberti, F., Derrington, A. M. (1999). Long range interactions modulate the contrast gain in the lateral geniculate nucleus of cats. Visual Neuroscience, 16, 943-956.

Felisberti, F., Derrington, A. M. (2001). Long-range interactions in the lateral geniculate nucleus of the New World monkey, Callithrix jacchus. Visual Neuroscience, 18, 209-218.

Felleman, D. J., Van Essen, D. C. (1991) Distributed hierarchical processing in the primate cerebral cortex. Cereb Cortex 1:1–47

Felsen, G., Shen, Y. S., Yao, H., Spor, G., Li, C., and Dan, Y. (2002). Dynamic modification of cortical orientation tuning mediated by recurrent connections. Neuron 36, 945–954.

Ferster, D. (1990). X- and Y-mediated current sources in areas 17 and 18 of cat visual cortex. Visual Neuroscience 4, 135-145.

Ferster, D., Miller, K. D. (2000). Neural mechanisms of orientation selectivity in the visual cortex. Annu Rev Neurosci.;23:441-71.

Field D. J., Hayes, A., Hess, R. F. (1993). Contour integration by the human visual system: evidence for a local "association field." Vision Res 33 :173–193.

Fiorani, M., Rosa, M. G. P., Gattas, R., Rocha-Miranda, C. E. (1992). Dynamic surrounds of receptive fields in primate striate cortex: a physiological basis for perceptual completion? Proc. Natl Acad. Sci. USA 89, 8547–8551.

Fiorentini, A. (1972). Mach Band Phenomena. Visual Psychophysics pp 188-201.

Fischer, B., Krüger, J. (1974). The shift effect in the cat's lateral geniculate neurons. Experimental Brain Research. 21, 225 221.

Fiser, J., Chiu, C., Weliky, M. (2004). Small modulation of ongoing cortical dynamics by sensory input during natural vision. Nature volume 431, 573–578.

Fisken, R., Garey, L., Powell, T. (1975). The intrinsic, association and commisural connections of area 17 of the visual cortex, Phil Trans R Soc Lond B 272: 487–536.

Fitzpatrick, D. (1996). The functional organization of local circuits in visual cortex: insights from the study of tree shrew striate cortex, Cereb Cortex 6: 329–341.

Foster, K. H., Gaska, J. P., Nagler, M., Pollen, D. A. (1985). Spatial and temporal frequency selectivity of neurones in visual cortical areas V1 and V2 of the macaque monkey, J Physiol 365: 331–63.

Fournier, J., Monier, C., Pananceau, M., Fregnac, Y. (2011). Adaptation of the Simple or Complex nature of V1 receptive fields to visual statistics. Nature Neuroscience. 14: 1053-1060.

Freedman, S. J., Marks, P. A. (1965). Visual imagery produced by rhythmic photic stimulation: Personality correlates and phenomenology. British Journal of Psychology, 56, 95–112.

Fregnac, Y. (2003). Neurogeometry and entoptic visions of the functional architecture of the brain. Journal of Physiology (Paris), pp. 97, 87–92.

Fregnac, Y. (2012). Reading out the synaptic echoes of low-level perception in V1. Lect Notes Comput Sci 7583:486–495.

Fregnac, Y., Bathellier, B. (2015). Cortical Correlates of Low-Level Perception: From Neural Circuits to Percepts.Neuron 88(1): 110-126.

Fregnac, Y., Baudot, P., Chavane, F., Lorenceau, J., Marre, O., Monier C., Pananceau, M., Carelli, P., Sadoc, G. (2010). Multiscale functional imaging in V1 and cortical correlates of apparent motion. In: Dynamics of visual motion processing (G. Masson and U. Ilg) Springer 73-94.

Fregnac, Y., Bringuier, V. (1996). Spatio-temporal dynamics of synaptic integration in cat visual cortical receptive fields, in A. Aertsen and V. Braitenberg (eds), Brain Theory - Biological and Computational Principles, Elsevier, pp. 143–199.

Fregnac, Y., Bringuier, V., Chavane, F. (1996). Synaptic integration fields and associative plasticity of visual cortical cells in vivo. J Physiol Paris 90:367–372.

Freund, T. F., Martin, K. A. C., Whitteridoe, D. (1985). Innervation of cat visual areas 17 and 18 by physiologically identified X- and Y-type thalamic afferents, I: Arborization patterns and quantitative distribution of postsynaptic elements. Journal of Comparative Neurology 141, 263-274.

Friston, K. (2009). The free-energy principle: a rough guide to the brain? Trends Cogn. Sci. (Regul. Ed.) 13, 293–301.

Fuchs, A. F. (1967). Saccadic and smooth pursuit eye movements in the monkey. J Physiol. 1967 Aug; 191(3): 609–631.

Funke, K., Nelle, E., Li, B., Worgotter, F. (1996). Corticofugal feedback improves the timing of retino-geniculate signal transmission. Neuroreport; 7:2130–2134.

Galuske, R. A., Schmidt, K. E., Goebel, R., Lomber, S. G., Payne, B. R. (2002). The role of feedback in shaping neural representations in cat visual cortex. Proc. Natl. Acad. Sci. U.S.A. 99, 17083–17088.

Garrido, M. I., Kilner, J. M., Kiebel, S. J., Stephan, K. E., Friston K. J. (2007). Dynamic causal modelling of evoked potentials: a reproducibility study. Neuroimage; 36:571–580.

Garrido, M. I., Kilner, J. M., Kiebel, S. J., Stephan, K. E., Friston K. J (2009). The mismatch negativity: a review of the underlying mechanisms. Clinical Neurophysiol; 120:453–463.

Geisler, W. S. (1999). Motion streaks provide a spatial code for motion direction. Nature, 400, pp. 65-69.

Geisler, W. S., Albrecht, D. G., Crane, A., Stern, L. (2001). Motion direction signals in the primary visual cortex of cat and monkey. Visual Neuroscience, 18, pp. 501-516.

Georges, S., Series, P., Fregnac, Y., Lorenceau, J. (2002). Orientation dependent modulation of apparent speed: psychophysical evidence. Vision Res. 42, 2757–2772.

Georgeson, M. A. (1976). Psychophysical hallucinations of orientation and spatial frequency. Perception, 5, 99–111.

Gerard-Mercier, F., Carelli, P. V, Pananceau, M, Troncoso, X. G, Fregnac Y. (2016). Synaptic Correlates of Low-Level Perception in V1. J Neurosci; 36(14):3925-42.

Gerrits, H. J. M., Vendrik, A. J. H. (1970). Simultaneous contrast, filling-in process and information processing in man's visual system. Exp. Brain Res. 11, 411–430.

Ghosh, A., Rho, Y., McIntosh, A. R., Kötter, R., & Jirsa, V. K. (2008). Noise during rest enables the exploration of the brain's dynamic repertoire. PLOS Computational Biology, 4, Article e1000196.

Gilbert, C. D. (1977). Laminar differences in receptive field properties of cells in cat primary visual cortex, J Physiol 268(2): 391–421.

Gilbert, C. D. (1998). Adult cortical dynamics, Physiol Rev 78(2): 467–85.
Gilbert, C. D, Kelly, J. P. (1975). The projections of cells in different layers of the cat's visual cortex. J Comp Neurol 63: 81-106.

Gilbert, C. D., Li, W. (2012). Adult visual cortical plasticity. Neuron 75(2) :250–264.

Gilbert, C. D., Li, W. (2013). Top-down influences on visual processing. Nat Rev Neurosci.,14(5):350-63.

Gilbert, C. D., Wiesel, T. N. (1979). Morphology and intracortical projections of functionally characterized neurons in the cat visual cortex. Nature.280: 120-125.

Gilbert, C. D., Wiesel, T. N. (1983a). Functional Organization of the Visual Cortex. Progress in Brain Research. vol 58 : 209-218.

Gilbert, C. D, Wiesel, T. N. (1983b). Clustered intrinsic connections in cat visual cortex. J Neurosci; 3:1116–1133.

Gilbert, C. D., Wiesel, T. N. (1985). Intrinsic connectivity and receptive field properties in visual cortex. Vision Research, 25, 365-74.

Gilbert, C. D, Wiesel, T. N. (1989). Columnar specificity of intrinsic horizontal and corticocortical connections in cat visual cortex. J Neurosci 9:2432–2442.

Gilbert, C. D, Wiesel T. N. (1990). The influence of contextual stimuli on the orientation selectivity of cells in primary visual cortex. Vision Res, 30, pp. 1689-1701.

Gilbert, C. D, Wiesel, T. N. (1992). Receptive field dynamics in adult primary visual cortex. Nature;356(6365):150–152.

Girard, P., Bullier, J. (1989). Visual activity in area V2 during reversible inactivation of area 17 in the macaque monkey. J Neurophysiol, 62(6):1287-302.

Girard, P., Salin, P. A., Bullier, J. (1992). Response selectivity of neurons in area MT of the macaque monkey during reversible inactivation of area V1. J Neurophysiol , 67(6):1437-46.

Girard, P., Hupe, J. M, Bullier, J. (2001). Feedforward and feedback connections between areas V1 and V2 of the monkey have similar rapid conduction velocities. J Neurophysiol. 85:1328–1331.

Girman, S. V, Sauve, Y, Lund, R. D. (1999). Receptive field properties of single neurons in rat primary visual cortex. J Neurophysiol; 82:301–311.

Glickfeld, L. L, Andermann, M. L., Bonin, V., Reid, R. C. (2013). Cortico-cortical projections in mouse visual cortex are functionally target specific. Nat Neurosci. 16, 219–226.

Goldberg, J. A., Rokni, U., Sompolinsky, H. (2004). Patterns of ongoing activity and the functional architecture of the primary visual cortex. Neuron, 42, 489–500.

Golubitsky, M., Schaeffer, D. G. (1985). Singularities and groups in bifurcation theory I. Berlin: Springer-Verlag.

Golubitsky, M., Stewart, I., Schaeffer, D. G. (1988). Singularities and groups in bifurcation theory II. Berlin: Springer-Verlag.

Goupillaud, P., Grossman, A., Morlet, J. (1984). Cycle-Octave and Related Transforms in Seismic Signal Analysis. Geoexploration.,23:85-102.

Gray, C. M., Konig, P., Engel, A. K., Singer, W. (1989). Oscillatory responses in cat visual cortex exhibit inter-columnar synchronization which reflects global stimulus properties. Nature 338:334-37

Grinvald, A., Lieke, E. E, Frostig, R. D, Hildesheim, R. (1994). Cortical point-spread function and long-range lateral interactions revealed by real-time optical imaging of macaque monkey primary visualcortex. J Neurosci. 14 :2545–2568.

Gu, H. G., Yang M. H., Li L., Liu Z. Q., Ren, W. (2003). Dynamics of autonomous stochastic resonance in neural period adding bifurcation scenarios. Physics Letters A, vol. 319, no. 1-2, pp. 89–96.

Gulyas, B., Orban, G. A., Duysens, J., Maes, H. (1987). The suppressive influence of moving textured backgrounds on responses of cat striate neurons to moving bars. Journal of Neurophysiology, 57, 1767–1791.

Haag, J., Borst, A. (2004). Neural mechanism underlying complex receptive field properties of motion-sensitive interneurons. Nat Neurosci.; 7(6):628-34.

Hadjikhani, N. Sanchez del Rio, M., Wu, O., Schwartz, D., Bakker, D., Fischl, B., Moskowitz, M. A. (2001). Mechanisms of migraine aura revealed by functional MRI in human visual cortex. PNAS, 98, 4687–4692.

Haider, B, Krause, M. R, Duque, A., Yu, Y., Touryan, J., Mazer, J. A, McCormick, D. A. (2010). Synaptic and network mechanisms of sparse and reliable visual cortical activity during nonclassical receptive field stimulation. Neuron; 65:107–121.

Han, F., Caporale, N., Dan, Y. (2008). Reverberation of recent visual experience in spontaneous cortical waves. Neuron, 60(2), 321–327.

Harrison, R., Balázs, P., Csaba, P., Stephen, G. O., Delneri. D. (2007). Plasticity of genetic interactions in metabolic networks of yeast. PNAS February 13,104 (7) 2307-2312.

Hashemi-Nezhad, M., Lyon, D. C. (2012). Orientation tuning of the suppressive extraclassical surround depends on intrinsic organization of V1. Cereb Cortex; 22:308–326.

Hammond, P., MacKay, D. M. (1981). Modulatory influences of moving textured backgrounds on responsiveness of simple cells in feline striate cortex. Journal of Physiology, London, 319. 431442.

Hedges, J. H., Stocker, A. A., Simoncelli, E. P. (2011). Optimal inference explains the perceptual coherence of visual motion stimuli. J Vis;11

Heeger, D. J. (1992). Normalization of cell responses in cat striate cortex. Vis Neurosci; 9: 181–197.

Heeger, D. J., Simoncelli, E. P., Movshon, J. A. (1996) Computational models of cortical visual processing. Proc Natl Acad Sci US A 93:623–627. Helmholtz, H. (1925). Physiological optics (Vol. 2). Rochester, NY: Optical Society of America.

Hengstenberg, R. (1982). Common visual response properties of giant vertical cells in the lobula plate of the blowfly Calliphora. Journal of comparative physiology. Volume 149, Issue 2, pp 179–193

Henry, C. A, Joshi, S., Xing, D., Shapley, R. M., Hawken, M. J. (2013). Functional characterization of the extraclassical receptive field in macaque V1: contrast, orientation, and temporal dynamics. J Neurosci; 33:6230–6242.

Henry, G. H., Salin, P. A., Bullier, J. (1991). Projections from areas 18 and 19 to cat striate cortex: divergence and laminar specificity. Eur. J. Neurosci. 3, 186–200.

Hess, R., Field, D. (1999) Integration of contours: new insights. Trends. Cogn. Sci. 3:480–486.

Hess, R. F., Hayes, A. (1993). The coding of spatial position by the human visual system. Effects of spatial scale and retinal eccentricity. Vision Research Volume 34, Issue 5, Pages 625-643.

Hess, R., McIlhagga, W., Field, D. J. (1997). Contour integration in strabismic amblyopia: the sufficiency of an explanation based on position uncertainty. Vision Res 37:3145–3161.

Hidaka, S., Manaka, Y., Teramoto, W., Sugita, Y., Miyauchi, R., Gyoba, J., Suzuki, Y., Iwaya, Y. (2009). Alternation of sound location induces visual motion perception of a static object. PLoS ONE 4, e8188.10.1371.

Hikosaka, O., Miyauchi, S., Shimojo, S. (1993). Focal visual attention produces illusory temporal order and motion sensation. Vision Res.,33, 1219–1240.

Hirsch, J. A., Alonso, J. M., Reid, R. C., Martinez, L. M. (1998). Synaptic integration in striate cortical simple cells. The Journal of Neuroscien*ce*, 18:9517–9528.

Hirsch, J. A, Gilbert, C. D. (1991). Synaptic physiology of horizontal connections in the cat's visual cortex. J Neurosci. 11:1800–1809.

Hoffman, K. P., Stone, J. (1971). Conduction velocity of afferents to cat visual cortex: a correlation with cortical receptive-field properties. Brain Research 32, 460-466.

Hollander, H., Vanegas, H. (1977). The projection from the lateral geniculate onto the visual cortex in the cat. A quantitative study with horseradish peroxidase. J. comp. Neurol.173, 519-536.

Horikawa, J., Nasu, M., Taniguchi, I. (1998). Optical recording of responses to frequency-modulated sounds in the auditory cortex. NeuroReport 9, 799–802.

Horton, J. C., Adams, D. L. (2005). The cortical column: a structure without a function. Philos. Trans. R. Soc. Lond. BBiol. Sci. 360, 837–862.

Hu, G*.,* Ditzinger, T*.,* Ning, C. Z*.,* Haken, H. (1993). Stochastic resonance without external periodic force. Phys*.* Rev*.* Lett*,* 71:807.

Huang, L., Chen X., Shou T. (2004). Spatial frequency-dependent feedback of visual cortical area 21a modulating functional orientation column maps in areas 17 and 18 of the cat. Brain Res. 998, 194–201.

Huang, J. Y., Wang, C., Dreher, B. (2007). The effects of reversible inactivation of postero-temporal visual cortex on neuronal activities in cat's area 17. Brain Res. 1138, 111–128.

Hubel, D. H., Wiesel, T. N. (1959). Receptive fields of single neurones in the cat's striate cortex. J Physiol. 148:574–591.

Hubel, D. H., Wiesel, T. N. (1960). Receptive fields of optic nerve fibres in the spider monkey. J.Physiol.154,572-580.

Hubel, D. H, Wiesel, T. N. (1962). Receptive fields, binocular interaction and functional architecture in the cat’s visual cortex. J Physiol (Lond) 160:106 –154.

Hubel, D. H., Wiesel, T. N. (1965). Receptive fields and functional architecture in two non-striate visual areas (18 and 19) of the cat, J Neurophysiol 28: 229–289.

Hubel, D. H, Wiesel, T. N. (1968). Receptive fields and functional architecture of monkey striate cortex. J Physiol (Lond) 195:215–243.

Hubel, D. H, Wiesel, T. N. (1974). Uniformity of monkey striate cortex: a parallel relationship beween field size scatter, and magnification factor. J Comp Neurol 158: 295–306.

Humphrey, A. L., Sur, M., Uhlrich, D. J., Sherman, S. M. (1985). Projection patterns of individual X- and Y-cell axons from the lateral geniculate nucleus to cortical area 17 in the cat. Journal of Comparative Neurology 233, 159-189.

Hunt, A. R., Cavanagh, P. (2009). Looking ahead: The perceived direction of gaze shifts before the eyes move. Journal of Vision, 9, ArtID: 1.

Hung, C. P., Kreiman, G., Poggio, T., DiCarlo, J. J. (2005). Fast readout of object identity from macaque inferior temporal cortex. Science, 310(5749), 863-866.

Hupe, J. M., James, A. C., Girard, P., Bullier, J. (2001a). Response modulations by static texture surround in area V1 of the macaque monkey do not depend on feedback connections from V2, J Neurophysiol 85(1): 146–63.

Hupe J. M., James, A. C., Girard, P., Lomber, S. G., Payne, B. R., Bullier, J. (2001b). Feedback connections act on the early part of the responses in monkey visual cortex. J Neurophysiol.; 85:134–145.

Hupe J. M., James, A. C., Payne, B. R., Lomber, S. G., Girard, P., Bullier, J. (1998). Cortical feedback improves discrimination between figure and background by V1, V2 and V3 neurons. Nature; 394:784–787.

Iacaruso, M. F., Gasler, I. T., Hofer, S. B. (2017*).* Synaptic organization of visual space in primary visual cortex. Nature; 547: 449–452.

Ichida J. M., Schwabe, L., Bressloff, P. C., Angelucci, A. (2007). Response facilitation from the "suppressive" receptive field surround of macaque V1 neurons. J Neurophysiol. 98:2168–2181.

Ikeda, H., Wright, M. J. (1972a). Receptive field organization of "sustained" and "transient" retinal ganglion cells which subserve different functional roles. Journal of Physiology, London, 227,769 - 800.

Ikeda, H., Wright, M. J. (1972b). Functional organization of the periphery effect in retinal ganglion cells. Vision Research, 12, I857 1879.

Ikeda, H., Wright, M. J. (1974). Effect of halothane-nitrous oxide anaesthesia on the behaviour of ’sustained’ and ’transient’ visual cortical neurones, J Physiol 237(2): 20P–21P.

Inase, M. et al. (1999) Functional connections between the monkey premotor and primary motor cortex revealed by the optical recording method. Neurosci. Res. S203.

Inase, M., Tokuno, H., Nambu, A., et al. (1999). Corticostriatal and corticosubthalamic input zones from the presupplementary motor area in the macaque monkey: comparison with the input zones from the supplementary motor area. BrainRes; 833: 191-201.

Ito, M., Gilbert, C. D. (1999). Attention modulates contextual influences in the primary visual cortex of alert monkeys. Neuron 22, 593–604.

Jancke, D. (2000) Orientation formed by a spot's trajectory: a two-dimensional population approach in primary visual cortex. J Neurosci 20:RC86, (1–6).

Jancke, D., Chavane, F., Naaman, S., Grinvald, A. (2004). Imaging cortical correlates of illusion in early visual cortex. Nature 428:423–426.

Jancke, D., Erlhagen, W. (2010). “Bridging the gap: a model of common neural mechanisms underlying the Fröhlich effect, the flash-lag effect, and the representational momentum effect,” in Space and Time in Perception and Action, chapter 25. (Cambridge: Cambridge University Press), 422–440.

Jin, D. Z., Dragoi, V., Sur, M., Seung, H. S. (2005). Tilt aftereffect and adaptation-induced changes in orientation tuning in visual cortex. Journal of Neurophysiology, 94, 4038–4050.

Johnson, R. R., Burkhalter, A. (1996). Microcircuitry of forward and feedback connections within rat visual cortex, J Comp Neurol 368(3): 383–98.

Jones. (1970). Responses of single neurons in cat visual cortex to a simple and more complex stimulus. Am. J. Physiol., pp. 1102-1107.

Jones, H.E., Andolina, I. M.; Grieve, K. L.; Wang, W.; Salt, T. E.; Cudeiro, J.; Sillito, A. M. (2013). Responses of primate LGN cells to moving stimuli involve a constant background modulation by feedback from area MT. Neuroscience 246, 254-264.

Jones, H.E., Andolina, I. M., Oakely, N. M., Murphy, P.C. and Sillito, A. M. (2000). Spatial summation in lateral geniculate nucleus and visual cortex. Exp. Brain Res., 135: 279–284.

Jones, H.E., Grieve, K. L., Wang, W., & Sillito, A. M. (2001). Surround suppression in primate V1. Journal of Neurophysiology, 86, 2011–2028.

Jones, S.R., Kerr, C. E., Wan. Q., Pritchett. D. L., Hämäläinen, M., Moore C. I. (2010). Cued Spatial Attention Drives Functionally Relevant Modulation of the Mu Rhythm in Primary Somatosensory Cortex. Journal of Neuroscience, 30 (41) 13760-13765.

Judge, S.J., Richmond, B. J., Chu, F. C. (1980). Implantation of magnetic search coils for measurement of eye position: An improved method Vision Research, pp. 535-538.

Jung, P., Cornell-Bell, A. H., Madden, K., Moss, F. (1998). Noise-induced spiral waves in astrocyte syncytia show evidence of self-organized criticality. J. Neurophys. 70, 1098-1101.

Kadar, S., Wang, J., Showalter, K. (1998). Noise-supported traveling waves in sub-excitable media. Nature (London), 391:770-772.

Kapadia, M.K., Ito, M., Gilbert, C.D., Westheimer, G. (1995). Improvement in visual sensitivity by changes in local context: Parallel studies in human observers and in V1 of alert monkeys. Neuron 15, 843–856.

Kapadia, M.K., Westheimer, G., Gilbert, C. D. (1999). Dynamics of spatial summation in primary visual cortex of alert monkeys. Proceedings of the National Academy of Sciences of the United States of America, 96, 12038–12073.

Kapadia, M.K., Westheimer, G., Gilbert, C. D. (2000). Spatial distribution of contextual interactions in primary visual cortex and in visual perception. J Neurophysiol 84: 2048–2062.

Kaplan, E., Benardete, E. (2001). The dynamics of primate retinal ganglion cells. Prog Brain Res; 134: 17-34. PMID: 11702542.

Kaplan, B. A., Lansner, A., Masson, G. S., Perrinet, L. U. (2013). Anisotropic connectivity implements motion-based prediction in a spiking neural network. Frontiers in Comput Neurosci; 7: 112.

Kaplan, D. A., Paudel, R., Cohen, M. J., Jawitz, J. W. (2012). Orientation matters: patch anisotropy controls discharge competence and hydroperiod in a patterned peatland. Geophys Res Lett 39(17).

Karube, F., Kisvarday, Z. F. (2011). Axon topography of layer 4 spiny cells to orientation map in the cat primary visual cortex (area 18). Cereb Cortex 21:1443–1458.

Karube, F., Sári, K., Kisvárday, Z. F. (2017). Axon topography of layer 6 spiny cells to orientation map in the primary visual cortex of the cat (area 18). Brain Struct Funct; 222(3):1401-1426.

Kasamatsu T, Miller R, Zhu Z, Chang M. Ishida Y. (2010). Collinear facilitation is independent of receptive-field expansion at low contrast. Experimental Brain Research;201(3):453–465.

Kastner, S., Schneider, K. A., Wunderlich, K. (2006). Beyond a relay nucleus: Neuroimaging views on the human LGN. Progress in Brain Research, 155, 125–143.

Kato, H., Bishop, P. O., Orban, G. A. (1978). Hypercomplex and simple/complex cell classifications in cat striate cortex, J Neurophysiol 41(5): 1071–95.

Keller A. J., Martin K. A. C. (2015). Local Circuits for Contrast Normalization and Adaptation Investigated with Two-Photon Imaging in Cat Primary Visual Cortex. Journal of Neuroscience; 35:(27) 10078-10087.

Kenet, T., Bibitchkov, D., Tsodyks, M., Grinvald, A., Arieli, A. (2003). Spontaneously emerging cortical representations of visual attributes. Nature 425: 954–956.

Khoei, M. A., Masson, G. S., Perrinet, L. U. (2013). Motion-based prediction explains the role of tracking in motion extrapolation, Journal of Physiology. Journal of Physiology, 107: 409-420.

Kilpeläinen, M., Donner, K., Laurinen, P. (2007). Time course of suppression by surround gratings: highly contrast-dependent, but consistently fast. Vision Res; 47:3298–3306.

Kisvarday, Z. F., Cowey, A., Hodgson, A. J., Somogyi, P. (1986). The relationship between GABA immunoreactivity and labelling by local uptake of [3H] GABA in the striate cortex of monkey. Exp Brain Res.;62(1):89-98.

Kisvarday Z. F, Beaulieu C, Eysel U. T. (1993b) Network of GABAergic large basket cells in cat visual cortex (area 18): implication for lateral disinhibition. J Comp Neurol 327:398–415.

Kisvarday, Z. F., Eysel, U. T. (1993a). Functional and structural topography of horizontal inhibitory connections in cat visual cortex. Eur. J. Neurosci. 5, 1558–1572.

Kisvarday, Z. F., Kim, D. S., Eysel, U. T., Bonhoeffer, T. (1994). Relationship between lateral inhibitory connections and the topography of the orientation map in cat visual cortex. Eur. J. Neurosci. 6, 1619–1632.

Kisvarday, Z. F, Toth, E., Rausch, M., Eysel, U. T. (1997). Orientation-specific relationship between populations of excitatory and inhibitory lateral connections in the visual cortex of the cat. Cereb Cortex 7:605– 618.

Kitano, M., Niiyama, K., Kasamatsu, T., Sutter, E. E., Norcia, A. M. (1994). Retinotopic and nonretinotopic field potentials in cat visual cortex. Visual Neuroscience, 11, pp. 953-977.

Kleinfeld, D. Delaney, K. R. (1996). Distributed representation of vibrissa movement in the upper layers of somatosensory cortex revealed with voltage-sensitive dyes. J. Comp. Neurol. 375, 89–108.

Klüver, H. (1967). Mescal and mechanisms of hallucinations. Chicago, IL: University of Chicago Press.

Knierim, D. C., Van Essen, D.C. (1992). Neuronal responses to static texture patterns in area V1 of the alert macaque monkey. Journal of Neurophysiology 67, 961–980.

Knill, D. C., Field, D., Kersten, D. (1990). Human discrimination of fractal images J. Opt. Soc. Am. A, 7, pp. 1113-1123.

Ko, Ho; Hofer, Sonja B.; Pichler, Bruno; Buchanan, Katherine A.; Sjöström, P. Jesper; Mrsic-Flogel, Thomas D. (2011). Functional specificity of local synaptic connections in neocortical networks. Nature, 473(7345), 87-91.

Kolb, H. (1997). Amacrine cells of the mammalian retina: Neurocircuitry and functional roles. Eye; 11: 904-923.

Komatsu, H. (2006). The neural mechanisms of perceptual filling-in. Nat Rev Neurosci.;7(3):220-31.

Komatsu, Y., Nakajima, S., Toyama, K., and Fetz, E. E. (1988). Intracortical connectivity revealed by spike-triggered averaging in slice preparations of cat visual cortex. Brain Res. 442, 359–362.

Komatsu, H., Murakami, I. & Kinoshita, M. (1996). Surface representation in the visual system. Brain Res. Cogn. Brain Res. 5, 97–104.

Komatsu, H., Kinoshita, M., Murakami, I. (2000). Neural responses in the retinotopic representation of the blind spot in the macaque V1 to stimuli for perceptual filling-in. J. Neurosci. 20, 9310–9319.

König, P., Engel, A. K., Löwel, S., Singer, W. (1993). Squint Affects Synchronization of Oscillatory Responses in Cat Visual Cortex. Eur J Neurosci; 5(5):501-8.

Kovacs, I., Julesz, B. (1993). A closed curve is much more than an incomplete one: effect of closure in figure-ground segmentation. Proc. Natl. Acad. Sci. USA 90, 7495-7497.

Krapp, H. G., Hengstenberg, R. (1996). Estimation of self-motion by optic flow processing in single visual interneurons. Nature; 384(6608):463-6.

Krapp, H. G., Hengstenberg, B., Hengstenberg, R. (1998). Dendritic structure and receptive-field organization of optic flow processing interneurons in the fly. J Neurophysiol; 79(4):1902-17.

Kravitz, D. J., Saleem, K. S., Baker, C. I., Ungerleider, L. G., Mishkin, M. (2013). The ventral visual pathway: an expanded neural framework for the processing of object quality. Trends Cogn. Sci. 17 26–49.

Krill, A. F., Alpert, H. J., and Ostfeld, A. M. (1963). Effects of a hallucinogenic agent in totally blind subjects, Archives of Ophthalmology 69, 180-185.

Krüger, J. (1977). The shift-effect in the lateral geniculate body of the rhesus monkey, Exp. Brain Res., 18,387–392.

Krüger. J. (1977). Stimulus dependent color specificity of monkey lateral geniculate neurons. Experimental Brain Research, 30. 297-311.

Krüger, J., Fischer, B. (1973). Strong periphery effect in cat retinal ganglion cells. Excitatory responses in ON- and OFF-center neurons to single grid displacement. Experimental Brain Research. 18.316-318.

Krüger, J., Fischer, B., Barth, R. (1975). The shift-effect in retinal ganglion cells in the rhesus monkey. Exp. Brain Res.,24;23(4):443-6.

Kuffler, S. W. (1952). Neurons in the retina: organization, inhibition and excitation problems. Symp.quant.Biol.27,281-292.

Lamme, V. A. F. (1995). The neurophysiology of figure–ground segregation in primary visual cortex. J. Neurosci. 15, 1605–1615.

Lamme, V. A. F., Super, H., Spekreijse, H. (1998a). Feedforward, horizontal, and feedback processing in the visual cortex. Curr Opin Neurobiol 8: 529–535.

Lamme, V. A. F., Super, H., Spekreijse, H. (1998b). Figure-ground activity in primary visual cortex is suppressed by anesthesia. Proc Natl Acad Sci USA 95 :3263–3268.

Lamme V. A. F., Rodriguez-Rodriguez, V., Spekreijse, H. (1999). Separate processing dynamics for texture elements, boundaries and surfaces in primary visual cortex of the macaque monkey. Cereb Cortex 9: 406–413.

Lamme, V. A. F., Roelfsema, P. R. (2000). The Distinct Modes of Vision Offered by Feedforward and Recurrent Processing. Trends in Neurosciences, 23, 571-579.

Lee, D, Malpeli, J. G. (1998a). Effects of saccades on the activity of neurons in the cat lateral geniculate nucleus. J Neurophysiol 79: 922–926.

Lee, B. B., Martin, P. R., Grünert, U. (2010). Retinal connectivity and primate vision. Prog Retin Eye Res; 29: 622-639.

Lee T. S., Mumford, D., Romero, R., Lamme, V. A. F. (1998b). The role of the primary visual cortex in higher-level vision. Vision Res 38: 2429–2454.

Lee, T. S., Nguyen, M. (2001). Dynamics of subjective contour formation in the early visual cortex. Proc. Natl. Acad. Sci. USA 98, 1907–1911.

Levay, S., Ferster, D. (1977). Relay classes in the lateral geniculate nucleus of the cat and the effects of visual deprivation. J. comp. Neurol. 172, 563-584.

Levay, S., Gilbert, C. D. (1976). Laminar patterns of geniculocortical projection in the cat. Brain Res;113(1):1-19.

Levick, W. R, Cleland, B. G, Dubin, M. W. (1972). Lateral geniculate neurons of the cat: retinal inputs and physiology. Inv Ophthalm. 11:302–311.

Levitt, J. B., Lund, J. S. (1997a) Contrast dependence of contextual effects in primate visual cortex. Nature, 387: 73-76.

Levitt, J. B., Lund, J. S. (1997b) Spatial summation properties of macaque striate neurons. Sot. Neurosci. Abstr., 23: 455.

Levitt, J. B, Lund, J. S. (2002). The spatial extent over which neurons in macaque striate cortex pool visual signals. Vis Neurosci; 19:439–452.

Li, C. Y., Li, W. (1994). Extensive integration field beyond the classical receptive field of cat's striate cortical neurons — classification and tuning properties. Vision Res., 34:2337-2355.

Li, W., Piëch, V., Gilbert, C. D. (2006). Contour saliency in primary visual cortex. Neuron. 50:951–962.

Li, W., Piëch, V., Gilbert, C. D. (2008) Learning to link visual contours. Neuron 57:442–451.

Liang, Z., Shen, W., Shou, T. (2007). Enhancement of oblique effect in the cat's primary visual cortex via orientation preference shifting induced by excitatory feedback from higher-order cortical area 21a. J. Neuroscience 145, 377–383.

Lim, H., Choe, Y. (2008). Extrapolative delay compensation through facilitating synapses and its relation to the flash-lag effect. Neural Netw. 19, 1678–1688.

Lin, B., Masland, R. H. (2006). Populations of wide-field amacrine cells in the mouse retina. J Comp Neurol; 499: 797-809.

Lindner, B.; García-Ojalvo, J.; Neiman, A.; Schimansky-Geier, L. (2004). Effects of noise in excitable systems. Physics Reports,392, 6, p. 321-424.

Liu, F., Wang, X. J. (2008). A common cortical circuit mechanism for perceptual categorical discrimination and veridical judgment. PLoS Comput.Biol.4: e1000253 10.1371/journal.pcbi.1000253.

Liu, L., Wang, k., Liao, B., Xu, L., Han, S. (2004). Perceptual salience of global structures and the crowding effect in amblyopia. Graefe's Archive Clinical Experimental Ophthalmology, 242 (7).

Loffler, G., Orbach, H. S. (2001). Anisotropy in judging the absolute direction of motion. Vision Research, 41, pp. 3677-3692

Lorenceau, J., Shiffrar, M., Wells, N., Castet, E. (1993). Different motion sensitive units are involved in recovering the direction of moving lines. Vision Research, 33, pp. 1207-1217

Luczak, A., Bartho, P., Harris, K. D. (2009). Spontaneous events outline the realm of possible sensory responses in neocortical populations. Neuron, 62, 413–425.

Luczak, A., Bartho, P., Marguet, S. L, Buzsaki, G., Harris, K. D. (2007). Sequential structure of neocortical spontaneous activity in vivo. Proc Natl Acad Sci U S A 104:347–352.

.

Lui, L. L, Bourne, J. A, Rosa, M. G. (2007). Spatial summation, end inhibition and side inhibition in the middle temporal visual area (MT). J Neurophysiol;97(2):1135-48.

Lund, J. S. (1973). Organization of neurons in the visual cortex, area 17, of the monkey (Macaca mulatta). J. Comp. Neurol. 147, 455—496.

Lund, J. S., Boothe, R. G. (1975). Interlaminar connections and pyramidal neuron organization in the visual cortex, area 17, of the macaque monkey. J Comp. Neurol. 159, 305-334.

Lund, J. S., Henry, G. H., MacQueen, C. L., Harvey, A. R. (1979). Anatomical organization of the primary visual cortex (area 17) of the cat. A comparison with area 17 of the macaque monkey, J. Comp. Neurol. 184:599–618.

MacKay, D. M. (1957a). Moving visual images produced by regular stationary patterns. Nature, 180, 849 – 850.

MacKay, D. M. (1957b). Some further visual phenomena associated with regular pattern stimulation. Nature, 180, 1145–1146.

MacKay, D. M. (1965). Visual noise as a tool of research. Journal of General Psychology, 72, 181–197.

MacKay, D. M. (1978). The time-course of induction of complementary images. Vision Research, 18, 913–916.

MacNeil, M. A., Masland, R. H. (1998). Extreme diversity among amacrine cells: Implications for function. Neuron;20: 971982.

Maffei, L., Fiorentini, A. (1973). The visual cortex as a spatial frequency analyser. Vision Research Volume 13, Issue 7, Pages 1255-1267.

Maffei, L., Fiorentini, A. (1976). The unresponsive regions of visual cortical receptive fields. Vision Research, 16, 1131-1139.

Malach, R., Amir, Y., Harel, M., Grinvald, A. (1993). Relationship between intrinsic connections and functional architecture revealed by optical imaging and in vivo targeted biocytin injections in primate striate cortex. Proc Natl Acad Sci USA; 90:10469–10473.

Mangini, N. J., Pearlman, A. L. (1980). Laminar distribution of receptive field properties in the primary visual cortex of the mouse. J Comp Neurol; 193:203–222.

Manookin, M. B., Puller, C., Rieke, F., Neitz, J., Neitz, M. (2015). Distinctive receptive field and physiological properties of a wide-field amacrine cell in the macaque monkey retina. J Neurophysiol. 114: 1606-1616.

Mante, V., Carandini, M. (2005). Mapping of stimulus energy in primary visual cortex. J. Neurophysiol., 94, pp. 788-798.

Markov, N. T., Ercsey-Ravasz, M. M., Ribeiro Gomes, A. R., Lamy, C., Magrou, L., Vezoli, J., Misery, P., Falchier, A., Quilodran, R., Gariel, M. A., Sallet, J., Gamanut, R., Huissoud, C., Clavagnier, S., Giroud, P., Sappey-Marinier, D., Barone, P., Dehay, C., Toroczkai, Z., Knoblauch ,K., Van Essen, D. C, Kennedy, H. (2014). A Weighted and Directed Interareal Connectivity Matrix for Macaque Cerebral Cortex Cerebral. Cerebral Corte; 24:17–36.

Markov, N.T., Ercsey-Ravasz, M., Van Essen, D.C., Knoblauch, K., Toroczkai, Z., and Kennedy, H. (2013). Cortical high-density counterstream architectures. Science 342, 1238406.

Markov, N. T., Vezoli, J., Chameau, P., Falchier, A., Quilodran, R., Huissoud, C., Lamy, C., Misery P., Giroud, P., Ullman, S., Barone, P., Dehay, C., Knoblauch, K., Kennedy, H. (2014 b) Anatomy of hierarchy: feedforward and feedback pathways in macaque visual cortex. J. Comp. Neurol. 522:225–259.

Marrocco, R. T., McClurkin, J. W., Young, R. A. (1982). Modulation of lateral geniculate nucleus cell responsiveness by visual activation of the cortico-geniculate pathway. Journal of Neuroscience, 2, 256-263.

Martin, A. B., Von Der Heydt, R. (2015). Spike synchrony reveals emergence of proto-objects in visual cortex. J Neurosci 35:6860–6870.

Martin, K. A .C, Roth, S., Rusch, E.S. (2014). Superficial layer pyramidal cells communicate heterogeneously between multiple functional domains of cat primary visual cortex. Nat. Comm.5: 5252: 1–13.

Martin, K. A. C., Schröder, S. (2013). Functional heterogeneity in neighboring neurons of cat primary visual cortex in response to both artificial and natural stimuli. J. Neurosci. 33, 7325–7344.

Martin, K.A.C., Whitteridge, D. (1984). Form function and intracortical projections of spiny neurons in the striate visual cortex of the cat, J Physiol (London) 353: 463–504.

Martinez-Conde, S., Cudeiron, J., Grieve, K., Rodriguez, R., Rivudalla, C. and na, C. A. (1999). Effects of feedback projections from area 18 layers 2/3 to area 17 layers 2/3 in the cat visual cortex, J Neurophysiol 82: 2667–2675.

Martinez-Conde, S., Otero-Millan, J., Macknik, S.L. (2013). The impact of microsaccades on vision: towards a unified theory of saccadic function. Nat Rev Neurosci 14: 83–96.

Mason, R. (1975). Cell responses in the medial interlaminar nucleus of the cat's lateral geniculate complex in relation to the transient/sustained classification. Expl Brain Re8. 22, 327-329.

Masson, G. S., Rybarczyk, Y., Castet, E., Mestre, D. R. (2000). Temporal dynamics of motion integration for the initiation of tracking eye movements at ultra-short latencies. Vis. Neurosci.;17(5):753-67.

Matsumoto, M., Komatsu, H. (2005). Neural. responses in the macaque V1 to bar stimuli with various lengths presented on the blind spot. J. Neurophysiol. 93, 2374–2387.

Maunsell, J. H. R., Van Essen, D. C. (1983). The connections of the middle temporal visual area (MT) and their relationship to a cortical hierarchy in the macaque monkey. J Neurosci; 3:2563–2586.

Maus, G. W; Nijhawan, R. (2008). Motion Extrapolation into the Blind Spot. Psychol Sci. ,19(11) :1087-91

McGuire, B. A., Gilbert, C. D., Rivlin P. K., Wiesel, T. N. (1991). Targets of horizontal connections in macaque primary visual cortex. J Comp. Neurol. 305:370–392.

McKeefry, D. J., Watson, J. D., Frackowiak, R. S., Fong, K., Zeki, S. (1997). The activity in human areas V1/V2, V3, and V5 during the perception of coherent and incoherent motion. Neuroimage;5(1):1-12.

Mcllwain, J. T. (1964). Receptive fields of optic tract axons and lateral geniculate cells: Peripheral extent and barbiturate sensitivity. Journal of Neurophysiology, 27, 1154-1173.

Mcllwain, J. T. (1966). Some evidence concerning the physiological basis of the periphery effect in the cat's retina. Experimental Brain Research, 1. 265-271.

Mendola, J. D. (2003). in Filling-in (eds Pessoa, L. & De Weerd, P.) 38–58 (Oxford Univ. Press, New York).

Mendola, J. D., Dale, A. M., Fischl, B., Liu, A. K., Tootell, R. B. (1999). The representation of illusory and real contours in human cortical visual areas revealed by functional magnetic resonance imaging. J. Neurosci. 19, 8560–8572.

Metin, C., Godement, P., Imbert, M. (1988). The primary visual cortex in the mouse: receptive field properties and functional organization. Exp Brain Res; 69:594–612.

Meyer, T., Olson, C. R. (2011). Statistical learning of visual transitions in monkey inferotemporal cortex. Proc Natl Acad Sci U S A 108:19401–19406.

Michalski, A., Gerstein, G. L., Czarkowska, J., Tarnecki, R. (1983). Interactions between cat striate cortex neurons. Exp. Brain Res. 51, 97–107.

Miezin et al., (1982). Antagonistic direction specific mechanisms in area MT in the owl monkey. Sot Neurosci Abstr 8:68 1

Mikami, A., Newsome, W. T., Wurtz, R. H. (1986). Motion selectivity in macaque visual cortex. I. Mechanisms of direction and speed selectivity in extrastriate area MT. Journal of Neurophysiology 55(6):1308-27.

Mitchell, D. E., Muir, D. W. (1976). Does the tilt after-effect occur in the oblique meridian? Vision Research, 16, 609–613.

Mitchison, G., Crick, F. (1982). Long axons within the striate cortex: their distribution, orientation, and patterns of connection, Proc Natl Acad Sci U S A 79(11): 3661–5.

Mizone, K., Polat, U., Kasamatsu, T., Norcia, A.M. (1996). Lateral masking reveals facilitation and suppression from the same single cells in cat area-17. Investigative Ophthalmology & Visual Science, p. 2188.

Mizobe, K., Polat, U., Pettet, M. W., Kasamatsu, T. (2001). Facilitation and suppression of single striate-cell activity by spatially discrete pattern stimuli presented beyond the receptive field. Visual. Neurosci; 18:377–391.

Molotchnikoff, S., Cérat, (1992) Responses from outside classical receptive fields of dorsal lateral geniculate cells in rabbits A. Exp Brain Res 92(1): 94-104.

Molotchnikoff, S., Delaunais, D., Casanova, C. (1986). Modulations of the lateral geniculate nucleus cell responses by a second discrete conditioning stimulus: implications of the superior colliculus in rabbits. Exp Brain Res;62(2):321-8.

Montaser-Kouhsari, L., Landy, M.S., Heeger, D.J., Larsson, J. (2007). Orientation-selective adaptation to illusory contours in human visual cortex. J. Neurosci. 27, 2186–2195.

Movshon J. A., Thompson I. D., Tolhurst D. J. (1978). Spatial and temporal contrast sensitivity of neurones in areas 17 and 18 of the cat's visual cortex. J. Physiol. 283, 101-120.

Muckli, L., Kohler, A., Kriegeskorte, N., Singer, W. (2005). Primary visual cortex activity along the apparent-motion trace reflects illusory perception. PLoS Biol. 3, e265.

Müller, J. R., Metha, A. B., Krauskopf, J., Lennie, P. (1999). Rapid adaptation in visual cortex to the structure of images. Science 285, 1405–1408.

Muller, L. E, Reynaud, A, Chavane, F, Destexhe, A. (2013). Propagating waves structure spatiotemporal activity in visual cortex of the awake monkey. BMC Neurosci; 14(Suppl 1): O8

Muller, L., Reynaud A., Chavane F., Destexhe. A. (2014). The stimulus-evoked population response in visual cortex of awake monkey is a propagating wave. Nat Commun, 5:3675.

Mumford, D. B. (1992). On the computational architecture of the neocortex II: The role of cortico-cortical loops. Biological Cybernetics, 66, 241-251.

Mumford, D. (1994). In Large-Scale Neuronal Theories of the Brain (eds Koch, C. & Davis, J.) 125–152 (MIT Press, Cambridge, Massachusetts).

Mundy-Castle, A. C. (1953). Electrical responses of the brain in relation to behavior. British Journal of Psychology, 44, 318–329.

Murakami, I. (1995). Motion aftereffect after monocular adaptation to filled-in motion at the blind spot. Vision Res. 35, 1041–1045.

Murray, J. D. (1989). Mathematical biology. Berlin, Germany: Springer-Verlag.

Murray, M.M., Molholm, S., Michel, C.M., Heslenfeld, D.J., Ritter, W., Javitt, D.C., Schroeder, C.E. Foxe, J. J (2004). Grabbing your ear: rapid auditory-somatosensory multisensory interactions in low-level sensory cortices are not constrained by stimulus alignment. Cereb Cortex.;15(7):963-74.

Murray, M. M., Wylie, G. R., Higgins, B. A., Javitt, D. C., Schroeder, C. E, Foxe, J. J. (2002). The spatiotemporal dynamics of illusory contour processing: combined high-density electrical mapping, source analysis, and functional magnetic resonance imaging. J Neurosci. 15;22(12):5055-73.

Naito, T., Sadakane, O., Okamoto, M., Sato, H. (2007). Orientation tuning of surround suppression in lateral geniculate nucleus and primary visual cortex of cat. Neuroscience;149(4):962-75.

Nassi J. J., Lomber S. G., Born R. T. (2013). Corticocortical feedback contributes to surround suppression in V1 of the alert primate. J. Neurosci. 33, 8504–8517.

Nauhaus, I., Busse, l., Carandini, M., Ringach, D.L. (2009). Stimulus contrast modulates functional connectivity in visual cortex. Nat. Neurosci., 12, pp. 70-76.

Nelson, J. I., Frost, B. J. (1978). Orientation-selective inhibition from beyond the classic visual receptive field, Brain Res 139(2): 359–65.

Nelson, J. I., Frost, B. J. (1985). Intracortical facilitation among co-oriented co-axially aligned simple cells in cat striate cortex. Experimental Brain Research, 61, 54-61.

Neri P., Morrone, M. C., Burr D. C. (1998). Seeing biological motion. Nature; 395:894–896.

Nothdurft, H. C., Gallant, J. L., Van Essen, D. C. (1999). Response modulation by texture surround in primate area V1: Correlates of “pop out” under anesthesia. Visual Neuroscience 16, 15–34.

Nijhawan, R. (2008). Visual prediction: psychophysics and neurophysiology of compensation for time delays. Behav. Brain Sci. 31, 179–198; discussion 198–239.

Nowak, L. G. Bullier, J. (1997). The timing of information transfer in the visual system, in Cerebral Cortex, Vol. 12: Extrastriate Cortex in primates, pp.205-241.

Nowak, L. G., Bullier, J. (1998). Axons, but not cell bodies, are activated by electrical stimulation in cortical gray matter. I. Evidence from chronaxie measurements. Exp. Brain Res. 118, 477–488.

Nowak L. G., Munk, M. H. J, Girard, P., Bullier J. (1995). Visual latencies in areas V1 and V2 of the macaque monkey. Visual Neuroscience, 12, 371-384.

Nurminen, L., Angelucci, A. (2014). Multiple components of surround modulation in primary visual cortex: multiple neural circuits with multiple functions? Vision Res; 0: 47–56.

Nurminen L., Peromaa, T., Laurinen, P. (2010). Surround suppression and facilitation in the fovea: very long-range spatial interactions in contrast perception. J. Vis.; 10(13):9.

O'Connor, D. H., Fukui, M. M., Pinsk, M. A., Kastner, S. (2002). Attention modulates responses in the human lateral geniculate nucleus. Nature Neuroscience, 5 1203-9.

Ohki, K., Chung, S., Ch'ng, Y. H., Kara, P., Reid, R. C. (2005). Functional imaging with cellular resolution reveals precise micro-architecture in visual cortex. Nature; 433:597–603.

Olshausen, B. A., Field, D. J. (1997). "Sparse coding with an overcomplete basis set: A strategy employed by V1?". Vision Research. 37 (23): 3311–3325.

O'Toole, B., Wenderoth, P. (1977). The tilt illusion: Repulsion and attraction effects in the oblique meridian. Vision Research, 17, 367–374.

Oram, M. W., Perrett, D. I. (1992). Time course of neural responses discriminating different views of the face and head. J Neurophysiol, 68(1), 70-84.

Orban, G. A, Kato, H., Bishop, P. (1979). Dimensions and properties of end-zone inhibitory areas in receptive fields of hypercomplex cells in cat striate cortex, J Neurophysiol. ;42(3):833-49.

Orban, G. A., Kennedy, H., Bullier, J. (1986). Velocity sensitivity and direction selectivity of neurons in areas V1 and V2 of the monkey: influence of eccentricity. J. Neurophysiol. Aug;56(2):462-80.

Orban, G. A, Kennedy, H., Maes, H. (1981). Response to movement of neurons in areas 17 and 18 of the cat: velocity sensitivity. J. Neurophysiol. 45: 1043–1058.

Ouellette, B. G., Casanova C. (2006). Overlapping visual response latency distributions in visual cortices and LP-pulvinar complex of the cat. Exp Brain Res 175: 332-341

Ozeki, H., Finn, I. M., Schaffer, E. S., Miller, K. D, Ferster, D. (2009). Inhibitory stabilization of the cortical network underlies visual surround suppression. Neuron; 62:578–592.

Ozeki, H., Sadakane, O., Akasaki, T., Naito, T., Shimegi, S., Sato, H. (2004). Relationship between excitation and inhibition underlying size tuning and contextual response modulation in the cat primary visual cortex. J Neurosci; 24:1428–1438

Pack, C. C., Born, R. T. (2001). Temporal dynamics of a neural solution to the aperture problem in visual area MT of macaque brain. Nature, 409: 1040-1042.

Packer, O. S., Dacey, D. M. (2002). Receptive field structure of H1 horizontal cells in macaque monkey retina. J Vis; 2: 272-292.

Packer, O. S, Dacey, D. M. (2005). Synergistic center-surround receptive field model of monkey H1 horizontal cells. J Vis; 5: 1038-1054.

Pan, Y., Chen, M., Yin, J., An, X., Zhang, X., Lu, Y., Gong, H., Li, W., Wang, W. (2012). Equivalent representation of real and illusory contours in macaque V4. J. Neurosci. 32, 6760–6770.

Paradiso, M. A. (1988). A theory for the use of visual orientation information which exploits the columnar structure of striate cortex. Biological Cybernetics, 58, 35–49.

Parnavelas, J. G, Burne, R. A, Lin, C. S. (1981). Receptive field properties of neurons in the visual cortex of the rat. Neurosci Lett; 27:291–296.

Pascual-Leone A., Walsh, V. (2001). Fast backprojections from the motion to the primary visual area necessary for visual awareness. Science; 292:510–512.

Passaglia, C. L., Enroth-Cugell, C., Troy, J. B. (2001). Effects of remote stimulation on the mean firing rate of cat retinal ganglion cells. J Neurosci; 21: 5794-5803.

Patterson, A. (1992). Rock art symbols of the greater southwest. Boulder, CO: Johnson Books.

Patterson, C. A., Duijnhouwer, J., Wissig, S. C., Krekelberg, B., Kohn, A. (2014). Similar adaptation effects in primary visual cortex and area MT of the macaque monkey under matched stimulus conditions. J. Neurophysiol. 111, 1203–1213.

Patterson, C. A., Wissig, S.C., Kohn, A. (2013). Distinct effects of brief and prolonged adaptation on orientation tuning in primary visual cortex. J. Neurosci. 33, 532–543.

Penfield, W., Perot, P. (1963) The Brain's Record of Auditory and Visual Experience. A Final Summary and Discussion. Brain, 86, 595-696.

Perin, R., Berger, T. K., Markram, H. (2011). A synaptic organizing principle for cortical neuronal groups. Proc. Natl. Acad. Sci. U.S.A. 108, 5419–5424.

Perkel, D. J., Bullier, J. and Kennedy, H. (1986). Topography of the afferent connectivity of area 17 in the macaque monkey: a double-labelling study., J Comp Neurol 253(3): 374–402.

Perlman, I., Normann, R. A. (1998). Light adaptation and sensitivity controlling mechanisms in vertebrate photoreceptors. Prog Retin Eye Res; 17: 523-563.

Perrett, D.I., Xiao, D., Barraclough, N.E., Keysers, C., Oram, M.W. (2009). Seeing the future: Natural image sequences produce "anticipatory" neuronal activity and bias perceptual report. The Quarterly Journal of Experimental Psychology, 62(11), 2081-2104.

Perrinet, L. U., Masson, G. S. (2012). Motion-based prediction is sufficient to solve the aperture problem. Neural Comput; 24(10):2726-50.

Pessoa, L., Thompson, E., Noe, A. (1998). Finding out about filling-in: a guide to perceptual completion for visual science and the philosophy of perception. Behav. Brain Sci. 21, 723–748; discussion 748–802.

Petitot, J. (2003). The neurogeometry of pinwheels as a sub-Riemannian contact structure. J. Phy siol., Paris 97., 265–309.

Pettigrew, J. D., Nikara, T., Bishop, P. O. (1968). Binocular interaction on single units in cat striate cortex: simultaneous stimulation by single moving slit with receptive fields in correspondence. Exp. Brain Res. 6: 391–410. PIOTROWSKI, L. N

Petrov, Y., McKee, S. P. (2006). The effect of spatial configuration on surround suppression of contrast sensitivity. J Vis ; 6:224–238.

Polat, U., Mizobe, K., Pettet, M. W., Kasamatsu, T., Norcia A. M. (1998). Collinear stimuli regulate visual responses depending on cell's contrast threshold. Nature, 391 (6667), 580–584.

Polat, U., Norcia, A. M. (1996). Neurophysiological evidence for contrast dependent long-range facilitation and suppression in the human visual cortex Vision Research, 36, pp. 2099-2109.

Polat, U., Sagi, D. (1993). Lateral interactions between spatial channels, suppression and facilitation revealed by lateral masking experiments. Vision Research 33, 993–999.

Polat, U., Sagi, D. (1994a). The architecture of perceptual spatial interactions. Vision Research 34, 73–78.

Polat, U., Sagi, D. (1994b). Spatial interactions in human vision, from near to far via experience-dependent cascades of connections. Proceeding of the National Academy of Sciences of the U.S.A. 91, 1206–1209.

Polat, U., Sagi, D. (1995). Plasticity of spatial interactions in early vision. In B. Jules z and I.kovacs (Eds.), Maturational windows and adult cortical plasticity, XXIV, pp. 1-15.

Polat, U., Tyler, C. W. (1999). What pattern the eye sees best. Vision Research, 39 (5), 887–895.

Priebe, N. J., Ferster, D. (2006). Mechanisms underlying cross-orientation suppression in cat visual cortex. Nat. Neurosci., 9, 552-561.

Priebe, N. J., Ferster D. (2012). Mechanisms of neuronal computation in mammalian visual cortex. Neuron ;75(2):194-208.

Purkinje, J. E. (1819/1823). Beobachtungen und versuche zur physiolgie der sinne: Beitrage zur kenntniss des schens in subjectiver hinsicht [Observations and experiments on the physiology of the senses: Contributions to the knowledge of vision in its subjective aspect]. Prague, Czechoslovakia: Calve.

Qiu, F. T., von der Heydt, R. (2005). Figure and ground in the visual cortex: V2 combines stereoscopic cues with gestalt rules. Neuron 47, 155–166.

Quiroga D.M. M., Morris, A. P., Krekelberg, B. (2016). Adaptation without plasticity. Cell Rep.;17(1):58-68.

Raiguel, S., Lagae, L., Gulyás, B., Orban, G.A. (1989). Response latencies of visual cells in macaque areas V1 V2 and V5. Brain Res, 493, pp. 155-159.

Raiguel, S., Van Hulle, M. M., Xiao, D. K, Marcar, V. L., Lagae, L., Orban G. A. (1997). Size and shape of receptive fields in the medial superior temporal area (MST) of the macaque. Neuroreport 8:2803-2808.

Raiguel, S., Van Hulle, M. M., Xiao, D. K., Marcar, V. L., Orban, G. A (1995). Shape and spatial distribution of receptive fields and antagonistic motion surrounds in the middle temporal area (V5) of the macaque. European Journal of Neuroscience, 7, pp. 2064-2082.

Rao, R. P. N., Ballard, D. H. (1999). Predictive Coding in the Visual Cortex: A Functional Interpretation of Some Extra-Classical Receptive Field Effects. Nature Neuroscience, 2, 79-87.

Rappel W. J., Strogatz S. H. (1994). Stochastic resonance in an autonomous system with a uniform limit cycle, Phys. Rev. E 50, 3249-3250.

Rees, G., Frith, C., Lavie, N. (2001). Processing of irrelevant visual motion during performance of an auditory attention task. Neuropsychologia;39(9):937-49.

Reid, R. C., Alonso, J. M. (1995). Specicity of monosynaptic connections from thalamus to visual cortex., Nature; 378,281-284

Reid, R. C; Alonso, J. M. (1996). The processing and encoding of information in the visual cortex. Curr. Op. Biol; 6, 475-480.

Remole, A. (1971). Luminance thresholds for subjective patterns in a flickering field: Effects of wavelength. Journal of the Optical Society of America, 61, 1164–1168.

Remole, A. (1973). Subjective patterns in a flickering field: Binocular vs monocular observation. Journal of the Optical Society of America, 63, 745–748.

Reynaud, A, Masson, G. S, Chavane, F. (2012). Dynamics of local input normalization result from balanced short- and long-range intracortical interactions in area V1. J Neurosci. 5;32(36):12558-69.

Reynaud, A., Takerkart, S., Masson, G. S, Chavane, F. (2011) Linear model decomposition for voltage-sensitive dye imaging signals: application in awake behaving monkey. Neuroimage 54:1196–1210.

Richards, W. (1971). The fortification illusions of migraines. Scientific American, 224(5), 88–96.

Ringach, D. L. (2009). Spontaneous and driven cortical activity: Implications for computation. Current Opinion in Neurobiology, 19, 439–444.

Ringach, D. L., Hawken, M. J., Shapley, R. (1997). Dynamics of orientation tuning in macaque primary visual cortex. Nature 387:281–284.

Riva, S. E., Agnati, L. F., Maioli, M. G., Galletti, C. (1973) Maintained activity of single neurons in striate and non-striate areas of cat visual-cortex. Brain Res; 54:225–242.

Rizzolatti, G., Camarda, R. (1977). Influence of the presentation of remote visual stimuli on visual responses of cat area 17 and lateral suprasylvian area. Experimental Brain Research, 29, 1077122.

Robinson, D. A. (1965). The mechanics of human smooth pursuit eye movement. J. Physiol. 180, 569-591.

Rockland, K. S. (2003). Feedback connections: splitting the arrow. In: Kaas, JH.; Collins, CE., editors. The primate visual system. CRC Press; p. 387-405.

Rockland, K. S. (2010). Five points on columns. Front. Neuroanat. 4:22.

Rockland, K.S., Knutson, T. (2000). Feedback connections from area MT of the squirrel monkey to areas V1 and V2. J Comp Neurol; 425:345–368.

Rockland, K. S, Lund, J. S. (1982). Widespread periodic intrinsic connections in the tree shrew visual cortex. Science; 215:1532–1534.

Rockland, K. S, Lund, J. S. (1983). Intrinsic laminar lattice connections in primate visual cortex. J Comp Neurol; 216:303–318.

Rockland, K. S., Pandya, D. N. (1979). Laminar origins and terminations of cortical connections of the occipital lobe in the Rhesus monkey. Brain Res; 179:3–20.

Rodieck, R. W., Stone, J. (1965). Analysis of receptive fields of cat retinal ganglion cells. J Neurophysiol; 28: 832-849. PMID: 5867882

Roe, A. W., Lu, H. D., Hung, C. P. (2005). Cortical processing of a brightness illusion. Proc. Natl Acad. Sci. USA 102, 3869–3874.

Roelfsema, P. R., Lamme, V. A., Spekreijse, H. (1998). Object-based attention in the primary visual cortex of the macaque monkey., Nature 395(6700): 376–81.

Roerig, B., Chen, B. (2002). Relationships of local inhibitory and excitatory circuits to orientation preference maps in ferret visual cortex. Cereb Cortex., Feb;12(2):187-98.

Roland, P. E. (2002). Dynamic depolarisation fields in the cerebral cortex. Trends Neurosci. 25. 183–190.

Rose, D. (1974). Proceedings: The hypercomplex cell classification in the cat's striate cortex, J Physiol 242(2): 123P–125P.

Rosenquist, A. L., Edwards, S. B., Palmer, L. A. (1974). An autoradiographic study of the projections of the dorsal lateral geniculate nucleus and posterior nucleus in the cat. Brain Res. 80, 71-93.

Royal, D. W., Sáry, G., Schall, J. D., Casagrande, V. A. (2005). Correlates of motor planning and postsaccadic fixation in the macaque monkey lateral geniculate nucleus. Exp Brain Res 168(1-2):62-75

Sadakane, O., Ozeki, H., Naito, T., Akasaki, T., Kasamatsu, T., Sato, H. (2006). Contrast-dependent, contextual response modulation in primary visual cortex and lateral geniculate nucleus of the cat. European Journal of Neuroscience, 23, 1633–1642.

Salin, P. A., Bullier, J. (1995). Corticocortical connections in the visual system: structure and function, Physiol Rev 75(1): 107–54.

Salin, P. A., Bullier, J., Kennedy, H. (1989). Convergence and divergence in the afferent projections to cat area 17. J Comp Neurol 283(4): 486–512.

Salin, P. A., Girard, P., Kennedy, H., Bullier, J. (1992) The visuotopic organization of corticocortical connections in the visual system of the cat. J. Comp. Neurol., 320: 415-434.

Salin, P. A. Prince, D. A. (1996). Electrophysiological mapping of GABAA receptor-mediated inhibition in adult rat somatosensory cortex, J Neurophysiol 75(4): 1589–600.

Sanchez-Vives, M. V., Nowak, L.G., McCormick, D. A. (2000). Membrane mechanisms underlying contrast adaptation in cat area 17 in vivo. J. Neurosci. 20, 4267–4285.

Sarti, A., Citti, G., Petitot, J. (2007). The symplectic structure of the primary visual cortex. Biol. Cybern; 98(1):33-48.

Sarti A., Citti G., Petitot, J. (2009). Functional geometry of the horizontal connectivity in the primary visual cortex, J. Physiol. (Paris) 103; 1-2, 37–45.

Sato, T. K., Nauhaus, I., Carandini, M. (2012) Traveling waves in visual cortex. Neuron. 2:218-29.

Sawaguchi, T. (1994) Modular activation and suppression of neocortical activity in the monkey revealed by optical imaging. NeuroReport 6, 185–189.

Sceniak, M. P., Chatterjee, S., Callaway, E. M. (2006). Visual spatial summation in macaque geniculocortical afferents. J Neurophysiol; 96:3474–3484.

Sceniak, M. P., Hawken, M. J., Shapley, R. M. (2001). Visual spatial characterization of macaque V1 neurons. J. Neurophysiol.,85: 1873-1887.

Sceniak, M. P., Ringach, D. L., Hawken, M. J., Shapley, R. M. (1999). Contrast's effect on spatial summation by macaque V1 neurons. Nat. Neurosci., 2: 733-739.

Schmidt, K. E., Goebel, R., Löwell, S., Singer, W. (1997a). The perceptual grouping criterion of colinearity is reflected by anisotropies of connections in the primary visual cortex. Eur J Neurosci 9:1083–1089.

Schmidt, K. E., Kim, D. S., Singer, W., Bonhoeffer, T., Löwel, S. (1997b). Functional specificity of long-range intrinsic and interhemispheric connections in the visual cortex of strabismic cats, J Neurosci 17: 5480–5492.

Schmolesky, M. T., Wang, Y., Hanes, D. P., Thompson, K. G., Leutgeb, S., Schall, J. D., Leventhal A. G. (1998). Signal timing across the macaque visual system. J. Neurophysiol. 79: 3272 – 3278.

Schölvinck, M. L., Rees, G. (2010). Neural correlates of motion-induced blindness in the human brain. J. Cogn. Neurosci; 22:1235–1243.

Schwabe, L., Ichida, J. M., Shushruth, S., Mangapathy, P., Angelucci, A. (2010). Contrast dependence of surround suppression in Macaque V1: experimental testing of a recurrent network model. Neuroimage 52, 777-792.

Schwarz, C., Bolz, J. (1991). Functional specificity of a long-range horizontal connection in cat visual cortex: a cross-correlation study. J Neurosci;11(10):2995-3007.

Segel, L. A., Jackson, J. L. (1972). Dissipative structure: An explanation and an ecological example. Journal of Theoretical Biology, 37, 545–559.

Segel, L. A., Levin, S. A. (1976). Application of nonlinear stability theory to the study of the effects of diffusion on predator-prey interactions. In R. A. Piccirrelli (Ed.), Topics in statistical mechanics and biophysics: A memorial to Julius L. Jackson (pp. 123–152).

Seghier, M. L., Vuilleumier, P. (2006). Functional neuroimaging findings on the human perception of illusory contours. Neurosci. Biobehav. Rev. 30,595–612.

Sengpiel, F., Hubener, M. (1999). Visual attention: spotlight on the primary visual cortex., Curr Biol 9(9): R318–21.

Sengpiel, F., Sen, A., Blakemore, C. (1997). Characteristics of surround inhibition in cat area 17. Experimental Brain Research, 116, 216–228.

Series, P., Georges, S., Lorenceau, J., Fregnac, Y. (2002). Orientation dependent modulation of apparent speed: a model based on the dynamics of feed-forward and horizontal connectivity in V1 cortex.Vision research 42 (25), 2781-2797.

Series, P., Lorenceau, J., Fregnac, Y. (2003). The ‘‘silent’’ surround of V1 receptive fields: Theory and experiments. Journal of Physiology (Paris), 97, 453–474.

Serre, T., Oliva, A., Poggio, T. (2007a) A feedforward architecture accounts for rapid categorization. Proc. Natl.Acad. Sci., 104(15): 6424–6429.

Shang C.F., Dan Y., Poo M. M., Wang Z. (2011). Periodic stimulation induces long-range modulation of cortical responses and visual perception. The Journal of Physiology. 589: 3125-33.

Shannon, C. E. (1948). A Mathematical Theory of Communication. (1948) Bell System Technical Journal, 27: 3. pp 379-423.

Shao, Z., Burkhalter, A. (1996). Different balance of excitation and inhibition in forward and feedback circuits in rat visual cirtex, J Neurosci 16(22): 7353–7365.

Shapley, R., Enroth-Cugell. (1984). C. Visual adaptation and retinal gain controls. Prog Retin Eye Res; 3: 263-346.

Shen W., Liang Z., Chen X., Shou T. (2006). Posteromedial lateral suprasylvian motion area modulates direction but not orientation preference in area 17 of cats. J. Neuroscience 142, 905–916.

Shen W., Liang Z., Shou T. (2008). Weakened feedback abolishes neural oblique effect evoked by pseudo-natural visual stimuli in area 17 of the cat. Neurosci. Lett. 437, 65–70

Sheth, B. R., Sharma, J., Rao, S. C., Sur, M. (1996). Orientation maps of subjective contours in visual cortex. Science 274, 2110–2115.

Shimojo, S., Kamitani, Y., Nishida, S. (2001). Afterimage of perceptually filled-in surface. Science 293,1677–1680.

Shipp S., Zeki, S. (1989). The organization of connections between areas V5 and V1 in macaque monkey visual cortex. Eur J Neurosci; 1:309–332.

Shmuel, A., Korman, M., Sterkin, A., Harel, M., Ullman, S., Malach, R., Grinvald, A. (2005). Retinotopic axis specificity and selective clustering of feedback projections from V2 to V1 in the owl monkey. J Neurosci; 25:2117–2131.

Shoham D., Glaser D. E., Arieli A., Kenet T., Wijnbergen C., Toledo Y., Hildesheim R., Grinvald A. (1999) Imaging cortical dynamics at high spatial and temporal resolution with novel blue voltage-sensitive dyes. Neuron 24, 791–802

Shulz, D. E., Fregnac, Y. (2010). From sensation to perception. In Encyclopedia of Behavioural Neuroscience, G. Koob, M. Le Moal, and R. Thompson, eds. (Elsevier), pp. 550–558.

Shushruth, S., Ichida, J. M, Levitt, J. B, Angelucci A. (2009). Comparison of spatial summation properties of neurons in macaque V1 and V2. J Neurophysiol; 102:2069–2083.

Shushruth, S., Mangapathy, P., Ichida, J. M., Bressloff, P. C, Schwabe, L., Angelucci, A. Strong recurrent networks compute the orientation-tuning of surround modulation in primate primary visual cortex. J Neurosci; 4:308–321.

Shushruth, S., Nurminen, L., Bijanzadeh, M., Ichida, J. M., Vanni, S., Angelucci, A. (2013). Different orientation-tuning of near and far surround suppression in macaque primary visual cortex mirrors their tuning in human perception. J Neurosci; 33:106–119.

Siegel, R. K. (1977). Hallucinations. Scientific American, 237(4), 132-140.

Siegel, R. K., West, L. J. (1975). (eds.): Hallucinations, Wiley, New York.

Siegel, R. K., Jarvik, M. E. (1975). Drug-induced hallucinations in animals and man. In R. K. Siegel, & L. J. West (Eds.), Hallucinations (pp. 81–162). New York, NY: Wiley.

Sillito, A. M., Cudeiro, J., Jones, H. E. (2006). Always returning: feedback and sensory processing in visual cortex and thalamus. Trends Neurosci; 29:307–316.

Sillito, A. M., Cudeiro, J., Murphy, P. C. (1993) Orientation sensitive elements in the corticofugal influence on centre-surround interactions in the dorsal lateral geniculate nucleus. Exp. Brain Res. 93(1):6-16.

Sillito, A. M., Grieve, K. L., Jones, H. L., Cuderio, J., Davis, J. (1995). Visual cortical mechanisms detecting focal orientation discontinuities. Nature, 378, pp. 492-496

Sillito A. M., Jones, H. E (1996). Context-dependent interactions and visual processing in V1. Journal of Physiology (Paris), Volume 90, Issues 3–4, Pages 205-209.

Simoncelli, E. P., Olshausen, B. A. (2001). Natural image statistics and neural representation. Annu Rev Neurosci.;24:1193-216.

Sincich, L. C., Blasdel, G. G. (2001). Oriented axon projections in primary visual cortex of the monkey. J Neurosci 21:4416–4426.

Sincich, L. C., Park, K. F., Wohlgemuth, M. J., Horton, J. C. (2004). Bypassing V1: a direct geniculate input to area MT. Nat Neurosci; 7:1123–1128.

Sit, Y. F., Chen, Y., Geisler, W. S., Miikkulainen, R., Seidemann, E. (2009). Complex dynamics of V1 population responses explained by a simple gain-control model. Neuron., 64(6):943-56.

Slovin, H., Arieli, A., Hildesheim, R., Grinvald, A. (2002) Long-term voltage-sensitive dye imaging reveals cortical dynamics in behaving monkeys. J Neurophysiol 88:3421–3438.

Smythies, J. R. (1959a). The stroboscopic patterns: I. The dark phase. British Journal of Psychology, 50, 106–116.

Smythies, J. R. (1959b). The stroboscopic patterns: II. The phenomenology of the bright phase and after-images. British Journal of Psychology, 50, 305–324.

Smythies, J. R. (1960). The stroboscopic patterns: III. Further experiments and discussion. British Journal of Psychology, 51, 247–255.

Sohya, K., Kameyama, K., Yanagawa, Y., Obata, K., Tsumoto, T. (2007). Gabaergic neurons are less selective to stimulus orientation than excitatory neurons in layer II/III of visual cortex, as revealed by in vivo functional Ca2+ imaging in transgenic mice. J Neurosci ;27 :2145–2149.

Solomon, S. G., Lee, B. B., Sun, H. (2006). Suppressive surrounds and contrast gain in magnocellular-pathway retinal ganglion cells of macaque. J Neurosci; 26:8715–8726.

Solomon, J. A., Morgan, M. J. (2000). Facilitation from collinear flanks is cancelled by non-collinear flanks. Vision Res. 40, 279–286.

Solomon, S. G., White, A., Martin, P. (2002). Extraclassical receptive field properties of parvocellular, magnocellular, and koniocellular cells in the primate lateral geniculate nucleus. J Neurosci; 22:338–349.

Somers, D. C., Dale, A. M., Seiffert, A. E., Tootell, R. B. (1999). Functional MRI reveals spatially specific attentional modulation in human primary visual cortex., Proc Natl Acad Sci USA 96(4): 1663–8.

Somers, D. C., Nelson, S. B., Sur, M. (1995). An emergent model of orientation selectivity in cat visual cortical simple cells. J. Neurosci. 15, 5448–5465.

Somers, D. C., Todorov, E., Siapas, A. G., Toth, L. J., Kim, D., Sur, M. (1998). A local circuit approach to understanding integration of long-range inputs in primary visual cortex, Cereb. Cortex 8: 204–217.

Song, S., Sjöström, P. J., Reigl, M., Nelson, S., Chklovskii, D. B. (2005). Highly nonrandom features of synaptic connectivity in local cortical circuits. PLoSBiol. 3(10): e350.

Song, X. M., Wang, Y., Zhu, Z., Li, C. Y. (2010). Morphological bases of suppressive and facilitative spatial summation in the striate cortex of the cat. PLoS ONE, e15025.

Spratling, M. W. (2010). Predictive coding as a model of response properties in cortical area v1. J. Neurosci. 30, 3531–3543.

Sterzer, P., Haynes, J. D., Rees, G. (2006). Primary visual cortex activation on the path of apparent motion is mediated by feedback from hMT+/V5; 32(3):1308-16.

Stettler, D. D, Das, A., Bennett, J., Gilbert, C. D. (2002). Lateral connectivity and contextual interactions in macaque primary visual cortex. Neuron; 36:739–750.

Stocker, A. A., Simoncelli, E. P. (2006). Noise characteristics and prior expectations in human visual speed perception. Nat Neurosci;9(4):578-85.

Summerfield, J. J., Rao, A., Garside, N., Nobre A.C. (2011). Biasing perception by spatial long-term memory. J Neurosci;31(42):14952-60.

Summerfield, C., Trittschuh, E. H., Monti, J. M., Mesulam, M. M., Egner, T. (2008). Neural repetition suppression reflects fulfilled perceptual expectations. Nat. Neurosci., 11, pp. 1004-1006.

Tanifuji, M., Sugiyama, T., Murase, K. (1994). Horizontal proagation of excitation in rat visual cortical slices revealed by optical Imaging. Science 266, 1057-1059.

Tass, P. (1995). Cortical pattern formation during visual hallucinations. J. Biol. Phys. 21, 177-210.

Tass, P. (1997). Oscillatory cortical activity during hallucination. Journal of Biological Physics, 23, 21–66.

Teich, A. F., Qian, N. (2003). Learning and adaptation in a recurrent model of V1 orientation selectivity. J. Neurophysiol. 89, 2086–2100.

Thoreson, W. B, Mangel, S. C. (2012). Lateral interactions in the outer retina. Prog Retin Eye Res.pp. 407-441.

Thorpe, S. J, Fize. D., Marlot, C. (1996). Speed of processing in the human visual system. Nature, 381(6582), 520-522.

Thorpe, S. J., Imbert, M. (1989). Biological constraints on connectionist models. In R. Pfeifer, Z. Schreter, F. Fogelman-Soulie, & I., Steels (Eds.), Connectionism in perspective (pp. 63-92). Amsterdam: Elsevier.

Tlapale, E., Masson, G. S., Kornprobst, P. (2010). Modelling the dynamics of motion integration with a new luminance-gated diffusion mechanism. Vision. Res. 50, 1676–1692.

Tootell, R. B. H., Hadjikhani, N. K., Vanduffel, W., Liu, A. K., Mendola, J. D., Sereno, M. I., and Dale, A. M. (1998). Functional analysis of primary visual cortex (V1) in humans. Proc Natl Acad Sci USA; 95(3):811-7.

Tootell, R. B. H., Silverman, M. S., Switkes, E., DeValois, R. L. (1982). Deoxyglucose Analysis of Retinotopic Organization in Primate Striate Cortex. Science, 218, p. 902 -904.

Tootell, R. B. H., Switkes, E., Silverman, M. S., Hamilton, S. L. (1988). Functional anatomy of macaque striate cortex. II. Retinotopic organization. J Neurosci., 8: 1531-1568.

Toth, L. J., Rao, S. C., Kim, D. S., Somers, D., Sur, M. (1996). Subthreshold facilitation and suppression in primary visual cortex revealed by intrinsic signal imaging, Proc Natl Acad Sci USA 93: 9869–9874.

Toyama, K., Matsunami, K., Ohno, T. (1969). Antidromic identification of association, commissural and corticofugal efferent cells in cat visual cortex. Brain Res. 14, 513–517.

Toyama, K., Tanifuji, M. (1991). Seeing excitation propagation in visual cortex. Biomedical Research, 12, 145-147.

Troncoso, X., Pananceau, M., Le Bec, B., Desbois, C., Gerard-Mercier, F., Fregnac, Y. (2015) Spatial synergy and temporal coherence requirements for binding the feedforward and horizontal waves in V1. American Society for Neuroscience Abstracts, Chicago, IL.

Ts'o, D., Gilbert, C., Wiesel, T.W. (1986). Relationships between horizontal interactions and functional architecture in cat striate cortex as revealed by cross-correlation analysis., J Neurosci 6(4): 1160–1170.

Turing, A. M. (1952). The chemical basis of morphogenesis. Philosophical Transactions of the Royal Society of London: Series B. Biological Sciences, 237, 37–72.

Tusa, R. J., Palmer, L. A., Rosenquist, A. C. (1978). The retinotopic organization of area 17 (striate cortex) in the cat. J Comp Neurol.15;177(2):213-35.

Tyler, C. W. (1978). Some new entopic phenomena. Vision Research, 18, 1633–1639.

Van Essen, D. C., Newsome, W. T., Maunsell, J. H. R. (1984). The visual field representation in striate cortex of macaque monkey: asymmetries, anisotropies, and individual variability. Vis. Res., 24: 429-448.

Verghese, P., McKee, S. P., Grzywacz, N. M. (2000). Stimulus configuration determines the detectability of motion signals in noise. Journal of Optical Society of America, 17, pp. 1525-1534.

Vetter, P., Edwards, G., Muckli, L. (2012). Transfer of predictive signals across saccades. Front. Psychology 3:176.

Vidyasagar, T. R., Buzas, P., Kisvarday, Z. F., Eysel, U. T. (1999). Release from inhibition reveals the visual past. Nature, 399, 422.

Voges, N., Perrinet, L. (2012). Complex dynamics in recurrent cortical networks based on spatially realistic connectivities. Front. Comput. Neurosci. 6:41 10.3389.

Von der Heydt, R., Friedman, H., Zhou, H. in Filling-in (eds Pessoa, L. & De Weerd, P.) 106–127 (Oxford Univ. Press, New York, 2003).

Von der Heydt, R., Peterhans, E., Baumgartner, G. (1984). Illusory contours and cortical neuron responses. Science 224, 1260–1262.

Von der Heydt, R., Peterhans, E. Dursteler, M. R. (1992). Periodic-pattern-selective cells in monkey visual cortex, J Neurosci 12(4): 1416–34.

Wacongne, C., Labyt, E., van, Wassenhove, V., Bekinschtein, T., Naccache, L., Dehaene, S. (2011) Evidence for a hierarchy of predictions and prediction errors in human cortex. Proc Natl Acad Sci USA 108:20754–20759.

Wagemans, J., Feldman, J., Gepshtein S., Kimchi, R., Pomerantz, J. R., Van Der Helm, P. A., Van Leeuwen, C. (2012). A century of Gestalt psychology in visual perception: II. Conceptual and theoretical foundations. Psychol Bull. 2012 Nov;138(6):1218-52.

Walker, G. A., Ohzawa, I., Freeman, R. D. (1999). Asymmetric suppression outside the classical receptive field of the visual cortex. Journal of Neuroscience, 19, 10536–10553.

Walker, G. A., Ohzawa, I., Freeman, R. D. (2000). Suppression outside the classical cortical receptive field. Visual Neuroscience 17, 369–379.

Walls, G. L. (1954). The filling-in process. Am. J. Optom. Arch. Am. Acad. Optom. 31, 329–341.

Walter, V. J., Walter, W. G. (1949). The central effects of rhythmic sensory stimulation. Electroencephalography and Clinical Neurophysiology, 1, 57–86.

Walter, W. G. (1956). Colour illusions and aberrations during stimulation by flickering light. Nature, 177, 710.

Wang, C., Bardy, C., Huang, J. Y., FitzGibbon, T., Dreher, B. (2009). Contrast dependence of center and surround integration in primary visual cortex of the cat. Journal of Vision, 9, 1–15.

Wang, C., Huang, J. Y., Bardy, C., FitzGibbon, T., Dreher, B. (2010). Influence of 'feedback' signals on spatial integration in receptive fields of cat area 17 neurons. Brain Res. 1328, 34–4810.1016.

Wang, J., Kádár, S., Jung, P., Showalter, K. (1999). Noise driven Avalanche behavior in subexcitable media. Physical Review Letters, 82, 855–858.

Wang, K. H., Majewska, A., Schummers, J., Farley, B., Hu, C., Sur, M., Tonegawa, S. (2006). In vivo two-photon imaging reveals a role of arc in enhancing orientation specificity in visual cortex. Cell; 126:389–402.

Wang, C., Waleszczyk, W. J., Burke, W., Dreher, B. (2000). Modulatory influence of feedback projections from area 21a on neuronal activities in striate cortex of the cat. Cereb. Cortex 10, 1217–1232.

Wang, C., Waleszczyk, W., Burke, W., Dreher, B. (2007). Feedback signals from cat's area 21a enhance orientation selectivity of area 17 neurons. Exp. Brain Res. 182, 479–490.

Watamaniuk, S. N. J., McKee, S. P., Grzywacz, N. M. (1995). Detecting a trajectory embedded in random-direction motion noise. Vision Research, 35, pp. 65-77

Webb, B. S., Dhruv, N. T., Solomon, S. G., Tailby, C., Lennie, P. Early (2005). Early and late mechanisms of surround suppression in striate cortex of macaque. J Neurosci; 25:11666–11675.

Webb, B. S., Tinsley, C. J, Barraclough, N. E, Easton, A., Parker, A., Derrington, A. M. (2002). Feedback from V1 and inhibition from beyond the classical receptive field modulates the responses of neurons in the primate lateral geniculate nucleus. Vis Neurosci.19:583–592.

Weber, B., Keller, A. L., Reichold, J., Logothetis, N. K. (2008). The microvascular system of the striate and extrastriate visual cortex of the macaque. Cerebral Cortex, Volume 18, Issue 10, Pages 2318–2330.

Weiss, Y., Simoncelli, E. P., Adelson, E. H. (2002). Motion illusions as optimal percepts. Nature Neuroscience volume5, pages 598–604.

Weliky, M., Kandler, K., Fitzpatrick, D. and Katz, L. C. (1995). Patterns of excitation and inhibition evoked by horizontal connections in visual cortex share a common relationship to orientation columns. Neuron 15(3): 541–52.

Wenderoth, P., Johnstone, S. (1988). The different mechanisms of the direct and indirect tilt illusions. Vision Research, 28, 301–312.

Werkhoven, P., Snippe, H.P., Koenderink, J. J. (1990). Effects of element orientation on apparent motion. Percept Psychophysics, 47, pp. 509-525

Westheimer, G. (1989). Neural mechanisms of visual perception. In Line orientation considered as a separate psychophysical domain. (pp. 237–246). Texas: The Woodlands, chapter 11.

Westheimer, G. (1990). Simultaneous orientation contrast for lines in the human fovea. Vision Research, 30, 1913–1921.

Westheimer, G., Shimamura, K., McKee, S. P. (1976). Interference with line-orientation sensitivity. Journal of the Optical Society of America, 66, 332–338.

White, L. E., Coppola, D. M., Fitzpatrick, D. (2001). The contribution of sensory experience to the maturation of orientation selectivity in ferret visual cortex. Nature, 411, pp. 1049-1052.

Wibral, M., Turi, G., Linden, D.E., Kaiser, J., Bledowski, C. (2008). Decomposition of working memory-related scalp ERPs: crossvalidation of FMRI-constrained source analysis and ICA. J Psychophysiol;67(3):200-11. Epub 2007 Aug 10.

Wiener, M. C. (1994). Hallucinations, symmetry, and the structure of primary visual cortex: A bifurcation theory approach. Unpublished doctoral dissertation, University of Chicago.

Wiesenfeld, Z., Kornel, E. E. (1975). Receptive fields of single cells in the visual cortex of the hooded rat. Brain Res; 94:401–412.

Wiesenfeld, K., Moss, F. (1995). Stochastic resonance and the benefits of noise: from ice ages to crayfish and SQUIDs. Nature 373, 33-36.

Wilkinson, F. (2004). Auras and other hallucinations: Windows on the visual brain. Progress in Brain Research, 144, 305–320.

Winters, W. D., Wallach, M. B. (1970). Drug-induced states of CNS excitation: A theory of hallucinosis. In Psychotomimetic Drugs, pp 193-214. Efron, D.H. (ed) New York: Raven Press.

Winterson, B. J., Robinson, D. A. (1975). Fixation by the alert but solitary cat. Vision Research, 15, 1349–1352.

Wissig, S. C., Kohn, A. (2012). The influence of surround suppression on adaptation effects in primary visual cortex. J. Neurophysiol. 107, 3370–3384.

Wörgotter, F., Eysel, U. T. (1989). Axis of preferred motion is a function of bar length in visual cortical receptive fields. Experimental Brain Research, 76, pp. 307-314

Wörgotter, F., Eysel, U. T. (1991). Correlations between directional and orientational tuning of cells in cat striate cortex. Exp. Brain Res., 83, pp. 665-669.

Wörgotter, F. Eysel, U. T. (2000). Context, state and the receptive fields of striatal cortex cells, Trends Neurosci 23(10): 497.

Wörgotter, F., Suder, K., Zao, Y., Kersher, N., Eysel, U. T., Funke, K. (1998). State-dependent receptive field restructuring in the visual cortex, Nature 396: 165–168.

Wunderlich K, Schneider K. A, Kastner S. (2005). Neural correlates of binocular rivalry in the human lateral geniculate nucleus. Nat. Neurosci ;8 :1595–1602.

Xu, X., Ichida, J. M., Allison, J. D., Boyd, J. D., Bonds, A. B., Casagrande, V. A. (2001). A comparison of koniocellular, magnocellular and parvocellular receptive field properties in the lateral geniculate nucleus of the owl monkey (Aotus trivirgatus).J. Physiol. 531 (Pt 1): 203–18.

Yabuta, N. H., Sawatari, A., Callaway, E. M. (2001). Two functional channels from primary visual cortex to dorsal visual cortical areas. Science, 292:297-300.

Yeonan-Kim J., Bertalmio, M. (2016) Retinal Lateral Inhibition Provides the Biological Basis of Long-Range Spatial Induction. PLoS ONE 11(12): e0168963.

Yi, D. J., Turk-Browne, N. B., Flombaum, J. I., Kim, M. S., Scholl, B. J., Chun, M. M. (2008). Spatiotemporal object continuity in human ventral visual cortex. PNAS; 105:8840–8845.

Yoshioka, T., Blasdel, G. G., Levitt, J. B. and Lund, J. S. (1996). Relation between patterns of intrinsic lateral connectivity, ocular dominance, and cytochrome oxidase-reactive regions in macaque monkey striate cortex. Cereb Cortex 6(2): 297–310.

Young, L., Stark, L. (1963). Variable feedback experiments testing a sampled data model for eye tracking movements. Institute of Electrical and Electronics Engineers, Transactions in Human Factors in Electronics HFE-4 pp. 38-51.

Yoshimura, Y., Sato, H., Imamura, K., Watanabe, Y. (2000). Properties of horizontal and vertical inputs to pyramidal cells in the superficial layers of the cat visual cortex. Journal of Neuroscience 20, 1931–1940.

Yousef, T., Bonhoeffer, T., Kim, D. S., Eysel, U. T., Tóth, E. and Kisvárday, Z. F. (1999). Orientation topography of layer 4 lateral networks revealed by optical imaging in cat visual cortex. Eur J Neurosci 11: 4291–4308.

Yousef, T., Toth, E., Raush, M., Eysel, U. T., Kisvárday, Z. F. (2001). Topography of orientation centre connections in the primary visual cortex of the cat, Neuroreport 12(8): 1693–1699.

Zhou, H., Friedman, H. S., von der Heydt, R. (2000). Coding of border ownership in monkey visual cortex. J. Neurosci. 20, 6594–6611.

Zipser, K., Lamme, V. A. F., Schiller, P. H. (1996). Contextual modulation in primary visual cortex. J. Neurosci. 15, 7376–7389.